Third International Workshop on Ion Mobility Spectrometry

John H. Cross, Editor
KRUG Life Sciences Inc.
Houston, Texas

1995

FOREWORD

In the past few years, rapid advancement in hardware development and applications has grown out of the basic research conducted in ion mobility spectrometry (IMS). It has been the goal of the Ion Mobility Spectrometry workshops to provide a forum for investigators to present the most recent results of both basic and applied IMS research. These unique meetings have assembled university, government, and industry researchers, users, and suppliers of IMS systems in a format that has encouraged discussion and high quality presentations.

The 3rd International Workshop on Ion Mobility Spectrometry continued the fine traditions established during the first two workshops with the presentation of 30 quality papers covering a wide breath of topics from hardware development to software development and user applications. Researchers new to the IMS field were evident in both software, hardware, and basic science areas which is indicative of the growth of IMS. Over 60 scientists attended the 3rd International Workshop on Ion Mobility Spectrometry comprised of 5 sessions. Participants agreed that the level of interest in IMS has advanced to the point where a steering committee was needed to help organize future workshops and insure smooth transitions between workshops.

The organizers would like to thank the authors for their prompt response in submitting manuscripts for these proceedings, and we look forward to seeing everybody in England next year at the 4th International Workshop on Ion Mobility Spectrometry.
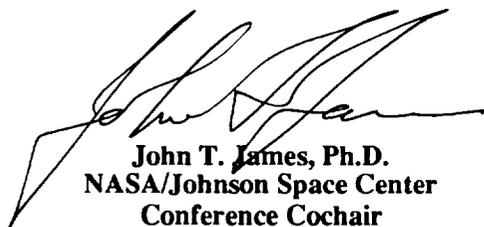
John T. James, Ph.D.
NASA/Johnson Space Center
Conference Cochair

Thomas F. Limero, Ph.D.
KRUG Life Sciences
Conference Cochair

KRUG
LIFE SCIENCES
A KRUG International Company

iii

ACKNOWLEDGEMENTS

CONTENTS

SESSION IV: **Applications**
Session Chair: **Dr. Robert Turner**

SESSION V: **Data Reduction and Signal Processing**
Session Chair: **Dr. Dennis Davis**

APPENDIX A:

Session I: Fundamental IMS Studies

Session Chair: Dr. André Lawrence

PROTON AFFINITY DETERMINATIONS AND

PROTON - BOUND DIMER STRUCTURE INDICATIONS IN

C2 TO C15, α,ω-ALKYLDIAMINES

Z. Karpas[a], C. S. Harden and P. B. W. Smith[b]
Edgewood Research, Development and Engineering Center,
Aberdeen Proving Ground, MD 21010, U. S. A.

ABSTRACT

The "kinetic method" was used to determine the proton affinity (PA) of α,ω-alkyldiamines from collision induced dissociation (CID) studies of protonated heterodimers. These PA values were consistently lower than those reported in the proton affinity scale. The apparent discrepancy was rationalized in terms of differences in the conformation of the protonated diamine monomers. The minimum energy species, formed by equilibrium proton transfer processes, have a cyclic conformation and the ion charge is shared by both amino-groups which are bridged by the proton. On the other hand, the species formed through dissociation of protonated dimers have a linear structure and the charge is localized on one of the amino-groups. Thus, the difference in the PA values obtained by both methods is a measure of the additional stability acquired by the protonated diamines through cyclization and charge delocalization.

The major collision dissociation pathway of the protonated diamine monomers involved elimination of an ammonia moiety. Other reactions observed included loss of the second amino-group and several other bond cleavages. CID of the protonated dimers involved primarily formation of a protonated monomer through cleavage of the weaker hydrogen bond and subsequently loss of ammonia at higher collision energies. As observed from the CID studies, doubly charged ions were also formed from the diamines under conditions of the electrospray ionization.

Permanent address:
a. Analytical Chemistry Department, Nuclear Research Center, Negev, P.O. Box 9001, Beer-Sheva, ISRAEL 84190
b. Geo-Centers, Inc., P.O. Box 68, Gunpowder Branch, Aberdeen Proving Ground, MD 21010-0068.

INTRODUCTION

The "kinetic method"

The "kinetic method" has been used to obtain thermodynamic data on ions, as described in detail elsewhere [1-11]. Originally it was used to study the dissociation of proton bound dimers in the field free region of a reverse geometry magnetic mass spectrometer, but subsequently collision induced dissociation (CID) methods were also successfully deployed [9-10]. The kinetic method was used to study the proton affinities (PAs) of aliphatic and aromatic amines [1-2], the acidity of carboxylate anions [3,10], alkoxide ions [4,11] and nitrates [5], to differentiate between stereo isomers and determine alkali ion affinities [6,7] and the PAs of amino acids [8,9].

The basis of the method is to compare the rates of competitive dissociation channels (1a) and (1b), as represented by reaction (1):

$$\text{A--H}^+\text{--B} \begin{cases} \text{---> A + BH}^+ & \text{(1a)} \\ \text{---> AH}^+ + \text{B} & \text{(1b)} \end{cases}$$
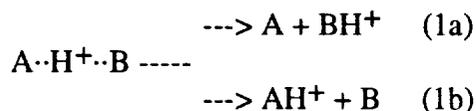
It was demonstrated that a linear relationship existed between the logarithm of the product ion peak height ratios AH^+/BH^+ and the proton affinities of the fragments, A and B. The underlying logic was that for similar species A and B the competitive fragmentation of the protonated dimer should have similar entropy changes and that the reverse activation energy would be small as the reaction involves a simple bond cleavage process. Therefore the rate of fragmentation in each channel should be controlled by the relative activation energies, i. e. it should be proportional to the proton affinity difference:

$$PA_{(A-B)} = \ln(AH^+/BH^+) * R T \qquad (2)$$

where, $PA_{(A-B)}$ is the difference between the proton affinities of compounds A and B, $\ln(AH^+/BH^+)$ is the natural logarithm of the intensity ratio of the protonated free bases (monomers) formed by dissociation of the mixed protonated dimer, R is the gas constant and T is the effective temperature.

However, some caution must be practiced as the site through which hydrogen bonding occurs in the proton bound dimer may not necessarily be the same as site of protonation in the free base. Whenever this is the case, discrepancies between PA values obtained by kinetic methods and by "classic" thermodynamic equilibrium or bracketing methods may occur.

It was shown recently that there was good agreement between these methods and the results obtained from CID studies [11]. It was also noted that special care had to be taken when the effective ion temperature was calculated, as, for example, differences in the temperature were observed between primary and secondary alcohols [11].

Diamines

Diamines, particularly α,ω-diamines, are placed close to the top of the NIST proton affinity (PA) scale, which is the most comprehensive compilation of such data [12]. The evaluated PAs from this compilation are shown in Table 1. Proton affinities of these compounds were calculated by Aue *et. al.* [13] who invoked intramolecular hydrogen bonding (proton bridging) to rationalize the high gas-phase basicities of the diamines. Experimental results from equilibrium measurements of four diamines, relative to dimethylamine and trimethylamine, in a high pressure ion source of a mass spectrometer were reported by Yamadagni and Kebarle [14]. The PA values of 1,2-

diaminoethane, 1,3-diaminopropane, 1,5-diaminopentane and 1,7-diaminoheptane were given as 234.9, 243.3, 243.3 and 243.3 kcal/mol, respectively, in that work. These high values arose, in part, from the high PA values assigned to the reference compounds (for example, the PA of n-butylamine was taken as 222.8 vs 218.4 kcal/mol in the NIST database [12]. Later Lau *et. al.* [15] reported the gas-phase basicity of 1,5-diaminopentane as being 26.2 kcal/mol above that of ammonia, i.e. (195.6+26.2) 221.8, quite close to the previously reported values. Using similar experimental methods, Meot-Ner *et. al.* [16] gave the PA values for 1,2-diaminoethane, 1,3-diaminopropane and 1,4-diaminobutane as 227.8, 235.3 and 239.5 kcal/mol, respectively.

EXPERIMENTAL

The work was carried out on an API-III triple quadrupole atmospheric pressure ionization mass spectrometer fitted with an Ionspray (pneumatically assisted electrospray ionization source) made by Sciex (Thornhill, Ontario, Canada) shown schematically in Figure 1. The triple quadrupole instrument and operating procedures were described in detail earlier [17]. The proton-bound monomers and dimers enter the vacuum system through a small orifice (OR) and are then introduced into the first mass spectrometer (Q1) via a quadrupole ion lens (Q0). The ion of interest was mass selected by appropriately tuning Q1 to allow only a single m/z ion to enter the collision region, the second quadrupole, Q2. This mass spectrometer is operated in the RF-only mode and acts as an ion-confining lens. By introducing controlled levels of argon into Q2 the mass-selected ions are forced to collide with the inert gas molecules and some of them undergo collision induced dissociation (CID). The third mass spectrometer, Q3, is used to measure the masses and intensities of the ions leaving Q2, i. e. the undissociated parent ion and the fragment (or product) ions formed through CID processes. The peak intensities are reported relative to the most abundant peak in the spectrum. It should be noted that the API-III has a unique pumping system, based on liquid helium cooled cryogenic surfaces.

All the compounds studied here, ranging from 1,2-diaminoethane to 1,10-diaminodecane, were commercially available from Aldrich and were used without purification. Protonated molecules and proton-bound clusters corresponding to heavier diamines, with 11 to 15 carbons, were also observed in the mass spectra of the longer chain diamines. Their presence made it possible to expand this study well beyond the range of the purchased chemicals. The compound, or compounds, of interest were dissolved in a 50:50 water-methanol mixture, and the solution was injected into the electrospray ionization source at a rate of 5 microliter/minute.

Procedure

The proton bound dimer was mass selected in the first mass spectrometer. The intensity ratio between the signals of the two protonated monomers into which it fragmented was measured. The natural logarithm of this ratio was multiplied by the effective temperature, T, and the gas constant, R (0.083 kJ/mole degree), and the result was taken as the difference in the proton affinity between the two monomers (in kJ/mole). Several such measurements were made between the same and different pairs of diamines. In some cases, the mass selected parent ion was a composite of several such pairs. For example, the CID spectrum of the parent ion at m/z 275 (nominally $C_{15}H_{39}N_4^+$) showed that it was made of three different pairs of protonated diamine monomers: 1,7-diaminoheptane and 1,8-diaminooctane (at m/z 131 and 145), 1,6-diaminohexane and 1,9-diaminononane (at m/z 117 and 159) and 1,5-diaminopentane and 1,10-diaminodecane (at m/z 103 and 173), as shown in Figure 2a. Another example is shown in Figure 2b for the parent ion at m/z 261 (nominally $C_{14}H_{37}N_4^+$). Note that the sum of each pair of product ions is always 1 dalton higher than that of the parent ion, which is an outcome of the fact that the proton from the parent ion may in some cases reside on the

3

one monomer and in other cases on the second monomer. Care was taken to calculate the intensity ratios only of ion pairs that complement each other to make up the parent ion.

RESULTS AND DISCUSSION

1. The effective temperature and proton affinity scale

Reference compounds were used to calibrate the effective temperature and to anchor the proton affinity values to the NIST proton affinity scale [12]. The compounds used for this purpose were di-isopropylamine $(iC_3H_7)_2NH$, triethylamine $(C_2H_5)_3N$, and tributylamine $(C_4H_9)_3N$, which have proton affinities of 230.2, 232.0 and 235.4 kcal/mol, respectively [12]. The heterodimer formed by each pair of amines was mass selected and the intensity ratio of the fragments (the corresponding protonated free bases) was used to calculate the effective temperature, according to equation 3:

$$T = PA_{(A-B)}/[\ln (AH^+/BH^+) * R] \qquad (3)$$

The results showed that the effective temperature was 60 K.

2. The proton affinity of diamines

The results for the diamines are summarized in Table 1, as are the evaluated proton affinities and the PAs of the equivalent normal primary aliphatic amines, taken from the NIST compilation [12]. The trend, observed in many homologous series [12], of increasing PA with the hydrocarbon chain length does not hold for the diamines once the number of carbon atoms exceeds 4 or 5 (Table 1).

Table 1: The proton affinities of diamines and aliphatic normal alkylamines.

Compound H2N(CH2)nNH2	n	This work	Proton Affinity Other[a]	CH3(CH2)nNH2[a]	D[b]
1,2-diaminoethane	2	223.6	225.9	217.9	2.3
1,2-diaminopropane	3	225.3			
1,3-diaminopropane	3	226.6	234.1	218.4	7.5
1,4-diaminobutane	4	230.6	237.6	218.9	7.0
1,5-diaminopentane	5	227.7	238.1	218.9	10.4
1,6-diaminohexane	6	227.0	237.7	219.0	10.7
1,7-diaminoheptane	7	225.7	238.0	220.4	12.3
1,8-diaminooctane	8	225.5			
1,9-diaminononane	9	226.6			
1,10-diaminodecane	10	228.1		220.7	
1,11-diaminoundecane	11	231.3			
1,12-diaminododecane	12	232.0			
1,13-diaminotridecane	13	232.4			
1,14-diaminotetradecane	14	233.0			
1,15-diaminopentadecane	15	231.9			

a) Reference 12.
b) - The stabilization energy of cyclization, i.e. the difference between NIST value and this work (cyclic and unbridged conformation).

There is a systematic difference, increasing with the chain length, between the proton affinity values obtained in this work and the NIST values, as shown in Table 1. The structure of protonated diamines, formed under equilibrium conditions [13-16] has been assumed to be that of an intramolecular proton bridged ring. A similar configuration, of proton induced cyclization, was proposed for diamines [18], amino-alcohols [19] and other polyamines [20] from ion mobility spectrometry (IMS) measurements at atmospheric pressure. The systematic difference in PAs indicates that the protonated diamines formed by fragmentation of the dimer species do not have the same structure, i.e. are not cyclic. It therefore appears that when the protonated dimer disintegrates the proton remains attached to one of the amino groups of the product ions and that rearrangement to the more stable, and thermodynamically favored conformation, does not take place in the time scale of the CID experiment. The fact that the site of protonation in the product ions is on a single amino group, indicates that the protonated dimer is formed by a proton bridge between the two monomer units that make up the dimer (schematic 1a). A more complex structure involving all four nitrogen atoms (amino groups) may also be visualized (schematic 1b). However, it would be sterically crowded with four amino-groups surrounding the proton, and the CID should yield the "normal" protonated diamines with the intramolecular ring, which evidently is not the case.
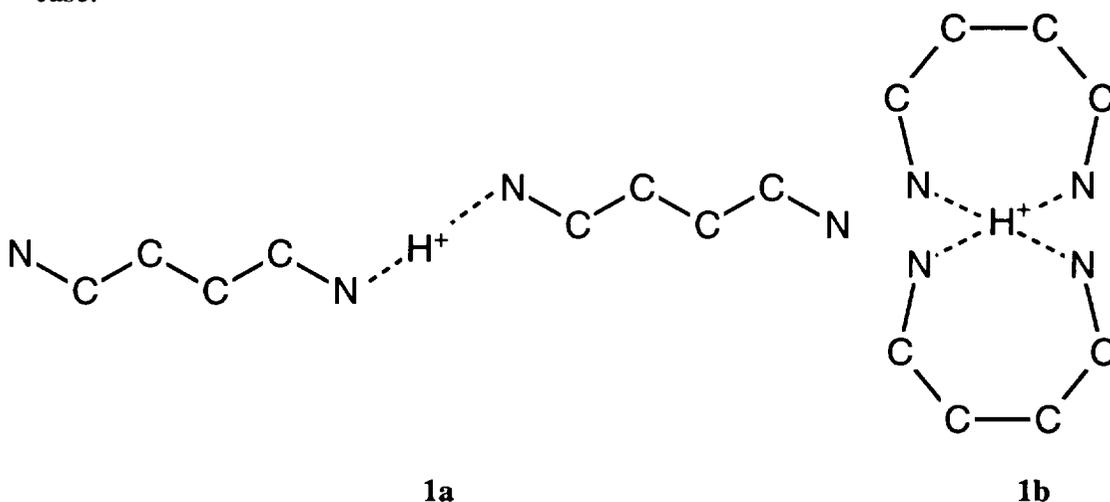
1a   **1b**
Schematic conformation of protonated diamine dimers

When the hydrogen bond that bridges the two monomer units is cleaved, as the outcome of a collision of the dimer with the inert gas, the proton may go either to one monomer unit or to the other. The ratio between these two fragments depends on the relative basicity at the binding site, i.e. the relative strength of the hydrogen bond to the local amino group. As Table 1 shows, the PA values obtained in this work for the diamines are higher than those of the corresponding normal aliphatic mono-amines, as expected for two compounds of this type [12].

These results indicate that CID may offer a novel method of producing ions, protonated molecules in this case, which have conformations which are not normally accessible by conventional methods.

The proton affinities of larger diamines, 1,11-undecanediamine through 1,15-pentadecanediamine, are also presented in Table 1. These compounds existed as trace impurities in the smaller diamines, but due to their higher proton affinities were preferentially protonated, and demonstrated a high tendency to participate in mixed dimer formation with the more abundant, but lower PA, diamines. Thus, it was possible to carry out CID studies on such mixed dimers and estimate the PA values of these large diamines.

3. Dissociation pathways of protonated diamine monomers and dimers

The active dissociation channels of the protonated monomers and dimers were also studied. The major dissociation channel, observed in all of the protonated diamine monomers, was loss of 17 mass units, corresponding to the elimination of ammonia:

$$H_2N(CH_2)_nNH_3^+ \longrightarrow (CH_2)_nNH_2^+ + NH_3 \qquad (4)$$

This could be followed by elimination of the second ammonia unit, leaving an ionized hydrocarbon skeleton. Other common dissociation channels in all of these diamines involved cleavage of C-C or C-N bonds, such as the formation of an ion at m/z 30 formed by cleavage of the C-C bond in the position alpha to the amino group:

$$H_2N(CH_2)_nNH_3^+ \longrightarrow CH_2NH_2^+ + CH_3(CH_2)_{n-2}NH_2 \qquad (5)$$

Other dissociation channels observed in these CID studies led to the formation of product ions by single bond cleavages in different parts of the hydrocarbon chain. A typical CID spectrum, in this case of protonated 1,5-diaminopentane is shown in Figure 3. Ammonia is eliminated from the parent ion at m/z 105, giving the product ion at m/z 86 and loss of both ammonia groups gives the product ion at m/z 69. Cleavage of an alpha C-C bond gives the product ion at m/z 30 (reaction 5), while other single C-C cleavages give the product ions at m/z 44 and 74, and the ion at m/z 41 which is probably $C_3H_5^+$ formed by additional cleavage of a C-C bond after elimination of one or two ammonia moieties.

The protonated dimers dissociated mainly by cleavage of the hydrogen bond at the protonation site, into either of the two protonated monomers, as shown in Figure 2. At higher collision gas thickness (CGT) values, ions corresponding to the elimination of ammonia from the protonated monomer were observed, accompanied by additional product ions as shown in reaction 4. In no case was cleavage of a covalent bond (C-C or C-N) observed without concomitant monomer formation, i. e. the hydrogen bond was always the first bond to be cleaved in the CID spectra of these protonated dimers and mixed dimers.

4. Collision dissociation cross sections of protonated dimers

The cross section for collision induced dissociation was determined by plotting the logarithm of the fraction of undissociated protonated dimers (the parent ion) as a function of the collision gas thickness. The slope of the line corresponds to the collision cross section. Figure 4 depicts such typical plots of this sort for pure protonated dimers of 1,7-diaminoheptane, 1,8-diaminooctane and 1,9-diaminononane. The general trend is that the slope of these plots, i.e. the cross sections, increase simply with the size (or mass) of the parent ion in the diamine homologous series.

5. Doubly charged ions

Under the conditions of electrospray ionization, multiply charged ions are frequently observed when polyamine bases are studied. In the present study doubly protonated, and doubly charged, diamines were observed, as shown in Figure 5 for diprotonated 1,9-diaminononane at m/z 79.9 (nominally 80). The identity of these ions was established from their mass (half of a diprotonated molecular ion), and by their CID spectrum which led to formation of ions with higher masses than the parent ion.

CONCLUSION

The results presented above demonstrate one of the pitfalls of using the "kinetic method" for deriving thermochemical data from the ratio of product ions in collision induced dissociation studies. The observed difference between proton affinity values of diamines obtained from equilibrium measurements (NIST data) and these CID studies was attributed to the fact that the conformation of the product ions in the latter method was with the proton attached to a single amino group and not to both groups in a cyclic structure as in the former experiments. Therefore, in this case the kinetic method may be used to estimate the proton affinities of unbridged protonated diamines. The stabilization energy resulting from cyclization may be derived from the difference between the PAs of the cyclic and unbridged diamines. Thus, the last column of Table 1 gives this stabilization energy, where data for the cyclic structures was available. The fact that this value increases with length of the hydrocarbon chain is indicative of the strain in the smaller cyclic structures, where part of the gain in stabilization energy is offset by the extra strain. This strain is also the reason that the difference between the PA of 1,2-ethanediamine and n-propylamine is smaller than between the corresponding larger homologues (see Table 1).

The CID results also give insights into the structure of the mixed and pure dimers, which may be elucidated as having a single hydrogen bond bridging the two monomer units. The CID studies of protonated diamine monomers showed that elimination of ammonia was the favored dissociation channel for these species. At higher CGT values other dissociation channels observed were loss of a second ammonia unit and cleavage of different C-C bonds in the hydrocarbon skeleton. The CID studies of all the protonated dimers, mixed or pure, showed that cleavage of the hydrogen bond was favored over breaking covalent bonds, which is expected from bond energy considerations.

7

REFERENCES

1. Cooks, R. G. and Kruger, T. L., Intrinsic Basicity Determination Using Metastable Ions, *J. Am. Chem. Soc.* **99**, 1279-1281 (1977).
2. McLuckey, S. A., Cameron, D. and Cooks, R. G., Proton Affinities and Dissociations of Proton-Bound Dimers, *J. Am. Chem. Soc.* **103**, 1313-1317 (1981).
3. Wright, L. G., McLuckey, S. A. and Cooks, R. G., Relative Gas-Phase Acidities from Triple Quadrupole Mass Spectrometers, *Intl. J. Mass Spectrom. Ion Phys.* **42**, 115-124 (1982).
4. Boand, G., Houriet, R. and Gaumann, T., Gas-Phase Acidity of Aliphatic Alcohols, *J. Am. Chem. Soc.* **105**, 2203-2206 (1983).
5. Burinsky, D. J., Fukuda, E. K. and Compana, J. E., Electron Affinities from Dissociations of Mixed Negative Ion Dimers, *J. Am. Chem. Soc.* **106**, 2770-2771 (1984).
6. Puzo, G., Fournie, J.-F. and Prome, J.-C., Identification of Stereoisomers of Some Hexoses by Mass Spectrometry Using Fast Atom Bombardment and Mass Ion Kinetic Energy, *Anal. Chem.* **57**, 892-894 (1985).
7. Fournie, J.-F. and Puzo, G., Stereoisomer Differentiation of 2-Acetamido-2-deoxyhexose by Mass Spectrometric Measurement of Relative Gas-Phase Alkali Ion Affinities, *Anal. Chem.* **57**, 2287-2289 (1985).

8. Bojesen, G., Relative Proton Affinities of the Four Common Basic L-α-Amino Acids. Analysis of Metastable Cluster Ions from Fast Atom Bombardment Mass Spectrometry, *J. Chem. Soc. Chem. Comm.* 244-245 (1986).
9. Greco, F., Liguori, A., Sindona, G. and Uccella, N., Gas-Phase Proton Affinity of Deoxyribonucleosides and Related Nucleobases by Fast Atom Bombardment Mass Spectrometry, *J. Am. Chem. Soc.* **112**, 9092-9096 (1990).
10. Graul, S. T., Schnute, M. E. and Squires, R. R., Gas-Phase Acidities of Carboxylic Acids and Alcohols from Collision-Induced Dissociation of Dimer Cluster Ions, *Intl. J. Mass Spectrom. Ion Proc.* **96**, 181-198 (1990).
11. Majumdar, T. K., Clairet, F., Tabet, J.-C. and Cooks, R. G., Epimer Distinction and Structural Effects on Gas-Phase Acidities of Alcohols Measured Using the Kinetic Method, *J. Am. Chem. Soc.* **114**, 2897-2903 (1992).
12. Lias, S. G., Liebman, J. F. and Levin, R. D., Evaluated Gas Phase Basicities and Proton Affinities of Molecules; Heats of Formation of protonated Molecules, *J. Chem. Phys. Ref. Data* **13**, 695-808 (1984).
13. Aue, D. H., Webb, H. M. and Bowers, M. T., Quantitative Evaluation of Intramolecular Strong Hydrogen Bonding in the Gas Phase, *J. Am. Chem. Soc.* **95**, 2699-2701 (1973).
14. Yamadagni, R. and Kebarle, P., Gas-Phase Basicities of Amines. Hydrogen Bonding in Proton-Bound Amine Dimers and Proton-Induced Cyclization of α,ω-Diamines, *J. Am. Chem. Soc.* **95**, 3504-3510 (1973).
15. Lau, Y. K., Saluja, P. P, Kebarle, P. and Alder, R. W., Gas-Phase Basicities of N-Methyl Substituted 1,8-Diaminonaphthalenes and Related Compounds, *J. Am. Chem. Soc.* **100**, 7328-7333 (1978).
16. Meot-Ner (Mautner), M, Hamlet, P., Hunter, E. P. and Field, F. H., Internal and External Solvation of Polyfunctional Ions, *J. Am. Chem. Soc.* **102**, 6393-6399 (1980).
17. Bruins, A. P., Atmospheric Pressure Ionization Mass Spectrometry, I. Instrumentation and Ionization Techniques, *Trends Anal. Chem.* **13**, 37-43 (1994); Bruins, A. P., Atmospheric Pressure Ionization Mass Spectrometry, II. Applications in Pharmacy, Biochemistry and General Chemistry, *Trends Anal. Chem.* **13**, 81-90 (1994).

18. Karpas, Z., Evidence of Proton-Induced Cyclization of α,ω–Diamines from Ion Mobility Measurements, *Intl. J. Mass Spectrom. Ion Proc.* **93**, 237-242 (1989).
19. Karpas, Z., The Mobility of Protonated Aminoalcohols: Evidence for Proton-Induced Cyclization, *Struct. Chem.* **3**, 139-141 (1992).

20. Karpas, Z., Bell, S. E., Wang, Y-F., Walsh, M., and Eiceman, G. A., The Structure of Protonated Diamines and Polyamines, *Struct. Chem.* **5,** 139-144 (1994).

ELECTROSPRAY IONIZATION
Sciex API-III "Ionspray" MS/MS
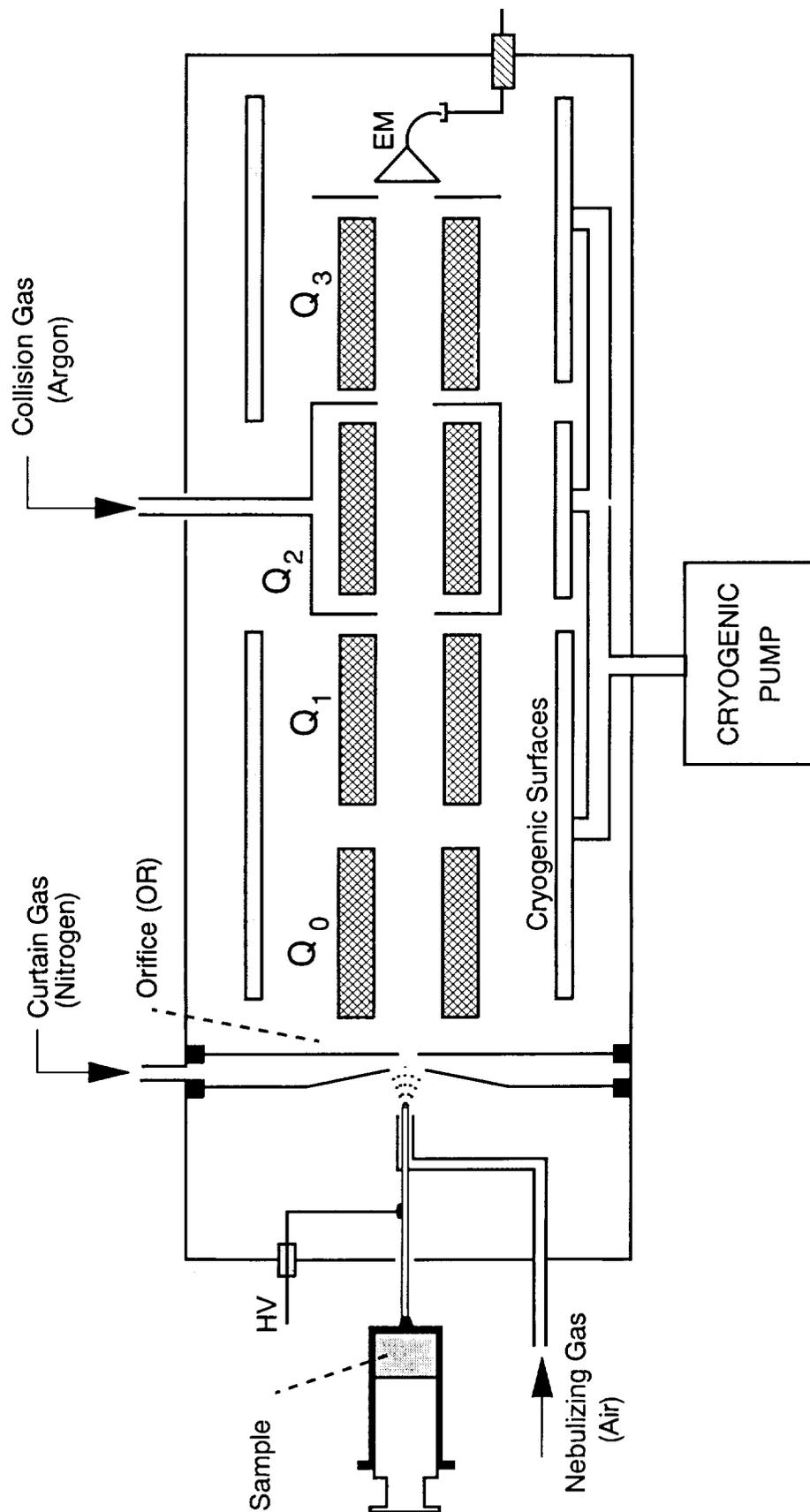
Figure 1. Schematic diagram of the API-III triple quadrupole mass spectrometer with the Ionspray (pneumatically assisted electrospray) atmospheric pressure ionization source.

Spectra

1,9-Nonanediamine
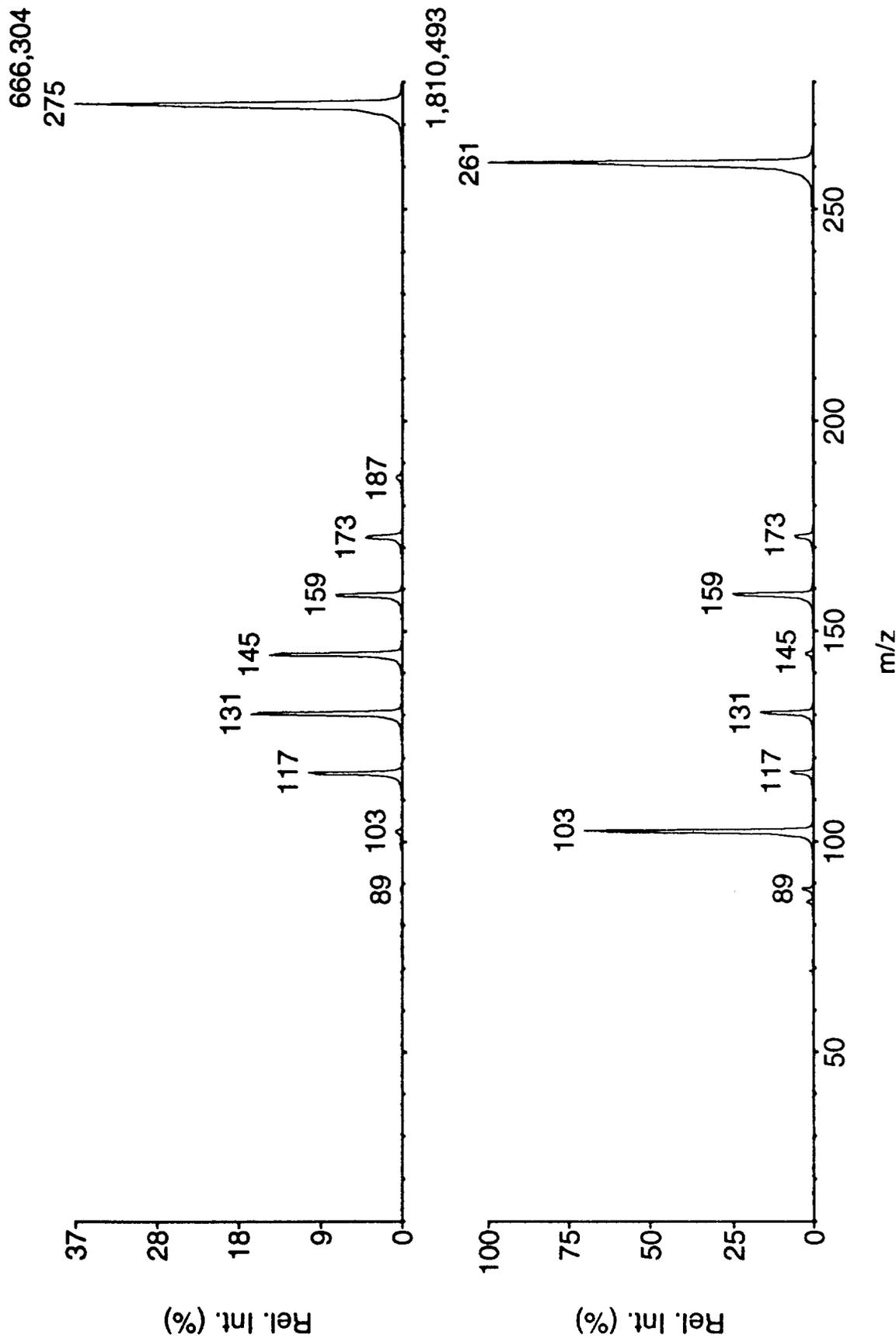
Figure 2a. The collision induced dissociation product ion mass spectrum of the parent ion at m/z 275 (nominally $C_{15}H_{39}N_4^+$). Note that pairs of protonated diamine monomers are produced through its dissociation: 1,7-diaminoheptane and 1,8-diaminooctane (at m/z 131 and 145), 1,6-diaminohexane and 1,9-diaminononane (at m/z 117 and 159) and 1,5-diaminopentane and 1,10-diaminodecane (at m/z 103 and 173)

12

CID Product Ion Mass Spectrum of Protonated Cadaverine (1,5-diaminopentane)
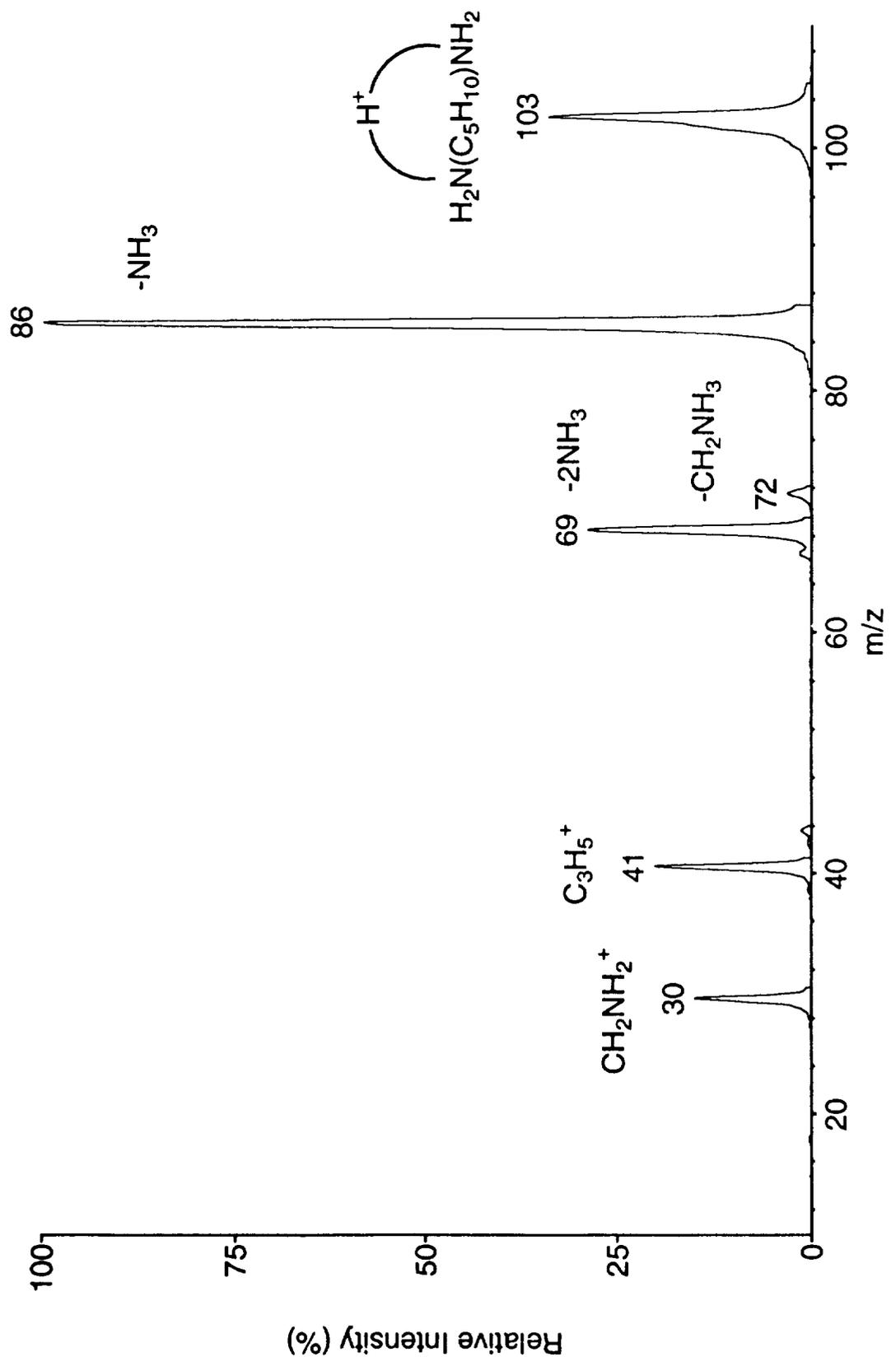
Figure 2b. The collision induced dissociation product ion mass spectrum of the parent ion at m/z mass 261 (nominally $C_{14}H_{37}N_4^+$).

13
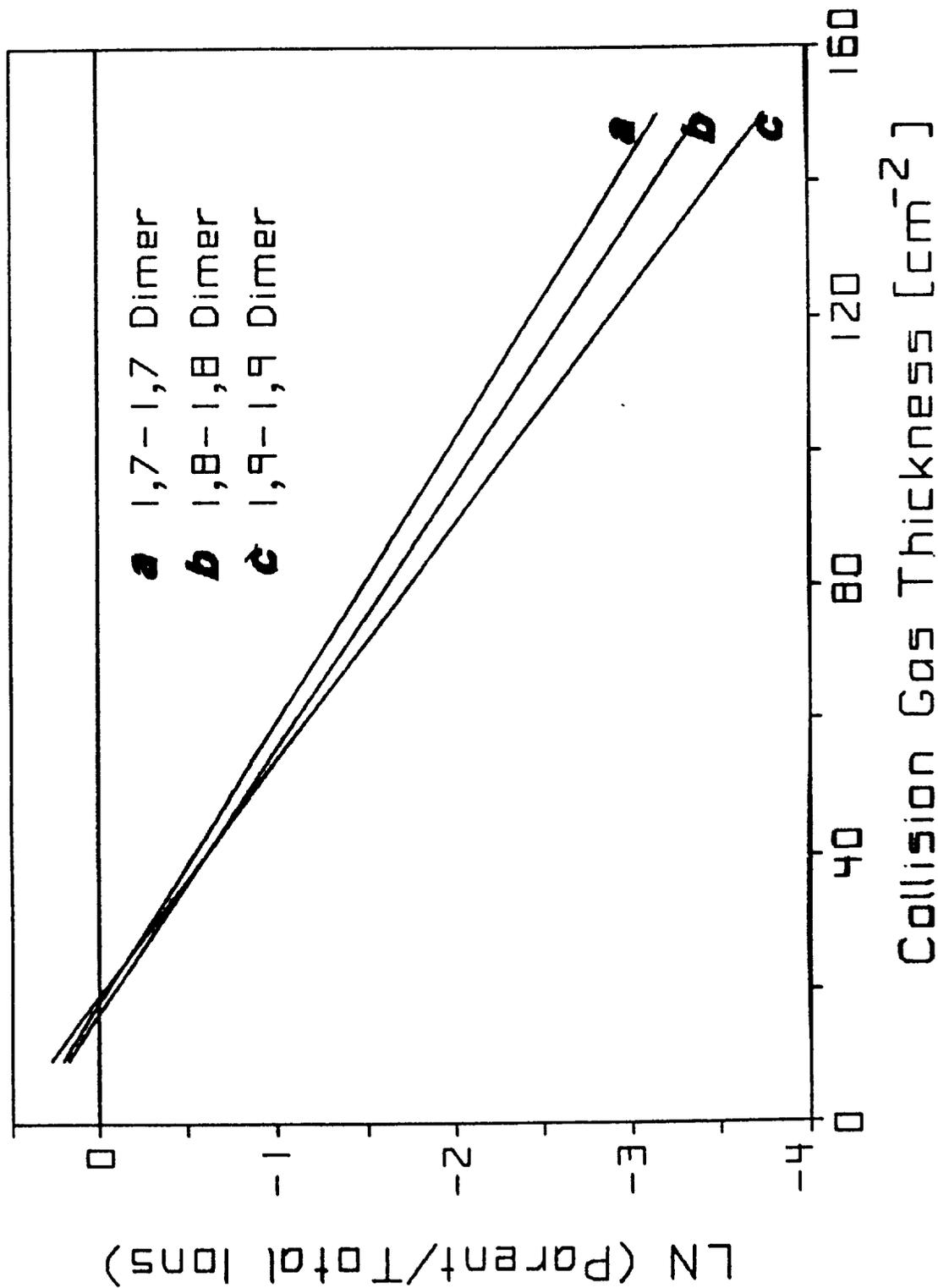
Figure 3. The CID product ion mass spectrum of the protonated monomer of 1,5-diaminopentane at m/z 105. The product ions at m/z 86 and 69 are produced by loss of one and two ammonia groups, respectively. The product ions at m/z 30, 44 and 74 are formed through single C-C cleavages.

14

CID Product Ion Mass Spectrum of Doubly Charged Parent [M+2H]2+ (Nonanediamine)
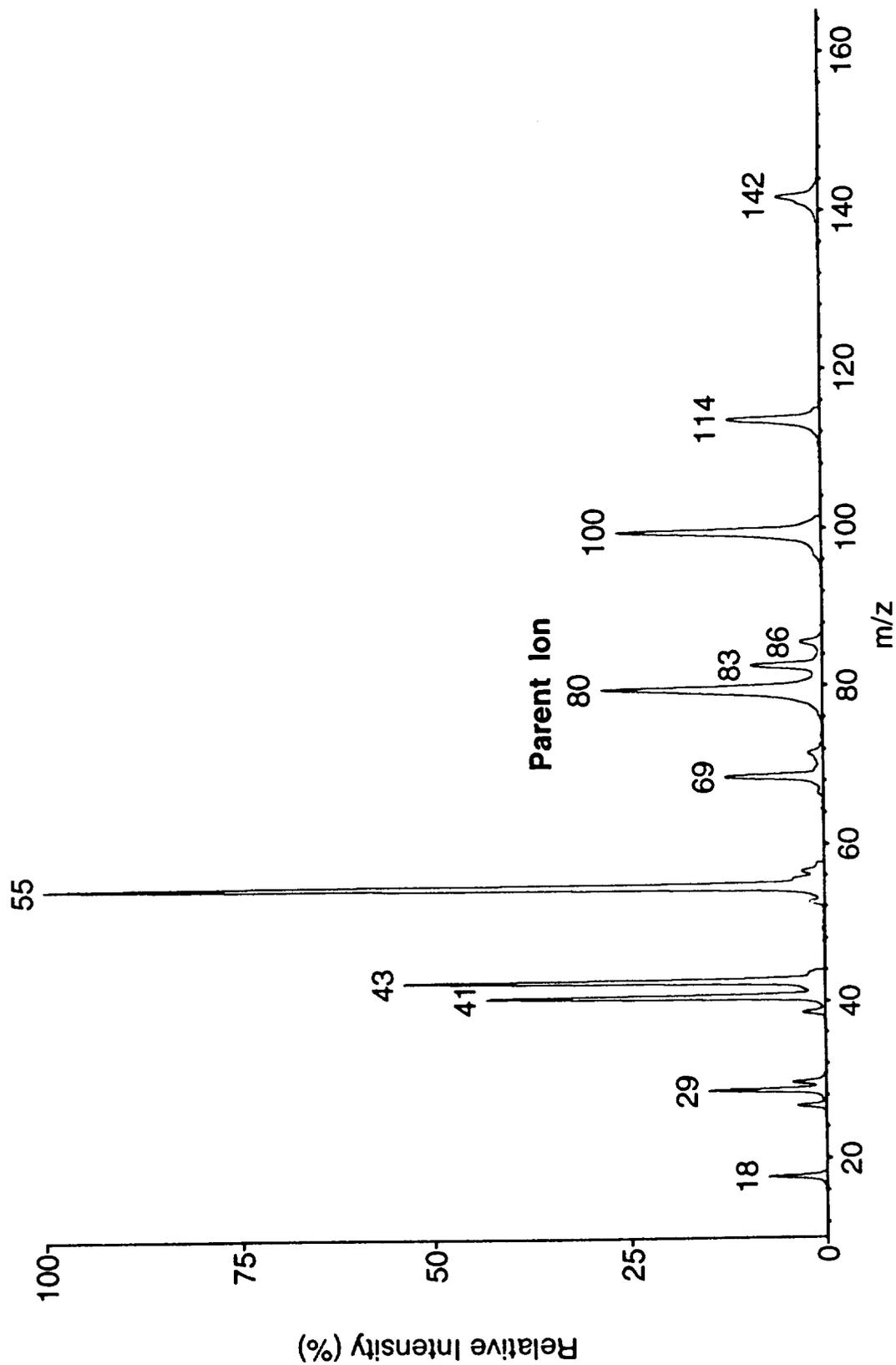
Figure 5. The CID product ion mass spectrum of the doubly charged parent ion at m/z 80 from 1,9-diaminononane [M+2H]²⁺. Product ions at higher m/z values than the parent ion arise from both mass and charge elimination. For instance, the product ion at m/z 142 represents loss of NH₄⁺ from the doubly charged dimer, or alternatively elimination of neutral ammonia from the singly charged monomer.

15

THE EFFECTS OF CO_2 ON THE
NEGATIVE REACTANT IONS OF IMS

Glenn E. Spangler[1]
Environmental Technologies Group, Inc., 1400 Taylor Ave., Baltimore, MD 21284-9840

ABSTRACT

In the presence of CO_2, the negative reactant ions of ion mobility spectrometry (IMS) are ion clusters of CO_4^- and CO_3^-. Methyl salicylate is ionized by the $CO_4^-(H_2O)_n(N_2)_m$ reactant ions, but not by the $CO_3^-(H_2O)_n(N_2)_m$ reactant ions. While the CO_4^- ions are formed by direct association, the CO_3^- ions require additional energy to be formed. The additional energy is provided by either excited neutral gas molecules in a metastable state or UV radiation.

INTRODUCTION

The effects of CO_2 on the composition of the negative reactant ions has been the subject of various investigations throughout the history of ion mobility spectrometry (IMS). The investigations started when Spangler and Collins added CO_2 to the carrier gas and noted an increase in the drift time for the negative reactant ion.[1] Then as Herbert Hill and his group began to couple supercritical fluid chromatography to IMS, the drift times for several straight-chain methyl ethers were investigated using CO_2 for both the carrier and drift gases.[2] While ion drift times were considerably longer, separation of both reactant and product ions was possible using normal operating temperatures for the IMS. More recently, Hayhurst et al. studied the composition of the negative reactant ions using IMS/MS and, similar to Spangler and Carrico, found contributions from CO_2.[3,4] The CO_2 can enter the system either through an improperly activated 13X scrubber used to precondition the carrier and drift gases or by permeating through a membrane inlet (or other opening) exposed to ambient air. Until now, there has been no indication that CO_2 affects significantly the ionization capabilities of IMS. In fact, a wide range of electronegative compounds can be ionized without adverse affects from CO_2.

This changed, however, when ETG, Inc. began to investigate non-radioactive ionization sources for IMS. During these investigations, it was found that certain compounds could be negatively ionized using a conventional ^{63}Ni ionization source, but not using a nonradioactive ionization source. For example, previous investigators reported the ionization of methyl salicylate to form $(M+O_2)^-$ product ions in the presence of a ^{63}Ni radioactive source, but this was not possible using a photoionization source.[5,6] When it was further discovered that methyl salicylate could not be ionized using argon for the carrier and drift gases, the mass spectrometer studies described in this paper were undertaken to investigate causes.

EXPERIMENTAL METHODS

The investigations were conducted using an IMS/MS system described previously in the open literature.[4] Improvements to the system included replacing the stacked-ring IMS cell with an all-ceramic IMS cell, upgrading the quadrupole mass spectrometer to an EXTREL C50 quadrupole mass spectrometer,[7] and installing a

---

turbomolecular pump in place of the 4-inch diffusion pump. These are shown in Figure 1. Since the flexible design of the new IMS cell was key to the success of the studies, it will be described in more detail.

The IMS cell was assembled on a base-plate which also served as a mounting flange when the cell was coupled to the mass spectrometer. Structurally, the cell was modular in design consisting of three parts:

- Reactor (approx. 2 cm long, 2.5 cm internal diameter, 1.16 megohm resistance)

- Drift Tube (11.4 cm long, 3.8 cm internal diameter, 11.08 megohm resistance)

- Membrane Inlet (OV-101 impregnated microporous Teflon membrane, 1.3 cm^2 area)[8]

The cell was attached to the base-plate using four support rods over which the three sections of the cell were slipped. Teflon sheet or ceramic tape impregnated with OV-17 silicone oil pneumatically sealed and electrically insulated the various sections. The assembly was compressed with nuts threaded on the four support rods. The reactor and drift tubes were conductive inlaid tubes (CITs) coated internally with thick film resistor ink and terminated with thick film conductive ink.[9] The cell was biased by attaching electrical leads to the conductive ink pads.

Two ionization sources were used for ionization: a ^{63}Ni radioactive source and a photoionization flashlamp. These were implemented by replacing the reactor section of the cell: one reactor containing the ^{63}Ni ionization source and the other containing the photoionization source as shown in Figure 1. The second reactor could also be assembled including a radioactive source so that the photoionization lamp irradiated the ions produced by the ^{63}Ni radioactive source. The radioactive source was a cylindrical ring of ^{63}Ni foil, approximately one inch in diameter and one centimeter long, mounted axially in the reactor.[10] It had a source strength of 15 millicuries and was mounted in a cup which also served as an ion repeller. The source cup was mechanically constrained within the ceramic reactor using "C"-rings which also made electrical contact with the thick film resistor fired on the inner surface of the drift tube. The photoionization source was an EG&G FK-1064 flashlamp (filled with 2 atm. krypton and sealed with a MgF$_2$ window) mounted perpendicular to the axis of the reactor.[11] The lamp was powered with an EG&G PS350 power supply through a FYD-507 lite pak. The flash rate for the flashlamp was controlled using a pulser assembled from a timer chip and optoisolators.

The shutter grid for the IMS cell was a parallel plane grid constructed from photoetched mesh purchased from Buckbee Mears.[12] This grid was deactivated during the experiments and biased to continuously conduct ion current. Since the ion current was measured using the electronics of the mass spectrometer, there was no ion collector.

The temperature of the IMS was measured using four thermocouples placed in contact with the pinhole mounted on the vacuum flange leading into the mass spectrometer, around the drift tube of the IMS halfway between the shutter grid and the mass spectrometer, and in contact with the reactor and membrane inlet of the IMS. Using strategically located heater tapes, the temperatures at these four locations were continuously monitored and automatically controlled with temperature controllers. Thermal gradients were minimized by preheating the carrier and drift gases before they entered the cell.

Purified air or argon (Matheson UN 1006)[13] was used for the carrier, drift and sample gases of the cell. The purified air was generated using a Balston CO$_2$ remover.[14] Before being introduced into the cell, both gases were passed through activated 13X molecular sieve scrubbers.[15] For some of the data, the 13X molecular sieve scrubbers were activated with a purging flow of prepurified nitrogen at 200 °C for 24 hours and for other of the data (including all of the argon data), the 13X molecular sieve scrubbers were activated with a purging flow of prepurified nitrogen at 300 °C for 24 hours. The water content of the gases was monitored using a DuPont 703

17

phosphorous pentoxide hygrometer[16] which indicated that the purified air contained 0.1 (est.) to 1.5 ppm water when the 13X scrubbers were activated at 300 °C and 2 to 4 ppm when the 13X scrubbers were activated at 200 °C. The argon contained 1.5 to 1.6 ppm water. The water content increased within these ranges as the scrubbers aged. Since the drift gas flowed between the mounting flange for the IMS and the vacuum flange for the mass spectrometer, it also served as a curtain gas for the pinhole. After flowing through a membrane inlet, the carrier gas entered the IMS cell near the shutter grid and exhausted with the drift gas through the reactor (i.e., unidirectional flow).

The CO_2 was Airgas syphon type CO_2 used without further purification.[17] The methyl salicylate was generated using reagent grade methyl salicylate in a diffusion tube standards generator. The generator was calibrated gravimetrically by periodically weighing the diffusion tube.

The remainder of the operating conditions for the mass spectrometer are given in Table 1.

TABLE 1: Operating Conditions for the IMS/MS

PARAMETER		VALUE
Pressures	Mass Spectrometer	2.6×10^{-6} Torr
	Focussing Lenses	1.8×10^{-4} Torr
Voltages	Reaction Region Hi Drift	- 2471 Volts (- 1549 Volts w Argon)
	Region Hi	- 1922 Volts (- 1000 Volts w Argon)
	Aperture Grid	- 129 Volts (- 67 Volts w Argon)
	Pinhole	Ground
	Focussing Lens #1	+ 44.3 Volts
	Focussing Lens #2	+ 17.5 Volts
	Focussing Lens #3	+ 80.2 Volts
	Focussing Lens #4	+ 30.4 Volts
	Focussing Lens #5	+ 45.0 Volts
	Pole Zero	+ 8.5 to - 1.5 Volts
Temperatures	Membrane Inlet	48 °C
	Reaction Region	45 °C
	Drift Region	54 °C
	Pinhole	53 °C
	Mass Spectrometer	Unheated
Gas Flows	Carrier Gas	210 cc/min
	Drift Gas	336 cc/min
	Sample Gas	240 cc/min

RESULTS

Using the radioactive source for ionization and purified air for the carrier, drift and sample gases, Figures 2 and 3 show mass spectra for the negative reactant ions and methyl salicylate for two qualities of the purified air. The methyl salicylate was introduced by challenging the membrane inlet with 0.02 - 0.03 mg/m³ methyl salicylate in purified air. While the purified air was passed through a 13X scrubber activated at 200 °C in both

instances, the data of Figure 2 were collected immediately (within several hours) after the scrubber was removed from the oven and reinstalled into the carrier/drift gas flow lines and the data of Figure 3 were collected after the 13X scrubber had aged for several days. The ions with masses 50, 60, 68, 78, 86, 88, 96 and 106 in Figure 2 are $O_2^-(H_2O)_n(N_2)_m$, n = 0 to 2 and m = 0 to 2 overlaying $CO_3^-(H_2O)_n(N_2)_m$, n = 0 to 2 and m = 0 to 1; the ions with masses 82, 100, 110, 128 and 138 are $O_4^-(H_2O)_n(N_2)_m$, n = 2 to 3 and m = 0 to 2; and the ions with masses 94, 122 and 150 are $O_2^-(CO_2)(H_2O)(N_2)_m$, m = 0 to 2. In Figure 3, an elevated CO_2 concentration increased the relative abundance of the $O_2^-(CO_2)(H_2O)(N_2)_m$ ions. For both cases, methyl salicylate was ionized by producing $O_2^-(MS)(N_2)_m$ ions at masses 184, 212, 240 and 268 and proton abstracted ions at mass 151. A comparison of the relative amplitudes in Figure 2 shows that methyl salicylate was ionized by reaction with the $O_2^-(CO_2)(H_2O)(N_2)_m$ reactant ions, but not the $CO_3^-(H_2O)_n(N_2)_m$ reactant ions.

Figure 4 compares the negative reactant ions when purified air versus argon was used for the drift gas. Purified air was used for the carrier and sample gases in both cases. Since the 13X scrubbers were activated at 300 °C, the extent of water clustering was reduced and the ions with masses 50 ($O_2^-(H_2O)$), 82 ($O_4^-(H_2O)$) and 76 ($O_2^-(CO_2)$) were much stronger. The water clusters at masses 68 ($O_2^-(H_2O)_2$), 94 ($O_2^-(CO_2)(H_2O)$) and 100 ($O_4^-(H_2O)_2$) increased when the drift gas was switched to argon. Two possible explanations are possible for this shift: (1) the argon drift gas was wetter than the purified air and (2) argon is less likely to collisionally dissociate the ion clusters as they drifted through the drift tube. Since the first possibility is supported by a higher reading on the hygrometer when argon was used as the drift gas and the second possibility is consistent with increased cluster stabilities which might accompany the lower drift fields used (to eliminate gas breakdown) to collect the argon results, the experimental evidence is inconclusive.

More significantly (and the reason why the data were collected), the results of Figure 4 show that the nitrogen clusters (e.g., masses 78, 96, 110 and 138) were observed independent of whether the drift gas was purified air or argon. Since an unidirectional flow scheme was used for the carrier and drift gases, nitrogen should not have built up in the argon drift gas. This means that the nitrogen clusters most likely formed in the reactor and not in the drift tube or the molecular beam issuing from the pinhole.

Instead of using purified air for the sample gas, Figure 5 shows the negative reactant ions when sampling 100% CO_2 with the membrane inlet. Unlike the results of Figures 2 and 4, the major reactant ions were $O_2^-(CO_2)(H_2O)_n$, masses 76 and 94, when purified air was used for the carrier and drift gases and $CO_3^-(Ar)_n$, masses 60, 100 and 140, when argon was used for the carrier and drift gases. As expected CO_2, made a significant contribution to the composition of the ions. The appearance of argon clusters of CO_3^- was surprising. It demonstrated that ligands do not have to be polar before they can cluster with an ion. The $CO_3^-(Ar)_n$ ions were persistent even when purified air or argon was used for the sample gas. This latter result demonstrates that the reactions leading to the $CO_3^-(Ar)_n$ ions are strongly exothermic.

Figure 6 shows the effects of adding purified air to the argon drift gas of Figure 5. As the purified air concentration increased, the amplitude of the $CO_3^-(Ar)_n$ ions decreased. With the introduction of as little as 1.1% purified air into the argon, the $O_2^-(CO_2)(H_2O)_n$ ions at masses 76 and 94 were the major reactant ions. While there was an ion at mass 116, corresponding to $O_2^-(CO_2)(Ar)$, in the 1.1% data, this ion disappeared when the purified air concentration rose to 6.3%.

Figure 7 shows mass spectra for the negative reactant ions and methyl salicylate when the UV photoionization flashlamp was used for ionization. Like Figures 2 and 3, the methyl salicylate was introduced by challenging the membrane inlet of the IMS cell with 0.02-0.03 mg/m³ methyl salicylate in purified air. The photoionization flashlamp produced only $CO_3^-(Ac)_x(N_2)_m$ ions at masses 60, 88, 116, 118 and 146 where x = 0 to 1 and m = 0 to 3. The acetone adduct (Ac) was present because 58 ppm acetone was in the reactor when the data were collected. Inconsistent with the results of Figures 2 and 3, the methyl salicylate was not ionized using these reactant ions.

To explore the lack of response to methyl salicylate, data were collected with a combination reactor where the ions produced by a radioactive source were irradiated by the UV photoionization flashlamp. Figure 8 shows the results when the membrane inlet was challenged with 0.02-0.03 mg/m^3 methyl salicylate. The top spectrum was collected with the flashlamp off. Similar to Figure 2, the methyl salicylate was ionized by forming $O_2^-(MS)(N_2)_m$ product ions. The bottom spectrum was collected with the flashlamp on. The $CO_3^-(Ac)(N_2)_m$ reactant ions reappeared, and the methyl salicylate was no longer ionized. Apparently the photoionization flashlamp altered the composition of the reactant ions sufficiently to prevent the ionization of methyl salicylate. This result was independent of the flash rate used for the flashlamp.

DISCUSSION

Carr has shown that the negative reactant ions in IMS are primarily $O_2^-(H_2O)_n$ when purified air is used for the carrier and drift gases.[18] In the presence of CO_2, Mohnen observed CO_4^- and its hydrate resulting from the following reactions.[19]

$$O_2^- + CO_2 \rightleftharpoons O_2^-(CO_2) \overset{+H_2O}{\rightleftharpoons} O_2^-(CO_2)(H_2O)$$
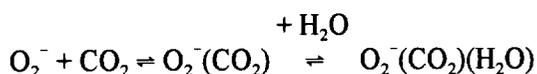
These ions appear in the mass spectrum at masses 76 and 94 and are noted in Figures 3 and 5. Hayhurst et al. found that the CO_4^- ions become important when the CO_2 concentration increases from about 2 ppm to 100 ppm.[3] Ab initio calculations show that the CO_4^- ion is a π-π* complex with oxygen bridging a C+O bond in CO_2 and that 0.8 ± 0.08 eV is required to dissociate $O_2^-(CO_2)$ into O_2^- and CO_2.[20,21] Since Fehsenfeld and Ferguson found that[22]

$$O_2^-(H_2O) + CO_2 \rightleftharpoons CO_4^- + H_2O \qquad\qquad - \Delta G^\circ{}_{296} = 2.1 \text{ kJ/mol}$$

$$CO_4^-(H_2O) + H_2O \rightleftharpoons O_2^-(H_2O)_2 + CO_2 \qquad\qquad - \Delta G^\circ{}_{296} = 6.7 \text{ kJ/mol}$$

the appearance of CO_4^- is more favorable in the presence of reduced water and/or elevated CO_2 concentrations.[23]

When the $O_2^-(H_2O)_n$ or $CO_4^-(H_2O)_n$ ions are formed under atmospheric pressure conditions, they may also contain nitrogen (N_2) adducts. This is evidenced by a series of ions separated by 28 mass units in the mass spectrum. Because CO also has a mass of 28 and is a more polar molecule than nitrogen, it can also contribute to the 28 mass unit differences in the mass spectrum. For the present data, however, there are several arguments against the CO assignment. First, CO was not intentionally introduced into the IMS; second, nitrogen was the major component when purified air was used for the carrier and drift gases; and third, the nitrogen adducts could be correlated with the presence of purified air in the reactor (see a companion paper given at this workshop).

When using a drift temperature of 50 °C, Spangler, et al. identified the presence of nitrogen adducts in both the positive and negative ion spectra using IMS/MS.[4,24] At the risk of oversimplifying the situation, as many as 3 nitrogens were attached to the positive ion (e.g., $H_3O^+(H_2O)_4$) and as many as 2 nitrogens were attached to the negative ion (e.g., $O_2^-(CO_2)$). This difference suggests that the affinity of the ion for the nitrogen adduct is greater when the ion contains a positive charge. If the attraction is due to an ion-induced dipole interaction, this means that a positive charge induces a stronger dipole in the adduct than a negative charge. While other factors relating to the distribution of the charge on the ion may also be important, this result is consistent with the fact that opposite charges attract and the positive nuclear charge is shielded by valence electrons.

The mechanism whereby CO_3^- is formed in IMS is less understood than CO_4^-. For purposes of

discussion, five possible mechanisms are proposed. The first two were first mentioned by Fehsenfeld and Ferguson who proposed that O^- is produced in the gas phase by dissociative attachment of electrons to O_2 or by ion pair production.[22,25] That is[26,27]

$$\beta^-(67\ keV) + O_2 \rightarrow O + O^-$$

$$O^- + n(H_2O) \rightleftharpoons O^-(H_2O)_n$$

$$O^-(H_2O)_n + CO_2 \rightleftharpoons CO_3^-(H_2O)_m + (n-m)H_2O$$

or

$$\beta^-(67\ keV) + O_2 \rightarrow O^+ + O^-$$

$$O^- + n(H_2O) \rightleftharpoons O^-(H_2O)_n$$

$$O^-(H_2O)_n + CO_2 \rightleftharpoons CO_3^-(H_2O)_m + (n-m)H_2O$$
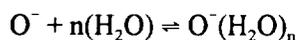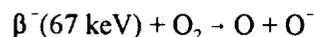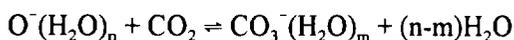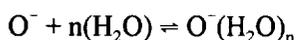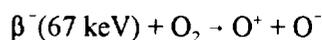
where $\beta^-(67\ keV)$ is the beta particle emitted by the ^{63}Ni radioactive source. The second three depend on the presence of metastable nitrogen (N_2^*) originating from the Vegard-Kaplan A $^3\Sigma_u^+ - X^1\Sigma_g^+$ transition with 6.3 eV of energy.[28,29]

$$O_2 + N_2^* \rightarrow 2O + N_2 + 1.1\ eV$$

$$e^-(thermal) + O \rightarrow O^-$$

$$O^- + n(H_2O) \rightleftharpoons O^-(H_2O)_n$$

$$O^-(H_2O)_n + CO_2 \rightleftharpoons CO_3^-(H_2O)_m + (n-m)H_2O$$

or

$$O_2^- + N_2^* \rightarrow O + O^- + N_2 + 2.2\ eV$$

$$O^- + n(H_2O) \rightleftharpoons O^-(H_2O)_n$$

$$O^-(H_2O)_n + CO_2 \rightleftharpoons CO_3^-(H_2O)_m + (n-m)H_2O$$

and

$$CO_4^- + N_2^* \rightarrow CO_3^- + O + N_2 + 3.4\ eV$$

$$CO_3^- + n(H_2O) \rightleftharpoons CO_3^-(H_2O)_n$$
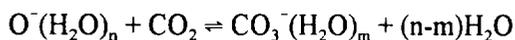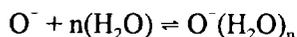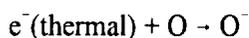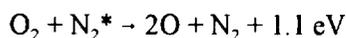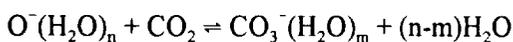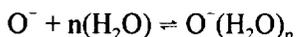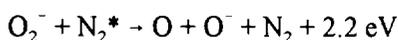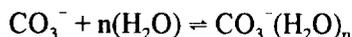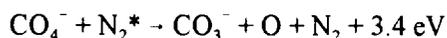
One source for the metastable nitrogen is recombination of N_2^+ which serves as a precursor ion to the formation of the positive reactant ions .[30]

The dissociative attachment and ion pair production mechanisms for O^- need no additional energy other than that provided by the β^--particle. Once the O^- is formed, it reacts readily with CO_2 with an exothermicity of 52 kcal/mol.[31,32,33] If the O^- should be clustered with water, the reaction is still exothermic since the enthalpy

21

of hydration is only 30 kcal/mol.[31] Because of the excess energy, the reactions proceed to completion and yield less CO_3^- when the oxygen content of the carrier and drift gases is reduced. This latter observation contradicts the findings of Carr who observed an increase in CO_3^- ions when the drift gas was changed from air to nitrogen at 210 °C.[18] Consequently, doubt is cast on the role which dissociative attachment and ion pair production play in the formation of CO_3^-.

During their studies on the negative reactant ions between 25 and 55 °C, Hayhurst, Watts and Wilders did not detect O^- ions.[3] On the other hand, they were able to identify the presence of CO_3^- ions using isotope dilution techniques. Using IMS data, they also found that "in a dry system, increasing the CO_2 concentration decreases the amount of CO_3^- formed; in a wet system, the CO_2 concentration has no marked effect on CO_3^- production." This water effect shows features similar to those observed by Fehsenfeld and Ferguson when they studied CO_4^- (see above).[22] Unlike Hayhurst, Watts and Wilders, however, Fehsenfeld and Ferguson noted an increased yield for CO_4^- the concentration of CO_2 was increased.

The involvement of metastable nitrogen in the formation of CO_3^- has not yet been hypothesized in the open literature. On the other hand, it is consistent with the experimental results for argon where a much greater tendency towards the formation of CO_3^- was observed. Metastable argon has an excitation energy of 11.6 eV.[28] In the presence of trace concentrations of oxygen and carbon dioxide, the following reactions can occur.

$$O_2 + Ar^* \rightarrow 2O + Ar + 6.4 \text{ eV}$$

$$e^-(\text{thermal}) + O \rightarrow O^-$$

$$O^- + n(H_2O) \rightleftharpoons O^-(H_2O)_n$$

$$O^-(H_2O)_n + CO_2 \rightleftharpoons CO_3^-(H_2O)_m + (n-m)H_2O$$

or

$$O_2^- + Ar^* \rightarrow O + O^- + Ar + 7.5 \text{ eV}$$

$$O^- + n(H_2O) \rightleftharpoons O^-(H_2O)_n$$

$$O^-(H_2O)_n + CO_2 \rightleftharpoons CO_3^-(H_2O)_m + (n-m)H_2O$$

and

$$CO_4^- + Ar^* \rightarrow CO_3^- + O + Ar + 8.7 \text{ eV}$$

$$CO_3^- + n(H_2O) \rightleftharpoons CO_3^-(H_2O)_n$$
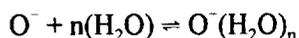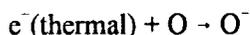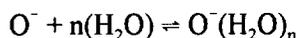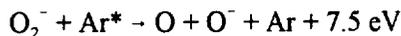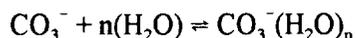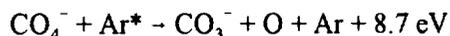
These are the same reactions proposed with nitrogen, except Ar^* replaces N_2^* in the equations. Because the excitation energy for metastable argon is greater than metastable nitrogen, the reactions are more exothermic. Hence less CO_2 sample gas is needed to saturate the CO_3^- response when argon is used for the carrier and drift gases than when purified air is used for the carrier and drift gases. Except to say that metastable neutral species play a role in forming CO_3^-, it is not yet possible to identify with confidence the set of reactions most responsible for the ionization. Because of its high energy, metastable argon may participate in all the reactions. Because its energy is low, metastable nitrogen may not participate as freely. This should become more so if cluster growth occurs in the presence of water.

In the presence of UV radiation, ozone is easily generated because of the large cross section offered by the Schumann-Runge system (complete absorption below 175.9 nm) of oxygen and the low heat of formation for ozone (34.1 kcal/mol).[34,35] Watts in his compilation of kinetic data for IMS noted that a pathway to CO_3^- from ozone might be[36]

$$O_2^-(H_2O)_n + O_3 \rightarrow O_3^-(H_2O)_{n-1} + O_2 + H_2O$$

$$O_3^-(H_2O)_n + CO_2 \rightarrow CO_3^-(H_2O)_{n-1} + H_2O + O_2$$
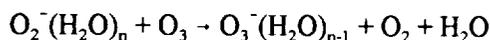
If this proposal is correct, it would seem that the results of Figures 7 and 8 can be explained on the basis that photoelectrons generated by the flashlamp are captured by ozone which then react with CO_2 to form CO_3^-. The reaction scheme is consistent with the fact that the results in Figures 7 and 8 are independent of the flash rate used for the flashlamp.

The inability to ionize methyl salicylate with $CO_3^-(H_2O)_n(N_2)_m$ reactant ions is related to the distribution of the charge on the ion. Ab initio calculations show that the ground state for CO_3^- ion is a $^2B_1$ state with C_{2v} symmetry and an OCO angle of $131.36°$.[37] The electronic configuration can be viewed as a resonating structure which spreads the ionic charge over the three legs of the ion. When the ion attacks a methyl salicylate molecule, the strength of the induced dipole interaction is weakened by the delocalized ionic charge. This causes the ion/molecule complex to be unstable towards dissociation with a lifetime short compared to the drift time for the ion. This is unlike the reaction of methyl salicylate with the dioxygen anion, O_2^-, which does form a stable $(M+O_2)^-$ complex.

CONCLUSIONS

The effects of CO_2 on the negative reactant ions in IMS is to form ion clusters of CO_4^- and CO_3^-. The CO_4^- ions are formed by direct association, but the CO_3^- ions require additional energy. This additional energy can be provided by either neutral metastable gas molecules or UV radiation. When metastable nitrogen is involved in the reactions, the reactions are mildly thermoneutral making the yield of CO_3^- is strongly temperature dependent. When metastable argon or UV irradiation are involved in the reactions, excess energy is generated and the ion/molecule reactions are saturated towards CO_3^-. Methyl salicylate can be ionized using CO_4^- reactant ions, but not CO_3^- reactant ions.

REFERENCES

1. Spangler, G.E. and Collins, C.I. Reactant Ions in Negative Ion Plasma Chromatography. *Anal. Chem.* **47**, 393-402 (1975).

2. Rokushika, S., Hatano, H. and Hill, H.H., Jr. Ion Mobility Spectrometry in Carbon Dioxide. *Anal. Chem.* **58**, 361-365 (1986).

3. Hayhurst, C.J., Watts, P. and Wilders, A. Studies on Gas-Phase Negative Ion-Molecule Reactions of Relevance to Ion Mobility Spectrometry: Mass Analysis and Ion Identification of the Negative Reactant Ion Peak in "Clean" Air. *Int. J. Mass Spectrom. Ion Proc.* **121**, 127-139 (1992).

4. Spangler, G.E. and Carrico, J.P. Membrane Inlet for Ion Mobility Spectrometry (Plasma Chromatography). *Int. J. Mass Spectrom. Ion Phys.* **52**, 267-287 (1983).

5. Nowak, D.M. Mobility and Molecular Ions of Dimethyl Methyl Phosphonate, Methyl Salicylate, and Acetone. Technical Report ARCSL-TR-83056, U.S. Army Armament R&D Command, Chemical Systems Laboratory, Aberdeen Proving Ground, MD, June 1983.

6. Spangler, G.E. and Roehl, J.E. Nonradioactive Source Development for the XM22 Automatic Chemical Agent Alarm and Auxiliary Equipment. Technical Report on Contract DAAA15-90-C-0030, U.S. Army Edgewood Research, Development and Engineering Center, Aberdeen Proving Ground, MD 21010 by Environmental Technologies Group, Inc., 1400 Taylor Avenue, Baltimore 21284-9840, December 1992.

7. Extrel Corporation, 240 Alpha Drive, Box 11512, Pittsburgh, PA 15238.

8. Spangler, G.E. Membrane Interface for Ion Mobility Detector Cells. U.S. Patent 4,311,699, The Bendix Corporation, Southfield, MI, January 1982.

9. Browning, D.R., Sima, G.R., Jr., Schmidt, J.C. and Sickenberger, D.W. One Piece Ion Accelerator for Ion Mobility Detector Cells. U.S. Patent 4,390,784, The Bendix Corporation, Southfield, MI, June 1983.

10. New England Nuclear, 549 Albany Street, Boston, MA 02118.

11. EG&G Electro-Optics, 35 Congress Street, Salem, MA 01970.

12. Interconics, Buckbee Mears, Inc., 245 E. 6th St., St. Paul, MN 55101.

13. Matheson Gas Products, 30 Seaview Dr., P.O. Box 1587, Secaucus, NJ 07096.

14. Balston, Inc., 260 Neck Rd., Haverhill, MA 01835.

15. W.R. Grace & Co., Davison Chemical Division, P.O. Box 2117, Baltimore, MD 21203.

16. Ametek, 455 Corporate Blvd., Pencador Corporate Ctr., Newark, DE 19702.

17. Airgas, 100 Matsonford Road, Suite 550, Radnor, PA 19087.

18. Carr, T.W. Comparison of the Negative Reactant Ions Formed in the Plasma Chromatograph by Nitrogen, Air, and Sulfur Hexafluoride as the Drift Gas with Air as the Carrier Gas. *Anal. Chem.* **51**, 705-711 (1979).

19. Mohnen, V.A. *Pure Appl. Geophys.* **100**, 123 (1972).

20. Hiraoka, K. and Yamabe, S. Formation of the Chelate Bonds in the Cluster $O_2^-(CO_2)_n$, $CO_3^-(CO_2)_n$ and $NO_2^-(CO_2)_n$. *J. Chem. Phys.* **97**, 643-650 (1992).

21. Pack, J.L. and Phelps, A.V. Electron Attachment and Detachment. II. Mixtures of O_2 and CO_2 and of O_2 and H_2O. *J. Chem. Phys.* **45**, 4316-4329 (1966).

22. Fehsenfeld, F.C. and Ferguson, E.E. Laboratory Studies of Negative Ion Reactions with Atmospheric Trace Constituents. *J. Chem. Phys.* **61**, 3181-3193 (1974).

23. Ellis, H.W., Pai, R.Y., Gatland, I.R., McDaniel, E.W., Wernlund, R. and Cohen, M.J. Ion Identity and Transport Properties in CO_2 Over a Wide Pressure Range. *J. Chem. Phys.* **64**, 3935-3941 (1976).

24. Kim, S.H. and Spangler, G.E. Ion Mobility Spectrometry/Mass Spectrometry (IMS/MS) of Two Structurally Different Ions Having Identical Ion Mass. *Anal. Chem.* **57**, 567-569 (1985).

25. Siegel, M.W. and Fite, W.L. Terminal Ions in Weak Atmospheric Pressure Plasmas. Application of Atmospheric Pressure Ionization to Trace Impurity Analysis in Gases. *J. Phys. Chem.* **80**, 2871-2881 (1976).

26. Chase, M.W., Jr., Davies, C.A., Downey, J.R., Jr., Frurip, D.J., McDonald, R.A. and Syverud, A.N. JANAF Thermochemical Tables, Third Edition. *J. Phys. Chem. Ref. Data* 14(Suppl. 1), 1-1856 (1985).

27. Rosenstock, H.M., Draxl, K., Steiner, B.W. and Herron, J.T. Energetics of Gaseous Ions. *J. Phys. Chem. Ref. Data* 6(Suppl. 1), 1-783 (1977).

28. Littlewood, A.B. Gas Chromatography: Principles, Techniques, and Applications. Academic Press, NY, 1970.

29. Herzberg, G. Molecular Spectra and Molecular Structure: I. Spectra of Diatomic Molecules. Van Nostrand Reinhold Company, NY, 1950.

30. Carroll, D.I., Dzidic, I., Stillwell, R.N. and Horning, E.C. Identification of Positive Reactant Ions Observed for Nitrogen Carrier Gas in Plasma Chromatograph Mobility Studies. *Anal. Chem.* **47**, 1956-1959 (1975).

31. Keesee, R.G. and Castleman, A.W., Jr. Thermochemical Data on Gas-Phase Ion-Molecule Association and Clustering Reactions. *J. Phys. Chem. Ref. Data* **15**(3), 1011-1071 (1986).

32. Moruzzi, J.L. and Phelps, A.V. Survey of Negative-Ion-Molecule Reactions in O_2, CO_2, H_2O, CO and Mixtures of These Gases at High Pressure. *J. Chem. Phys.* **45**, 4617-4627 (1966).

33. Bohme, D.K., Dunkin, D.B., Fehsenfeld, F.C. and Ferguson, E.E. Flowing Afterglow Studies of Ion-Molecule Association Reactions. *J. Chem. Phys.* **51**, 863-872 (1969).

34. Handbook of Optics, W.G. Driscoll, W. Vaughan, Eds. McGraw Hill, NY, 1978.

35. CRC Handbook of Chemistry and Physics, D.R. Lide, Ed. CRC Press, Boca Raton, FL, 1994.

36. Watts, P. Studies on Gas-Phase Negative Ion-Molecule Reactions of Relevance to Ion Mobility Spectrometry: Kinetic Modeling of the Reactions Occurring in "Clean" Air". *Int. J. Mass Spectrom. Ion Proc.* **121**, 141-158 (1992).

37. So, S.P. Ground Electronic State and Geometry of the CO_3^- Radical Anion. *J. Chem. Phys., F. Trans. II* **72**, 646-650 (1976).
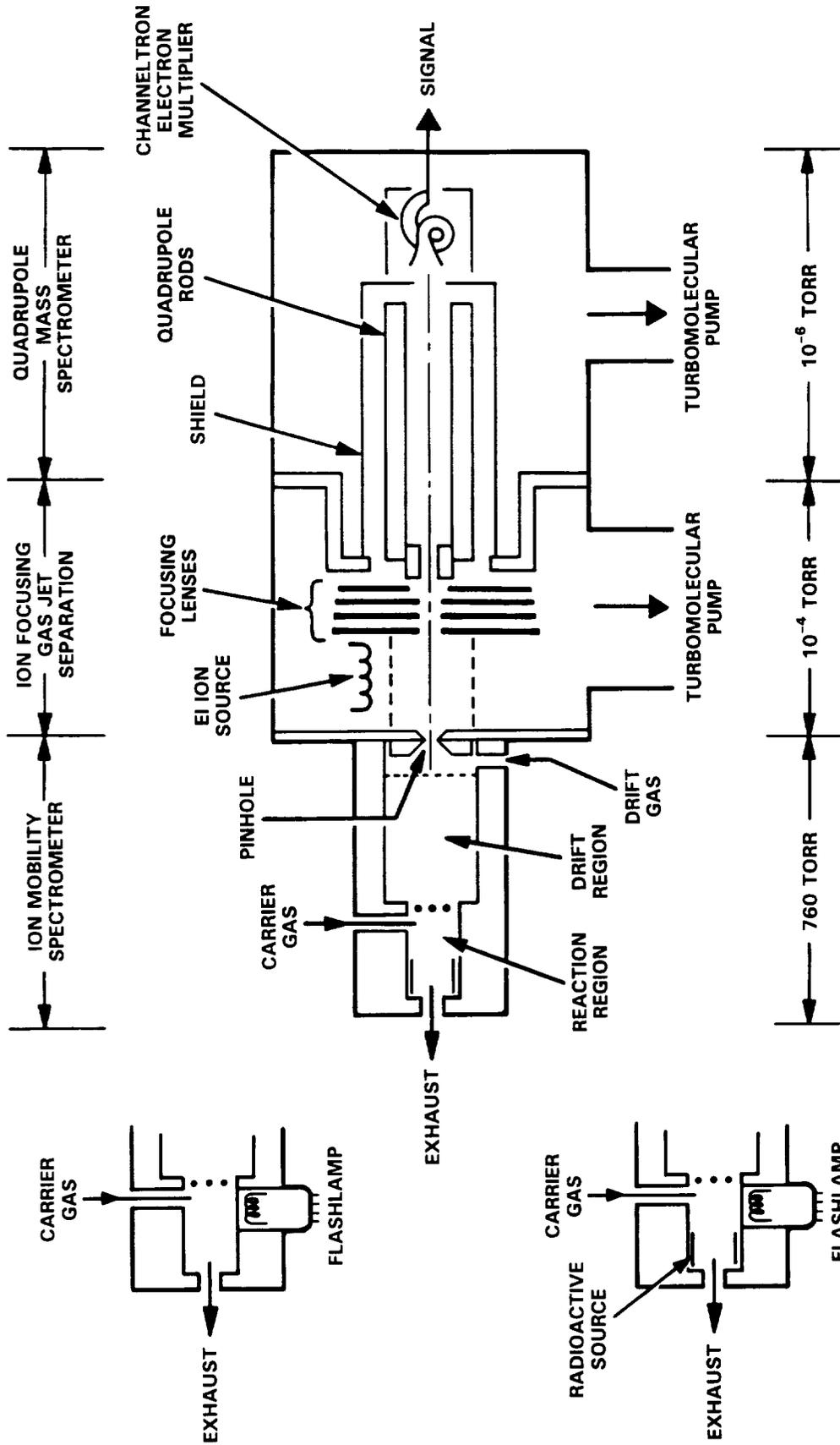
Figure 1. Functional Diagram for the Ion Mobility Spectrometer/Mass Spectrometer System. The Photoionization Reactor (top) and the Photoionization Reactor Equipped with a Radioactive Source (bottom) Are Shown on the Left.
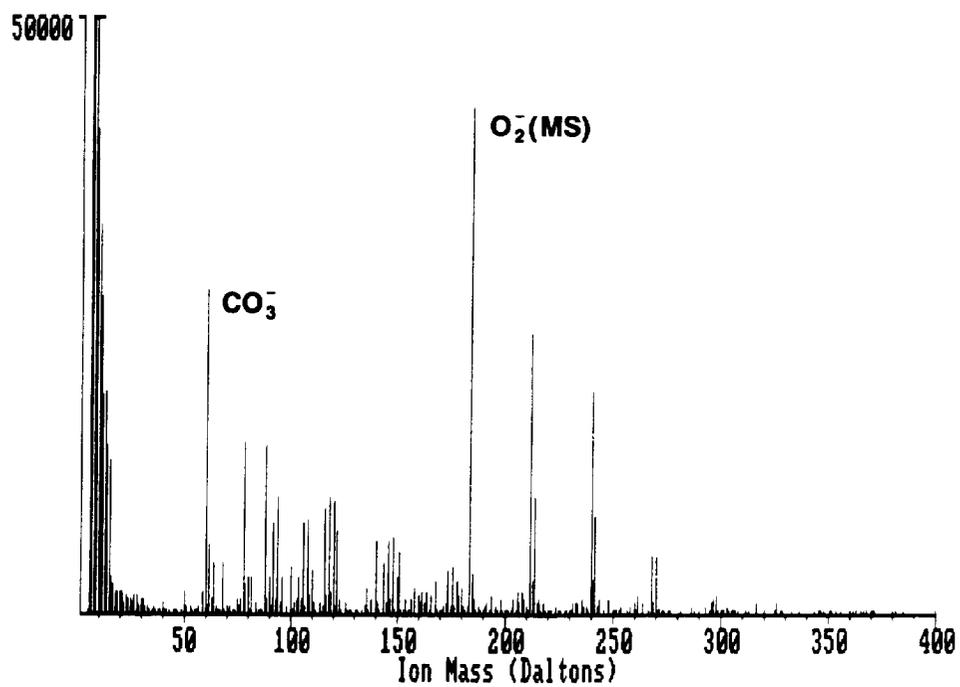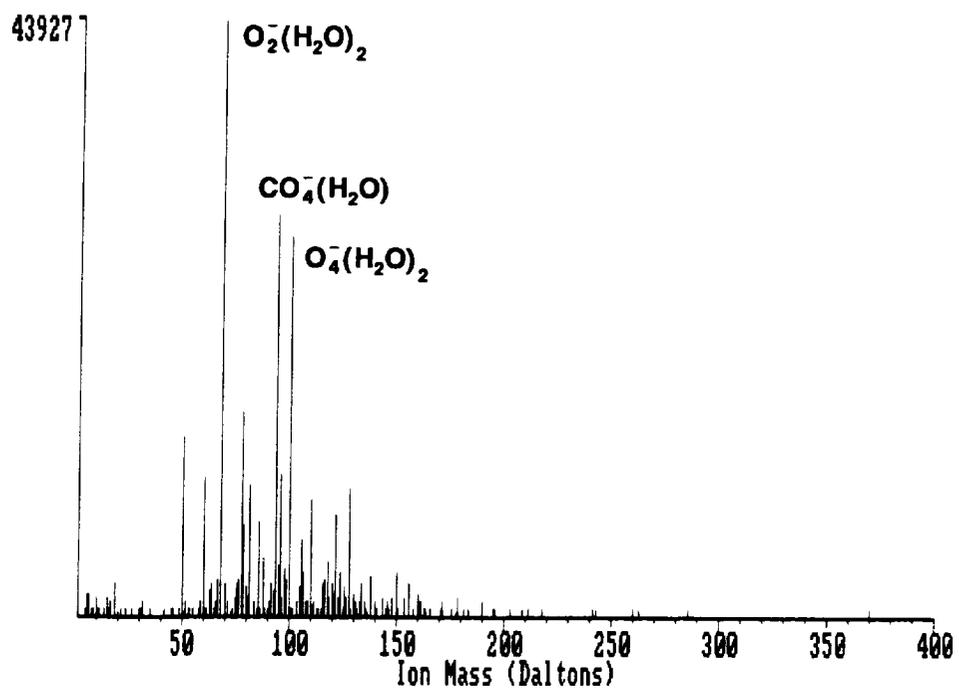
Figure 2. Negative Reactant Ions (top) and the Negative Ionization of Methyl Salicylate (bottom) using a 13X Scrubber Immediately after Reactivation at 200 °C.

27
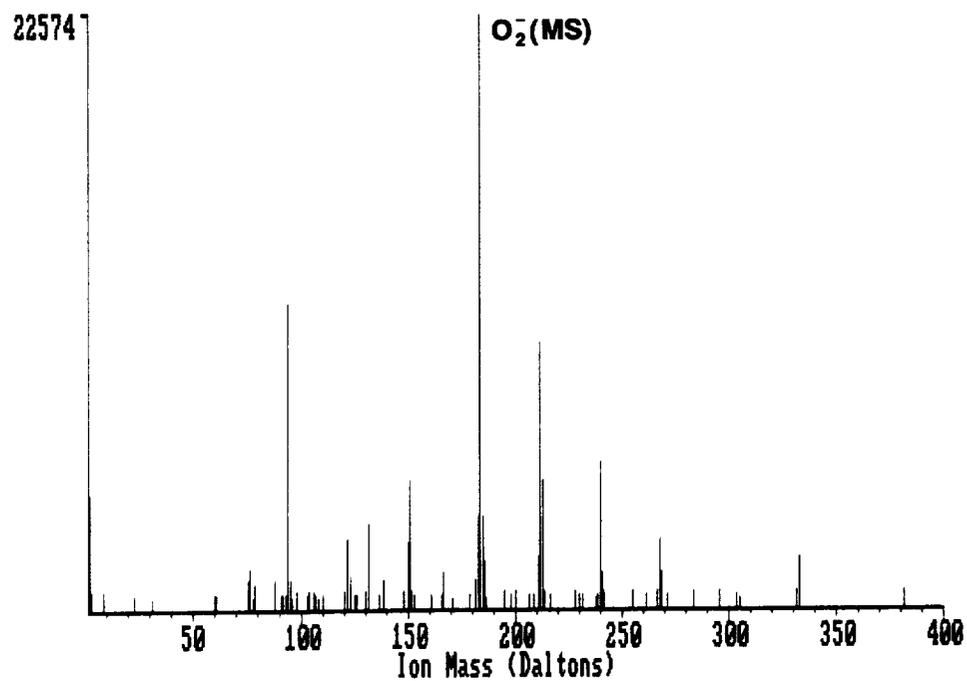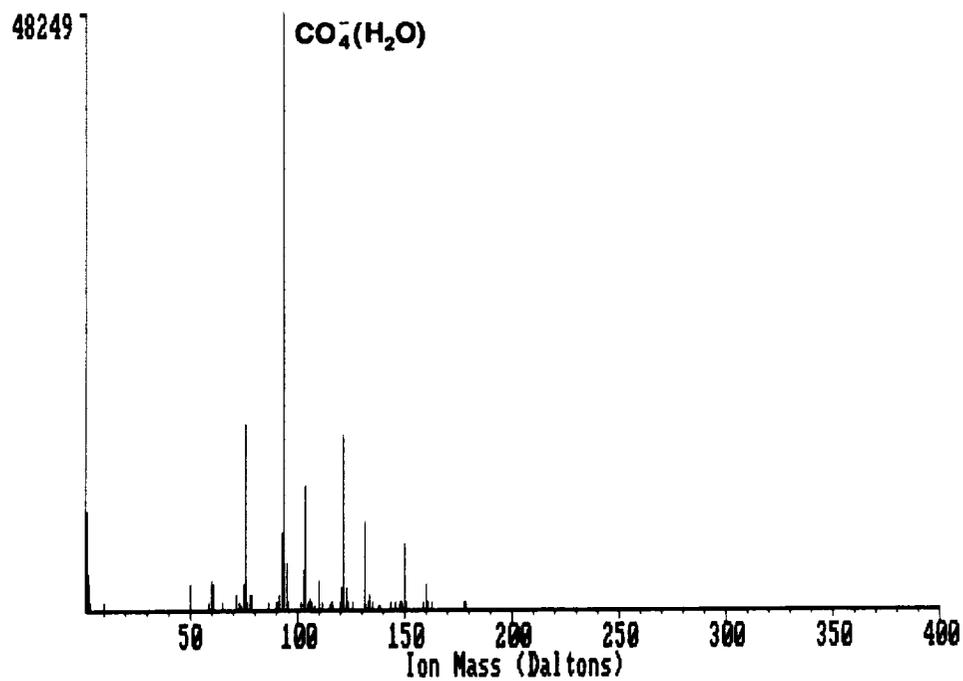
Figure 3. Negative Reactant Ions (top) and the Negative Ionization of Methyl Salicylate (bottom) using an Aged 13X Scrubber Several Hours after Reactivation at 200 °C.
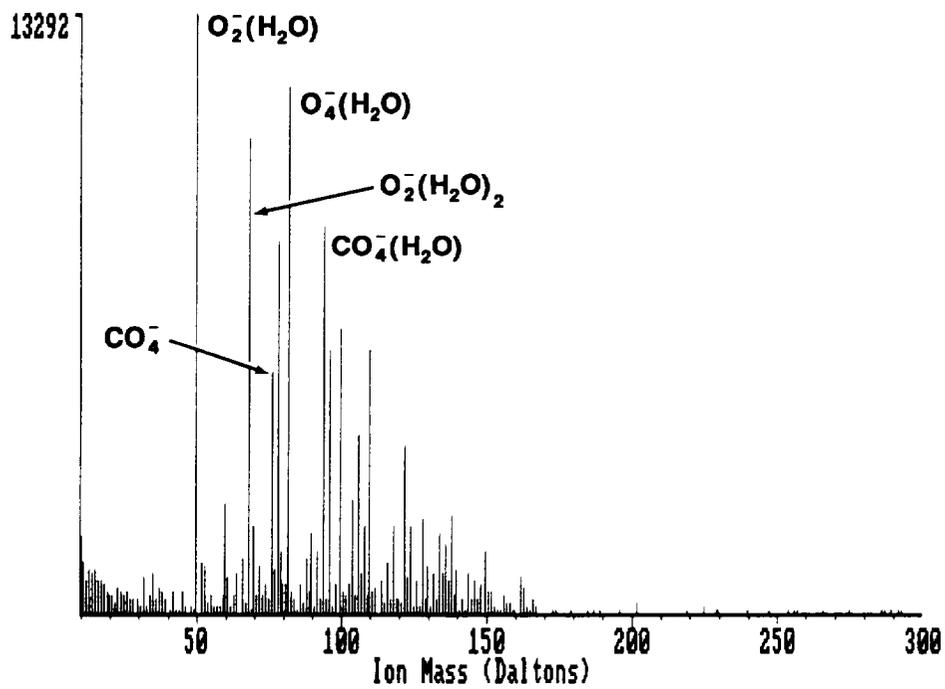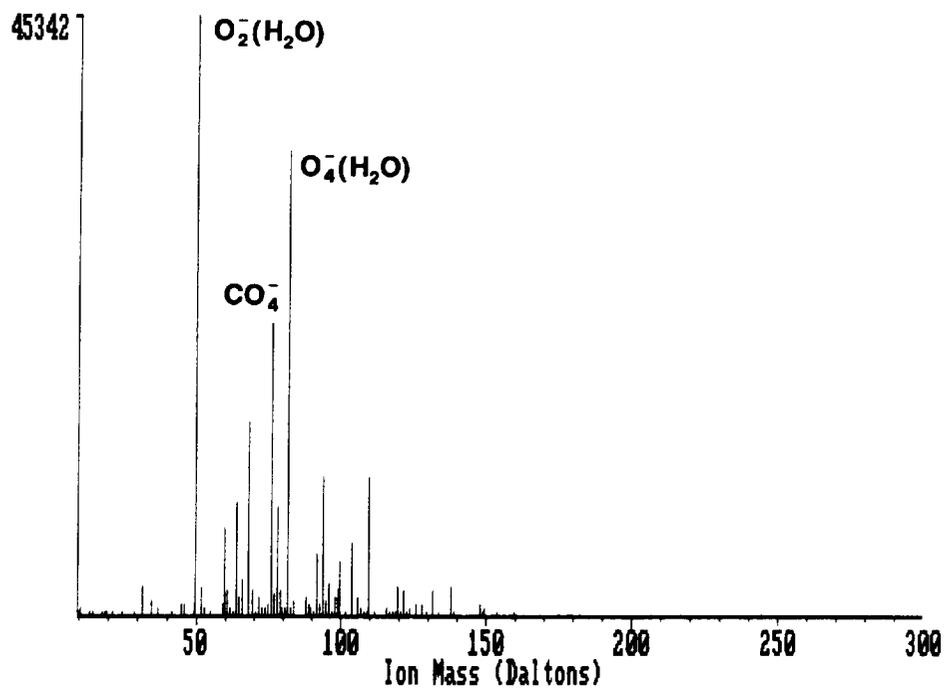
Figure 4. Negative Reactant Ions Using Purified Air (top) and Argon (bottom) for the Drift Gas. Purified Air was used for the Carrier and Sample Gases.
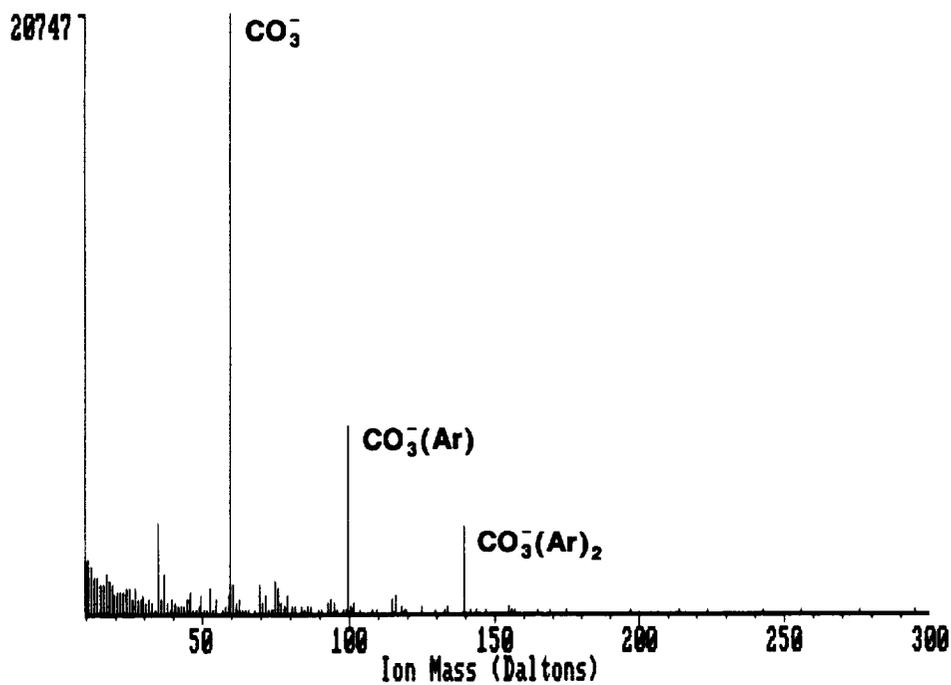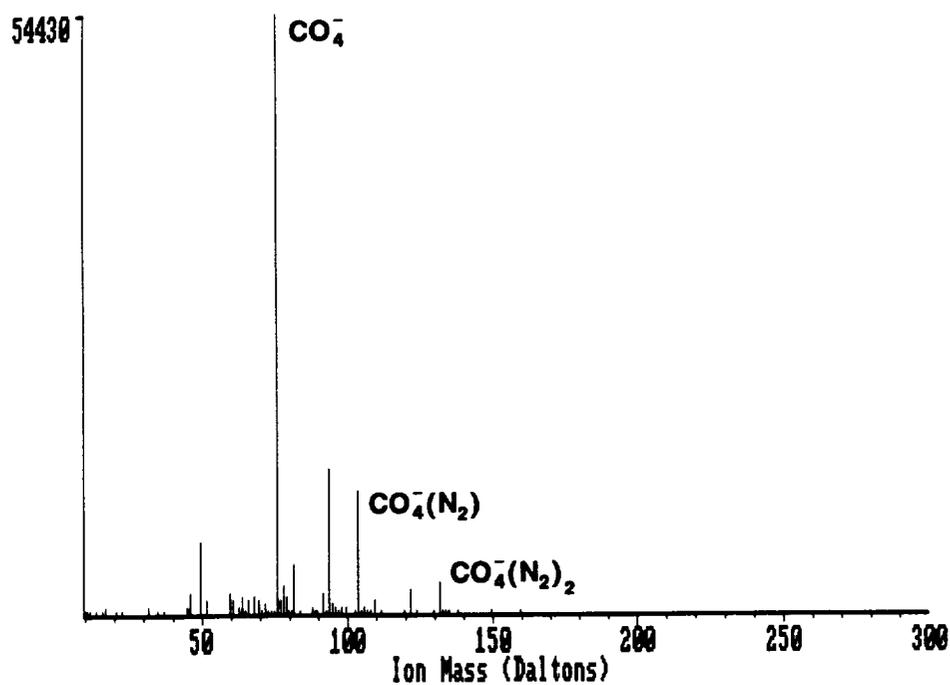
Figure 5. Negative Reactant Ions Using Purified Air (top) and Argon (bottom) for the Carrier and Drift Gases. The Membrane Inlet was challenged with CO_2.
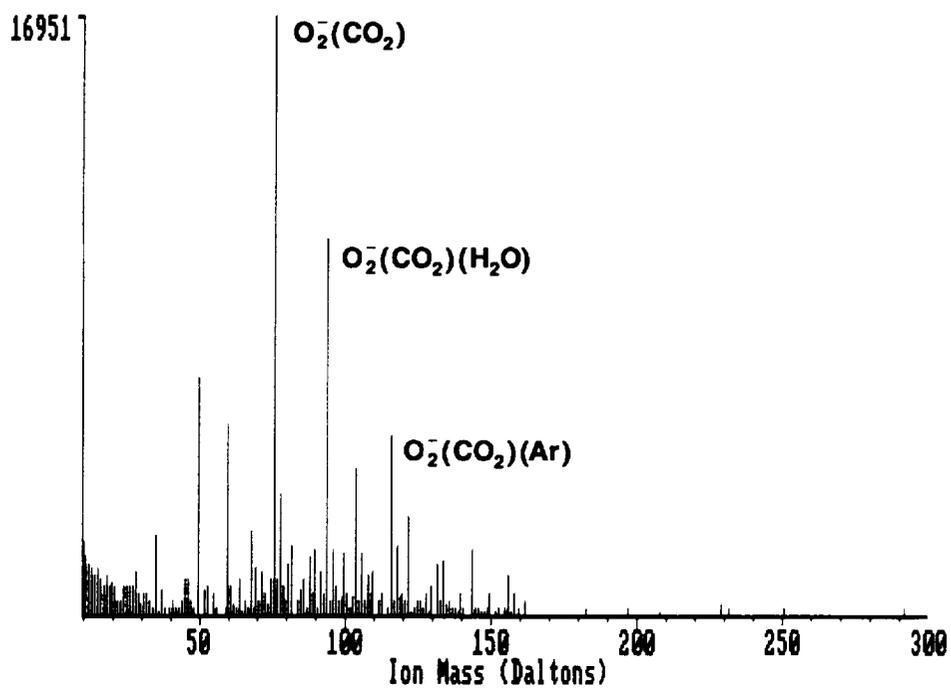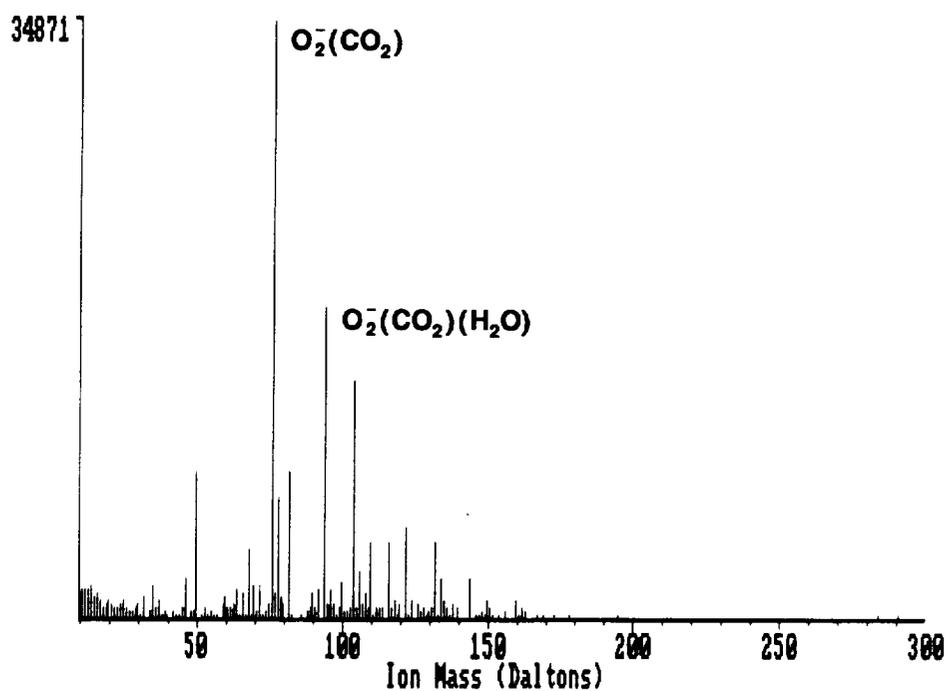
Figure 6. Negative Reactant Ions Using Argon for the Carrier and Drift Gases and CO_2 for the Sample Gas. 1.1% Purified Air (bottom) and 6.3% Purified Air (top) was introduced into the Argon Drift Gas.
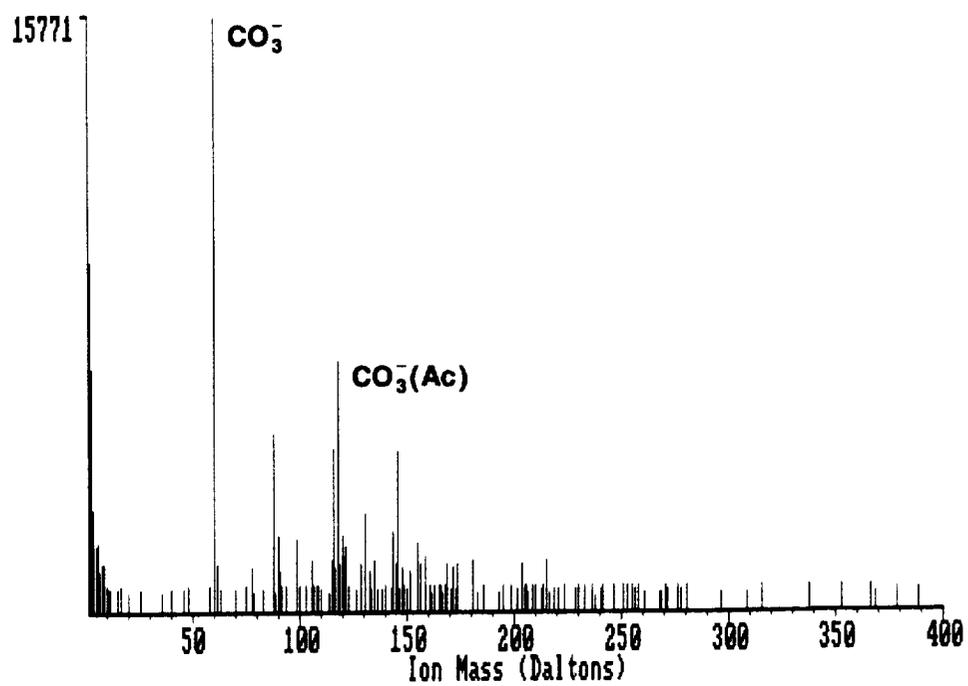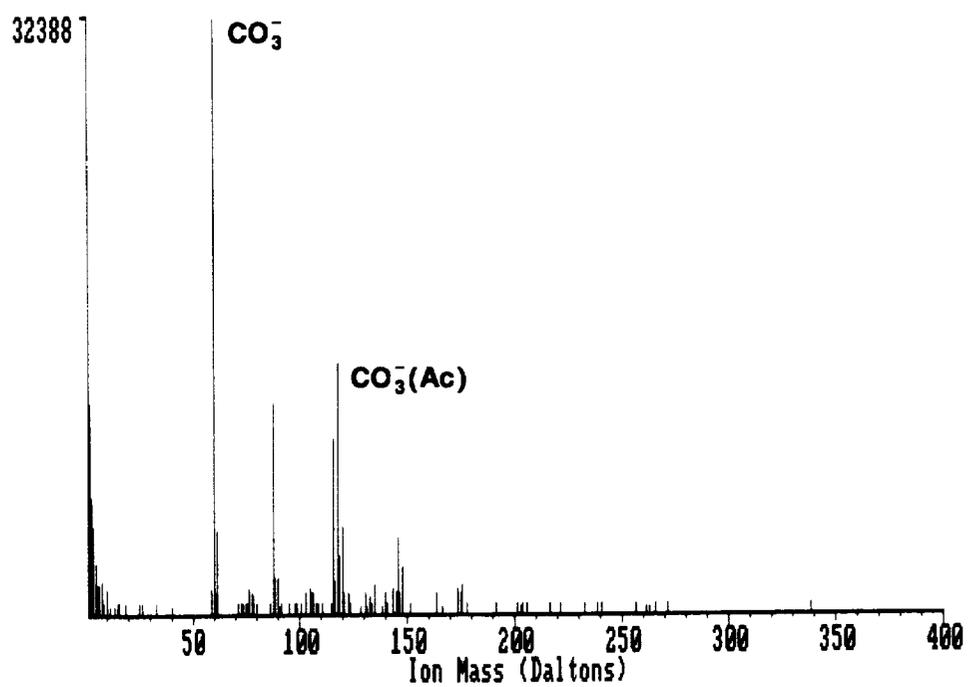
Figure 7. **Negative Reactant Ions (top) and the Negative Ionization of Methyl Salicylate (bottom) using a** Photoionization Source.
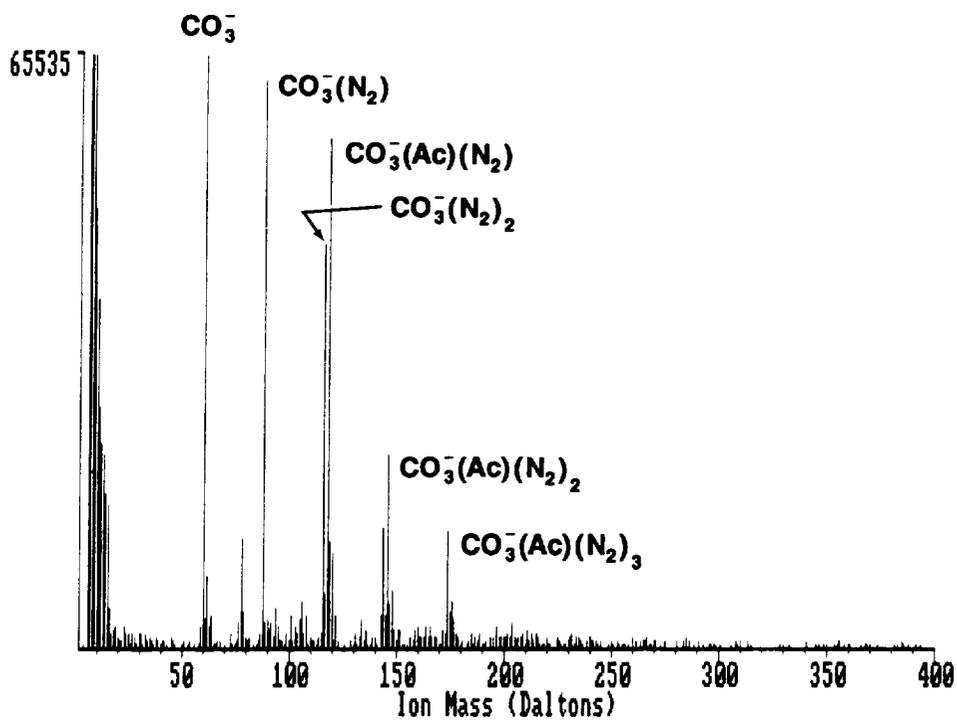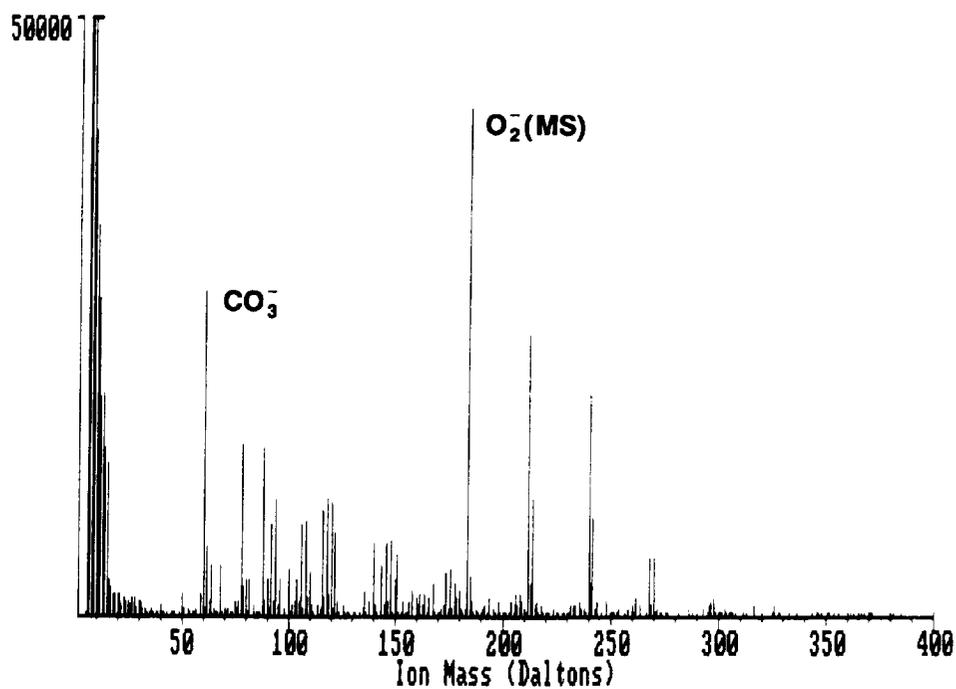
Figure 8. Negative Ionization of Methyl Salicylate using a Radioactive Source with (bottom) and without (top) the Product Ions being Irradiated with UV Radiation from the Photoionization Source.

33

FUNDAMENTAL STUDIES OF GAS PHASE IONIC REACTIONS BY ION MOBILITY SPECTROMETRY

K. Giles, W.B. Knighton, K.E. Sahlstrom and E.P. Grimsrud
Department of Chemistry, Montana State University, Bozeman, MT

ABSTRACT

Ion mobility spectrometry (IMS) provides a promising approach to the study of gas phase ionic reactions in buffer gases at unusually high pressures. This point is illustrated here by studies of the Sn2 nucleophilic displacement reaction, $Cl^- + CH_3Br \rightarrow Br^- + CH_3Br$, using IMS at atmospheric pressure. The equilibrium clustering reaction, $Cl^-(CHCl_3)_{n-1} + CHCl_3 \rightleftharpoons Cl^-(CHCl_3)_n$, where n = 1 and 2, and the effect of clustering on the Sn2 reaction with CH_3Br have also been characterized by this IMS-based kinetic method. Present problems and anticipated improvements in the application of ion mobility spectrometry to studies of other gas phase ionic processes are discussed.

INTRODUCTION

While the field of gas phase ion chemistry (GPIC) has received a great deal of attention during the last 3 decades, kinetic studies of ionic reactions have been successfully performed primarily under conditions in which the total system pressure is relatively low and has rarely exceeding a few torr. In fact, less than 15 reports have appeared in the literature, to date, in which the use of an instrumental method for the kinetic characterization of a gas phase ion-molecule reaction in a buffer gas near atmospheric pressure is described[1-13]. This omission in the field of GPIC is clearly due to instrumental reasons, rather than a lack of interest. The principal methods of GPIC have been based almost exclusively on various forms of mass spectrometry which have been most easily adapted to the study of reactions systems at relatively low pressure.

It is important that we gain increased understanding of the effects of elevated pressures on GPIC for a variety of reasons. One practical reason is that several modern instrumental methods of analysis are based on ionic reactions occurring within an atmospheric pressure buffer gas. These methods include atmospheric pressure ionization mass spectrometry[14], ion mobility spectrometry[15], and the electron capture detector for gas chromatography[16]. In addition, certain lasers depend on the manipulation of ionic reactions under conditions of elevated pressures[1]. Perhaps the most compelling motivation for increased research in GPIC under conditions of elevated pressure, however, is simply that such studies are needed in order to understand more completely the nature of reactions between ions and neutrals in the gas phase. Consider, for example, the following issue which has recently gained much attention in the field of GPIC. Even relatively simple bimolecular ion-molecule (IM) reactions are generally thought to occur by the following set of individual steps in the gas phase[17],

$$A^\pm + B \; \rightleftharpoons \; A^\pm(B)^* \; \overset{\ddagger}{\rightleftharpoons} \; (A)B^{\pm^*} \; \rightleftharpoons \; A + B^\pm \qquad (1)$$
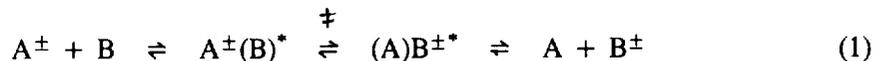
in which the ion and molecule first combined to form an excited entrance-channel ion complex, $A^\pm(B)^*$, prior to passing through a transition-state ($\pm$) that leads to an excited exit-channel ion complex, $(A)B^{\pm^*}$, and, finally, to the products of the reaction. In interpreting kinetic data obtained under low pressure conditions for reactions of this type, a formidable complexity is becoming increasingly recognized. That is, that the internal energy within the collision

complex, $A^{\pm}(B)^*$, does not necessarily get rapidly distributed among its vibrational and rotational modes of freedom, prior to its continued motion (either forward or backward) along the reaction coordinate[18-21]. This means that the well-developed statistical theories (RRKM theory, for example) for describing kinetic processes involving excited species are probably not applicable to these systems. For some IM reactions (such as the one to be illustrated below), energy transfer within the entrance-channel complex is actually thought to be the rate-limiting step of the overall reaction when performed under low pressure conditions. Therefore, for these cases, some of the basic parameters of interest in a mechanistic study, such as the structure and energy of the transition state along the reaction coordinate, can not be reliable deduced from low pressure kinetic data and existing theory.

The impasse described above could be avoided if the reaction of interest could be studied under conditions of relatively high pressure where the reaction system is moved to what is known as its high pressure (HP) limit of kinetic behavior. In the HP limit, the entrance- and exit-channel ion complexes shown in Reaction 1 would be brought into thermal equilibrium with the buffer gas by collisions prior to their continued motion along the reaction coordinate. In representing an IM reaction occurring in the HP limit, the asterisks shown in Reaction 1 would be removed, indicating that the entrance- and exit-channel ion complexes do not have the extra internal energy imparted to them by their exothermic formation processes. Instead, these intermediates would have normal Boltzman distributions of energies, that would be determined only by the temperature of the buffer gas and would be continuously maintained by collisions. Kinetic data for systems that are clearly operating in their HP limit should be relatively simple to interpret using well-established transition-state theory.

For the reason highlighted above and for other fundamental reasons[5], as well, new methods for the study of GPIC at elevated pressures are needed. In this paper, we describe recent efforts in our laboratory to apply an ion mobility spectrometer (IMS) to this task. We will focus here on one specific reaction system that has received a great deal of attention by others in recent years. This is the Sn2 nucleophilic displacement reaction of chloride anion with methyl bromide, as shown in Reaction 2.

$$Cl^- + CH_3Br \rightarrow CH_3Cl + Br^- \qquad (2)$$

This reaction is thought to proceed by the general mechanism expressed in Reaction 1, in which the behavior of its entrance-channel ion complex, $Cl^-(CH_3Br)$, is expected to determine the rate of the overall reaction. Others have shown that the entrance- and exit-channel intermediates of this reaction behave in a distinctly non-statistical manner under low pressure conditions[20,21]. Therefore, a comparison of the kinetic behavior of this system under low pressure and high pressure conditions is of considerable interest.

EXPERIMENTAL METHODS

The IMS instrument that we have developed for kinetic studies is shown in Figure 1. Since this instrument has been previously described in detail[10-12], only a brief summary of its operation will be provided here. The instrument consists of an IMS, a mass spectrometer (MS) and a gas handling plant (GHP). The walls of the IMS are defined by a Pyrex glass tube that is terminated at both ends by glass-to-metal seals and stainless-steel flanges. The electric field for the IMS is created by 19 stainless-steel rings (common hose clamps) that are strapped around the glass tube. Ions are created in a movable ion source containing a 15 mCi ^{63}Ni-on-Pt radioactive foil. Nitrogen flows continuously through the ion source (about 50 mL min^{-1}) from a 1-L dilution volume. A movable Bradbury-Nielson gate is located about 0.5 cm in front of the ion source. A counterflow of nitrogen gas (about 500 mL min^{-1}) enters at the left end of

the IMS. Ions are detected by a stainless-steel Faraday plate that has an MS sampling aperture (50 μm) at its center. By the MS, the ions under any mobility peak of interest can be positively identified. The entire IMS is enclosed in an oven and can be heated up to 175°C. The GHP provides a means of accurately seeding the nitrogen drift gas with the reagent compounds of interest. It includes a 4-L stainless volume that is pressurized to about 2500 torr.

RESULTS AND DISCUSSION

Rate Constants for Ion Molecule Reactions

In Figure 2, typical ion mobility spectra obtained for the purpose of rate constant measurements for Reaction 2 in an atmospheric pressure buffer gas are shown. In Figure 2A, a small amount of CCl_4 was added to the ion source gas so that the Cl^- ion is formed in the ion source by dissociative electron capture. This provides the major ion observed at about t = 25 ms. It is also seen in Figure 2A that other ions of minor relative intensity contribute to a broad baseline between 25 and 30 ms. Parallel MS measurements indicate that these unwanted ions are due to the clustering of various protic neutrals to Cl^-. These neutrals include HCl, HCOOH, and CH_3COOH and are thought to be formed by the radiation chemistry occurring within the ion source. These neutrals are not present in the drift region of the IMS.

In Figures 2B-2D, the effects of adding various amounts of CH_3Br to the drift gas are indicated. A new peak is thereby formed due to the formation of Br^- by Reaction 2 at all points along the drift tube. This peak is skewed, has a maximum intensity at about t = 27 ms, and is progressively increases in intensity with increased CH_3Br concentration. By analysis of these waveforms, the rate constants for Reaction 2 is obtained. Kinetic determinations such as these have been made over a range of temperatures and are plotted in Figure 3 (solid squares with uncertainty bars). Also shown in Figure 3 are previous measurements of the rate constant for Reaction 2 made under various conditions of lower pressure[17,20,22-27].

It is seen in Figure 3 that the rate constants measured at atmospheric pressure are distinctly greater than those that have been measured at the lower pressures. We believe that this effect with increased pressure is due to changes in the nature of the entrance-channel ion complexes of this reactions, as suggested in the INTRODUCTION. That is, at atmospheric pressure a significant portion of the entrance-channel ion complexes suffer collisions with the buffer gas, thereby altering both the amount of internal energy and the distribution of energy within the vibrational and rotational modes of the entrance-channel ion complexes. It is interesting to note that while the average amount of energy in the entrance-channel ion complexes can be assumed to be decreased by use of higher pressure, the rate of the overall reaction is nevertheless significantly increased at atmospheric pressure. This rate enhancement illustrates the importance of the change in the distribution of energy within complexes that is caused by their increased collisions with buffer gas molecules at atmospheric pressure. Also shown in Figure 3, are predictions of the rate constants for Reaction 2 derived by transition state theory under the assumption that the HP limit has been reached. The fact that the predictions are about twice as great as the measurements at atmospheric pressure suggests that the HP limit for this reaction has not been reached at atmospheric pressure. This suspicion is reinforced by recent calculations by Hase and coworkers[28] indicating that some of the excited entrance-channel ion complexes for this reaction have lifetimes shorter than the time of collisions at atmospheric pressure. Furthermore, their calculations suggest that in order to bring this reaction system clearly into the HP limit, the pressure of the buffer gas would have to be raised to about ten atmospheres. Therefore, it presently appears that the data in Figure 3 indicate the reaction system under study has been moved towards, but not onto, the HP limit

of behavior by the pressure increase to one atmosphere.

Ion Clustering Equilibrium Constants

Ion clustering equilibrium constants can also be measured by IMS as illustrated in Figure 4 for the clustering of Cl^- ion by $CHCl_3$. In this figure, it is noted that the drift time of the major Cl^--containing ion packet is increased by increasing the concentration of the clustering agent, $CHCl_3$. This is because equilibrium Reaction 3 is shifted to the right by increased $CHCl_3$ concentration.

$$Cl^-(CHCl_3)_{n-1} + CHCl_3 \rightleftharpoons Cl^-(CHCl_3)_n \tag{3}$$
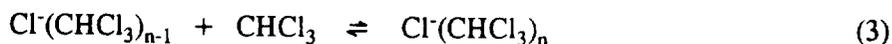
By the analysis of data such as these, equilibrium constants for the individual steps, $n = 1$ and $n = 2$ have been determined at three temperatures and these are listed in Table I. Also shown in Table I are other fundamental parameters that were obtained from these measurements, including reduced single ion mobilities and the ion-buffer gas interaction cross sections for the bare and clustered Cl^- ions.

An important advantage of the IMS approach to equilibrium measurements is that a major problem experienced in equilibrium measurements by high pressure mass spectrometric measurements is entirely avoided. That problem is the perturbation of relative ion intensities that can be associated with aperture-sampling of a high pressure ionized gas[29,30].

Rate Constants for Reactions Involving Sets of Clustered Ions

A useful feature of kinetic measurements by the IMS is that the reactions of a set of ions, that are coupled by fast equilibrium reactions, can be observed. In Figure 5, for example, a series of ion mobility spectra are shown which reflect the reaction of a set of $Cl^-(CHCl_3)_n$ cluster ions with CH_3Br. As opposed to the spectra shown previously in Figure 2, it is noted in Figure 5 that the Br^- product ion appears to have a drift time that is less than that of the reactant Cl^- ion. This is due to the fact that clustering of Br^- by $CHCl_3$ is less extensive than clustering of Cl^- under the conditions of this experiment. By analysis of waveforms such as these, the rate constants for the reaction of any selected set of $Cl^-(CHCl_3)_n$ cluster ions with CH_3Br can be determined. Some of these determinations have been plotted in Figure 6 along with a curve indicating the net rate constants that were predicted under the assumption that only the bare Cl^- ion is reactive with CH_3Br. These results indicate that the reaction is essentially shut off by any clustering of the reactant Cl^- ion. This result is interesting in view of the fact that the reaction,

$$Cl^-(CHCl_3)_1 + CH_3Br \rightarrow CH_3Cl + Br^-(CHCl_3)_1 \tag{4}$$
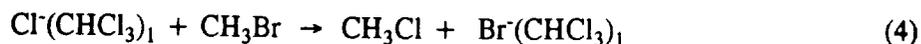
would be exothermic by about 6 kcal/mol. A possible reason why Reaction 4 is not fast is the following. In a concerted Sn2 transition state that might be envisioned for this reaction, the solvent molecule, $CHCl_3$, would have to migrate from one region of decreasing negative charge density at the Cl atom to the other region of increasing negative charge density at the Br atom. Since these two regions would be located at opposite ends of the Sn2 transition state and the $CHCl_3$ molecule has only one proton for interaction with negative charge, migration of the $CHCl_3$ molecule to the Br end of the transition-state probably does not occur during the very short lifetime of this species.

37

CONCLUSIONS AND FUTURE DIRECTIONS

We have demonstrated here that IMS provides a means of measuring various types of ion molecule processes under conditions of much higher buffer gas pressures than has been possible by the conventional, mass spectrometry-based methods of GPIC. The general procedures described here should be applicable to many reaction systems of interest within the field of GPIC. We have also learned, however, that several formidable problems must be either acknowledged or overcome in future studies of GPIC at very high pressures. One of the most significant of these is that it will be difficult to study the reactions of ions that react readily with ubiquitous buffer gas impurities, such as water, unless the concentration of that impurity can be reduced to about one part per billion. Since the reduction of water to that level is extremely difficult, the reactions of numerous high-energy positive and negative ions that react with water will not be easily studied by the IMS approach. In addition, improved ion sources are needed by which the detrimental effects of the reactive neutrals produced by radiation chemistry within the presently utilized beta sources can be minimized. We have also learned that the internal surfaces of the stainless-steel GHP presently used for our IMS are not sufficiently inert as to allow the quantitative introduction of many compounds. For example, CH_3I and substituted nitrobenezenes have been found to either decompose or adsorb on the surfaces of our GHP. More inert GHP surfaces that are also capable of withstanding superambient pressures (several atmospheres) are needed. Finally, gas phase kinetic measurements are needed over a very wide and continuously varied range of pressures, from about 10 torr to 10 atmospheres. In addressing this need, it presently appears that IMS offers the most promising approach.

REFERENCES

1. Lee, F.W., Collins, C.B. and Waller, R.A., *J. Chem. Phys.* **65**, 1605 (1976).
2. Collins, C.B. and Lee, F.W., *J. Chem. Phys.*, **68**, 1391 (1978).
3. Collins, C.B. and Lee, F.W., *J. Chem. Phys.*, **71**, 184 (1979).
4. Collins, C.B, and Lee, F.W., *J. Chem. Phys.*, **72**, 5381 (1980).
5. Collins, C.B., Lee, F.W., Tepfenhart, W.M., and Stevefelt, J., *J. Chem. Phys.*, **78**, 6079 (1983).
6. Matsuoka, S, Nakamura, H. and Takaaki, T., *J. Chem. Phys.*, **79**, 825 (1983).
7. Matsuoka, S. and Nakamura, H., *J. Chem. Phys.*, **89**, 5663 (1988).
8. Matsuoka, S, Nakamura, H. and Tamura, T., *J. Chem. Phys.*, **75**, 681 (1981).
9. Matsuoka, S. and Ikesoe, Y., *J. Phys. Chem.*, **92**, 1126 (1988).
10. Giles, K. and Grimsrud, E.P., *J. Phys. Chem.*, **96**, 6680 (1992).
11. Giles, K. and Grimsrud, E.P., *J. Phys. Chem.*, **97**, 1318 (1993).
12. Knighton, W.B., Bognar, J.A., O'Connor, P.M. and Grimsrud, E.P., *J. Am. Chem. Soc.*, **115**, 12079 (1993).
13. Strode, K.S. and Grimsrud, E.P., *Int. J. Mass Spectrom. and Ion Proc.*, **130**, 227 (1994).
14. Carroll, D.I., Dzidic, I., Horning, E.C. and Stillwell, R.N., *Appl. Spectros. Rev.*, **17**, 337 (1981).
15. Carr, T.W. *Plasma Chromatography*, Plenum Press: New York, NY (1984).
16. Zlatkis, A. and Poole, C.F., *Electron Capture, Theory and Practice in Chromatography*, Elsevier: New York (1981).
17. Olmstead, W.N. and Brauman, J.I., *J. Am. Chem. Soc.*, **99**, 4219 (1977).
18. Vande Linde, S.R. and Hase, W.L., *J. Am. Chem. Soc.*, **111**, 2349 (1989).
19. Vande Linde, S.R., and Hase, W.L., *J. Phys. Chem.*, **94**, 6148 (1990).
20. Viggiano, A.A., Morris, R.A., Paschkewitz, J.S. and Paulson, J.F., *J. Am. Chem. Soc.*,

114, 10477 (1992).

21. Graul, S.T. and Bowers, M.T., *J. Am. Chem. Soc.*, **113**, 9696 (1991).
22. Caldwell, G., Magnera, T.F and Kebarle, P., *J. Am. Chem. Soc.*, **106**, 959 (1984).
23. Gronert, S., DePuy, C. and Bierbaum, V. *J. Am. Chem. Soc.*, **113**, 4009 (1991).
24. Ingemann, S. and Nibbering, N.M.M., Can. J. Chem., **62**, 2273 (1984).
25. Depuy, C.H., Gronert, S., Mullin, A. and Bierbaum, V.M., *J. Am. Chem. Soc.*, **112**, 8650 (1990).
26. Tanaka, K., Mackay, G.I., Payzant, J.D. and Bohme, D.K., *Can. J. Chem.*, **54**, 1643 (1976).
27. Bohme, D.K. and Raksit, A.B., *Can. J. Chem.*, **63**, 3007 (1985).
28. Wang, H., Perlherbe, G.H. and Hase, W.L, *J. Phys. Chem.*, in press.
29. Kebarle, P. *Ann. Rev. Phys. Chem.*, **28**, 445 (1977).
30. Zook, D.R. and Grimsrud, E.P., *J. Phys. Chem.*, **92**, 6374 (1988).

ACKNOWLEDGEMENT

Table I. Results Obtained from IMS Measurents of $Cl^-(CHCl_3)_n$ Clustering Reactions

	Temperature (°C)		
	75°	100°	125°
t_0 [a] (msec)	40.80	36.84	33.99
t_1	63.84	57.88	54.35
t_2	82.64		
$K_{o,0}$ [b] ($cm^2\ V^{-1}\ s^{-1}$)	2.725	2.820	2.883
$K_{o,1}$	1.742	1.795	1.803
$K_{o,2}$	1.346		
Ω_0 [c] (nm^2)	0.919	0.858	0.813
Ω_1	1.168	1.095	1.056
Ω_2	1.461		
K_1 [d] (atm^{-1})	3.7E6	6.1E5	1.41E5
K_2	1.43E4		
ΔH^0_l [e] ($kcal\ mol^{-1}$)			-18.1
ΔS^0_l [f] ($cal\ deg^{-1}\ mol^{-1}$)			-21.8

[a] Drift time, t_i, of single ion $Cl^-(CHCl_3)_i$.

[b] Reduced mobility, $K_{o,i}$, of single ion $Cl^-(CHCl_3)_i$.

[c] Ion-buffer gas interaction cross section, Ω_i, for single ion $Cl_i(CHCl_3)_i$.

[d] Equilibrium constant, K_n, for reaction, $Cl^-(CHCl_3)_{n-1} + CHCl_3 = Cl^-(CHCl_3)_n$

[e] Enthalpy of $Cl^-(CHCl_3)_1$ formation determined from temperature dependence of K_1.

[f] Entropy of $Cl^-(CHCl_3)_1$ formation determined from temperature dependence of K_1.
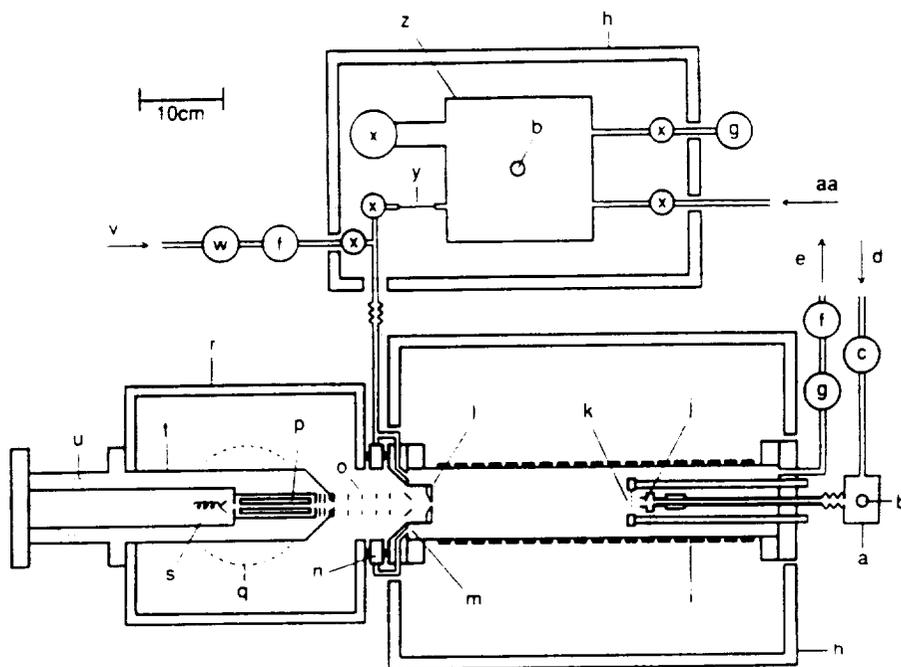
Figure 1. Diagram of the IMS apparatus: (a) stainless-steel source gas dilution volume, (b) septum inlet, (c) needle valve, (d) N_2 source gas supply, (e) source and drift gas exhaust, (f) flow meter, (g) pressure transducer, (h) insulated box, (i) drift tube, (j) ion source, (k) Bradbury-Nielson gate, (l) Faraday plate / MS aperture, (m) drift gas inlet, (n) universal joint, (o) electrostatic lens element, (p) quadrupole mass filter, (q) 6" diffusion pump, (r) first vacuum envelope, (s) channeltron electron multiplier, (t) second vacuum envelope, (u) 3" diffusion pump, (v) N_2 drift gas supply, (w) leak valve, (x) on/off valve, (y) fused silica capillary, (z) 4-liter stainless steel dilution volume, (aa) N_2 gas supply.

40
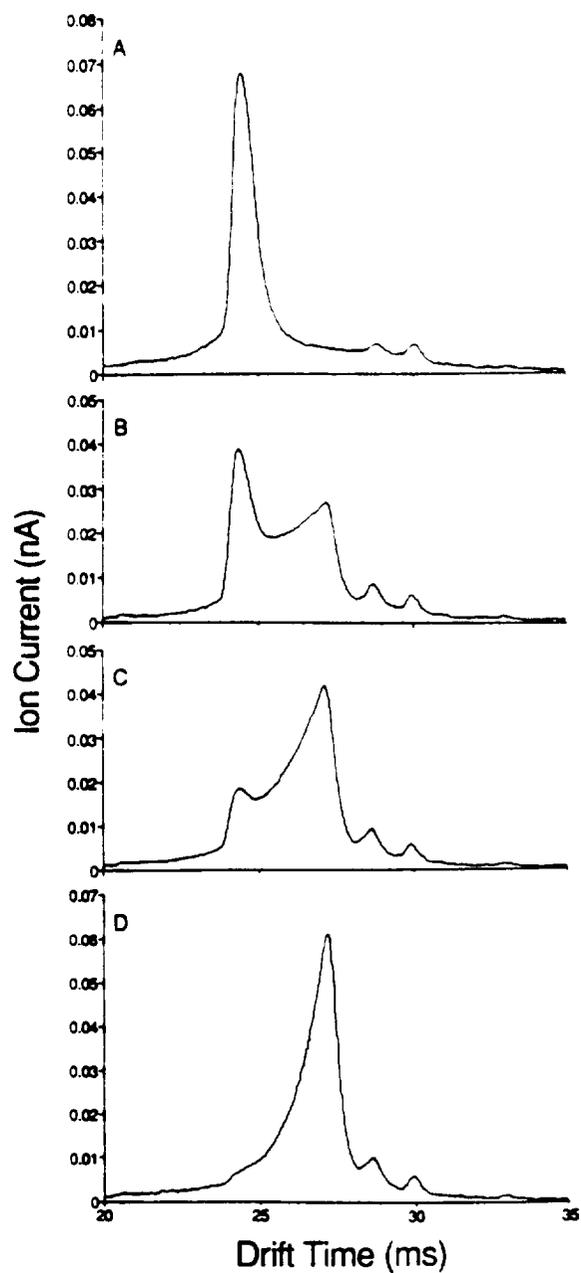
Figure 2. Ion mobility spectra modified by the reaction, $Cl^- + CH_3Br \rightarrow Br^- + CH_3Cl$, using the following concentrations of CH_3Br in the drift tube: (A) none, (B) 1.29 x 10^{12}, (C) 2.60 x 10^{12}, and (D) 5.27 x 10^{12} molecules cm^{-3}. Temperature is 125°C.
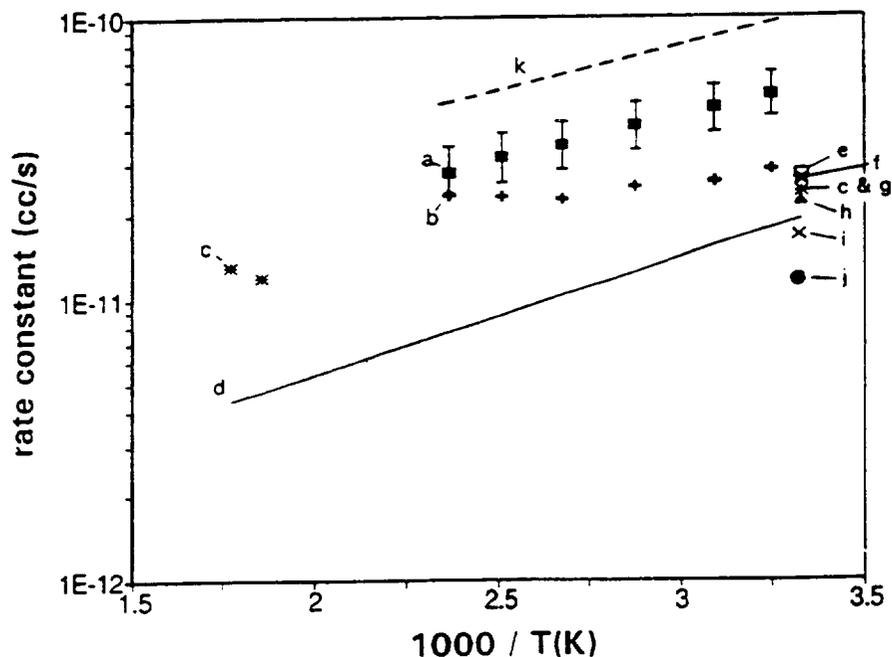
Figure 3. Rate constants observed for the reaction of Cl⁻ with CH_3Br under a variety of different temperature and pressure conditions. The present IMS measurements at 640 Torr (a) and measurements by pulsed high pressure mass spectrometry at 3 Torr also made in our lab (b) have been plotted in the Arrhenius form. Error bars indicate the estimated uncertainties of the IMS measurements (±20%). Also shown are previous measurements of this reaction system by the following techniques and pressures: (c) SIFT (ref. 20) at 0.5 Torr, (d) PHPMS (ref. 22) at 4 Torr, (e) SIFT (ref. 23) at 0.5 Torr, (f) FTMS (ref. 24) at < 10⁻⁵ Torr, (g) SIFT (ref. 25) at 0.5 Torr, (h) FA (ref. 26) at 0.5 Torr, (i) FA (ref. 27) at 0.5 Torr, and (j) ICR (ref. 17) at < 10⁻⁵ Torr. The dashed line (k) provides a prediction for the rate constants in the HP limit of kinetic behavior obtained from transition-state theory.
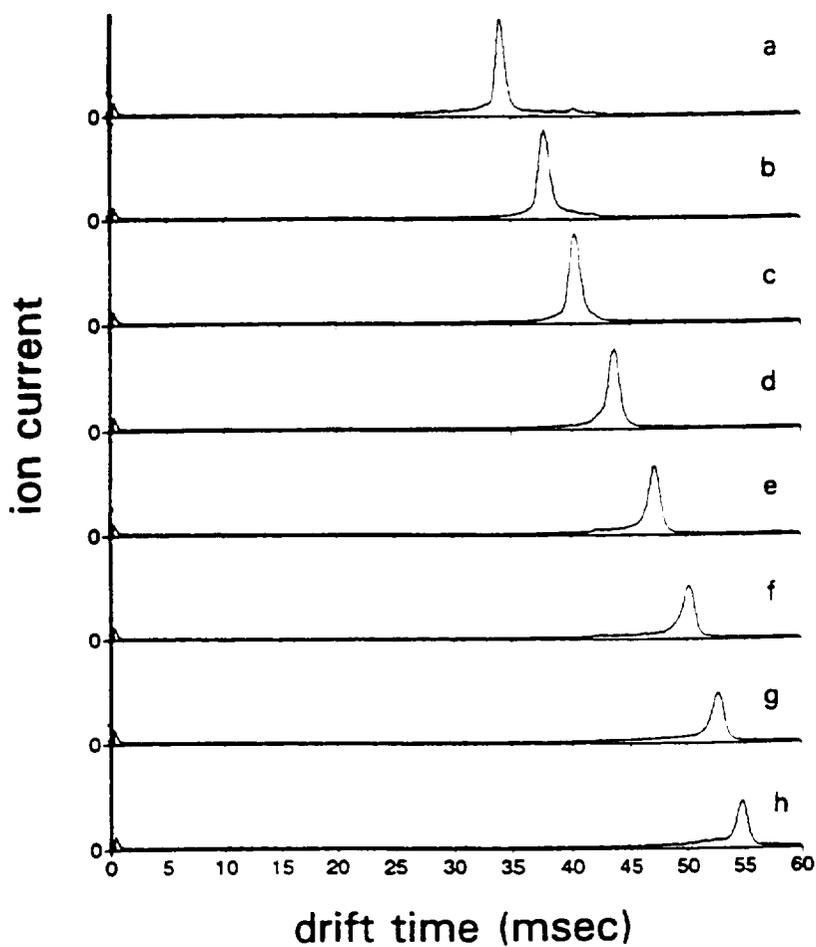
Figure 4. Ion mobility spectra obtained by the production of Cl⁻ by electron capture to CCl_4 in the ion source with the following partial pressures of $CHCl_3$ added to the drift gas: (a) none, (b) 1.61 x 10^{-6}, (c) 3.2 x 10^{-6}, (d) 6.5 x 10^{-6}, (e) 1.29 x 10^{-5}, (f) 2.6 x 10^{-5}, (g) 5.2 x 10^{-5}, and (h) 1.03 x 10^{-4} atm. Ion source and drift regions contain nitrogen buffer gas at 640 torr and 125°C.
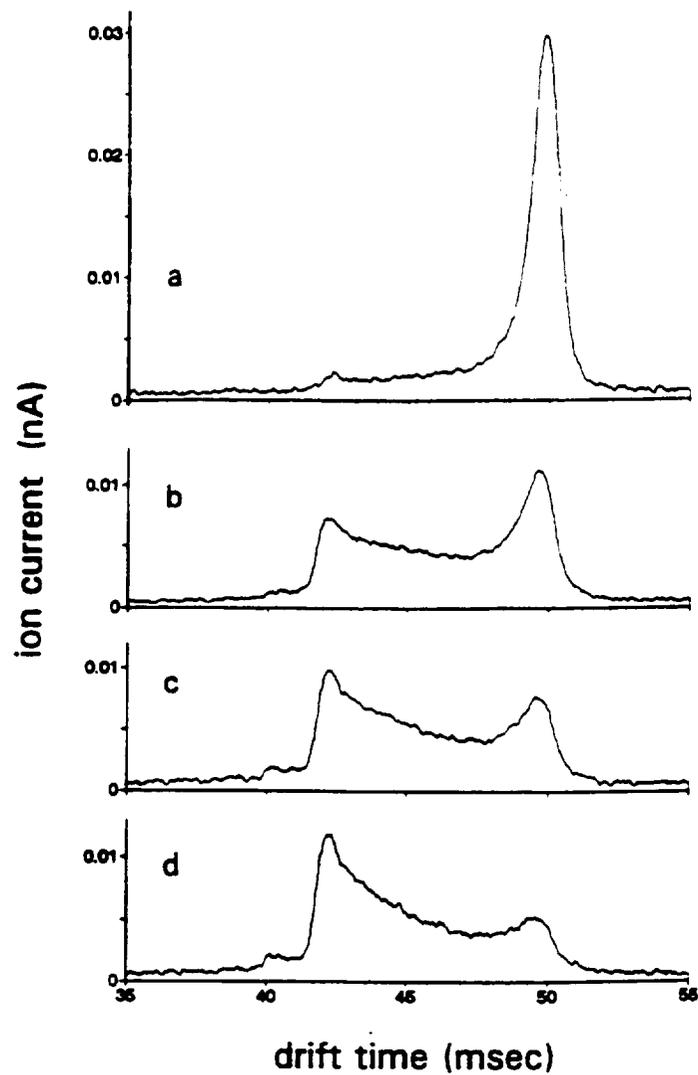
Figure 5. Ion mobility spectra of source-produced Cl$^-$ ions with 2.22 x 10^{-5} atm of the clustering agent, CHCl$_3$, present in the drift gas along with the following amounts of the reagent neutral, CH$_3$Br: (a) none, (b) 2.6 x 10^{12}, (c) 3.9 x 10^{12}, and (d) 5.3 x 10^{12} molecules cm^{-3}. Temperature is 125°C. Under these conditions, only 24% of the reagent ions are present as uncomplexed Cl$^-$ ions.
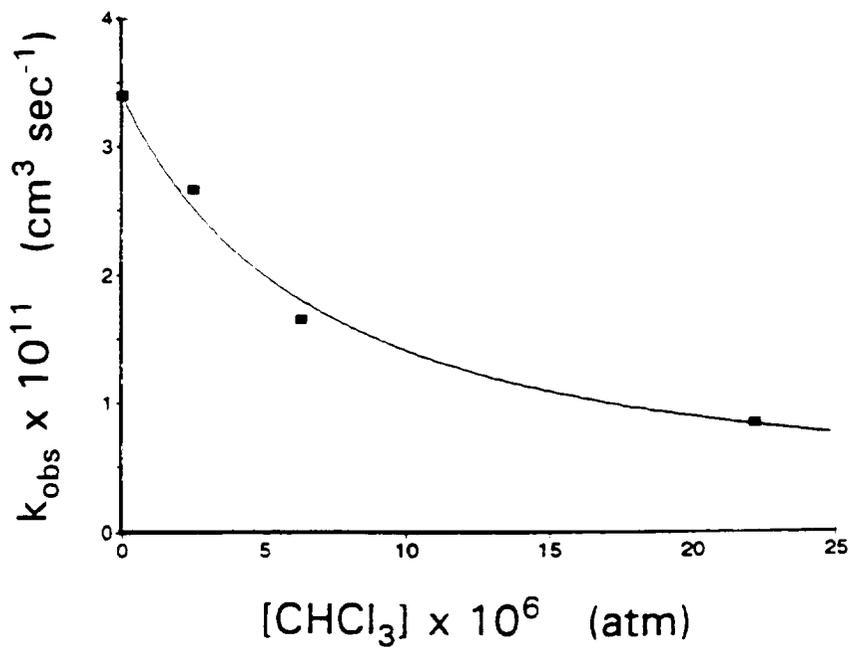
Figure 6. Rate constants observed for the reactions of $Cl^-(CHCl_3)_{0-2}$ ions with CH_3Br as a function of $CHCl_3$ concentration in the drift gas. Temperature is 125°C. The solid line shown is a prediction for k_{obs} based on the assumption that only the uncomplexed Cl^- ion reacts with CH_3Br.

Session II: Instrument Development

Session Chair: Dr. Steve Harden

Determination of Benzene, Toluene, and Xylene by means of an Ion Mobility Spectrometer Device using Photoionization

J.W. Leonhardt[1], H. Bensch[1], D. Berger[1], M. Nolting[2], J.I.Baumbach[3]

[1] Institut für Umwelttechnolgien, Berlin, Germany
[2] AUERGESELLSCHAFT/MSA, Berlin, Germany
[3]Institut für Spektrochemie und angewandte Spektroskopie,
Dortmund, Germany

ABSTRACT

The continuous monitoring of changes on the quality of ambient air is a field of advantage of ion mobility spectrometry. Benzene, Toluene, and Xylene are substances of special interest because of their toxicity. We present an optimised drift tube for ion mobility spectrometers, which uses photo-ionisation tubes to produce the ions to be analysed. The actual version of this drift tube has a length of 45 mm, an electric field strength established within the drift tube of about 180 V/cm and a shutter-opening-time of 400 µs. With the hydrogen tube used for ionisation a mean flux of 10^{12} photons/cm^{2}s was established for the experiments described.

We discuss the results of investigations on Benzene, Toluene, and Xylene in normal used gasoline SUPER. The detection limits obtained with the ion mobility spectrometer developed in co-operation are in the range of 10 ppbv in this case. Normally, charge transfer from Benzene ions to Toluene takes place. Nevertheless the simultaneous determination in mixtures is possible by a data evaluation procedure developed for this case. The interferences found between Xylene and others are rather weak. The ion mobility spectra of different concentrations of gasoline SUPER are attached as an example for the resolution and the detection limit of the instrument developed. Resolution and sensitivity of the system are well demonstrated. A hand-held portable device produced just now is to be tested for special environmental analytical problems in some industrial and scientific laboratories in Germany.

KEY WORDS

Benzene, gas analysis, gasoline, ion mobility spectrometry, Toluene, UV-ionisation, Xylene

INTRODUCTION

Ion mobility spectrometry is a very sensitive method that can be applied to monitoring of air pollutants at sub-parts per million concentrations in ambient air and at ambient pressure. An application tool is the continuos determination of cancer Benzene in air at work places and environmental protection. The addition of aromatics to petrol lies in the percent range. The dangerous risk follow immediately. Thus, a selective, portable and hand-held device must be able to detect the substances under control in the range of legal limit (in Germany called maximum permitted exposure level of pollution at the place of work [MAK]). In the case of Benzene, the instrument must be able to detect Benzene in an environment of Toluen and Xylene with MAK values 400 times higher then Benzene.

In this work, we present an UV-lamp supported ion mobility spectrometer to detect Benzene in such an environment and spectra of different gasolines.

EXPERIMENTAL SECTION.

The ion mobility measurements were carried out using a prototype of a UV-lamp supported drift tube. The schematic diagram of the experimental arrangement to detect Benzene, Toluene, and Xylene is given in Figure 1. Details of the geometrical parameters are summarised in figure 2. The parameters chosen for the instrumentation of the ion mobility spectrometer are presented in Table 1. In the ionisation range a H_2-lamp was used as source for ionisation, and standard power supplies were employed to establish an electrostatic electric field in the drift region. At the

Table 1: Main operation parameter of the UV-lamp ion mobility spectromter used in the experiments	
temperature	ambient (25°C)
pressure	ambient air
drift gas flow	500 ml/min
sample gas flow	50 ml/min
shutter	duplex-shutter
shutter open time	500 μs
amplifier	$5 \cdot 10^9$ V/A
ion source	H_2 - lamp, MgF-window
mean flux	10^{12} photons/cm²s
interior diameter	30 mm
drift path	45 mm
electric field strength	170 - 230 V/cm
water content	<= 50 ppmv
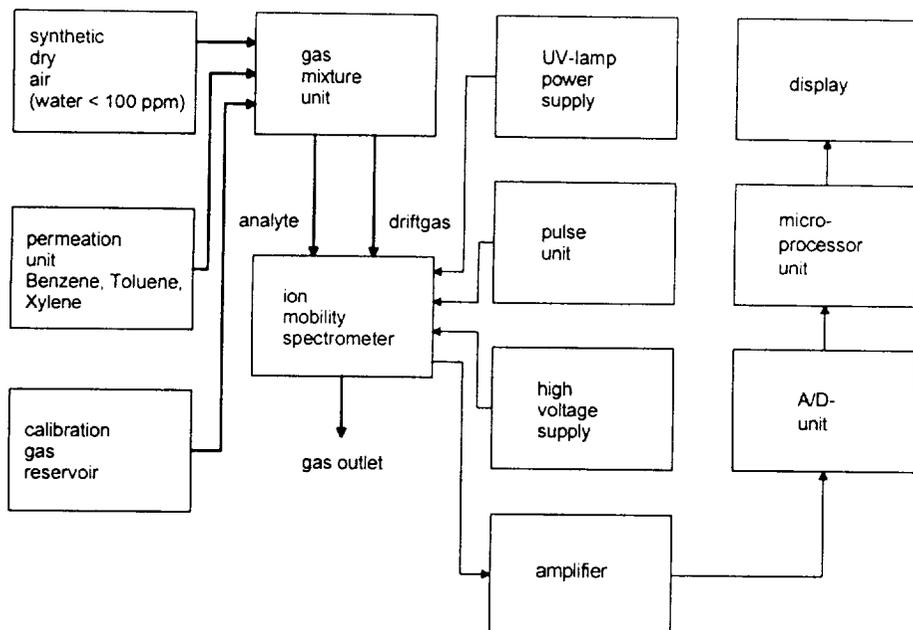
duplex-shutter ion swarms are created for time intervals less then 500 μs. Through this short gate time all ions start to travel in a plane of the drift field. The control unit for the shutter pulse drive circuit and the A/D-converter are on-line connected with a computer.

Figure 1:

Schematic diagram of the experimental arrangement to detect Benzene, Toluene, and Xylene using UV-ion mobility spectrometer
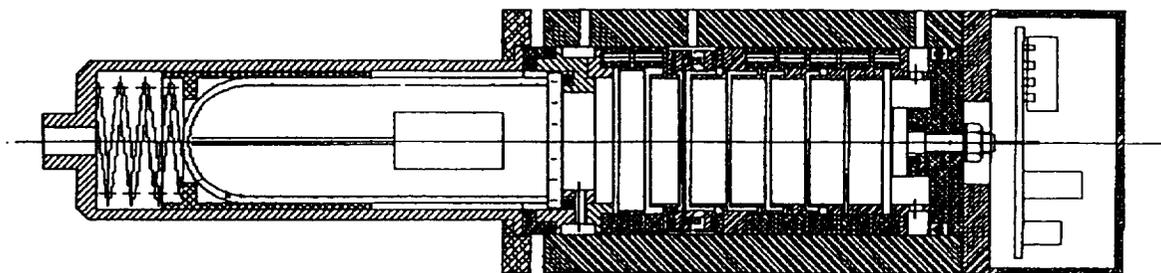
Figure 2:

Picture of the ion mobility spectrometer with UV-lamp, drift tube and data acquisition board (from left)

RESULTS AND DISCUSSION

The spectra of samples of different content of pure Benzene, Toluene, and Xylene are presented in figure 3, 4, and 5, respectively. In the case of Benzene we take 8 peaks, for Toluene 7 and Xylene 3. In Table 2 we consider these substances, the drift times correlated with different peaks and reduced mobility values belong to the drift times.
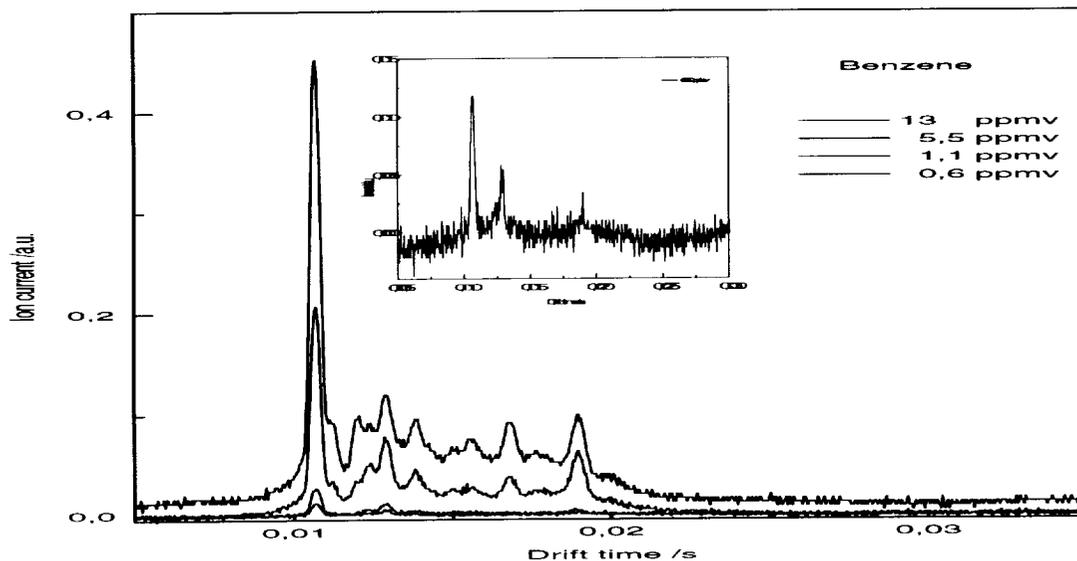
Figure 3:

Ion mobility spectra of different concentrations of pure Benzene
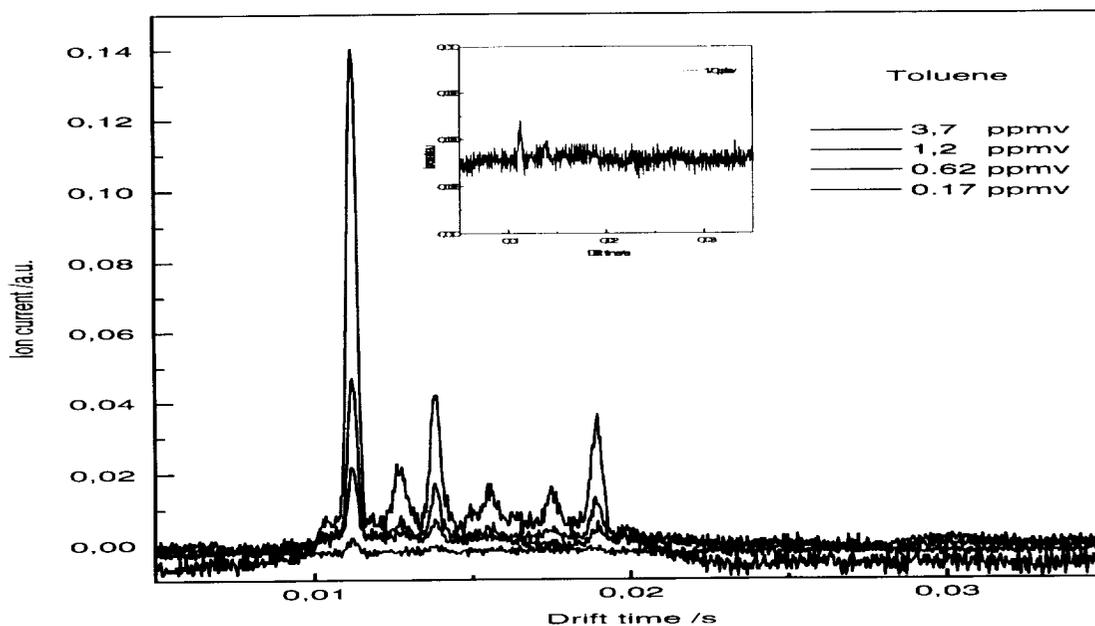
Figure 4:

Ion mobility spectra of different concentrations of pure Toluene
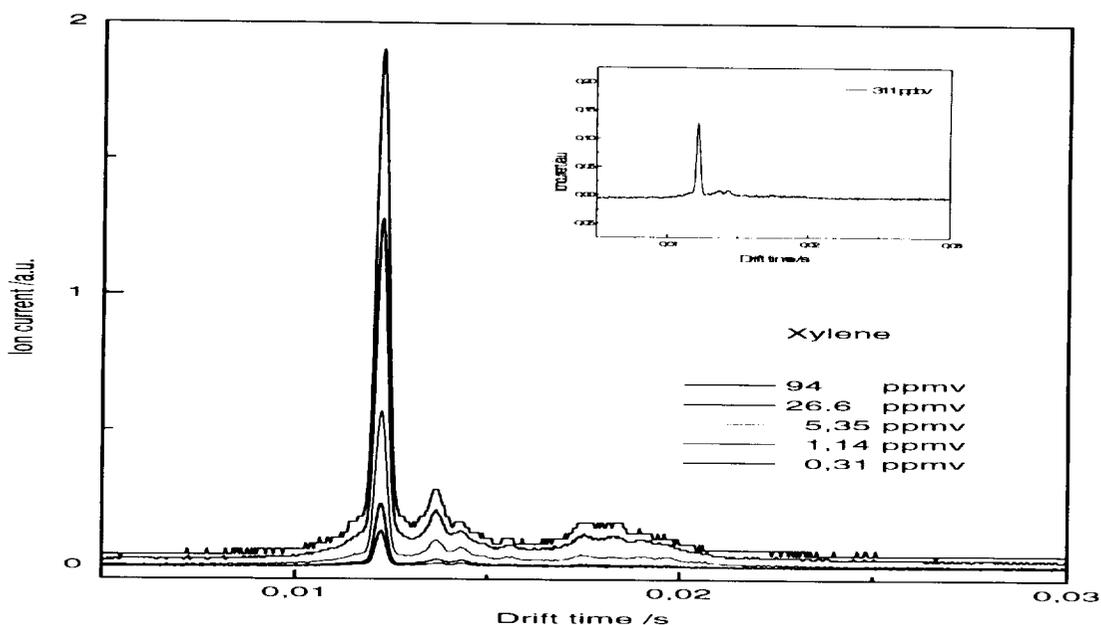
Figure 5:

Ion mobility spectra of different concentrations of pure Xylene

Table 2: Correlation between measured drift times and reduced mobilities in the case of pure Benzene, Toluene, and Xylene					
Substance	Benzene		Toluene		Xylene	
peak number	drift time	reduced mobility	drift time	reduced mobility	drift time	reduced mobility
	ms	cm^2/V s	ms	cm^2/V s	ms	cm^2/V s
1	10.66	2,27	10.04	2,33	11.81	2,96
2	11.20	2,16	11.20	2,16	13.18	1,84
3	11.96	2,03	12.72	1,91	13.85	1,75
4	12.88	1,88	13.82	1,75		
5	13.84	1,75	15.56	1,56		
6	15.56	1,56	17.50	1,39		
7	16.80	1,45	18.94	1,28		
8	18.96	1,28				

The spectra in the case of mixtures of Benzene and Toluene, as well as Benzene and Xylen are presented in Figure 6 and 7, respectively. It was observed an intensive charge transfer reaction between the positive charged Benzene ion and Toluene. The presence of Toluol is visible as increased peak height. In all cases a little peak of Benzene is present. This represents a short amount of Benzene in all cases is available as residual peak. It comes out, that in the

case of small concentrations of Toluene up to 1 ppmv the detection of Benzene can be re-alised in case of excess of Toluen quantitatively. In the case of very high concentrations of Toluene over 10 ppmv the detection of small amounts of Benzene the detection problem gets into difficulties. Thus, the simultaneous determination in the range of the MAK-value of Benzene and the MAK-value of Toluene needs further investigations and an optimal arrangement of the ionisation and the drift tube.
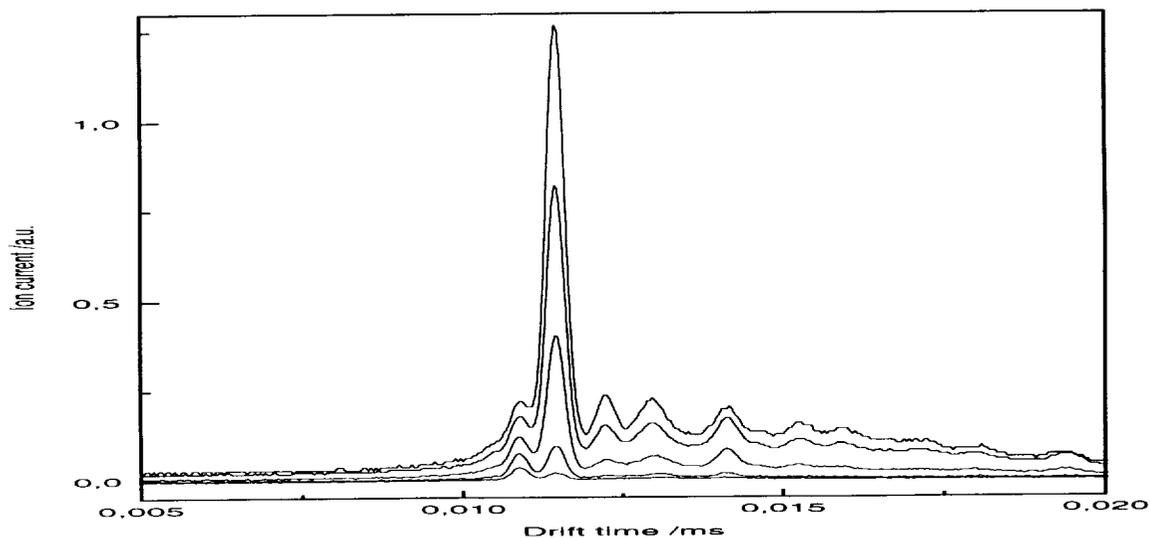
Figure 6:

Ion mobility spectra of different concentrations mixtures of Benzene and Toluene
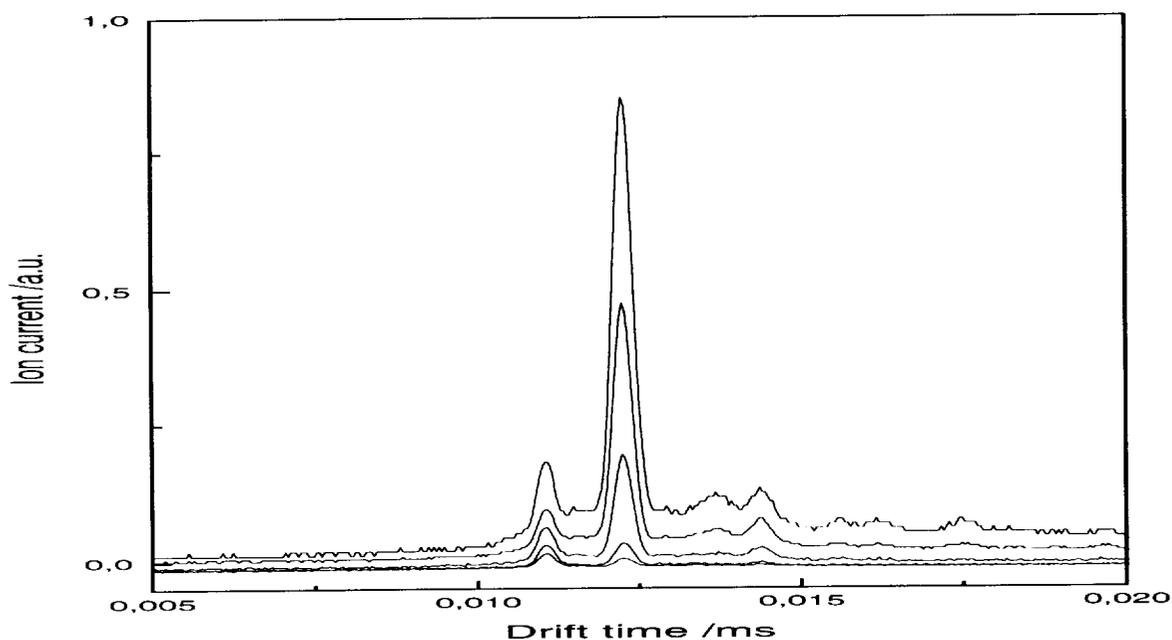
Figure 7:

Ion mobility spectra of different concentrations mixtures of Benzene and Xylene

The charge transfer rate between ions of Benzene and Xylene is lower the in the case of Benzene and Toluene. With regard of this fact a correction factor is useful.

In Figure 8 and 9 we present the first applications of the experimental device to detect gasoline SUPER UNLEADED and BENZIN UNLEADED available from a conventional petrol station in Germany.
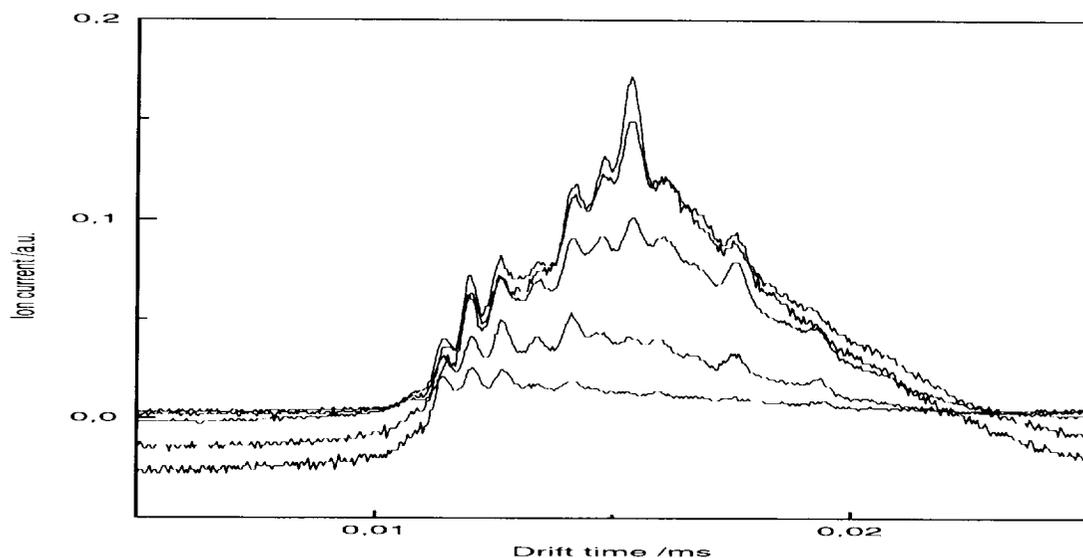
Figure 8:

Ion mobility spectra of gasoline SUPER UNLEADED.
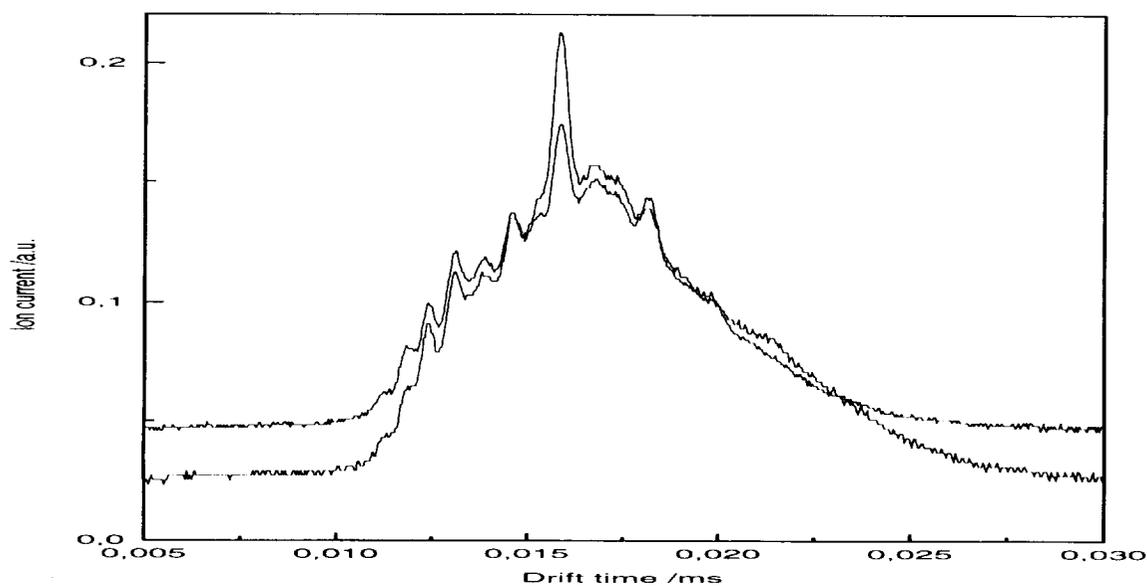
Figure 9:

Ion mobility spectra of gasoline BENZIN UNLEADED.

CONCLUSIONS

The main conclusions of the first experiments with Benzene, Toluene, and Xylene of the UV-lamp supported ion mobility spectrometer are the following:

1) A method for simultaneous determination of the concentrations of Toluene and Xylen is available.

2) The determination of Benzene in the range of the MAK-value is possible in the case of additional Xylene, also at higher Xylol concentrations.

3) The determination of Benzene in the case of additional Toluene is possible if the concentrations of both are lower then 1 ppmv.

4) The continuos monitoring of Benzene arising from petrol stations using UV-lamp supported ion mobility spectrometer is an new application field for the method presented.

REFERENCES

1) T.Carr (Ed.): Plasma Chromatography (Plenum, New York, 1984) 249pp

2) H.H.Hill; W.F.Siems; R.H.St. Louis: Anal.Chem. 62 (1990) 210A-1209A

3) R.H.St. Louis; H.H.Hill: Crit.Rev.Anal.Chem. 21 (1990) 321-355

4) H.M.Widmer: Chimia 43 (1989) 268-277

5) J.E.Roehl: Appl.Spectrosc.Rev. 26 (1991)1-57

6) G.A.Eiceman: Crit.Rev.Anal.Chem. 22 (1991)17-36

7) J.Adler; G.Arnold; J.I.Baumbach; R.Döring: ZfI-Mitt. 154 (1992) 1-11

8) J.I.Baumbach; D.Berger; J.W.Leonhardt; D.Klockow: Int.J.Environm.Anal. Chem.52 (1993) 189-193

9) R.E.Clement; K.W.M.Siu; H.H.Hill (Ed.): Instrum. Trace Org. Monit. (Lewis Publ., Chelsea, Mich., 1992) 300pp.

10) G.E.Spangler; K.N.Vora; J.P.Carrico: J.Phys. E19 (1986) 191-198

THE MINI-CIDEX GC/IMS: ANALYSIS OF COMETARY ICE AND DUST.

Daniel R. Kojiro, Glenn C. Carle, NASA-Ames Research Center, Moffett Field, CA 94035, **Donald E. Humphry and Maxine Shao**, SETI Institute, 2035 Landings Dr., Mountain View, CA 94043, **Nori Takeuchi**, TMA/Norcal, 2030 Wright Ave., Richmond, CA 94804.

ABSTRACT

Comets are recognized as among the most scientifically important objects in the solar system. They are presumed relics of the early primitive material in the solar nebula and are believed to have provided a general enrichment of volatiles to the inner solar system. The Cometary Coma Chemical Composition (C4) Mission, a proposed Discovery-Class Mission, will analyze materials released into the coma, providing information leading to the understanding of the chemical composition and make-up of the cometary nucleus. As one of two scientific instruments in the C4 spacecraft, an advanced and streamlined version of the Cometary Ice and Dust Experiment (CIDEX), a mini-CIDEX, will employ an X-Ray Fluorescence (XRF) spectrometer to determine bulk elemental composition of cometary dust grains and a Gas Chromatograph / Ion Mobility Spectrometer (GC/IMS) for determination of the molecular composition of dust and ices following stepwise pyrolysis and combustion. A description of the mini-CIDEX IMS will be provided as well as data from analyses conducted using the mini-CIDEX breadboard instrument.

INTRODUCTION

Comets are of enormous scientific interest for many reasons. They are primitive bodies that date back to the earliest stages of solar system formation and, because of their small size and because they have been stored in the outer reaches of the solar system, their pristine nature has been preserved better than for any other class of body. They are extremely rich in highly volatile elements, many in the form of ices, and are richer in organic matter than any other known solar system body It is strongly suspected that in addition to their content of primordial solar nebular material, they also incorporate unprocessed matter from the interstellar medium. Impacts by comets occur onto all the planets and satellites, often with major consequences (e.g., the dinosaur extinction event at the K/T boundary), or sometimes just providing a spectacular cosmic event (e.g., the collision of comet Shoemaker-Levy 9 with Jupiter). Much continues to be learned by ground-based photo and spectroscopic studies of the more than 100 comets that have been perturbed into the inner solar system. Comets have major surface heterogeneities and exhibit a rich diversity of activity due to the emissions and associated plasma phenomena of the comae and tails.

Planetary geochemistry, atmospheric science, astrophysics, cosmochemistry, space physics, interplanetary dust, and exobiology all have a stake in the advances that can be made by reading the chemical tapestry embedded in the cometary nucleus. Comets may have played a strong role in the origin of the atmospheres of the planets, in the compositional content of their crusts, and even in the origin and early evolution of life 3.5 X 10^9 years ago on Earth and the continuing extinction of species since that time.

The C4 Mission

The Cometary Coma Chemical Composition (C4) Mission, a proposed Discovery class mission, provides a unique opportunity for studying the make up of the cometary nucleus, details of cometary activity, and chemical characteristics of the comet's various morphological and stratigraphic units. C4 can perform the direct *in situ* measurements to provide valuable data to greatly increase our understanding of the nature of comets and provide the key to better interpretations of the continuing program of ground-based observations by astronomers using spectroscopic imaging.

To provide the maximum scientific return, a number of specific goals have been defined for C4. The goals of the C4 Mission are: to determine the elemental, molecular, and isotopic composition of a cometary nucleus; to characterize the chemical composition and processes in a cometary coma; and to determine the size, shape, morphology, mass, density, and rotational properties of a cometary nucleus.

Accomplishing these goals requires the fulfilling of a number of mission objectives. These can be divided into several categories depending on their importance to directly address the mission goals. The core objective of the C4 Mission is to determine the composition of a cometary nucleus by measuring the composition of the coma dust, including both the organic and silicate fractions, and the coma volatiles, including neutral gases, ions and ice grains. In addition, C4 will measure the dust-to-gas ratio for the comet and cosmochemically significant isotopic ratios.

Secondary objectives of the C4 Mission are to characterize the cometary nucleus by measuring its size, shape, surface morphology, mass, bulk density, and rotational properties, and to look for variations in coma composition as a function of time and nucleus activity.

Lower priority, opportunistic objectives are to observe the sources of nucleus activity, i.e., jets, and their variation over time, and to search for compositional heterogeneity on the cometary nucleus. In addition, as part of its baseline mission, the C4 spacecraft will fly by and observe the main belt, asteroids 598 Octavia and 2232 Altaj en route to the rendezvous with periodic comet Tempel 2.

C4 Instrumentation

To obtain the data necessary for fulfilling the mission objectives, C4 will carry four instruments. The organic and inorganic chemical composition of the grains and gases emitted from the cometary nucleus will be analyzed by two science instruments: a mass spectrometer for the gas-phase constituents and a combined gas chromatograph and x-ray fluorescence analyzer for particulates. Both the Neutral Gas and Ion Mass Spectrometer (NGIMS) and the Cometary Ice and Dust Experiment (CIDEX)[1] instruments were under intensive development for the Comet Rendezvous/ Asteroid Flyby (CRAF) mission, and had been not only chosen for the mission in the original selection process, but survived all peer-reviewed instrument cuts prior to the mission cancellation. NGIMS will analyze molecules and ions over the mass range 1 to 150 AMU via quadrapole mass spectrometry. The C4 mini-Cometary Ice and Dust Experiment (m-CIDEX), an advanced, streamlined version of the CRAF CIDEX, captures and analyzes dust and ice grains streaming from the comet using X-Ray Fluorescence(XRF) and pyrolysis Gas Chromatography-Ion Mobility Spectrometry (GC-IMS). Two engineering instruments are also included in the C4 payload, the mini-Cometary Dust Experiment (mini-CODEM) and a Navigation Camera (NavCam), both of which will return extremely important science data as well. The

CRAF-derived mini-Comet Dust Environment Monitor (CODEM)[2], will make extensive measurements of the dust flux and size distribution at the spacecraft, both as a means of assessing spacecraft safety and to obtain temporal and spatial data about the activity of the comet. The NavCam, although primarily to support optical navigation in the vicinity of the comet (and for asteroid flybys), will obtain extensive temporal morphology and topography of the comet nucleus and coma as well as identify active areas and rotational properties.

EXPERIMENTAL

Mini-Cometary Ice and Dust Experiment (m-CIDEX)
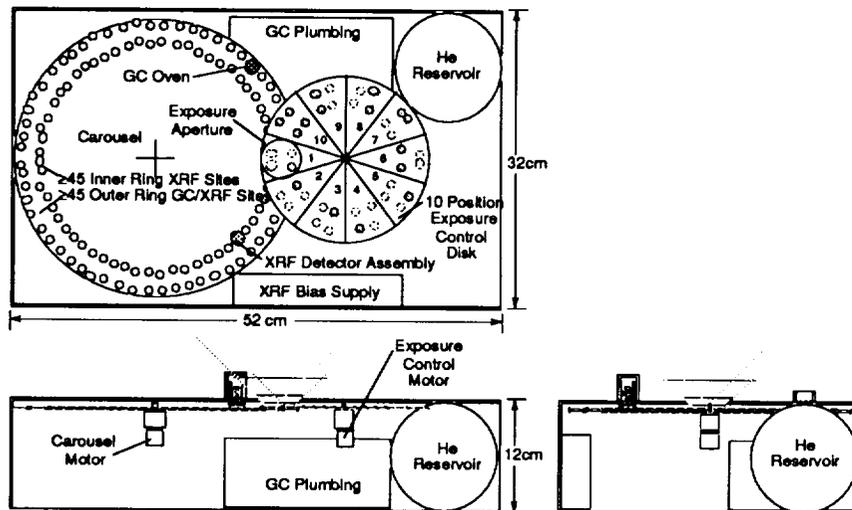
Figure 1.   m-CIDEX Apparatus.

The m-CIDEX, shown in figure 1, will return data obtained from the collection and analysis of cometary dust and ice released from the comet. Using highly developed dust collection technology developed by Clark[3], multiple samples representative of temporal and spatial distributions about the comet are collected. These samples are correlated to the dust flux measurements and orbital position. Collection Planchets utilize specially selected viscid surfaces and metal maze traps as universal particle collectors for the XRF and GC analyses, respectively. Other collectors include accordion traps, ultraclean metal foils, and a unique oil-impregnated filter combination. After collection periods from hours to days, the dust is subjected to analysis by X-Ray Fluorescence (XRF) spectrometry to obtain elemental composition of the bulk dust sample. The mini-CIDEX XRF determines elemental composition for carbon and all higher elements in the periodic table, with detection limits as low as 10 ppm for some elements. That sample or a similar sample can then be subjected to pyrolysis Gas Chromatography - Ion Mobility Spectrometry (GC-IMS) to obtain chemical composition, with particular emphasis given to the analysis of volatiles and organic molecules. The m-CIDEX GC-IMS (figure 2) detects less than 1 ppm of many inorganic and organic species, spanning the range from 2-atom molecules up to typical 8-carbon complex molecules. The sample can be step-wise pyrolyzed at various temperatures up to 1100K and then be returned to the XRF spectrometer after treatment to further enrich the analytical data. Table 1 shows the science requirements and capabilities of m-CIDEX. Molecular species in the cometary ice and dust grains that the GC-IMS experiment in m-CIDEX will focus its analyses on are shown in Table 2.

Feature	Requirements and Capabilities
m-CIDEX Sample Collection And Transportation (SCAT) equipment:	
GC Sample Collection Sites	$\geq$45 Sites Heatable to $\geq$800°C in GC oven with temperature measurement.
XRF Sample Collection Sites:	$\geq$45 Low Temperature Sites
Site Collection Temp.:	-110C$\leq$ T$\leq$50C°
m-CIDEX X-Ray Fluorescence (XRF) spectrometer:	
Targeted Measurable Elements:	C, O, Na, Al, Cl, K, Ti, Zn, Mg, Si, S, Ca, Mn, Cr, Ni, Fe, Br, Sr, Zr, Ga, Se, Ge, V
Sample Quantity:	0.1 to 10,000 μg/cm^2
Accuracy:	$\pm$10% from 0.5 to 10,000 μg/cm^2
Sensitivity:	0.1 to 10 μg/cm^2 of O, Mg, Si, S, Ca, Cr, Mn, Fe, Ni
m-CIDEX Gas Chromatograph - Ion Mobility Spectrometer (GC-IMS):	
Measureable Species:	Hydrocarbons, nitriles, fixed gases, alcohols, aldehydes, amines, amino acids
Sensitivity:	1×10^{-14} moles/s or 1ppm in collected samples
Dynamic Range:	10^7 for light gases, 10^4 for medium organic compounds
Accuracy:	$\pm$ 1% @ > 100 X sensitivity

Table 1. Science Requirements and Capabilities of m-CIDEX.

Hydrocarbons		Nitriles	Inorganics	Alcohols, Aldehydes	Amines, Amino Acids
CH_4	C_2H_2	CH_3CN	H_2, N_2, O_2	CH_3OH	CH_3NH_2
C_2H_4	C_2H_6	CH_3CH_2CN	NH_3, H_2O	CH_3CH_2OH	NH_2CH_2COOH
CH_2CCH	$CH_3CH_2CH_3$	CHCCN	HCN, CO, NO	CH_2O	$CH_3CH_2NH_2$
CH_2CHCH_3	$CH_2CH_2CH_2$	C_2N_2	H_2S, Ar,	CHOOH	$NH_2CH_2CH_2NH_2$
1,3-CH_2CCHCH_3	1-CHCCH$_2$CH$_3$		SO_2, CO_2, Ne	CH_3CH_2OH	
1-$CH_2CHCH_2CH_3$	$CH_3CH_2CH_2CH_3$				
$CH_2CHCH_2CH_3$	C_6H_6				

Table 2. Some Candidate Molecular Species in Cometary Grains.

m-CIDEX GC-IMS Breadboard

Laboratory versions of the m-CIDEX GC-IMS functional components are assembled in a breadboard for testing and evaluation. As shown in figure 2, the m-CIDEX GC-IMS breadboard currently uses three columns: 1) a light gas column; 2) an organic column; and 3) a polar column. Operating parameters for the columns and their associated detectors are shown in figure 3. The detectors are NASA developed, Modulated Voltage[4] Tri-axial Metastable Ionization Detectors (MIDs)[5]. A Keithly 247 supplies power to the MIDs and a Keithly 642 Electrometer monitors and displays detector current. Stock helium is used to purge the VICI 8 port valve used for sample introduction. GC carrier gas is Research Grade (99.9999%) helium passed through a VICI gas purifier. The IMS is a PCP Model 111, Dry Helium IMS[6] using a drift gas flow of 100ml/min and operating at 100°C. IMS drift gas is Research Grade helium (99.9999%) passed through a Mol. Sieve trap (cooled by a NessLab Cryocool CC-100II to -84° C) for further removal of water. Sample introduction to the IMS is via the GC column and MID. Data from the GC are interfaced through a Nelson Analytical Series 900 to PC Work Stations. PE Nelson Mod. 2600 Multiple Inst. Chromatography Software and Graseby Analytical Ltd. System V200 are used for the GC and IMS data, respectively.
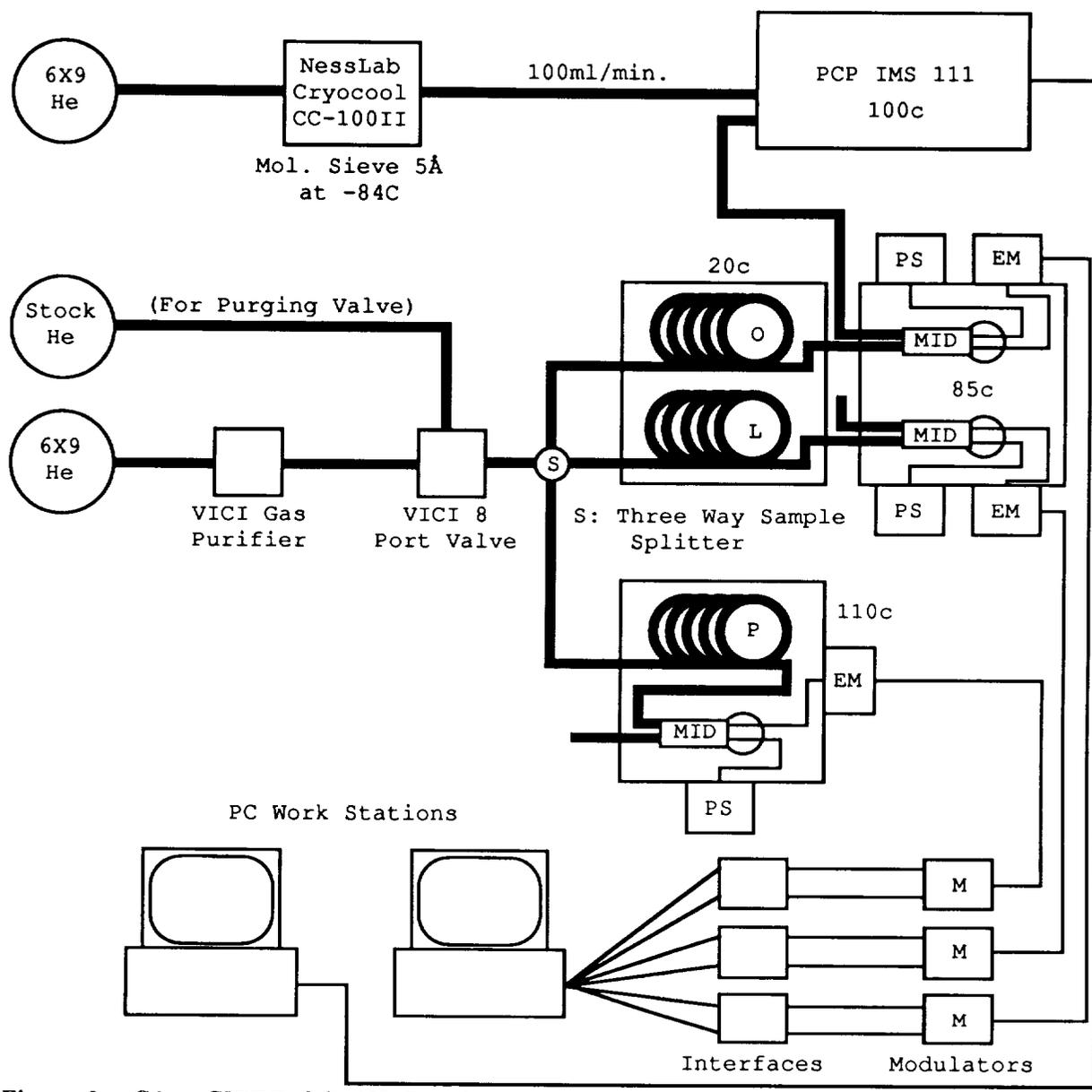
Figure 2. C4 m-CIDEX GC-IMS Breadboard.

61

L (Light Gas)

Hayesep A, 100/120 mesh,

7.3m(L) x 1.08mm(ID), 304 SS

Carrier Gas Flow Rate: 12.5ml/min.

Column Temperature: Room.

Detector Temperature: 85C.

Applied Voltage: -320V.

O (Organic)

P-tolylisocyanate Porasil C, 100/200 mesh,

1.15m(L) x 1.08mm(ID), 304 SS Column.

Carrier Gas Flow Rate: 11.6ml/min.

Column Temperature: Room.

Detector Temperature: 85C.

Applied Voltage: -275V

P (Polar)

Hayesep P, 140/170 mesh,

2.13m(L) x 1.08mm(ID), Nickel column.

Carrier Gas Flow Rate: 12.4ml/min.

Column Temperature: 110C.

Detector Temperature: 110C.

Applied Voltage: -300V

Figure 3. GC operating parameters.

Samples are prepared in 1 to 3 liter stainless steel gas cylinders by simple dilution using Research Grade helium. An Exponential Dilution Flask sample dilution system will be used for wide range calibration studies. A 250µl sample loop is loaded and then flushed with carrier gas to introduce sample to the GC. The carrier gas, with sample, is then split into three streams, one for each column.

RESULTS AND DISCUSSION

The maturity of the C4 analytical instruments is very high, largely due to extensive research and development in preparation for the CRAF Mission. For the m-CIDEX in particular, there is no further significant instrument development planned. Various versions of GC columns are now being tailored for this specific mission. The columns now being used are all of the packed variety, but other types of columns, such as *in situ* polymerized PLOT columns[7] are being considered. Although the IMS was not a part of the CRAF development efforts, it was developed through NASA's Small Business Innovative Research Program to analyze extraterrestrial volatiles from a gas chromatograph for planetary missions[8], and was an analytical component on the Titan Aerosol and Gas Experiment (TAGEX) proposed for the Cassini Mission to Saturn and its moon Titan.

Current research efforts on the m-CIDEX GC-IMS are focused on the various combinations of molecular species that must be analyzed during C4's encounter with the comet. The GC-dry helium IMS has been successfully used to detect and provide spectra of samples in each of the target groups: Hydrocarbons, Nitriles, Inorganics, Alcohols and Amines. The first mixtures to be separated and analyzed on the m-CIDEX GC-IMS were hydrocarbons. Figures 4 and 5 show the IMS spectra of Butane and Ethylene during an analysis of 10 hydrocarbons by the m-CIDEX GC-IMS. The response of the IMS in these cases is typical for dry helium IMS response to simple hydrocarbons. A full chromatogram, showing the MID response, of this analysis is shown in figure 6

surrounded by the IMS spectra of all the components. In this case the column performed well and made the jobs of the MID and IMS easy. However, future analyses will combine sample species from more than one group, complicating the analysis and making complete gas chromatographic resolution of every component unlikely.

As the flight column(s) are selected, further tests of the GC-IMS on various, more complex, mixtures will done. Addition of the sample collection system and pyrolysis ovens will then enable a full simulation of C4 m-CIDEX GC-IMS analyses to be performed.

REFERENCES

1. Carle, G. C., O'Hara, B. J. and Clark, B. C. Publ. Astron. Soc. Pac. 1985, **97**, 895-896.

2. Alexander, W. M., Tanner, W. G., McDonnell, J. A. M., Clark, W. C., Green, E., Goertz, C.K., Burton, W. M., Schaub, G.E. and Farmer, B.J., (19-91) A Cometary Dust Environment Monitor : CoDEM D1 Principal Investigator Experiment Implementation Plan for Comet Rendezvous and Asteroid Flyby Mission : CRAF, Confirmation Design Review at the Jet Propulsion Laboratory.

3. Clark, B. C. and Clair, D. W. Collection and Analysis of Cometary Dust from a Rendezvous Mission. Acta Astromica, Vol. 7, 531-541, 1980.

4. Carle, G. C., Kojiro, D. R. and Humphry, D. E. Modulated Voltage Metastable Ionization Detector. United States Patent Number: 4,538,066 August 27, 1985.

5. Woeller, F. H., Kojiro, D. R. and Carle, G. C. A Reliable Miniature Triaxial Metastable Ionization Detector for GC Trace Analysis of Extraterrestrial Volatiles. Anal. Chem. **56**, 860-862 (1984).

6. Kojiro, D. R., Cohen, M. J., Stimac, R. M., Wernlund, R. F., Humphry, D. E. and Takeuchi, N. Determination of C1 - C2 Alkanes by Ion Mobility Spectrometry. Anal. Chem. **63**, 2295-2300, (1991).

7. Shen, T.C. In-situ Polymerization PLOT Columns I: Divinylbenzene. J. Chrom. Sci. **30**, 239-240, (1992).

8. Cohen, M. J., Stimac, R. M. and Wernlund, R. F. Ion Mobility Sensing of Extraterrestrial Volatiles From a Gas Chromatograph. SBIR Phase II Final Report. Contract No. NAS2-13276, March 1993.
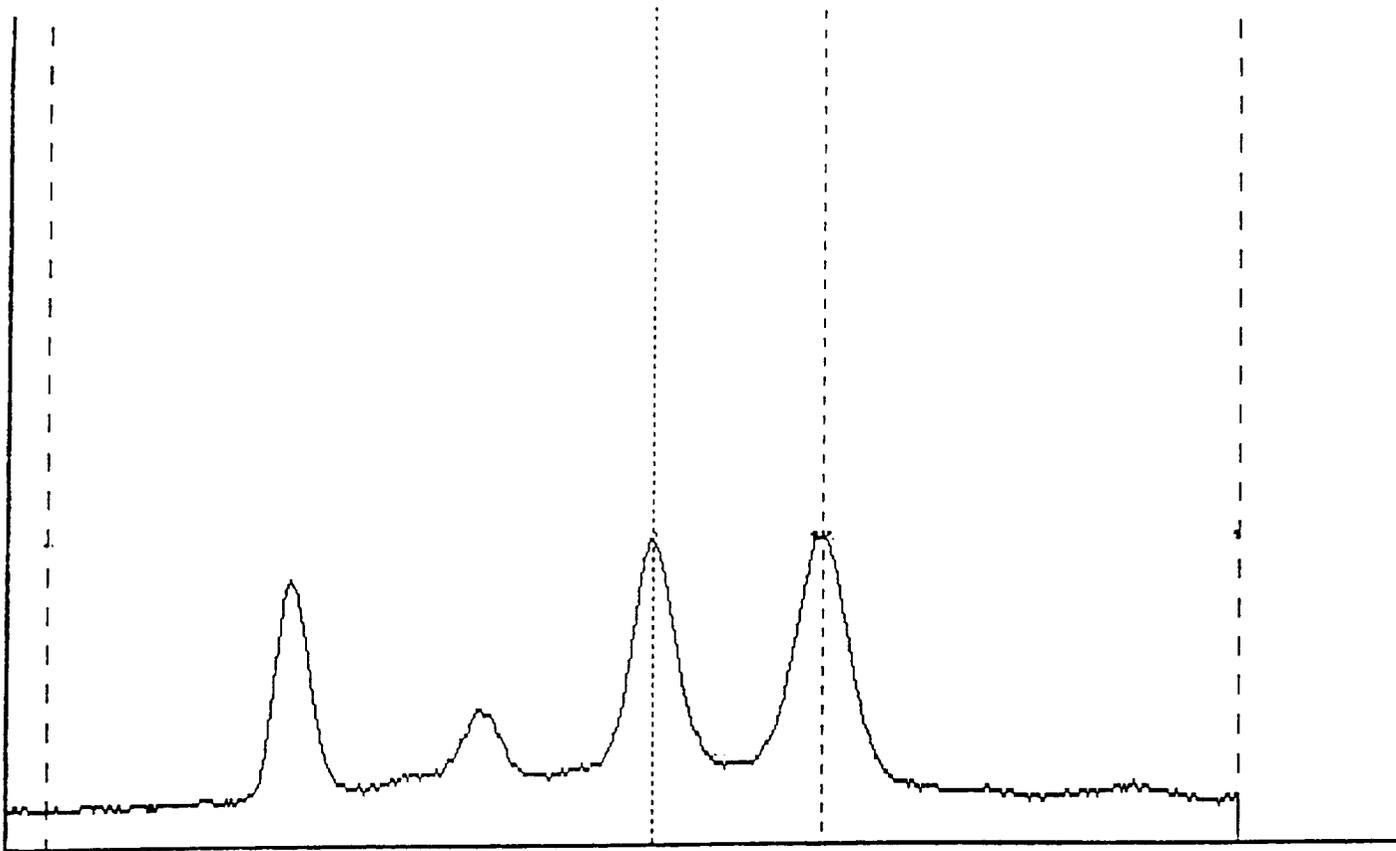
Figure 4. Butane IMS spectrum taken from ten hydrocarbon mixture.
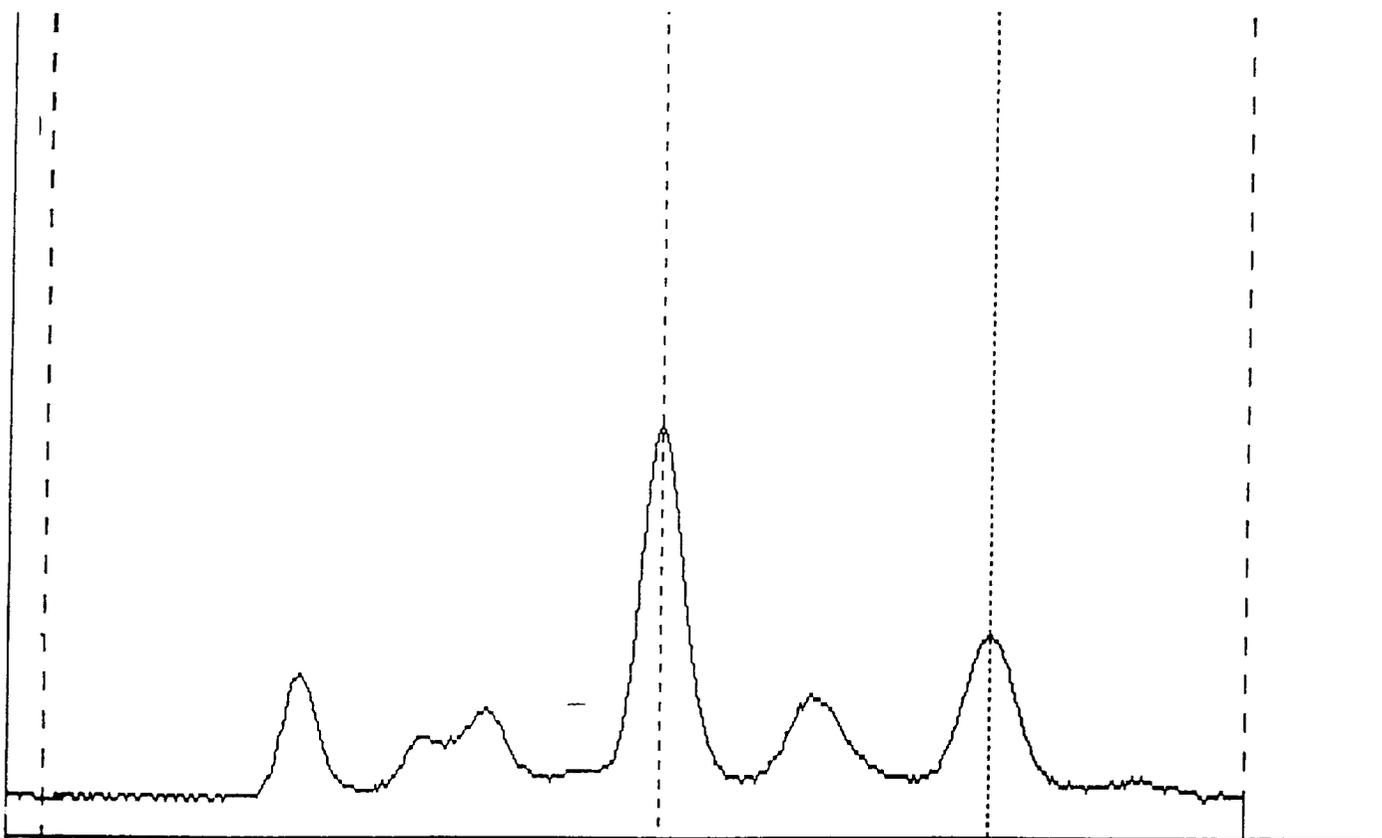
Figure 5. Ethylene IMS spectrum taken from ten hydrocarbon mixture.

4 Propane   5-Acetylene   6-Isobutane   7-N-Butane

3-Ethylene   8-Propylene

2-Ethane   9-Propadiene

1-Methane   10-Methylacetylene

MID Chromatogram of Hydrocarbon Mixture
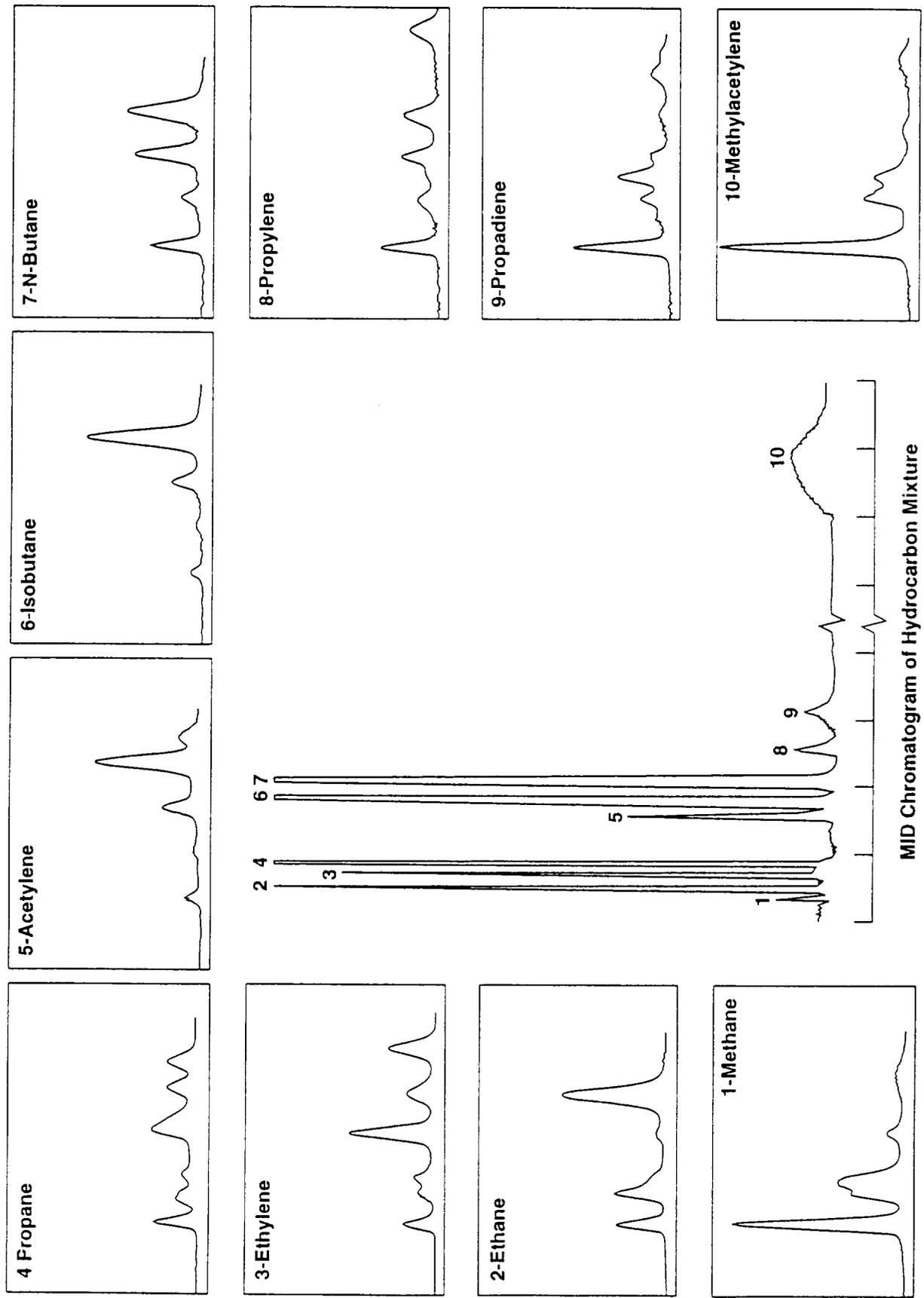
Figure 6. M-CIDEX GC-IMS analysis of ten hydrocarbon mixture.

65

ENGINEERING APPROACHES AND COMPROMISES IN THE DESIGN OF SMALL ION MOBILITY SPECTROMETERS.

R.F.D.Bradshaw, Bulstrode Technology, 17 Avebury Court, Mark Road, HEMEL HEMPSTEAD , HP2 7TA UK

ABSTRACT

The engineering approaches in the design phase of small portable I.M.S.-based instruments are discussed. The choices available are described, and their effect on instrument dimensions analysed. Possible future developments are outlined.

INTRODUCTION

The motive for miniaturisation of IMS devices is primarily to address the perceived market for small, portable detection devices, and secondarily to take advantage of the fact that smaller devices tend in general to cost less and to be more robust.

TARGET DIMENSIONS

There is little point in miniaturisation for its own sake. There comes a point beyond which further size reduction is counter-productive. The target has to be a device of which the user will not be constantly aware if he has it about his person, which has sufficient surface area to carry the necessary user interfaces, and which can be held comfortably in the hand.

The first target, comfort in carrying, is met by pocketbooks and diaries. These can be relatively large in two dimensions as long as they are thin and flexible. Complex user interfaces are used on Calculators and Mobile Phones, which tend to have their plan area defined by these interfaces.

The need to hold an instrument comfortably in the hand requires that its girth does not much exceed nine inches; however a three inch diameter cylinder would be unacceptable. It becomes clear that, within the girth restriction, plan area is not of prime importance; the critical dimension is thickness. Length should not exceed the depth of a pocket. All these considerations taken together lead to the conclusion that an instrument having a rectangular plan form of about seven inches by two point five inches would be acceptable; the thickness should be no more than one inch, and preferably much less.

CRITICAL COMPONENTS

In any device there is likely to be one component that will set a minimum value on the critical outside dimension. In an IMS-based device a natural assumption is that this critical component is the Drift Cell. This assumption should not go unquestioned; the other candidate is the Battery. System studies must be done to check that adequate battery life is available considering the mode of operation of the instrument and the volume available.

Cell Dimensions

Assuming the cell to be the critical component, it is clear that typical cell lengths can easily be accommodated within the plan areas being considered. The drift length of a CAM cell is just over an inch.

More difficult is the cell diameter. This may be the primary constraint on thickness reduction. The Graseby Ionics 'Mini' embodies a standard CAM electrode structure; its thickness represents the best that can be achieved without cell re-design.

Cell diameter, or rather thickness if non-circular geometries are considered, is governed primarily by the aperture of the central drift region. Reduction of this aperture results, with a given maximum ion concentration, in reduction of the collected current and consequent degradation in signal-to-noise ratio. With a circular cross-section this degradation goes as the square of diameter. Some reduction of the outside diameter, which is what matters, can be achieved by careful electrode design.

Increase of Ion concentration, even if allowed by the nature of the ionisation source, is of limited use, as space-charge effects begin to give trouble at charge densities much above those currently employed. The problem is not so much one of lateral expansion of the ion pulse, leading to a requirement of increased drift region diameter, as of axial expansion, leading to loss of resolution in the output spectrum.

There is thus a rather fundamental limitation placed by minimum drift-space cross-section. Some relief might be found in high-aspect-ratio rectangular cross-sections, but these bring problems in ionisation source design.

A typical thickness contribution for a circular cross-section may be 0.4 inches. By itself, this would allow a satisfactorily thin device. However, to this figure must be added allowances for the field-defining electrode structure, clearances for electrical insulation, and the space required for the gas-tight containment of the cell. Depending on the design choices made, there may also need to be room for lead-throughs and resistor chains.

OTHER COMPONENTS

Having established a feasible cell thickness (which may in fact be increased somewhat if that allows the adoption of a low-cost assembly method - a trade-off of cost against size) other components of the system can be considered. These will fall into three classes: ancillaries of the cell, electronic components, and batteries.

Cell Ancillaries

Cell ancillaries will include Drying agent and its containment, pumps (if used), sample inlet means and dopant sources. In most cases these will be specifically designed for the equipment and the need to be no higher than the cell will be a primary design requirement.

Electronics

Electronic components similarly will be chosen with thickness in mind.

Two points need to be made here. The first is that in concentrating on thickness, plan area must not be forgotten; the second is that due note should always be taken of the *next* highest component, which may be an electronic component, when considering schemes for reduction in the height of the cell.

Batteries.

A miniature instrument will not have much room for batteries. Since an IMS cell operates in principle on nanoamperes of current, the cell power used is almost all wasted and will be substantially independent of cell size. The principle of demand sampling, exemplified by the Graseby Ionics Mini and made possible by the use of passive pumping, allows substantial scope for power economy in that the instrument is only turned on when a sample is to be taken. Also, due to the sequential nature of operation, savings can be effected by careful scheduling of supplies to power-hungry areas.

Demand sampling allows good battery life with battery volume comparable to that of the cell module. The effect of other types of operation on power demand should be considered

very carefully. System studies may show that battery size and weight may become dominant, negating the value of miniaturisation in other areas, unless very stringent power-management techniques are adopted.

CASE AND USER INTERFACE

Having generated a design and layout of suitably small dimensions, two other related matters remain; the outer case, and the operator interface.

Case

Sophisticated designs in other fields tend to combine the case and the main structure, often in the form of elaborate plastic mouldings. In the current stage of IMS-based instrument development it is more likely that a scheme in which self-supporting internals are housed within a separate hard protective case will be chosen, the advantage being low tooling cost and easier and more flexible design. It is galling to find that this latter approach, if plastics are used. can add 0.25" to the thickness of an instrument.

A major consideration in case design is accommodating the User Interface. In terms of input this may be simple, being one or two push-buttons; the output is likely to be the ubiquitous LCD Display. This in itself requires little more than a viewing aperture in the case, but space conflicts can arise when considering its location. In an instrument in which the sampling probe is at one end, the natural position for both cell and display is close to that end. If the display is located on a major face of the instrument it will add its thickness, which may be a quarter of an inch, to that of the cell, causing a corresponding local increase in instrument thickness.

Sample Interface

The sample interface itself should not present a space problem, except in that if a pump or flow inducer is required it can have a secondary effect on battery volume, depending on its mode of use, continuous or intermittent.

Any requirement for continuous heating is bound to have a serious effect on battery volume.

THE DESIGN PROCESS

The smaller the target envelope, the more complex the design process. It becomes increasingly difficult to segregate the design into independent areas to be worked on by specialists; design must proceed in an iterative manner, with the effect of each choice on all other areas being considered. It calls for strong overall project management with detail involvement.

System engineering nevertheless remains vital; the operating regime of the detector will determine the battery size/battery life trade-off.

EXAMPLES

Three examples of miniaturisation are shown (*Fig.1*). The CAM instrument was in fact a remarkable achievement for its day and set a standard for emulation. The Graseby Ionics 'Mini' is an interim design, using standard CAM cell components, and is being used to explore the concepts of passive pumping and demand sampling. Its design evades the issues of display location. The current Bulstrode Mini is a more integrated design in which a revised cell structure allows a character display to be used, but in which concessions have been made for ease of manufacture and lower cost.

FUTURE DEVELOPMENTS

The experience gained in these designs allows reasonable estimates to be made of achievable sizes of future products. An informed guess would be that an overall thickness of about 0.7" should be attainable. Whether or not the necessary investment in development and tooling will be justified will become apparent from the market reaction to the present generation of instruments.

Fig. 1

CAM™

Cell
Battery
Display

Inches

Bulstrode Mini

GI-Mini™

© Bulstrode Technology 1994
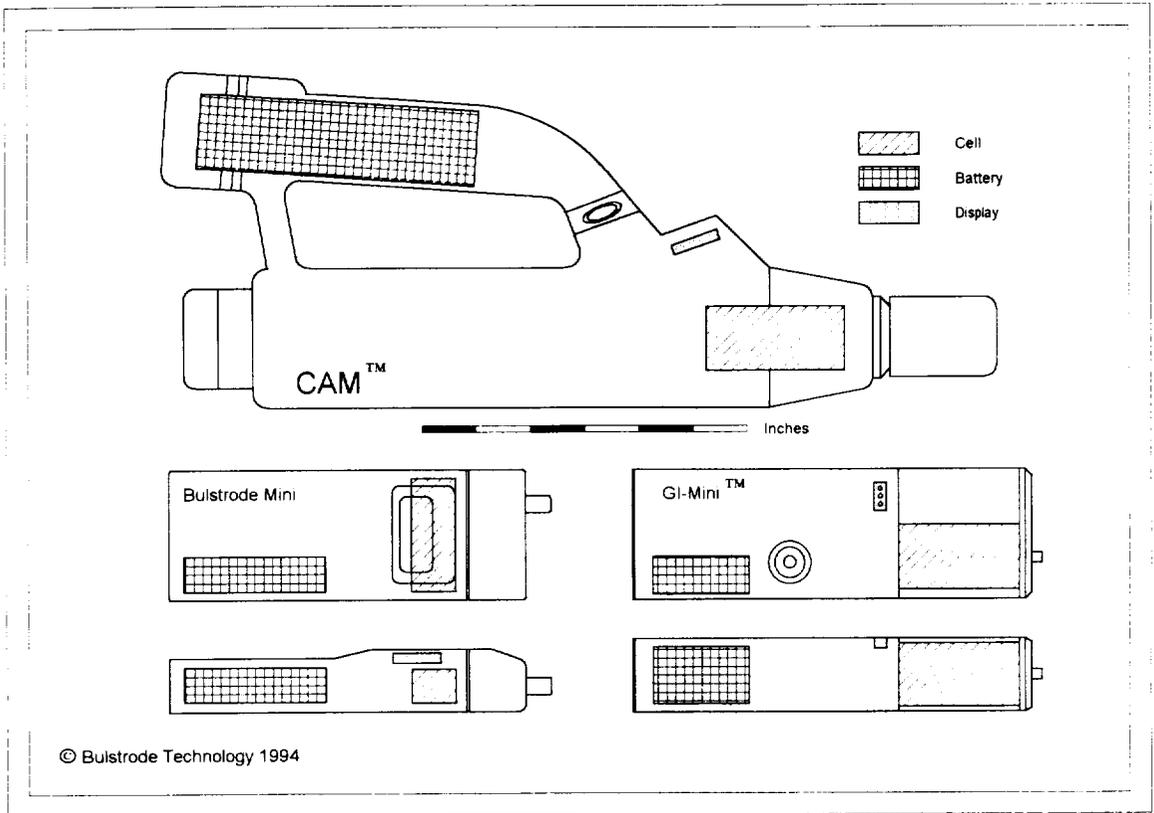
APPLICATION OF ^{63}Ni, PHOTO- AND CORONA DISCHARGE IONIZATION FOR THE ANALYSIS OF CHEMICAL WARFARE AGENTS AND TOXIC WASTES

J. Stach, J. Adler, M. Brodacki and H.-R. Döring

BRUKER-Saxonia Analytik GmbH, Permoserstr. 15, 04318 Leipzig, F.R.G.

1. INTRODUCTION

Over the past decade, advances in instrumental design and refinements in the understanding of ion molecule reactions at atmospheric pressure enabled the application of Ion Mobility Spectrometry (IMS) as a simple inexpensive and sensitive analytical method for the detection of organic trace compounds [1-6]. Positive and negative gas-phase ions for ion mobility spectrometry have been produced by a variety of methods, including photo-ionization [7], laser multiphoton ionization [8], surface ionization [9], corona discharge ionization [10]. The most common ion source used in ion mobility spectrometry is a radioactive ^{63}Ni foil which is favoured due to simplicity, stability, convenience, and high selectivity. If reactant ions like $[(H_2O)_nH]^+$ or $[(H_2O)_nO_2]^-$ dominate in the reaction region, nearly all kinds of compounds with a given proton or electron affinity are ionized. However, the radioactivity of the ^{63}Ni foil is one disadvantage of this ion source that stimulates the development and application of other ionization techniques.

In this paper, we report analyses of old chemical warfare agents and toxic wastes using Bruker RAID ion mobility spectrometers. Due to the modular construction of the measuring cell, the spectrometers can be equipped with different ion sources. The combined use of ^{63}Ni, photo- and corona discharge ionization allows the identification of different classes of chemical compounds and yields in most cases comparable results.

2. EXPERIMENTAL

Spectra were recorded with BRUKER RAID ion mobility spectrometers equipped with ^{63}Ni, photo- and corona discharge ion sources. A scheme of the RAID-1 is shown in Fig. 1. Further details were given elsewhere [11,12].

Most of the samples were investigated with field and laboratory methods. Whereas in field analyses air above soil samples (from surface or drill holes) and contaminated parts of production buildings were measured, the head space technique was used in the lab.

GAS AND CURRENT FLOW DIAGRAM

1. Ni^{63} - beta source **12.** membrane inlet
2. reaction region   **13.** gas flow sensor
3. shutter grid   **14.** pump
4. drift region   **15.** filter
5. screen grid   **16.** filter
6. collector   **17.** magnetic valve
7. amplifier   **18.** pump
8. microcontroller   **19.** gas flow sensor
9. display LCD   **E** sample gas inlet
10. shutter grid driver **A** sample gas outlet
11. high voltage source **S** backflush gas inlet
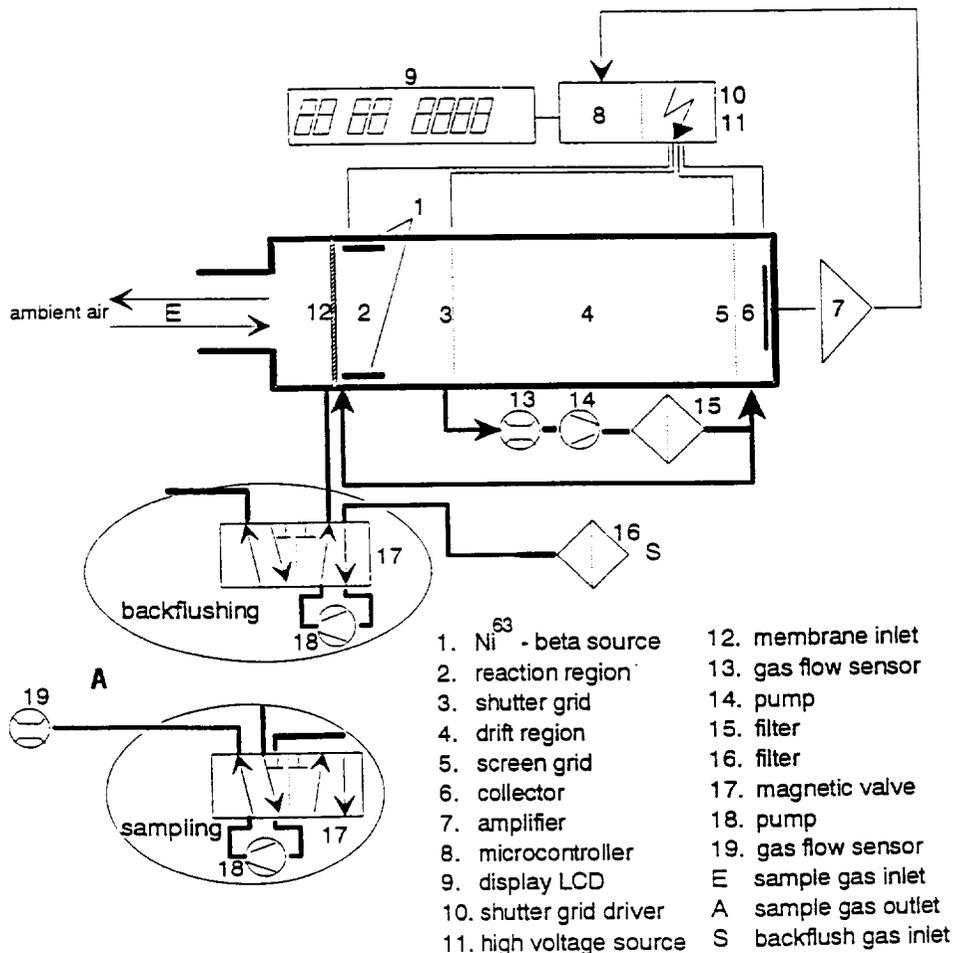
Fig.1: Gas and current flow diagram of the BRUKER RAID-1 IMS instrument

Head space analyses were carried out using 50 g of contaminated soil or 0.5 ml of liquids in glass flasks which were connected with the IMS by means of a Teflon tube. The samples were heated during 5 minutes from room temperature to 80°C. During the hole time, every 10 seconds, ion mobility spectra were recorded.

Results of the IMS investigations were confirmed by means of head space GC/MS (HP-5972) measurements using the following conditions: GC - column - DB-5, 30 m; carrier gas - helium; temperature program - 60°/2min. - 6°/min. - 280°C; injector temperature - 280°C; source temperature - 200°C; mass range - 40-400 amu; scan time - 1 sec.

1	Chlorobenzene	62.4 %
2	Phenol	6.6 %
3	Dichlorobenzene	1.0 %
4	Sulfur mustard	0.2 %
5	Dichlorobiphenyl	23.8 %
6	Clark I	2.8 %
7	Triphenylarsine	0.5 %
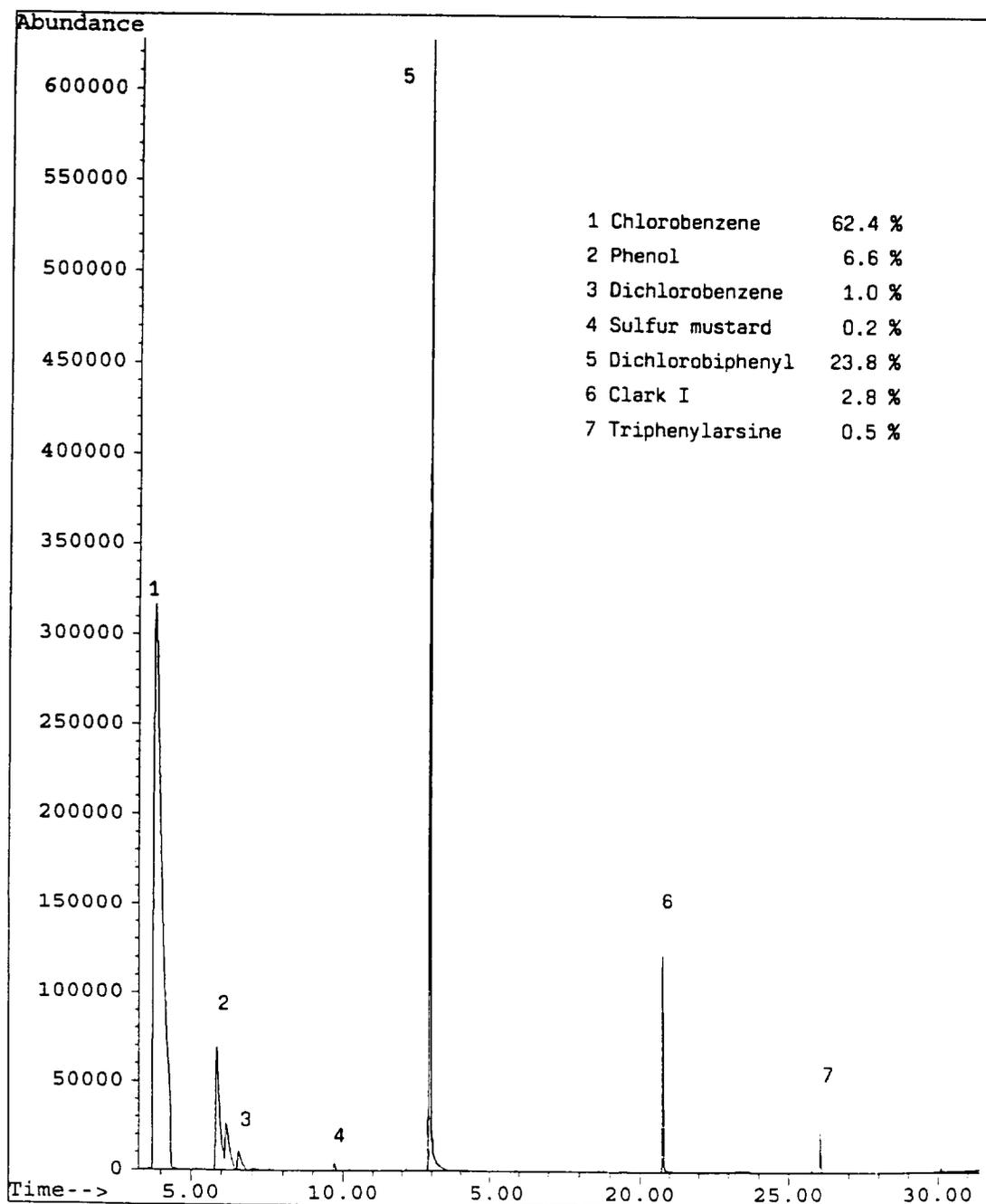
Fig. 2: Total ion chromatogram of the "Arsinöl" obtained by head space measurements

73

3. RESULTS

Usually old chemical warfare agents or residues resulting from production processes of warfare agents consist of a mixture of hazardous compounds. A typical example is that of sulfur or oxygen mustard which was used in mixtures with the German "Arsinöl" and other additives. The "Arsinöl" itself consists of 50 % phenyldichloroarsine, 35 % diphenylchloroarsine, 5 % triphenylarsine and 5 % trichloroarsine. Fig. 2 shows a total ion chromatogram obtained by head space GC/MS of a sample found on a production site for chemical warfare agents from the second world war. Maine components of this sample are chlorobenzene, dichlorobenzene, phenol, chlorobiphenyl, chlorodiphenylarsine and triphenylarsine. Sulfur mustard is present in traces. The gas phase composition of the sample is given in the Fig 2.

The head space GC/MS investigations confirm the results of ion mobility spectrometry obtained with ^{63}Ni ß-ionization in the negative ion mode. The corresponding spectrum (Fig. 3) shows typical signals with reduced ion mobilities $K_0 = 1.89$, 1.51, 1.31 and 1.17 cm^2/Vs. As indicated in Fig 3, these signals are mainly caused by chlorodiphenylarsine (Clark I) and triphenylarsine. Sulfur mustard could not be identified because its concentration (0.2 %) in presence of the arsenic containing compounds is too small.

^{63}Ni - ß-IMS   ION MOBILITY SPECTRA OF NEGATIVE IONS
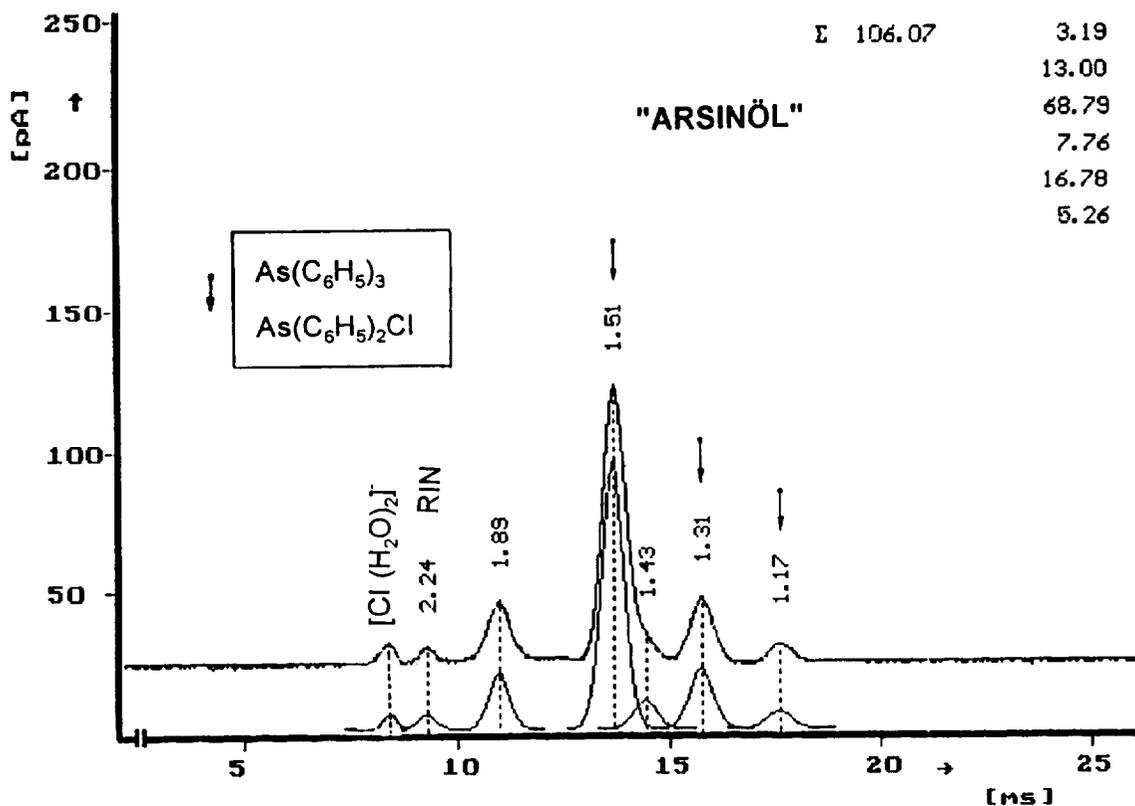
Fig. 3: Ion mobility spectrum (negative ions) of the "Arsinöl" obtained with ^{63}Ni ß-ionization

74

The ion mobility spectrum recorded in the positive ion mode using a ^{63}Ni ß-ion source shows a very complicated structure. However, using the information obtained from the negative ion mobility spectrum and the results of the GC/MS investigations, some peaks can be assigned to the arsenic containing compounds, chlorobenzene and the dichlorobiphenyl. The spectrum is shown in Fig. 4.

^{63}Ni - ß-IMS ION MOBILITY SPECTRA OF POSITIVE IONS
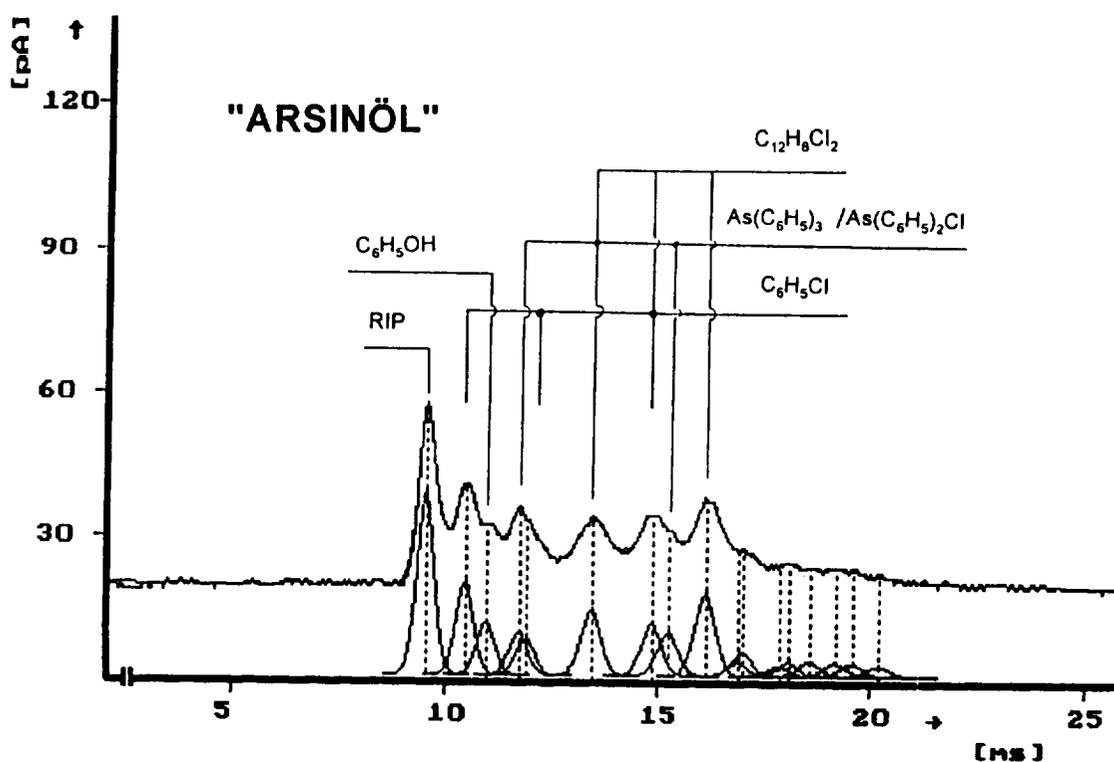
Fig. 4: Ion mobility spectrum (positive ions) of the "Arsinöl" recorded with a ^{63}Ni ion source

The GC/MS and IMS investigations suggest that this sample should be well suited for the application of photo-ionization because all components of the mixture are aromatic compounds. However, ion mobility spectra of the sample obtained in the positive ion mode by means of photo-ionization show very small signals. The intensity can be increased using a reagent gas[13]. The improvement in intensity is shown by means of a series of ion mobility spectra given in Fig. 5. Beside the signal caused by the reagent gas, peaks in the ion mobility spectra can be assigned to chlorobenzene, dichlorobiphenyl and the arsenic containing compounds.

UV-IMS ION MOBILITY SPECTRA OF POSITIVE IONS

"ARSINÖL"

ADDITION OF REAGENT GAS

Kr-Lampe

SAMPLING

ADDITION OF
REAGENT GAS
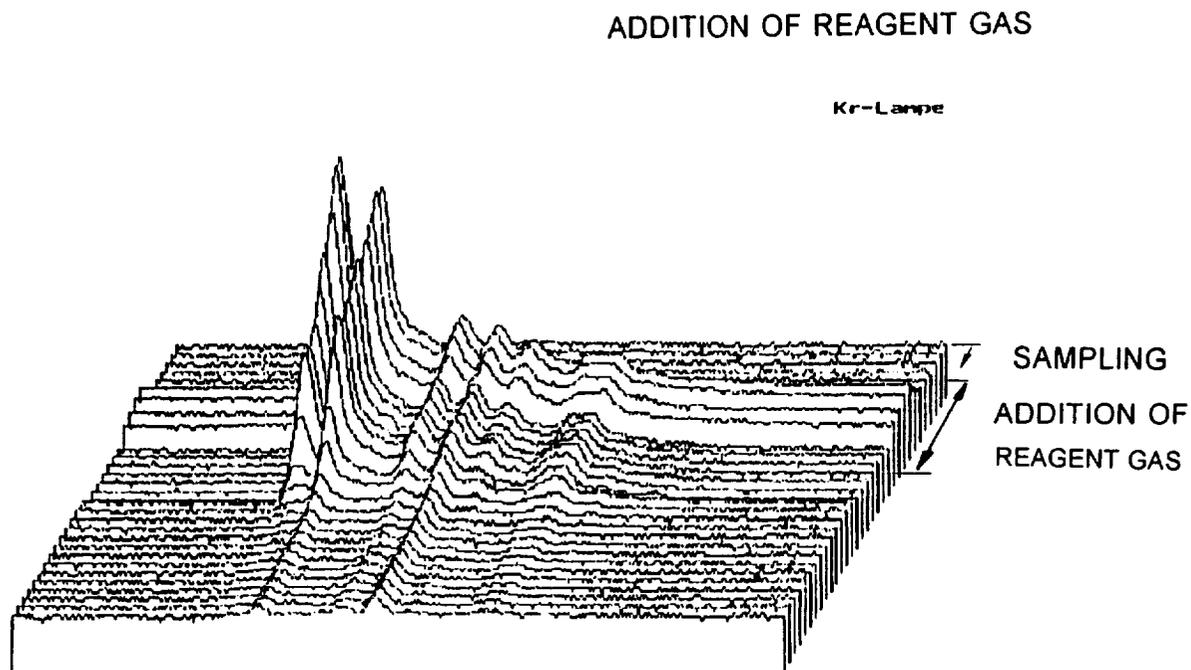
Fig. 5: Series of ion mobility spectra (positive ions) obtained by photo-ionisation and addition
of reagent gas

Ion mobility spectra of negative ions recorded on spectrometers equipped with a photo-ionization source show reactant ions like CO_3^-, CO_4^- or $(H_2O)_2O_2^-$ as known from ^{63}Ni ion sources. It is therefore not surprising that the spectra obtained for the "Arsinöl" are similar to those obtained by ^{63}Ni ß-ionization. The spectrum is shown in Fig. 6. Peaks due to arsenic containing compounds are marked with arrows.

The corona discharge ion source which is still in process of development is considered as a substitute for the ^{63}Ni ion source. However, the formation of reactant and product ions depends on the applied field strength and geometrical arrangements of the electrodes. If both parameters are optimized, spectra as known from instruments with ^{63}Ni ion sources can be obtained. Fig. 7 shows a spectrum of positive ions recorded for the "Arsinöl". The shape of the measured spectrum comes close to that obtained with a ^{63}Ni ion source. The same is true for spectra recorded in the negative ion mode. However, in this case a pulsed corona discharge ion source has to be applied.

76

UV-IMS   ION MOBILITY SPECTRA OF NEGATIVE IONS
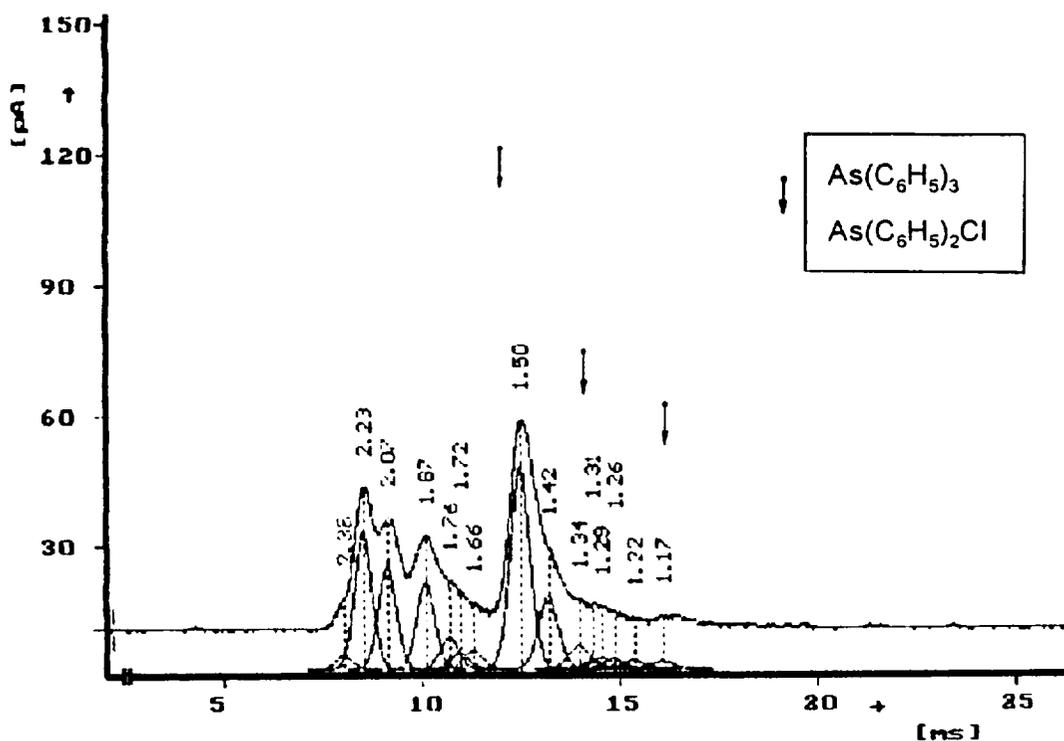
Fig. 6: Photo-ionization spectrum of negative ions of the "Arsinöl"
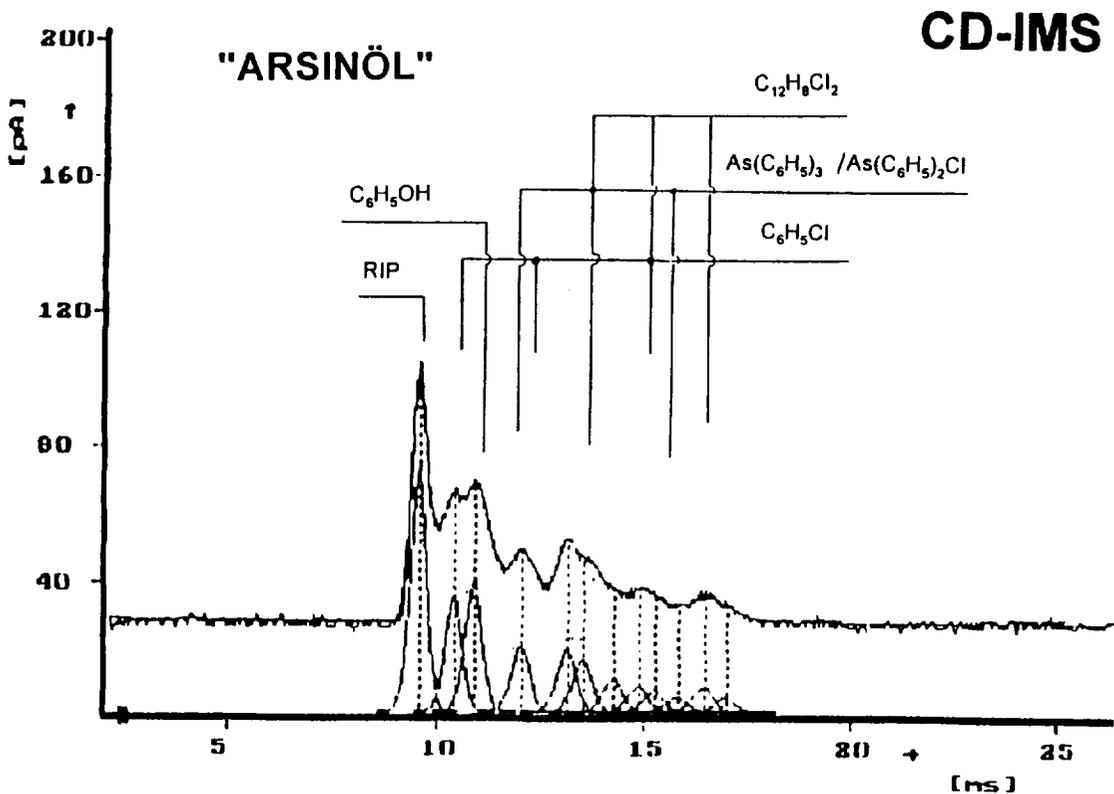
Fig.7: Corona discharge ion mobility spectrum (positive ions) of the "Arsinöl"

4. DISCUSSION

A comparison of the results obtained with three ionization techniques shows that the investigated sample can be characterized in each case. As shown by the above described measurements, also in the case of old chemical warfare agents, which contain many additives or degradation products, the main components can be identified easily. However, up to now the ^{63}Ni ion source gives the best results for the detection of chemical warfare agents. The ionization processes are well known and the detection limits for compounds with given proton or electron affinity reach the lower ppb level. A disadvantage is the small linear range. From a practical point of view the high stability and life time of the ion source and the low power consumption of the instruments should be mentioned.

If photo-ionization is applied, reactant gases have to be used to get comparable results. Because of the formation of additional adduct ions, the spectra are not well resolved sometimes. Thedetection limits are found in the higher ppb or ppm level.

The sensitivity of the corona discharge ionization is comparable or better than that obtained with ^{63}Ni ion sources. The long time stability and the power consumption of the ion sources prevent a broad application in on-site analyses up to now.

4. LITERATURE

[1]   Morrisey, M.A. and Widmer H., Chimia 43 (1989) 268.

[2]   Hill, H.H., Jr., Siems W.F. and Luis, R.H.St., Anal. Chem.62 (1990) 1201A.

[3]   Luis, R.H.St. and Hill, H.H., Jr., Crit. Rev. Anal. Chem. 21 (1990) 321.

[4]   Eiceman G.A., Crit. Rev. Anal. Chem. 22 (1991) 471.

[5]   Roehl J.E., Appl. Sectr. Rev. 26 (1991) 1.

[6]   Eiceman, G.A. and Karpas, Z., Ion Mobility Spectrometry, CRC Press, Boca Raton FL, 1994.

[7]   Baim, M.A., Eatherton, R.L. and Hill, H.H.,Jr., Anal. Chem. 55 (1983)1761.

[8]   Lubman, D.M. and Kronick, M.N., Anal. Chem. 54 (1982) 1546.

[9]   U.S. Patent 581398, August 3, 1984.

[10]   Shumate, C. and Hill, H.H., Jr.,Anal. Chem. 61 (1989) 601.

[11]   Starrock, V., Krippendorf, A. and Döring, H.-R., Second International Workshop on Ion Mobility Spectrometry, Quebec City, Canada, 15.-18.8.1993.

[12]   Döring, H.-R., Adler, J., Stach, J., Krippendorf, A., Int. Workshop on Doctrine and Instruments for Detection and Monitoring of Chemical Warfare Agents, Riksgränsen, Sweden, 8-10 November 1993.

[13]   U.S. Patent, WO 93/22033, November 11, 1993

IMS R&D PROGRAM AT CANADA CUSTOMS.

Pierre Pilon, Tony Mungham, Lay-Keow Ng, André Lawrence.

Revenue Canada, Customs Excise and Taxation,
Laboratory and Scientific Services Directorate,
Research and Development Division,
79 Bentley Avenue, Ottawa, Ontario, Canada, K1A 0L5

ABSTRACT

Over the last few years, Revenue Canada, in collaboration with Barringer Instruments Limited, has been involved in the development of a field-usable ion mobility spectrometer (IMS) for the detection of drugs of abuse. This work has culminated in the manufacturing and commercialization by Barringer of the Ionscan 350 instruments, now in use by various law enforcement agencies worldwide.

Although IMS exhibits a very strong and distinctive response toward some nitrogen containing drugs, e.g., cocaine, like all separation techniques it has inherent limitations, namely moderate resolution and low chemical signal to noise ratio which may affect the reliability of IMS-based drug detectors. A programme is in place at the Laboratory and Scientific Services Directorate (LSSD) to investigate the applicability of various digital signal processing (DSP) techniques to IMS output signals. The application of neural network techniques to overlapping IMS peaks is presented.

INTRODUCTION

The Research and Development Division of the Laboratory and Scientific Services Directorate (LSSD) of Revenue Canada, Customs, Excise and Taxation, has a mandate to perform the following tasks:

- identify and develop technology and instrumentation for the detection of drugs to be used by Customs officers at points of entry into Canada; and

- develop new methods for the Customs Laboratory and the Excise Laboratory.

The work described in this paper gives a brief review of the work performed at LSSD on the development of a drug detection system based on IMS, outlines possible applications of IMS for the Customs or Excise Laboratories, describes modifications performed on the drug detector for other applications and gives details on digital signal processing which may be useful in all applications of ion mobility spectrometry.

Drug Detection

Between 1983 and 1991, LSSD was involved in the development and testing of the IONSCAN series of instruments for the detection of cocaine and heroin in Customs scenarios, in conjunction with Barringer Research Limited (BRL)[1-7]. In 1993 and 1994, Revenue Canada purchased four IONSCAN instruments from BRL, one used for on-going testing in the laboratory and three for field implementation. Two of the field instruments are presently in use at airports in Toronto and

Montreal; these have been instrumental in a number of drug seizures.

Customs, Excise Applications

The Customs Laboratory of Revenue Canada is responsible for the analysis of imported goods into Canada for tariff classification while the Excise Laboratory is involved in the analysis of alcohol and tobacco products for the determination of excise tax. The R&D Division has worked in conjunction with these laboratories to develop methods using ion mobility spectrometry. The samples chosen for analysis by IMS met at least one of the following requirements:

- the sample consists of an analyte of interest present in a well known matrix which is relatively inert to the IMS detector;

- the existing method of analysis for the sample involves a long preparation step; and

- no satisfactory analytical techniques are available at our laboratory.

Some preliminary work on a BRL Ionscan 250 instrument has indicated that IMS can be used for the determination of the presence of additives in polymers, and the presence of cocaine and/or heroin in drug seizures. In addition, IMS can be used to analyze bitrex in denatured alcohol.

RESULTS AND DISCUSSION

Modifications to Ionscan 250.

The Ionscan 250 has been developed for the sampling and analysis of solid samples collected in the field. The instrument uses pumped, purified room air for the drift and carrier gas. An exhaust pump evacuates the drift and carrier gas to avoid the creation of a vacuum or pressurization inside the drift tube. The software of the Ionscan 250 gives an indication of the presence of a substance of interest by monitoring a number of windows across the spectrum. In order to use the BRL Ionscan 250 instrument for laboratory applications, a number of modifications were required. These modifications were performed in conjunction with BRL.

The modified instrument uses zero air from a cylinder and does not require pumps for the drift or carrier gas. The exhaust pump from the Ionscan 250 is still used. Zero air is also used as a make-up gas.

For a more reproducible introduction of samples as solutions, the inlet of the Ionscan 250 was modified, as shown in Figure 1. When no sample tube is inserted into the inlet, a make-up gas is introduced into the IMS; the rate is adjusted so that 15 to 20 cm^3/min of gas come out of the inlet, thus not allowing unpurified room air to enter the drift tube. The sample is injected into the glass wool of a glass sample tube, and the tube is brought into the inlet of the instrument, close to the repeller grid of the drift tube to ensure good transfer of the sample to the reactant region. The carrier gas is set at 200 cm^3/min and is pumped out of the drift tube, along with the drift gas, set at 300 cm^3/min, by the exhaust pump. The make-up gas is flushed out of the front end of the inlet since no tight seal is made between the sample tube and the inlet. The BRL temperature controls were used for the new inlet.

A data acquisition system was developed to increase the flexibility of the instrument. The software has a variable acquisition rate (20 to 125 KHz), allows for a maximum of 512 data point

per scan, has a 30 msec gate firing, a 4 msec delay time for data processing, hand shaking and data transfer. It has the capability of storing individual raw scans and displaying 128 individual traces. 4 megabytes of memory are available for data storage. Figure 2 shows a partial display of 16 traces, chosen from the full display to investigate certain features in the spectrum. From the partial display, single traces can be plotted, where the drift time and amplitude information can be obtained.

Signal Processing

The output signal of the spectrometer is made up peaks embedded in noise, each peak indicating the presence of a specific component in a mixture. Previous analyses of experimental data[8] have shown the following:

-    the peak shapes of IMS signals are Gaussian; and

-    the noise is band limited, shows no clear repetitive pattern and is Gaussian.

From this information, an IMS signal simulator was developed to artificially generate IMS-like signals with any desired peak parameters (amplitude and standard deviation (σ)), peak separation and signal to noise ratio (SNR)[8]. The simulated signals were subsequently used to test the detection limits and the selectivity of peak detection algorithms. The detection limit of an algorithm is measured by determining how well a low signal can be detected in the presence of noise, without false detection. The selectivity is determined by the minimum peak separation that can be correctly detected by the algorithm. The resolution is a function of the peak separation, the standard deviation of the peak, the relative amplitude and the SNR. A number of packages have been tested previously[8,9]; the results obtained are summarized below. Finally, recent results obtained with neural networks are described.

Derivative Methods

This involves the differentiation of the IMS signal. Any slight variation in the slope of the original signal due to overlapping peaks can be detected using this technique. However, because of this capability to recognize slight variations, this method is susceptible to noise. It must therefore be preceded by precise filtering to remove out of band noise. The results obtained on simulated signals are the following:

-    in a high signal to noise environment, with a 1:1 signal ratio, a differentiation of peaks separated by 1.7 σ can be achieved using double differentiation;

-    with an amplitude ratio of 6:1, the minimum separation must be 2.2 σ;

-    single peaks can be detected at 18 dB SNR;

-    single peaks could be detected at lower SNR at the expense of selectivity; and

-    the detection of multiple peaks can be achieved at lower separation by using higher order differentiation (1.4 σ using 6th order differentiation, 1.25 σ using 10th order differentiation), at the expense of high false detection probabilities.

Cross-Correlation Method

This method involves cross-correlating two vectors of length n (an IMS signal and a Gaussian curve) for relative shifts of -n up to +n. When the two vectors are normalized, the cross-correlation function is a maximum when the two signals are identical and is zero when the two vectors are uncorrelated. This method is very efficient for the detection of single peaks in low SNR environments and may therefore improve the detection limit of an IMS system. The method has a negative impact on selectivity since it is a perfect filter, blocking all other noises, including irregularities due to the presence of other peaks.

Curve Fitting Methods

In this method, the signal is resolved into distinct bands which are fitted to an n-order polynomial using least squares. The polynomial coefficients are then used to estimate the parameters of the peak. In IMS, a quadratic equation can be used since the peaks are Gaussian. This kind of algorithm is very accurate at estimating the position of a peak.

Hopfield Neural Network

An IMS signal can be thought of in terms of the following equation:

$$r(t) = x(t) + z(t)$$

where $x(t)$ is the signal of interest, assumed to be made up of Gaussian pulses and $z(t)$ is a noise term. The Gaussian pulses can be represented by:

$$g(t;l,k,m) = a_l \exp \frac{-(t-c_k)^2}{2\sigma_m^2}$$

$\{a_l\}$ is a set of discrete amplitudes
$\{c_k\}$ is a set of discrete centers
$\{\sigma_m\}$ is a set of standard deviations

$x(t)$ can then be represented by

$$x(t) = \Sigma \Sigma \Sigma A_{lkm} \, g(t;l,k,m)$$

where A_{lkm} is 1 if $g(t;l,k,m)$ is present in the signal and A_{lkm} is 0 otherwise.

Our objective is to obtain the values of $\{A_{lkm}\}$ from the noisy signal. This is a set of cross-coupled equations for which it is hard to obtain analytical solutions. Thus, it was decided to use a neural network approach to find the solution iteratively.

This problem can be thought of as a multi-input multi-output process where the input is the N-dimensional recorded signal and the output is a binary vector. The system structure is very similar to a well known neural network structure called the Hopfield net. The network consists of a single layer of Q neurons. Each neuron adds up all its inputs and compares the sum to a threshold value. If the sum > threshold, the output of the neuron is 1, if the sum < threshold, the output is 0.

Each neuron output is fed back to the inputs of all neurons except its own. Feedback connections are called weights. The neuron also receives signals from an external source. The weights are determined by minimizing an artificial energy function which is a measure of how far the value of the output vector is from an acceptable solution. The setup of the Hopfield Network is shown in Figure 3.

In order to test the network's sensitivity to noise and its resolving power, simulation studies were performed using an input vector consisting of 1024 points, made up of Gaussian pulses with different amplitudes, centers and sigma, with different SNR. Signals collected on the modified Ionscan unit described above were also used as input into the network. The vector (simulated signal or actual IMS spectra) was fed into the neural network and compared to a set of 12 basis functions, Gaussian functions with varying distances between two consecutive functions and varying standard deviations (see Figure 4). The network calculates the error between the signal and the basis functions with different parameters and displays the best fit between the input and the basis functions.

The system's sensitivity to noise was tested by creating one Gaussian pulse using the signal simulator. The noise level of the signal was increased until the network failed to produce the correct output. The minimum SNR was found to be -3dB, as shown in Figure 5. At this level, the noise power is twice the signal power. Reducing SNR below this level resulted in multiple peaks, as shown in Figure 6 for a blank sample introduced into the modified Ionscan.

The network's resolving power was tested by analyzing two pulses which are synchronized to the positions of their basis Gaussian pulses counterparts. These pulses were delayed by one standard deviation. At equal amplitudes, two peaks were observed for a signal to noise ratio as low as 3 dB (Figure 7). The amplitude of one pulse was then reduced gradually until the network failed to produce the correct output. The limit of amplitude ratio was approximately 0.6 with a signal to noise ratio down to 10 dB. The time separation between two peaks was then reduced. A time resolution of 0.65 σ could be obtained, at a SNR of 30 dB, as shown in Figure 8. Tests on various combinations of delay and amplitude differences indicate that the limit is 0.65 σ at an amplitude ratio of 0.8. An example of the output of the Hopfield Network for the separation of cocaine and tetracaine, injected as a mixture in solution, is shown in Figure 9. These two substances have amplitude maxima separated by approximately 0.65 σ.

We are presently investigating the capabilities of the Hopfield Network in more details, along with the possibility of using a combination of algorithms to lower the detection limits, and to help in the peak location and peak resolution capabilities of ion mobility spectrometers.

ACKNOWLEDGMENT

REFERENCES

1. Barringer Research Limited. "A Feasibility Study for the Detection of Heroin and Cocaine Using Ion Mobility Spectrometry (IMS)." D.S.S. File No. 21ST.32032-4-0330M., June, 1985.

2. Barringer Research Limited. "Development of a Prototype Ion Mobility Spectrometer (IMS) Pre-prototype Narcotic Detector Using Air Sampling and Trace Particulate Analysis Techniques." December, 1986.

3. Barringer Research Limited. "Development of the IMS Prototype Narcotics Detector"., D.S.S. 25ST.32032-7-3271., August, 1988.

4. Barringer Research Limited. "Development of an Improved Portable Ion Mobility Spectrometer Narcotics Detector." D.S.S. 038ST.32032-9-N174EX00PT01., January, 1990.

5. Chauhan, M., Hamois, J., Kovar, J., Pilon, P., Trace Analysis of Cocaine and Heroin in Different Customs Scenarios Using a Custom-Built Ion Mobility Spectrometer. Can. Soc. Forens. Sci. J., **24**, No. 1, 43-49 (1991).

6. Hamois, J., Kovar, J., Pilon, P., Detection of Cocaine and Heroin Using a Custom-Built Ion Mobility Spectrometer, Customs Laboratory Bulletin, **4**, No. 1, 11-31 (1992).

7. Fytche, L.M., Hupé, M., Kovar, J.B., Pilon, P., Ion Mobility Spectrometry of Drugs of Abuse in Customs Scenarios: Concentration and Temperature Study., Journal of Forensic Sciences, **37**, No. 6, 1550-1566 (1992).

8. Goubran, R.A., Lawrence, A.H., Experimental Signal Analysis in Ion Mobility Spectrometry., International Journal of Mass Spectrometry and Ion Processes, **104**, 163-178 (1991).

9. Goubran, R.A., Peak Detection of IMS Signals, NRC Contract No. 990-1266/1045, March, 1991.

C-2 .
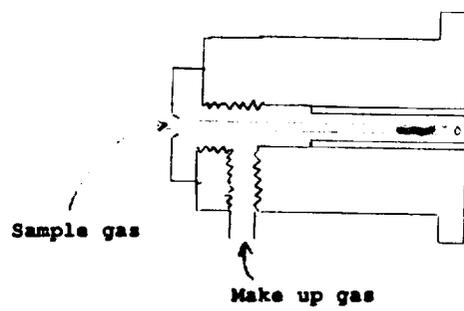
Figure 1. Modified Ionscan Inlet.
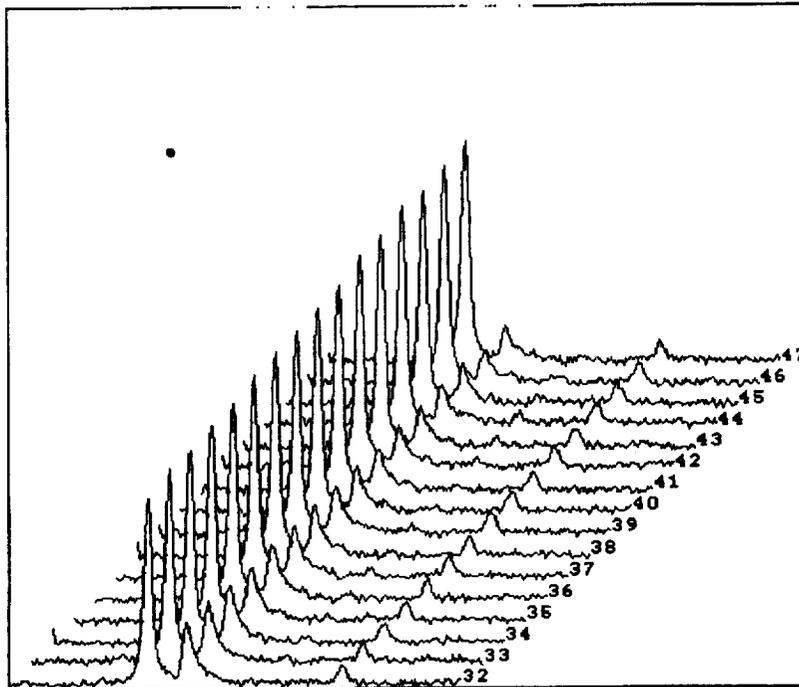
TIMING PARAMETERS
Start Time: 4 msec   End Time: 19 msec   Gate Time: 30 msec

DATA PARAMETERS
Data Points: 512   Scans: 8   Traces: 128

Figure 2. Modified Data Acquisition System: Partial Display
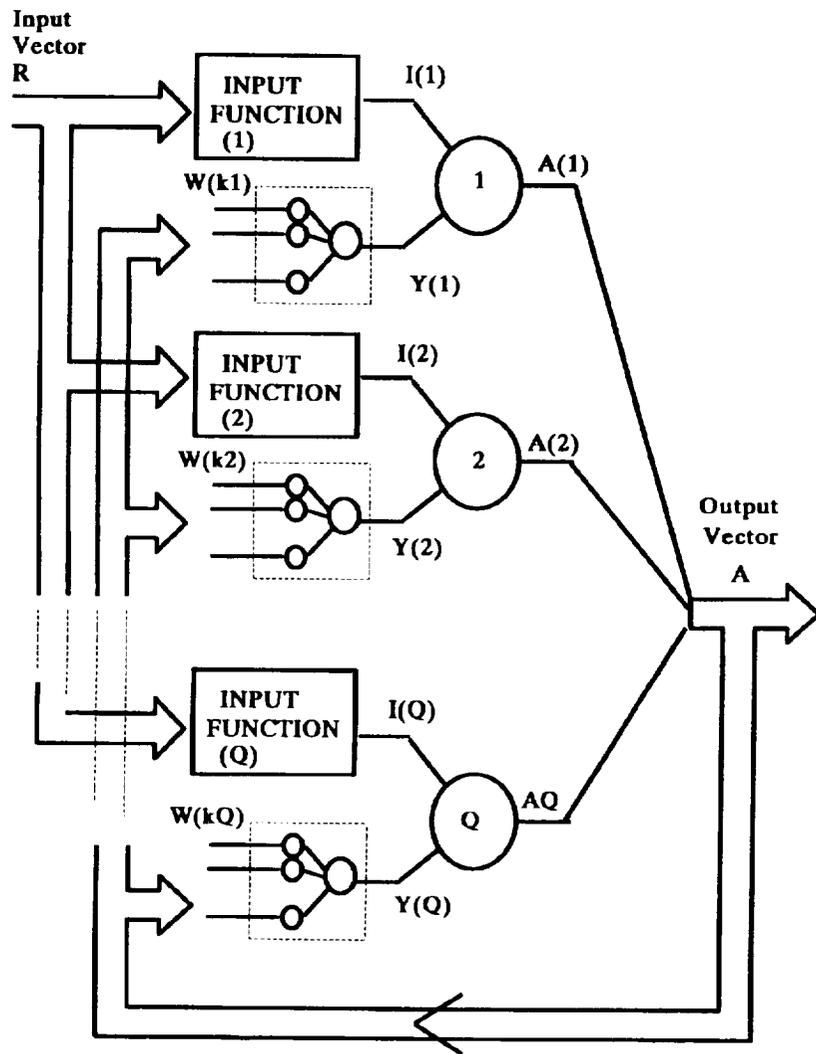
Figure 3. Setup of a Hopfield Network
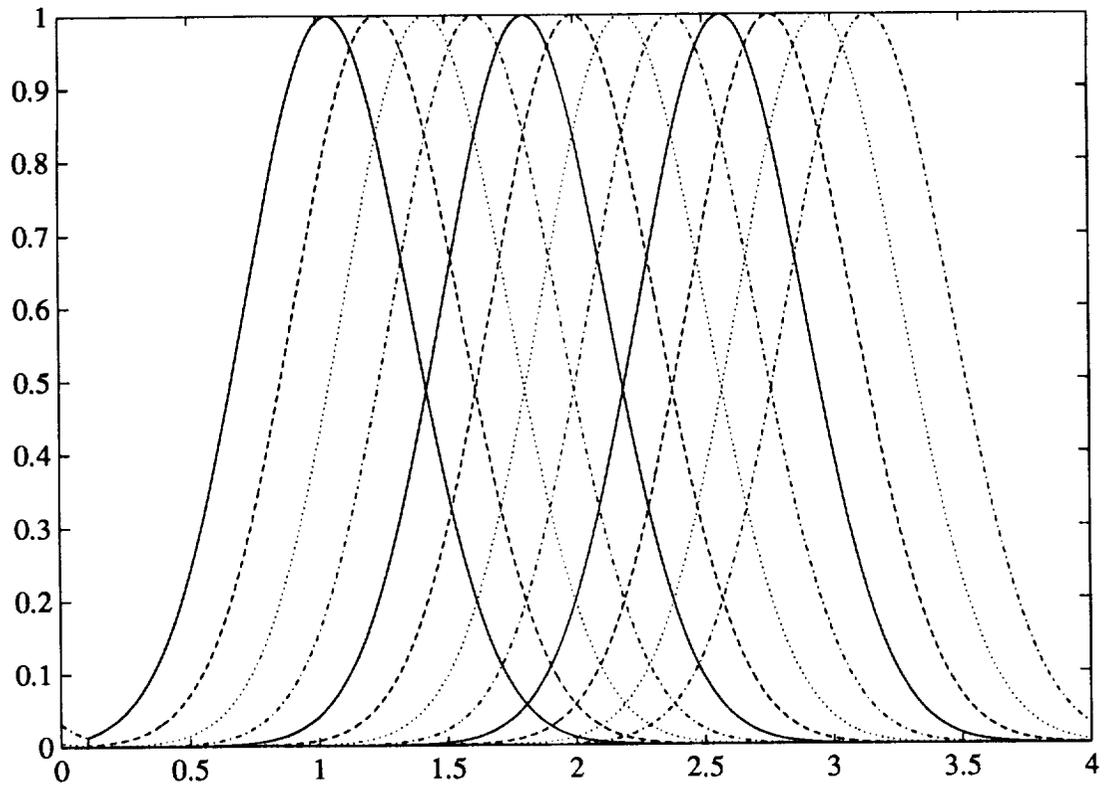
Figure 4. Example of Basis Function
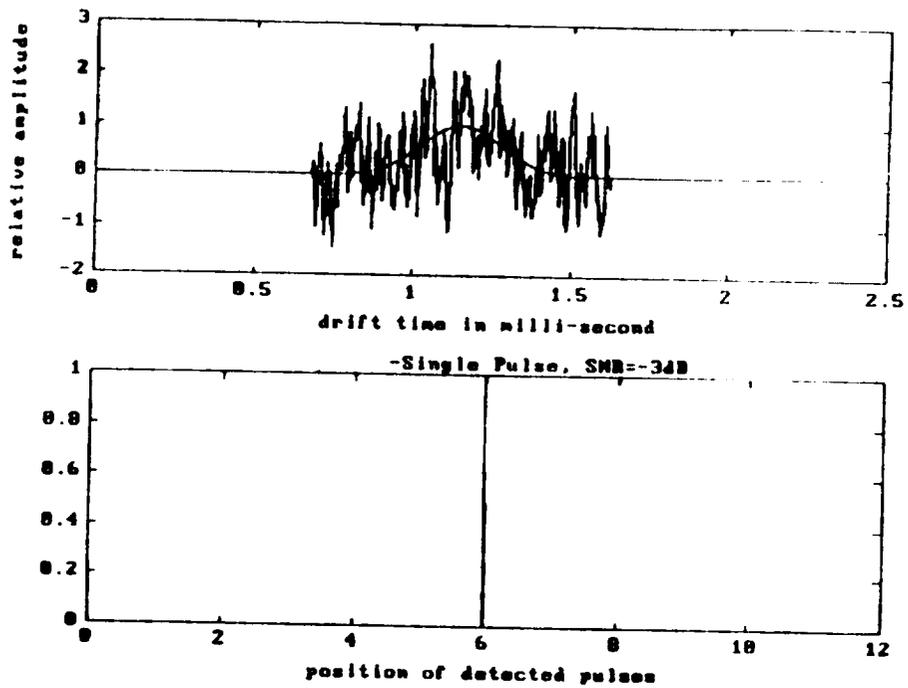
Figure 5. Hopfield Network Sensitivity to Noise: Simulated Signal
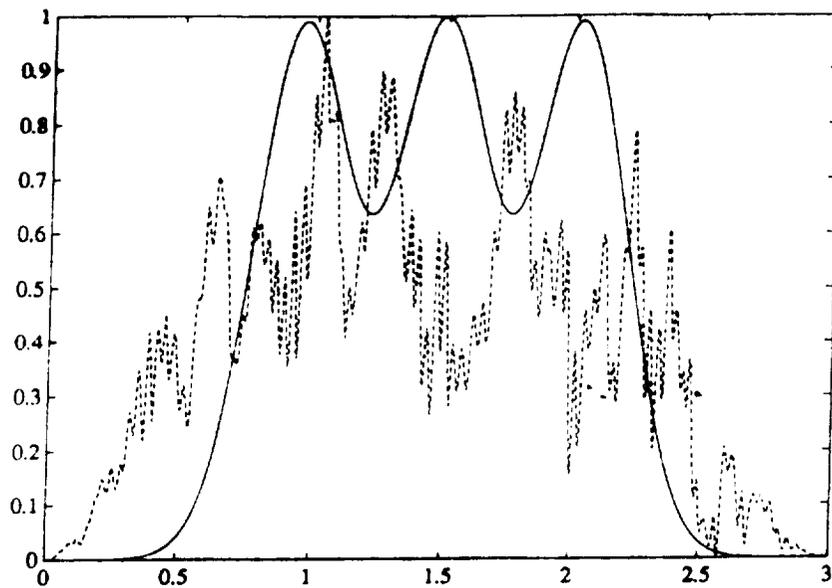
Figure 6. Hopfield Network Result on Blank Signal from Ionscan Instrument
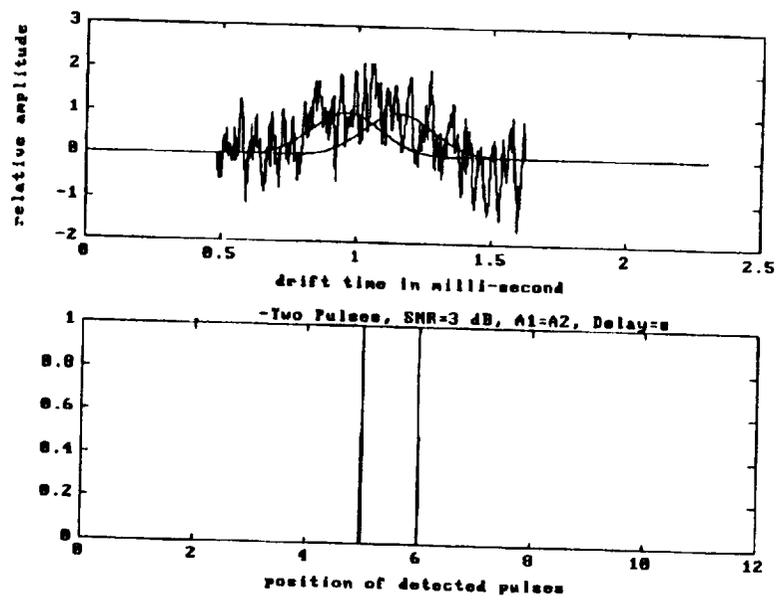
Figure 7. Resolving Power of Hopfield Network:
Equal Amplitudes, SNR = 3 dB
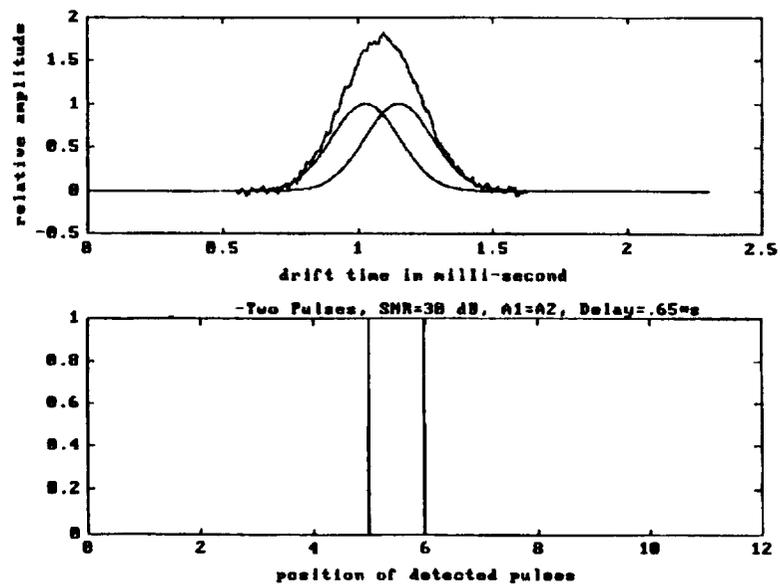
Figure 8. Resolving Power of Hopfield Network:
Time Resolution of 0.65 σ
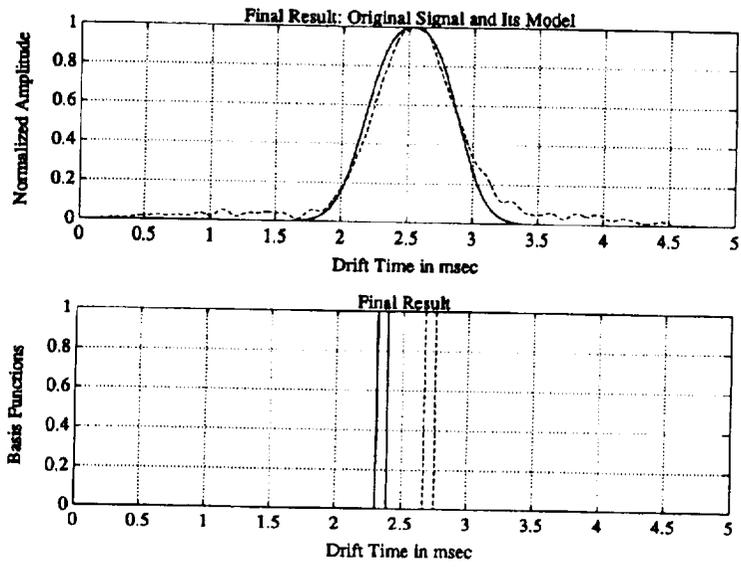
Figure 9. Resolving Power of Hopfield Network:
Separation of Cocaine and Tetracaine.

Exchange, interpretation, and database-search
of ion mobility spectra supported by data format JCAMP-DX

J.I. Baumbach, A.N. Davies, A.v. Irmer, P.H. Lampen

Institut für Spektrochemie und angewandte Spektroskopie,
Bunsen-Kirchhoff-Str. 11, D-44139 Dortmund, Germany

ABSTRACT

To assist peak assignment in ion mobility spectrometry it is important to have quality reference data. The reference collection should be stored in a database system which is capable of being searched using spectral or substance information. We propose to build such a database customized for ion mobility spectra. To start off with it is important to quickly reach a critical mass of data in the collection. We wish to obtain as many spectra combined with their IMS parameters as possible. Spectra suppliers will be rewarded for their participation with access to the database. To make the data exchange between users and system administration possible, it is important to define a file format specially made for the requirements of ion mobility spectra. The format should be computer readable and flexible enough for extensive comments to be included. In this document we propose a data exchange format, and we would like you to give comments on it.

For the international data exchange it is important, to have a standard data exchange format. We propose to base the definition of this format on the JCAMP-DX protocol, which was developed for the exchange of infrared spectra. This standard made by the Joint Committee on Atomic and Molecular Physical Data is of a flexible design. The aim of this paper is to adopt JCAMP-DX to the special requirements of ion mobility spectra.

KEY WORDS
Data exchange, ion mobility spectrometry, JCAMP-DX

1 INTRODUCTION

JCAMP-DX is a file based format using ASCII characters (American Standard Code of Information Interchanging) reduced to the printable character. This guarantees the acceptance on all computer systems. The main components to describe the ion mobility spectrometer and the spectra are shown in Figure 1:

Figure 1:

##.FLUX=
##.ELEKTRIC FIELD=
##.CARRIERGAS=
##SAMPLE DESCRIPTION=
##CAS NAMES=
##NAMES=
##CONCENTRATIONS=
##.REDUCED MOBILITY=
##.IONISATION TEMPERATURE=
##.IONISATION CHAMBER=
##.DRIFT TEMPERATURE=
##PRESURE=
##.DRIFT CHAMBER=
##.IONISATION MODE=
##.IONISATION ENERGY=
##.DRIFT GAS=
##.REPETITION RATE=
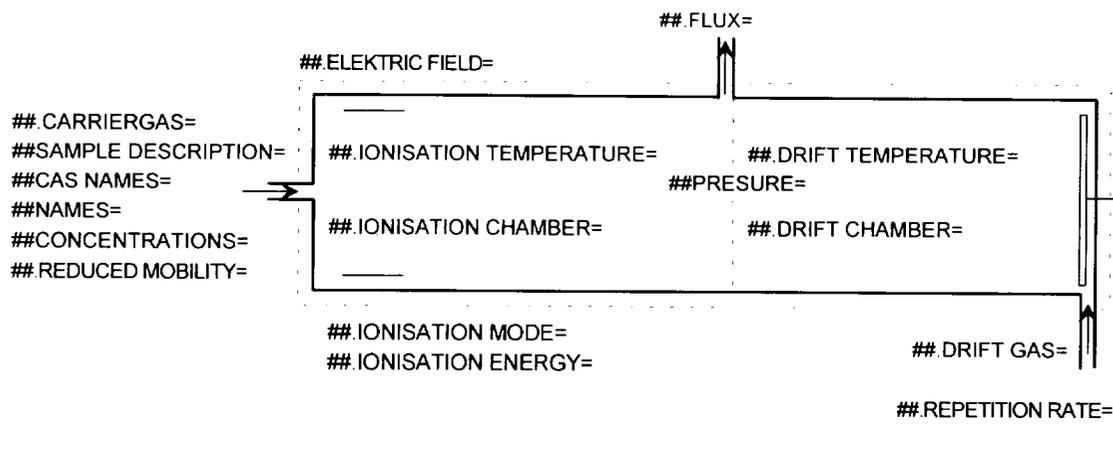
Main declarations to connect ion mobility spectrometry and JCAMP-DX

2 DEFINITIONS

The following definitions are important for the unterstanding of the JCAMP-DX protocol:

2.1 LDR

Labeled-Data-Records (LDR) consists of 80 characters (or less) starting with Data-Labels delimited by ## and terminated with =. For example ##TITLE= is a data lable for the definition of the working title of the following spectrum. There are two kinds of LDR: Core and Note. Core LDRs are required. Notes are optional. Every defintion of an LDR should include if it's a core or a note.

2.2 TEXT

The LDR contain descriptive information for humans, not normally intended to be parsed by computers, i.e., title, comments, origin, etc.

2.3 STRING

Some LDR contain pre-defined text fields intended to be parsed by computers and read by human. The form of each string field is specified under the LDR in which it is used.

2.4 AFFN

The easiest way to write the data is to use the ASCII free format numeric. This format is important to simplify direct user input. It is a format similar to freeform input in BASIC. A field starts either with +, -, decimal point or digit. E is the only allowed character to give the power of 10 by witch the field must be multiplied. It is followed by + or - and up to three digits. The numeric field is terminated either by E, comma or blank.

2.5 ASDF

This is the ASCII sqeezed difference form. Tabular data using JCAMP-DX data compression scheme. (see section 3.2.9)

3 JCAMP-DX LABELED-DATA-RECORDS (LDR)

The main structure of a JCAMP-DX file consist of

- equipment parameter
- header which includes all file informations
- parameter of spectrum
- sample parameters

3.1 Equipment Parameter

Many LDR are already defined by JCAMP-DX. They can be easy adapted for IM-Spectrometer. But in the case of the equipment parameters the special requirements of this technology call for some special LDRs. The JCAMP-DX standard is easy to expand. Any new LDR starts with "##.". In the following part a conglomerate of definitions coming from IR-, NMR-, MS-JCAMP and special for IMS defined LDR will allow a precise description of the equipment parameters.

3.1.1 ##DATA SYSTEM= (TEXT)

This LDR allows a description of the data acquisition and the treatment of the data. *(Note)*

3.1.2 ##DATA PROCESSING= (TEXT)

Here all mathematical procedures used before storing the data in JCAMP-DX file are described. Even for a peak assignment table this LDR is important. *(Note)*

3.1.3 ##PRESSURE= (STRING)

Pressure inside the IMS-System is ment (in SI-units). *(Note in JCAMP-DX but in this case strongly recommended)*

3.1.4 ##.CARRIERGAS= (TEXT)

A description of the carrier gas is required here. *(Core)*

3.1.5 ##.REDUCED MOBILITY= (AFFN)

In addition of the sample description seen above in this LDR the known reduced mobility can be given. *(Note)*

3.1.6 ##.ELECTRIC FIELD= (AFFN,AFFN)

The electric field description is divided in two parts: The filed in the ionisation chamber and the one in the drift chamber (in Volt / cm). *(Core)*

3.1.7 ##.IONISATION MODE= (STRING)

How does the system ionise the gas? The following keywords are defined:

UV   ultraviolet source

BR   beta-radiation source

For detailed information it is possible to give a comment like $$Ni63-source. *(Core)*

3.1.8 ##.IONISATION ENERGY= (AFFN)

To have the information, witch part of the probe is ionised the ionisation energy is needful (eV is used). *(Note)*

3.1.9   ##.IONISATION TEMPERATURE= (STRING) and ##.DRIFT
         TEMPERATURE= (STRING)

Here the temperature in the ionisation/drift chamber is meant (in °C). *(Core)*

3.1.10   ##TEMPERATURE= (STRING)

The sample temperature in °C should only be given if there is a significant different to room

temperature. *(Core)*

3.1.11   ##.IONISATION CHAMBER= (STRING, AFFN, AFFN[, AFFN]) and
         ##.DRIFT CHAMBER= (STRING, AFFN, AFFN[, AFFN])

Different geometrical parameters of the ionisation/drift chamber are distinguished by the

following keywords:

RECT   This means a rectangular chamber. It is followed by the size of the three

        dimensions length, width and height in mm.

CYL   Stands for a cylindrical form of the chamber. It is followed by its length and

        radius.

(Note)

3.1.12   ##.FLUX= (AFFN, AFFN)

This LDR is divided in two fluxes. The first value is linked to the ionisation chamber and the

second to the drift chamber. All values have the unit liter/minute. *(Note)*

After having discussed the IMS equipment LDR´s we now come to the LDR´s which already

defined in JCAMP-DX. The header of a file, the spectrum parameter and the sample

parameter are nearly the same for other analytical processes. This allows us to adapt most of

the standart LDR from the existing JCAMP-DX with some small changes only. For more

information see [1], [2] and [3].

3.2   Header

3.2.1   ##TITLE= (TEXT)

Title and/or reason of the measurement. *(Core)*

3.2.2   ##JCAMP-DX= (STRING)

The version number of the used format is 5.00 *(Core)*

3.2.3   ##DATA TYPE= (STRING)

Keywords: ION MOBILITY SPECTRUM or

                         IMS PEAK TABLE

Give a possibility to distinguish between different kinds of data like NMR- or IR-data. The string ION MOBILITY SPECTRUM reports a continuous spectrum located at the ##XYDATA=-LDR and IMS PEAK TABLE reports distinct and analysed peak's located in the ##PEAK TABLE=-LDR. *(Core)*

3.2.4   ##DATA CLASS= (STRING)

Keywords: XYDATA or

                         PEAK TABLE

This lable defines the type of tabular data within the data block and is not to be used for link blocks. *(Core)*

3.2.5   ##ORIGIN= (TEXT)

Here the name of organisation, address, telephone number, name of individual contributor etc. must be added. This information is <u>not</u> optional.*(Core)*

3.2.6   ##OWNER= (TEXT)

It is possible to set here a copyright linked to the spectrum that has the form: "COPYRIGHT (C) <year> by <name>". If ##OWNER= contains "PUBLIC DOMAIN", the implication is that the data may be copied without permission on the authority of the one is named under ##ORIGIN=.*(Core)*

3.2.7   ##DATE= (STRING)

Date of measurement is required here in the form: YY/MM/DD. *(NOTE)*

3.2.8   ##TIME= (STRING)

Time of measurement in the form: HH:MM:SS. *(NOTE)*

3.2.9 ##BLOCK_ID= (AFFN) and ##BLOCKS= (AFFN)

These records are to be used in compound JCAMP-DX files to provide inter-block refering. A unique positve integer must be given to each block within a compound file. This number must not necessarily be sequential. For ease of use it is recommended to use separate files for each data block. *(Core only for compound files)*

EXAMPLE:

##TITLE=	´title of the whole compound file´
##JCAMP-DX=	5.00 $$name & Version No. of JCAMP-DX software
##DATA TYPE=	LINK
##BLOCKS=	´n´
##ORIGIN=	´name of contributor, organisation, address, telephone etc.´
##OWNER=	COPYRIGHT (C) ´year´ by ´name´ $$ or PUBLIC DOMAIN
##TITLE=	´title of the first data block´
##JCAMP-DX=	5.00
##DATA TYPE=	ION MOBILITY SPECTRUM
##DATA CLASS=	XYDATA
##BLOCK_ID=	1
##ORIGIN=	´name of contributor, organisation, address, telephone etc.´
##OWNER=	COPYRIGHT (C) ´year´ by ´name´ $$ or PUBLIC DOMAIN
##CROSS REFEERENCE=	IMS PEAK TABLE:BLOCK_ID=2

. . .

##END=

##TITLE=	´title of the second data block´
##JCAMP-DX=	5.00
##DATA TYPE=	IMS PEAK TABLE
##DATA CLASS=	PEAK TABLE
##BLOCK_ID=	2

```
##ORIGIN=                 'name of contributor, organisation,
                          address, telephone etc.'
##OWNER=                  COPYRIGHT (C) 'year' by 'name'
                          $$ or PUBLIC DOMAIN
##CROSS REFEERENCE=       ION MOBILITY SPECTRUM: BLOCK_ID=1
. . .
##END=
```

3.2.10 ##SOURCE REFERENCE= (TEXT)

Here an identification to locate the original spectrum file or library name and serial number is possible. *(Note)*

3.2.11 ##CROSS REFERENCE= (TEXT)

If there's additional data for the same sample like peak assignments or other types of spectra, this LDR gives the linkage to them. *(Note)*

EXAMPLE:
```
##CROSS REFERNCE= ION MOBILITY SPECTRUM:
                      EXTERNAL_FILE= FILENAME.DX
                      IMS PEAK TABLE: BLOCK_ID=16
```

3.2.12 ##END=

It's important to have a mark at the end of file in the data format to know that it is complete received and to distinguish between the blocks of a multi spectrum file. *(Core)*

3.3 Parameters of the spectrum

3.3.1 ##XUNITS= (STRING) and ##YUNITS= (STRING)

Here the units of the axis can be given. The following keywords are defined:
SECONDS, MILLISECONDS, NANOSECONDS, MILLIAMPERS, NANOAMPERS. *(Core)*

3.3.2   ##FIRSTX= (AFFN) and ##LASTX= (AFFN)

First and last actual abscissa values of ##XYDATA=. First tabulated abbscissa times ##XFACTOR= should equal ##FIRSTX=. *(Core for spectrum files)*

3.3.3   ##FIRSTY= (AFFN)

Here the actual Y-value corresponding to ##FIRSTX= is ment. ##FIRSTY= should be equal ##YFACTOR= times the first Y-value in ##XYDATA=. *(Core for spectrum files)*

3.3.4   ##XFACTOR= (AFFN) and ##YFACTOR= (AFFN)

The values of spectrum have to be integer to save space and allow the DIFDUP format (see 3.2.6). For that the ##XFACTOR=- and ##YFACTOR=-LDR contain a floatingpoint number to be multiplied by the ##XYDATA= values. For example if ##XFACTOR= 0.0001 the following ##XYDATA= 9999 means an X-value of 0.9999. *(Core for spectrum files)*

3.3.5   ##NPOINTS= (AFFN)

Here the numbers of points are required for both cases: IMS-Peak table and IM-Spectrum. *(Core)*

3.3.6   ##XYDATA= (STRING)

This LDR contains spectral data. It is followed by the form of the tabular data like: (X++(Y..Y)) where .. indicate indefinite repeat of Y-values until the end of line and ++ indicates that X is incremented by (##LASTX=-##FIRSTX=)/(##NPOINTS=-1) between two Y. For discrete point the indication (XY..XY) is useable. (See the following example)

This format creates on one hand large files, but is one the other hand readable.

To have a better data compression it is possible to use the squeezed form (SQZ) in witch the delimiter, the leading digit and sign are replaced by a pseudo-digit from Table I.

For a better compression, it is possible to use the difference form (DIF) where the delimiter, leading digit and sign of the difference between adjacent values are transformed in a pseudo-digit from Table I. To check data, each line starts with the absolute x- and y-value,

witch is the same as the last calculated value of the previous line. The last line of a block of DIF data contains only abscissa and ordinate for y-value check of the last ordinate.

Another possible format is duplicate suppression (DUP) replaces two or more adjacent and identical numbers with pseudo-digits written in Table I. For example 50 50 50 50 becomes 50V. The two formats DIF and DUP can be combined to the most compressing but less readable format called DIFDUP. In this format the duplicate count is obtained by counting identical differences. The example above becomes 50 % % % in DIF form and 50%U in DIFDUP form. *(Core for spectrum files)*

Table I:

<u>Pseudo digits used to compress spectra data in SQS-, DIF- and DUP-format</u>

ASCII digits	0	1	2	3	4	5	6	7	8	9
Postive SQZ	@	A	B	C	D	E	F	G	H	I
Negative SQZ		a	b	c	d	e	f	g	h	i
Positive DIF	%	J	K	L	M	N	O	P	Q	R
Negative DIF		j	k	l	m	n	o	p	q	r
DUP		S	T	U	V	W	X	Y	Z	s

Example for normal data storage

<u>Normal form:</u>

```
##YUNITS= NANOAMPER
##XUNITS= MILLISECONDS
##XFACTOR= 1
##YFACTOR= 0.1
##XYDATA= (X++(Y..Y)
4        0  0  0  0  2  4  4  4  7
12       5  4  4  5  5  7 10 11 11
21       6  5  7  6  9  9  7 10 10
31       9 10 11 12 15 16 16 14 17
39      38 38 35 38 42 47 54 59 66
48      75 78 88 96 104 110 121 128
```

witch is the same as the last calculated value of the previous line. The last line of a block of DIF data contains only abscissa and ordinate for y-value check of the last ordinate.

Another possible format is duplicate suppression (DUP) replaces two or more adjacent and identical numbers with pseudo-digits written in Table I. For example 50 50 50 50 becomes 50V. The two formats DIF and DUP can be combined to the most compressing but less readable format called DIFDUP. In this format the duplicate count is obtained by counting identical differences. The example above becomes 50 % % % in DIF form and 50%U in DIFDUP form. *(Core for spectrum files)*

Table I:

Pseudo digits used to compress spectra data in SQS-, DIF- and DUP-format

ASCII digits	0	1	2	3	4	5	6	7	8	9
Postive SQZ	@	A	B	C	D	E	F	G	H	I
Negative SQZ		a	b	c	d	e	f	g	h	i
Positive DIF	%	J	K	L	M	N	O	P	Q	R
Negative DIF		j	k	l	m	n	o	p	q	r
DUP		S	T	U	V	W	X	Y	Z	s

Example for normal data storage

Normal form:

```
##YUNITS= NANOAMPER
##XUNITS= MILLISECONDS
##XFACTOR= 1
##YFACTOR= 0.1
##XYDATA= (X++(Y..Y)
4         0  0  0  0  2  4  4  4  7
12        5  4  4  5  5  7 10 11 11
21        6  5  7  6  9  9  7 10 10
31        9 10 11 12 15 16 16 14 17
39       38 38 35 38 42 47 54 59 66
48       75 78 88 96 104 110 121 128
```

Example for DIFDUP-form

```
##YUNITS= NANOAMPER
##XUNITS= MILLISECONDS
##XFACTOR= 1
##YFACTOR= 0.1
##XYDATA= (X++(Y..Y)
4@VKT%TLkj%J%KLJ%njKjL%kL%jJULJ%kLK1%1LMNPNPRLJ0QTOJ1P
56A28
```

3.3.7 ##PEAK ASSIGNMENT= (STRING)

Keywords: (XA),(XYA) or (XYWA)

After this LDR a list of peak's and their assignments for each components are given in the following form:

$$(X_1[,Y_1][,W_1],<A_1>)$$

$$....$$

$$(X_i[,Y_i][,W_i],<A_i>)$$

X and Y indicates the location and height of each peak in units given by ##YUNITS= and ##XUNITS=. W stands for width and A represents a string describing the assignment enclosed in angle brackets.

The parentheses are just to get a beginning and ending flag of each assignment. Square backets indicate optional information. It is important for the technical readability to have the same format for the whole peak assignment table and describe it after the ##PEAK ASSIGNMENT= -LDR with (XA),(XYA) or (XYWA). This LDR should be followed by a comment, which gives the method of finding the peak. *(Core for peak assignments)*

3.3.8 ##XLABEL= (TEXT) and ##YLABEL= (TEXT)

These LDRs give the possibility of labelling the axis. *(Note)*

3.4 Sample information

At least one of the optional LDRs described in this section should be included in each JCAMP-DX file.

3.4.1 ##SAMPLE DESCRIPTION= (TEXT)

If the sample is not a pure compound, this field should contain its description, i.e., composition, origin, appearance, results of interpretation, etc. If the sample is a known compound, the following LDRs specify structure and properties, as appropriate. *(Note)*

3.4.2 ##CAS NAME= (STRING)

Name according to Chemical Abstracts naming conventions as described in Appendix IV of the 1985 CAS Index Guide is required here. Examples can be found in Chemical Abstracts indices or the Merck Index. Greek letters are spelled out, and standard ASCII capitals are used for small capitals. Sub-/Superscribts are indicated by prefixes / and $\wedge$. Example: alpha-D-glucopyranose, 1-(dihydrogen phosphate).*(Note)*

3.4.3 ##NAMES= (STRING)

Here the common, trade or other names are allowed. Multiple names are placed on separate lines.*(Note)*

3.4.4 ##MOLFORM= (STRING)

Another possibility of describing the sample is to write down the Molecular formular. Elemental symbols are arranged with carbon first, followed by hydrogen, and then remaining element symbols in alphabetic order. The first letter of each elemental symbol is capitalised. The second letter, if required, is lower case. One-letter symbols must be separated from the next symbol by a blank or digit. Sub-/Superscripts are indicated by the prefixes: / and $\wedge$, respectively. Sub- and superscripts are terminated by the next nondigit. Slash may be omitted for subscripts. For readability, each atomic symbol may be separated from its predecessor by a space. For substances that are represented by dot disconnected formulas (hydrates, etc.), each fragment is represented in the above order, and the dot is represented by *. Isotopic mass is specified by a leading superscript. D and T may be used for deuterium and tritium. *(Note)*

Examples:

C2H4O2 or C2 H4 O2	(acetic acid)
C6 H9 Cr O6 * H2 O	(chromic acetate monohydrate)
H2 $\wedge$ 17O	(water, mass 17 oxygen)

3.4.5   ##CONCENTRATIONS= (STRING)

The list of the known components and their concentrations has the following form, where N stands for the name and C for the concentration of each component in units given with U. *(Note in JCAMP-DX but in this case strongly recommended)*

```
##CONCENTRATIONS=  (NCU)
(N ,C ,U )
    1   1
    .  .  .
(N ,C ,U )
   i   i   i
```

The group for each component is enclosed in parentheses. Each group starts a new line and may continue on following lines.

4   SUMMERY

In the following tables all discussed LDR´s are shown with their basic Parameters:

Equipment Parameter:

LDR	Parameter	Keyword	Status	Location
##DATA SYSTEM=	(TEXT)		Note	3.1.1
##DATA PROCESSING=	(TEXT)		Note	3.1.2
##PRESSURE=	(STRING)		Note in JCAMP-DX but in this case strogly recommended	3.1.3
##.CARRIERGAS=	(TEXT)		Core	3.1.4
##.REDUCED MOBILITY=	(AFFN)		Note	3.1.5
##.ELECTRIC FIELD=	(AFFN, AFFN)		Core	3.1.6
##.IONISATION MODE=	(STRING)	UV or BR	Core	3.1.7
##.IONISATION ENERGY=	(AFFN)		Note	3.1.8
##.IONISATION TEMPERATURE=	(STRING)		Core	3.1.9
##.DRIFT TEMPERATURE=	(STRING)		Core	3.1.9
##TEMPERATUR=	(STRING)		Core	3.1.10
##.IONISATION CHAMBER=	(STRING, AFFN, AFFN [, AFFN])	RECT or CYL	Note	3.1.11
##.DRIFT CHAMBER=	(STRING, AFFN, AFFN [, AFFN])	RECT or CYL	Note	3.1.11
##.FLUX= (AFFN, AFFN)	(AFFN, AFFN)		Note	3.1.12

Header

LDR	Parameter	Keyword	Status	Location
##TITLE=	(TEXT)		Core	3.2.1
##JCAMP-DX=	(STRING)	5	Core	3.2.2
##DATA TYPE=	(STRING)	ION MOBILITY SPECTRUM or IMS PEAKTABLE	Core	3.2.3
##DATA CLASS=	(STRING)	XYDATA or PEAK TABLE	Core	3.2.4
##ORIGIN=	(TEXT)		Core	3.2.5
##OWNER=	(TEXT)		Core	3.2.6
##DATE=	(STRING)		Core	3.2.7
##TIME=	(STRING)		Note	3.2.8
##BLOCK_ID=	(AFFN)		Core for compound files	3.2.9
##BLOCKS=	(AFFN)		Core for compound files	3.2.9
##SOURCE REFERENCE=	(TEXT)		Note	3.2.10
##CROSS REFERENCE=	(TEXT)		Note	3.2.11
##END=			Core	3.2.12

Parameter of Spectrum

LDR	Parameter	Keyword	Status	Location
##XUNITS=	(STRING)	SECONDS, MILLISEC-ONDS, NANOSECONDS	Core	3.3.1
##YUNITS=	(STRING)	MIL-LIAMPERS, NANOAMPERS	Core	3.3.1
##FIRSTX=	(AFFN)		Core for spectrum files	3.3.3
##LASTX=	(AFFN)		Core for spectrum files	3.3.4
##FIRSTY=	(AFFN)		Core for spectrum files	3.3.5
##XFACTOR=	(AFFN)		Core for spectrum files	3.3.6
##YFACTOR=	(AFFN)		Core for spectrum files	3.3.7
##NPOINTS=	(AFFN)		Core for spectrum files	3.3.8
##XYDATA=	(STRING)	(X++(Y..Y)), (XY..XY)	Core for spectrum files	3.3.9
##PEAK ASSIGNMENT=	(STRING)	(XA),(XYA) or (XYWA)	Core for peak assignments	3.3.10
##XLABLE=	(TEXT)		Note	3.3.11
##YLABLE=	(TEXT)		Note	3.3.12

Header

LDR	Parameter	Keyword	Status	Location
##TITLE=	(TEXT)		Core	3.2.1
##JCAMP-DX=	(STRING)	5	Core	3.2.2
##DATA TYPE=	(STRING)	ION MOBILITY SPECTRUM or IMS PEAKTABLE	Core	3.2.3
##DATA CLASS=	(STRING)	XYDATA or PEAK TABLE	Core	3.2.4
##ORIGIN=	(TEXT)		Core	3.2.5
##OWNER=	(TEXT)		Core	3.2.6
##DATE=	(STRING)		Core	3.2.7
##TIME=	(STRING)		Note	3.2.8
##BLOCK_ID=	(AFFN)		Core for compound files	3.2.9
##BLOCKS=	(AFFN)		Core for compound files	3.2.9
##SOURCE REFERENCE=	(TEXT)		Note	3.2.10
##CROSS REFERENCE=	(TEXT)		Note	3.2.11
##END=			Core	3.2.12

Parameter of Spectrum

LDR	Parameter	Keyword	Status	Location
##XUNITS=	(STRING)	SECONDS, MILLISEC-ONDS, NANOSECONDS	Core	3.3.1
##YUNITS=	(STRING)	MIL-LIAMPERS, NANOAMPERS	Core	3.3.1
##FIRSTX=	(AFFN)		Core for spectrum files	3.3.3
##LASTX=	(AFFN)		Core for spectrum files	3.3.4
##FIRSTY=	(AFFN)		Core for spectrum files	3.3.5
##XFACTOR=	(AFFN)		Core for spectrum files	3.3.6
##YFACTOR=	(AFFN)		Core for spectrum files	3.3.7
##NPOINTS=	(AFFN)		Core for spectrum files	3.3.8
##XYDATA=	(STRING)	(X++(Y..Y)), (XY..XY)	Core for spectrum files	3.3.9
##PEAK ASSIGNMENT=	(STRING)	(XA),(XYA) or (XYWA)	Core for peak assignments	3.3.10
##XLABLE=	(TEXT)		Note	3.3.11
##YLABLE=	(TEXT)		Note	3.3.12

Sample information

LDR	Parameter	Keyword	Status	Location
##SAMPLE DESCRIPTION=	(TEXT)		Note	3.4.1
##CAS NAME=	(STRING)	Names defined by CAS Index Guide	Note	3.4.2
##NAMES=	(TEXT)		Note	3.4.3
##MOLFORM=	(STRING)	see Def.	Note	3.4.4
##CONCENTRATIONS=	(STRING)		Note in JCAMP-DX butin this case strogly recommended	3.4.5

EXAMPLE JCAMP-DX-FILE FOR IMS DATA EXCHANGE

##TITLE=EXAMPLE FOR A JCAMP-DX FILE FOR IMS
##JCAMP-DX=500
##DATA-TYPE=ION MOBILITY SPECTRUM
##DATA CLASS=XYDATA
##ORIGIN=A.v.Irmer, ISAS Dortmund, Germany
##OWNER=COPYRIGHT (C) 1994 by ISAS Dortmund, Germany
##DATE=94/09/12
##TIME=12:37:23
##SOURCE REFERENCE=C:\VONIRMER\AVIJIBB.ASC
##DATA SYSTEM=PCI28000
##DATA PROCESSING=AVIJIBBOVERSAMPLING
##PRESSURE=101
##.CARRIERGAS=ARGON
##.ELECTRIC FIELD=(250,333)
##.IONISATION MODE=BR $$Ni63
##.IONISATION TEMPERATURE=25
##.DRIFT TEMPERATURE=25
##TEMPERATURE=25
##.IONISATION CHAMBER=(CYL,2,2)
##.DRIFT CHAMBER=(CYL,5,2)
##.FLUX=(2,5)
##XUNITS=MILLISECONDS
##YUNITS=AMPERS
##FIRSTX=10
##LASTX=25
##FIRSTY=4.096E11
##XFACTOR=1
##YFACTOR=1E7
##POINTS=151
##XYDATA=(X++(YY))
 10   4096,4352,4608,4352,4352,4864,4608,4864,4608,4352
 11   4096,4096,4352,4352,4096,4096,4096,4352,4512,4608
 12   4352,4096,4352,4352,4608,4352,4096,4096,4864,512

110

```
13  512,4864,4608,4096,4096,4096,4096,4096,4096,4352
14  4352,4608,4608,4864,4864,4608,4608,512,512,4864
15  4864,4608,4608,4608,512,512,4864,4608,4608,4864
16  5376,4864,4352,4096,4352,4608,4864,512,4864,512
17  512,5376,5376,512,4608,4608,4608,4864,4864,512
18  512,4864,4864,512,5376,5376,512,512,512,512
19  5376,5376,5888,6144,6912,8448,107520,135680,168960,20480
20  225280,245760,245760,23040,207360,176640,151040,133120,122880,107520
21  104960,107520,122880,133120,156160,174080,184320,186880,181760,174080
22  163840,14080,122880,107520,9472,896,896,896,8704,8704
23  9216,104960,122880,130560,14080,145920,143360,138240,1280,112640
24  9472,8192,6912,6656,64,6656,64,6144,5888,5888
25  512
##XLABLE=Drifttime /ms
##YLABLE=Ion Current /A
##END=
```

5   REFERENCES

[1] JCAMP-DX: A Standard Form for Exchange of Infrared Spectra

in Computer Readable Form

Robert S.McDonald and Paul A. Wilks, Applied Spectroscopy **42** (1988) 151-162

[2] JCAMP-DX for Mass Spectrometry

Peter Lampen, Heinrich Hillig, Antony N.Davies and Micheal Linscheid, accepted for

publication in Applied Spectroscopy

[3] JCAMP-DX for NMR

Antony N. Davies and Peter Lampen, Applied Spectroscopy **47** (1993) 1093-1099

Session III: Hyphenated IMS Techniques

Session Chair: Dr. Gary Eiceman

THE PINHOLE INTERFACE FOR IMS/MS

Glenn E. Spangler[1]

Environmental Technologies Group, Inc., 1400 Taylor Avenue, Baltimore, MD 21204-9840

ABSTRACT

An important supplementary technique for ion mobility spectrometry (IMS) is mass spectrometry (MS). A mass spectrometer coupled to an ion mobility spectrometer (IMS/MS) can provide significant information on the composition of the ions contributing to an ion mobility peak. On the other hand, the interpretation of IMS/MS results requires knowledge of processes which can occur at the pinhole interface. When the ion composition is a mixture of ion clusters, the observed cluster distribution may not be an accurate representation of the ion clusters in the IMS. Depending on the buffer gas, lower clusters can form by equilibrating with reduced concentrations in the continuum regime of the expansion and larger clusters can form by collisional stabilization in the cooled jet stream. Besides water, nitrogen molecules can also add to the ion clusters. Even though nitrogen is non-polar, this addition is made possible by an ion-induced dipole interaction between the ion and molecule.

INTRODUCTION

A favorite activity in ion mobility spectrometry (IMS) is to correlate ion mobility with the molecular weight and structure of ions.[1,2,3] The motivation behind these activities is that the mobility of an ion colliding with a gas is inversely proportional to the ion's reduced mass and collision cross section.[4,5] While many interesting observations have been made on ion structures using this approach,[6,7,8,9,10,11] one cannot be assured that the ions formed in IMS are bare ions. Rather the ions are often clusters containing neutral molecules other than the analyte.[12] Mass spectrometry is invaluable in identifying the composition of these ion clusters.

An IMS/MS is a IMS coupled to a mass spectrometer in such a way to allow sampling of the ions formed in the IMS by the MS. This is accomplished by providing a hole in the collector plate of the IMS and passing the ions through a pinhole interface into the vacuum system containing the mass spectrometer. Immediately behind the pinhole are focussing lenses which focus the ions unto the entrance aperture of the mass spectrometer. The pinhole interface is very similar to jet samplers used to sample ions in atmospheric pressure ionization mass spectrometry.[13,14] While the pinhole is very efficient in transmitting ions into the vacuum system, it also has a tendency to distort ion distributions. Since ion mobilities in IMS are dependent upon ion cluster distributions, this tendency interferes with the original purpose for collecting IMS/MS data.[15] Without knowledge of the processes leading to the distortion, absolute certainty concerning ion composition is lacking. Although the difficulty has not gone unnoticed in the open literature, approaches to IMS research have not been addressed.

Because the mean free path for an ion at 1 atmosphere is three orders of magnitude less than the diameter of a typical pinhole (20 - 50 micrometers), there will be many collisions between the molecules (and ions) as they enter the vacuum system of an IMS/MS. The current theory for the gas flow through a pinhole is isentropic free-jet expansion.[16,17,18,19] In the jet, the density of the gas decreases monotonically and the enthalpy of the source gas is converted into directed flow.[20] According to Miller, the fluid mechanical structure of a jet is dependent not only on hydrodynamic parameters (e.g., stagnant pressure, initial temperature, orifice area, etc.), but also the

---

[1]Current Address: 1209 Malbay Drive, Lutherville, MD 21093

length scale of the apparatus into which the jet is expanding.[21] For an unconstrained jet, the flow becomes supersonic and the expansion is surrounded by a concentric barrel shock terminated by a perpendicular shock known as the Mach disc.[22] This shock structure protects the expansion region from collisions with the background gas and the degree of ionization remains frozen to that of the source.[22] On the other hand when Searcy and Fenn used a 100 micron pinhole diameter to sample a 4.6 torr partial pressure of water, they noticed a sampling error which was dependent on stagnant pressure and buffer gas composition.[23,24,25] Ion clusters were formed which tended towards supersaturation. When Zook and Grimsrud reduced the pinhole diameter to 25 microns, the cluster distribution was dependent upon source temperature (125-250 °C) and could be accurately determined using a helium or hydrogen buffer gas.[26]

This paper describes experiments conducted to characterize the sampling capabilities of a pinhole interface between an IMS and an MS. When performing studies of this type, it is necessary to eliminate collisional dissociation mechanisms. Collisionally induced dissociation (i.e., "cluster buster") is often used to simplify mass spectra obtained from an atmospheric pressure ionization source.[27,28,29] This is accomplished by exposing the ion clusters to an elevated potential drop as they enter the vacuum region. While this may be a good way to prepare an ion sample for subsequent mass analysis, the conditions of the ionization source are forgotten in the process. This issue will be addressed.

EXPERIMENTAL METHODS

The investigations were conducted using an IMS/MS previously described in the open literature.[30] Improvements to the system included replacing the stacked-ring IMS cell with an all-ceramic IMS cell, upgrading the quadrupole mass spectrometer to an EXTREL C50 quadrupole mass spectrometer,[31] and installing a turbomolecular pump in place of the 4-inch diffusion pump. These are shown in Figure 1.

Structurally, the IMS cell contained three main parts:

a. Reactor (approx. 2 cm long, 2.5 cm internal diameter, 1.16 megohm resistance)

b. Drift tube (11.4 cm long, 3.8 cm internal diameter, 11.08 megohm resistance)

c. Membrane inlet (OV-101 impregnated microporous Teflon membrane, 1.3 cm^2 area).[32]

The ionization source was a cylindrical ring of ^{63}Ni foil approximately one inch in diameter and one centimeter long.[33] Although the IMS cell contained a shutter grid between the reactor and drift tube, it was biased open during the experiments so that it continuously conducted ion current. Since the ion current was measured using the electronics of the mass spectrometer, the IMS cell contained no ion collector. The temperature was measured using four thermocouples placed in contact with the pinhole mounted on the vacuum flange leading into the mass spectrometer, around the drift tube of the IMS halfway between the shutter grid and the mass spectrometer, and in contact with the reactor and membrane inlet of the IMS. Using strategically located heater tapes, the temperature at these four locations were continuously monitored and automatically controlled using temperature controllers. Thermal gradients were minimized by preheating the carrier and drift gases before they entered the cell.

Purified air or argon (Matheson UN 1006)[34] was used for the carrier, drift and sample gases of the cell. The purified air was generated using a Balston CO$_2$ remover.[35] Before being introduced into the cell, both gases were passed through activated 13X molecular sieve scrubbers.[36] The 13X molecular sieve scrubbers were activated with a purging flow of prepurified nitrogen at 300 °C for 24 hours before each experiment. The water content of the gases was monitored using a DuPont 703 phosphorous pentoxide hygrometer.[37] Typically the purified air contained 0.1 to 1.5 ppm water and the argon contained 1.5 to 1.6 ppm water. The water content

increased within these ranges as the scrubbers aged. Since the drift gas flowed between the vacuum flange of the mass spectrometer and the mounting flange for the IMS, it also served as a curtain gas for the pinhole. After flowing through the membrane inlet, the carrier gas entered the IMS cell near the shutter grid and exhausted with the drift gas through the reactor (i.e., unidirectional flow).

Since this paper is about processes that occur at the pinhole, this part of the IMS/MS is very important. An expanded sketch is shown in Figure 2. The ion sampling pinhole was mounted at the apex of a conical extension to the vacuum flange leading into the mass spectrometer. The angle for the cone was 50° with a height of 2.2 cm. These dimensions placed the pinhole 4.18 cm from the focussing lens assembly of the mass spectrometer. Immediately behind the pinhole was a 2.45 cm diameter by 2.27 cm long wire basket. This wire basket was mechanically and electrically attached to the first ion focussing lens and served to focus the ions entering the mass spectrometer onto the lens assembly. The wire basket also allowed gas entering the pinhole to freely expand into the vacuum system. With a bubble flowmeter, the volumetric flow of air passing through the pinhole was measured as 5.3 cc(RTP)/min. For the rated 450 L/s pumping speed for the turbomolecular pump behind the pinhole, this air flow corresponds to a baseline pressure of 1.5×10^{-4} Torr in the inlet chamber (i.e., the chamber that contained the focussing lenses). The actual pressure was 1.8×10^{-4} Torr as indicated by a vacuum gauge attached to the pumping line. When averaged across the area of the pinhole, the measured air flow corresponds to a linear air velocity of 179.3 m/s (<350 m/s, the velocity of sound in dry air).

The remainder of the operating conditions for the mass spectrometer are shown in Table 1.

RESULTS

Figures 3 and 4 show the positive and negative reactant ions generated in purified air using two potential distributions for the ion focussing lenses. The two potential distributions are given in Table 1 and were selected in an effort to influence the energy of the ions as they entered the vacuum system. The water content of the purified air was 1.5 ppm. The major positive ions were $H^+(H_2O)_n(N_2)_m$ with masses 55, 73, 83, 91, 101, 111, 129, 139 and 157 corresponding to n = 3 to 5 and m = 0 to 3. The major negative ions were $O_2^-(H_2O)_n(N_2)_m$ with masses 32, 50, 68, 78, 86, 96 and 124 corresponding to n = 0 to 3 and m = 0 to 2. Also the negative ions with masses 82, 100, 110, 118 and 138 are due to $O_4^-(H_2O)_n(N_2)_m$ with n = 1 to 4 and m = 0 to 2. All these ions are clusters involving water and nitrogen adducts.

A problem with these ion assignments is that the mass 28 difference assigned to nitrogen could also be carbon dioxide. Nitrogen has a zero dipole moment while carbon monoxide has a 0.10×10^{-18} e.s.u. dipole moment.[38] Although carbon monoxide was not added intentionally to the present experiments and nitrogen was a major component of the carrier and drift gases, it cannot be argued that carbon monoxide was not present as a trace contaminant during the experiments. This issue will be addressed when the data of Figure 5 are discussed.

The amplitude ratios between neighboring clusters are shown in Table 2. These amplitude ratios are proportional to the equilibrium constant for

$$I^\pm + S \rightleftharpoons I^\pm(S)$$
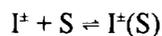
where $I^\pm$ is the ion and S is the solvating molecule. Except for the large unexplained discrepancy for the $O_2^- + H_2O \rightleftharpoons O_2^-(H_2O)$ reaction, the data for the two of lens potential distributions are in basic agreement. These results demonstrate that the potential distribution on the focussing lenses does not cause the clusters to dissociate as they enter the vacuum region.[28,29] Considering the fact that the potential applied to lens #1 located immediately behind the pinhole was increased an order of magnitude, a considerable margin of safety is indicated. Because there was nearly an order of magnitude more ion signal when the higher lens potentials were used, the remainder

TABLE 1: Operating Parameters for the IMS/MS

PARAMETER		VALUE
Pressures	Mass Spectrometer Focussing Lenses	2.6×10^{-6} Torr 1.8×10^{-4} Torr
Voltages	Reaction Region Hi Drift Region Hi Aperture Grid Pinhole Focussing Lens #1 Focussing Lens #2 Focussing Lens #3 Focussing Lens #4 Focussing Lens #5 Pole Zero	$\pm$ 2471 Volts ($\pm$ 1549 Volts w Argon) $\pm$ 1922 Volts ($\pm$ 1000 Volts w Argon) $\pm$ 129 Volts ($\pm$ 67 Volts w Argon) Ground $\mp$ 44.3 Volts or $\mp$ 4.7 Volts $\mp$ 17.5 Volts or $\mp$ 1.2 Volts $\mp$ 80.2 Volts or $\mp$ 20.1 Volts $\mp$ 30.4 Volts or $\mp$ 17.9 Volts $\mp$ 45.0 Volts or $\mp$ 14.8 Volts $\mp$ 8.5 to $\pm$ 1.5 Volts, or $\mp$ 21 to $\mp$ 11 Volts
Temperatures	Membrane Inlet Reaction Region Drift Region Pinhole Mass Spectrometer	48 °C 45 °C 54 °C 53 °C Unheated
Gas Flows	Carrier Gas Drift Gas Sample Gas	210 cc/min 336 cc/min 240 cc/min

of the data in this report were collected using that potential distribution. This means that lens #1 was biased at $\pm$ 44.3 Volts and the quadrupole mass analyzer was near ground potential.

Figure 5 compares positive ion spectra when purified air was used for the carrier, drift and sample gases; when argon was used for the carrier, drift and sample gases; and when purified air was used for the carrier and sample gases and argon was used for the drift gas. These data show that the ions with masses 101, 129 and 157 previously attributed to nitrogen adducts were observed only when purified air was used for the carrier and sample gases. They were not observed when argon was used for all the gases. When argon was used for the carrier gas, ions with mass 55, 73, 95, 113, 135 and 153 were observed which can be assigned the structures $H^+(H_2O)_n(Ar)_m$ with n = 3 and 4 and m = 0 to 2. It is clear from this result that the nitrogen adducts are formed in the reactor and that the nitrogen adducts are not CO adducts. Because CO has a dipole moment greater than argon, CO adducts should have been observed in the presence of the argon carrier gas.

Recorded in Table 3 are the amplitude ratios observed when purified air, and then argon, were used for the drift gas. While several of the ratios are larger for argon to indicate that larger clusters are formed in argon, this result may be due to differences in water content between the two gases. Experiments were not run with a known concentration of water introduced in both gases. While Zook and Grimsrud report extensive cluster

Table 2: Amplitude Ratio Between Various Reactant Ion Clusters

Positive Reactant Ions			Negative Reactant Ions		
Reaction	Lens Potentials		Reaction	Lens Potentials	
	High	Low		High	Low
$H^+(H_2O)_3 \rightleftharpoons H^+(H_2O)_4$	4.9	4.3	$O_2^- \rightleftharpoons O_2^-(H_2O)$	21	4.9
$H^+(H_2O)_4 \rightleftharpoons H^+(H_2O)_5$	0.06	0.09	$O_2^-(H_2O) \rightleftharpoons O_2^-(H_2O)_2$	1.6	1.9
$H^+(H_2O)_3 \rightleftharpoons H^+(H_2O)_3(N_2)$	0.69	0.78	$O_2^-(H_2O)_2 \rightleftharpoons O_2^-(H_2O)_3$	0.07	0.07
$H^+(H_2O)_3(N_2) \rightleftharpoons H^+(H_2O)_3(N_2)_2$	0.81	0.48	$O_2^-(H_2O) \rightleftharpoons O_2^-(H_2O)(N_2)$	0.29	0.34
$H^+(H_2O)_3(N_2)_2 \rightleftharpoons H^+(H_2O)_3(N_2)_3$	0.66	0.73	$O_2^-(H_2O)_2 \rightleftharpoons O_2^-(H_2O)_2(N_2)$	0.15	0.15
$H^+(H_2O)_4 \rightleftharpoons H^+(H_2O)_4(N_2)$	0.47	0.43	$O_2^-(H_2O)_2(N_2) \rightleftharpoons O_2^-(H_2O)_2(N_2)_2$	0.19	0.21
$H^+(H_2O)_4(N_2) \rightleftharpoons H^+(H_2O)_4(N_2)_2$	0.38	0.32	$O_4^- \rightleftharpoons O_4^-(H_2O)$	5.45	7.29
$H^+(H_2O)_4(N_2)_2 \rightleftharpoons H^+(H_2O)_4(N_2)_3$	0.20	0.21	$O_4^-(H_2O) \rightleftharpoons O_4^-(H_2O)_2$	0.71	0.82
			$O_4^-(H_2O)_2 \rightleftharpoons O_4^-(H_2O)_3$	0.07	0.05
			$O_4^-(H_2O) \rightleftharpoons O_4^-(H_2O)(N_2)$	0.37	0.43
			$O_4^-(H_2O)(N_2) \rightleftharpoons O_4^-(H_2O)(N_2)_2$	0.31	0.32

growth when analyzing higher water concentrations using an argon buffer gas, the current data cannot be used to either confirm or deny their results.[26] Certainly, Amirav et al. report that cooling increases in the order of Xe > Kr > Ar > Ne > He for jet expansions, a trend reflected in Zook and Grimsrud's data.[39]

Finally, the carrier gas flow was removed from the IMS cell and purified air was used for the drift gas. Since the drift gas exhausted through the reactor of the cell, the IMS cell was being totally purged with purified air. Next, the 13X scrubber in line with the purified air was reactivated and all fittings checked for leak tightness. When this was completed, the cell exhaust was drier than could be reliably measured with the hygrometer. Using estimation procedures described in the hygrometer manual, the water content of the exhausting air was probably on the order of 100 ppb. The positive and negative reactant ions collected for this condition are shown in Figure 6.

Immediately after the data of Figure 6 were collected, a 5 mm bore by 7.5 cm long diffusion tube of deionized water was placed in line with the drift gas line of the cell. This caused the water content of the gas exhausting from the cell to increase to 13.1 ppm. This hygrometer reading agreed with gravimetric measurements performed on the diffusion tube which indicated 12.0 to 13.4 ppm water was being added to the drift gas. When the water concentration stabilized, the IMS signatures of Figure 7 were collected. The effects of the increased water concentration were immediately obvious. In the positive ion mode, the amplitude ratio for the $H^+(H_2O)_4/H^+(H_2O)_3$ ions increased from 0.9 to 8.1 and in the negative ion mode, the amplitude ratio for the $O_2^-(H_2O)_2/O_2^-(H_2O)$ ions increased from 0.16 to 3.1. These amplitude ratios are shown in Table 4.

Table 3: Amplitude Ratios for Reactant Ion Clusters Using Two Drift Gases

Reaction	P.A. Drift Gas	Ar Drift Gas	Reaction	P.A. Drift Gas	Ar Drift Gas
$H^+(H_2O)_3 \rightleftharpoons H^+(H_2O)_4$	1.5	3.2	$O_2^- \rightleftharpoons O_2^-(H_2O)$	18.5	15.1
$H^+(H_2O)_4 \rightleftharpoons H^+(H_2O)_5$	0.05	0.07	$O_2^-(H_2O) \rightleftharpoons O_2^-(H_2O)_2$	0.32	0.79
$H^+(H_2O)_3 \rightleftharpoons H^+(H_2O)_3(N_2)$	0.92	1.0	$O_2^-(H_2O)_2 \rightleftharpoons O_2^-(H_2O)_3$	-	0.06
$H^+(H_2O)_3(N_2) \rightleftharpoons H^+(H_2O)_3(N_2)_2$	0.91	0.72	$O_2^-(H_2O) \rightleftharpoons O_2^-(H_2O)(N_2)$	0.19	0.63
$H^+(H_2O)_3(N_2)_2 \rightleftharpoons H^+(H_2O)_3(N_2)_3$	0.39	0.73	$O_2^-(H_2O)(N_2) \rightleftharpoons O_2^-(H_2O)(N_2)_2$	0.17	0.49
$H^+(H_2O)_4 \rightleftharpoons H^+(H_2O)_4(N_2)$	0.05	0.08	$O_2^-(H_2O)_2 \rightleftharpoons O_2^-(H_2O)_2(N_2)$	0.19	0.56
$H^+(H_2O)_4(N_2) \rightleftharpoons H^+(H_2O)_4(N_2)_2$	0.33	0.63	$O_4^- \rightleftharpoons O_4^-(H_2O)$	4.0	12.7
$H^+(H_2O)_4(N_2)_2 \rightleftharpoons H^+(H_2O)_4(N_2)_3$	0.24	0.26	$O_4^-(H_2O) \rightleftharpoons O_4^-(H_2O)_2$	0.12	0.55
			$O_4^-(H_2O)_2 \rightleftharpoons O_4^-(H_2O)_3$	0.12	0.54
			$O_4^-(H_2O) \rightleftharpoons O_4^-(H_2O)(N_2)$	0.30	0.50
			$O_4^-(H_2O)(N_2) \rightleftharpoons O_4^-(H_2O)(N_2)_2$	0.21	0.39

If it is assumed that the water clusters are in equilibrium and their concentrations are related to each other through previously measured thermochemical data, it is possible to estimate the water concentration in the IMS cell using the mass spectrometer data. This is done using the relationship

$$C_{H2O} = [I^\pm(H_2O)_{n+1}]/[I^\pm(H_2O)_n]\{\exp(\Delta G/RT)\}$$

where $[I^\pm(H_2O)_n]$ is the amplitude of the n-th ion cluster and ΔG is the free energy for

$$I^\pm(H_2O)_n + H_2O \rightleftharpoons I^\pm(H_2O)_{n+1}$$
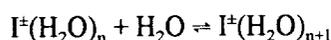
These estimates are also shown in Table 4.

Table 4 shows a large discrepancy between the calculated values and the actual value of 13 ppm. The calculated values obtained from smaller clusters underestimate the water concentration, while the calculated values obtained from larger clusters overestimate the water concentration. Efforts to adjust the values by raising or lowering the temperature or by including an extra energy term in the exponential were unsuccessful. If the thermochemical data are correct, it is apparent that the processes occurring behind the pinhole are complex and cannot be explained in terms of simple cooling or collisional dissociation.

DISCUSSION

Because it was shown that the lens potentials have little effect on ion distributions, the results of Table 4 must be

Table 4: Comparison of 13 ppm Water Concentration with Thermodynamic Values
Calculated from Peak Amplitude Ratios.*

Positive Reactant Ions			Negative Reactant Ions		
Reaction	Ampl Ratio	C_{H2O} (ppm)	Reaction	Ampl Ratio	C_{H2O} (ppm)
$H^+(H_2O)_2 + H_2O \rightleftharpoons H^+(H_2O)_3$	13	0.04	$O_2^- + H_2O \rightleftharpoons O_2^-(H_2O)$	30	0.37
$H^+(H_2O)_3 + H_2O \rightleftharpoons H^+(H_2O)_4$	8.1	54	$O_2^-(H_2O) + H_2O \rightleftharpoons O_2^-(H_2O)_2$	3.1	0.49
$H^+(H_2O)_4 + H_2O \rightleftharpoons H^+(H_2O)_5$	0.16	126	$O_2^-(H_2O)_2 + H_2O \rightleftharpoons O_2^-(H_2O)_3$	0.14	10
$H^+(H_2O)_5 + H_2O \rightleftharpoons H^+(H_2O)_6$	0.12	885			

* P. Kebarle, S.K. Searles, A. Zolla, J. Scarborough, M. Arshadi *J. Amer. Chem. Soc.* 1967, *89*, 6393; M. Arshadi, P. Kebarle *J. Phys. Chem.* 1970, *74*, 1483.

due to gas dynamics accompanying ion sampling. As mentioned in the introduction, the current accepted theory for the flow of gas through a 25 micrometer pinhole into vacuum is isentropic free-jet expansion.[40] Isentropic expansions are expansions in which the entropy remains constant and the various degrees of freedom (translation, rotation, vibration) of the gas remain in equilibrium.

Another characteristic of jet expansions is that there is a narrowing of the velocity distribution. This narrowing arises from those statistically favored molecules which have a velocity component in the direction of the expansion as they pass through the pinhole and from geometric channeling by the pinhole.[40] Accompanying the narrowing of the velocity distribution is a lowering of the temperature. As the temperature drops, so does the velocity of sound which leads to a change in conditions required to establish supersonic expansion.

For the present experiments, the linear air velocity through the pinhole was 179.3 m/s. While this velocity is significantly less than the standard velocity of sound in dry air (350 m/s), it does correspond to the velocity of sound at a reduced temperature and pressure. Assuming a square root dependence for the velocity of sound on temperature,[41] the required temperature is 26% of the standard temperature, or approximately 84 °C. To maintain isentropic conditions for the expansion, this temperature corresponds to a pressure of 26 Torr immediately behind the pinhole.

Assuming that supersonic expansion was occurring, it is possible to roughly locate the Mach disc. Theoretically, the location (x_M) is given by[42]

$$x_M = 0.67D[P_o/P]^{1/2}$$

where D is the pinhole diameter and P is the background pressure in the expansion chamber. Since the pinhole diameter was 25 microns and the background pressure was 1.8×10^{-4} torr, x_M was 3.4 cm. Because the distance between the pinhole and first focussing lens in the mass spectrometer was 4.2 cm, this location for the Mach disc was within the wire basket (see Figure 2) used to pull the ions towards the focussing lenses. If this is the case, then all the ions analyzed by the mass spectrometer had to pass through the Mach disc. The literature is undecided on what might happen to an ion cluster if this should occur.[22]

It turns out, however, that this may not be a problem because Miller notes that in a system were the background pressure is 10^{-4} and the stagnation pressure is atmospheric, "the continuum pressure just upstream of the Mach disc would be predicted to be $P_M \sim 10^{-9}$ torr, and the upstream mean free path about 25 cm!"[21] If this should occur, the mean free path would be greater than the 2.45 cm diameter for the wire basket, meaning the mean free path is much greater than the instrument dimension. Since shock wave thicknesses are on the order of the mean free path, it is doubtful that a Mach disc could form. For such a condition, a smooth transition from continuum to free-molecular flow would occur; the jet rays being attenuated by the background gas and surface reflected molecules in a Beer's Law like fashion. Hayes claims the expansion can be broken down into three distinct regimes: (1) continuum flow, (2) transition flow and (3) free molecular flow.[40]

The results of Table 4 show that when the ions participate in the expansion, there are opposing tendencies for cluster growth (as evidenced by the high concentration derived from the $H^+(H_2O)_5 + H_2O \rightleftharpoons H^+(H_2O)_6$ reaction) and desolvation (as evidenced by the low concentration derived from the $H^+(H_2O)_2 + H_2O \rightleftharpoons H^+(H_2O)_3$ reaction). In their studies Zook and Grimsrud observed similar tendencies.[26] They noted that the "MS$^-$ and M$^-$ ion density ratios *for dimethyl sulfoxide (DMSO)* were actually somewhat less than the expected ion intensity abundance ratio, suggesting that cluster growth due to a cooling effect in the aperture was not the dominant force in perturbing the ion distribution."[26] When describing their results using methane and nitrogen buffer gases, they claimed that "two opposing processes are operative within the jet expansions for the proton hydrates. One of these causes cluster growth, as evidenced by the prominent ions of n = 8 and the other leads to smaller clusters, as evidenced by the prominent ions at n = 4."

Zook and Grimsrud tried to interpret their data in terms of Searcy's kinetic model based on Buckle's suggestions for neutral clustering.[24,43] This model assumes that all radiative transitions have long time constants compared with collision frequency, and equilibrium is maintained by the following series of reactions.

increasing n (parallel three body and energetic cluster formation reactions),

$$H^+(H_2O)_n + H_2O + A \rightarrow H^+(H_2O)_{n+1} + A^*$$

$$H^+(H_2O)_n + H_2O \rightleftharpoons H^+(H_2O)_{n+1}{}^*$$

$$H^+(H_2O)_{n+1}{}^* + A \rightleftharpoons H^+(H_2O)_{n+1} + A^*$$
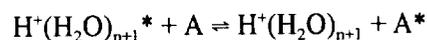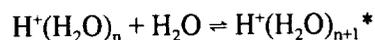
decreasing n (unimolecular decay),

$$H^+(H_2O)_n + A \rightleftharpoons H^+(H_2O)_n{}^* + A$$

$$H^+(H_2O)_n{}^* \rightarrow H^+(H_2O)_{n-1} + H_2O$$
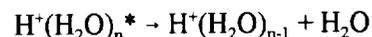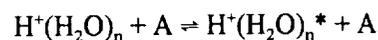
A is a third body and the asterisk indicates that a particle has sufficient energy to make it inherently unstable. While Zook and Grimsrud gave an excellent argument for cluster growth using this model, they realized that they needed another mechanism to explain the smaller-than-expected cluster ions. They proposed collisional dissociation even though they noted, similar to the results of Figures 3 and 4, that the cluster distributions were independent of the potentials applied to the focussing lenses.

Before expanding on this model, it is necessary to first note that cluster distributions can be distorted by instrumental effects in mass spectrometry. One of these is diminished ion transmission due to mass discrimination by the quadrupole filter; another is fragmentation of the cluster during its flight through the mass analyzer; and still another is fractionation of species as a result of different speed ratios perpendicular to the expanding jet.[44] The first two favor enhanced yields for lower molecular weight clusters, while the latter favors the sampling of higher molecular

weight clusters. In modern quadrupole mass spectrometers, adjustments can be and are made to minimize the effects of mass discrimination. On the EXTREL C50 mass spectrometer, this is accomplished using the "resolution" and "ΔM" controls. The cluster fragmentation and species fractionation processes, however, are beyond simple adjustments. Their effects can only be minimized by carefully selecting the original design used to construct the mass spectrometer.

To the extent that instrumental effects do not effect cluster distributions, gas dynamic mechanisms can be used to explain the results of Table 4. The most obvious feature for a gas expansion under isentropic conditions is that gas density and translational temperature decrease (except for local regions of supersaturation) with increasing distance from the nozzle.[44] In the continuum flow regime where equilibrium conditions are collisionally maintained, this means that ion cluster distributions are adjusting to decreasing water concentrations until the distribution is "frozen" by a lack of collisions. This "frozen" state will contain "smaller-than-expected" ion clusters if water concentrations in the source are used for calculations. Competing with this apparent desolvation mechanism is cluster growth precipitated by the reduced temperature created by the expansion. In terms of Buckle's model, this arises from the intermediate ion, $H^+(H_2O)_{n+1}$*, having a lower internal energy and having a longer lifetime within which it can be stabilized by collision with a neutral gas molecule.[26] Both processes depend upon the buffer gas used for the expansion. Heavier buffer gases will lead to slower expansions and lighter buffer gases will lead to faster expansions. There are more opportunities for the development of distortions in slow expansions than in faster expansions because more collisions are possible and the terminal translational temperature is higher. For faster expansions, reduced residence times may also minimize the effects expected for lower temperature. Consequently, Zook and Grimsrud found cluster distributions equivalent to equilibrium conditions when using a helium buffer gas.

CONCLUSIONS

Mass spectrometry is an invaluable tool in characterizing the ion composition of ion mobility peaks in ion mobility spectrometry. When the ion composition is found to be a mixture of ion clusters, the observed cluster distribution may not be an accurate representation of the ion clusters in the IMS. Depending on the buffer gas, lower clusters can form by equilibrating with reduced concentrations in the continuum regime of the expansion and larger clusters can form by collisional stabilization in the cooled jet stream. Besides water, nitrogen molecules can also add to the ion clusters created in ion mobility spectrometry. Even though nitrogen is non-polar, this addition is made possible by an ion-induced dipole interaction between the ion and molecule.

REFERENCES

1. Griffin, G.W., Dzidic, I., Carroll, D.I., Stillwell, R.N. and Horning, E.C. Ion Mass Assignments Based on Mobility Measurements: Validity of Plasma Chromatographic Mass Mobility Correlations. *Anal. Chem.*, **45**, 1204-1209 (1973).

2. Lin, S.N., Griffin, G.W., Horning, E.C. and Wentworth, W.E. Dependence of Polyatomic Ion Mobilities on Ionic Size. *J. Chem. Phys.*, **60**, 4994-4999 (1974).

3. Wessel, M.D. and Jurs, P.C. Prediction of Reduced Ion Mobility Constants from Structural Information Using Multiple Linear Regression Analysis and Computational Neural Networks. *Anal. Chem.* **66**, 2480-2487 (1994).

4. Revercomb, H.E. and Mason, E.A. Theory of Plasma Chromatography/Gaseous Electrophoresis - A Review. *Anal. Chem.* **47**, 970-983 (1975).

5. Mason, E.A. Ion Mobility: Its Role in Plasma Chromatography. In Plasma Chromatography, Carr, T.W., Ed. Plenum, NY, 1984, chapt. 2.

6. Spangler, G.E. and Lawless, P.A. Ionization of Nitrotoluene Compounds in Negative Ion Plasma Chromatography. *Anal. Chem.* **50**, 884-892 (1978).

7. Hagen, D.F. Characterization of Isomeric Compounds by Gas and Plasma Chromatography. *Anal. Chem.* **51**, 870-874 (1979).

8. Karpas, Z., Stimac, R.M. and Rappoport, Z. Differentiating Between Large Isomers and Derivation of Structural Information by Ion Mobility Spectrometry Mass-Spectrometry Techniques. *Int. J. Mass Spectrom. Ion Processes* **83**, 163-175, (1988).

9. Karpas, Z. Ion Mobility Spectrometry of Aliphatic and Aromatic Amines. *Anal. Chem.* **61**, 684-689 (1989).

10. Karpas, Z. The Structure and Mobility in Air of Protonated Ketones. *Int. J. Mass Spectrom. Ion Processes* **107**, 435-440 (1991).

11. Karpas, Z. and Pollevoy, Y. Ion Mobility Spectrometric Studies of Organophosphorus Compounds. *Anal. Chim. Acta* **259**, 333-338 (1992).

12. Karasek, F.W., Kim, S.H. and Rokushika, S. Plasma Chromatography of Alkyl Amines. *Anal. Chem.* **50**, 2013-2016 (1978).

13. McKeown, M. and Siegel, M.W. Atmospheric Pressure Ionization for Mass Spectrometry. *Amer. Lab.* **7**(11), 89-99 (1975).

14. Carroll, D.I., Dzidic, I., Horning, E.C. and Stillwell, R.N. Atmospheric Pressure Ionization Mass Spectrometry. *Appl. Spectros. Rev.* **17**, 337-406 (1981).

15. Preston, J.M. and Rajadhyax, L. Effect of Ion/Molecule Reactions on Ion Mobilities. *Anal. Chem.* **60**, 31-34 (1988).

16. Ashkenas, H. and Sherman, F.S. Experimental Methods in Rarefied Gas Dynamics. In Rarified Gas Dynamics, 4th Symposium, Vol. II, DeLeeuw, J.H., Ed. Academic Press, NY, 1966, p. 84.

17. Fite, W.L. Expansion of Gases from Molecular Beam Sources. Research Note #1, Extranuclear Laboratories, Inc., Pittsburgh, PA, 1971.

18. Fricke, J., Jackson, W.M. and Fite, W.L. Mass and Phase Spectrometry of a Water Vapor Jet. *J. Chem. Phys.* **57**, 580-582 (1972).

19. Mitchum, R.K. and Korfmacher, W.A. Atmospheric Pressure Ionization Mass Spectrometry. *Anal. Chem.* **55**, 1485A-1499A (1983).

20. Anderson, J.B. and Fenn, J.B. Velocity Distributions in Molecular Beams from Nozzle Sources. *Phys. Fluids* **8**, 780-787 (1965).

21. Miller, D.R. Free Jet Sources. In Atomic and Molecular Beam Methods, G. Scoles, Ed. Oxford Univ. Press, Oxford, England, 1988, chapt. 2.

22. Douglas, D.J. and French, J.B. Gas Dynamics of the Inductively Coupled Plasma Mass Spectrometry Interface. *J. Anal. At. Spectrom.* **3**, 743-747 (1988).

23. Searcy, J.Q. and Fenn, J.B. Clustering of Water on Hydrated Protons in a Supersonic Free Jet Expansion. *J. Chem. Phys.* **61**, 5282-5288 (1974).

24. Searcy, J.Q. A Kinetic Model for Clustering of Water on Hydrated Protons in a Supersonic Free Jet Expansion. *J. Chem. Phys.* **63**, 4114-4119 (1975).

25. Carlon, H.R. and Harden, C.S. Mass Spectrometry of Ion Induced Water Clusters: An Explanation of the Infrared Continuum Absorption. *Appl. Opt.* **19**, 1776-1786 (1980).

26. Zook, D.R. and Grimsrud, E.P. Measurement of Ion Clustering Equilibria of Proton Hydrates by Atmospheric Pressure Ionization Mass Spectrometry. *J. Phys. Chem.* **92**, 6374-6379 (1988).

27. Kambara, H. and Kanomata, I. Ionization Characteristics of Atmospheric Pressure Ionization by Corona Discharge. *Mass Spectrom.* **24**, 229-236 (1976).

28. Kambara, H. and Kanomata, I. Determination of Impurities in Gases by Atmospheric Pressure Ionization Mass Spectrometry. *Anal. Chem.* **49**, 270-275 (1977).

29. Kambara, H., Mitsui, Y. and Kanomata, I. Identification of Clusters Produced in an Atmospheric Pressure Ionization Process by a Collisional Dissociation Method. *Anal. Chem.* **51**, 1447-1452 (1979).

30. Spangler, G.E. and Carrico, J.P. Membrane Inlet for Ion Mobility Spectrometry (Plasma Chromatography). *Int. J. Mass Spectrom. Ion Phys.* **52**, 267-287 (1983).

31. Extrel Corporation, 240 Alpha Drive, Box 11512, Pittsburgh, PA 15238.

32. Spangler, G.E. Membrane Interface for Ion Mobility Detector Cells. U.S. Patent 4,311,699, The Bendix Corporation, Southfield, MI, January 1982.

33. New England Nuclear, 549 Albany Street, Boston, MA 02118.

34. Matheson Gas Products, 30 Seaview Dr., P.O. Box 1587, Secaucus, NJ 07096.

35. Balston, Inc., 260 Neck Rd., Haverhill, MA 01835.

36. W.R. Grace & Co., Davison Chemical Division, P.O. Box 2117, Baltimore, MD 21203.

37. Ametek, 455 Corporate Blvd., Pencador Corporate Ctr., Newark, DE 19702.

38. CRC Handbook of Chemistry and Physics, R.C. Weast, Ed. CRC Press, Boca Raton, FL, 1983.

39. Amirav, A., Even, U. and Jortner, J. Cooling of Large and Heavy Molecules in Seeded Supersonic Beams. *Chem. Phys.* **51**, 31-42 (1980).

40. Hayes, J.M. Analytical Spectroscopy in Supersonic Jets. *Chem. Rev.* **87**, 745-760 (1987).

41. Noggle, J.H. Physical Chemistry. Little, Brown and Company, Boston, MA, 1985.

42. Ashkenas, H. and Sherman, F.S. Experimental Methods in Rarefied Gas Dynamics. In Rarefied Gas Dynamics, 4th Symposium, Vol. II, J.H. de Leeuw, Ed. Academic Press, NY, 1966, pp. 89-91.

43. Buckle, R.E. A Kinetic Theory of Cluster Formation in the Condensation of Gases. *Trans. Faraday Soc.* **65**, 1267-1288 (1969).

44. Kappes, M. and Leutwyler, S. Molecular Beams of Clusters. In Atomic and Molecular Beam Methods, Vol. 1, G. Scoles, Ed. Oxford University Press, Oxford, 1988, chapt. 15.
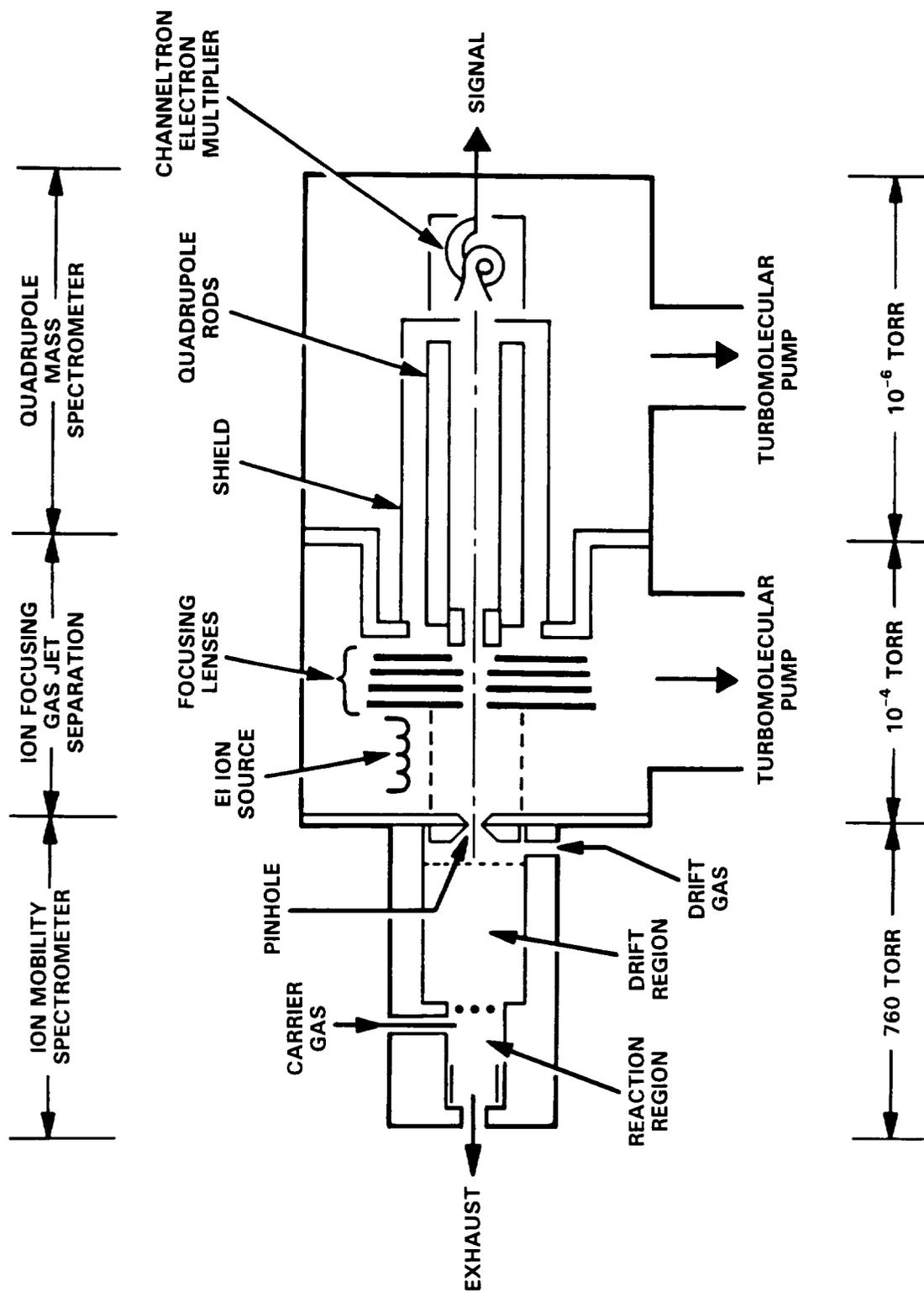
Figure 1. Functional Diagram for the Ion Mobility Spectrometer/Mass Spectrometer System.
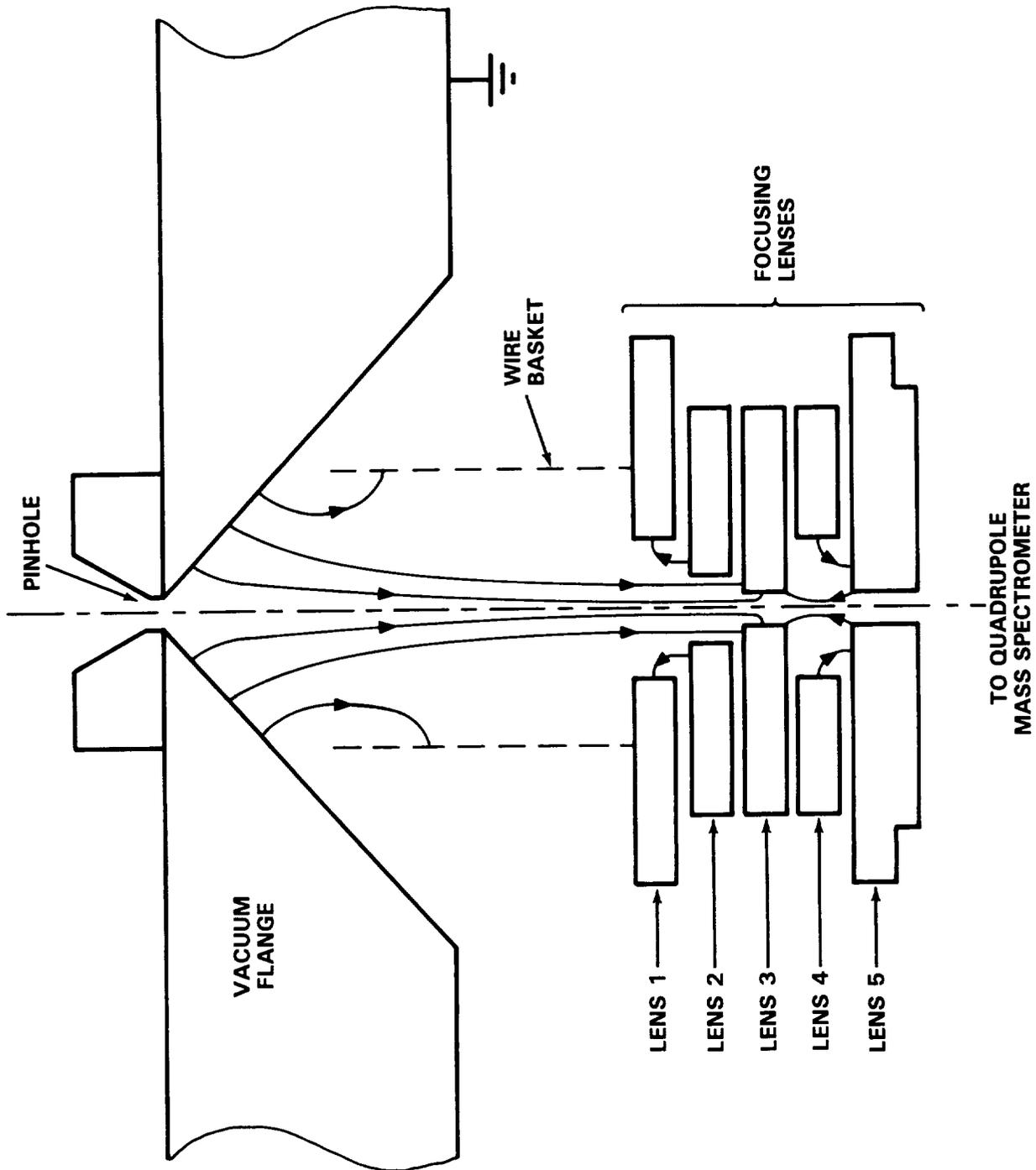
Figure 2. Expanded Sketch for the Pinhole Ion Sampler and Mass Spectrometer Focussing Lens Assembly.
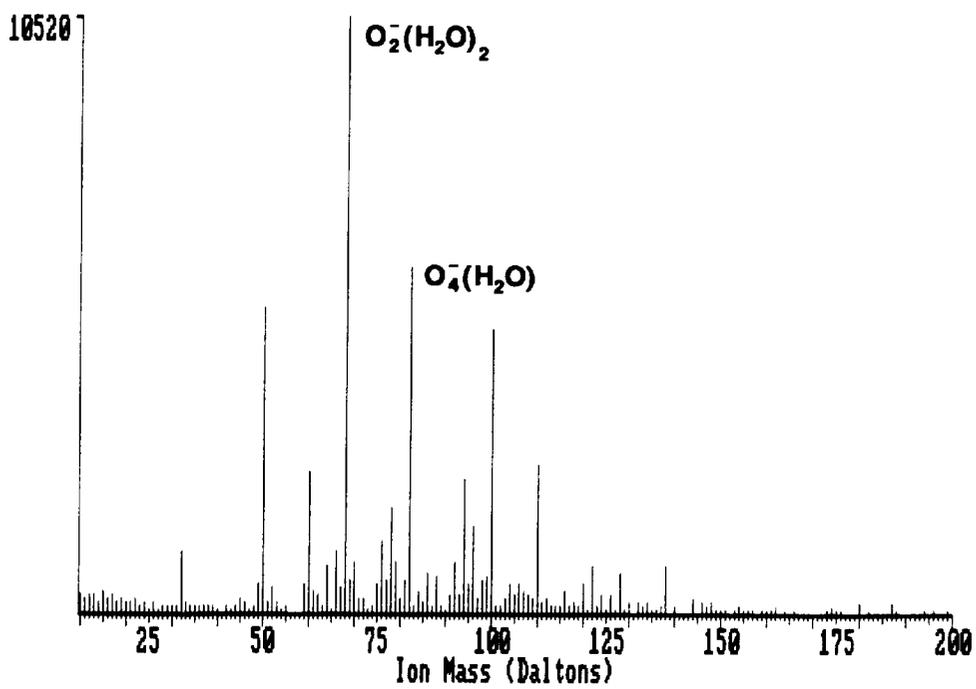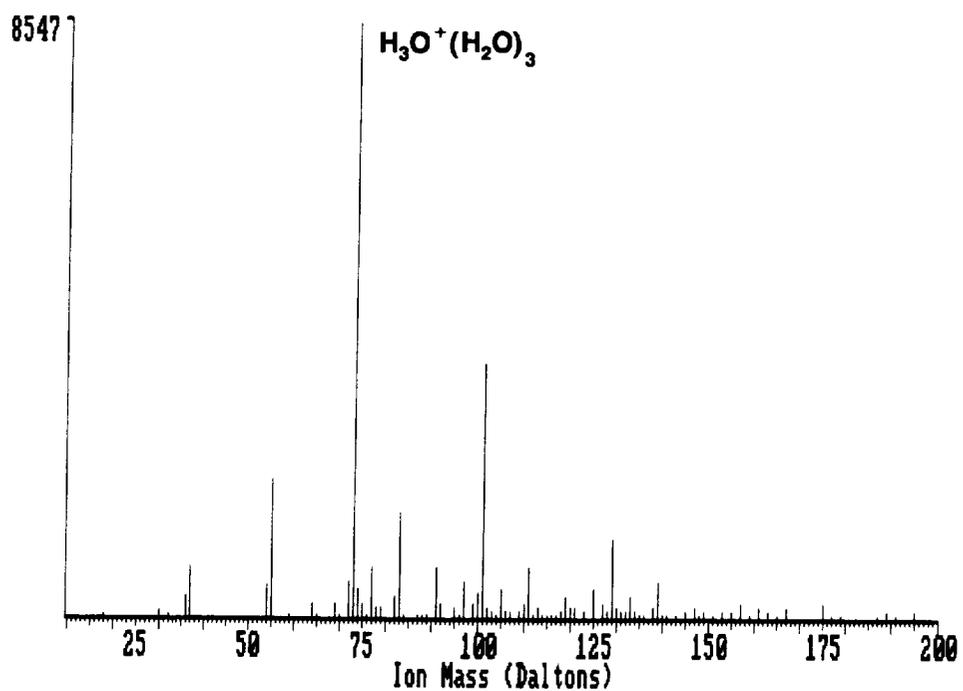
Figure 3. Positive (top) and Negative (bottom) Reactant Ions Using the Lower Voltages for the Ion Focussing Lens Assembly.
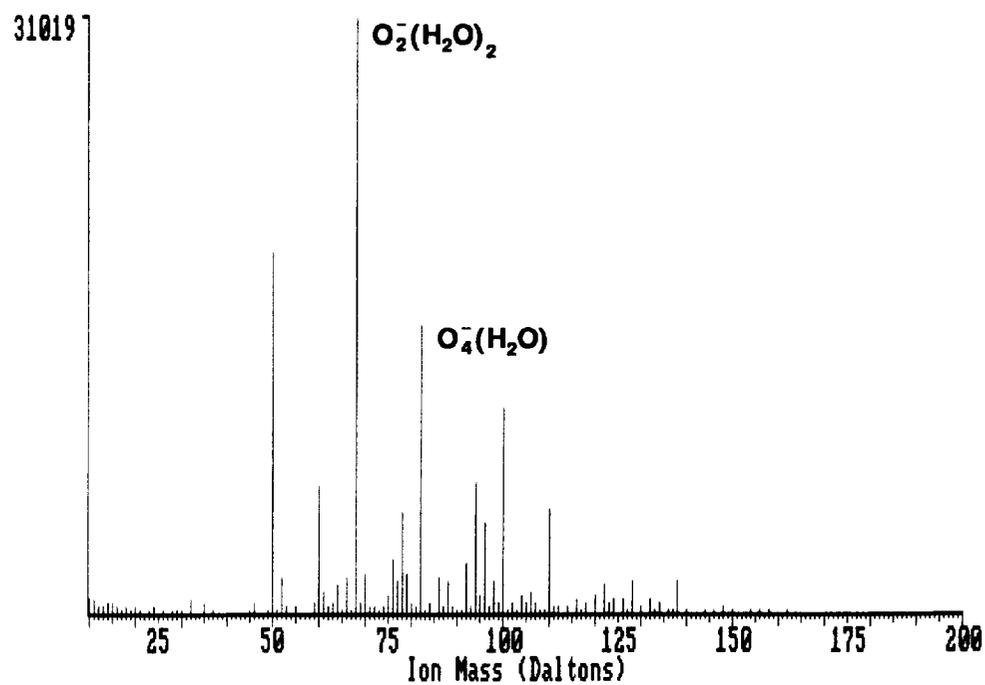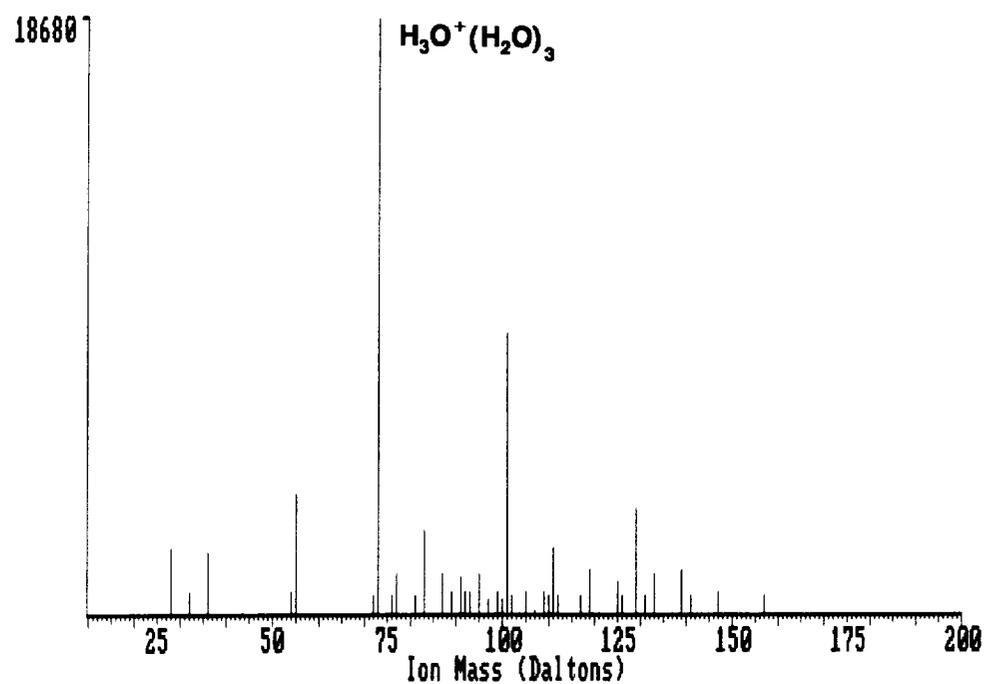
Figure 4. Positive (top) and Negative (bottom) Reactant Ions Using the Higher Voltages for the Ion Focussing Lens Assembly.

130
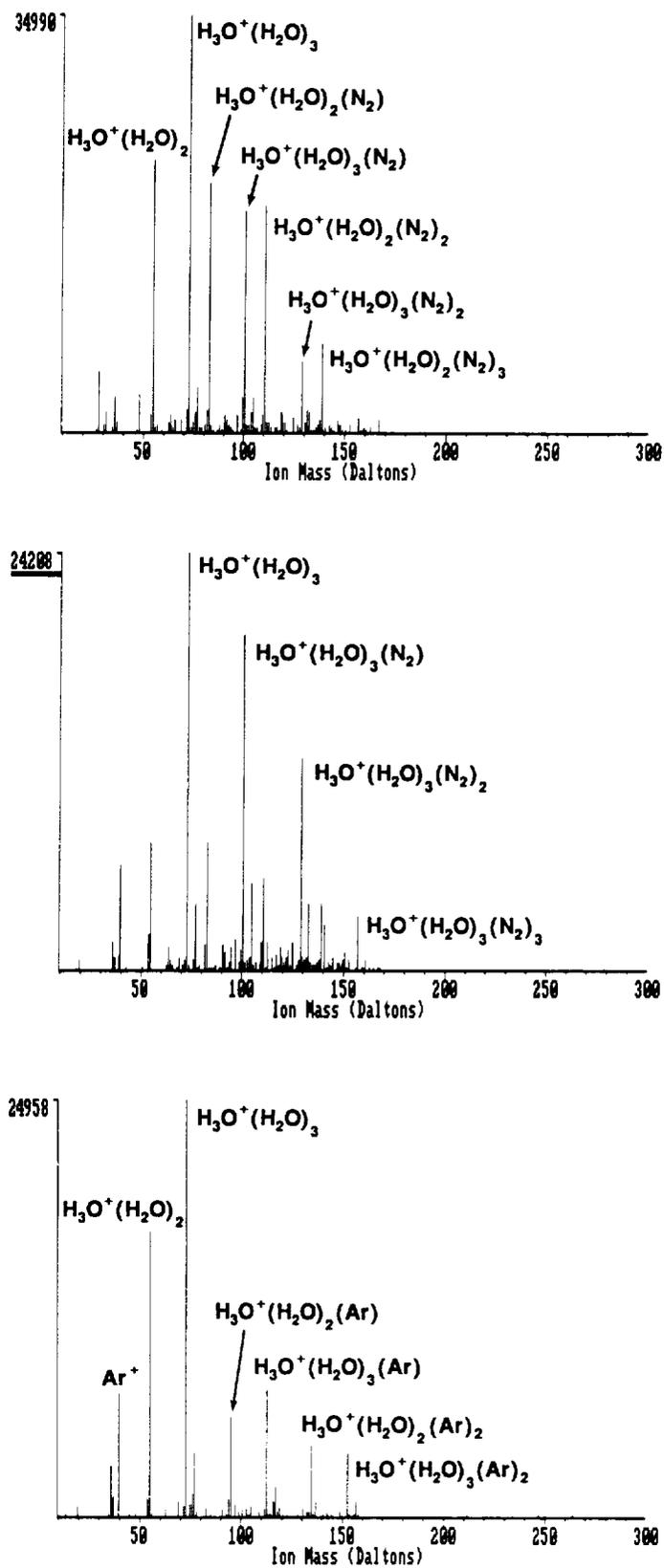
Figure 5. Positive Reactant Ions Using Purified Air for the Carrier, Drift and Sample Gases (top); Argon for the Carrier, Drift and Sample Gases (bottom); and Purified Air for the Carrier and Sample Gases and Argon for the Drift Gas (middle).

131
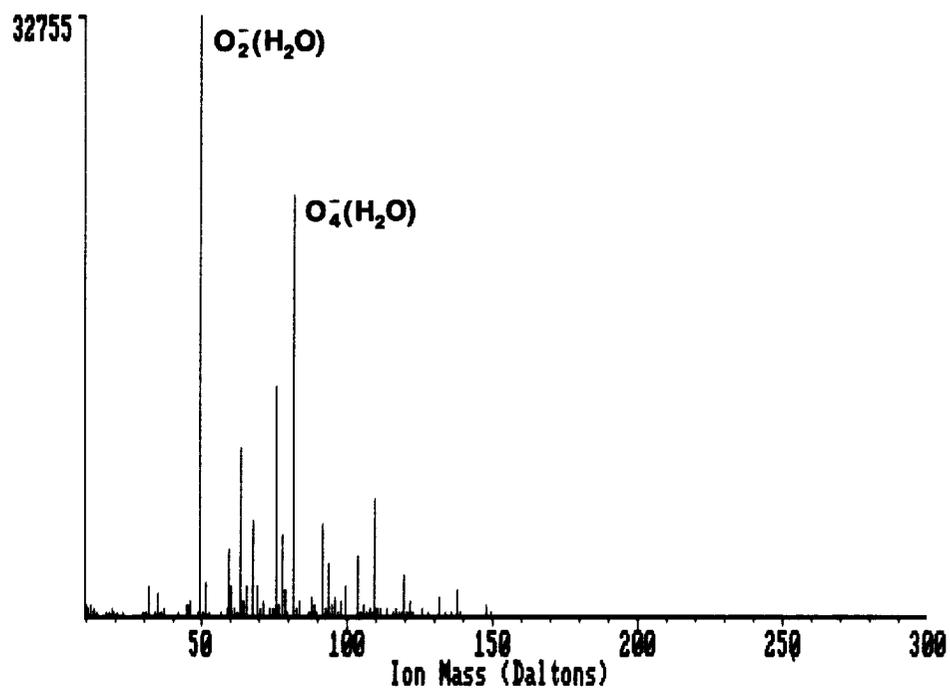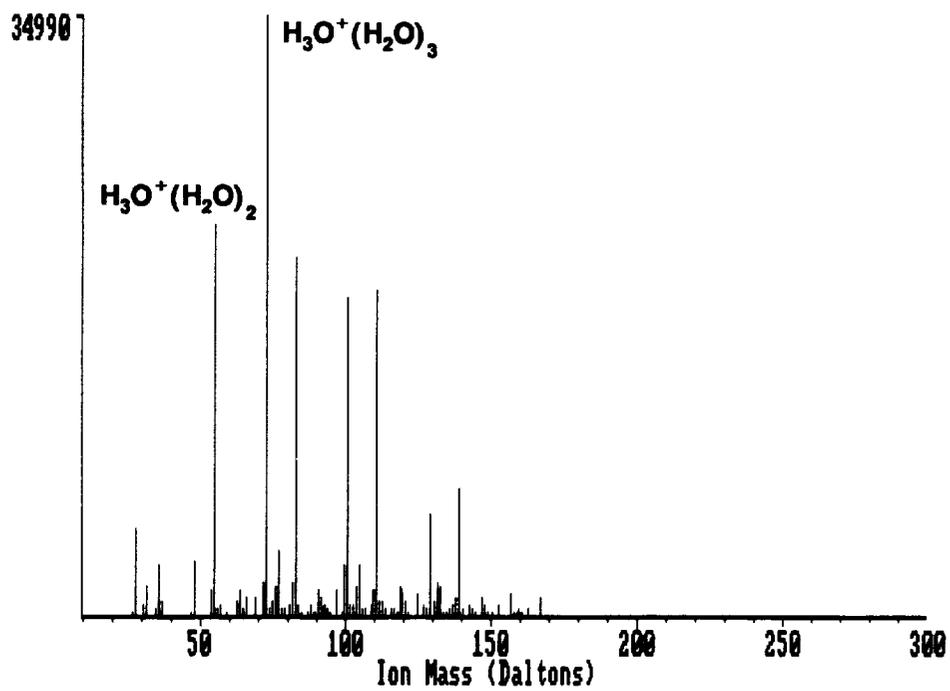
Figure 6. Positive (top) and Negative (bottom) Reactant Ions Before 13 ppm Water Introduced into the IMS.

132
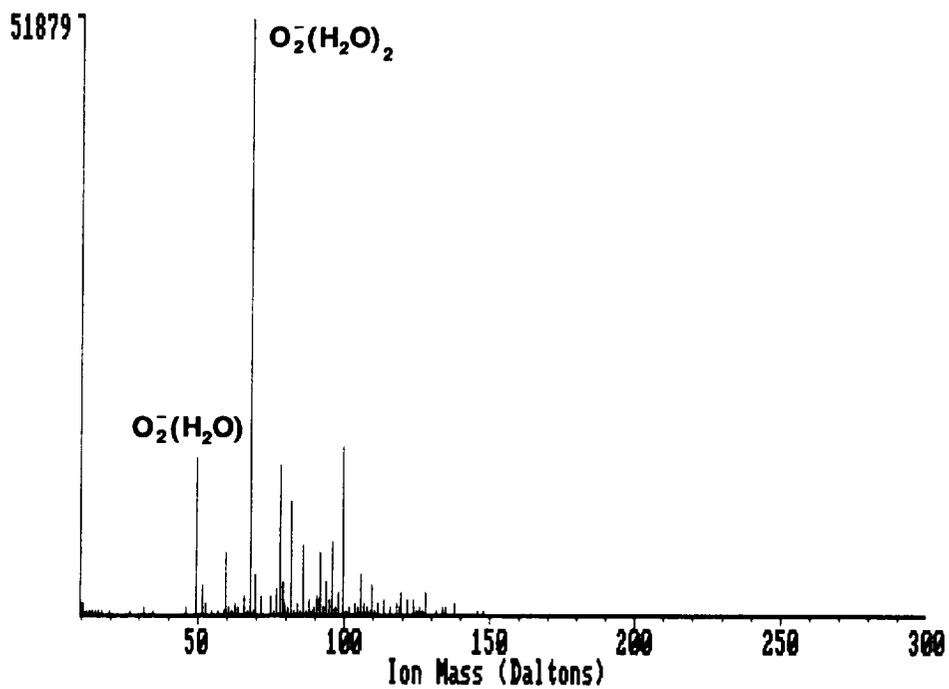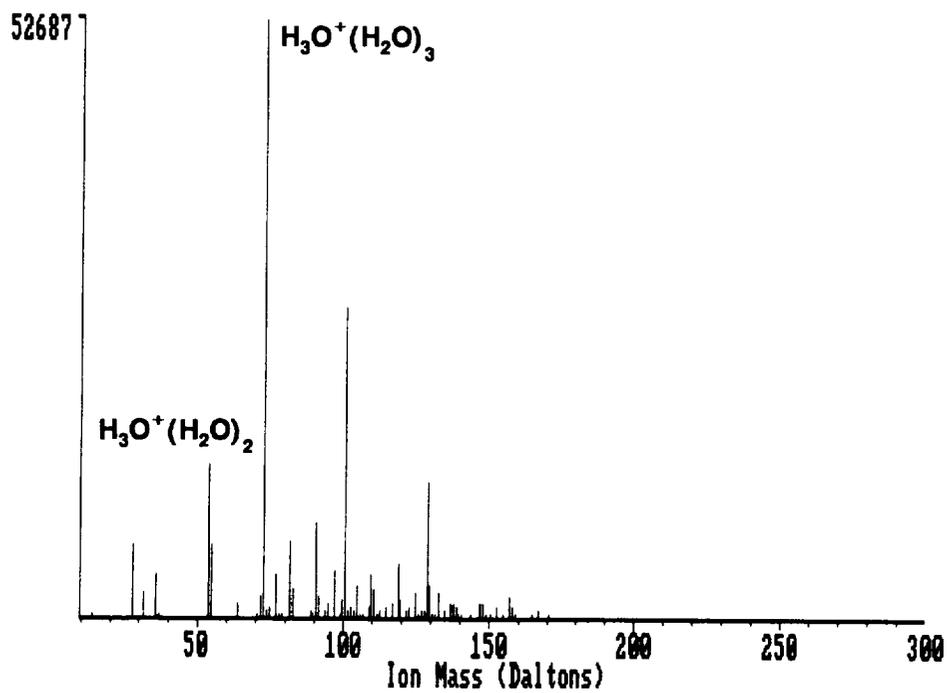
Figure 7: Positive (top) and Negative (bottom) Reactant Ions After 13 ppm Water Introduced into the IMS.

THE USE OF ION MOBILITY SPECTROMETRY AND GAS CHROMATOGRAPHY/MASS SPECTROMETRY FOR THE DETECTION OF ILLICIT DRUGS ON CLANDESTINE RECORDS.

Brian Donnelly, Ph.D., Thomas Jourdan, Ph.D., Dean D. Fetterolf, Ph.D.
and James O. Beasley, II, MPA
Federal Bureau of Investigation, Laboratory Division, Washington, D.C. 20535

INTRODUCTION

Illicit drug distribution has over the past decade grown tremendously from simple "drug pushing" where drugs were distributed from poorly organized individuals to today's well organized and well financed "drug cartels." This change to a more "corporate-like" atmosphere has resulted in a greater use of record keeping to monitor the profits generated. The use of record keeping by drug distributors is not restricted to high level drug smugglers but is used at all levels within the distribution network. Dealers at all levels including street dealers are generally "fronted," given on consignment quantities of drugs that they in turn sell to customers thereby requiring the need for records to keep track of drug sales versus liabilities. These records because of their illicit nature are often encrypted to hide the fact that they are indeed records of drug transactions.

The creation of a handwritten notation concerning a drug transaction is normally brought on because of a purchase or sale. In a sale, this is commonly accomplished through a consignment, or the designation of a quantity to a customer to whom that amount has been "fronted." Because this activity generates a debt, it follows that an accounting for payments made, as well as new transactions completed, is only logical. One of the most common means of representing these is through an "accounting flow," in which payments are subtracted from a running balance while new sales are added to it.

The examination of illicit drug records has been they key to the prosecution of numerous federal, state and local drug cases for a number of years. The Document Section of the FBI Laboratory, through its Racketeering Records Analysis Unit (RRAU), has been involved in such analytical efforts since 1983. Detailed analytical research brought about an evolution in the systematic approach utilized in the RRAU since that time. (1-3)

The close proximity of the drugs to the records often results in trace drug evidence being transferred to the records. The detection of trace drug residue on surfaces by ion mobility spectrometry (IMS) is well documented in the literature. Ion mobility spectrometry (IMS), first introduced by Cohen and Karasek in 1970 (4), is experiencing a resurgence of interest in specific purpose detection systems because of its analytical flexibility (5). A recent book thoroughly describes the fundamentals and applications of IMS (6). Forensic applications of IMS technology from 1970 to 1989 have been thoroughly reviewed by Karpas (7).

The probative value of IMS as an investigative and forensic tool is exemplified in recent applications which have included the detection of drug micro-particulates on hands (8,9), determining cocaine in injection molded plastic (10), and use in customs scenarios (11).

The following procedure will deal primarily with the newer techniques of trace drug analysis and drug record analysis developed by the Chemistry/Toxicology Unit of the FBI Laboratory since the more traditional techniques of latent finger print analysis and document analysis are well known.

EXPERIMENTAL PROCEDURE

Document Analysis:

The initial visual examination consists of studying the documents to determine if the notations thereon relate to the buying and/or selling of a product. Figure 1 shows a typical clandestine drug record. If the answer is yes, the procedure then calls for a closer look at the type of product involved. In the case of illicit drug records, the drug(s) are not normally identified, at least to the extent that a legitimate commodity would be. However, a relationship is often found between units and corresponding prices that may be consistent with certain quantities of illicit drugs. This relationship is one of the class characteristics of illicit drug records. If the weight can be decided, this may lead to the identification of the drug that is an example of an individual characteristic. Coded or abbreviated customer names (ref. to herein as "account designation"), partial dates, and lack of product and weight identifiers are all used to compare and contrast clandestine drug records with legitimate business records.

The relationships between and among various notations are frequently found mathematically. These relationships are then carefully studied, along with application of knowledge about how illicit drugs are bought and sold. For example, conversions from one weight system to another are accomplished through commonly applied formulas recognized in these examinations. The determination of the system used may also aid in the identification of the drug involved but often requires many numerical comparisons in order for a conclusion to be reached.

Besides numerical notations, slang terms, simple accounting terminology, as well as references to weights (grams, ounces, kilos, pounds, etc.) may provide clues as to the "flow" of quantities of drugs between supplier and distributor, between distributor and customer, or among employees of a drug business. These words or abbreviations commonly include "paid," "owed," "balance," "delivered," "returned," "profit," "expenses," "incoming," and "outgoing," usually in English or Spanish. Slang terms may aid in identification of the drug, and include references to the drugs ("pot," "weed," "rocks," "crank," "crack," etc.) or descriptive terms ("mold," "wet," "shake," etc.)

Class Characteristics. In maintaining illicit drug records, dealers frequently use 28 as the approximate number of grams in one ounce. Related conversions include 14 grams in 1/2 ounce, 7 grams in 1/4 ounce, 3.5 grams in 1/8 ounce ("eightball"), and 1.75 grams in 1/16 ounce. Multiples of 28 may suggest ounce equivalents in larger quantities, i.e., 56 grams in 2 ounces, 84 grams in 3 ounces, 112 grams in 4 ounces, etc. In even larger quantities, 224 grams equals 8 ounces (1/2 pound), and 448 grams equals 16 ounces (1 pound). One pound may also be suggested by the more accurate (though still not precise) equivalent of 453 or 454 grams. Such variations may be encountered even within the same set of documents.

In like fashion, the breakdown of kilogram weights into gram quantities is often made in easily recognized patterns. With 1,000 grams in a kilogram and 500 grams in 1/2 kilo, it follows that 1/4, 1/8, and 1/16 of a kilo could be recorded as 250, 125, and 62.5 grams respectively. Actually, these types of references are noted frequently in clandestine drug records.

In records of large-scale, multi-kilo cocaine distribution records, three general types of documents are often encountered. First, an inventory of incoming and outgoing kilos may provide a summary of the quantities received and distributed by the business over a specific period. Second, individual account pages show the debts incurred and payments made by various customers. Third, the business's cash ledger may show payments received from customers or employees as well as expenditures by the business. These may include office transportation and utility expenses as well as larger amounts deducted as payments to the business's cocaine supplier or for laundering purposes.

Individual characteristics. Sometimes the markings on kilo packages of cocaine (which serve as product identifiers, or brand names) are recorded as part of the inventory procedure. These may be studied for possible relationships between various search locations and links to seizures of cocaine or records seized in connection with previously unrelated investigations. These markings may consist of stickers, logos, symbols, or names (some common ones include "Rolex," "Baby," "Cartier," and "Leon.") Such specific indicators as these are examples of individual characteristics of illicit cocaine distribution records.

Marijuana records may detail inventories and distribution of hundreds or even thousands of pounds. Marijuana package weights in such documents often show pounds recorded to the left of a decimal point and ounces to the right. For example, 10 1/4 pounds might be expressed as "10.4" or "10.04." A determination that this is so might entail repeated checks of the computations noted to compare totals. If totals are in dispute, this may explain how the totals were calculated in ways unique to illicit marijuana distribution businesses.

Coded Records. Although illicit drug records are not always deliberately encoded, they often appear cryptic in nature. This is usually due to the absence of certain notations that would make them more meaningful. For example, writers often drop zeros in recording large amounts of money, possibly because including them is simply too cumbersome and time-consuming. Thus, $23,500 as a price for one kilo of cocaine might be written as "23.5." Mathematical proof that zeros have been dropped may be found when the writer mistakenly records the full notation, or through calculations made to show partial payments such as "$21,357."

In addition, simple substitution ciphers may be utilized by drug dealers or their bookkeepers. These are frequently based on 10-letter key words that contain no repeated letters. These may then be used to substitute for digits in telephone numbers or in the accounting records themselves. For example, the letters "M-O-N-E-Y-T-A-L-K-S" might be substituted for the numbers 1 through 9 and 0. Breaking such codes may be possible through mistakes made by the writer or through mathematical computations.

Instrumental Analysis

Ion Mobility Spectrometry. A sample to be examined is vacuumed using a standard vacuum with an attachment specifically designed to allow the collection of drug residue on a Teflon filter (4 micron mesh). Following the collection of the residue from the subject document the filter is removed from the vacuum and placed (see figure 2) into the sample holder in the Ionscan, an ion mobility spectrometer for analysis. Analysis is accomplished by heating of the filter at a temperature of 250 degrees Centigrade for four seconds to volatilize the analyte. Figure 3 shows a block diagram of the IMS. The analyte enters a chamber where ionization of the drug is accomplished under atmospheric conditions. The ions that are formed are then pulsed into at drift tube (see where they are separated in time and detected at the collector. Identification of a drug is determined by the time in milliseconds that an ion takes to transverse the drift tube in relation to an internal standard, nicotinamide that is analyzed simultaneously. The collection and display (see figure 4) of data are accomplished using a notebook computer linked to the Ionscan via an interface card.

Gas Chromatography/Mass Spectrometry. After a sample is determined to contain a drug the filter is again placed into the vacuum and the specimen in question is vacuumed a second time and the filter extracted with methanol. The extraction of the filter is accomplished by removing the filter from the filter holder and placing it into a small test tube. To the test tube is added approximately two milliliters of methanol and the test tube vortexed for thirty seconds. After vortexing of the sample the filter is removed and the methanol evaporated to dryness under a stream of nitrogen at sixty degrees centigrade. The resulting residue is reconstituted using fifty microliters of methanol and analyzed via GC/MS utilizing a Finnigan 4500 fitted with a six-foot 3% OV-17 and programmed from 60 to 270 degrees Centigrade at 25 degrees Centigrade per minute. The mass spectrometer is operated in the chemical ionization mode, using

methane as a reagent gas. Figure 5 shows the positive ion chemical ionization mass spectrum of cocaine.

Confirmation of cocaine is also accomplished through solid probe-tandem mass spectrometry. The cocaine residue is introduced into the ionization chamber through a direct solids' probe. The probe is heated from 0 to 300 degrees Centigrade at a rate of 100 degrees Centigrade per minute thereby volatilizing the cocaine and ionization in the presence of the reactant gas methane. The resulting M + 1 ion, m/z 304, is subsequently separated by the first quadrapole from the other ions formed. After separation the 304 m/z ion is accelerated and collided into argon gas in the second quadrapole causing fragmentation (daughter spectrum) which is detected in the third quadrapole. Figure 6 shows the daughter spectrum of cocaine.

CONCLUSION

It should be noted that forensic examinations of illicit drug records are made exclusively through comparison of all of the documents contained in a given submission taken as a whole. Isolating individual notations outside their contextual relationships to other notations in a group of documents may lead to difficulties in interpretation and severely limit the benefits to the investigating agency.

Forensic techniques of the types described above have been used effectively in many so-called "no-dope" conspiracy cases, and it is in these investigations that they can become the most important element of the prosecution. Expert testimony in this area has proven helpful in providing summaries of the activities of many illicit drug businesses as well as in describing the scope of such organizations, often in great detail. Coupled with other items of factual and circumstantial evidence, it can be a powerful tool for both investigators and prosecutors.

The analysis of the records themselves for traces of the drug being distributed lends further evidence that the notations determined by visual inspection are indeed records of drug transactions and not related to some other type of business records. The combination of these with other forensic techniques such as hair and fiber analysis, latent fingerprint analysis and traditional document analysis offer new techniques to combat the increasingly more sophisticated drug distribution networks.

REFERENCES

1. Jensen, C.J. The Forensic Analysis of Clandestine Drug Records. *Forensic Science International* **66**, 33-40 (1994).

2. Beasley, J.O. The Analysis of Illicit Drug and Money Laundering Records. *The Narc Officer*, October 1990.

3. Beasley, J.O. The Forensic Examination of Illicit Drug & Money Laundering Records, January/February 1992.

4. Cohen, M.J., Karasek, F.W. Plasma Chromatography - A New Dimension for Gas Chromatography and Mass Spectrometry. *J. of Chromatogr. Sci.* **8**, 330-337 (1970).

5. Hill, H.H., Siems, W.F., St. Louis, R.H., Ion Mobility Spectrometry. *Anal. Chem.*, **62**, 1201-1209 (1990).

6. Eicman, G.A. and Karpas, Z. Ion Mobility Spectrometry. CRC Press, Boca Raton, Fl, 1994, pp 148-149.

7. Karpas, Z., Forensic Applications of Ion Mobility Spectrometry. *Forensic Sci. Rev.* 1, 104-119, (1989).

8. Lawrence, A.H., Detection of Drug Residue on the Hands of Subjects by Surface Sampling and ion Mobility Spectrometry. *Forensic Sci. Int.*, 34, 73-78 (1987).

9. Nanji, A.A., Lawrence, A.H., Mikhael, N.Z., Use of Skin Sampling and Ion Mobility Spectrometry as a Preliminary Screening Method for Drug Detection in an Emergency Room. *Clin. Toxicol.*, 25, 501-515 (1987).

10. "Cocaine Smuggled as Ingredient in Plastic," *Chemical and Engineering News*, July 8, 1991.

11. Chauhan, M, Harnois, J., Kovar, J., Pilon, P., Trace Analysis of Cocaine and Heroin in Different Customs Scenarios Using a Custom-Built Ion Mobility Spectrometer. *Canadian Soc. of Forensic Sci. J.*, 24, 43-49 (1991).

Lunes

Ventas | **Dieta** | **Casa** | **Residuo** | **Entrega**

```
Ventas                          Dieta   Casa   Residuo    Entrega
7 = x 135    4½ = x 90                          12·5
4½ = x 103   6 = x 120          40     20       16         500
1 = x 20     45 x 900                           22         200
1½ = x 35    5 = x 100                          22         1,000
3 = x 60     1 = x 25                           13         400
1 = x 20                                        22         300
4 = x 100                                       22         500
2 = x 44                                        22         500
1 = x 25                                        22         900
14 = x 294                                      22
2 = x 44                                                   4,300
½ = x 11                                        217½       169
48 = x 1055                                     22
4½ = x 90                                       239½       4,469
2 = x 50
6 = x 120                        GRAMO
1 = x 25
2 = x 50     TOTAL              210
2 = x 50                        26
1 = x credito 4389             236
3½ = x 71
6 = x 115                                  Quedo 4f. vende x 26
2 = x 40
2.8 = x 560                                4f x 26.   martin
½ = x cash
X = x 12                                    quedo 16 + 1 f.
1 = x 25                                     comida 120
```

Figure 1. A typical clandestine drug record.
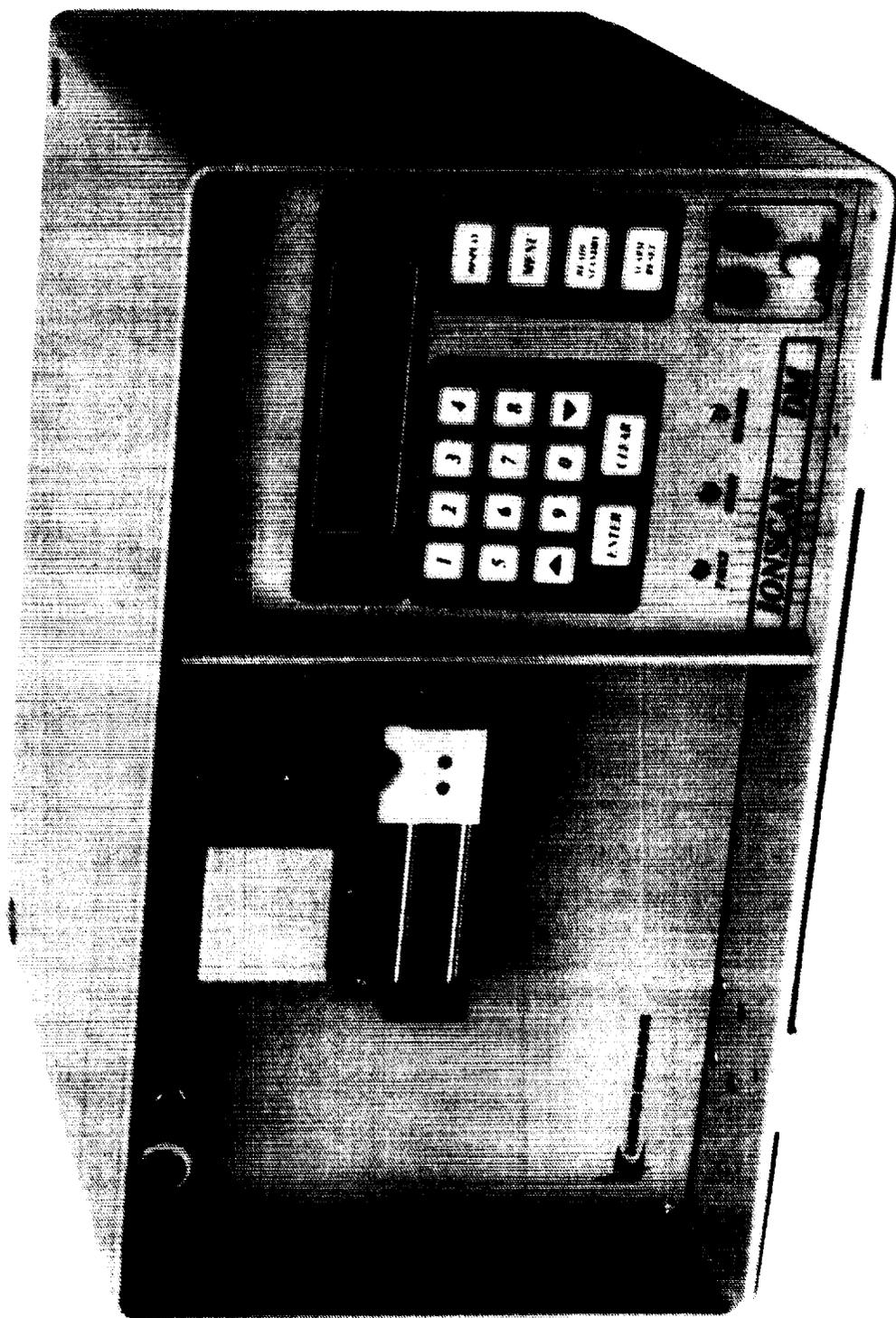
Figure 2. Photograph of the ion mobility spectrometer.
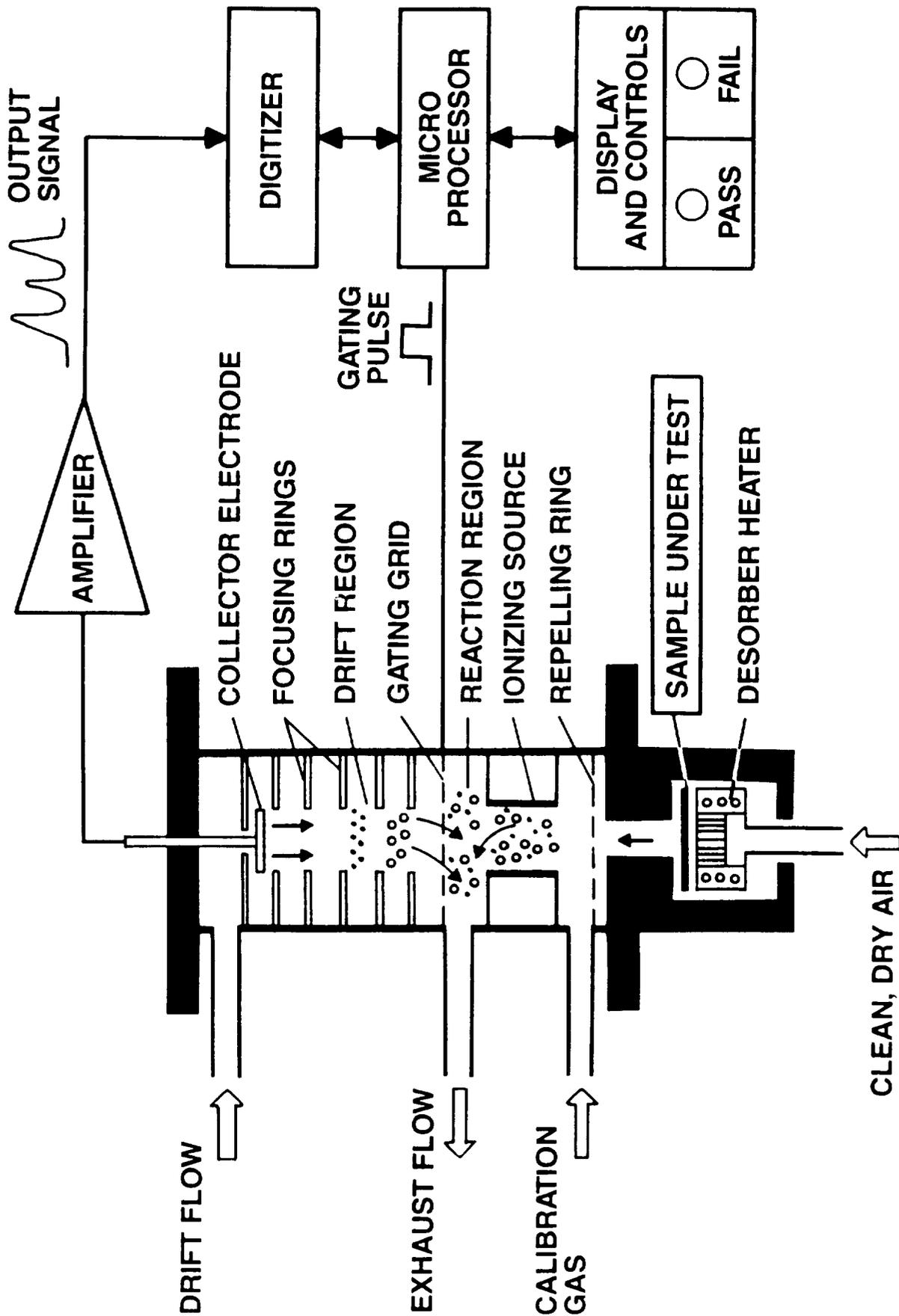
Figure 3. Block diagram of the ion mobility spectrometer.

141

Figure 4. Plasmagram showing the detection of cocaine.

1147 du
Winds: 1-14

Pk#	PeakID	Ko	DTime
0*	Cal	1.8725*	9.555
1	COCAINE	1.1600*	15.424 *
2	HEROIN	1.0407*	17.192
3	AMPH-S	1.6758*	10.677
5	METHAMPH	1.6431*	10.889
7	MDMA	1.4706*	12.166
8	THC	1.0475*	17.080
9	PROCAINE	1.3085*	13.673
10	PCP	1.2683*	14.107
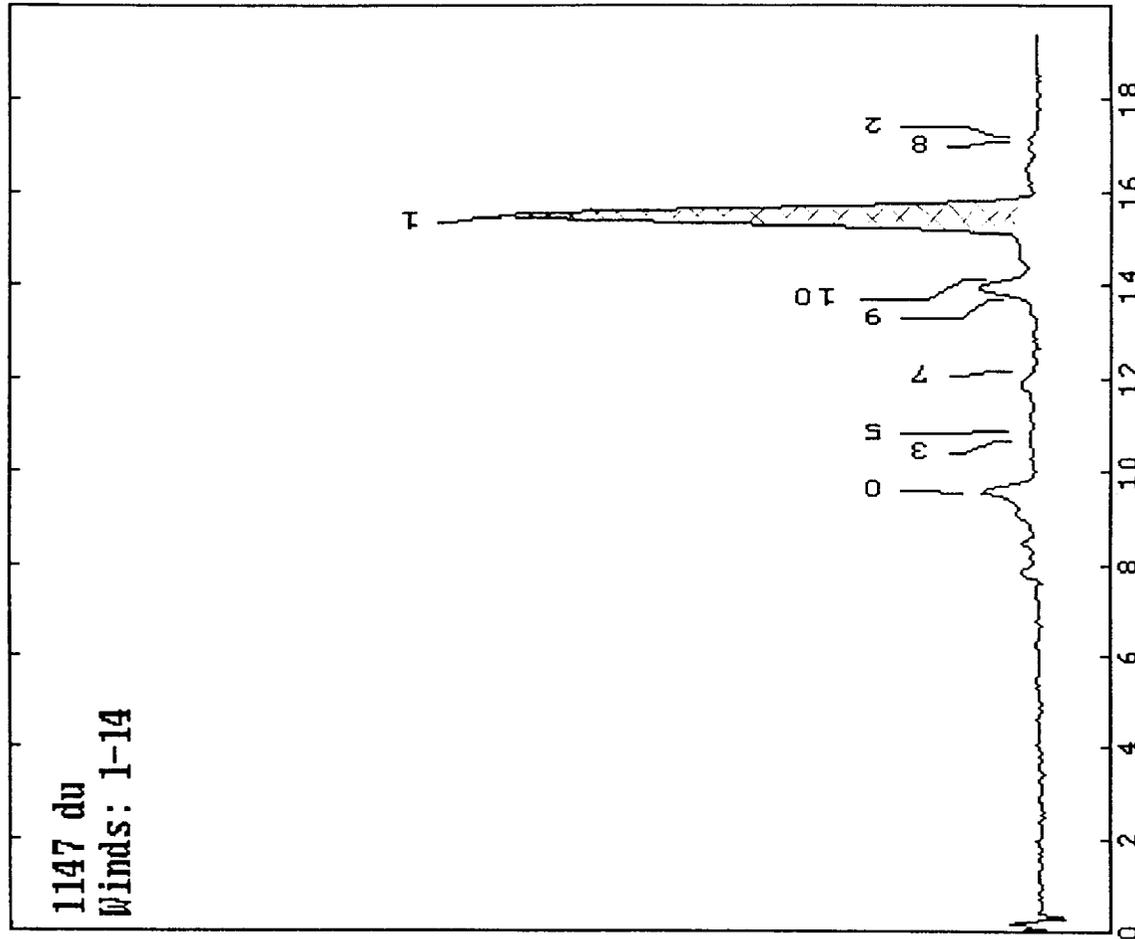
Ion Drift Time (ms) ———▶
Wnds: 14 Scans: 16 Pts: 776 Per: 25µs T: 20ms Alg: 0 Time: 23:05:27 10/14/90
Desc: Model 250-8391 Pos Mode; 235,295,296 degC; 300,200,494 cc/min;

Figure 5. Chemical ionization mass spectrum of cocaine.

Figure 6. MS/MS daugher ion spectrum of cocaine.

SPEC: EH ver 13 on UIC 002002   5-OCT-94 Elapse: 00:01:19** 71
Samp: COCAINE   Start : 15:09:37   85
Comm: STANDARD
Mode: CI +DAU 304.0 @ -15eV LMR SYNTH GAS UP LR   Inlet :
Oper: EH   Masses: 80 > 310
Base: 182.1   Inten : 1520884   # peaks: 79
Norm: 182.1   RIC : 3403998
Peak: 1000.00 mmu

144

HAND-PORTABLE GAS CHROMATOGRAPHY - ION MOBILITY SPECTROMETER FOR THE DETERMINATION OF THE FRESHNESS OF FISH

A. Peter Snyder, Charles S. Harden, Dennis M. Davis and Donald B. Shoff
U.S. Army Edgewood Research, Development and Engineering Center, Aberdeen Proving Ground, MD 21010-5423

Waleed M. Maswadeh
GEO-CENTERS, Gunpowder Branch, P.O. Box 68, Aberdeen Proving Ground, MD 21010-0068

ABSTRACT

A hand-held, portable gas chromatography-ion mobility spectrometer (GC-IMS) device was used to detect the presence of volatile amine compounds in the headspace of decomposing fish. The Food and Drug Administration (FDA) largely relies on olfactory discrimination with respect to fresh and spoiled, frozen and unfrozen fish. The fish are delivered at ship docks on pallets, and each pallet of fish can range from $30-40K in value. Fresh fish were placed in a teflon bag and the direct headspace was interrogated. In the first three days, only low molecular weight volatile amines were detected. On the fourth day, a number of spectral signatures were observed which indicated the presence of 1,5-diaminopentane, cadaverine. Analyses typically took from 0.5-1 minute.

INTRODUCTION

Recently, a hand-held device has been introduced which embodies two separate analytical stages for separation in the detection and identification of chemical species [1,2]. The first stage is a gas chromatograph (GC) and the second stage is an ion mobility spectrometer (IMS). This hand-held GC-IMS was shown to provide for the rapid (seconds to minutes) separation of a number of compounds belonging to different chemical classes including phosphoryl species, chlorophenols, ketones and aromatic amines. The concept was to take two analytical techniques, that have been mated in the laboratory since the early 1980's, and produce a GC-IMS system that could have potential as a field screening or environmental compound monitor. Thus, this system would be able to produce two separate, yet concurrent (or hyphenated), dimensions of information which has greater information content with respect to a one-dimensional or parallel instrumental arrangement.

GC is a widely used analytical technique and its fundamentals as well as its combinations with other instruments can be found in many places in the literature. IMS has shown a resurgence in popularity in the late 1980s and early 1990s and was the topic of a number of recent reviews [3,4] and a book on its fundamentals, theory and applications [5].

One of the charges of the U.S. Food and Drug Administration is to administer inspections of commercial catches of fish when they are delivered at dockyards and ship ports as well as in storage areas. A pallet of fish can cost over $30,000, and as such, inspections are performed on fresh and frozen fish in order to ensure that no spoilage of the seafood has taken place. Inspections routinely take the form of

organoleptic characterization, by inspectors who are trained to use their sense of smell for these purposes. This procedure can de-sensitize or overwhelm nasal discrimination in a very short time. A hand-held analytical instrument that could discriminate between fresh and spoiled fish would be a welcome tool for the FDA inspection personnel.

There are important characteristics that a hand-held instrument should have when considering that a person should be relatively unhindered and unencumbered when performing investigations of seafood quality in a dockyard scenario. Some of these include lightweight, portability (considered to be one-hand portability), ease of use, information production of the unit and speed of response.

A desirable characteristic of analytical instrument interrogation is where there is a minimal to negligible handling/processing of the sample. This is especially true for outdoor or away-from-the-laboratory situations. The literature shows that various classes of compounds have been investigated from fresh and decomposing fish for their degree of freshness and include saturated and unsaturated low and high molecular weight free fatty acids, aldehydes, ketones, mono- and polyamines, selected amino acids, alcohols and C_2-C_4 esters. The esters and carbonyl containing compounds appear to have utility as indicators of the freshness of fish in the long term (greater than 2 months) under frozen conditions [6]. However, in the short term, the only reliable chemical compound indicators have been the amine class of compounds that produce an odor [6, 7-9]. Virtually all investigations in the determination of the freshness of fish have utilized extensive processing and handling methods, culminating in the analyses of extracts and/or the chemical derivatization of extracts [10-13]. The few experiments that dealt with headspace of vapors entailed sparging homogenates [6,9] or steam distillation [14] of a sample of fish and directing the vapors onto the head of a GC column. The latter studies reported on non-amine compounds and the former provided no information on the identification of the volatile compounds.

The present study addressed the possibility of determining volatile biochemical markers with a hand-held, two-dimensional GC-IMS system from freshly caught fish. Volatile compounds were sought in order to alleviate for sample handling and processing procedures. Direct headspace was used in sampling for volatiles from the fish, and the mono- and di- amine classes of compounds were targeted.

EXPERIMENTAL

Gas Chromatography -Ion Mobility Spectrometry

A modified Environmental Vapor Monitor, EVM, (Graseby Ionics, Ltd., Watford, Herts, UK) was used (Figure 1). The EVM is comprised of a capillary gas chromatograph integrated with a hand-held ion mobility spectrometer, IMS [1,2]. The IMS operates with an internal sample gate repetition rate of 33 Hz. The gating pulse was 180 microseconds in duration and provided the trigger for the data collection. The modifications include the introduction of temperature and pressure sensors inside the IMS cell and the construction of a modular, easy-to-replace and disposable GC module with temperature programming. The modifications in the GC-IMS system were designed to allow a more complete separation, improved detection and identification of chemical compounds, increased ease of maintenance of the system, and a more robust hand-held detector. Typical experimental conditions used for the GC-IMS are shown in Table 1. Sample introduction to the GC column was accomplished by using an Automated Vapor Sampling unit (AVS) [15]. Conventional power supplies were used to provide power to the GC-IMS unit. The sample pulse was user controlled, with a range of 0.2 seconds to 20 seconds duration.

The IMS data was collected using an AT-MIO-16X multifunction I/O board (National Instruments Corporation, Austin, TX). The data collection algorithms for the GC-IMS were written using Labwindows

Software Version 2.2 (National Instruments, Austin, TX) in both C and QuickBasic programming languages. The programs were compiled using Microsoft C Version 5.1 and Microsoft QuickBasic as appropriate. The compiled versions of the software were then run under Microsoft DOS Version 6.0. Labwindows versions of the executable code were all created using the Labwindows Run Time System.

Gas Chromatography - Mass Spectrometry

A Finnigan-MAT Magnum GC-ion trap MS system was used to assist in confirmation of GC-IMS data. GC parameters were: 10 m DB-1, 0.25 mm ID, 0.25 um film thickness, 35-280°C or 50-280°C at 25°C/min column temperature. The GC value was splitless for the first one-half minute and then switched to split mode. The injector and transfer line were both set at 280°C.

Fish Samples

Fish (bluegill, perch) were caught from local streams (by DBS) and were placed in a teflon bag equipped with a septum sampling port. The headspace of the bag containing one or two fish was sampled periodically either directly by the GC-IMS or by injection of 1, 10 or 20 ul volumes into the GC-MS with a gas-tight syringe.

Standards

Chemical amine standards were purchased from either Aldrich (Milwaukee, WI) or Alfa (Ward Hill, MA).

RESULTS AND DISCUSSION

The decay of fish occurs in the form of different biological processes and as such produces different metabolic products. Two key processes are muscle and fat (rancidity) decay. Muscle decay produces monoamine and polyamine by-products and results from proteolysis caused by the decarboxylase enzymes in microorganisms. Fat decay (phospholipid oxidation) produces volatiles such as aldehydes, ketones, fatty acids and alcohols [10, 11, 16].

Monoamines

Currently, the presence of the amine class of decomposition analyte is the most reliable indicator of fish spoilage, because they correlate most closely with organoleptic (nasal) judgment of fish freshness. Very low molecular weight monoamines are known to be produced by muscle amino acid decay. In the various GC-IMS experiments, whether there was one or two fish in a teflon bag, headspace sampling of the volatiles at various intervals from 1-3 days produced spectra typical of that as shown in Figure 2. In addition to the water reactant ion peak (RIP), a mobility peak at shorter times was observed. This phenomenon is typical of low molecular weight amine compounds. Table 2 shows that compounds such as ammonia, dimethylamine and trimethylamine all have drift times in the 5.23-5.35 msec range, which is faster than the water RIP of 5.56 msec. They also have very short GC retention times on the order of 0.7 sec. Therefore, any or all of these compounds could comprise the 5.23-5.35 msec peak.

GC-MS analyses of the fish headspace confirmed this hypothesis. A representative total ion current (TIC) GC-MS profile of a headspace injection of fish volatiles is shown in Figure 3a. Essentially a broad air void volume and low molecular weight fish volatiles were found in the first minute and small amounts of column degradation silane products were found later in the run at temperatures greater than

170°C. The TIC of an equivalent volume of laboratory air injected into the GC-MS (Figure 3b) is very similar in appearance to that of the fish headspace (Figure 3a). Upon close inspection for low molecular weight amine compounds, Figure 4 shows relative intensities of m/z 40, 44 and 45. m/z 40 is that of the background atmospheric argon gas, and m/z 44, 45 are characteristic of dimethylamine. Note that m/z 40 is the base peak in the air blank mass spectrum while it is relatively lower in intensity with respect to m/z 44 and 45 in the fish samples. In other words, m/z 44 and 45 increase significantly with respect to m/z 40 in a fish headspace sample. Figure 5 shows a TIC of dimethylamine and note that it elutes in the same time frame as the air peak. Figure 6 shows a series of mass spectra. Figures 6a and 6b show pure dimethylamine and the fish headspace, respectively, from scan numbers 21-30 of the TIC in Figure 3a. Figures 6c-e are library compound mass spectra. N-methyl methanamine (dimethylamine) appears to give a good match (compare Figure 6a-b) while the low operating temperatures of the GC preclude decomposition of the silane phase coating to produce methysilane.

The possibility of the presence of trimethylamine was investigated. Figure 7 shows that the pure compound also elutes in the air background window of time and Figure 8a-d shows a series of mass spectra including pure trimethylamine and its library mass spectrum. Characteristic masses are m/z 58 and 59 in a roughly 2:1 intensity ratio, respectively. Figure 9 shows reconstructed ion chromatograms of m/z 58 and 59, with the approximate 2:1 ratio in the features between 20-40 sec. This ratio was a typical occurrence in the 21-30 mass scan number interval as shown in Figure 3a. However, the relative intensities of the peaks indicative of trimethylamine (Figure 9) are approximately 10-100 times lower than that of dimethylamine (Figure 4).

An enlargement of Figure 6b is shown in Figure 10 to indicate the relative intensities of m/z 44, 45, and 58, 59. If trimethylamine was present, it was only in very low quantities. It is possible that in the teflon bag-enclosed headspace, trimethylamine decomposed to dimethylamine.

Polyamines

The monoamine analysis was indicative of the sampled fish headspace in the 1-3 day timeframe. Polyamines also indicates fish spoilage and their appearance follows microbial muscle degradation and the deleterious organoleptic odor evaluations. Putrescine $NH_2(CH_2)_4NH_2$, cadaverine $NH_2(CH_2)_5NH_2$, spermidine $NH_2(CH_2)_4NH(CH_2)_3NH_2$, and spermine $NH_2(CH_2)_3NH(CH_2)_4NH(CH_2)_3NH_2$ are included among these compounds. Standard analyses with the GC-IMS are found in Table 2.

Table 3 presents a retention time and drift time summary on the fourth day of the fish volatile characterization study; a complete gas chromatogram - ion mobility spectrum is shown in Figure 11. The first IMS peak consists of the low molecular weight amines (5.20 msec drift time) as observed in the first three days of the study. A second set of ion mobility peaks elutes at a retention time of 5-7 sec with K_0 of 1.73 and 1.40 cm/V*sec. Table 2 shows that a standard cadaverine sample has a component that elutes at 7.14 sec with a K_0 of 1.73 cm/V*sec and Figure 12 shows a GC-IMS record of pure cadaverine (summarized in Table 2). There is a close match of the second eluting peak in Table 3 (peak marked "a" in Figure 11) to that of the peak marked "a" in Figure 12. The K_0 1.40 CM/V*sec peak from the second eluting compound in Table 3 was not observed in the cadaverine standard. The third and fourth eluting peaks in Table 3 were unidentified in that they did not match any of the suspected amine compounds in Table 3. Unfortunately, confirmation assistance of the fish headspace vapor by GC-MS did not take place because of instrumental failure. Later, another experiment with one fish in a teflon bag failed to show the information shown in Figure 11 in a one week time frame analysis, either by GC-IMS or GC-MS.

Despite the relatively high boiling points of the polyamines (up to 180°C) and the relatively low 126°C temperature limit of the column in the GC-IMS device, these compounds can elute from the GC and be observed by the IMS due to the short column length and relatively high flow rates.

CONCLUSIONS

The hand-held GC-IMS system was capable of detecting spoilage/decomposition amine compounds of fish stored at room temperatures in a teflon bag by sampling the headspace vapors over a period of one week. Volatile amines are the most indicative substances of fish spoilage. GC-MS confirmation of dimethylamine and trimethylamine was used to implicate their presence in GC-IMS experiments of fish stored at room temperature. Ion mobilities of these compounds fell in a drift time window which was faster than that of the RIP and were consistently present after the first day of fish decomposition. One GC-IMS experiment indicated the presence of cadaverine, among other unidentified compounds, that produced ion mobilities slower than that of the RIP and was observed at the fourth day of fish decomposition. This correlates with the observation that trimethylamine and volatile amine compounds appear to a relatively greater extent after the second day of fish storage under room temperature conditions [7].

Further experimentation needs to be done. For example, better characterization of the potential for hand-held GC-IMS utility in the determination of fish decomposition products would be to sample the headspace of containers with more than 2 fish, e.g. - 10-15 fish. This would be closer to actual conditions where pallets of fresh fish are routinely screened. This would necessarily increase the amount of analyte available in the vapor phase for instrumental monitoring.

ACKNOWLEDGEMENT

REFERENCES

1.   Snyder, A.P., Harden, C.S., Brittain, A.H., Kim, M.-G., Arnold, N.S. and Meuzelaar, H.L.C., *Anal. Chem.* **1993**, *65*, 299-306.

2.   Snyder, A.P., Harden, C.S., Brittain, A.H., Kim, M.-G., Arnold, N.S. and Meuzelaar, H.L.C., *Am. Lab.* **1992**, 32B-H.

3.   Hill, H.H., Jr., Siems, W.F., St. Louis, R.H. and McMinn, D.G., *Anal. Chem.* **1990**, *62*, 1201A-1209A.

4.   Eiceman, G.A., *Crit. Rev. in Anal. Chem.* **1991**, *22* (471-490).

5.   Eiceman, G.A. and Karpas, Z., Ion Mobility Spectrometry, CRC Press, Boca Raton, FL, 1994.

6.   Bencsath, F.A., Jester, E.L.E., Mowdy, D.E and McPhearson, R.M., Examination of Volatile Compounds in Fresh and Decomposed Oysters, Proceedings of the 42nd ASMS Conference on Mass Spectrometry, 1994, p. 45.

7.   Hillig, F., Shelton, L.R., Jr., Loughrey, J.H. and Eisner, J., *J. Assoc. Off. Anal. Chem*, **1958**, *41*, 763-776.

8.   Rosier, J. and Peteghem, C.V., *Z. Lebensm. Unters. Forsch.*, **1988**, *186*, 25-28.

9.   Przybylski, R., Eskin, N.A.M. and Malcolmson, L.J., *Can. Inst. Sci. Technol. J.*, **1991**, *24*, 129-135.

10.   Wood, G., Hintz, L. and Salwin, H., *J. Assoc. Off. Anal. Chem*, **1969**, *52*, 904-910.

11.   Staruszkiewicz, W.F., Jr. and Bond, J.F., *J. Assoc. Off. Anal. Chem.*, **1981**, *64*, 584-591.

12.   Yamamoto, S., Itano, H., Kataoka, H. and Makita, M., *J. Agric. Food Chem.*, **1982**, *30*, 435-439.

13.   Carlucci, F.V. and Karmas, E., *J. Assoc. Off. Anal. Chem.*, **1988**, *71*, 564-568.

14.   Dupuy, H.P., Legendre, M.G., Rayner, E.T., Grodner, R.M. and Novak, A.F., Instrumental Analysis of Volatiles in Seafood, Proceedings of the 3rd Annual Trop. Subtrop. Fish Technol. Conf. Am., **1978**, 354-358.

15.   Dworzanski, J.P., Kim, M.-G., Snyder, A.P., Arnold, N.S. and Meuzelaar, H.L.C., *Anal. Chim. Acta*, **1994**, *293*, 219-235.

16.   Yen, G.-C. and Hsieh, C.-L., *J. Food Sci.*, **1991**, *56*, 158-160.

TABLE 1
EXPERIMENTAL OPERATING CONDITIONS OF THE GC-IMS

Disposable GC Module:

GC Column:

	Liquid Phase:	DB-1 (0.25 micrometer)
	Temperature (°C):	45°C/min programmable
	Carrier Gas:	Clean dry air
	Flow Rate:	2.1 ml/min
	Length:	1 m
	Sample injection:	0.2 sec
	AVS unit:	90°C

Ion Mobility Spectrometer:

Ionization Source:	^{63}Ni
Gating Pulse Repetition Rate:	30 Hz
Cell Temperature:	30°C
Cell Pressure:	640 torr
Drift Gas:	Clean dry air
Drift Gas Flow:	400 ml/min
Positive Mode	

TABLE 2
GC retention times and ion mobility values of various amines,
Drift Time of the RIP was 5.56 msec

K_0 relative to 2,4-Lutidine at $K_0 = 1.95$ cm^2/V*sec

Chemical Name	MW	bp°C	R.T. (sec)	t_{Drift}	K_0
Ammonia NH$_3$	17	--	.7-.8	5.23	2.20
Dimethylamine	45	7	.7-.8	5.35	2.15
Trimethylamine	59	3	0.71	5.27	2.19
Diethylamine	73	55	1.1	5.78	1.99
Diisopropylamine	101	84	1.3	6.07	1.90
Butylamine	73	78	1.37	6.26	1.84
1,4 Diaminobutane; putrescine	88	160	1.32	6.36	1.81
1,3 Diaminopropane	74	140	2.8	6.65	1.73
1,5 Diaminopentane; cadaverine	102	180	1.54	6.35	1.81
			3.46	5.93	1.94
				7.05	1.63
			7.14	6.68	1.73
			13.1	6.13	1.88
				7.68	1.50
2,4 Lutidine	107	159	7.2	5.91	1.95
				7.57	1.52

153

TABLE 3
GC retention times and ion mobility values of
a head space sample of two, 4-day old fish
Drift time of the RIP was 5.55 msec

K_0 relative to 2,4-Lutidine at $K_0 = 1.95$ cm^2/V*sec

Fish component	R.T. (sec)	t_{Drift}	K_0
#1	0.71	5.20	2.22
#2	5-7	6.65	1.73
		8.23	1.40
#3	7-8.5	5.88	1.96
		7.58	1.52
#4	21.5-22.5	6.80	1.69
		7.31	1.58

154
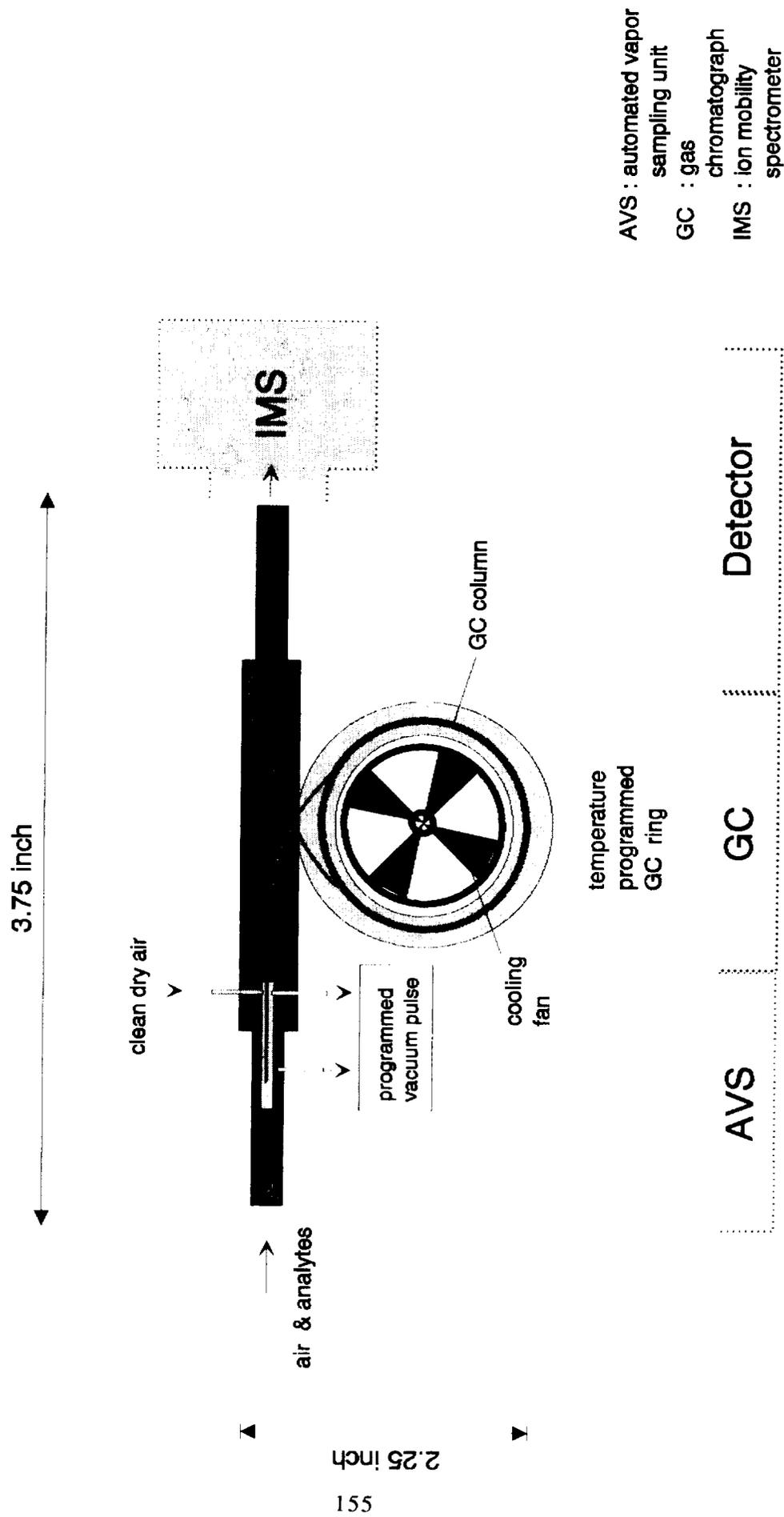
Figure 1. Schematic of the improved GC-IMS device.

AVS : automated vapor
      sampling unit
GC : gas
      chromatograph
IMS : ion mobility
      spectrometer

155
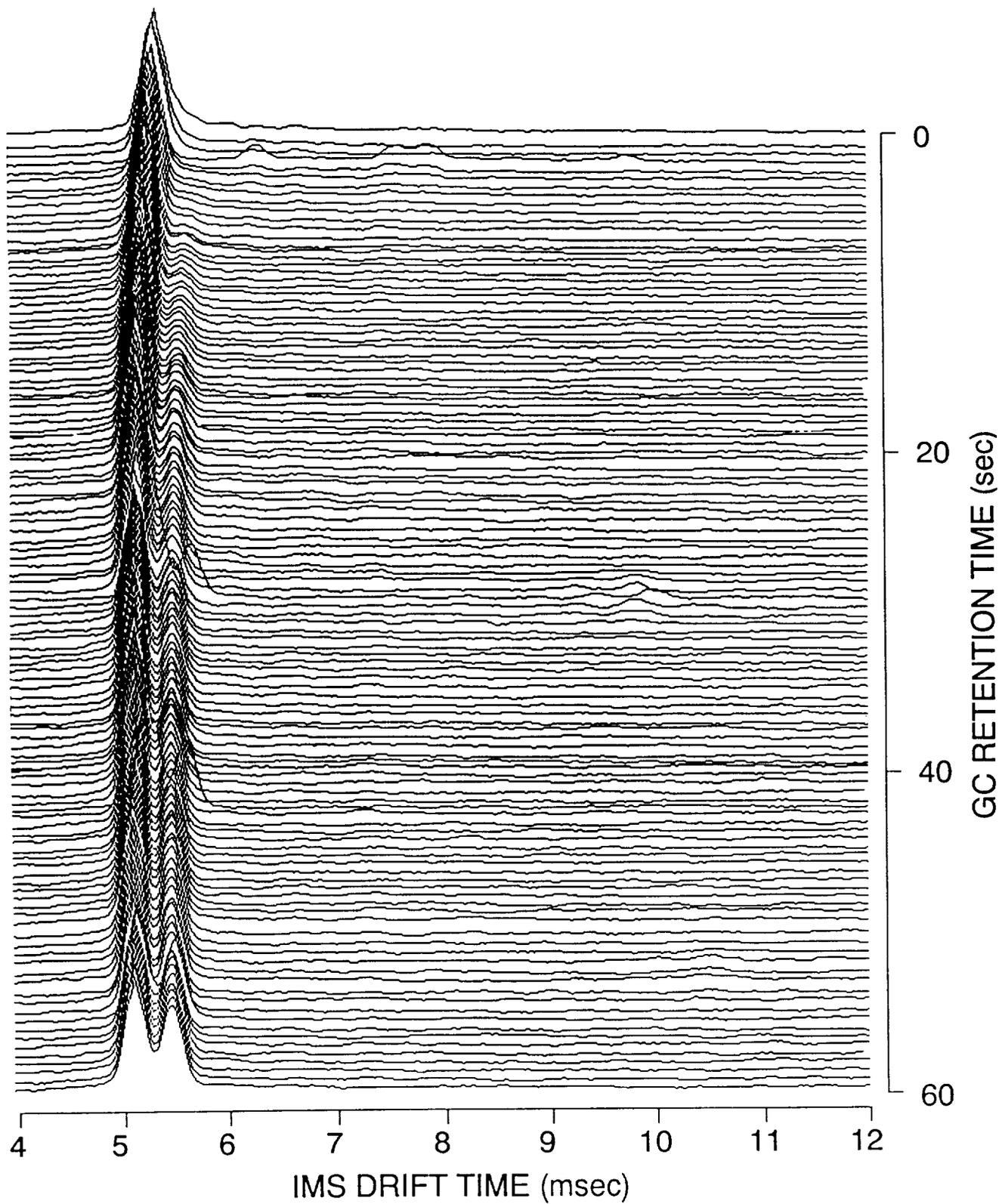
Figure 2. GC/IMS chromatogram of the headspace of a 3-day old fish sample in a teflon bag. Note the faster volatile amine drift time (5.14 msec) with respect to the water RIP (5.47 msec).
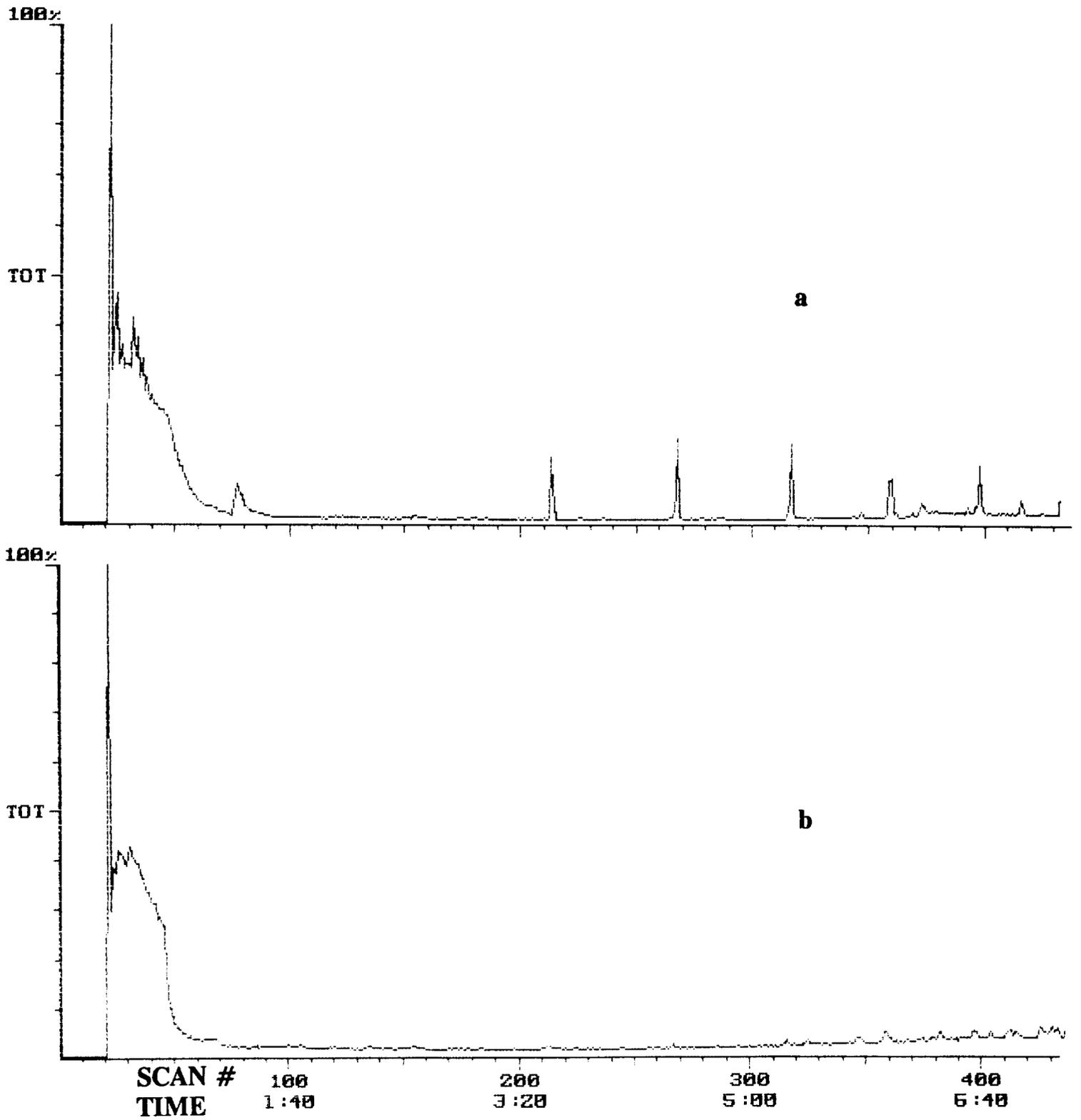
Figure 3. GC-MS TICs of (a) fish headspace and (b) air blank.
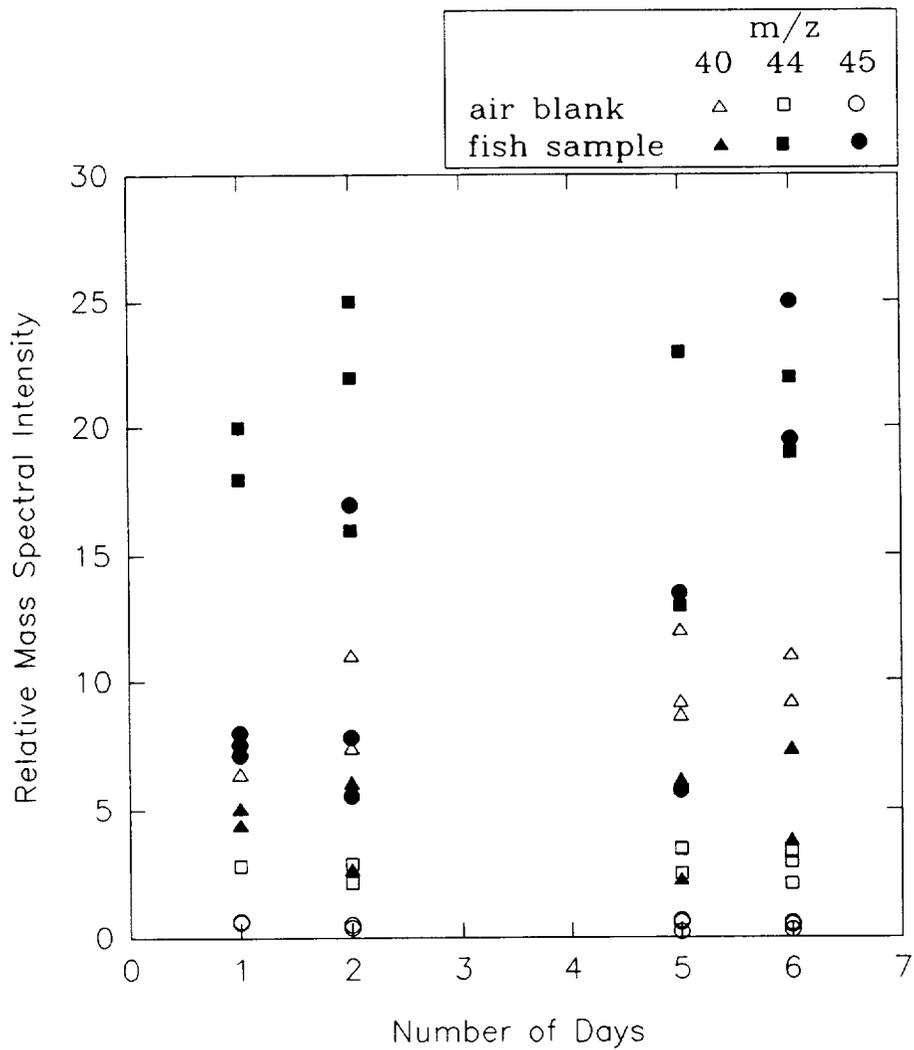
Figure 4. Graph of the maximum value of the reconstructed ion currents of m/z 40, 44 and 45 in air blank and fish headspace GC-MS analyses.
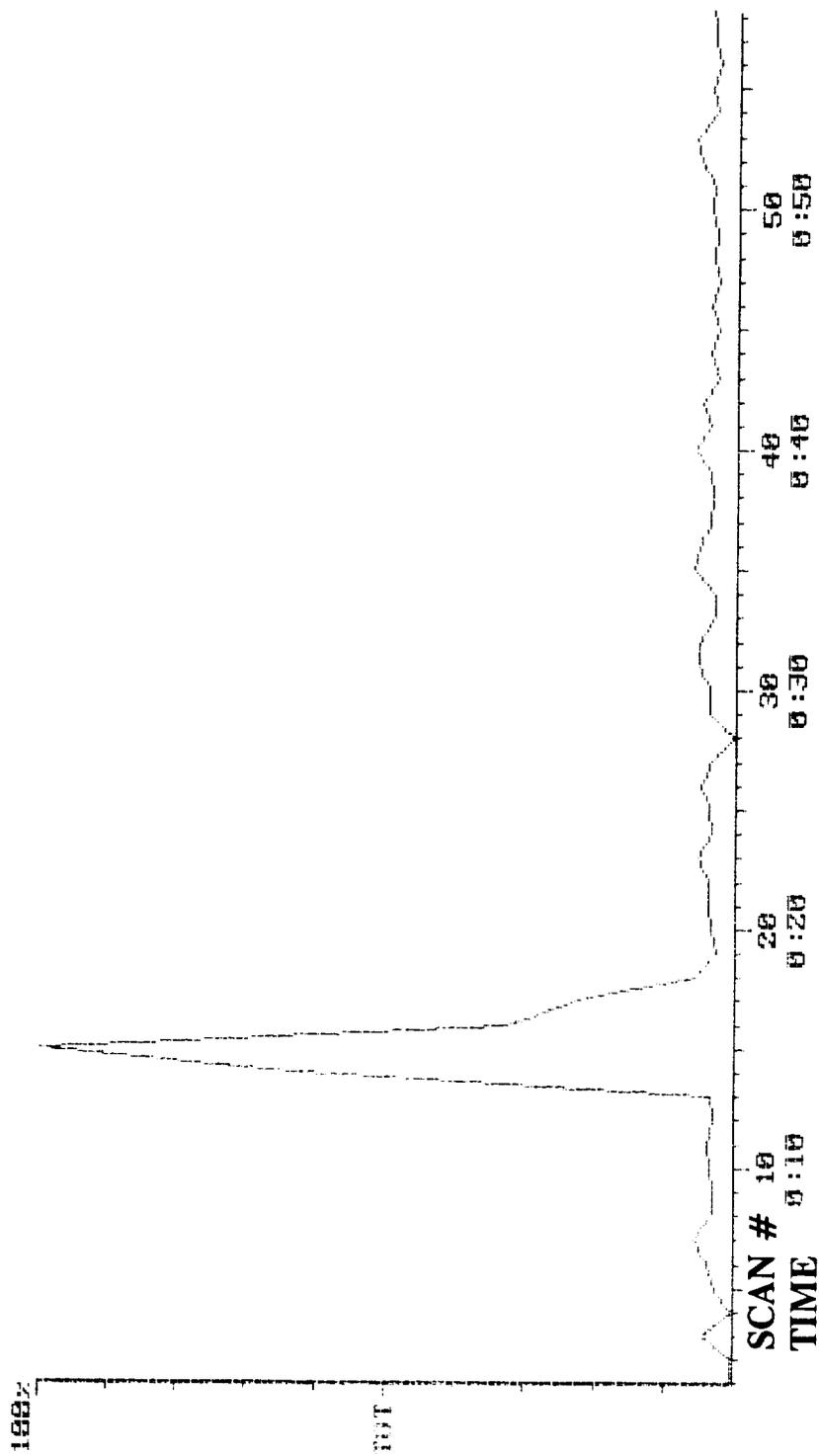
Figure 5. GC-MS TIC of pure dimethylamine.

159
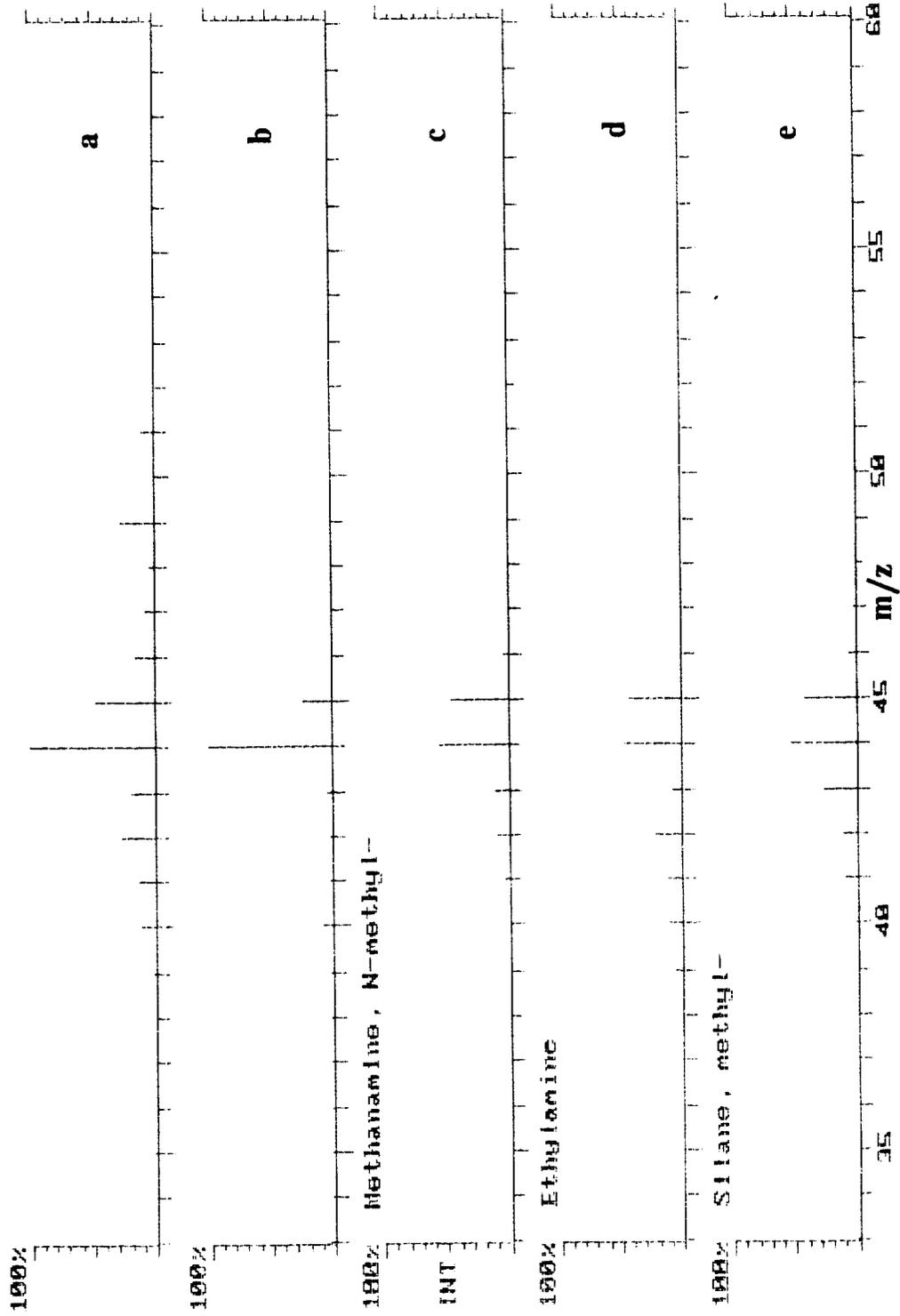
Figure 6. Mass spectra of (a) pure dimethylamine, (b) fish headspace and library mass spectra of (c) N-methylmethanamine, (d) ethylamine and (e) methylsilane.

160
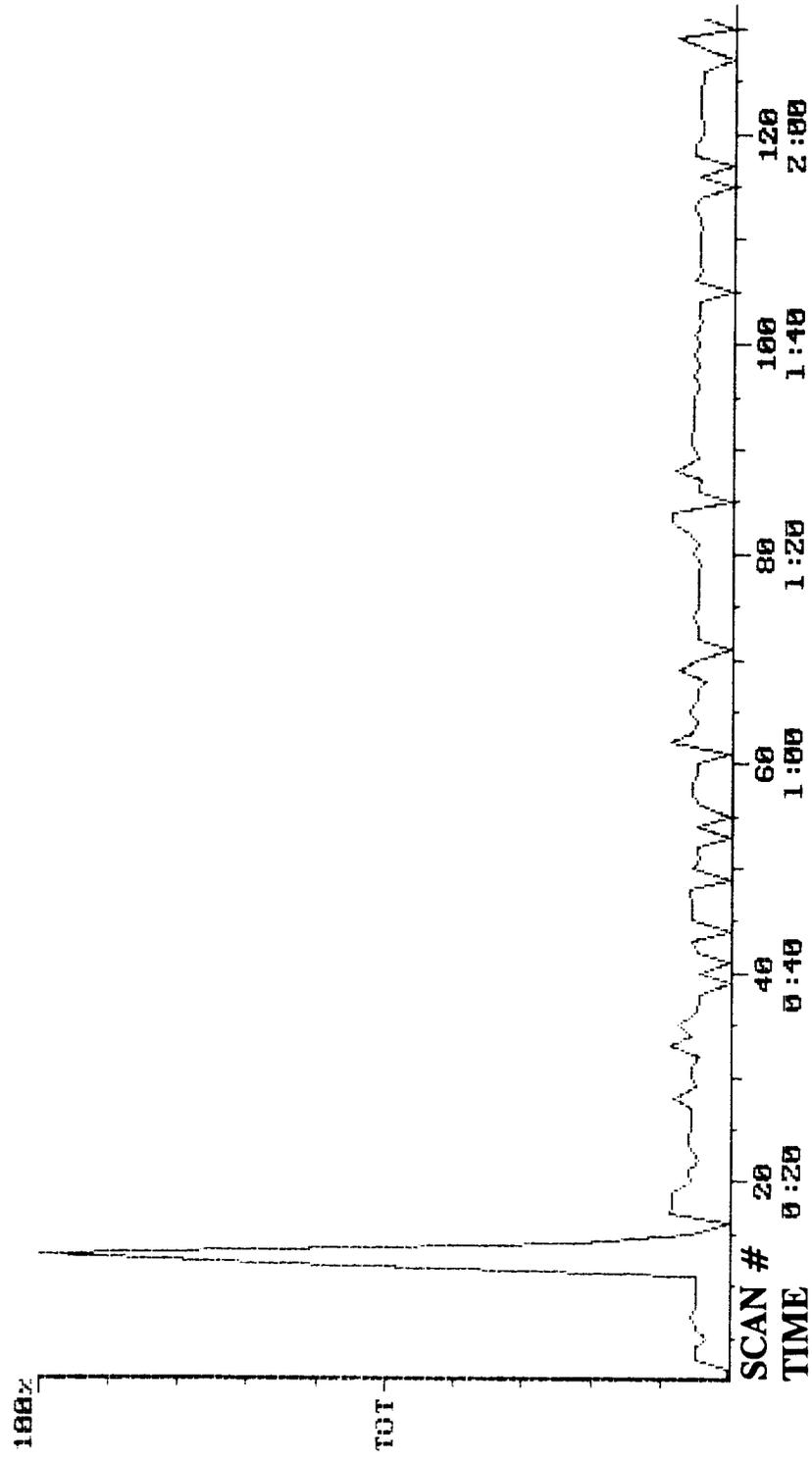
Figure 7. GC-MS TIC of pure trimethylamine.
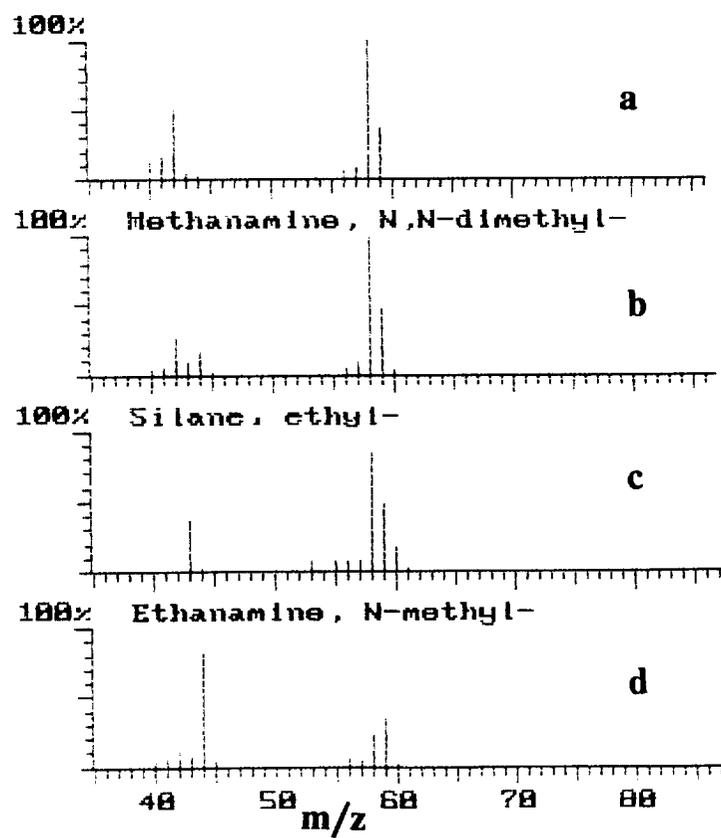
Figure 8. Mass spectra of (a) pure trimethylamine standard, and library mass spectra of (b) trimethylamine, (c) ethylsilane and (d) N-methylethanamine.
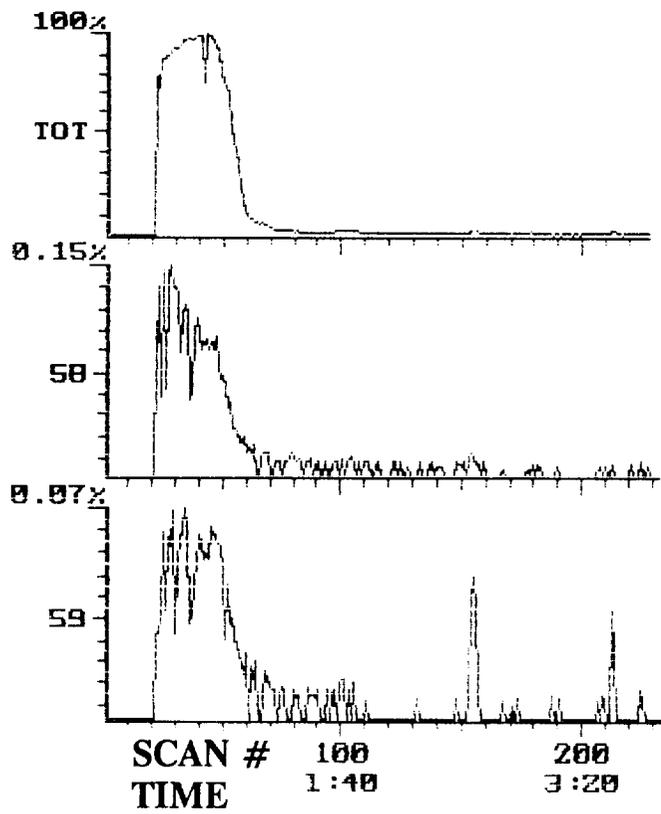
Figure 9. TIC and reconstructed ion chromatograms of m/z 58 and 59 in a fish headspace analysis.
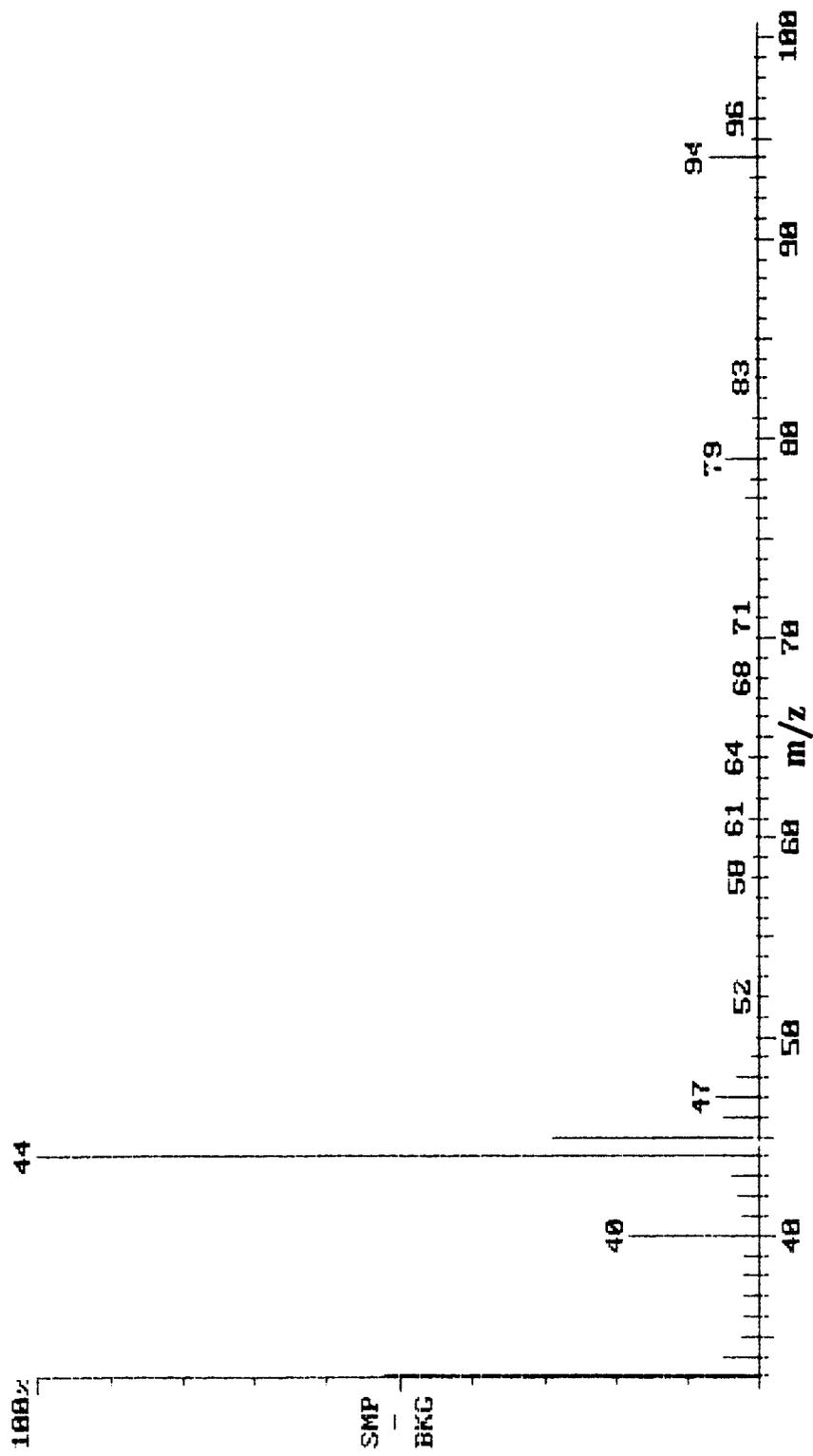
Figure 10. Mass spectrum of the 21-30 scan number interval in Figure 3a.
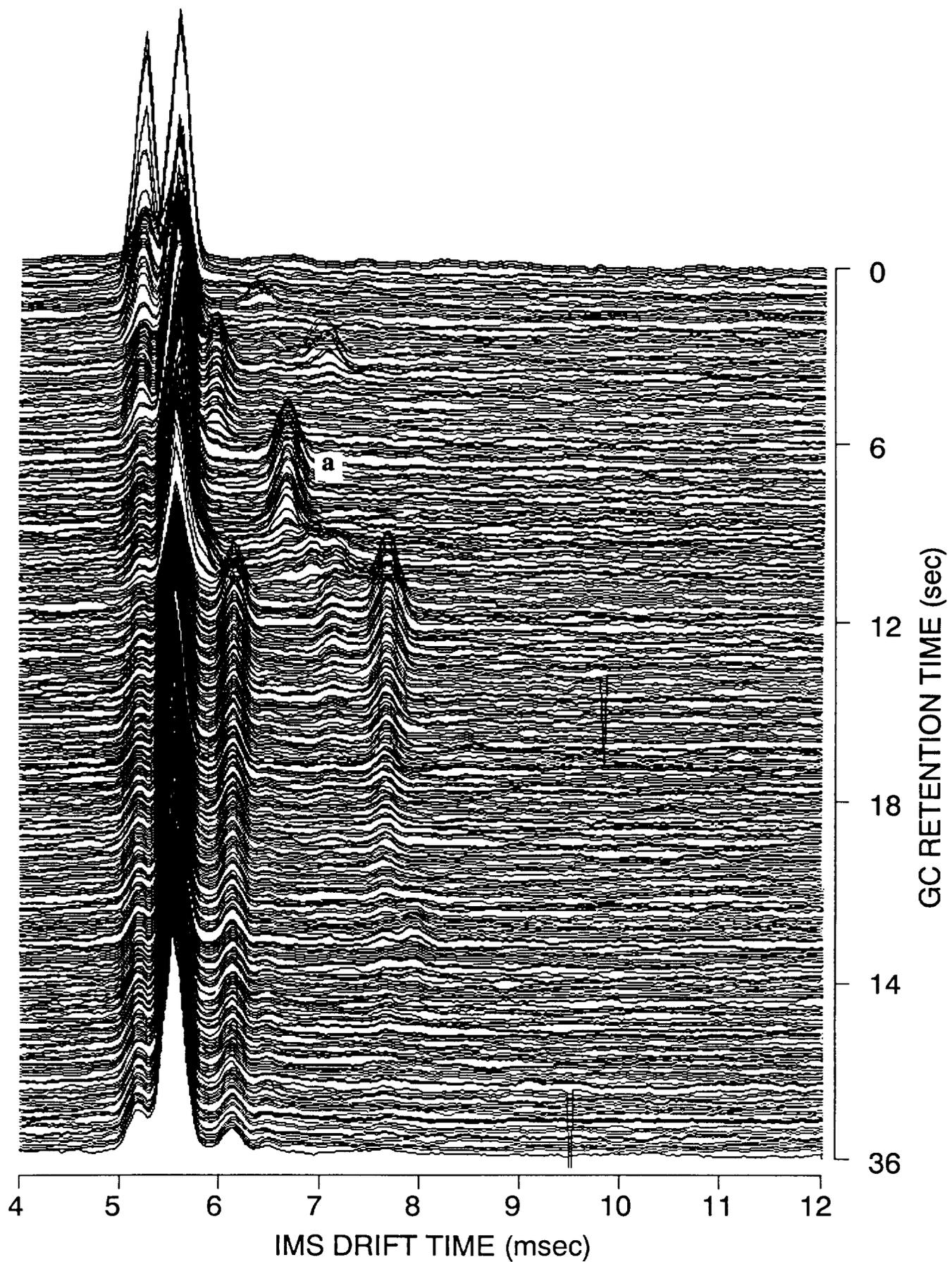
Figure 11. GC-IMS chromatogram of fish headspace on the fourth day of the study.
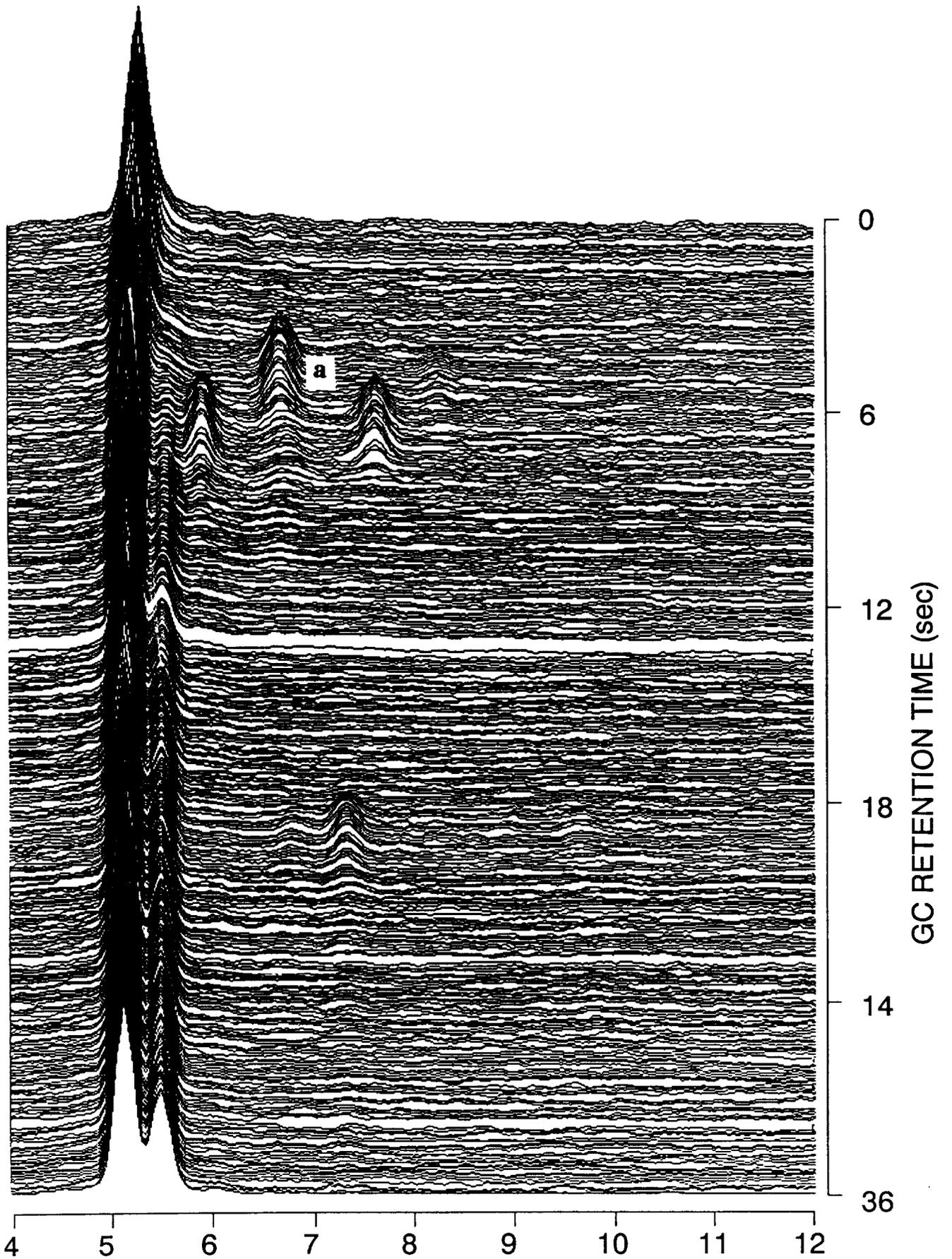
Figure 12. GC-IMS chromatogram of pure cadaverine.

166

GAS CHROMATOGRAPHY/ION MOBILITY SPECTROMETRY AS A HYPHENATED TECHNIQUE FOR IMPROVED EXPLOSIVES DETECTION AND ANALYSIS

Al Mercado
Federal Aviation Administration Technical Center, Atlantic City, New Jersey 08405

Paul Marsden
Science Applications International Corporation, 4161 Campus Point Court, San Diego, California 92121

BACKGROUND - DEFINITION OF THE PROBLEM

Ion Mobility Spectrometry and Explosives

Ion Mobility Spectrometry is currently being successfully applied to the problem of on-line trace detection of plastic and other explosives in airports and other facilities. The methods of sample retrieval primarily consist of batch sampling for particulate residue on a filter card for introduction into the IMS The sample is desorbed into the IMS using air as the carrier and negative ions of the explosives are detected, some as an adduct with a reagent ion such as CL⁻ Based on studies and tests conducted by different airport authorities, this method seems to work well for low vapor pressure explosives such as RDX and PETN, as well as TNT that are highly adsorptive and can be found in nanogram quantities on contaminated surfaces. Recently, the changing terrorist threat and the adoption of new marking agents for plastic explosives has meant that the sample introduction and analysis capabilities of the IMS must be enhanced in order to keep up with other detector developments. The IMS has sufficient analytical resolution for a few threat compounds but the IMS Plasmogram becomes increasingly more difficult to interpret when the sample mixture gets more complex.

The current list of compounds that need to be targeted for detection in addition to the plastics explosives and TNT, now include the MNT isomers ortho and para MNT and DMNB. Most of theses compounds have been previously characterized in the IMS with different known conditions for detection as well separation of all the compounds [1]. Spangler et al found out in previous studies, while nitrotoluene compounds such as 2,4,6 TNT and 2,4 DNT can be separated according to their ion mobilities, the MNT isomers cannot [2]. In addition, EGDN which has been extensively studied as a vapor constituent in dynamite can only be detected as and EGDN-Cl⁻ or EGDN-NO3⁻ ion cluster at IMS cell temperatures below 100°C as pointed out by Lawrence and Neudorl [3]. However, this is inconsistent with the optimum IMS operating conditions of 160 °C with hydrated NO_2 as the reagent gas when RDX, PETN , and TNT are directly introduced from air. The detection of DMNB by the IMS has been reported as the formation of ion clusters DMNB-H⁻, DMNB- CL⁻, and DMNB-NO₃⁻ that are separable according to their ion mobility spectra, but no additional fragmented species were found at cell temperatures above 100°C [4]. The idea of using dual IMS detectors with different front end separators and operating conditions to make up for the different species has been proposed, but there is the added complexity of effectively splitting the sample in a ratio that reflects the difference in available concentrations of the various compounds without taking multiple replicates.

There is also the added complication of knowing the actual ionization processes for all nitroester and nitroaromatic compounds in air at atmospheric pressure [5]. More ionized species have

been reported with air as the carrier as opposed to nitrogen with differences in resolution as well as sensitivity for some the compounds. Lawrence and Neudorfl found more broader peaks coming from other chemical interferants in the atmosphere , which caused the EGDN-CL⁻ peak to vary enormously and disappear. While others have noted that the response to TNT is much lower by an order of magnitude in nitrogen as opposed to air, additional TNT isomers as well as DNT have been detected and they are available for sampling along with the primary TNT isomer in the explosive. The primary concern is the stability of the ions in air as opposed to nitrogen and the species' thermal stability and concentration prior to sample introduction. Non one has reported conditions in air for the detection of all the targeted taggants and explosives. It is possible to seed the remotely collected sample in a nitrogen carrier gas into the IMS, but that would not be efficient for the sample transfer. Direct air sampling onto an intermediate preconcentrator for trapping upstream of the IMS would be more effective in reducing ambient atmospheric effects, but that might also be selective as well to only one class of the targeted compounds.

One potential system design would be to interface a capillary GC to an IMS with a front end membrane separator to selectively introduce the sample without the oxygen. The benefits would be obvious in that the IMS resolution could be increased to selectively monitor the MNT isomers product ions in a drift time window after column separation. The GC column would be able to reduce any potential interference from halogenated compounds such as trichloroethane and tetrachloroethane that would be greatly accumulated in a preconcentrator along with the explosives. The GC limited sample introduction would also reduce the surface decomposition and adsorption effects on some of the compounds by allowing more rapid analyses in the IMS [6]. This design has been successfully employed in portable GC-ECD detection devices that are used for explosives detection as well as a handheld GC-IMS analyzer for chemical warfare agents. However in today's screening scenario, applying any of these designs poses additional problems for the IMS being used for explosives detection. The disadvantages arise from the additional front end components that reduce the current low level detection capabilities of the IMS itself which have made it a successful analytical technique used for trace plastic explosives detection.

Membrane Separators
In the past, the use of semi-permeable membranes to selectively introduce explosives sample into an ion mobility spectrometer has not had the effect of enriching the concentration of the explosive vapors over oxygen and other atmospheric constituents such as water which complicate the ionization process. The explosives molecules which are already present in low concentrations had to permeate through the membrane material primarily through its greater solubility in the polymethylsilicone substrate than the other lighter molecules Even with operation at elevated temperatures the adsorption desorption process governing the selectivity were not very efficient, so the sensitivity of the IMS tended to be diminished by as much as two orders of magnitude even though a high percentage of other non-organic molecules were rejected [7]. In addition , since the permeability of the explosives was not primarily dependent on the diffusion through the rubbery polymer membrane, a substantial pressure differential had to be applied over a thick membrane wall, usually in the form of a interstage pump to speed up the enrichment process for explosives sample in the membrane. In effect, the explosive molecules tended to have long residence times in the membrane separator which led to its retention in the membrane structure. In order to process large volumes of the air that contained the explosive sample, membrane separators with large surface area to volume ratios were built to permeate the explosives primarily through diffusion, with the use of compressors and vacuum pumps to establish the pressure differential over the membrane module [8]. When such a membrane preconcentrator was built and tested for coupling with an explosives detector its time constant for detection was

demonstrated to be several minutes to effectively enrich the level of TNT, which was woefully inadequate for real time explosives detection.

GC-IMS Integration

Even though a GC column has been successfully integrated to the IMS, one must consider that the IMS is a relatively large volume detector which makes it more suitable for larger sample screening of explosives in comparison to other detectors such as an ECD. This presents a pneumatic impedance mismatch due to the lower GC effluent flow rates and the larger IMS reaction volume of typically 7 cc. Baim and Hill found that in order to effectively integrate the GC column to the IMS without degrading the column resolution, the IMS ionization cell volume had to be reduced to match the GC effluent volume [9]. In another method that did not change the reaction region size, the GC effluent flow was increased with a makeup flow to fill most of the IMS reaction volume in real time and subsequently purged out with an even greater counter current drift flow to prevent lingering memory effects, as demonstrated by PCP in figure 1. However, this ultimately has the effect of reducing the concentration of explosives in the GC peaks to maintain the chromatographic separation between peaks. With the limited sample capacity of the capillary column most of the air sample containing the explosives would have to be split off in the first place before directly introducing it directly into the GC column for separation. The pneumatic impedance mismatch is even more severe between a high volume preconcentrator used at the front end and the capillary column.

Recent developments in GC column technology and membrane separators can be applied to the IMS to overcome any of the previous drawbacks to their use. The objective of this work was to come up with a preliminary design that would incorporate these components with an IMS for the purposes of enhanced explosives and taggant detection.

APPLICATION OF NOVEL EQUIPMENT TO THE IMS

Ultra Thin Hollow Fiber Membranes

Hollow fiber silicone tubing in membranes has been proposed in the past to selectively permeate large molecules, such as explosives, instead of air or an inert carrier gas into a mass spectrometer. However, Lucero et al determined that the permeation of the carrier gas (i.e. hydrogen) instead of the heavier organics was more efficient, by as much as 100% through a tubular palladium alloy electrolytic separator that was designed for a GC-MS interface [10] , as long as the pressure was substantially lower on the permeate side than the retentate side. The high diffusivity of carrier gases, such as hydrogen and helium, and the use of a membrane with greater selectivity over organic penetrants makes it possible to achieve a substantial enrichment of the sample over the carrier at lower time constants. This enrichment would be easy to achieve in a compact GC-MS membrane module since the MS inlet would be operating at pressures below a millitorr and the GC effluent would be fed in at low flow rates of 10 cc/min. However, this would not be the case for the high air sampling flow rates that are required of a membrane preconcentrator for an atmospheric pressure and large volume detector such as an IMS. The membrane sheet thickness would have to be much thinner to avoid the need to pressurize the sample on the feed side and the total surface area to volume ratio for the module would have to be reduced for a good pneumatic interface with the IMS.

Recently coiled membrane sheets made up of a thin membrane selective film on a porous support structure have been successfully manufactured and tested as membrane preconcentrators[11] These modules were tested by blowing different carrier gases including air into several types of membrane selective layers along with a dilute amount of toluene (which has a similar diffusion coefficient as some of the explosives). The results of selectivity, membrane area and enrichment are displayed in table 1 for a predetermined feed flow rate, residue flow rate and required enrichment. While the spiral wound membrane module surface area may be too large for the demonstrated enrichment of the toluene simulant the area can be reduced much further with the use of a hollow fiber membrane module.

The hollow fiber membrane module of figure 2 is composed of a polymer selective layer that is deposited from solution with water being forced through the inner core to form a fiber. The necessary surface area is obtained by stacking bundles of the fibers together in a heating mantle to provide the maximum surface area and minimum volume for the carrier gas and explosive vapor mixture that is being fed into the preconcentrator. The air, water, and ammonia permeate through the selective layer under the pressure differential being created by a vacuum pump while the retentate organics flow directly into the detector or other down stream separator. The membrane module design is dependent on the enrichment and flow rates necessary for the detector which continuously takes in the retentate flow that is separated from air as described in figure 2. The operating temperature can go up in excess of 100 °C and a coating with a low surface energy can be applied to cover adsorption sites and plug up defects. This structure is similar to some of the early designs for preconcentrators made up of bundles of capillary tubes for trapping the explosives. However, the inefficiency in purging out the sample during a desorption flow limited the use of those designs. With a hollow fiber membrane preconcentrator operating in continuous mode, there would be no additional inefficiencies arising from the adsorption/desorption processing of the sample flow. Ultimately a GC can be incorporated downstream of the preconcentrator before the detector to separate any background levels being produced by the polymer emissions from the membrane. However, such a GC column would have to be more pneumatically compatible with the retentate flow output of the preconcentrator than a standard capillary GC.

Multi-capillary Columns

The drawback of long retention times and limited sample capacity when using capillary GC columns with the IMS has limited its application to real time explosives detection. High speed chromatography for a field instrument generally requires reduced thermal mass, cold trapping, low injection bandwidths, and faster detector response, all of which are difficult to achieve with a gas sampling IMS. And shortening the column and ramping the temperature to reduce the analysis time does not produce an adequate resolution of some of the compounds that is worth the additional sample introduction problems for the IMS. Packed columns, which have a higher sample capacity and thus are more pneumatically compatible for integration than a narrow bore capillary, have been used in the past with the IMS, but there have been problems with the column bleed and the resolution. Ideally for an IMS, the sample capacity of the GC column would have to be increased to fill the reaction region of the IMS while retaining the high resolution of the narrow bore capillary under isothermal conditions.

The idea of bundling several capillaries within a larger tube to increase capacity is not new. The peaks are broader because of a difference in phase ratios in each capillary, but for an IMS which has a typical scan time of 20 msec depending on repetion rate, this would not be the limiting factor, since the scan time is well within a factor of 0.1 of the peak width. The problem has

been in effectively manufacturing and testing these columns. However, Ertl et al demonstrated that with a hexagonally shaped tube containing about 1200, narrow bore (50 to 200 micron) capillaries, they were able to get effective separations of compounds in less than a minute that took several minutes in a single capillary [12]. The conditions under which they established their separations included column lengths of 0.3 m, injection volumes up to 10 microliters, and carrier gas flow rates up to 300 ml/min. While the resolution is lower, Berkley noted that these polycapillary columns shown in figure 3, that were developed by the Limnological Institute in Irtutsk, Russia would be still be effective for separating high molecular weight compounds such as pesticides [13]. These bundled parallel capillary columns had specifications that were variable but included:

Efficiency: 8000 - 12000 TP/m (Theoretical Plates/meter)
Column Length: 150 mm - 1000 mm
Carrier Gas Flow Rate: 20 -120 ml/min depending on the detector
Gaseous Sample Volume: Up to 1 ml
Working Temperature Range: 20 - 200 °C

They were available in a selection of liquid phases and could be bundled and coated for the required sample capacity and desired analysis time.

These columns would be more ideal for the application of the real time detection of explosives as long as column specifications such as the maximum gaseous sample volume, the length, the operating temperature and the choice of phase can be traded off to achieve the desired separation. Separations of the high volatile and low volatile explosives EGDN, TNT, PETN, and RDX have been done within 22 seconds with an Ekho GC-ECD running isothermally at temperatures typically around 172 °C [14]. The specifications with the multi-capillary column that was run with the system included 1,000 parallel capillaries, 40 micron diameter, 25 cm length. The samples were collected from air onto a trap that injected the sample through a gas sampling valve connected to the multicapillary GC. A chromatograph obtained directly from headspace vapor sample of dynamite is shown in figure 4. It seems that of all the targeted compounds the higher volatile taggants or explosives such as EGDN o-MNT, and p-MNT would be the most difficult to separate with the multicapillary GC than the plastic explosives at isothermal temperatures over a short analysis time.

For operation with an IMS the retention times and widths of the sample peaks can be optimized for complete separation by the either the column itself or in conjunction with successive ion mobility separation by an IMS. The lower pressure drop over the length of the column because of the reduced impedance to the flow also means that this type of column would constitute a better pneumatic match with the IMS, with the carrier flow rate coming directly from the column. There would be no need for additional pumping in the IMS cell to make up for the pressure loss as long as the preconcentrator module supplies a continuous carrier flow rate into the column with a pulsed sample. The total analytical capability for a GC-IMS combination would still have to specified with the peak shape specifications of the IMS in question specially its efficiency or height equivalent theoretical plate. Assuming that this is adequate for the analysis of explosives, then the limiting factor would be the integration and time of response of the preconcentrator.

DESIGN SECTION

Ion Mobility Spectrometer Instrumentation

Any Minimum Detectable Limits (MDL) generated for low levels of explosives should be qualified. Factors such as the number of signal averages taken, the carrier flow rate, the integrator time constant, the gain setting, play a role in the S/N ratio observed for any IMS. Generally the IMS sensitivity will be the best the longer a sample concentration can be injected into the IMS and the longer the noise can be averaged out [15]. However, the sample will be injected for some explosives as a pulse and therefore have a shorter time constant. The concentration of the sample going into the IMS will have to be higher to make up for the shorter measurement times. This has resulted in the many different results reported as minimum detectable limits for the IMS to explosives. Some of the determinations have been made with the use of a continuous source which took long time constants to stabilize - which usually meant overcoming irreversible surface adsorption effects before the measured S/N ratio would stabilize. These minimum concentration levels reported for some of the low vapor pressure explosives over long time constants may never be available for direct sampling without some form of preconcentration.

For the purpose of on-line screening the analysis should take no more than 15 seconds for one replicate. The IMS will produce a different MDL for each explosive depending on the preferential adduct formation of the reagent ion with one particular explosive for enhancement of the signal. Various groups have reported that the use of methylene chloride in atmospheric pressure ionization will increase the signal response of nitroesters and cyclic nitramines such as RDX and PETN. Davidson et al conducted studies of chloride ion clustering in an API MS/MS system and identified the increases in sensitivity gained for several groups[16]. The ion clustering tended to suppress the response of the nitrotoluenes and the PETN nitroester peak tended to be diminished in comparison with the enhanced RDX nitramine peak with the chloride ion. Even though the IMS ionization process can be modified to detect most of the different taggants and explosives with high specificity, the differing concentrations can have an effect on the sensitivity of one explosive over the other. EGDN which would have the highest concentration in any sample matrix, can deplete the reactant ion to the point where the response to other less concentrated explosive species that have a short time constant such as PETN is suppressed. For this reason a GC column can act as a front end sample gate for the IMS to reduce any matrix effects on the response from the complexity of the sample.

Design Considerations

The IMS that will be specified for its potential integration with the other front end separators such the hollow fiber membranes and the multi-capillary GC is the PCP-110, because of the extensive information that exists on its performance for three explosives. The reported MDL of the PCP-110 IMS to all the explosives has been reported to be the best with hydrated NO_2 as the reagent gas. Its operating conditions for the optimal detection of three of the primary explosives, RDX, TNT, and PETN has been established as follows [17]:

Cell Temperature - 160°C
Carrier Gas (Air) - 100 cc/min
Drift Gas (Air)- 500 cc/min
Reagent Gas- Hydrated NO_2
Scan Time for Plasmogram - 25 msec
Gate Pulse Width - 0.50 msec
Number of sweeps averaged - 150 .

The signal levels are shown in figure 6 for the three explosives. In this case the MDL for the explosive PETN , which is the least stable and at a lower concentration than TNT, should be taken as the limiting factor in the response of the IMS.

With a multicapillary GC column as a quantitative sample introduction system to the IMS the sample pulse profile of the specific peak can be matched to the concentration dependent response and the reaction volume of the IMS. This width is much more narrower than some thermal desorption profile which would be further broadened and attenuated by the interface to the IMS detector. For the IMS the average concentration of PETN that needs to be maintained in the reaction volume is 10.7 pg/cc before detection is possible with a short time constant. If the GC column is treated as a quantitative generator of explosives, the average concentration within the peak width at FWHM would have to be 10.7 pg/cc. The preconcentrator would have to produce the needed concentration level at this time interval as well as minimize the dead volume, outlet surface area and pressure drop to keep from diluting it before introducing it into an IMS. None of these limitations would necessarily be encountered in reproducing a similar quantitative concentration level with the GC.

The emphasis on meeting performance specifications for explosives detection with the overall design, would now shift to the front end membrane preconcentrator. If 1 ml of gaseous sample is pulsed into the multi-capillary GC column inlet from the membrane preconcentrator, then the sample concentration of PETN at the head of the column before dilution by the carrier gas and additional sample broadening by the GC column would have to be 75 pg/cc. This can be used to determine the enrichment factor necessary with a membrane preconcentrator for a predetermined sampling time and flow rates that is inclusive of all sample transfer inefficiencies. Given a maximum concentration that can be expected to be found in the sample flow of:

$$6.92 \times 10^{-12} PPT (314 \text{ g/mole})/(22,400 \text{ ml/mole}) = 97 \text{ fg/cc}$$

then the minimum enrichment required of the preconcentrator for PETN can be determine by the following ratio:

$$\text{Enrichment} = 75 \text{ pg/cc} / 97 \text{ fg/cc} = 773$$

This is a critical piece of information that can now be used to guide the design of a complete system that includes the membrane preconcentrator, the multicapillary GC, and the IMS.

We can now determine all relevant system operating conditions for these specifications that we have now set. From the flow rates and sampling time intervals other conditions, such as the preconcentrator structural and pneumatic requirements, can be determined for the required

174

enrichment and detection[18]. A nitrogen carrier flow rate of at least 100 cc/min through the multi-capillary GC would be required to provide the make-up carrier flow rate going into the IMS. The enriched sample flow rate or retentate flow rate coming out of the precocentrator would have to be matched to the current GC gaseous injection volume of 1 ml and the required pulse width for separation. Assuming that any pneumatic switching can be done in less than one second and the peak width of an explosive after real time separation is less than a maximum of 2 seconds, then the required retentate flow rate is 60 ml/min for one second pulsing. This 1 ml of gaseous sample volume would be made up of explosives and other organics as well as any residual air. These specifications are variable depending on the allowable capacity of the column and its efficiency. If a sampling time interval of 6 seconds is used for the preconcentrator then the feed flow rate of 7732 ml/min might seem apparent as the required sampling flow rate based on the following estimate:

$$7732 \text{ ml/min (6 sec) /60 ml/min (1 sec)} = \text{Enrichment.}$$

However, this figure does not take into account transport inefficiencies through the outlet of the hollow fiber membrane module or the membrane material itself. A required inefficiency of 0.5 for vapor loss into the GC can be specified for the module depending on pressure, flows, surface area, temperature, and dead volumes involved. In this case the enrichment required would be 1546 to compensate for these losses. Depending on the mode of sampling the available concentration would be more dilute by an order of magnitude. This increase in the requirement necessary for enrichment to 1546, means that the sampling flow rate would have to be increased by an order of magnitude to 150 l/min. This is concurrent with the needs of high flow sampling portals and can be attained with a design presented.

Once again there will be a time constant in the response of the hollow fiber membrane preconcentrator and there will be a time constant associated with the pneumatic switching and sample injection into the GC. The main requirement is that it is established within real time. For a membrane preconcentrator that is operating continuously at elevated temperatures there would be no temperature cycles involved in trapping and desorbing the sample that change the condition of the equilibrated surfaces which in the end affect the time constants. The determining factor in the time constant would be the rate of the adsorption/desorption processes that govern the solubility in the membrane material, which would be low for organics like explosives in the membrane structure, since the polymer is not selective to permeating explosives. Once we have outlined the operating requirements and specifications we can sketch a preliminary design of key areas of the overall system such as the integration of all front end components.

RESULTS AND DISCUSSION

Preconcentrator/GC/IMS Interface Design

We have discussed how the multicapillary GC can be included as a low loss element in the system design. IMS instruments have been previously modified successfully to incorporate a GC. The PCP-110 can accept a capillary GC column axially with an effluent make-up flow and a purge gas to sweep it out, as seen in Figure 1. With a multi-capillary GC there would be no need for a make-up flow to be added to the effluent coming out of the column and into the transfer line to the ionization region. The mass transfer of the sample in the carrier coming out of the column can be matched to the reaction volume and drift flow of an IMS. Now the objective would be to come up with a design that does not trade off some of the current advantages of the IMS for explosives detection on the field, which include no carrier gases, large detector volumes, and low

time constants for response to explosives. This is largely dependent on the preconcentrator interface to the GC and operation which would be the limiting factor. The following design incorporates the requirements of the preconcentrator and the GC for operation, but it impacts the operation of the IMS in the least.

In the preliminary design proposed, the operation of the preconcentrator with the known requirements of the multi-capillary GC and IMS is shown in figure 6. The feed flow would come into the hollow fiber membrane preconcentrator enrich the organics over the air and dump the retentate flow directly to a drain behind the valve. The permeate mixture can flow through a secondary membrane module to further separate the residual nitrogen from the oxygen in the air permeate before introducing it into the column. The retentate flow from the secondary module would act as the carrier for the organic enriched retentate or residue flow that would be pulsed into the column. The nitrogen enriched residue stream can provide the necessary dynamic pressure for the carrier flow upstream of the multicapillary GC column. Downstream valves would provide a pneumatic switching of flows to pulse the sample from the organic enriched retentate flow out of the preconcentrator and into the carrier flow of the GC column. All the transfer lines from the outlet of the first hollow fiber membrane preconcentrator would be kept heated and have low dead volume. Under this scenario the next sample of the explosives enriched retentate flow would be taken once the column separation is completed (typically 10 sec.). But, the sample would be enriched to match the concentration MDL of the IMS.

The preconcentrator/GC sample introduction system would operate under two modes of operation; a purge cycle and a sampling cycle. In the purge condition the first valve would be open downstream to act as a drain for the retentate flow out of the membrane preconcentrator and the second valve would be closed. A portion of the N_2 enriched retentate flow from the secondary membrane would be diverted down the same drain. This would sweep out any organic remnants out of the line leading to the GC column before beginning the sample pulsing.

In the sampling condition, the first valve would be closed and the second valve open to divert the flow into the GC column. Through the action of some slight pumping the majority of the explosives enriched retentate flow would be diverted to the other drain created by opening up the second valve. The sample would then be swept into the GC column by the continuos nitrogen flow going into the column. Some of the nitrogen retentate flow may be diverted down the second drain but the residual flow going into the column can be set to prevent the diffusion of the explosives flow.

In another more simplified design as shown in figure 7, the explosives enriched retentate flow would go directly at the head of the column. And during the purge cycle the nitrogen sweep flow would be flowing past the hollow fiber membrane outlet to dump the sample to a drain when it is not being introduced to the inlet of the GC column. The nitrogen flow rate would have to be set at a much higher rate to prevent organics from diffusing through this flow barrier. At the same time a separate continuous nitrogen stream would have to be established to make up the continuous carrier flow going into the GC column. When the valve is closed during the sampling period all the sample and nitrogen retentate flow would be diverted directly into GC column and any residual nitrogen flow would be dumped to atmosphere or go to the IMS to be used in the drift gas. However, in this design the flows would be less steady and some of the sample from the last pulse might bleed into the column with a portion of the nitrogen flow sweeping through the line between the outlet of the preconcentrator and the inlet of the GC column during the purge condition.

Potential Problems and Improvements

Some additional calculations are required to further assess the feasibility of the design. The required dynamic pressures have to be determined to establish more exact flow rates. In addition the pneumatic impedances of key components in the system such as the multicapillary GC and any lines where the flow is split have to be determined. In order to make the valveless flow switching process more predictable, the pneumatic impedances across each transfer line would have to be fixed against these other specifications to maintain the proper flow rate [19]. For instance the impedance seen by the explosives flow would have to be much greater over the line to the drain than the impedance over the line representing the multicapillary GC. A representative pneumatic flow network would have to be determined to set all the flows and impedances for proper operation. In addition, most of the design assumes that the time for establishing these conditions would happen quickly, But in reality, even with fast switching solenoid valves (< 1 sec) and reduced dead volume, the flow switch would take at least one second. This would mean that a 2 sec sample pulsing of a 3 sec time constant for switching flows on and off must be taken into account. The concentration of the explosives stream must be great enough to overcome any time lag in response.

The estimates given for the makeup of the flow going into the GC and IMS needs to be better defined experimentally. It may not be possible to effectively enrich nitrogen over air in the secondary membrane module, so the carrier flow may not be that pure. In this case, a nitrogen generator would have to be used instead of the second module to provide the constant carrier flow. The width of the sample pulse and necessary separation time before the next pulse makes inefficient use of the explosive sample available in the enriched retentate flow that is being dumped to the drain . In this case, an actual adsorbing trap possibly made up of bundled glass capillary tubes can be used downstream at the outlet of the hollow fiber membrane preconcentrator to trap the low vapor pressure explosives such as RDX and PETN while the other organics that are more volatile flow directly through the intermediate trap down to the drain. When the sampling cycle is turned on the trap could be quickly ramped in temperature to desorb the plastic explosives without degrading taggants or other less stable explosives. However, the design would have to incorporate a low pressure drop collector so as not to impede the remainder of the flow during pulsing and switching. And it would have to be thermally isolated to be continuously cooled, while the sample is being accumulated and heated quickly to desorb during the switch of flows. The nitrogen enriched carrier flow into the GC would also have to be controlled with mass flow meters and a servo loop so as not to affect the stability of the chromatographic peaks. The long term degradation and hang-up of sample by the GC would also have to be included as a factor, since a system such as this is assumed to be operating on line for a long period of time.

In the designs proposed the method of sample introduction may be more complex because of the addition of the GC, but the end result would be a more efficient concentration of the sample to enhance the resolution and detection of the IMS.

Conclusions

The main objective was to present a preliminary design based on known operating conditions and a set of assumptions. The intention was to increase analytical and chemical resolution of the IMS based on a certain set of criteria and specifications. However, there is the possibility for tradeoffs in the design depending on changes in the sampling time interval, the GC sample capacity, and the required membrane selectivity. These tradeoffs can now be evaluated

against this preliminary design to meet the same requirements but additional modeling of the membrane preconcentrator design would have to be done as well as optimizing GC conditions for the best separation and shortest analysis time. The design has been shown to be feasible and as long as other components such as valves, pumps, flow lines, can be better defined and selected from the requirements set forth, then it will be possible to build such a system at low risk.

Acknowledgments

The authors wish to thank Dr.Cs.Giam of Texas A & M University for his help in providing some of the data and support that made this paper possible, and Dr.Martin Cohen of PCP, Inc. for supplying some of the insight and information on ion mobility spectrometry.

References

1) Eiceman, G.A. and Karpas, Z., Ion Mobility Spectrometry, CRC Press, Boca Raton, FL 1994 pp 153-157

2) Spangler, G.E. and Lawless,P.A., "Ionization of Nitrotoluene Compounds in Negative Ion Plasma Chroamtography"Anal. Chem. 50 (7), 884 (1978)

3)Lawrence A.H. and Neudorfl P., "Detection of Ethylene Glycol Dinitrate Vapors by Ion Mobility Spectrometery Using Chloride Reagent Ions," Anal. Chem. 60 (2), 104 (1988)

4) Danyleywych-May, L.I. ,"Modifications to the Ionization Process to Enhance the Detection of Explosives by IMS" Proc. 1st. Int. Symp.Explosives Det. Tech., Paper C-10, Atlantic city, N.J. Nov. 1991

5) Eiceman, G.A. and Karpas, Z. Ion Mobility Spectrometry, CRC Press, Boca Raton, FL 1994 pp 38-42

6)Cram, S.P. and Chesler S. N., "Coupling of High Speed Gas Chromatography with Plasma Chromatography" J. Chromatographic Sci., 11, 391-401, (1973)

7) Elias L and Neudorfl, P.,"Laboratory Evaluation of Portable and Walk Through Explosive Detectors"proc. 3rd. Symp. Anal. Detec. Explos. Manheim Neuostheim,Frg, Paper # 43, 1987

8) Pinnau, I. , " Gas Transport Through Integral Asssymetric Membranes: A comparison to Dense Fiml Properties", J. Appl. Pol. Sci. in press (1993)

9)Baim , M.A. and Hill, H.H., "Tunable Detection for Capillary Gas Chromatography by Ion Mobility Monitoring" Anal. Chem. 54 (1) 38 (1982)

10) Lucero, D.P. " Design of Palladium Alloy elkectrolytic Separator for GC=Ms analysis Systems", J. Chrom. Sci., 9, 106-115 (1971)

11) Pinnau I, " Membrane Concentrator for Explosives Detection: Final Report, DTRS-57-92-C-00091 DOT/Transportation Systems Center, Cambridge, MA, July 1993

12) Ertl, H and Breit, U et al. "New Separation Device tha Allows Fast Chromatography of Large Samples" Proc. Conf. of Cargo Inspection Tech., in Press, San Diego, CA, 1994

13) Brochure and Application Notes of the Ekho Gas Chromatograph and Multi-Capillary Columns by Mine Safety Applicances, Lyons, CO

14) Whitehurst, F., Private Communication with A. Mercado, Atlantic City, NJ, October 1994

15) Application Notes on the PCP-100 "Minimum Detectable Sample Levels in a Standard IMS", Sept. , 1992, by PCP Inc., West Palm Beach, Fl.

16) Davidson, W.R. et al., " Modifications to the Ionization Process to Enhance the Detection of Explosives by API/MS/MS" Proc. 1st. Int. Symp.Explosives Det. Tech., pp 653-662, Atlantic city, N.J. Nov. 1991

17) Manual of the PCP-100/Graseby ASP configuration Menu for Explosives, 1991, by PCP, Inc., West Palm Beach Florida

18) Lucero, DP, "Design of a High Performance Gas-Phase Explosives Vapor Preconcentrator" Proc. 3rd Symp. Anal. Detect. Explos., Manheim-Neuostheim, FRG, Paper #41, 1989

19) Arnold J.T. "Recent Developments for Trace Vapor Detection" Proc. Conf. of Cargo Inspection Tech., in Press, San Diego, CA 1994
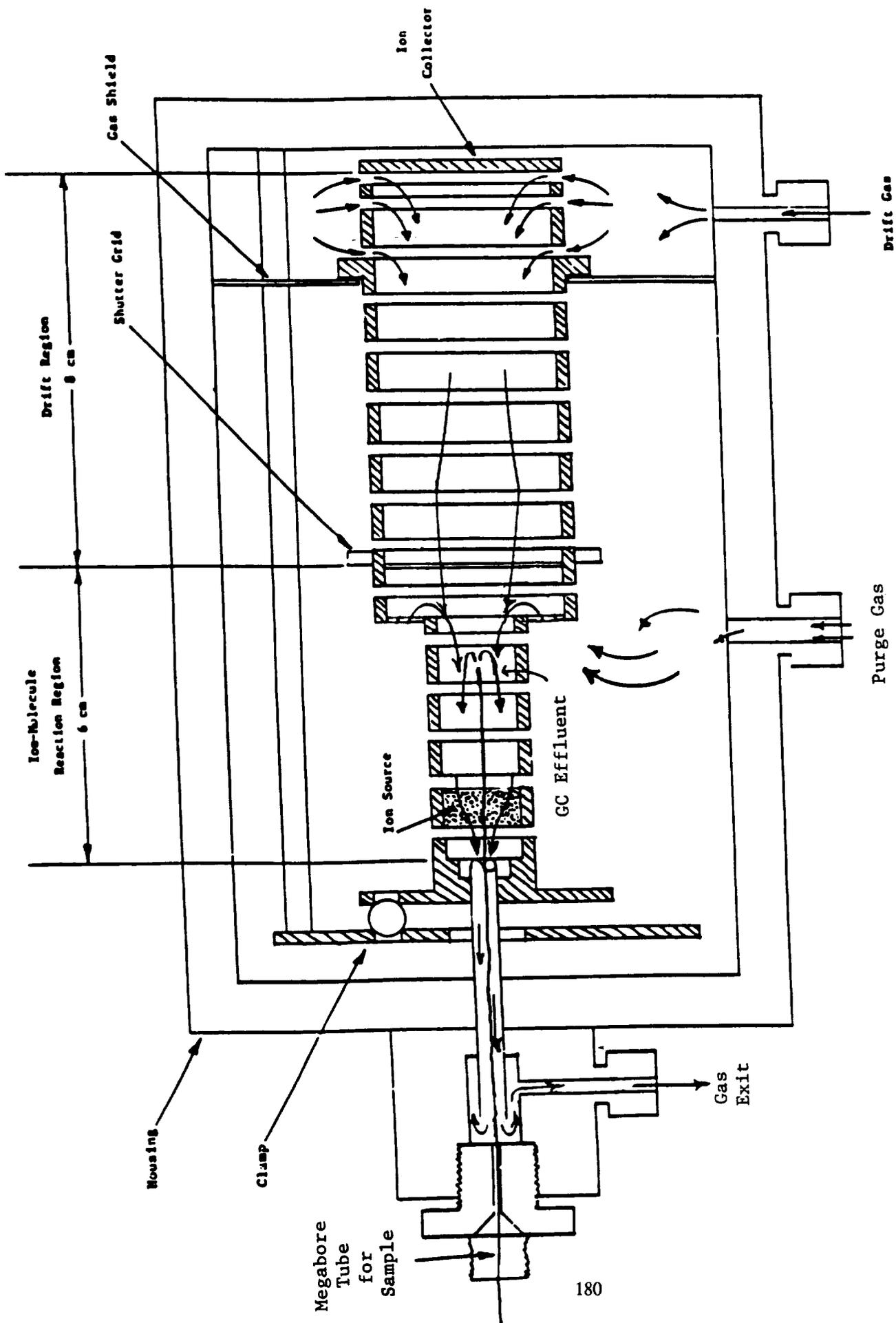
Figure 1. Ion Mobility Cell Modified for GC Inlet for Transfer Line

180

Carrier gas	Carrier gas pressure-normalized permeation flux ($10^{-6} cm^3/cm^2 \cdot s \cdot cmHg$)	Selectivity gas/toluene	Enrichment	Membrane area (m^2)
Nitrogen	2	14	700	108
Air	4	29	850	53
Carbon dioxide	50	360	987	4.3
Helium	140	1,000	995	1.5

Table 1. Table of vapor enrichment at feed flow rate of 10 L/min, residue flow rate of 10 ml/min, and Temperature of 22 °C.
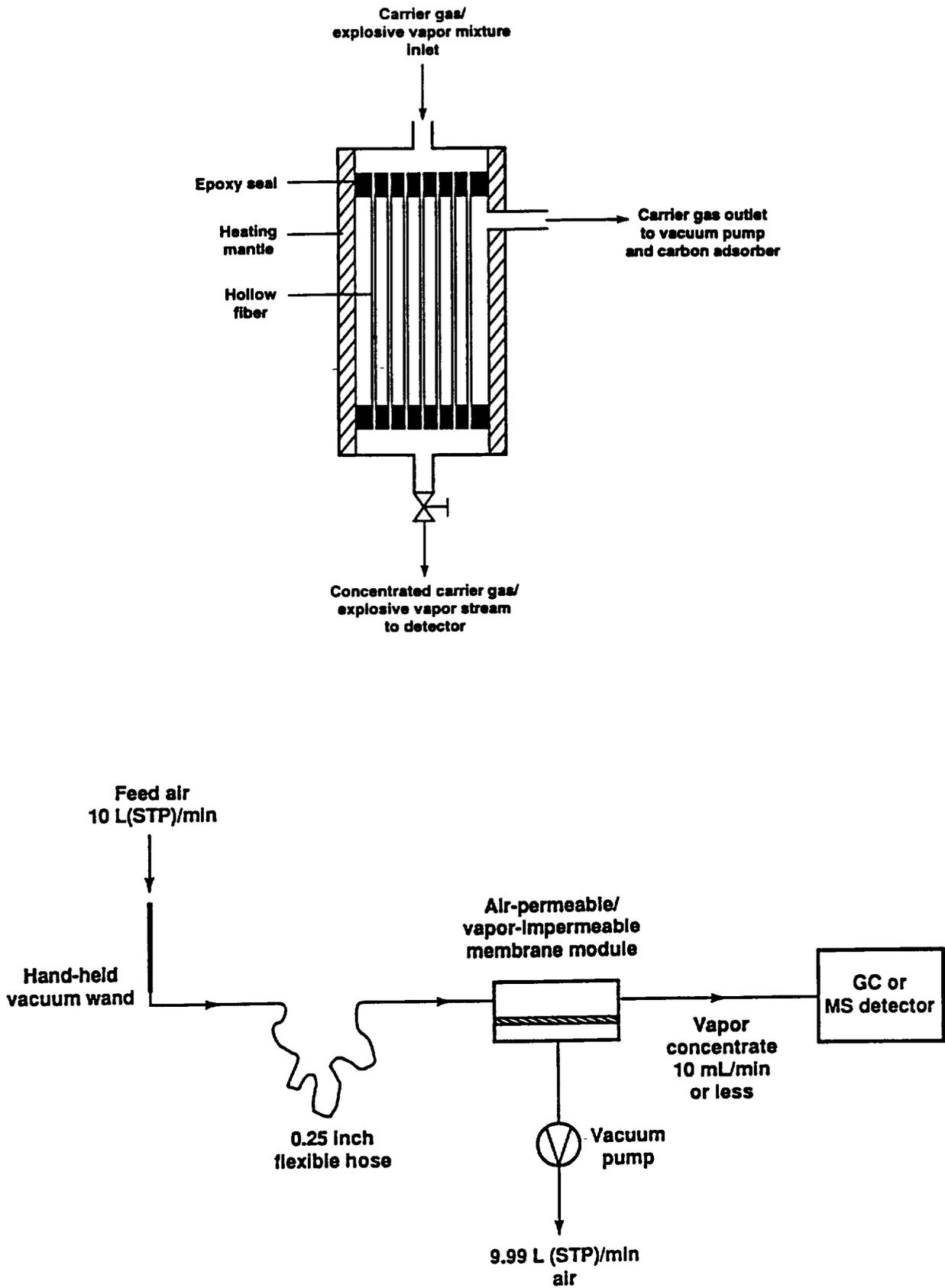
Figure 2. Schematic of a Hollow Fiber Membrane and its Use as a Preconcentrator

182
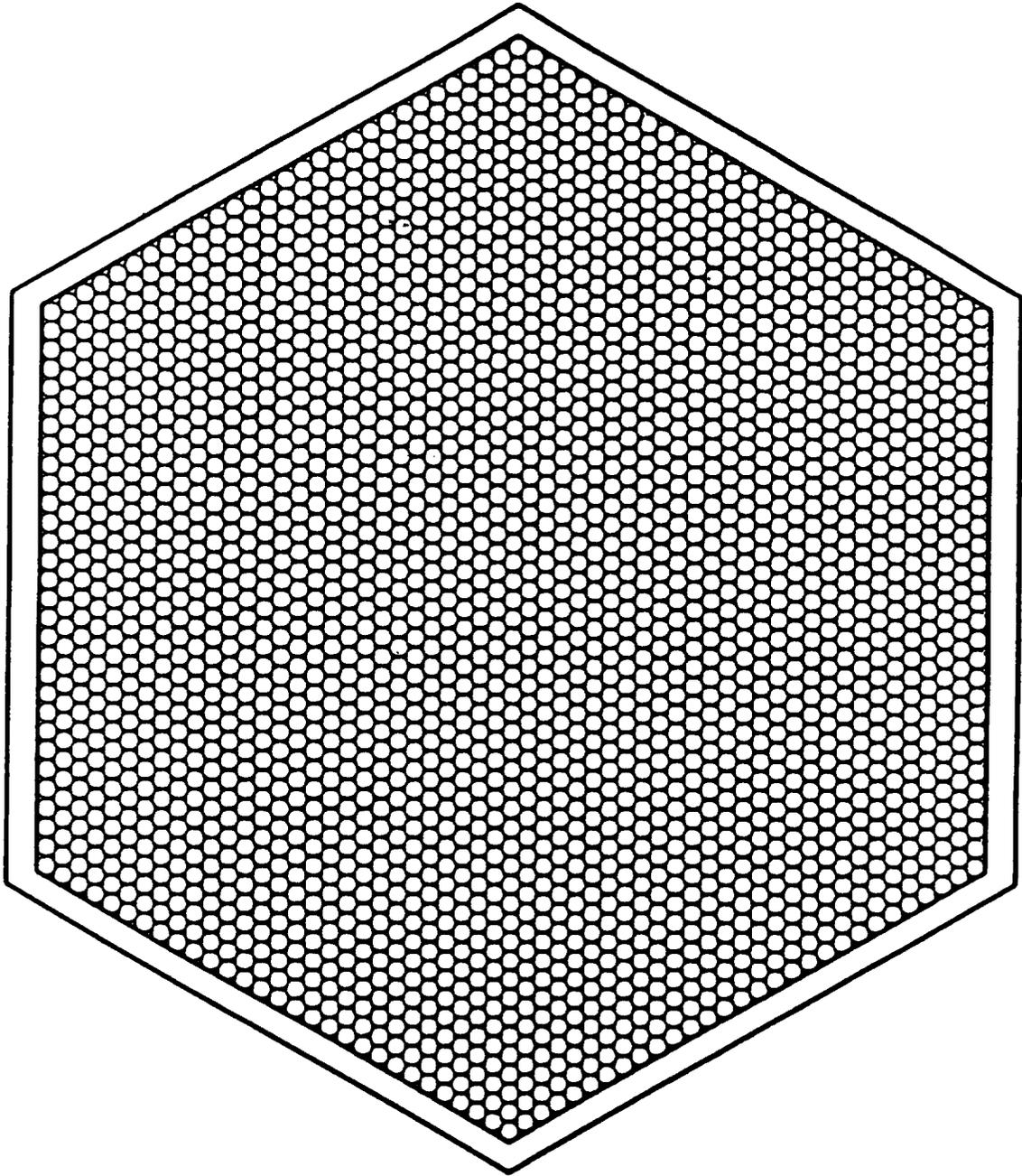
Figure 3. Cross section of a polycapillary column 6 mm width , 20 cm length

GC-Runs of Explosive Vapors (1mg in a 1l-Bottle) and Room-Air-Background
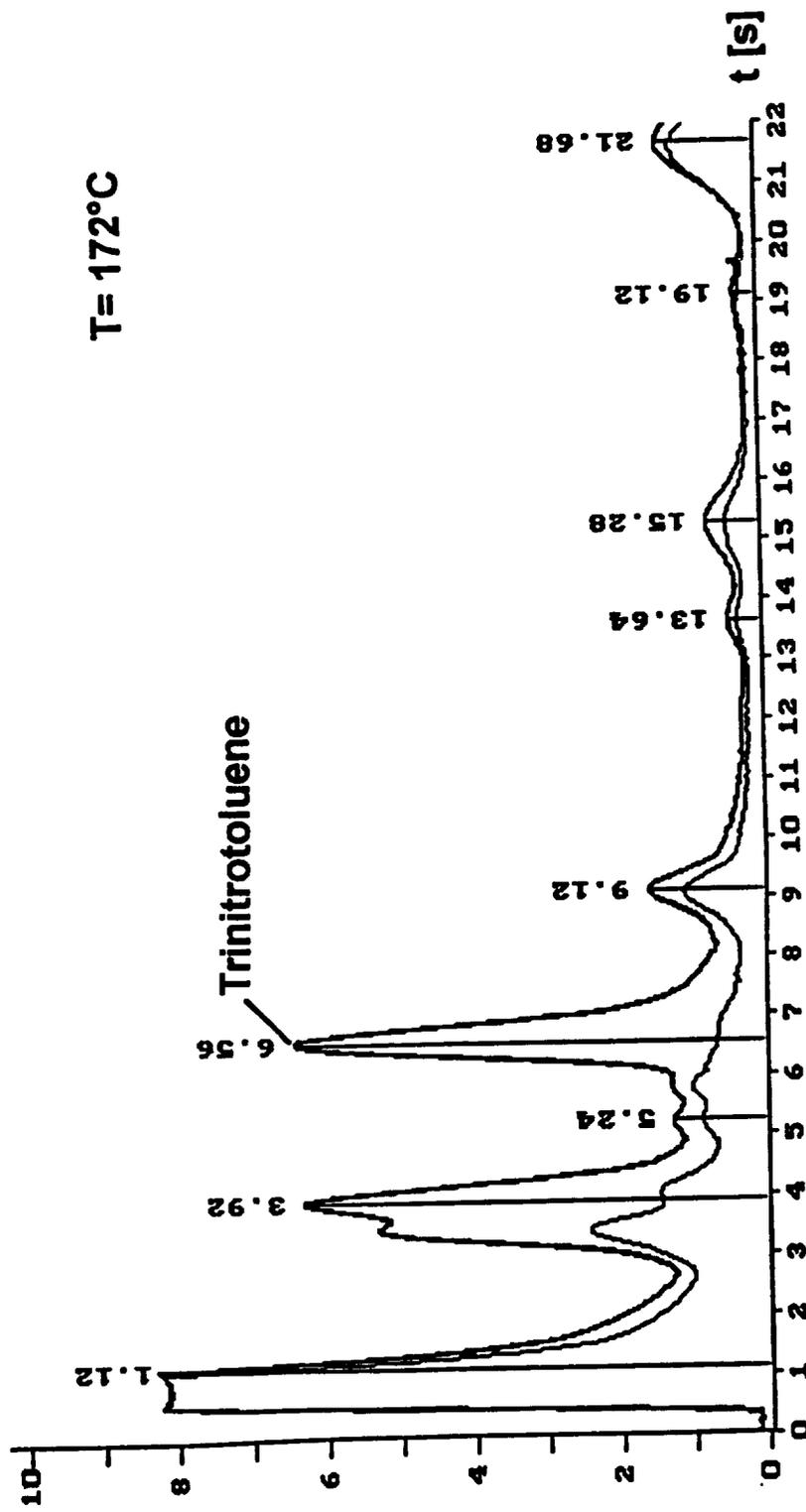
Figure 4. GC Chromatogram: Explosive Vapors sampled directly from room air
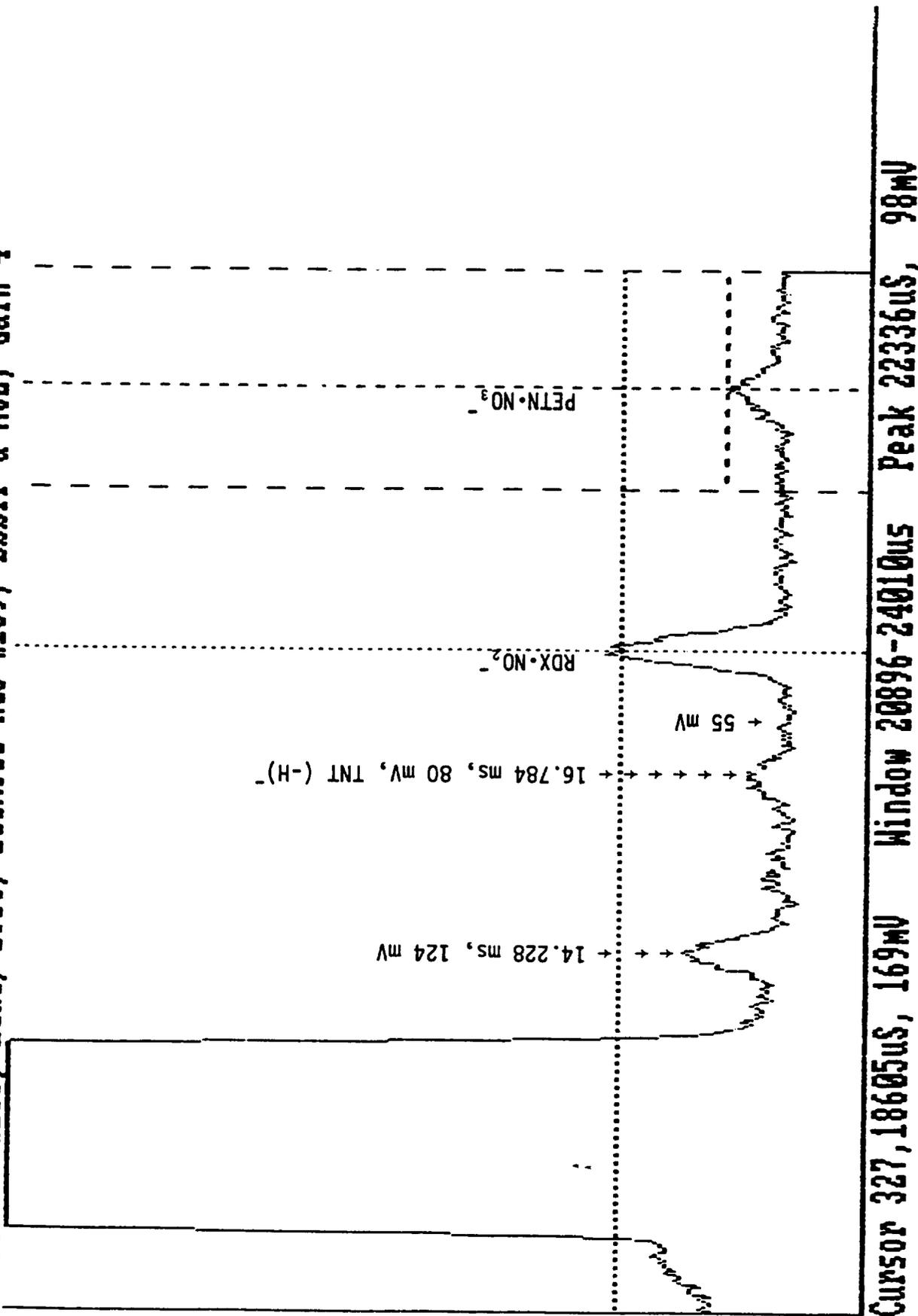
Figure 5. Injection of Solution Containing 50 pg TNT, 50 pg RDX, 75 pg PETN, @ 764 Torr

Figure 6. Preconcentrator/GC Interface Schematic
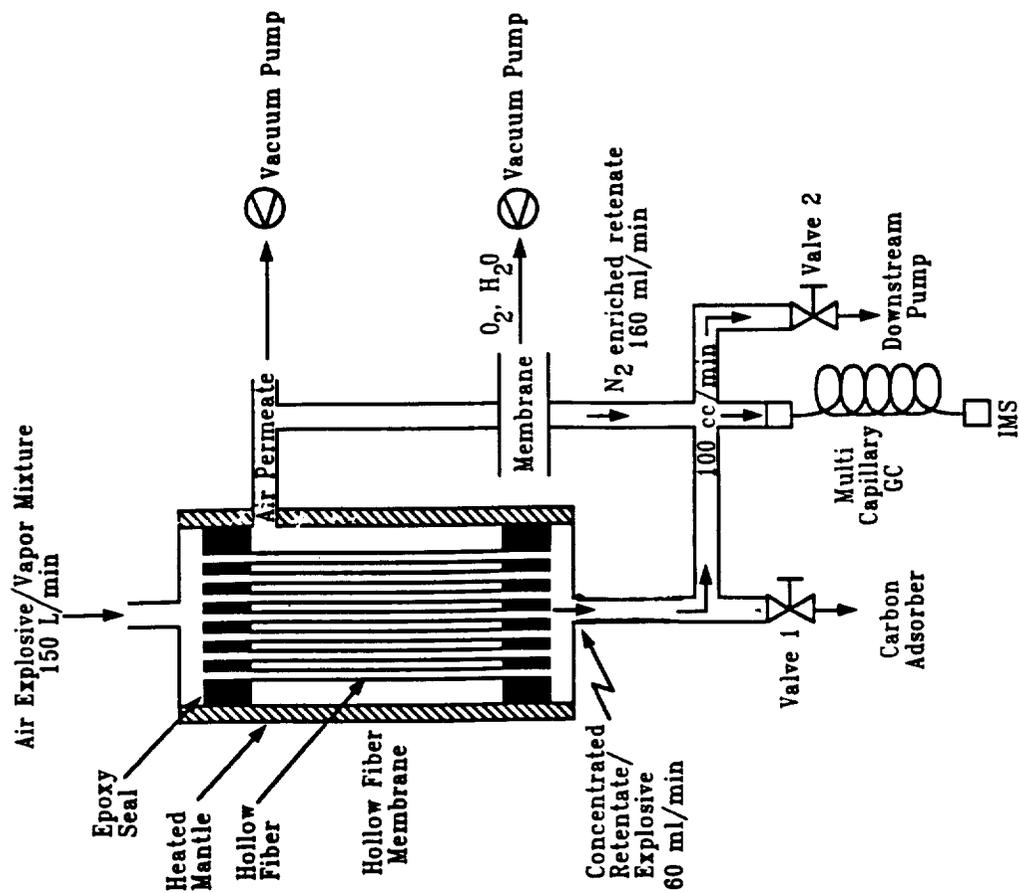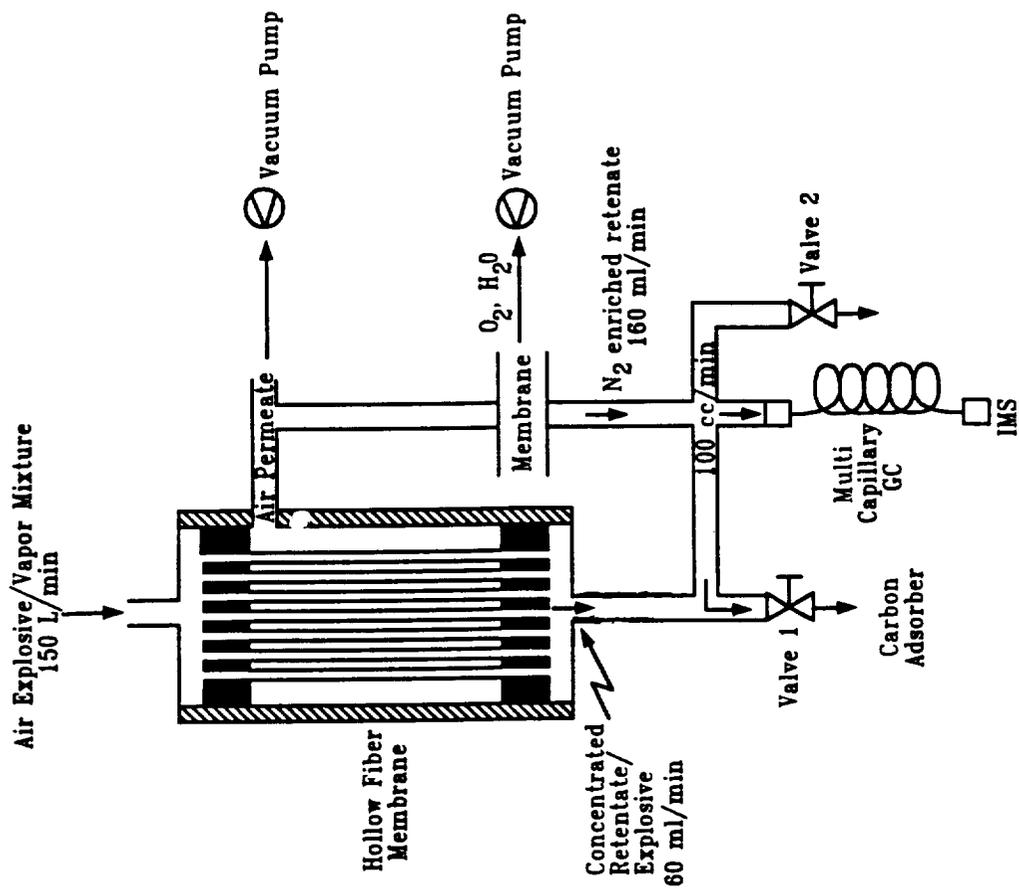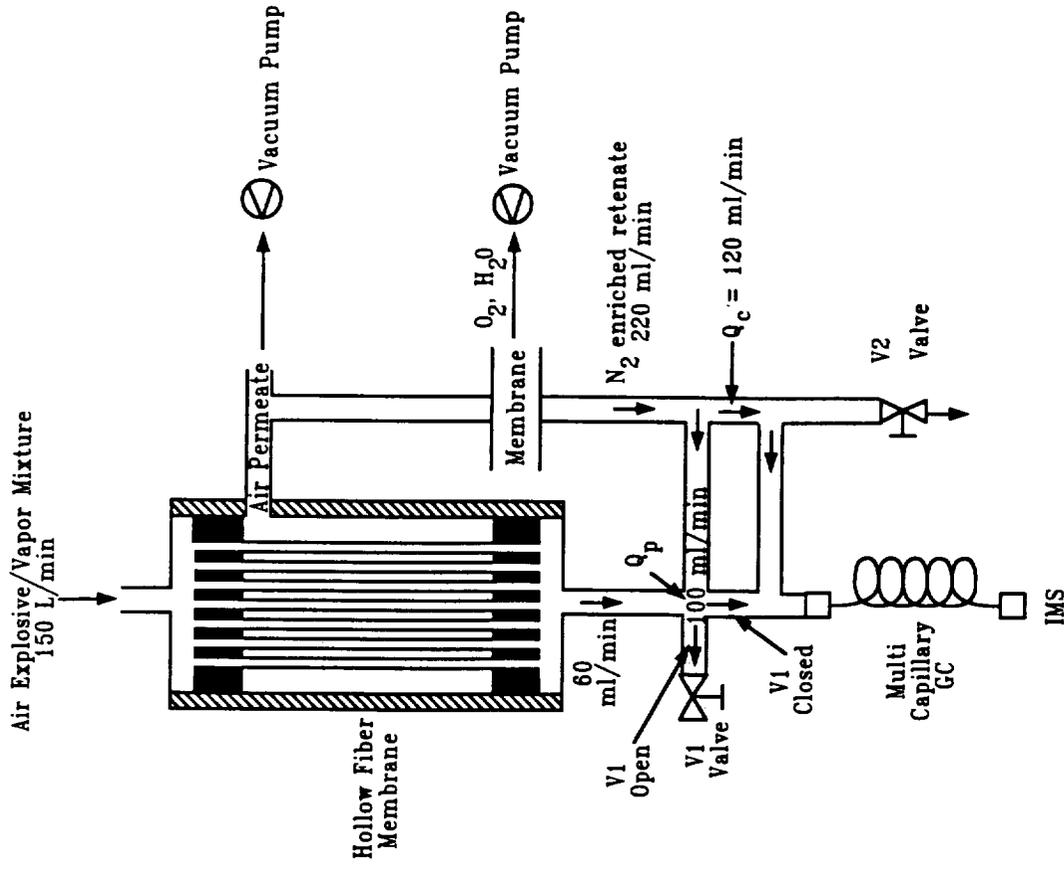
Figure 7. Preconcentrator/GC Interface Schematic

PURGE CONDITION: V1 Open, V2 Closed

Purge Flow Q_p to drain

Carrier Flow Q_c to GC Cloumn

SAMPLE CONDITION: V1 Closed, V2 Open Slightly

Purge Flow Q_p to GC Column

Carrier Flow Q_c to GC Column and Drain

Figure 6. Preconcentrator/GC Interface Schematic

188

Figure 7. Preconcentrator/GC Interface Schematic

Air Explosive/Vapor Mixture
150 L/min

Vacuum Pump

Air Permeate

O_2, H_2O

Vacuum Pump

N_2 enriched retenate
220 ml/min

Membrane

Q_c = 120 ml/min

V2
Valve

Q_p

100 ml/min

60
ml/min

V1
Open

V1
Valve

V1
Closed

Multi
Capillary
GC

IMS

Hollow Fiber
Membrane

PURGE CONDITION: V1 Open, V2 Closed

Purge Flow Q_p to drain

Carrier Flow Q_c to GC Cloumn

SAMPLE CONDITION: V1 Closed, V2 Open Slightly

Purge Flow Q_p to GC Column

Carrier Flow Q_c to GC Column and Drain

189
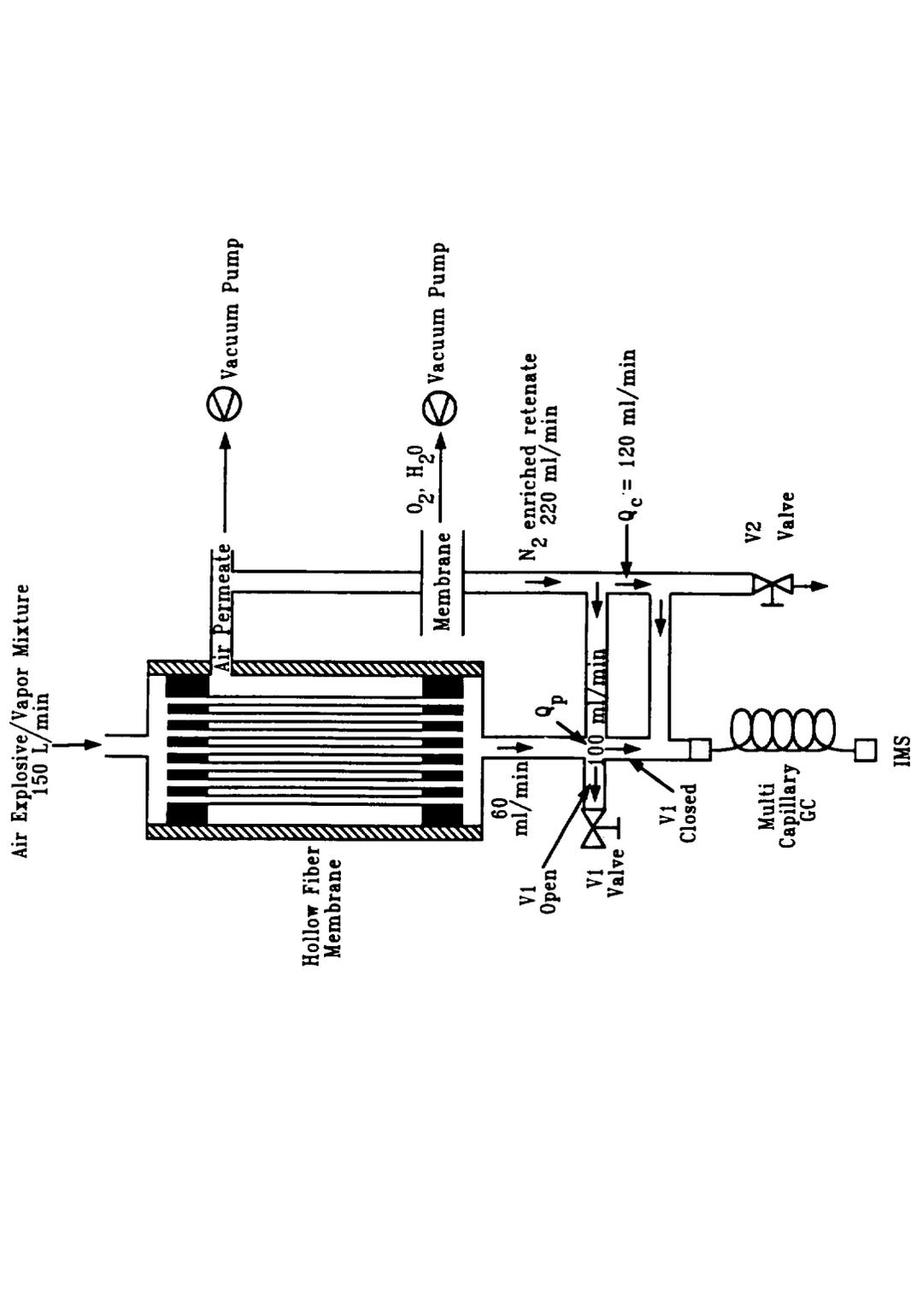
Session IV: Applications

Session Chair: Dr. Robert Turner

ENVIRONMENTAL APPLICATIONS FOR ION MOBILITY SPECTROMETRY

Robert K. Ritchie and Andreas Rudolph
Barringer Research Limited
304 Carlingview Drive, Rexdale, ON, Canada M9W 5G2

ABSTRACT

The detection of environmentally important polychlorinated aromatics by ion mobility spectrometry (IMS) was investigated. Single polychlorinated biphenyl (PCB) isomers (congeners) having five or more chlorine atoms were reliably detected in isooctane solution at levels of 35 ng with a Barringer IONSCAN ion mobility spectrometer operating in negative mode; limits of detection (LOD) were extrapolated to be in the low ng region. Mixtures of up to four PCB congeners, showing characteristic multiple peaks, and complex commercial mixtures of PCBs (Aroclors) were also detected. Detection of Aroclors in transformer oil was suppressed by the presence of the antioxidant BHT (2,6-di-t-butyl-4-methylphenol) in the oil. The wood preservative pentachlorophenol (PCP) was easily detected in recycled wood shavings at levels of 52 ppm with the IONSCAN; the LOD was extrapolated to be in the low ppm region.

INTRODUCTION

The Barringer IONSCAN ion mobility spectrometer is a proven instrument for the detection of trace amounts of explosives and illicit drugs. Current research efforts at Barringer are aimed at new IONSCAN applications, including the analysis of environmentally important compounds. IONSCAN systems require minimal or no sample preparation, are easy to use, and are very selective towards high electron affinity compounds such as polychlorinated aromatics. This presentation describes initial research to develop the IONSCAN into a rapid and on-site PCB and PCP detector.

Polychlorinated Biphenyls

PCBs are non-flammable, non-conductive, chemically quite inert, and have high boiling points; these properties make the commercial Aroclor mixtures desirable for use as insulator fluids or oil additives in electrical utility equipment such as transformers and capacitors. Unfortunately they have also been identified as major environmental pollutants, because high application temperatures can generate dangerous levels of dioxins and chlorinated dibenzofurans in the insulating fluids. Programs to remove PCBs from service usually either replace the whole transformer assembly (in case of high PCB content), or exchange the PCB containing oil with clean fluids (in case of lower PCB content). The present cutoff level for transformer replacement vs. oil exchange in Ontario is 50 ppm PCB in the oil. Analysis methods able to detect PCBs at levels below 50 ppm are needed to select the appropriate PCB removal action.[1]

PCB analysis is usually carried out by expensive and time consuming GC or GC/MS techniques. Recently, immunoassay[2] and colorimetric techniques aimed at on-site analysis have been developed; however, these require several handling and analysis steps, and are prone to interferences from other chlorinated organics or inorganic chlorides.

Wood Preservatives

Growing environmental awareness has led to a different attitude towards preservative-treated wood. It constitutes hazardous waste at the end of its life cycle, and it cannot be burned or landfilled due to release of the potentially dangerous preservatives. Manufacturers and users of this wood, faced with "cradle-to-grave" responsibility for these products, are looking for disposal alternatives. [3] Recycling is one important possibility, and in the case of wooden utility poles can result in almost complete recovery of the preservative (mostly creosote or PCP).

The patented TWT Technologies recycling process first removes the outer preservative-containing layer from the pole, and the somewhat smaller pole can then be reused, possibly for less demanding applications. The outer layer is subjected to a precisely defined heat treatment, dependent on the preservative used, which reclaims the preservative by distillation, and also produces a clean wood shaving product. [4]

Operational requirements are that the preservatives be identified before processing, and that the clean wood shaving product be declared non-hazardous (<40 ppm PCP, possibly reducing to 5 ppm). Fast, low-cost alternative methods to GC/MS are required, and again IMS appears to be a promising technique. [5]

EXPERIMENTAL METHODS

Table 1 details the analysis conditions that were employed on a Barringer IONSCAN Model 350 for the analyses of PCBs and PCP.

Table 1

	PCB Analysis	PCP Analysis
Ion Mode	Negative [a]	Negative [a]
Chloride Reactant Addition	No	Yes
Drift Tube Temperature	115°C	120°C
Inlet Temperature	300°C	300°C
Desorber Temperature	300°C	300°C

[a] explosives mode

PCB standard solutions (35 µg/ml in isooctane) were obtained from AccuStandard. Of the 209 different congeners, the following were chosen for analysis: 2-Chlorobiphenyl (#1), 3,3'-Dichlorobiphenyl (#11), 2,4,5-Trichlorobiphenyl (#29), 2,2'4,4'-Tetrachlorobiphenyl (#47), 2,3',4,5',6-Pentachlorobiphenyl (#121), 2,2',3,3',6,6'-Hexachlorobiphenyl (#136), 2,2',3,4,5,5',6-Heptachlorobiphenyl (#185), 2,2',3,3',4,4',5,5'-Octachlorobiphenyl (#194), 2,2',3,3',4,4',5,5',6-Nonachlorobiphenyl (#206), and Decachlorobiphenyl (#209). The numbers in parentheses represent the Ballschmiter-Zell numbering method.

Aroclor standard solutions in Volt-Esso 35 (a hydrocarbon transformer oil) and in isooctane were provided by Ontario Hydro and Barringer Laboratories, respectively. The following Aroclors were investigated: Aroclor 1254 (54% chlorine by weight, 75 ppm in Volt-Esso 35, and 35 µg/ml in isooctane) and Aroclor 1260 (60% chlorine by weight, 50 ppm in Volt-Esso 35, and 5 mg/ml in isooctane). BHT was available in-house.

1 µl aliquots of the PCB or Aroclor solutions in isooctane were applied to a standard

IONSCAN Teflon filter, and the solvent was allowed to evaporate (ca. 30 s) before IMS analysis. Aroclor analysis from transformer oil was carried out by applying ca. 10 μl of the oil solutions onto a standard Teflon filter, followed by desorption.

PCP samples supplied by TWT Technologies included a 5% solution in oil (a typical solution used in applying PCP to utility poles), and wood shavings containing 52 ppm PCP.

Barringer Ionscan System Manager Software Version 2.209 was used to acquire and handle the data.

RESULTS AND DISCUSSIONS

Polychlorinated Biphenyls

PCBs have been investigated by IMS by Karasek et al. as early as 1971.[6,7] He identified the species giving rise to the observed peaks as $(C_{12}H_{10-x}Cl_x)(H_2O)H^+$ for the positive ions and as $(C_{12}H_{10-x}Cl_x)^-$ for the negative ions. He also noted that the response of his instrument to the PCBs increased with degree of chlorine substitution in the negative mode and decreased in the positive mode, both due to increasing electron affinity with higher degree of chlorine substitution.

Under our analysis conditions, the PCBs with less than five chlorine atoms did not lead to an IONSCAN response, but the PCBs containing five or more chlorine atoms gave strong signal responses for 35 ng PCB. Typical plasmagrams and growth curves (the signal response plotted vs. desorption time) are shown in Figures 1 - 4. (Note: Since the negative mode in the IONSCAN is the explosives mode, all figures illustrations are titled Explosives Plasmagrams) The results are summarized in Table 2.

Table 2

PCB	K_o	Drift Time (ms)	Peak Area [a]	Max. Peak Height [b]	Estimated LOD (ng)
Penta-Cl	1.1813	15.265	288	320	<5 ng
Hexa-Cl	1.1572	15.566	49	70	#
Hepta-Cl	1.1004	16.373	396	371	<5 ng
Octa-Cl	1.0443	17.267	274	238	<5 ng
Nona-Cl	1.0182	17.734	389	244	<5 ng
Deca-Cl	0.9964	18.127	221	193	<5 ng

see text [a] in digital units * ms [b] in digital units

(1 digital unit corresponds to ca. 1.4×10^9 ions)

Unlike Karasek, we did not observe an increase of response with higher chlorine substitution. All PCBs investigated gave rise to single peak plasmagrams with a reasonable correlation between inverse reduced mobility ($1/K_o$) and molecular mass as shown in Figure 5. The growth curves show that the PCBs desorb relatively quickly under the conditions used, despite their high boiling points. The relatively poor response to the hexachlorobiphenyl is likely to be due to an impurity in this standard suppressing the ionization of the biphenyl. From Table 2 data, limits of detection (LOD) for the single PCB isomers are estimated to be in the low ng region.

Figures 6 - 8 depict plasmagrams of examples of binary, ternary, and quaternary mixtures of PCBs (35 ng for each individual compound) and show the expected multiple peaks. Unless not available due to partial peak overlap, the integrated and maximum peak heights of each component in the mixtures were calculated and compared to the equivalent data from the single isomer analysis; the data are listed in Table 3. There is not an appreciable degree of suppression of the responses if mixtures are analyzed except in mixtures containing the hexachlorobiphenyl where the impurity in that solution seems to suppress responses of the other isomers as well. The comparisons are also less reliable if there is peak overlap.

Figures 9 and 10 show Aroclor 1254 and Aroclor 1260, respectively, analyzed from isooctane solutions. Aroclors are highly complex mixtures of PCBs, and the plasmagrams show peaks that can be interpreted as sums of the individual responses. Based on the results of the single PCB isomer analyses, the observed peaks in the plasmagram of Aroclor 1254 can be assigned to pentachlorobiphenyls (peak 110), and hexachlorobiphenyls or possibly a mixture of hexa- and heptachlorobiphenyls (peak 111). In the analysis of Aroclor 1260, the peaks 120 - 123 are most likely derived from penta-, hexa-, hepta-, and octachlorobiphenyls, respectively. The distribution of the peaks reflect the different components in these Aroclors, with 1260 having a higher proportion of more substituted PCB isomers. It is thus possible to distinguish different Aroclors with an IONSCAN, without the need for a lengthy GC profiling analysis.

IMS analysis of blank (unspiked) Volt-Esso 35 transformer oil, shown in Figure 11, reveals the presence of a large peak (peak 100). Such a large peak must be due to an additive, since Volt-Esso 35 is a hydrocarbon oil, and hydrocarbons do not give good responses in IMS. Further investigation confirmed that the oil contains 0.03% of 2,6-di-t-butyl-4-methylphenol (BHT), a common antioxidant. The plasmagram of BHT is shown in Figure 12, confirming that this additive to Volt-Esso 35 is responsible for the large peak. Unfortunately presence of this compound in PCB containing oil suppresses the ionization of PCBs by an order of magnitude, as demonstrated in the plasmagram of Volt-Esso 35 spiked with 350 ng of heptachlorobiphenyl (Figure 13). IMS data on transformer oil samples are summarized in Table 4.

Figures 14 and 15 show plasmagrams of Aroclors 1254 and 1260, respectively, dissolved in Volt-Esso 35. Again it can easily be seen by comparison with Figures 9 and 10 that the presence of BHT suppresses any PCB response. Further research will be conducted into ways to eliminate the interference and suppression from BHT, e.g. possibly a quick sample filtration to selectively adsorb BHT on basic media.

Table 3

Mixture of PCBs (# of Cl)	Compounds	Int. Peak Area [a]	Max. Peak Height [b]	Individual Int. Peak Area [a]	Individual Max. Peak Height [b]
5+6	Penta-Cl	n.a.	83	288	320
	Hexa-Cl	n.a.	59	49	70
5+7	Penta-Cl	187	209	288	320
	Hepta-Cl	273	244	396	371
5+8	Penta-Cl	193	304	288	320
	Octa-Cl	331	204	274	238
5+9	Penta-Cl	176	278	288	320
	Nona-Cl	326	243	389	244
5+10	Penta-Cl	232	305	288	320
	Deca-Cl	284	202	221	193
6+7	Hexa-Cl	90	89	49	70
	Hepta-Cl	152	149	396	371
7+8	Hepta-Cl	211	284	396	371
	Octa-Cl	248	172	274	238
8+9	Octa-Cl	n.a.	111	274	238
	Nona-Cl	n.a.	133	389	244
9+10	Nona-Cl	n.a.	148	389	244
	Deca-Cl	n.a.	98	221	193
5+7+9	Penta-Cl	141	232	288	320
	Hepta-Cl	147	185	396	371
	Nona-Cl	204	165	389	244
7+8+10	Hepta-Cl	223	256	396	371
	Octa-Cl	252	139	274	238
	Deca-Cl	168	122	221	193
8+9+10	Octa-Cl	n.a.	103	274	238
	Nona-Cl	n.a.	70	389	244
	Deca-Cl	n.a.	53	221	193
5+7+8+10	Penta-Cl	119	208	288	320
	Hepta-Cl	166	166	396	371
	Octa-Cl	190	117	274	238
	Deca-Cl	136	107	221	193

[a] in digital units * ms   [b] in digital units

n.a. not available due to partial peak overlap

Table 4

Compound	35 ng in isooctane		35 ng in Volt-Esso		350 ng in Volt-Esso	
	Peak Area [a]	Max. Peak Height [b]	Peak Area [a]	Max. Peak Height [b]	Peak Area [a]	Max. Peak Height [b]
Penta-Cl	288	320	#	#	#	#
Hexa-Cl	49	70	#	#	#	#
Hepta-Cl	396	371	39	62	382	645
Octa-Cl	274	238	&	&	&	&
Nona-Cl	389	244	&	&	&	&
Deca-Cl	221	193	27	49	166	233

[a] in digital units * ms   [b] in digital units

no detection due to direct overlap with BHT   & not carried out

Wood Preservatives

Figure 16 shows a plasmagram for the IMS analysis of a 5% PCP solution in oil, and Figure 17 depicts a plasmagram from wood chips containing 52 ppm PCP. Both demonstrate that PCP gives rise to strong single peak plasmagrams in the IONSCAN. The weaker adjacent peak 130 in Figure 17 is most likely a tetrachlorophenol, and a previously conducted GC/MS analysis of this sample had shown the presence of ca. 3 ppm of this substance.

Figure 17 shows that the LOD for PCP is much lower than 52 ppm; it is extrapolated to be in the neighbourhood of 1 ppm, making IMS ideally suited for the wood recycling application for which the PCP levels of product shavings should be less than 40 ppm, or possibly less than 5 ppm.

Further experiments with more samples will be conducted to enable calibration of the IONSCAN for PCP in the region between 0 and 50 ppm; also, tetrachlorophenols will be analyzed to confirm the identity of the extra peak in Figure 17.

CONCLUSIONS

It was shown that Barringer's IONSCAN is in principle useful in environmental analysis since it is able to detect PCBs and PCP at low levels; however, in the case of PCB analysis the presence of BHT in transformer oil presents a major problem that has to be solved before this application can be developed any further. On the other hand PCP analysis in wood recycling applications presents no problems, and the development of this application is continuing.

ACKNOWLEDGMENTS

Peter Fransham of TWT Technologies for the PCP and wood samples.

REFERENCES

1.   Massey, R. Personal communication.

2.   Harrison, R.O., Carlson, R.E., Weiss, A.J. Analysis of PCBs in Soil, Sediments, and Other Matrices by Enzyme Immunoassay. *Proceedings:* 1993 U.S. EPA/A&WMA International Symposium on Field Screening Methods for Hazardous Wastes and Toxic Chemicals, Las Vegas, Nevada, pp. 462-471.

3.   Meil, J. Exploring the Resource - Timber Supplies & Life Cycle Analysis. Canadian Institute of Treated Wood: Treated Wood Life Cycle Workshop, Toronto, ON, June 1994.

4.   Fransham, P. Chemical Extraction Processes. Canadian Institute of Treated Wood: Treated Wood Life Cycle Workshop, Toronto, ON, June 1994.

5.   Lawrence, A.H. Rapid Characterization of Wood Species by Ion Mobility Spectrometry. *J. Pulp Pap. Sci.* **15**, J196-J199 (1989).

6.   Karasek, F.W. Plasma Chromatography of the Polychlorinated Biphenyls. *Anal. Chem.* **43**, 1982-1986 (1971).

7.   Karasek, F.W., Tatone, O.S., and Kane, D.M. Study of Electron Capture Behaviour of Substituted Aromatics by Plasma Chromatography. *Anal. Chem.* **45**, 1210-1214 (1973).

BARRINGER

IONSCAN™ Explosives Plasmagram

SampID: cl5bi-2 Cls: pcb WTime: 0.88 - 1.32 s
Sample: 1 ul (35 ng)

419 du
Wind: 3

Pk2	PeakID	K_0	DTime
0	Cal	1.6520 *	10.901
5	Cl5-PCB	1.1813 *	15.215
6	Cl6-PCB	1.1572 *	15.562
7	Cl7-PCB	1.1004 *	16.365
8	Cl8-PCB	1.0443 *	17.245
9	Cl9-PCB	1.0182 *	17.687
10	Cl10-PCB	0.9964 *	18.074

Ion Drift Time (ms)

Wnds: 15 **Scans:** 20 **Pts:** 856 **Per:** 25µs **T:** 22ms **Alg:** 1 **Time:** 14:04:16 07/29/94
Desc: Model 350-8812 Neg Mode; 115,298,300 degC; 351,302,643 cc/min;

No. of IONSCAN windows: 15

RESULTS OF IONSCAN ANALYSIS   *** FAIL ***

Penta-Cl ALARM! Substances found: Cl5-PCB

Chn	ChanID	Ko	DTime (µs)	Max Amp	Delta (µs)	# of Hits	Detected Substances (Partly) Dependent upon this Channel
0	Cal	1.6520	10901	215	N/A	N/A	
5	Cl5-PCB	1.1813	15253	320	+9	4	Cl5-PCB

Directory Pathname: g:\research\pcb\negmode
IONSCAN Model No: 350   Serial No: 8812
Comments:

Figure 1
IMS analysis of 2,3',4,5',6-pentachlorobiphenyl

BARRINGER

IONSCAN™ Explosives Growth Curves

SampID: cl5bi-2 Cls: pcb
Sample: 1 ul (35 ng)

419 du

Pk2	PeakID	K_0	DTime
0	Cal	1.6520 *	10.901
5	Cl5-PCB	1.1813 *	15.215
6	Cl6-PCB	1.1572 *	15.562
7	Cl7-PCB	1.1004 *	16.365
8	Cl8-PCB	1.0443 *	17.245
9	Cl9-PCB	1.0182 *	17.687
10	Cl10-PCB	0.9964 *	18.074

Desorption Time (s)

Wnds: 15 **Scans:** 20 **Pts:** 856 **Per:** 25µs **T:** 22ms **Alg:** 1 **Time:** 14:04:16 07/29/94
Desc: Model 350-8812 Neg Mode; 115,298,300 degC; 351,302,643 cc/min;

No. of IONSCAN windows: 15

RESULTS OF IONSCAN ANALYSIS   *** FAIL ***

Penta-Cl ALARM! Substances found: Cl5-PCB

Chn	ChanID	Ko	DTime (µs)	Max Amp	Delta (µs)	# of Hits	Detected Substances (Partly) Dependent upon this Channel
0	Cal	1.6520	10901	215	N/A	N/A	
5	Cl5-PCB	1.1813	15253	320	+9	4	Cl5-PCB

Directory Pathname: g:\research\pcb\negmode
IONSCAN Model No: 350   Serial No: 8812
Comments:

Figure 2
Growth curve of 2,3',4,5',6-pentachlorobiphenyl

IONSCAN™ Explosives Growth Curves

BARRINGER

SampID: cl10bi-2 Cls: pcb
Sample: 1 ul (35 ng)

PK2	PeakID	K₀	DTime
	Cal	1.6520	10.943
5	Cl5-PCB	1.1813*	15.289 *
6	Cl6-PCB	1.1572*	15.608 *
7	Cl7-PCB	1.1004*	16.413 *
8	Cl8-PCB	1.0443*	17.295 *
9	Cl9-PCB	1.0182*	17.738 *
10	Cl10-PCB	0.9964	18.127

250 du

Desorption Time (s)

Wnds: 15 Scans: 20 Pts: 856 Per: 25µs T: 22ms Alg: 1 Time: 12:27:35 07/29/94
Desc: Model 350-8812 Neg Mode: 115,298,300 degC: 351,302,643 cc/min;

*** FAIL *** No. of IONSCAN windows: 15

RESULTS OF IONSCAN ANALYSIS

Deca-Cl ALARM! Substances found: Cl10-PCB

Chn	ChanID	Ko	DTime (µs)	Max Amp	Delta (µs)	# of Hits	Detected Substances (Partly) Dependent upon this Channel
0	Cal	1.6520	10933	249	N/A	N/A	
10	Cl10-PCB	0.9964	18121	193	-5	4	Cl10-PCB

Directory Pathname: g:\research\pcb\negmode
IONSCAN Model No: 350 Serial No: 8812
Comments:

Figure 4
Growth curve of decachlorobiphenyl

IONSCAN™ Explosives Plasmagram

BARRINGER

SampID: cl10bi-2 Cls: pcb WTime: 1.76 - 2.20 s
Sample: 1 ul (35 ng)

PK2	PeakID	K₀	DTime
	Cal	1.6520	10.943
5	Cl5-PCB	1.1813*	15.289 *
6	Cl6-PCB	1.1572*	15.608 *
7	Cl7-PCB	1.1004*	16.413 *
8	Cl8-PCB	1.0443*	17.295 *
9	Cl9-PCB	1.0182*	17.738 *
10	Cl10-PCB	0.9964	18.127

250 du
Wind: 5

Ion Drift Time (ms)

Wnds: 15 Scans: 20 Pts: 856 Per: 25µs T: 22ms Alg: 1 Time: 12:27:35 07/29/94
Desc: Model 350-8812 Neg Mode: 115,298,300 degC: 351,302,643 cc/min;

*** FAIL *** No. of IONSCAN windows: 15

RESULTS OF IONSCAN ANALYSIS

Deca-Cl ALARM! Substances found: Cl10-PCB

Chn	ChanID	Ko	DTime (µs)	Max Amp	Delta (µs)	# of Hits	Detected Substances (Partly) Dependent upon this Channel
0	Cal	1.6520	10933	249	N/A	N/A	
10	Cl10-PCB	0.9964	18121	193	-5	4	Cl10-PCB

Directory Pathname: g:\research\pcb\negmode
IONSCAN Model No: 350 Serial No: 8812
Comments:

Figure 3
IMS analysis of decachlorobiphenyl

201

Figure 6
IMS analysis of a mixture of 2,3',4,5',6-pentachlorobiphenyl and decachlorobiphenyl

Figure 5
Correlation between inverse reduced mobility ($1/K_o$, in Vs/cm^2) and molecular mass of PCBs

BARRINGER   **IONSCAN™ Explosives Plasmagram**

Pk2	PeakID	K_0	DTime
0 ·	Cal	1.6520 ·	10.899
5	C15-PCB	1.1813 ·	15.212
6	C16-PCB	1.1572*	15.559 *
7	C17-PCB	1.1004*	16.362 *
8	C18-PCB	1.0443*	17.241 *
9	C19-PCB	1.0182*	17.683 *
10	C110-PCB	0.9964*	18.070 *

SampID: 3mixbi-1   Cls: pcb   WTime: 1.32 - 1.76 s
Sample: 1 ul penta, 1 ul hepta, 1 ul nona

227 du
Wind: 4

Ion Drift Time (ms)
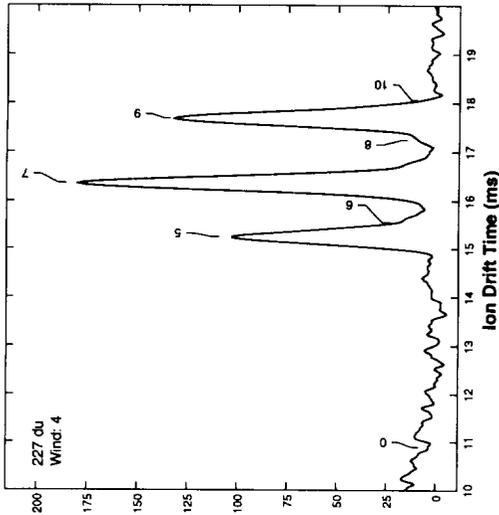
Wnds: 15   Scans: 20   Pts: 856   Per: 25µs   T: 22ms   Alg: 1   Time: 14:50:34 07/29/94
Desc: Model 350-8812 Neg Mode; 115,298,300 degC; 351,302,643 cc/min;

RESULTS OF IONSCAN ANALYSIS   * FAIL ***   No. of IONSCAN windows: 15**

Penta-Cl ALARM!   Substances found: C15-PCB
Hepta-Cl ALARM!   Substances found: C17-PCB
Nona-Cl ALARM!   Substances found: C19-PCB

Chn	ChanID	Ko	DTime (µs)	Max Amp	Delta (µs)	# of Hits	Detected Substances (Partly) Dependent upon this Channel
0	Cal	1.6520	10899	214	N/A	N/A	
5	C15-PCB	1.1813	15248	232	+7	2	C15-PCB
7	C17-PCB	1.1004	16365	185	+3	4	C17-PCB
9	C19-PCB	1.0182	17687	165	+4	4	C19-PCB

Directory Pathname: g:\research\pcb\negmode
IONSCAN Model No: 350   Serial No: 8812
Comments:
35 ng of 2,3',4,5',6-Pentachlorobiphenyl plus
35 ng of 2,2',3,4,5',6-Heptachlorobiphenyl plus
35 ng of 2,2',3,3',4,4',5,5',6-Nonachlorobiphenyl

Figure 7

IMS analysis of a mixture of 2,3',4,5',6-pentachlorobiphenyl, 2,2',3,4,5',6-heptachlorobiphenyl, and 2,2',3,3',4,4',5,5',6-nonachlorobiphenyl

---

BARRINGER   **IONSCAN™ Explosives Plasmagram**

Pk2	PeakID	K_0	DTime
0 ·	Cal	1.6520 ·	10.898
5	C15-PCB	1.1813 ·	15.210
6	C16-PCB	1.1572*	15.558 *
7	C17-PCB	1.1004*	16.361 *
8	C18-PCB	1.0443*	17.210 *
9	C19-PCB	1.0182*	17.682 *
10	C110-PCB	0.9964*	18.069 *

SampID: 4mixbi-1   Cls: pcb   WTime: 1.32 - 1.76 s
Sample: 1 ul each of penta, hepta, octa, deca

186 du
Wind: 4

Ion Drift Time (ms)
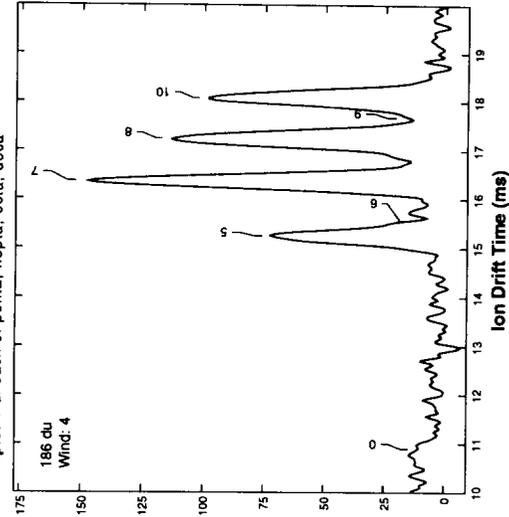
Wnds: 15   Scans: 20   Pts: 856   Per: 25µs   T: 22ms   Alg: 1   Time: 15:12:12 07/29/94
Desc: Model 350-8812 Neg Mode; 115,298,300 degC; 351,302,643 cc/min;

RESULTS OF IONSCAN ANALYSIS   * FAIL ***   No. of IONSCAN windows: 15**

Penta-Cl ALARM!   Substances found: C15-PCB
Hepta-Cl ALARM!   Substances found: C17-PCB
Octa-Cl ALARM!   Substances found: C18-PCB
Deca-Cl ALARM!   Substances found: C110-PCB

Chn	ChanID	Ko	DTime (µs)	Max Amp	Delta (µs)	# of Hits	Detected Substances (Partly) Dependent upon this Channel
0	Cal	1.6520	10898	218	N/A	N/A	
5	C15-PCB	1.1813	15258	208	+18	3	C15-PCB
7	C17-PCB	1.1004	16361	166	+1	4	C17-PCB
8	C18-PCB	1.0443	17239	117	+0	4	C18-PCB
10	C110-PCB	0.9964	18080	107	+12	4	C110-PCB

Directory Pathname: g:\research\pcb\negmode
IONSCAN Model No: 350   Serial No: 8812
Comments:
35 ng of 2,3',4,5',6-Pentachlorobiphenyl plus
35 ng of 2,2',3,4,5',6-Heptachlorobiphenyl plus
35 ng of 2,2',3,3',4,4',5,5'-octachlorobiphenyl plus
35 ng of Decachlorobiphenyl

Figure 8

IMS analysis of a mixture of 2,3',4,5',6-pentachlorobiphenyl, 2,2',3,4,5',6-heptachlorobiphenyl, 2,2',3,3',4,4',5,5'-octachlorobiphenyl, and decachlorobiphenyl

IONSCAN™ Explosives Plasmagram

SampID: 1260-1   Cls: pcb   WTime: 2.64 - 3.08 s
Sample: 5 ug Aroclor 1260 in isooctane

161 du
Wind: 7

Ion Drift Time (ms)

Wnds: 15   Scans: 20   Pts: 856   Per: 25µs   T: 22ms   Alg: 1   Time: 15:35:10 07/29/94
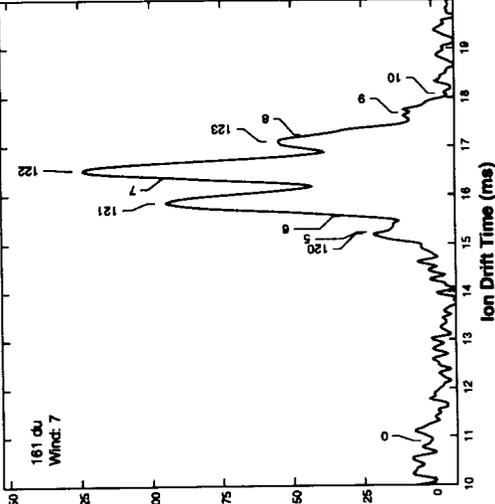
Pk2	PeakID	Ko	DTime
5	Cl5-PCB	1.1813*	15.243 *
6	Cl6-PCB	1.1572*	15.561 *
7	Cl7-PCB	1.1004*	16.364 *
8	Cl8-PCB	1.0443*	17.243 *
9	Cl9-PCB	1.0182*	17.685 *
10	Cl10-PCB	0.9964*	18.072 *
120		1.1843*	15.205 *
121		1.1364*	15.846 *
122		1.0905*	15.513 *
123		1.0529*	17.103 *

RESULTS OF IONSCAN ANALYSIS   *** PASS ***   No. of IONSCAN windows: 15

Desc: Model 350-8812 Neg Mode; 115,298,300 degC; 351,302,643 cc/min;

Chn	ChanID	Ko	DTime (µs)	Max Amp	Delta (µs)	# of Hits	Detected Substances (Partly) Dependent upon this Channel
0	Cal	1.6520	10900	222	N/A	N/A	

Directory Pathname: g:\research\pcb\negmode
IONSCAN Model No: 350   Serial No: 8812
Comments:

Figure 10
IMS analysis of Aroclor 1260 in isooctane

IONSCAN™ Explosives Plasmagram

SampID: 1254-1   Cls: pcb   WTime: 1.32 - 1.76 s
Sample: 35 ng Aroclor 1254 in isooctane

149 du
Wind: 4

Ion Drift Time (ms)

Wnds: 15   Scans: 20   Pts: 856   Per: 25µs   T: 22ms   Alg: 1   Time: 15:30:41 07/29/94

Pk2	PeakID	Ko	DTime
5	Cl5-PCB	1.1813*	15.233 *
6	Cl6-PCB	1.1572*	15.551 *
7	Cl7-PCB	1.1004*	16.353 *
8	Cl8-PCB	1.0443*	17.232 *
9	Cl9-PCB	1.0182*	17.674 *
10	Cl10-PCB	0.9964*	18.060 *
		1.1855*	15.179 *
111		1.1338*	15.872 *

RESULTS OF IONSCAN ANALYSIS   *** PASS ***   No. of IONSCAN windows: 15

Desc: Model 350-8812 Neg Mode; 115,298,300 degC; 351,302,643 cc/min;

Chn	ChanID	Ko	DTime (µs)	Max Amp	Delta (µs)	# of Hits	Detected Substances (Partly) Dependent upon this Channel
0	Cal	1.6520	10893	222	N/A	N/A	

Directory Pathname: g:\research\pcb\negmode
IONSCAN Model No: 350   Serial No: 8812
Comments:

Figure 9
IMS analysis of Aroclor 1254 in isooctane

BARRINGER

IONSCAN™ Explosives Plasmagram

SampID: BHT1 Cls: oil WTime: 0.88 - 1.32 s
Sample: Butylated hydroxytoluene

Pk2	PeakID	K₀	DTime
	Cal	1.6520	15.031
5	Cl5-PCB	1.1813*	15.301 *
6	Cl6-PCB	1.1572*	15.619 *
7	Cl7-PCB	1.1004*	16.425 *
8	Cl8-PCB	1.0443*	17.308 *
9	Cl9-PCB	1.0182*	17.751 *
10	Cl10-PCB	0.9964*	18.140 *
100	BHT	1.2034*	15.020 *

1390 du
Wlnd: 3

Ion Drift Time (ms)
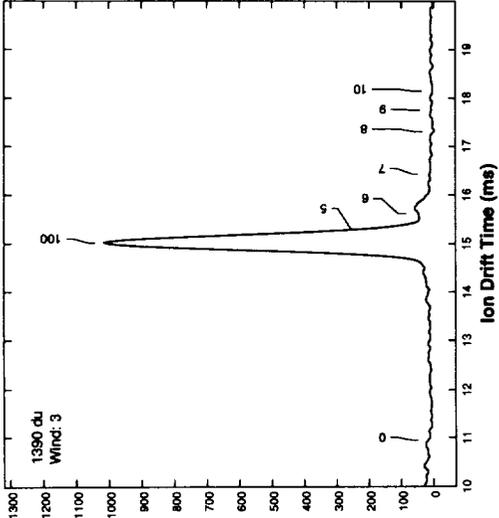
Wnds: 15 Scans: 20 Pts: 856 Per: 25μs T: 22ms Alg: 1 Time: 15:35:05 09/30/94
Desc: Model 350-8867 Neg Mode; 115,298,300 degC; 351,302,647 cc/min;

RESULTS OF IONSCAN ANALYSIS *** PASS *** No. of IONSCAN windows: 15

Chn	ChanID	Ko	DTime (μs)	Max Amp	Delta (μs)	# of Hits	Detected Substances (Partly) Dependent upon this Channel
0	Cal	1.6520	10941	421	N/A	N/A	

Directory Pathname: c:\ism\pcb
IONSCAN Model No: 350 Serial No: 8867
Comments:
2,6-Di-tert.butyl-4-methylphenol, antioxidant

Figure 12
IMS analysis of BHT (2,6-di-t-butyl-4-methylphenol)

BARRINGER

IONSCAN™ Explosives Plasmagram

SampID: blank1 Cls: oil WTime: 0.88 - 1.32 s
Sample: Blank transformer oil

Pk2	PeakID	K₀	DTime
	Cal	1.6520	15.031
5	Cl5-PCB	1.1813*	15.264 *
6	Cl6-PCB	1.1572*	15.582 *
7	Cl7-PCB	1.1004*	16.386 *
8	Cl8-PCB	1.0443*	17.287 *
9	Cl9-PCB	1.0182*	17.709 *
10	Cl10-PCB	0.9964*	18.097 *
100	BHT	1.2013*	15.010 *

963 du
Wlnd: 3

Ion Drift Time (ms)

Wnds: 15 Scans: 20 Pts: 856 Per: 25μs T: 22ms Alg: 1 Time: 16:22:49 09/29/94
Desc: Model 350-8867 Neg Mode; 113,298,300 degC; 351,302,647 cc/min;

RESULTS OF IONSCAN ANALYSIS *** PASS *** No. of IONSCAN windows: 15

Chn	ChanID	Ko	DTime (μs)	Max Amp	Delta (μs)	# of Hits	Detected Substances (Partly) Dependent upon this Channel
0	Cal	1.6520	10915	356	N/A	N/A	

Directory Pathname: g:\research\pcb\negmode
IONSCAN Model No: 350 Serial No: 8867
Comments:
from Ontario Hydro

Figure 11
IMS analysis of blank Volt-Esso 35 transformer oil

Figure 13

BARRINGER

Pk2	PeakID	K₀	DTime
0	Cal	1.6520*	15.224
5	C15-PCB	1.1813*	15.224
6	C16-PCB	1.1572*	15.541
7	C17-PCB	1.1004*	16.075
8	C18-PCB	1.0443*	17.221
9	C19-PCB	1.0182*	17.662
10	C110-PCB	0.9964*	18.049
100	BHT	1.1963*	15.033 *

IONSCAN™ Explosives Plasmagram

SampID: blank_7   Cls: oil   WTime: 1.32 - 1.76 s
Sample: 350 ng of Hepta-Cl PCB in Volt-Esso 35

RESULTS OF IONSCAN ANALYSIS   *** FAIL ***   No. of IONSCAN windows: 15

Hepta-Cl ALARM! Substances found: C17-PCB

Chn	ChanID	Ko	DTime (μs)	Max Amp	Delta (μs)	# of Hits	Detected Substances (Partly) Dependent upon this Channel
0	Cal	1.6520	10886	404	N/A	N/A	
7	C17-PCB	1.1004	16350	645	+8	5	C17-PCB

Directory Pathname: g:\research\pcb\negmode
IONSCAN Model No: 350   Serial No: 8867
Comments:

Wnds: 15   Scans: 20   Pts: 856   Per: 25μs   T: 22ms   Alg: 1   Time: 17:00:49 09/29/94
Desc: Model 350-8867 Neg Mode; 115,298,300 degC; 351,302,647 cc/min;

Figure 13
IMS analysis of 2,2′,3,4,5,5′,6-heptachlorobiphenyl in Volt-Esso 35

BARRINGER

Pk2	PeakID	K₀	DTime
0	Cal	1.6520*	15.012
5	C15-PCB	1.1813*	15.246 *
6	C16-PCB	1.1572*	15.564 *
7	C17-PCB	1.1004*	16.367 *
8	C18-PCB	1.0443*	17.246 *
9	C19-PCB	1.0182*	17.688 *
9	C110-PCB	0.9964*	18.075 *
100	BHT	1.2007*	15.000 *
110		1.1855*	15.192 *
111		1.1338*	15.885 *

IONSCAN™ Explosives Plasmagram

SampID: 1254-1   Cls: oil   WTime: 0.88 - 1.32 s
Sample: 75 ppm Aroclor 1254 in Volt-Esso 35

RESULTS OF IONSCAN ANALYSIS   *** PASS ***   No. of IONSCAN windows: 15

Chn	ChanID	Ko	DTime (μs)	Max Amp	Delta (μs)	# of Hits	Detected Substances (Partly) Dependent upon this Channel
0	Cal	1.6520	10902	384	N/A	N/A	

Directory Pathname: g:\research\pcb\negmode
IONSCAN Model No: 350   Serial No: 8867
Comments:
Peaks 110 and 111 refer to the Aroclor 1254 peaks in Figure 9

Wnds: 15   Scans: 20   Pts: 856   T: 22ms   Alg: 1   Time: 16:25:42 09/29/94
Desc: Model 350-8867 Neg Mode; 114,298,300 degC; 351,302,647 cc/min;

Figure 14
IMS analysis of Aroclor 1254 in Volt-Esso 35

Figure 15
IMS analysis of Aroclor 1260 in Volt-Esso 35

Figure 16
IMS analysis of pentachlorophenol in oil

BARRINGER

IONSCAN™ Explosives Plasmagram

Pk2	PeakID	K₀	DTime
0	Cal	1.6520	10.852
21	PCPhenol	1.4764	12.754
130	7	1.4760 *	12.146 *

SampID: twt_5   Cls: pcp   WTime: 1.32 - 1.76 s
Sample: Processed wood shavings (52 ppm PCP)

918 du
Wind: 4

800
700
600
500
400
300
200
100
0

10   11   12   13   14   15   16   17   18

Ion Drift Time (ms)
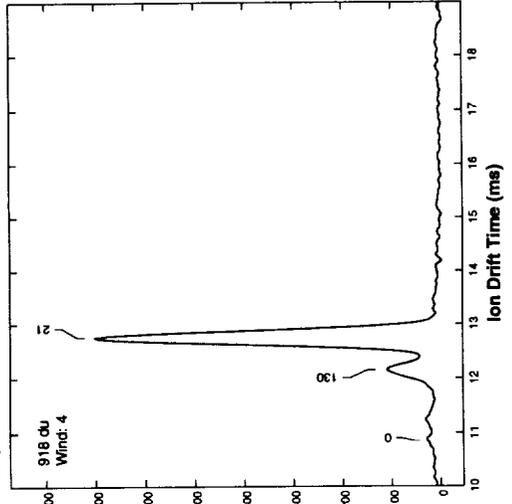
Wnds: 15   Scans: 20   Pts: 856   Per: 25µs   T: 22ms   Alg: 1   Time: 12:16:39 07/18/94
Desc: Model 350-8812 Neg Mode: 115,298,300 degC; 351,302,643 cc/min;

RESULTS OF IONSCAN ANALYSIS   *** FAIL ***   No. of IONSCAN windows: 15

PCPhenol ALARM!   Substances found: PCPhenol

Chn	ChanID	Ko	DTime (µs)	Max Amp	Delta (µs)	# of Hits	Detected Substances (Partly) Dependent upon this Channel
0	Cal	1.6520	10852	270	N/A	N/A	
21	PCPhenol	1.4053	12744	769	-13	15	PCPhenol

Directory Pathname: g:\research\wood
IONSCAN Model No: 350   Serial No: 8812
Comments:

Figure 17
IMS analysis of wood shavings containing 52 ppm PCP

208

DIRECT ANALYSIS OF ORGANIC PRIORITY POLLUTANTS BY IMS

C.S. Giam*, G.E. Reed, T.L. Holliday, L. Chang, and B.J. Rhodes
Environmental Analytical Research Laboratory, Texas A&M University at Galveston, 5007 Avenue U, Galveston, Texas 77551, U.S.A.

ABSTRACT

Many routine methods for monitoring of trace amounts of atmospheric organic pollutants consist of several steps. Typical steps are: (1) **collection** of the air sample, (2) **trapping** of organics from the sample, (3) **extraction** of the trapped organics, and (4) **identification** of the organics in the extract by GC (gas chromatography), HPLC (High Performance Liquid Chromatography), or MS (Mass Spectrometry). These methods are often cumbersome and time consuming. A simple and fast method for monitoring atmospheric organics using an IMS (Ion Mobility Spectrometer) is proposed. This method has a short sampling time and does not require extraction of the organics since the sample is placed directly in the IMS. The purpose of this study was to determine the responses in the IMS to organic "priority pollutants." Priority pollutants including representative polycyclic aromatic hydrocarbons (PAHs), phthalates, phenols, chlorinated pesticides, and polychlorinated biphenyls (PCBs) were analyzed in both the positive and negative detection mode at ambient atmospheric pressure. Detection mode and amount detected are presented.

INTRODUCTION

Our research group has, for several years, been detecting and quantitating organic pollutants, particularly anthropogenic ones, in very clean (open ocean) air at very low concentrations, picograms or less.[1-4] Very often, this analysis would require collection of large volumes of air using trapping materials for these organics, such as adsorbents like Amberlite and Florisil, followed by extraction of the trapped organics and then identification and quantitation by GC-ECD and GC-MS. This is a cumbersome, tedious, time consuming process and often contaminants are introduced into the samples. When we were kindly provided with a PCP IMS 100 by the FAA for explosive analysis, we took the opportunity to determine the scope and limitations of IMS (ion mobility spectrometry) as a faster way of direct analysis of real-time, real-life air samples. In order to see if IMS is suitable for detecting priority pollutants, we needed to first screen these compounds. Although detection of organics using IMS has been carried out for a number of years, often the reports in the literature are incomplete and usually the IMS operating conditions vary from report to report.

(*To whom all correspondences should be addressed.)

The goal of this research is to develop a fast and simple method for monitoring atmospheric organic priority pollutants using IMS. The objective for this study was to determine if different classes of semi-volatile organic priority pollutants give an IMS response. There are 128 priority pollutants, of these 110 are organic compounds, 80 of which are semi-volatile organics. We have analyzed over 90% of the semi-volatile organic priority pollutants. The IMS response for each compound studied was determined at atmospheric pressure in the negative detection mode with nitrogen and the positive detection mode with air. This paper will present an overview of general IMS responses for the different classes. Subsequent publications will emphasize methods that can be used to distinguish the different pollutants, reduced mobilities of the semi-volatile priority pollutants (studies are continuing to determine the purity of the compounds and peaks in the spectra due to impurities), and the use of IMS in monitoring atmospheric organics.

EXPERIMENTAL METHODS

IMS spectra of individual organic pollutants were obtained using a PCP-100 (from PCP, Inc., 2155 Indian Road, West Palm Beach, Florida, 33409-3287) and the instruments instructions, including the use of its sample holder (a quartz tube 4.0 mm + 0.4 mm i.d. x 1.5" long, with a small plug of glass wool). IMS conditions for both modes were: IMS temperature of 200°C, polarity of 3000 volts, drift flow of 600 ml/min, carrier flow of 400 ml/min and atmospheric pressure. For the negative detection mode, negative polarity, nitrogen and a delay of 2000 us were used. For the positive detection mode, positive polarity, air and a delay of 6000 us were used.

U.S. EPA Standards (100-500 ng/ul) in methanol were diluted to provide concentrations of 50 ng/ul. 2-4 ul of the diluted solution were placed in the IMS quartz sample holder; after the solution had evaporated (30 seconds), the sample holder was placed in the IMS. Detection limits vary from low nanograms to 400 ng. Any compound requiring more than 400 ng was considered unresponsive to IMS.

RESULTS AND DISCUSSION

Results are summarized in Table 1. The major findings were as follows. All of the PAHs investigated were detectable only in the positive mode. PAHs were very responsive even at low amounts. The phenols were detected only in the negative mode with the exception of 2,4-dimethylphenol which was only detected in the positive mode. Most of the phenols were very

responsive in the negative mode even at low amounts. In general, the ubiquitous PCBs were detected in the negative mode with the exception of PCB 1221, which was detected in both modes. A prominent chloride peak was observed in the negative mode with nitrogen for all of the PCBs analyzed. IMS spectra of the PCBs contained several peaks. This could be expected since PCB mixtures may contain as many as several hundred isomers. The ubiquitous phthalates were detected in both the positive and negative modes. However, phthalate detection was more sensitive in the positive mode.

Most of the chlorinated pesticides were detected in both modes with the exception of aldrin, heptachlor epoxide and toxaphene which were detected only in the negative mode. Most of these highly chlorinated compounds gave a large chloride peak in the negative mode. Many of the compounds gave more than one peak indicating one or more product ions from the parent molecule as well as the chloride ion.

IMS analysis of <u>some</u> of these compounds using different operating conditions have been reported by other researchers[5-12]. Published results were similar to our findings for phenanthrene[6,8], fluoranthene[6,8,9,12], dimethyl phthalate[5,7,11,12], chrysene[5,7], diethyl phthalate[7,11], fluorene[9,12], dieldrin[12], and 2,4-dichlorophenol.[10] Reported results for dibutyl phthalate[11], anthracene[8,9,12], endrin[12], and acenaphthalene[8] differed from our findings but may have been due to a difference in IMS operating conditions.

Experiments are continuing to obtain IMS spectra and reduced mobilities for the remaining semi-volatile organic priority pollutants. Once these experiments have been completed, field studies using the IMS air sampling and detection method will be conducted.

ACKNOWLEDGEMENTS

REFERENCES

1. Atlas, E., Sullivan, K. and Giam, C.S. Widespread Occurrence of Poly-halogenated Aromatic Ethers in the Marine Atmosphere. *Atmos. Environ.* **20**(6), 1217-1220 and references therein (1986).

2. Giam, C.S., Chan, H.S., Neff, G.S. and Atlas, E.L. Phthalate Ester Plasticizers: A New Class of Marine Pollutant. *Science.* **199**, 419-421 and references therein (1978).

3. Atlas, E. and Giam, C.S. Sea-air Exchange of High Molecular Weight Synthetic Organic Compounds: Results from the SEAREX Program. *Chem. Ocean.*, **10**, 340-378 and references therein (1989).

4. Atlas, E. and Giam, C.S. Sampling Organic Compounds fore Marine Pollution Studies. Strategies and Advanced Techniques in Marine Pollution Studies. NATO Advanced Studies Institute Symposium Series. 1986, pp 209-230.

5. Hagen, D.F. Characterization of Isomeric Compounds by Gas and Plasma Chromatography. *Anal. Chem.* **51**, 870-874 (1979).

6. Clement, R.E., Siu, K.W.M., and Hill, H.H., Jr., eds. Instrumentation for Trace Organic Monitoring. Lewis Publishers, Chelsea, MI, 1992, pp 27-48.

7. Carr, T.W., ed. Plasma Chromatography. Plenum Press, New York ,1984, pp 1-214.

8. Griffin, G.W., Dzidic, I., Carroll, D.I., Stillwell,R.N. and Horning, E.C. Ion Mass Assignments Based on Mobility Measurements. *Anal. Chem.* **45**, 1204-1209 (1973).

9. Lubman, D.M. Temperature Dependence of Plasma Chromatography of Aromatic Hydrocarbons. *Anal. Chem.* **56**, 1298-1302 (1984).

10. Moye, H.A. Plasma Chromatography of Pesticides. *J. Chrom. Sci.* **13**, 285-291 (1975).

11. Pozlomek, E.J. and Eiceman, G.A. Solid-Phase Enrichment, Thermal Desorption, and Ion Mobility Spectrometry for Field Screening of Organic Pollutants in Water. *Environ. Sci. Technol.* **26**, 1313-1318 (1992).

12. Shumate, C., St. Louis, R.H. and Hill, H.H., Jr. Table of Reduced Mobility Values from Ambient Pressure Ion Mobility Spectrometry. *J. Chrom.* **373**, 141-173 (1986).

TABLE 1. Summary of IMS Responses of the Different Priority Pollutant Classes

PRIORITY POLLUTANT	AMOUNT DETECTED (nanograms)	
	POSITIVE MODE	NEGATIVE MODE
Polycyclic Aromatic Hydrocarbons		
Acenaphthene	200	ND
Acenaphthylene	100	ND
Anthracene	25	ND
Chrysene	100	ND
Fluoranthene	50	ND
Fluorene	100	ND
Phenanthrene	100	ND
Pyrene	100	ND
Phenols		
2-Nitrophenol	ND	ND
4-Nitrophenol	ND	100
2,4-Dichlorophenol	ND	200
2,4-Dimethylphenol	400	ND
2,4-Dinitrophenol	ND	100
2,4,6-Trichlorophenol	ND	100
Pentachlorophenol	ND	50
Polychlorinated Biphenyls		
PCB 1221	400	400
PCB 1242	ND	400
PCB 1254	ND	100
PCB 1260	ND	100
Phthalates		
Butyl Benzyl Phthalate	50	200
Di-n-butyl Phthalate	50	400
Di(2-ethylhexyl) Phthalate	50	200
Diethyl Phthalate	25	400
Dimethyl Phthalate	50	400
Di-n-octyl Phthalate	50	200
Chorinated Pesticides		
Aldrin	ND	100
Chlordane	150	100
Dieldrin	100	100
Endosulfan Sulfate	200	100
Endrin	250	100
Endrin Aldehyde	400	100
Heptachlor	250	300
Heptachlor Epoxide	ND	200
Toxaphene	ND	100

ND = Not detected, > 400 ng

AN AMMONIA MONITOR FOR THE WATER INDUSTRY

J.L.Brokenshire and C.A.Cumming,
Graseby Dynamics Ltd., Watford, UK.

HISTORICAL BACKGROUND

Following the emergence of the European Community as a unified trading and economic entity, the various member states are required to follow certain directives governing their social affairs. Many of these directives concern the quality of the air we breathe, and the water that we use for consumption or in industrial processes. In order to comply with these directives a major overhaul of the water industry in the UK was required. For example, in many coastal towns and resorts there has never been any formal sewage treatment since, traditionally, all waste was dumped at sea through outfall pipes. Because this is no longer acceptable, whole new treatment systems are required.

CURRENT ORGANIZATION OF THE UK WATER INDUSTRY

For reasons which one can probably surmise, the first part of this overhaul was to privatize the industry. This consisted of creating ten individual Water Authorities according to geographical location within England and Wales with separate Authorities for Scotland and Northern Ireland. Each authority is responsible for the supply of drinking water and water for domestic and industrial consumption, and the treatment of all wastewaters, to the required standards laid down by both UK legislation and the appropriate EC directives. Compliance is monitored by the National Rivers Authority which has overall responsibility for all the freshwater supplies in the UK. The financial side of the industry is monitored on behalf of the consumer by OFWAT a quasi-government organization or Quango, which has the power to limit the water rates charged by the individual Authorities.

COST REDUCTION AND REMOTE MONITORING

The ten UK Water Authorities are autonomous companies listed on the UK stock exchange. They currently face a difficult time in undertaking a huge capital investment programme to update entire systems, and demonstrate compliance with legislative requirements, while being limited in the price increases that they can pass on to the consumer. Part of the solution is to increase efficiency and reduce costs, the latter inevitably entailing manpower reduction. The intention is to reduce manpower by automating treatment processes and monitoring them remotely from a central system.

In order to automate a process it is necessary to control it; in order to exercise control the process has to be monitored, and in order to monitor certain fundamental measurements are required. In order to make these measurements, it is essential that the critical variables are known, and that there exists a reliable means of measuring each of these variables which is amenable to long term unattended operation, and can be interrogated remotely. A considerable number of drinking water treatment facilities have been essentially unmanned for many years, but large sewage treatment works have not, and this is where the first serious look at demanning is taking place.

SEWAGE TREATMENT

The first task is to identify the critical parameters in the sewage treatment process. Sewage is the waste waters and excreta of both domestic and industrial processes, and is an undefined, complex mixture of chemical and biological components. It is a highly turbid liquid, greyish in color, which normally putrefies quickly using up any dissolved oxygen. The treatment of sewage must convert this mixture to relatively clean water prior to returning it to the freshwater system.

The first stage involves removal of large solid objects, and grit derived from road and roof surfaces during heavy rainfall. After grit separation and screening the sewage is subjected to sedimentation in which impurities in the form of suspended solids gradually settle and are removed in the form of a liquid sludge. Secondary treatment involves the use of biological filters in which bacteria, protozoa, fungi, worms, larvae and flies convert the impurities in the settled sewage. The final process involves a further settling or filtering referred to as 'polishing', before the final effluent is returned to the receiving watercourse.

ESSENTIAL PARAMETERS

In order to monitor and control the entire process for the majority of the time, excluding accidents and emergencies, there are several parameters which can be used to give guidance on the state of the treated sewage. These include temperature, flowrate, dissolved oxygen content, pH, and turbidity. The quality of the final effluent depends upon its biological and chemical activity, and historically these are determined by the chemical and biological oxygen demand, however there are certain specific components which require more detailed measurement, and one of these is ammonia.

THE ROLE OF AMMONIA

Ammonia is present in natural body wastes and is formed by microbial action on the organic nitrogen containing chemical species present in the sewage. In the time it takes the sewage to reach the treatment works, virtually all of the nitrogenous species have been converted to ammonia. In addition the run-off from farmland introduces ammonia directly or more nitrogenous material to the watercourses. Ammonia levels are reduced in the sewage treatment process by 'nitrification', the process by which particular bacteria convert ammonia to nitrate in the presence of oxygen. Ammonia causes specific problems if the levels are too high in freshwater supplies. Firstly, it is toxic to fish. Fish kills are immediately obvious and prompt swift action by the public and the NRA. Secondly, ammonia prevents effective disinfection of water by chlorination, resulting in drinking water supplies with high bacteriological activity. If a Water Authority returns treated sewage with a high ammonia content to the river, kills a lot of fish, then abstracts the water downstream and fails to disinfect it effectively before supplying it as drinking water, the local populace tends to take a pretty dim view. The concentration of ammonia in water is therefore regarded as a critical parameter.

AMMONIA IN WATER

Ammonia in water is subject to an acid-base equilibrium:

$$NH_3(g) + H_2O(l) \Leftrightarrow NH_4^+ + OH^-$$
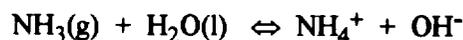
for which   *1:* $K_b = [NH_4^+][OH^-] / [NH_3]$

Since water is also ionized:

$$H_2O \Leftrightarrow H^+ + OH^-$$

for which   **2:** $K_w = [H^+][OH^-]$

For simplicity all activity coefficients have been assumed to be unity.

Equations 1 and 2 can be combined to give:

     3: $[NH_3] / [NH_4^+] = K_w / K_b [H^+]$

from which   **4:** $\log [NH_3] / [NH_4^+] = \log K_w - \log K_b + pH$

The ratio of free to ionized ammonia is crucial, since it is neutral ammonia which is toxic to fish[1].

If virtually all the ammonia is present in the free form, i.e. at least 99%, then $\log [NH_3] / [NH_4^+]$ would be >2. Since K_w is typically 3×10^{-15} and K_b is 1.6×10^{-5} then the pH would be have to be at least 11.5. By adding KOH to the sample to raise the pH to at least this level, the total ammonia concentration in the sample can be determined. Knowing the original pH of the sample prior to the addition of KOH, allows the level of free ammonia in the sample to be calculated.

At the present time the total ammonia level is measured and the neutral ammonia calculated, with varying degrees of complexity, using the measured temperature, pH and a knowledge of the typical level of total dissolved solids in the sample. The accuracy of this method is limited primarily by the accuracy of pH measurement. Tables of data are available[2] which relate the percentage of unionized ammonia to pH, temperature and total dissolved solids, and also give the total ammonia concentration which would breach the EC directives for protection of fish stocks as a function of these variables. Table 1 gives a selection of percentages of unionized ammonia as a function of pH and temperature with a total dissolved solid level of 400mg/l, while Table 2 gives selected concentrations of total ammonia having a free ammonia level of 0.021mg/l (the current mandatory EC limit) as a function of pH and temperature for the same level of total dissolved solids.

Table 1:   **Percentage unionized ammonia as a function of pH and Temperature**

pH	Temperature (°C)			
	5	15	25	35
5.5	0.0036	0.0078	0.0162	0.0321
6.5	0.0355	0.0778	0.1616	0.3196
7.5	0.3542	0.7727	1.5924	3.1063
8.5	3.4330	7.2250	13.928	24.276
9.5	26.226	43.781	61.806	76.224

Table 2: Concentration of Total Ammonia (mg/l) containing an unionized ammonia level of 0.021 mg/l as a function of pH and temperature with 400mg/l total dissolved solids.

pH	Temperature(°C)			
	5	15	25	35
5.5	579.1	264.4	127.2	64.24
6.5	57.93	26.46	12.74	6.443
7.5	5.812	2.664	1.293	0.663
8.5	0.600	0.285	0.148	0.085
9.5	0.079	0.047	0.033	0.027

REQUIREMENTS FOR AN AMMONIA ANALYZER

The majority of Ammonia analyzers currently use ion-specific electrodes with pH reference electrodes to perform the ammonia measurements. The typical life of electrodes in continuous operation is 3 months. The total ion measurement is performed by raising the pH using caustic solutions until virtually all of the ammonia is present in the unionized form. The ion-specific electrodes are subject to drift and therefore require calibration on a continuous basis. This type of analyzer is very expensive to maintain in terms of the cost of consumables, frequency of replacement and required routine maintenance. In addition the accuracy of the final result is subject to question.

Any replacement analyzer would need to demonstrate improved performance capabilities in terms of data reliability, while showing marked improvements in the cost and consumption of consumables, together with significant reductions in required maintenance. It would also need to be capable of long-term unattended operation with all data available for transmission to remote locations on demand.

THE NEED FOR SAMPLE PREPARATION

The initial stages of proof of the viability of a new analyzer involve demonstrable performance, under controlled conditions, using known solutions of ammonia in clean water, at different pH levels over a range of temperature. These initial studies assess accuracy, precision, stability, consumables and maintenance with a view to estimating the potential whole life costs of the analyzer.

Having successfully negotiated this phase of the evaluation, the next step is to undertake field trials. It is at this point that all previous problems pale into insignificance. The actual real world sample is an unstable liquid of unknown chemical and biological activity, containing a variety of suspended species. The presence or absence of light encourages bacterial growth as does temperature, and any surface acts as a growth medium. The only guarantee is that the major component will be water.

The analyzer is required to sample this liquid 24 hours per day for long periods without any maintenance and without any degradation of analyzer performance. In order to do this some form of continuous sample preparation is essential.

SAMPLE TREATMENT

The initial step is to transfer the sample to the analyzer. This has to be done on a continuous basis and, if a free ammonia measurement is being made, without changing the relevant conditions of the sample. This usually entails transfer at high velocity through smooth bore, light proof pipework using an appropriate long life pump.

In order to prevent degradation of the analyzer it is necessary to reduce the amount of suspended material and to prevent biofouling. Biofouling is caused by the initial coating of surfaces by active organic materials, followed by the use of these organics as a source of food by bacteria which subsequently multiply forming films of slime. As these films build up, the bacteria on the original surface wall are starved of dissolved oxygen in the liquid and die, causing sections of slime to detach from the walls and flow with the liquid. Biofouling can lead to the loss of ammonia by nitrification resulting in inaccuracies in the recorded measurements, and also to alteration of flowrates and blockages within small bore tubing in the analyzer. It is necessary to have a means of continuous filtration together with biocidal and algaecidal treatment. All of these processes must be done on a continuous basis, involve minimal low cost consumables and operate for long periods without maintenance. In addition, none of these processes must affect the concentration of ammonia in the liquid, nor the ratio of free to ionized ammonia.

Ideally this whole treatment process is continuous and uninterrupted, so that sample is constantly available for transfer to the analyzer to determine the ammonia concentration.

FREE VERSUS TOTAL AMMONIA

On the assumption that an improved analyzer measures both free and total ammonia, rather than measuring one and calculating the other; then, provided the concentration of ammonia is effectively unchanged by the pre treatment process, and that the ratio of free to ionized ammonia is unaltered, a measurement of the free ammonia content may be made on the treated sample. In order to perform the total measurement, the pH of the sample must be increased so that all of the ionized ammonia is converted to free ammonia and the measurement repeated.

Table 3 lists some of the proposed Environmental Quality Standards for ammonia in water in connection with EC directives[3], where * indicates mandatory limits.

Table 3 WRC recommended EQS values for Total and Unionised Ammonia.

Type	Usage		Total mg/l	Unionised mg/l
Fresh	Abstraction to Potable Supply			
	Treatment	A1	0.04	
		A2	1.17*	
		A3	3.1*	
	EC designated Salmonid and Cyprinid waters		0.78*	0.021*
	Non-EC designated waters			0.015
	Industrial abstraction for Food Processing		0.04	
Salt	Protection of saltwater fish and shellfish			0.021

218

The required ranges for detection of total ammonia are 0 - 1 mg/l for drinking water treatment processes and 0 - 20 mg/l for sewage treatment processes[2]. Recorded mean total ammonia levels in UK freshwaters vary from 0.007 to 8.2 mg/l[1]. Published data indicate that in many other EC member States permitted levels are also exceeded. Similar trends are observed in EC tidal estuaries. Although considerable data are available there is not always corresponding information on the fishery status at these sites, and the effects of high ammonia levels on these ecosystems cannot be assessed.

Because of the conservative nature of the Water Industry, the fact that legislation currently requires the measurement of total ammonia, that the Industry has no experience of IMS as a measurement technique, and that Graseby is not known as a supplier to the Water Industry; it has been decided that the first monitor will be completely conventional and measure total ammonia. Once IMS, the technique and Graseby have been accepted, a free ammonia monitor can then be made available, since there are moves within the NRA and the WRC to change from measuring total ammonia to free ammonia.

IMS DETECTION OF AMMONIA

As everyone skilled in the art of IMS knows, ammonia is readily detectable, however there have always been problems associated with obtaining fast response and recovery characteristics. In addition the ammonia monitor for water is going to be sampling ammonia in liquid water and inevitably high humidity levels will be present. Although high humidity levels are normally regarded as anathema in IMS, they do assist in the desorption of ammonia from surfaces. A careful choice of dopant is required to eliminate interferences and give acceptable ammonia peak resolution and sensitivity, while having a high tolerance to humidity. Careful attention to the design of the detector front end, the choice of materials, the design of the water/air interface and the optimization of flow characteristics are all of vital importance in achieving the required performance characteristics combined with stability and long life.

PERFORMANCE

When we embarked on this project and did a preliminary assessment, we set ourselves a design goal of 6 months for operating periods between maintenance for the complete system, based on what we thought could be achieved realistically with an IMS system and what we assumed a bought in pre treatment system would deliver. When we spoke to the WRC and to manufacturers of Ammonia Analyzers and Filter Systems, the scheduled maintenance for Analyzers ranged from twice daily to two to three weeks at best, while that for Filter Systems ranged from a few days to a maximum of one month. All of the required maintenance activities and costs were significant, involving expensive consumables such as chemicals and filters. The reaction to our proposed design goal was one of incredulity. Our first experience of a bought-in Filter System enabled us to understand this attitude.

The manufacturer had tailored the system to our requirements and recommended that we use a cross-flow filter system with a compressed air backflush facility. Two filters were incorporated, one active and one in standby mode. A daily backflush cycle had was recommended. After installation at our test site and extensive modification resulting in the backflush cycle being carried out every three minutes, the longest period of continuous operation achieved was 2 days. At the end of this period the entire filter system had to be stripped down and manually cleaned.

At the present time after extensive laboratory testing of the analyzer, and approaching a year of field testing for the analyzer and pre treatment system, we believe that the 6 months maintenance cycle for the analyzer is achievable, while that for the pre treatment system is currently being pushed towards this figure.

ACKNOWLEDGMENTS

REFERENCES

1   Mallett, M.J., Review of the Toxicity of Common Pollutants to Indigenous Species of Freshwater Fish. I. Ammonia, Arsenic and Cadmium. NRA Report No. 2541, August 1990.

2   Seager, J., Wolff, E.W. and Cooper, V.A. Proposed Environmental Quality Standards for List II Substances. Ammonia. ESSL TR260, 1988, WRC, UK.

3   Water Industry Specifications, Information and Guidance Notes, No. 7-08-01 Ammonia, 1990, Water Research Council, UK.

THE EFFECT OF SAMPLE HOLDER MATERIAL ON
ION MOBILITY SPECTROMETRY REPRODUCIBILITY

J. Richard Jadamec and Chih-Wu Su
U.S. Coast Guard Research and Development Center
1082 Shennecossett Road
Groton, CT 06340

Stephen Rigdon
Analysis & Technology, Inc.
258 Bank Street
New London, CT 06320

LaVan Norwood
Tectonic Technologies, Inc.
468 Wells Road
Wethersfield, CT 06109

ABSTRACT

When a positive detection of a narcotic occurs during the search of a vessel, a decision has to be made whether further intensive search is warranted. This decision is based in part on the results of a second sample collected from the same area. Therefore, the reproducibility of both sampling and instrumental analysis is critical in terms of justifying an in depth search. As reported at the 2nd Annual IMS Conference in Quebec City, the U.S. Coast Guard has determined that when paper is utilized as the sample desorption medium for the Barringer IONSCAN, the analytical results using standard reference samples are reproducible. A study was conducted utilizing papers of varying pore sizes and comparing their performance as a desorption material relative to the standard Barringer 50 micron Teflon. Nominal pore sizes ranged from 30 microns down to 2 microns. Results indicate that there is some peak instability in the first two to three windows during the analysis. The severity of the instability was observed to increase as the pore size of the paper is decreased. However, the observed peak instability does not create a situation that results in a decreased reliability or reproducibility in the analytical result.

BACKGROUND

Vessel search for the presence of contraband is one aspect of the US Coast Guard's Law Enforcement mission. Rapid detection of the presence of a narcotic is one of the primary requirements of Law Enforcement Agents engaged in field operations, especially in the maritime environment.

Since 1991, the USCG R&D Center has been actively conducting studies on non-canine contraband detection technologies for illicit drug detection. Two technologies have been

extensively tested and evaluated side by side during the past three years. Both systems analyze collected samples without any sample pretreatment which is an important criterion for field systems. IONSCAN, an Ion Mobility Spectrometer manufactured by Barringer Instruments, is one of these two systems. A sample, collected on a sampling medium, is placed into the IONSCAN sample entrance slot and is then subsequently heated, vaporized and passed into the analytical train in a heated air stream. Any material which is porous, gas permeable, and capable of withstanding the heat generated during the vaporization step can be used as the medium to transfer a collected sample into the IONSCAN for analysis. Filter paper and porous Teflon sheet are two common materials used by the U.S. Coast Guard for transferring the collected sample into the IONSCAN.

When a positive detection of a narcotic occurs during the preliminary search in any situation, a decision has to be made concerning whether a further intensive search is warranted. The impact of an intensive search will be substantially different dependent on the situation. If the positive detection is from a passenger at a port of entrance the delay at a check point and the search of his/her private belongings result in minimal delays and inconvenience. If the suspicious object is cargo, a vehicle, or a vessel, the potential of a destructive and time consuming search could occur. Detaining a vessel for one or more days in not unheard of. Resampling the suspicious area before a further intensive search is undertaken is the normal procedure employed to justify the need to conduct further detailed searching. The same procedure is employed if two canines are available in that verification of an alert is obtained using a second canine. Therefore, reproducibility of sampling and instrumental analysis is critical in justifying an in depth search based upon the analytical data. This is especially true in searches of maritime vessels because of the vessel size, the difficulty of sampling introduced by the multitude of objects and areas, and the limited time available during at-sea boardings.

INTRODUCTION

As reported at the 2nd Annual IMS Conference in Quebec City, it has been determined that when paper is utilized both as the sample collection and transfer material, the Ionscan analytical results for the determination of cocaine are reproducible. Field results from the last twelve months have supported this conclusion.

The logical extension of this research was to determine what effect, if any, different types of paper with different median porosities have on the Ionscan analysis for cocaine. There are two different directions this research could follow. The first is the investigation of several types of paper with varying physical properties and chemical compositions. The second is the investigation of one type of paper composition with varying physical characteristics (i.e. effective pore size, strength, wetability, etc.). For the purpose of this study, we chose to investigate the second condition. This decision was based on the fact that this particular type of paper has been proven effective in the field while introducing no known interferents in the Ionscan analysis for cocaine.

This paper presents the results of our study on the effects of a constant paper formulation with varying pore sizes on the Ionscan analysis for cocaine. Effects on the linear dynamic range of the calibration curve and cocaine peak drift time stability are presented. Teflon membrane, purchased from Barringer Instruments, was used as a sample holder material for comparison purposes.

EXPERIMENTAL METHODS

For the purpose of this study, three papers having similar compositions but of varying pore sizes in addition to Teflon were examined. Material specifications are as follows:

Sample Transfer Material	Nominal Pore Size
- Paper Sheet, Grade 404, purchased from Schleicher and Schuell, Inc.	20-30 micron
- Paper Sheet, Grade 497 purchased from Schleicher and Schuell, Inc.	8-12 micron
- Paper Sheet, Grade 402 purchased from Schleicher and Schuell, Inc.	2-5 micron
- Teflon Sheet Purchased from Barringer Instruments	50 micron

Aside from the different effective pore sizes, the three filter papers purchased from Schleicher and Schuell, Inc. are composed of the same material, 100 percent cotton linters. They are all hardened qualitative low-ash filter papers used primarily for the filtration of precipitates ranging in size from very fine (grade 402) to coarse (grade 404). Grades 404 and 402 contain an additive to increase the wet strength of the material. This additive (not identified by the manufacturer) has been observed not to introduce any interferent peak(s) to the Ionscan analysis. At present, the U.S. Coast Guard uses grade 404 paper in the field.

Calibration curves for each of these sample collection and transfer materials were run on the Ionscan. Standards of cocaine in methanol were used to spot the test materials. The test materials were loaded with concentrations of cocaine ranging from 5ng through 80ng, with five trials being accomplished at each concentration level.

RESULTS

Figure 1 details the calibration curves of the four materials tested. The amplitude of the cocaine peak is somewhat reduced when paper is used as the sample transfer medium relative to Teflon. However, there does seem to be an increase in the linear dynamic range for cocaine when paper is used relative to Teflon. When Teflon is used, it is generally accepted that the linear dynamic range for cocaine extends from the sub-nanogram range to approximately 10 nanograms, as shown in Figure 1. When using paper, this linear dynamic range is extended out to approximately 20 nanograms. The pore size of the paper does not affect the linear dynamic range.

Cocaine Calibration Curve
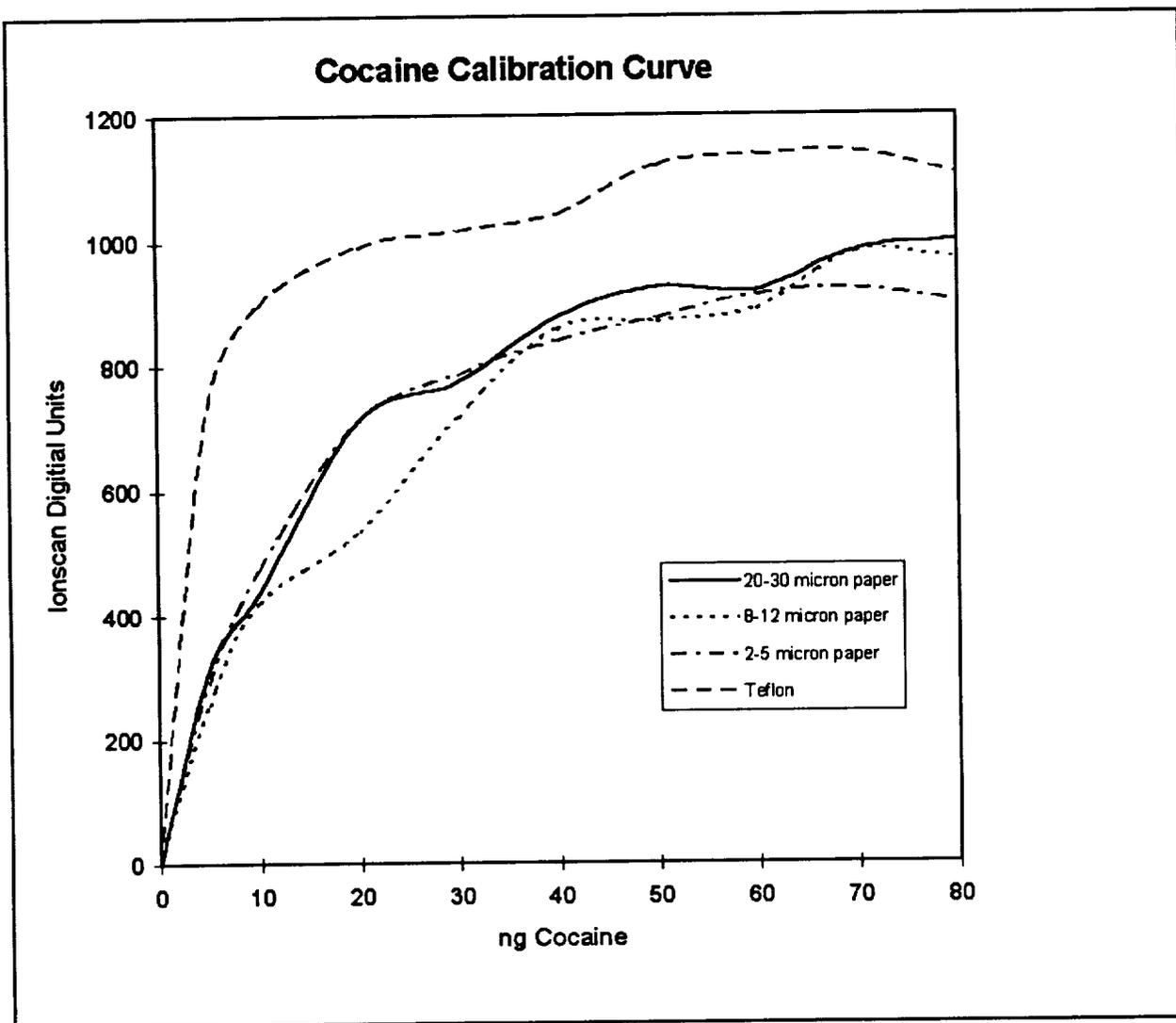
Figure 1
Cocaine Calibration Curves

Figure 2 depicts the calibration curves of the four materials tested as they relate to the number of Ionscan "windows" in which cocaine has been detected. These windows refer to the number of scans (out of a maximum possible 14 based on current instrumental setup parameters) that the Ionscan recognized the peak in question as a valid cocaine peak (i.e., a "hit"). As shown in Figure 2, at lower concentrations the number of windows in which a "hit" was recorded was, at times, reduced when using paper relative to Teflon. Although there is not a discernable difference between different types of paper used in this study, the general trend is that until the concentration level reaches approximately 25 nanograms a decrease in the number of windows in which cocaine is detected is exhibited.

Cocaine Calibration Curve
Ionscan Windows vs ng Cocaine
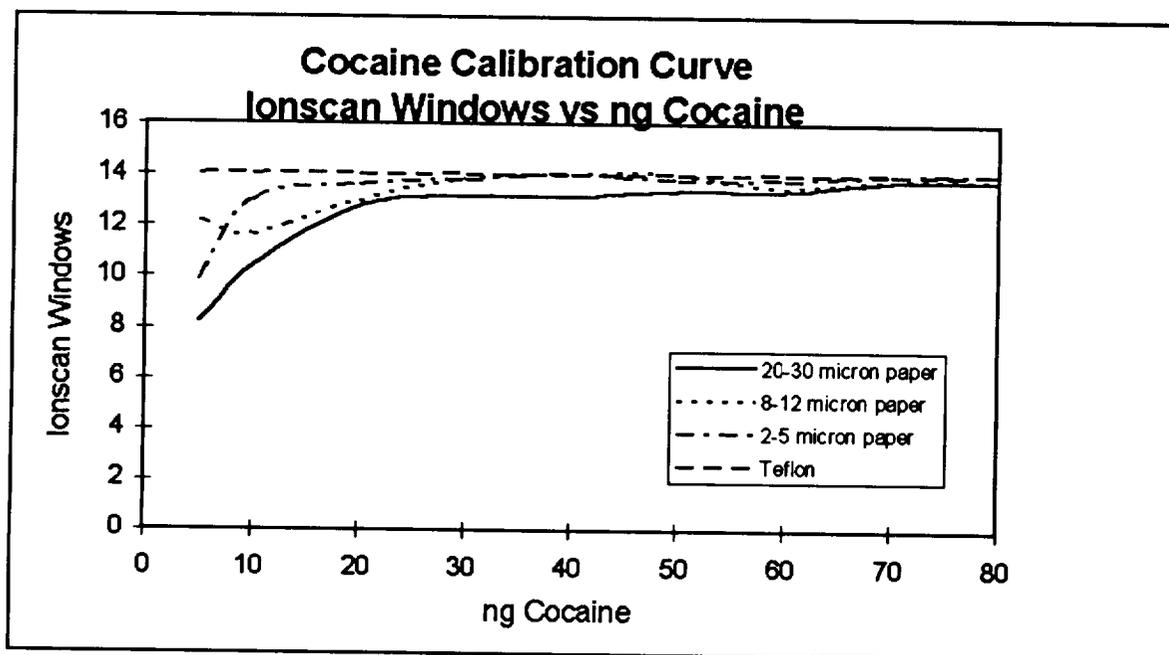
Figure 2
Cocaine Calibration Curve - Ionscan Windows vs. ng Cocaine

When using paper as a desorption media, the greatest concern is whether or not cocaine peak instability is introduced rendering accurate identification of cocaine questionable. The cause for this concern is due to the possibility that the paper impacts on the balanced heated air stream used for sample desorption and within the drift tube. Since the Ionscan is dependent on balanced desorb and drift gas flows, the possibility exists that a partial vacuum may be created in the drift tube if the desorb gas flow is partly blocked. As the mass flow controller struggles to balance the two flows, this partial vacuum will fluctuate as a balanced condition is being achieved. The magnitude of the fluctuation will decrease as a steady state condition is achieved. The net result could be that the cocaine ion is changing drift rates as the analysis progresses with the end result being a cocaine peak with shifting drift times between the early scans and the late scans. This would be detrimental if the cocaine peak "drifted" out of the target window. Figure 3 details the drift of the cocaine peak about the average drift time for the entire analysis. Since any peak instability is already included in the Ionscan algorithm for the average drift time, this is not a perfect analysis. It does, however, give a good representation of the amount of instability that is introduced.

As shown in Figure 3, a certain degree of peak instability is introduced when paper is used as the desorption media. There appears to be an inverse correlation between the pore size and the severity of the peak instability with the smaller pore size paper producing the greatest peak drift. A plot of the peak drift as a function of windows number exhibits a sinusoidal type curve about the average drift time. This may be due to the mass flow controller struggling to balance the flow by constantly adjusting the flow up and down as flow fluctuations are sensed.
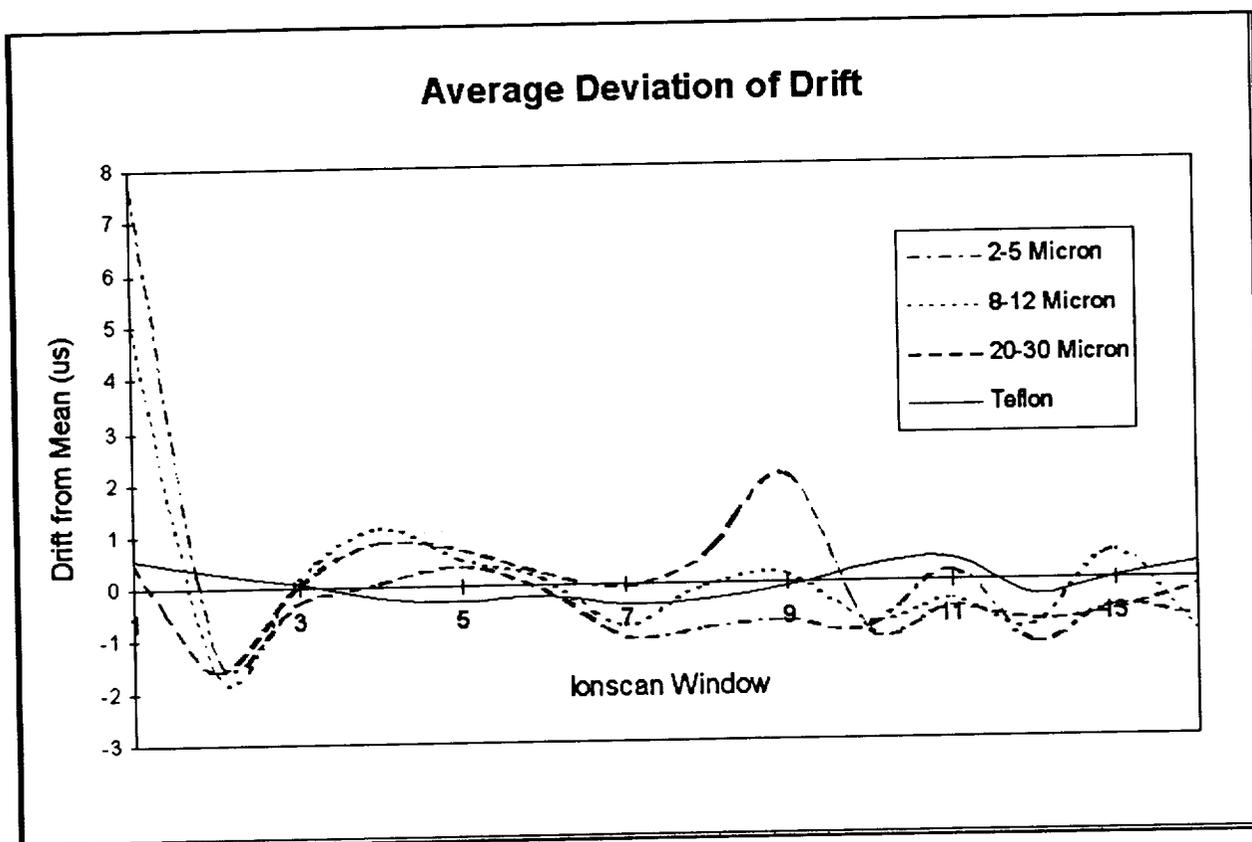
Figure 3
Average Deviation of Drift of Cocaine Peak

DISCUSSION

As evidenced by the results of this study, there is an effect on the Ionscan analysis when paper is utilized as the sample holder material for cocaine. The question that remains is whether this effect is great enough to preclude one from using paper as a sample holder material.

Due to the inherent design characteristics of the Ionscan, and in general IMS technology, quantitation of results has proven to be, at best, questionable over a wide linear dynamic range. IMS technology for cocaine analysis is also affected by sample matrix phenomenon [1]. While quantitation of results is not paramount, there seems to be an aspect of the human nature that always wants to know, "How much was analyzed?" When utilizing paper as a desorption medium, the concentration range in which quantification is possible is increased relative to Teflon. When using Teflon, one has only the amplitude of the response as information to use for quantification purposes since the number of windows is more likely to be at the maximum of fourteen. When using paper, however, the increased linear dynamic range of the amplitude of response coupled with the affected growth curve pattern in this

226

same range give two pieces of information to use for identification purposes. The results have shown that the windows that are not analyzed as a "hit" are usually the early windows of the analysis. This may be related to the capillary action of the paper which disperses the standard solution within the matrix of the paper as opposed to Teflon. While the total number of windows may be used for identification purposes, examination of the growth pattern of the earlier windows may lend some help in quantifying the result. The overriding fact that must be kept in mind, however, is that quantification with IMS can only be achieved when known, laboratory type samples are being analyzed on known background matrices. When analyzing a field sample, there is an unknown multitude of compounds present. Each one of these unknown compounds, with its corresponding proton affinity, could affect the amplitude of the compound of interest through competition in the ionization "reaction zone". Quantitation in the field is, basically, impossible and may be best performed by the classical standard addition method. However, this classical standard addition method is limited as due to the limited linear dynamic range of the system.

When using paper as a sample transfer material, a gas flow imbalance may be established. The design of the Ionscan calls for a heated air stream to be pushed through the sample transfer material at a rate of approximately 300cc/min. In addition, a heated anvil makes contact with the sample transfer medium during desorption. In combination, the anvil and the heated air stream desorb the compounds on the sample transfer material and transport them into the reaction chamber and eventually into the drift tube. When utilizing paper as the sample transfer material, a certain portion of the desorb air flow may not be allowed to pass through the paper. The effective flow through the paper would therefore be diminished. The mass flow controller within the Ionscan, however, would try to maintain the desorb flow into the Ionscan at the preset level. For this reason, room air would most likely be pulled through the side of the sample holder and sucked into the Ionscan. At the same time, cocaine molecules on the surface of the sample holder material would be vaporized by the heat of desorption and carried into the Ionscan by the rushing room air. This "flow balance" would not be achieved instantaneously, as a perfectly sealed and unhindered desorb air flow region would be. This may explain the increased peak instability observed in the earlier windows as evidenced in Figure 3. The time required for this equilibrium to be established may, in fact, cause a peak not to be recognized or not be present at all in the earlier windows. This is evidenced in Figure 2, with the greatest effect occurring at lower concentration ranges when the population of cocaine ions is reduced. This "blocked flow" condition may also occur when samples are collected with a vacuum device using Teflon as the sample collector. The massive air flow and increased number of particulates may result in passageways of the Teflon filter membrane becoming clogged and effectively "blocked". This same condition may also occur when wipe sampling any material that is greasy, dirty, etc. if the material in question becomes imbedded in the matrix of the sampling material.

Over the last eighteen months, it has been shown that surface wipe sampling is the most effective means of collecting samples in the maritime environment. Vacuum sampling has been judged to be too cumbersome. In addition to the logistical and safety concerns of carrying a vacuum apparatus around a ship, a hand held sampling system of some sort can reach many places that a vacuum cannot. When collecting samples by wiping, Teflon has proven to be not rugged enough. The Teflon filter breaks apart in most instances. Paper, however, has been shown to withstand the rigors of wiping in every conceivable type of maritime environment. The only other material that equals paper in this aspect is cotton gloves. Since the cotton glove itself cannot be analyzed by the Ionscan, some type of transfer to a sample holder material must be accomplished. The transfer efficiency in this

227

method (estimated to be 10-15%) will reduce the overall detection level capability. Research on new materials that are rugged enough to withstand the rigors of shipboard sampling and can also be used as a sample transfer material are presently being investigated by other law enforcement agencies. An example is the Canadian Customs "Gerry Bag". Until these materials are fully tested in the maritime environment, paper will remain the best option.

The overall conclusion remains that paper is the sample holder material that is best suited for use in the maritime environment. While its analytical properties are not as ideal as Teflon, its field adaptability is far superior. If cost is factored in, it becomes even more superior.

This study was conducted utilizing cocaine as the compound of interest. Therefore, the conclusions drawn herein pertain only to compounds whose drift times approximate cocaine. Further studies should be conducted on other narcotics having shorter drift times. One suggestion would be the study of the behavior of methamphetamine when subjected to the same experimental conditions.

REFERENCES

[1] Fytche, L.M., Hupe, M., Kovar, J.B., and Pilon, P., "Ion Mobility Spectrometry of Drugs of Abuse in Customs Scenarios: Concentration and Temperature Study," Journal of Forensic Sciences, JFSCA, Vol. 37, No. 6, November 1992, pp.1550-1566.

A NOVEL APPROACH TO INCREASING COCAINE DETECTION CONFIDENCE UTILIZING ION MOBILITY SPECTROMETRY

J. Richard Jadamec and Chih-Wu Su
U.S. Coast Guard Research and Development Center
1082 Shennecossett Road
Groton, CT 06340

Stephen Rigdon
Analysis & Technology, Inc.
258 Bank Street
New London, CT 06320

LaVan Norwood
Tectonic Technologies, Inc.
468 Wells Road
Wethersfield, CT 06109

ABSTRACT

When a positive detection of a narcotic occurs during the search of a vessel, a decision has to be made whether further intensive search is warranted. In terms of unwarranted delays of vessels and possible property damage, the accuracy of the analytical determination is very important. Analytical accuracy becomes critical when the data may be used in court actions as evidence. For this purpose, the U.S. Coast Guard has been investigating several confirmatory ion mobility spectrometry (IMS) field methods for the detection and identification of cocaine. This paper presents the findings of our investigations on the use of catalytic pyrolysis and base hydrolysis as confirmatory methods. The catalytic effects of various metals on the pyrolysis reaction are reported. In addition, the effects of several different ion mobility spectrometer sample transfer mediums and varying laboratory conditions on the base hydrolysis of the cocaine molecule are also be reported.

BACKGROUND

The U.S. Coast Guard (USCG) R&D Center has conducted extensive tests and evaluations (T&E) of commercially available contraband detection systems in both laboratory and field environments since 1991. The objective of these T&E studies was to determine if commercially available illicit drug detection systems could be effectively used in the search of maritime vessels for the presence of smuggled narcotics. Criteria used in selecting appropriate systems for test and study included: minimal sample preparation and pretreatment; speed of sample analysis; low nanogram narcotic detection levels; portability; ease of operation; and affordability. As the amount of laboratory and field T&E data increased, with respect to system performance under actual field situations and the effects of natural environmental backgrounds on analytical results, the accuracy of a positive

contraband detection became increasingly important. If a positive detection occurs a decision as to whether or not an in-depth search of a vessel should be undertaken has to be made. Therefore, with respect to unwarranted delays of vessels and possible property damage, the accuracy of a determination is very important. Furthermore, accuracy is critical when the analytical data may be used in court actions as evidence.

Acceptance of an analytical determination is based on the proven reliability of a given method or in the use of multiple technologies to confirm the results obtained by each system. Gas Chromatography/Mass Spectrometer (GC/MS) is an accepted analytical method employed by the EPA for organic pollutant and hazardous material analyses. In the urine drug testing program, NIDA, DOD and USCG require the use GC/MS to confirm and quantitate the level of narcotic or narcotic metabolite detected in the sample. DEA and FBI use GC/MS for both the identification of a seized narcotic and possible matching of the seized narcotic with a source of origin. However, present day GC/MS instrumentation and methodologies lack most of our selection criteria as mentioned above for use in the search of vessels for the detection of illicit drugs.

Other accepted means of verifying analytical results exist. These alternative methods require that a given sample be analyzed by different analytical methods, e.g., on different GC columns, and/or by different analytical technologies. This approach has been used by and recommended for use by the EPA in organic pollutant and hazardous chemical analysis; by the U.S. Coast Guard in oil identification analysis; by the DEA in the laboratory analysis of narcotics; and is recommended for cocaine and heroin analysis by the United Nations, Division of Narcotic Drugs.

IONSCAN (an ion mobility spectrometer), and SENTOR (a gas chromatographic system equipped with dual GC Columns and a chemiluminescence detector) are two of the contraband detection systems which have been extensively tested by the U.S. Coast Guard R&D Center under both laboratory and field conditions. Based on the knowledge acquired from these field T&E studies, two distinct modes of operation evolved for the use of these two systems in the detection of contraband aboard maritime vessels, a search mode and a forensic mode[1]. The forensic mode pertains to situations where the analytical results may be used as evidence in court or other legal actions. In order to generate reliable and scientifically acceptable results, these two systems are used in parallel which, in essence, is equal to a multimethod approach. To date, the analytical results obtained in the use of these two systems in actual searches of maritime vessels have been accepted in the Federal Courts as evidence, and have successfully withstood the challenges in court as to their reliability and accuracy.

INTRODUCTION

To improve the confidence of contraband detection results, specifically when only one detection system is used due to some uncontrollable and unavoidable situation, the use of additional confirmatory methods for the detection and identification of cocaine have been investigated.

Pyrolysis and hydrolysis reactions are two methods which have frequently been used by the analytical chemist to identify a compound, to verify the chemical structure of the compound, and to confirm the analytical result. Methylecgonidine has been reported to be the major pyrolysis product of both cocaine hydrochloride and crack (cocaine base)[2,3].

Methylecgonidine has also been reported in the analysis of cocaine samples by GC methods and is attributed to thermal degradation occurring in the GC injection port[4]. Carbomethoxycycloheptatrienes have also been identified as the main pyrolysis product of cocaine hydrochloride[3].

The cocaine molecule contains two ester groups which can be hydrolyzed to form acid(s) and alcohol(s) under certain conditions. Hydrolysis of cocaine in samples at a pH of 5.5 and higher has been observed to produce benzoylecgonine[5]. In human blood or plasma, the esterase metabolizing of cocaine to methylecgonine has been reported[6].

Both IONSCAN and SENTOR systems utilize heat to desorb collected samples containing cocaine into its vapor form at approximately 280° C. The desorbed cocaine vapor is then carried into the analytical system in a heated gas stream. Occasionally, small amounts of cocaine degradation products have been observed during the routine operation of these two system by the USCG. This suggests that pyrolysis reactions may have occurred during sample analysis by both systems since heat is present, and that hydrolysis reactions may also have occurred as a result of cocaine being smuggled in the maritime environment.

Based on the above observations, a study to determine whether pyrolysis and hydrolysis reactions could be utilized to confirm the Ionscan detection of cocaine was undertaken. Pyrolysis reactions can be enhanced by applying a catalyst and hydrolysis reactions can be controlled by pH and reactants. This paper will present the results of our study and their application as a field confirmation.

EXPERIMENTAL METHOD

Methanol solutions (1 mg/mL) of cocaine hydrochloride, benzoylecgonine, ecgonine and methylecgonine were purchased from Alltech Associates Inc. Methylecgonidine was synthesized in our laboratory and identified by comparing its mass spectra with the published mass spectra of methylecgonidine. Material used as sample holders were: filter paper, obtained from Schleicher & Schuell (S&S), having a nominal pore size of 20 to 30 um ; glass fiber filters having a nominal pore size less than 50 um obtained from both SKC Inc. and Omega Specialty Instrument Co.; and quartz glass filters having a nominal pore size less than 50 um obtained from Pallflex Products Corp., Putnam CT.

1) Catalytic pyrolysis: Copper, iron, steel and aluminum were selected as candidate catalysts. Fresh, fine powders of each metal were prepared by filing. Each metal powder was spread on an S&S filter paper and analyzed to ensure that no interferent responses were present in the cocaine and cocaine degradation regions of the ion mobility spectrum. Standard cocaine hydrochloride solutions (1 uL of a 5ug/mL standard) prepared in methanol, were deposited on top of each powder. The methanol was evaporated at room temperature. Normal routine IONSCAN analytical procedures were then followed in the analysis of these samples. The same amount of cocaine hydrochloride was also deposited on gold coated nickel screen obtained from Barringer Instruments Inc. (BII) and analyzed by the same procedures.

2) Base hydrolysis: Filter paper was selected for this study as a result of the water repellant properties of Teflon material. Three different sets of standard test conditions were employed as follows:

a) 1 uL of 5 ug/mL or 20 ng/mL standard cocaine hydrochloride in methanol was deposited on S&S filter paper. Methanol was evaporated at room temperature.

b) 1 uL of 5 ug/mL or 20 ng/mL standard cocaine hydroxide in methanol was deposited on S&S filter paper. After the methanol evaporated, 3 uL of 2% sodium hydrochloride in water solution was spotted on top of the cocaine hydrochloride.

c) 1 uL of 5 ug/mL or 20 ng/mL standard cocaine hydrochloride in methanol was deposited on S&S filter paper. After the methanol evaporated, 3 uL of 2% sodium hydroxide in methanol solution was spotted on top of the cocaine hydrochloride.

Standards prepared from (b) and (c) were then air dried at room temperature. All standard samples were analyzed by the same IONSCAN procedures. Black burned spots were observed to be present on the filter paper after IONSCAN analysis where the sodium hydroxide had been added . In order to determine whether the burning phenomenon affected the formation of the degradation products observed, quartz and glass fiber (brands A and B) filters were used for comparison purposes.

RESULTS AND DISCUSSION:

Figure 1 shows the IONSCAN ion mobility spectra (IIMS) of cocaine, benzoylecgonine, methylecgonine, methylecgonidine and ecgonine standards deposited on filter paper. As can be seen in this figure, each compound is readily identified by its reduced ion mobility spectrum. The results obtained in our pyrolysis and hydrolysis studies are summarized below:

1) Catalytic pyrolysis: Figure 2 shows the IIMS of 5 ng of cocaine hydrochloride on copper and iron powder. Table 1 lists the IONSCAN analytical results of 5 ng of cocaine hydrochloride deposited on the different metal powders used in this study. No cocaine degradation products were detected when copper and gold coated nickel screen were used as a catalytic surface. The ratio of the methylecgonidine amplitude to that of cocaine ranged from 20% to 26% when iron, steel and aluminum were present. The thermal conductivities (watt/cmC at 25° C) of copper, aluminum and iron are 3.98, 2.37 and 0.803, respectively. This suggests that the observed decrease in the cocaine amplitude may be related to the thermal conductivity of these metals. Unfortunately, the lack of enough standard methylecgonidine material prevented us from performing further semiquantitative calculations on the production of methylecgonidine under these experimental conditions.

Fytche et al., reported that the IONSCAN detection level for cocaine was substantially reduced when cocaine was deposited on silica[7]. The reduction in the detection level of cocaine was considered to be the result of the slow heat conduction property of silica. Whether the decreasing amount of cocaine observed in our studies is the result of the slow heat transfer of the metal powders, similar to that reported by Fytche et. al.[7], or if it is due to the conversion reaction of cocaine to methylecgonidine needs further investigation.

2) Base hydrolysis: The results of Ionscan analysis of cocaine on paper, quartz and glass fiber (brands A and B) filters are listed in Table 2. Except for filter paper, methylecgonidine was observed to be the major compound detected when 5 ng of cocaine was spotted on all types of sample holding material used in this study . When 20 ng of cocaine was spotted on quartz and glass fiber filters, only methylecgonine was observed for brand A glass fiber filters. However, when brand B Quartz and glass fiber filters were used

both methylecgonidine and cocaine were detected. Table 3 shows that the addition of 3 uL of 2% sodium hydroxide on cocaine produced subtle changes in the relative response of these compounds as seen in comparing the data contained in Tables 2 and 3. However, when 20 ng of cocaine was spotted on quartz the cocaine response diminished but the amount of methylecgonidine did not increase. Table 4 shows that the addition of 3 uL of 2% sodium hydroxide in methanol did not hydrolyze cocaine when filter paper was used as the sample holder. However, methylecgonine was the dominant product detected for all other test conditions except for the test in which 20 ng cocaine was deposited on brand B glass fiber filters. The contradiction between the results obtained when 5 ng and 20 ng of cocaine were spotted on brand B glass fiber filters requires further investigation.

Methylpseudoecgonine is produced when cocaine is hydrolyzed by sodium hydroxide and subsequent esterification occurs in the presence of methanol[8]. Methylecgonine and methylpsuedoecgonine differ only in structure, i.e., whether the 2-carboxylic methyl ester is located in the exo or endo position. Therefore their reduced mobilities should be approximately the same. Whether the methylecgonine detected in our study is actually methylpsuedoecgonine requires further investigation.

The structure of cocaine is a 8-methyl-8-azabicyclo[3.2.1]octane with both the 2-carboxylic methyl ester and 3-benzoyloxy groups located at exo positions. The elimination of benzoic acid from the cocaine molecule produces a double bond between the 2- and 3-carbon positions of the ring structure and forms the molecular structure of methylecgonidine. The double bond between the 2 and 3 carbons reduces the free rotation of the ring structure. However, the ring structure has less steric hindrance due to the elimination of exo-locatedfunctional groups located at the 2- and 3- carbon positions. These two chemicals, cocaine and methylecgonidine, are likely to have approximately the same ground state energies based on their ring structures. Although a six membered ring structure (a favorable transition state for a concerted reaction) can be formed by the connection of the exo benzoyloxy group and the endo hydrogen at the 2 carbon position (Figure 3) in the cocaine molecule coupled with the elimination of the benzoic acid, this study showed that at temperatures up to 280° C the cocaine molecule is very stable. This indicates that the activation energy required to convert cocaine to methylecgonidine is high.

Glass, with the main component being silica, is a common material for containers used to store organic chemicals due to its inertness toward most organic compounds. Quartz is a pure form of silica. It is well known that the surface of both quartz and glass contain many surface active sites, such as silanols (Si-OH) and siloxanes (Si-O-Si)[9]. These surface active sites frequently affect the quality of analytical separations of gas chromatographic glass columns, especially when capillary columns are used to separate polar compounds. The catalysis reaction leading to the conversion of cocaine to methylecgonidine on or in the presence of quartz and glass fiber filters suggests that the transition state might involve a cyclic ring structure larger than a six membered ring as shown in Figure 4.

When 1 uL of a liquid solution is deposited on quartz or glass fiber filter, the liquid does not disperse horizontally to the same degree as on filter paper, but penetrates downward. This is related to the different capillary properties of paper and glass filters. After the methanol has been removed by evaporation, the cocaine coats the surface of individual quartz or glass fibers that have been wetted by the methanol solution containing cocaine. As the concentration of cocaine in the solution increases, the residual coating thickness increases. Therefore, some of cocaine molecules are not in direct contact with a quartz or a glass fiber

233

surface. As soon as sufficient heat is supplied, the cocaine molecule evaporates (vaporizes) and migrates through the filter without a decomposition reaction occurring since the active sites of the glass fibers are already coated with cocaine or involved in a reaction with cocaine vapor.

Glass structures also contain various trace metal impurities. Low level concentrations of trace metals impurities still exist even after the glass filter has been acid leached. However, the catalysis reaction of cocaine resulting in the decomposition of cocaine to methylecgonidine is unlikely due to the presence of these trace metals, since our results of intentionally using large amounts of metal, as discussed previously, did not indicate that this decomposition reaction occurred (Table 1).

In order to determine whether this elimination reaction of benzoyl acid from cocaine can occur only through contact of cocaine vapors with the surfaces of glass fibers, rather than through the direct contact of solid cocaine with the glass fiber during the sample desorption stage, the following study was performed. 1 uL of 5ug/nL standard cocaine hydrochloride in methanol was deposited on filter paper positioned in the Barringer sample holder and a glass fiber filter was placed above the sample holder. In this configuration a 2 mm space exists between the filter paper and the glass fiber filter. Figure 5 clearly shows that under this condition methylecgonidine is generated by the contact of cocaine vapor with the glass fiber filter at a desorption temperature of 280° C .

APPLICATION AND PRECAUTIONS

This reaction and formation of methylecgonidine under these conditions has been observed to be repeatable and therefore has the potential of being used as a method for the confirmation of the presence of cocaine in a collected sample.

Filler materials are commonly added to paper and glass fiber filters. Manufacturers of paper and glass fiber use binders and fillers to obtain specific performance characteristics of these materials for their intended use as filtering mediums. The kinds of material added depend on the desired performance characteristics of the filter membrane and are dependent on the manufacturing process. Some of these fillers may dramatically alter the pyrolysis reaction product(s) observed in this study. The source of material used to perform this confirmation reaction should be screened and tested prior to its use.

REFERENCES

[1] Jadamec, J.R., Su, C., Rigdon, S., Norwood, L., and Kaplain, C., "Confidence in the Detection of Cocaine Particulates," Presented at the Society of PhotoOptical Instrumentation Engineers 1994 International Symposium, San Diego, CA, July 1994.

[2] Martin, B.R., Lue, L.P., and Boni, J.P., "Pyrolysis and Volatization of Cocaine," Journal of Analytical Toxicology, Vol. 13, 1989, pp. 158162.

[3] LeBelle, M.J., Dawson, B., Lauriault, G., and Savard, C., "Identification of Nformylnorcocaine and NBenzoylnormethylecgonine in Illicit Cocaine," Analyst, Vol. 116, 1991, pp. 10631065.

[4] Lukaszewski, T., and Jeffery, W.K., "Impurities and Artifacts of Illicit Cocaine," Journal of Forensic Sciences, Vol. 25, 1980, pp. 499507.

[5] Gupta, Das V., "Stability of Cocaine Hydrochloride Solutions at Various pH Values as Determined by Highpressure Liquid Chromatography," International Journal of Pharmaceutics, Vol. 10, 1982, pp. 249257.

[6] Baselt, R.C., "Stability of Cocaine in Biological Fluids," Journal of Chromatography, Vol. 268, 1983, pp. 502505.

[7] Fytche, L.M., Hupe, M., Kovar, J.B., and Pilon, P., "Ion Mobility Spectrometry of Drugs of Abuse in Customs Scenarios: Concentration and Temperature Study," Journal of Forensic Sciences, JFSCA, Vol. 37, No. 6, November 1992, pp.1550-1566.

[8] Sinnema, A., Matt, L., Van Der Gugten, A.J., and Beyerman, H.C., "Configuration and Conformation of All Four Cocaines from NMR Spectra," Recueil des Travaux Chimiques des PaysBas, Vol. 87, 1968, pp. 10271041.

[9] Dorsey, J. G., and Cooper, W. T. "Retention Mechanisms of BondedPhase Liquid Chromatograohy" Analytical Chemistry, Vol. 66, 1994, pp.857A.

Table 1. Detections of Cocaine and Methylecgonidine by Ionscan When Cocaine Deposited on Different Metal Powders

| | Filter Paper | | Metal Powder on Filter Paper | | | | | | | | | |
| | | | Copper | | Iron | | Steel | | Aluminum | | Gold Screen* | |
	Max Amp	# of Hit	Max Amp	# of Hit	Max Amp	# of Hit	Max Amp	# of Hit	Max Amp	# of Hit	Max Amp	# of Hit
1 cocaine	904	14	871	13	476	13	227	12	516	13	464	14
2 methylecgonidine	63	5	0		104	9	58	5	94	10	0	
3 Me-Ecgd**/cocaine	0.07		0		0.22		0.26		0.18		0	
4 Relative amptitue	1.00		0.96		0.53		0.25		0.57		0.51	

* : Gold coated nickel screen

** : Methylecgonidine

236

Table 2. Compounds Dectected by Ionscan when Cocaine Deposited on Paper, Quartz or Glass Fiber Filter

Sample holding material	Amount of cocaine added (ng)	Treat with NaOH	Solvent for NaOH	Cocaine		Methyl ecgonine		Methyl ecgonidine	
				Max Amp	# of Hit	Max Amp	# of Hit	Max Amp	# of Hit
paper	5	no	-	807	14	-		74	7
quartz	5	no	-	trace		-		438	13
glass (a)	5	no	-	-		-		535	9
glass (b)	5	no	-	trace		-		300	13
quartz	20	no	-	582	14	-		623	14
glass (a)	20	no	-	-		-		761	14
glass (b)	20	no	-	444	6	-		562	14

237

Table 3. Compounds Detected by Ionscan When Cocaine Was Deposited on Paper, Quartz or Glass Fiber Filter And Then Treated With 2% NaOH (in Water)

Sample holding material	Amount of cocaine added (ng)	Treat with NaOH	Solvent for NaOH	Cocaine		Methyl ecgonine		Methyl ecgonidine	
				Max Amp	# of Hit	Max Amp	# of Hit	Max Amp	# of Hit
paper	5	yes	water	809	14	-		61	2
quartz	5	yes	water	-		-		348	8
glass (b)	5	yes	water	63	2	-		247	13
quartz	20	yes	water	98	2	-		582	14
glass (a)	20	yes	water	-		-		725	14
glass (b)	20	yes	water	342	5	-		504	14

Table 4. Compounds Detected by Ionscan When Cocaine Was Deposited on Paper, Quartz or Glass Fiber Filter And Then Treated With 2% NaOH (in Methanol)

Sample holding material	Amount of cocaine added (ng)	Treat with NaOH	Solvent for NaOH	Cocaine		Methyl ecgonine		Methyl ecgonidine	
				Max Amp	# of Hit	Max Amp	# of Hit	Max Amp	# of Hit
quartz	5	yes	methanol	-		647	6	-	
glass (b)	5	yes	methanol	141	3	472	2	122	2
paper	20	yes	methanol	1061	14	-		trace	
quartz	20	yes	methanol	144	4	1016	6	-	
glass (b)	20	yes	methanol	519	5	-		150	4

239

Figure 1. Ion Mobility Spectra of

a) Ecgonine

b) Methylecgonidine

c) Methylecgonine

d) Benzoylecgonine
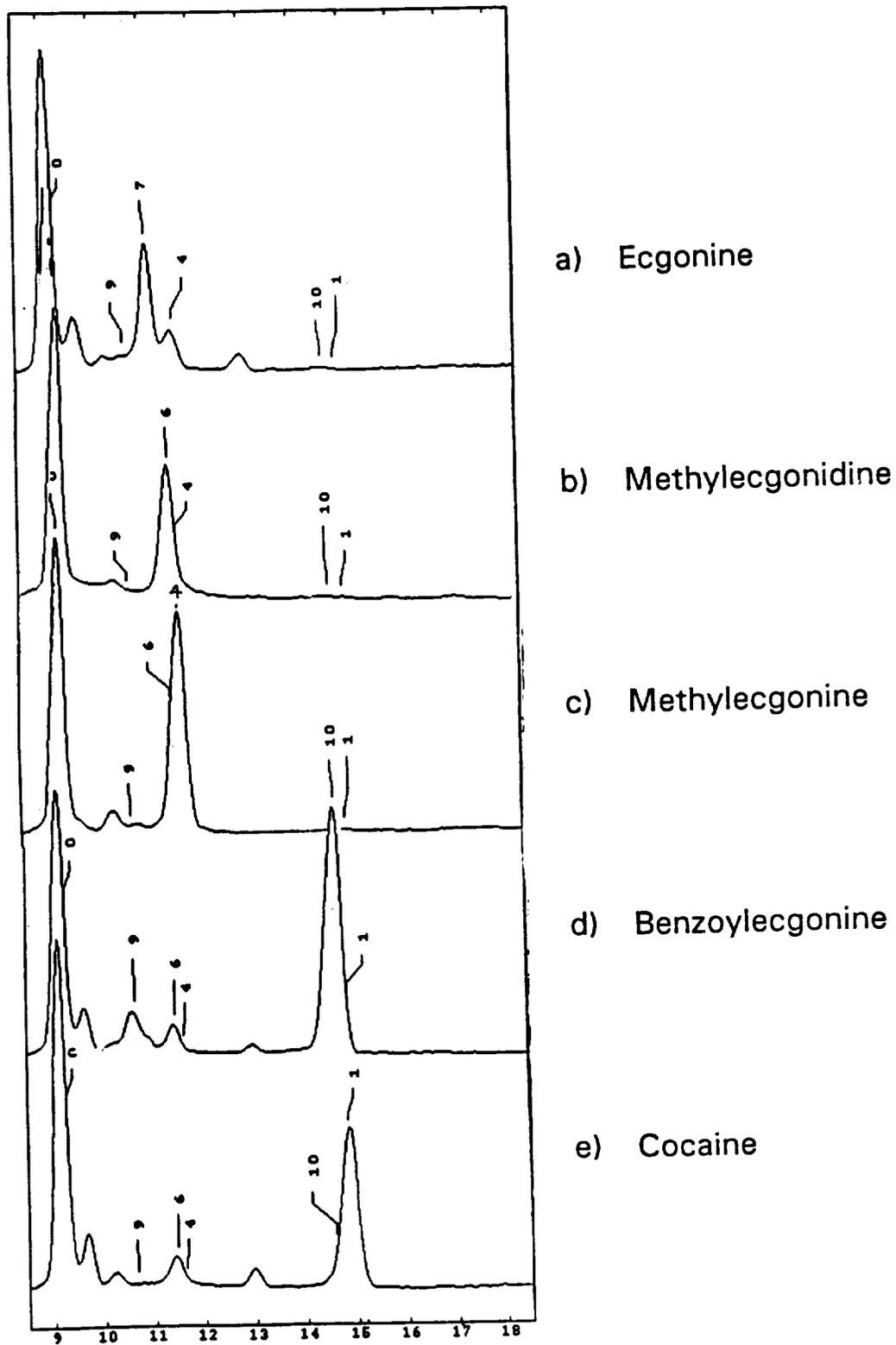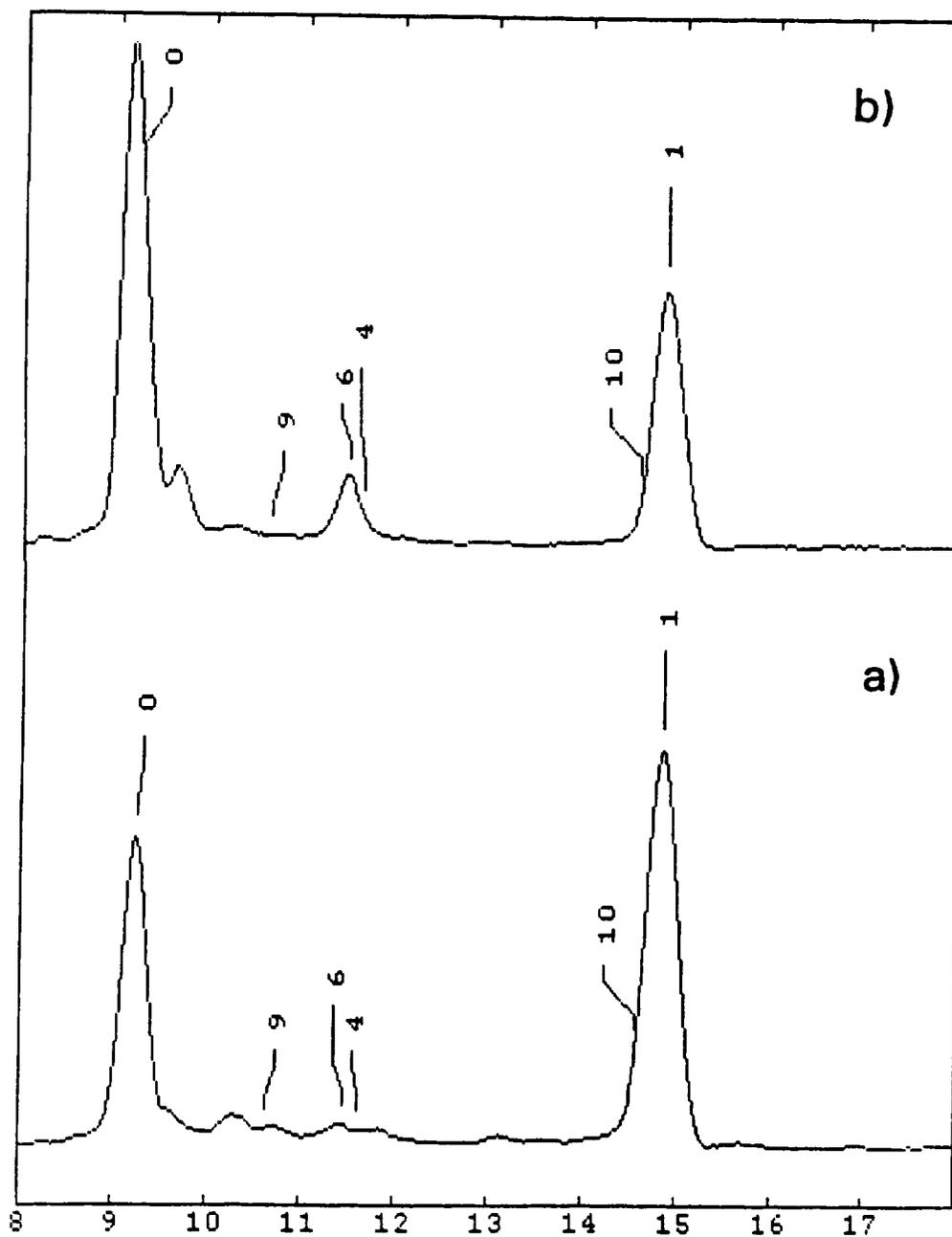
e) Cocaine

Figure 2.   Ion Mobility Spectra of

a) 5 ng of cocaine on copper powder
b) 5 ng of cocaine on iron powder
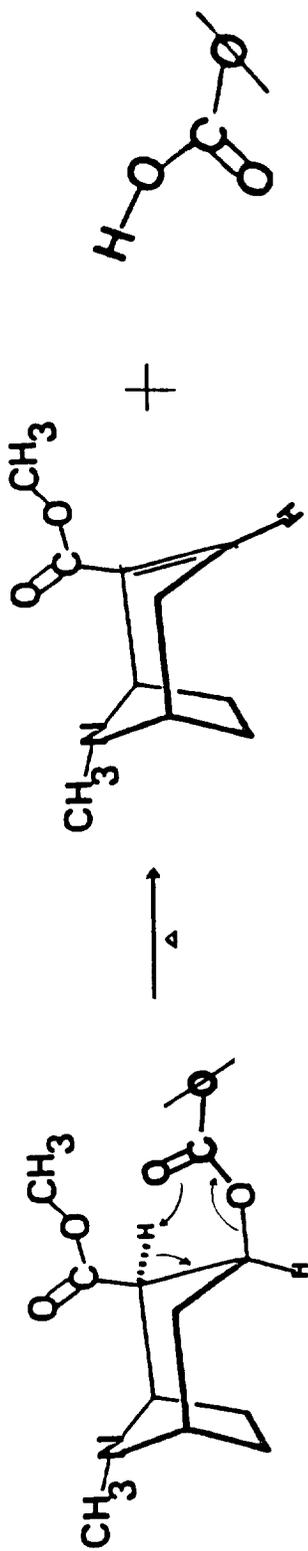
Cocaine   Methylecgonidine   Benzoic Acid

Figure 3. Elimination of Benzoic Acid From Cocaine Throught a Conserted Reaction Mechanism

242
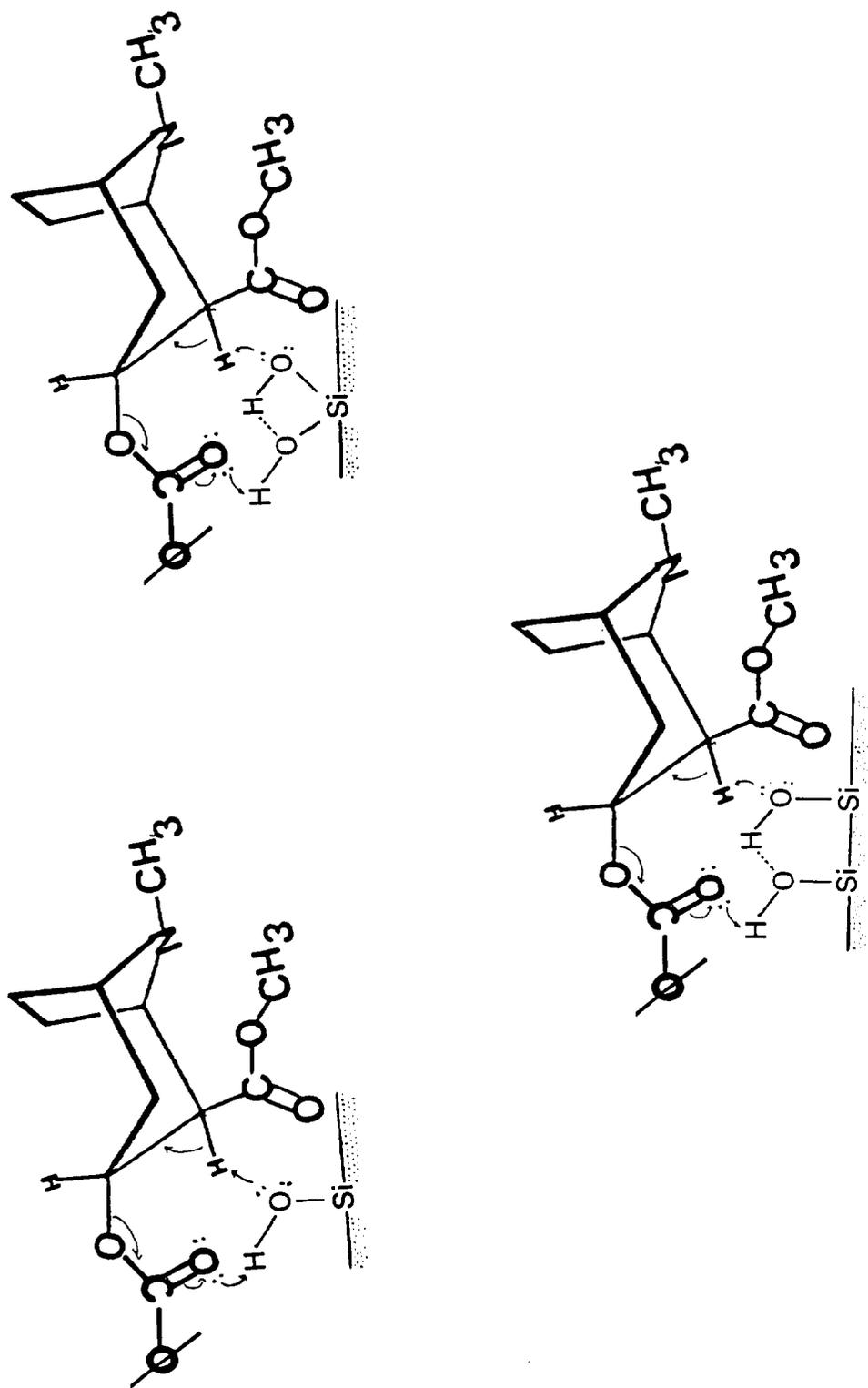
Figure 4. Catalytic Elimination of Benzoic Acid From Cocaine by Quartz or Glass Surface Active Sites
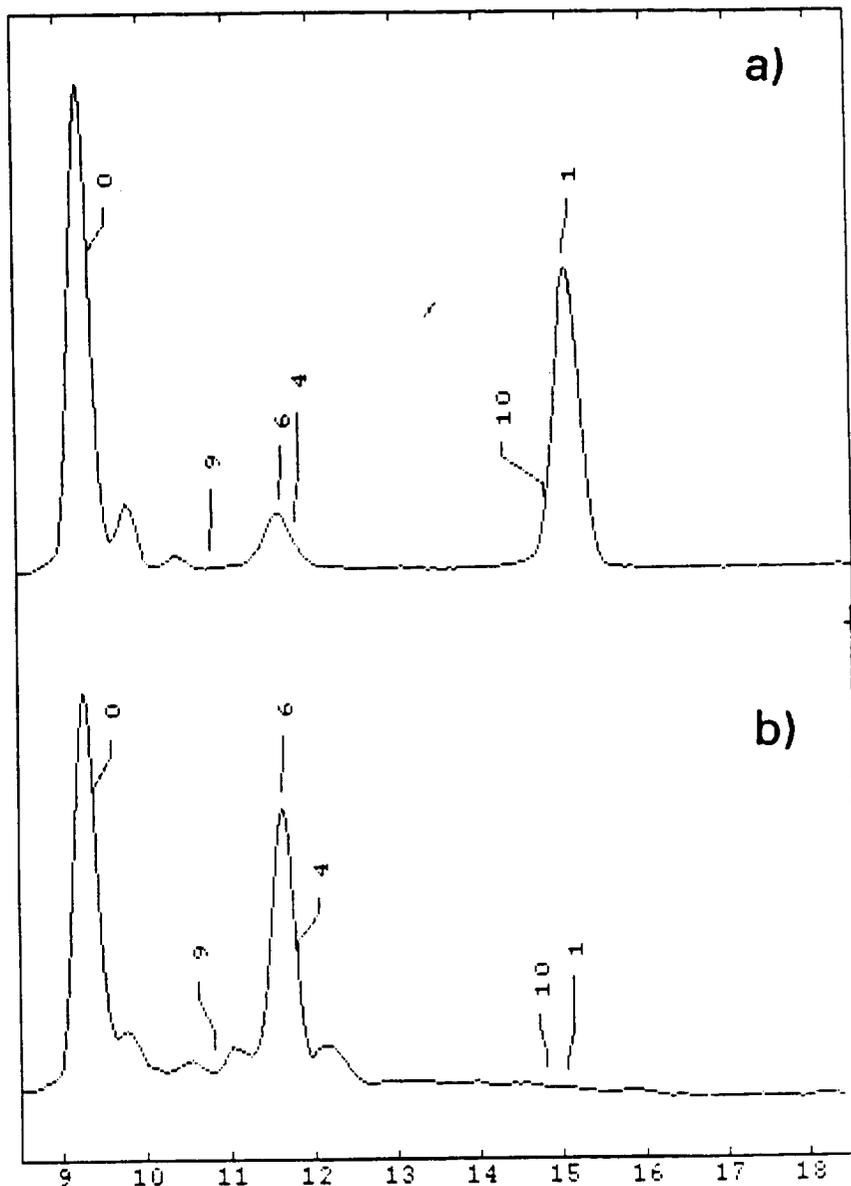
Figure 5. Ion Mobility Spectra of

a) 5 ng of cocaine on paper filter
b) 5 ng of cocaine on paper filter
then covered with glass fiber filter (brand a)

Application of the Ionscan for the Detection of Methamphetamine and Ephedrine in Abandoned Clandestine Laboratories.

Patricia A. Brown and Jeffrey H. Comparin

Drug Enforcement Administration, Southwest Laboratory, 410 W. 35th Street, National City California, 91950

ABSTRACT

Clandestine methamphetamine laboratories are prevalent in southern California. The most common encountered synthesis results in vapor release, and drug residue being left behind. The suspected manufacturing area can be vacuumed and/or methanol wiped and screened immediately at the lab site using the Ionscan. Positive results are confirmed by obtaining vacuum sweep samples with subsequent analysis at the DEA Laboratory. This procedure has been utilized successfully for identifying methamphetamine and ephedrine from clandestine laboratories that have been abandoned and/or remodeled.

INTRODUCTION

Ion Mobility Spectrometry (IMS) is the characterization of chemical substances by measurement of their gas-phase ion mobilities[1]. Chemical substances are heated to vaporization, ionized, and allowed to drift within a controlled electric field. Depending on molecular size and structure, the ions move at different speeds[2]. The measured ion mobility, or drift time, is characteristic of the substance from which the ions came. When compared to a known standard, drift time can be used as a presumptive test.

This technology has been used for approximately fifteen years for drug detection. Drugs such as barbiturates[3], cocaine, and heroin[4] dissolved in solution have been studied. Until recently, little work has been done on solid samples. With the introduction of the Barringer Ionscan, solid samples have been studied by Canadian Customs[5], U.S. Customs[6], and the FBI[7]. Their work on smuggled drugs has led to increased use of the Ionscan for drug detection throughout law enforcement.

Southern California, especially San Diego, has been known as the methamphetamine capital of the world. The most common synthesis used by clandestine operators in this area is the reduction of ephedrine with hydriodic acid and red phosphorus[8]. The "cooking process" is carried out in round bottom flasks with or without condensors. The extraction and crystallization steps are completed using large tanks, buckets or any other suitable container available. This results in vapor release and liquid spillage. Therefore, in most cases, methamphetamine and ephedrine residues are present at clandestine laboratory sites. Pursuant to clandestine laboratory

investigations, there is often a need to determine the existence and location of suspected lab sites that have been abandoned or remodeled. This had been done previously by conducting vacuum sweeps of the entire suspected manufacturing area with subsequent analysis for drug residue. The process was time consuming and resulted in a large number of samples to analyze. On-site utilization of the Ionscan allows for small areas to be vacuumed and/or wiped and immediately screened for the presence of drug residue.

EXPERIMENTAL SECTION

Instrumentation

Ionscan. The Ionscan used was a Barringer model 250 with a Toshiba laptop computer. Ionscan operating conditions were: drift region length, 6.9cm; drift heater temperature, 225°C; inlet heater temperature, 293°C; desorber heater temperature, 286°C; drift and sample gas, purified ambient air; drift gas flow, 300cc/min.; sample gas flow, 200cc/min.; exhaust gas flow, 502cc/min.; scan peroid, 20 microseconds; calibrant, niacinamide; desorber time, 4.4 seconds.

Gas Chromatograph. The gas chromatograph (GC) used was a Hewlett-Packard 5890 Series II equipped with a flame ionization detector. It was operated in the split mode (30:1) using a 5M x 0.32mm i.d. capillary column with a 5% phenyl methyl siloxane liquid phase (0.52um film thickness). The injector temperature was maintained at 280°C. The oven temperature was programmed as follows: initial temperature, 100°C; initial hold, 1min.; temperature program rate, 30°C/min.; final temperature, 270°C; final hold, 5min. Helium was used as the carrier gas at a column flow rate of 1ml/min.

Gas Chromatograph with an Infrared Detector. The vapor phase infrared spectra were obtained on a Hewlett-Packard 5965B Infrared Detector interfaced to a Hewlett-Packard 5890 Series II gas chromatograph (GC-IRD). The gas chromatograph was operated in the splitless mode with a 35 second purge delay then split 40:1 using a 25M x 0.32mm i.d. capillary column with 5% phenyl methyl siloxane liquid phase (0.52um film thickness). The injector temperature was maintained at 280°C. The oven temperature was programmed as follows: initial temperature, 40°C; initial hold, 0.5min.; temperature program rate, 30°C/min.; final temperature, 270°C; final hold, 5min. Helium was the carrier gas with a flow rate of 5ml/min. The spectra were acquired at 8 wavenumber resolution.

Gas Chromatograph-Mass Spectometer. Mass spectra were obtained on a Finnigan Incos XL mass spectrometer interfaced to a Hewlett-Packard 5890 Series II gas chromatograph (GC-MS). The gas chromatograph was operated in the split mode (50:1) using a 5M x 0.2mm i.d. capillary column with 5% phenyl methyl siloxane liquid phase (0.25um film thickness). The injector temperature was maintained at 280°C and the oven was programmed as follows: initial

246

temperature, 100°C; initial hold, 1 min.; temperature program rate, 30°C/min.; final temperature, 270°C; final hold, 5 min. The ion source temperature was maintained at 180°C under electron impact conditions at 70eV. The mass scanning range was 50-500amu with a rate of 0.5 seconds per scan. Helium was the carrier gas with a column flow rate of 1ml/min.

Materials and chemicals

The cocaine hydrochloride was obtained from Merck, West Point, PA, and the methamphetamine hydrochloride was obtained from Sigma Chemical Co., St. Louis, Mo. The cocaine and methamphetamine were each dissolved in reagent grade methanol to concentrations of 100μg/ml, and 10μg/ml respectively. The teflon filters and holder cards were obtained from Barringer Instruments Inc. A Hamilton ten microliter syringe was utilized for solution delivery.

Procedures

Prior to sample analysis, the Ionscan was calibrated with 100ηg cocaine, and 10ηg methamphetamine. At various times during sample analysis the instrument was checked, and recalibrated as necessary. Filter cards were run on the Ionscan to ensure they were blank. The cards were then placed into the vacuum holder and a vacuum sample was obtained to ensure the ability to obtain a blank air sample in the sampling area, and the cleanliness of the apparatus. After determination that the filters and vacuum blanks were negative for the presence of drugs, analysis of suspected manufacturing areas was done. A small area was vacuumed, and the filter was run on the Ionscan. If the sample screened positive for the presence of methamphetamine or ephedrine, the area was vacuumed intensely and the filter was placed into a clean clear plastic ziplock bag and further placed into an evidence envelope. The previously obtained blank filter was also placed into a clean clear plastic ziplock bag and an evidence envelope. Both envelopes were sealed and submitted to the DEA laboratory for analysis. After a positive Ionscan run, the vacuum holder was rinsed with water and methanol. Blank samples were obtained to ensure the apparatus was not contaminated with drug residue.

The vacuum samples, and vacuum blanks, and a reagent blank were analyzed at the DEA laboratory using an acid/base extraction procedure. Sufficient acidic water was added to the clear plastic ziplock bag to soak the filter. The solution was poured into a new clean glass vial, made basic, and extracted with diethyl ether. The ether fractions were screened on the gas chromatograph, and methamphetamine and ephedrine were identified utilizing GC-IRD or GC-MS.

RESULTS AND DISCUSSION

Table 1 shows the results of the samples screened using the Ionscan. In 21 out of 25 samples taken, the substance presumptively identified by the Ionscan was confirmed in the laboratory through analysis. Table 2 lists the drift time and K_0 for the substances of interest. The

x-axis of the plasmagram is the drift time in milliseconds (ms) and the y-axis is set in arbitrary display units. Figures 1 and 2 are the plasmagrams for methamphetamine and ephedrine. Figures 3-5 show the vacuum blank and two confirmed samples. The remaining four samples could not be confirmed. For methamphetamine and ephedrine, the criteria for collecting a sample for positive identification is that the sample peak height must exceed the calibrant peak height. The closer the two are in size, the more difficult it is to positively identify the substance. This could be seen in two non-confirmed samples (figures 6 and 7). In both plasmagrams, the sample peak and the calibrant are similar in size. This suggests that the amount of substance present was too small to detect or not enough sample was collected to confirm the presence of the substance. In no case was another substance identified that had interferred or caused a false positive.

Table 2. -Substances of Interest

Peak Number	Substance	K_0	Drift Time
0	Calibrant	1.8400	9.435
1	Cocaine	1.1600	14.966
4	Ephedrine	1.5812	10.979
5	Methamphetamine	1.6441	10.559
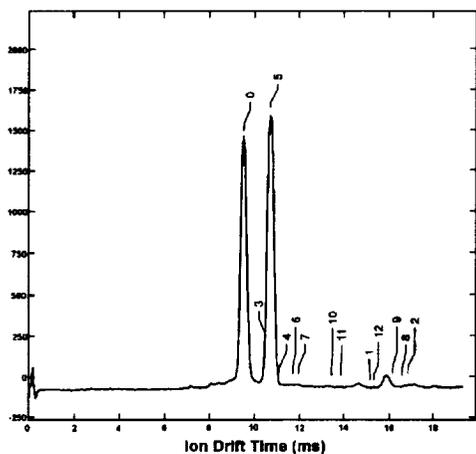
Figure 1.- Plasmagram of methamphetamine
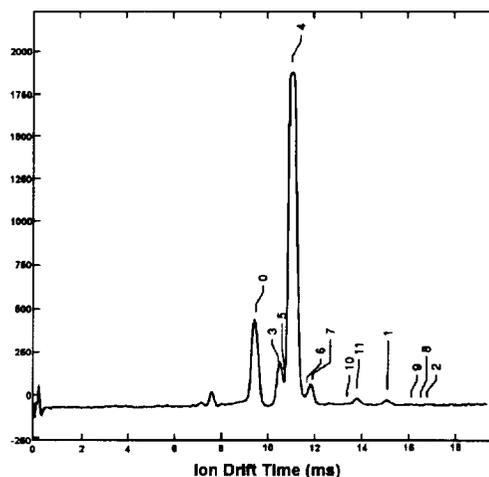
Figure 2.- Plasmagram of ephedrine

Conclusion

The results displayed in this paper show that the Ionscan is a very useful tool for screening samples taken from an abandoned clandestine laboratory. If our criteria for the size of sample peak is met, then confirmation through analysis is not a problem.
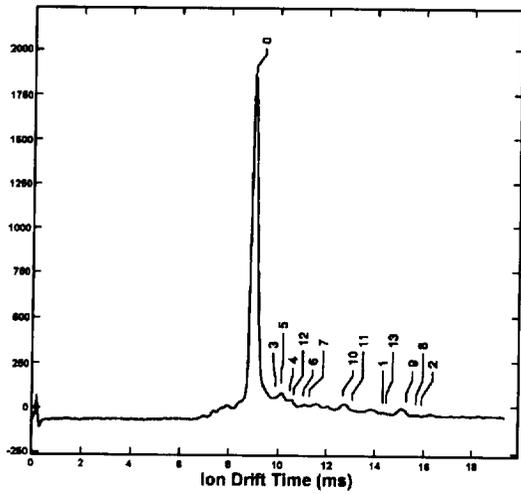
Figure 3- Plasmagram of vacuum blank.
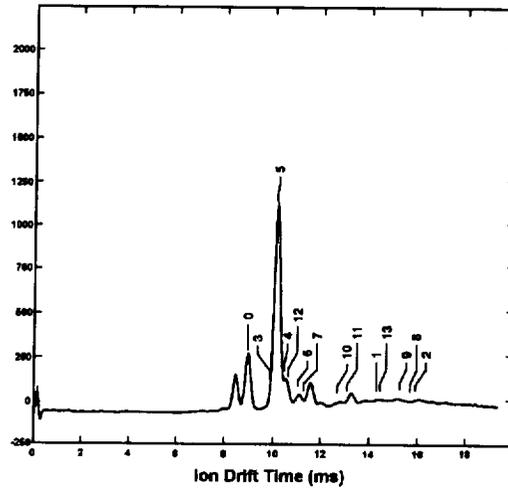
Figure 4- Plasmagram of white circle under rug (Sample 24).
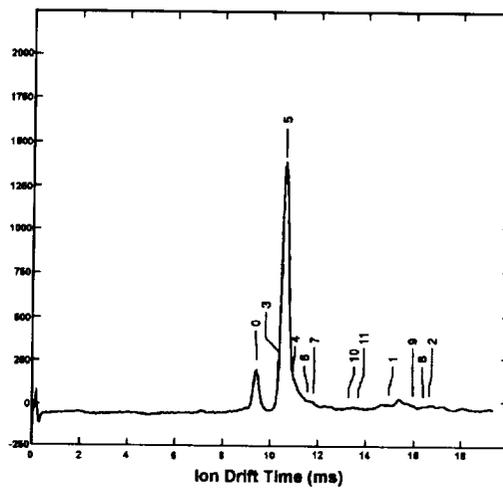
Figure 5- Plasmagram of the shirt (Sample 22).
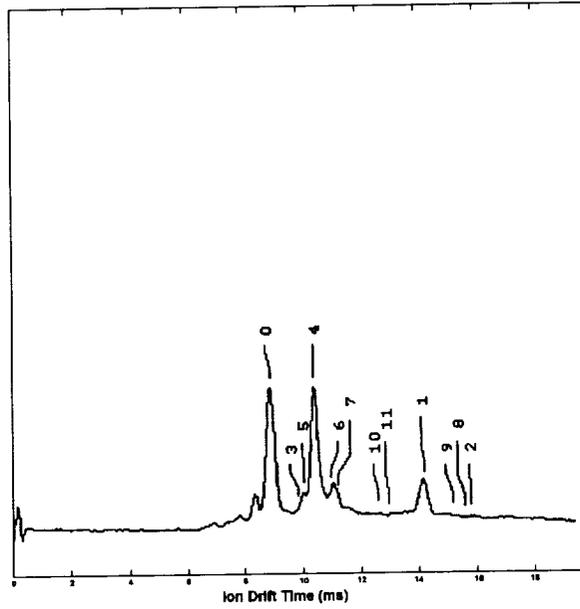
Figure 6-Plasmagram of a vacuum sample from a concrete garage floor (Sample 15).
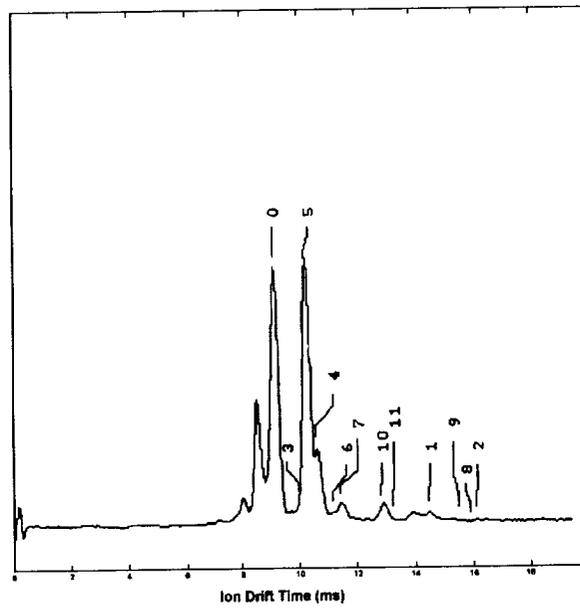
Figure 7-Plasmagram of an alcohol wipe of the register in the downstairs bathroom (Sample 14).

Acknowledgements

Reference

1. Eiceman, G.A. and Karpas, Z. Ion Mobility Spectrometry. CRC Press, Boca Raton, Fl. 1994 p.2.

2. Ionscan® Operators Manual Barringer Instruments Limited, Rexdale, Ontario, Canada, January 1993, p.2-1.

3. Ithakissos, D.S. Plasmagram Spectra of Some Barbiturates. *J. of Chromatographic Sciences*, 18,88-92 (1980).

4. Karasek, F.W., Hill Jr.., H.H., and Kim, S.H. Plasma Chromatography of Heroin and Cocaine with Mass-Identified Mobility Spectra. *J. of Chromatography*, 117, 327-336 (1976).

5. Harnois, J., Kovar, J., and Pilon,P. Detection of Cocaine and Heroin Using a Custom Built Ion Mobility Spectrometer. *Customs Laboratory Bulletin*, Vol. 4, No. 1, 11-31 (1992).

6. Smith, D., Hoglund, D., Hood, L., Flor, R., Erikson, C., and Trinh, T. A Field Evaluation of Drug Detection Technologies: Laboratory Confirmation of Drug Residues. Presented at Contraband and Cargo Technology International Symposium, Washington, D.C. October 28-30,1992.

7. Fetterolf, D. D., Donnelly, B., and Lasswell, L. D. Portable Analytical Instrumentation : New Weapons in the War on Drugs. Presented at Contraband and Cargo Technology International Symposium, Washington, D.C. October 28-30,1992.

8. Skinner, H.F., Methamphetamine Synthesis Via Hydriodic Acid/Red Phosphorus Reduction of Ephedrine. *Forensic Science International*, 48, 123-134 (1990).

Table 1. Information from various Clandestine Laboratory Sites.

Sample	Date Cooked	Date Collected	Area Sampled	Type Of Sample	Presumptive Identification	Confirmed
1	11-91	11-92	Ocean Facing Window	Vacuum	Methamphetamine	Yes
2	11-91	11-92	Floor Under Window	Vacuum	Methamphetamine	Yes
3	11-91	11-92	Remaining Floor Area	Vacuum	Methamphetamine	Yes
4	1-93	8-93	Shed Floor	Vacuum	Methamphetamine	Yes
5	8-93	10-93	Wooden Work Bench	Alcohol Wipe	Methamphetamine	Yes
6	8-93	10-93	Concrete Garage Floor	Alcohol Wipe	Methamphetamine	Yes
7	8-93	10-93	Concrete Garage Floor	Alcohol Wipe	Methamphetamine	No
8	8-93	10-93	Trunk Of Car	Vacuum	Ephedrine And Methamphetamine	Yes
9	6-93	10-93	Air Return Register	Alcohol Wipe	Methamphetamine	Yes
10	6-93	10-93	Laundry Room Exhaust Fan	Alcohol Wipe	Methamphetamine	Yes
11	6-93	10-93	Bathroom Air Register	Alcohol Wipe	Methamphetamine	Yes
12	6-93	10-93	Bathroom Exhaust Fan	Alcohol Wipe	Methamphetamine	Yes
13	6-93	10-93	Air Register	Alcohol Wipe	Methamphetamine	Yes
14	6-93	10-93	Register In Downstairs Bathroom	Alcohol Wipe	Ephedrine And Methamphetamine	No
15	6-93	10-93	Concrete Garage Floor	Vacuum	Ephedrine	No
16	6-93	10-93	Counter Top	Vacuum	Ephedrine And Methamphetamine	No
17	6-93	10-93	Separatory Funnel	Vacuum	Methamphetamine	No
18	3-92	11-93	Garage Door Opener	Vacuum	Methamphetamine	Yes
19	3-92	11-93	Ceiling Fan	Vacuum	Methamphetamine	Yes
20	3-92	11-93	Ventilation Fan	Vacuum	Methamphetamine	Yes
21	3-92	11-93	Safe Interior	Vacuum	Methamphetamine	Yes
22	3-92	11-93	Shirt	Vacuum	Methamphetamine	Yes
23	3-92	11-93	Pvc Pipe	Vacuum	Methamphetamine	Yes
24	8-92	3-94	White Circle Under Rug	Vacuum	Methamphetamine	Yes
25	8-92	3-94	Yellow Stain On Wooden Floor	Vacuum	Ephedrine And Methamphetamine	No

Application of Ion Mobility Spectrometry (IMS) in Forensic Chemistry and Toxicology with focus on biological matrices

Werner Bernhard, Thomas Keller[*] , Priska Regenscheit

Department of Forensic Chemistry and Toxicology

Institute of Forensic Medicine[**]
Buehlstr. 20
CH-3012 Berne, Switzerland

ABSTRACT

The IMS instrument "Ionscan" takes advantage of the fact that trace quantities of illicit drugs are adsorbed on dust particles on clothes, in cars and on other items of evidence. The dust particles are collected on a membrane filter by a special attachment on a vacuum cleaner. The sample is then directly inserted into the spectrometer and can be analyzed immediately. We show casework applications of a forensic chemistry and toxicology laboratory. One new application of IMS in forensic chemistry is the detection of psilocybin in dried mushrooms without any further sample preparation.

KEY WORDS: Ion mobility spectrometry, forensic chemistry, forensic toxicology, illicit drugs, psilocybin, instrumental thin layer chromatography

INTRODUCTION

At the Department of Forensic Chemistry and Toxicology at the Institute of Forensic Medicine at the University of Berne two ion mobility spectrometers (Ionscan, Model 250 and 350, Barringer, Toronto, Canada) are used to help law enforcement and government agencies of several Swiss cantons to combat drug-related crimes. In the department IMS is used for the analysis of illicit street drug samples obtained by the police. Analysis is performed of evidentiary items like clothing, cars, apartments, balances, knives, pipes, etc. If these items had got contact with illegal or controlled substances the objects give off tiny particles that cling to their surface. These particles are collected onto a Teflon membrane filter by vacuuming the objects or by swabbing them with a dry cotton swab. The filter is then directly inserted into the Ionscan. The results are obtained immediately [1, 2]. Also in some cases IMS is used to obtain rapid preliminary results in forensic toxicology as well as in forensic investigations.

Applications of IMS in forensic casework

Illicit substances, including all of the most commonly used drugs (e.g. heroine, cocaine, amphetamines, MDMA, MDEA, LSD, etc.) are detected on clothes, money, in vehicles, apartments as well as on various items used to portionate drugs (e.g. balances and knives). Packages sent to prisoners are also examined by IMS. In those special cases a main advantage of IMS is, that the outside of an unopened package can easily be screened. If a negative result is obtained, the probability that the package contains illicit or controlled substances is very small. To confirm trace analysis with IMS for court cases we use electron impact GC/MS. For illicit heroine and cocaine samples, positive results with IMS are always confirmed by a

---

second independent method, mostly instrumental TLC. The chromatograms are run in the system cyclohexane/toluene/diethylamine 85:5:10. Differentiation between the free base and the hydrochloride is done by FT/IR-spectroscopy. Illicit heroine samples are compared either by GC/FID, GC/PND or GC/MSD. The comparison of cocaine samples is performed by GC/MS after derivatization [3].

In one case the police seized a package of Psilocybe mushrooms. We were asked to examine the mushrooms for illicit or controlled substances. Examination of the mushrooms by IMS showed that they were contaminated with cocaine. In addition, without any sample preparation we were also able to detect psilocybin. Small amounts of ground mushrooms were put onto the membrane filter and directly inserted into the Ionscan. Blank dried mushrooms bought from a food store were used as a negative control. Figure 1 shows the plasmagram of this negative control. Figure 2 shows the plasmagram of the seized Psilocybe mushrooms.
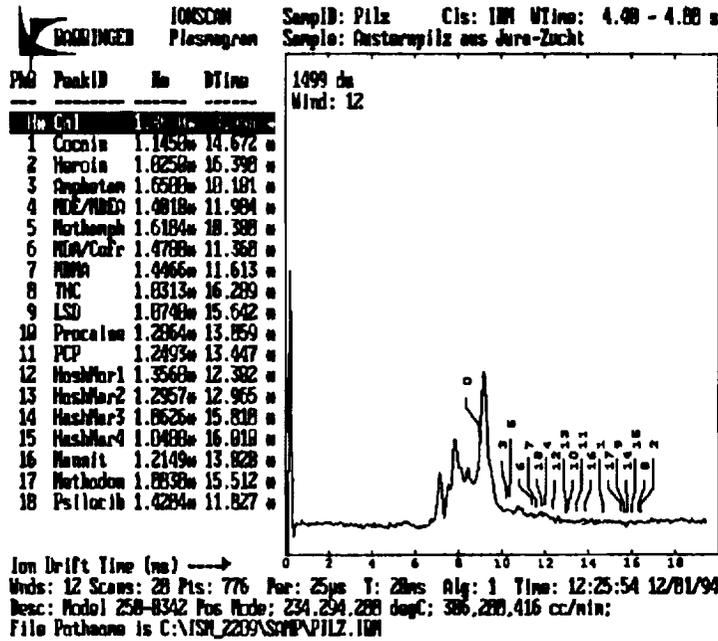
Fig. 1:   Plasmagram of negative control
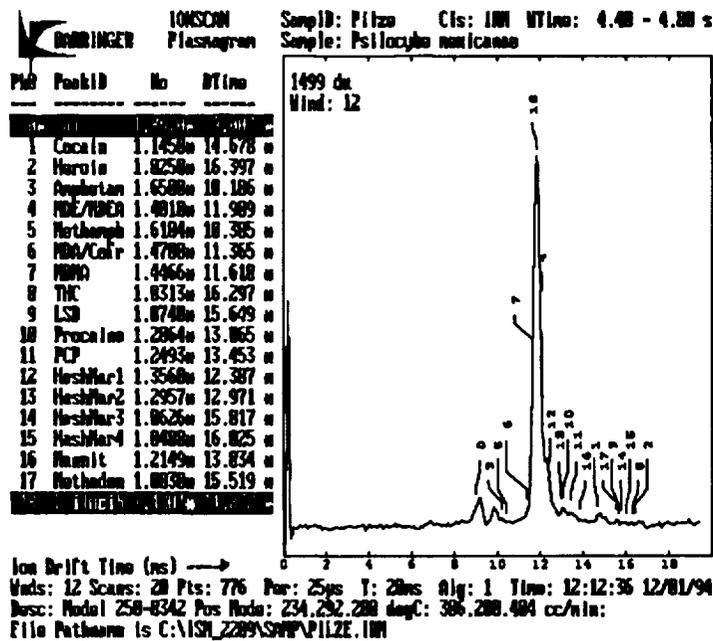
Fig. 2: Plasmagram of Psilocybe mushrooms

To verify that the observed signal at DTime = 11.83 ms stands for psilocybin a psilocin and psilocybin standard solution was also examined. Figure 3 and Figure 4 show the plasmagrams of the corresponding standard solutions.
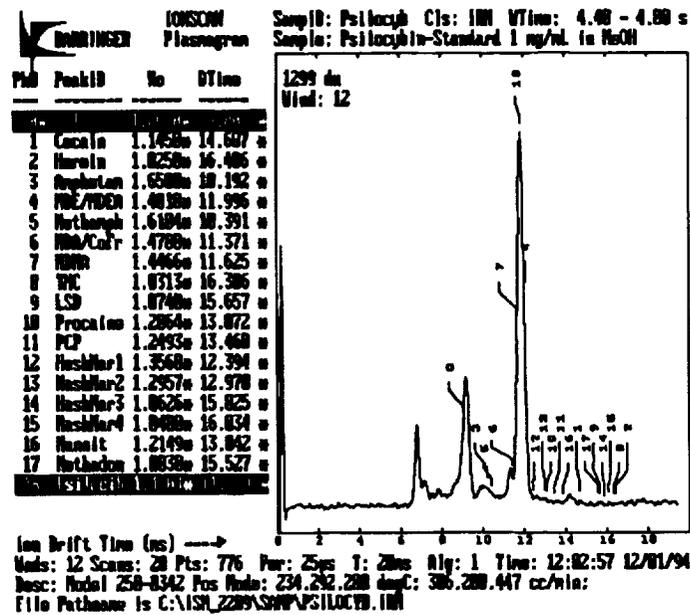
Fig. 3: Plasmagram of the psilocybin standard solution
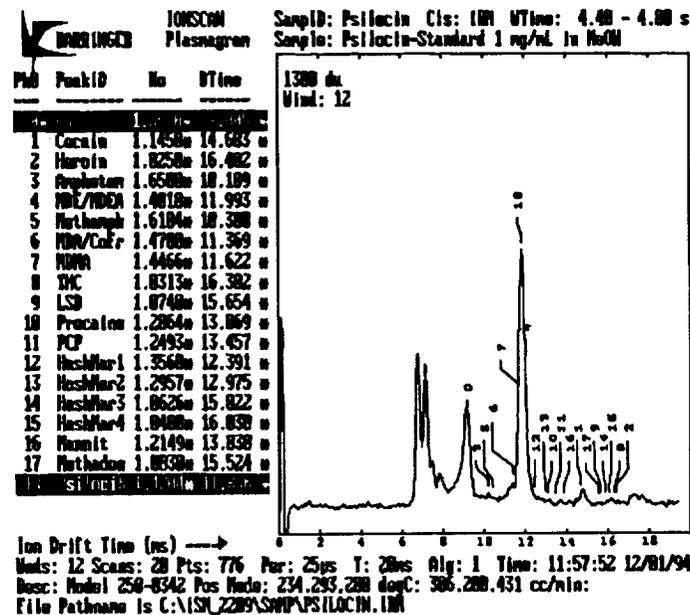
Fig. 4: Plasmagram of the psilocin standard solution

Comparison of Figure 3 and 4 shows that the plasmagrams of both standard solutions give the same drift time for the two substances. The appearance of a signal at DTime = 11.83 ms indicates that in the IMS ion source psilocybin is converted into psilocin.

Confirmation of the presence of both psychotropic substances was done by TLC.

A 1 mg/mL psilocin and psilocybin standard solution were used as reference. The ground mushrooms were extracted with methanol. The organic layer was separated from the residue through a filter and the clear solution was completely evaporated. The residue was then redissolved in 100 µL methanol. TLC was performed on a silica plate in the system methanol/acetic acid/water 75:10:15. As spray reagent 0.25 g of 4-Dimethlyaminocinnamaldehyd and 5 mL concentrated HCl in 25 mL methanol was used. After the development of the plate it was sprayed and heated up to 120 °C. Psilocybin yielded a violet spot at R_f = 0.47 whereas psilocin yielded a green spot at R_f = 0.71.

For instrumental TLC the system MeOH/H$_2$O 9:1 was used. In contrast to the procedure described above the plate was neither sprayed nor heated after development. Psilocin and psilocybin yielded spots under the UV light (254 nm) at R_f = 0.10 and R_f = 0.22 respectively. These spots were then detected with a Camag TLC Scanner II at 268 nm. Figure 5 shows the densitogram of the psilocin calibration curve. For the calibration curve (STD 1 - STD 4) 0.2, 0.4, 0.6 and 0.8 µg psilocin/µL was used. Psilocin could not be detected in the extracted mushrooms (S 1).
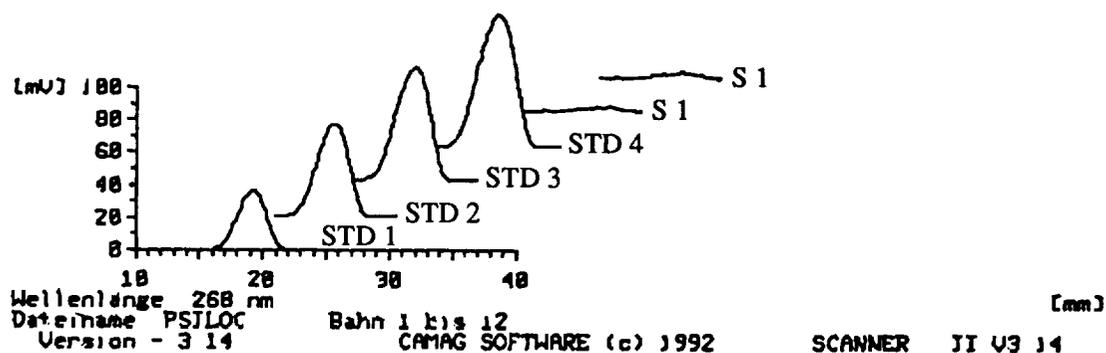
Fig. 5: Densitogram of the psilocin standard solution and extracted Psilocybe mushrooms

Figure 6 shows the densitogram of the psilocybin calibration curve (STD 1 - STD 4) and extracted Psilocybe mushrooms. For the calibration curve 0.5, 0.75, 1.0 and 1.25 µg psilocybin/µL was used. Psilocybin could be detected in the crude mushroom extract (S 1) as well as in its 1:10 dilution (D 1).
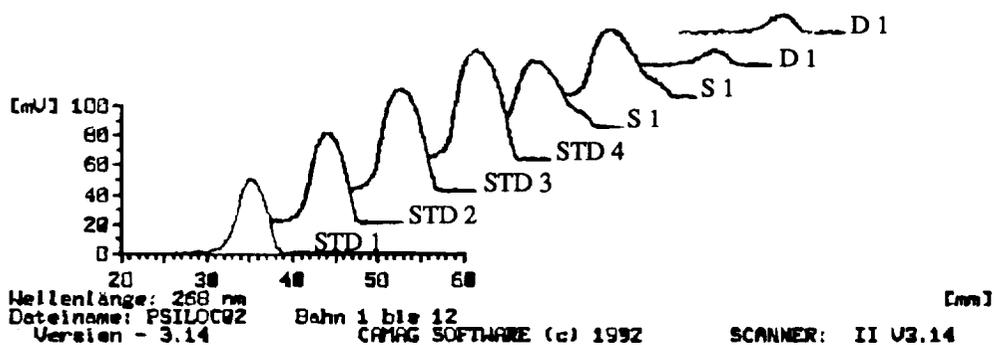
Fig. 6: Densitogram of the psilocybin standard solution and extracted Psilocybe mushrooms

257

A further application of IMS in forensic toxicology is the rapid detection of illicit or controlled substances (mostly heroine and cocaine) in biological samples like nose smears and fingernail dirt. The examination of fingernail dirt from people suspected to handle or deal with drugs is of great importance. Therefore our police officers are equipped with cotton swabs and requested to wipe the suspect's fingernails. For each hand one cotton swab moistened with methanol is used. Particles that cling to the cotton swab are either put directly onto the membrane filter or are eluted onto the filter with methanol. The solvent is evaporated in a gentle stream of air and the filter is then inserted into the Ionscan.

In forensic toxicology and forensic investigations quick answers for the route of intake of drugs into the body can also be obtained by IMS. In one case a person was found dead after a beer party. Since the medical examiners were unable to find the cause of death during the autopsy, nose smear was taken with the cotton swabs and also examined with IMS. The procedure of the examination was the same as described above. In both nostrils heroine could be found. With this quick analysis that was performed during the autopsy we were able to give indications for the direction of further investigations. Confirmation analysis done by GC/MS later, showed heroine, monoacetylmorphine and procaine present in the nose smear. Morphine could be found in the blood with a concentration of 0.7 mg/L. In addition the blood-alcohol concentration was 1.5 ‰. So the cause of death was determined as an intoxication with sniffed heroine in combination with ethanol [4].

CONCLUSIONS

We showed a number of interesting IMS applications in the daily casework of a forensic laboratory. IMS is a powerful tool to detect trace quantities of illicit or controlled substances on various surfaces and items of evidence. For most commonly encountered drugs (mostly heroine and cocaine) we observed excellent specificity and sensitivity. In the field of forensic toxicology the examination of fingernail dirt by IMS has proven extremely useful and successful. In a case of fatal heroine intoxication in combination with alcohol by examining the nose smear of the victim we could give indications for the direction of further police investigations. We also showed that the detection of psilocybin in Psilocybe mushrooms can rapidly be done by IMS without any sample preparation.

<u>References</u>

[1]   L.M. Fytche, M. Hupe, J.B. Kovar and P. Pilon, Journal of Forensic Sciences, <u>37</u>, p. 1550-1566 (1992).

[2]   D.D. Fetterolf and T.D. Clark, ibid. , <u>38</u>, p. 28-39 (1993).

[3]   G. Fritschi, Cocain-Profiling, Eine Methode zur Materialvergleichsuntersuchung von illegalen Cocainproben, Archiv fuer Kriminologie, <u>Band 188</u>, S. 87-95, (1991)

[4]   W. Bernhard, 13th Meeting, International Association of Forensic Sciences IAFS, Düsseldorf, Germany, 1993.

Session V: Data Reduction and Signal Processing

Session Chair: Dr. Dennis Davis

259

DATA COLLECTION IN IMS :
IT'S NOT AS EASY AS IT LOOKS

Dennis M. Davis[1], Waleed Maswadeh[2], Donald B. Shoff[1], Charles S. Harden[1], A. Peter Snyder[1]

[1]U.S. Army Edgewood Research Development and Engineering Center, Lightweight Chemical Detector Team, Aberdeen Proving Ground, MD 21010-5423, [2]GEO-CENTERS, Inc., P.O. Box 68, Gunpowder Branch, Aberdeen Proving Ground, MD 21010-5423

ABSTRACT

Data collection in Ion Mobility Spectrometry (IMS) is not as easy an endeavor as it appears. Despite the advent of high speed personal computers and fast analog-to-digital converters (ADC's), care must be taken to ensure that reliable data is obtained in a timely fashion. This is especially true in hyphenated techniques, e.g. GC-IMS, where the amount of data increases dramatically when gas chromatography-ion mobility spectrometry (GC-IMS) data is being collected. Using the Graseby GC-IMS, with a gate repetition rate of 33 Hz, it is theoretically possible to collect 33 spectra per second. This collection rate is not realistically obtained due to a number of factors. Among these factors are inaccuracy of the timing signal from the IMS, the necessity to store the data, disk input/output limitations, disk operating system limitations, and program overhead. Taking these factors into account, we have achieved a data collection rate of 20 spectra per second. This paper will describe these problems, demonstrate the practical effects these problems present, and present methods for minimizing these effects.

INTRODUCTION

One of the most important aspects of ion mobility spectrometry (IMS) studies, and too often the least understood, is data collection and data storage. Detection, identification and determination of the concentration of the chemical species present are all affected by the data collection. Yet, as important as data collection is, many researchers do not take the time to collect and store IMS data properly, either because they use routines written by others, or they are not fully aware of the limitations under which they must operate. The limitations may be classified into one of three categories: hardware related, software related, or data related. The limitations which most affect the data collection and data storage are as follows:

Hardware related:
(1) inaccuracy of the timing signal from the IMS,
(2) disk input/output limitations,
(3) computer limitations,

software related:
(4) disk operating system limitations,
(5) program overhead, and

data related:
(6) the necessity to store the data,
(7) the nature of the data itself.

261

EXPERIMENTAL

Hardware.

For this work, we used an improved Environmental Vapor Monitor, EVM, (Graseby Ionics, Ltd. Watford, Herts, UK). The EVM, a hand-held GC-IMS, is comprised of capillary gas chromatograph, GC, integrated with a hand-held ion mobility spectrometer, IMS[1]. The IMS operates with an internal sample gate repetition rate of 33 Hz. The gating pulse has an amplitude of 5 volts and is 180 microseconds in duration. This gating pulse provides the trigger for the data collection. The improvements include the introduction of temperature and pressure sensors inside the IMS cell and the construction of a disposable GC module. The disposable GC module offers some important features: 1) an easily replaceable GC module which facilitates changes in column types and lengths, as dictated by the compounds being studied, 2) easy replacement of the GC column when the column is spent, and 3) a GC column that can be easily heated from room temperature to 130°C in two minutes. The improvements in the GC-IMS system design ensure better separation characteristics, improved detection and identification of chemical compounds, increased ease of maintenance of the system, and a more robust hand-held detector. Typical experimental conditions used for the hand-held GC-IMS are shown in Table I. Sample introduction to the GC column was accomplished by using an Automated Vapor Sampling unit, AVS[2]. The sample pulse is user controlled with a range of 0.2 seconds to 2 seconds duration.

TABLE I
EXPERIMENTAL OPERATING CONDITIONS OF THE GC-IMS

Disposable GC Module:

GC Column:	Liquid Phase:	DB-1 (0.25 micrometer I.D.)
	Temperature (°C):	45°C/min programmable
	Carrier Gas:	Clean dry air
	Flow Rate:	2.1 ml/min
	Length:	1 m

Sample Injection:	User-software controlled
	typically 0.2 sec duration

Ion Mobility Spectrometer:

Ionization Source:	^{63}Ni
Gating Pulse Repetition Rate:	33 Hz
Cell Temperature:	30 °C
Cell Pressure:	640 torr
Drift Gas:	Clean dry air
Drift Gas Flow:	400 ml/min

Data was collected on a Dell 486D personal computer operating at a processor speed of 33MHz, with 8 KB of internal cache memory, 32 MB of system memory (RAM), a 230 MB IDE hard disk drive with 16 ms average seek time, and VGA monitor. The data was collected using an AT-MIO-16X multifunction I/O board (National Instruments Corporation, Austin, TX). The AT-MIO-16X has a 10 microsecond, 16 bit, sampling ADC. Typical data collection parameters are shown in Table II.

TABLE II.
TYPICAL DATA COLLECTION PARAMETERS USED WITH THE GC-IMS

Ion Mobility Spectrometer Parameters:

Spectral Mode:	Positive Ion
Points Per Spectrum:	640
Sampling Frequency:	33 Khz
Delay to Start of Sampling:	0 microseconds

GC Parameters:

GC Delay:	0 seconds
GC Heating Time:	30 seconds
AVS Temperature:	Room
AVS Pulse Duration:	100 ms

Data Acquisition Board Parameters:

PC Slot Number:	1
Digital I/O Port Address:	A
IMS Analog Input Channel:	0
IMS Mode Detect Channel:	0
GC Digital Trigger Channel:	1
Cell Temperature Input Channel:	4
AVS Temperature Input Channel:	5
Column Temperature Input Channel:	6
Cell Pressure Input Channel:	3

Software.

The data collection algorithms were written using Labwindows Software Version 2.2 (National Instruments, Austin,TX) in both C and QuickBasic programming languages. The programs were compiled using Microsoft C Version 5.1 and Microsoft QuickBasic as appropriate. The compiled versions of the software were then run under Microsoft DOS Version 6.0. Labwindows versions of the executable code were all created using the Labwindows Run Time System.

DISCUSSION

Hardware Related Limitations.

Of all the limitations, the hardware related limitations are the ones over which the researcher has the least direct control. The most severe limitations are caused by inaccuracy of the timing of the gating pulse, disk input/output limitations, and computer limitations. Each of these may be overcome to some extent, but each extracts a price.

Inaccuracies in the timing signal from the IMS. The gating pulse on the IMS is used as the trigger to start the data collection. The accuracy of the timing of the gating pulse is directly related to the accuracy of the clock used to time the pulse. While the gating pulse repetition rate of the GC-IMS is 33 Hz, there are inconsistencies in the gating pulse rate as shown in Figure 1. These inconsistencies, or inaccuracies, affect the data collection. The data collection is not affected by the gating pulse repetition rate being slower than the 33 Hz as much as it is when the rate is faster than 33 Hz. Since 640 data points are collected at a frequency of 33 kHz, the total time necessary to collect one spectrum is 21.12 milliseconds. At a gating pulse repetition rate of 33 Hz, this leaves 8.88 milliseconds between the end of data collection and the start of the next spectrum to write the data to the disk. Slowing of the data gating pulse repetition rate provides more time to complete the transfer of data to the disk. Thus, the effect of slowing the data rate by a slight amount is negligible. However, when the data rate is increased slightly, the amount of time available to transfer the data to the disk is decreased. Thus, the chance of getting a trigger pulse to start data collection during the data transfer to disk is increased. Since the program has not issued the commands to initiate the data collection, the spectrum is lost and the program waits for the next trigger pulse. Thus, it is possible to envision a decrease in the sampling rate of 33 Hz to 15 Hz without taking other limitations into account.

A sequence of ion mobility scans is shown in Figure 2 and demonstrates another problem which may be encountered. It is noted that although the repetition rate of the gating pulse and data is approximately 33 Hz, there are periods in which no trigger signal, and thus, no data is available. The GC-IMS produces eight trigger pulses and spectral data sets, skips four pulses and data sets, then repeats the pattern. The source of this periodicity is internal to the GC-IMS, and therefore beyond control of the experimenter. This problem may be unique to those IMS devices which are designed to provide averaged spectra. In actuality, with the GC-IMS, there are at most 24 spectra available for collection per second. The effect that the non-uniformity of the gating pulse has on the data collection is shown in Figure 3, which is a contour plot of the first 11 spectra collected in a GC-IMS run, with each spectrum in Figure 3 being represented by a bar. The GC retention time reflects the inaccuracy in the timing of the gating pulse. There should be consistent spcaing, retention time difference, between consecutive bars in Figure 3. This problem may be overcome by issuing the trigger pulse from the computer rather than the IMS. This generally entails a reworking of the IMS electronics. If one uses more than one IMS, the time and energy spent on this solution becomes burdensome.

Disk input/output limitations. The second of the hardware limitations, and the least understood, are the disk input/output limitations. These limitations include disk access time, disk cluster size, and disk access procedures. Typically, disk access times range from 13 to 21 milliseconds, with the time being a function of disk size. Some of the more common drives and their disk access times are given in Table III. The data in Table III was compiled from a variety of sources including manufacturer data sheets, computer system documentation, and computer shopper magazines. A complete description of drive types may be found elsewhere[3]. To improve the speed of the disk drive, one must usually increase the size of the drive, resulting in increased computer costs. However, when speed is of the essence, it is a price well spent.

The next disk input/output limitation, disk cluster size, is more insidious than the other limitations, because it is generally hidden from the programmer. The disk cluster size is a function of the disk size, as shown in Table IV. While the disk cluster size does not directly affect the speed of data collection, its effects are nevertheless present. For example, when collecting individual IMS spectra, which have a typical size of 1300 bytes, collecting a large number of individual spectra on a 200 MB drive results in a waste of disk space of almost 75 percent. Thus, when each subsequent spectrum is saved to disk, there are fewer clusters in which to save data, the clusters are generally scattered across the surface of the disk, and the disk access time slows as free clusters are located. This problem is easily overcome by collecting all spectra to a single spectral file, thus ensuring that at most 1 disk cluster is lost

TABLE III.
DISK TYPES AND ACCESS TIMES

MANUFACTURER	DRIVE TYPE	DRIVE SIZE	DISK ACCESS TIME
Conner	SCSI	212 MB	12 ms
Conner	SCSI	170 MB	17 ms
Conner	IDE	42 MB	25 ms
Conner	IDE	212 MB	12 ms
Seagate	IDE	43 MB	28 ms
Seagate	IDE	245 MB	12 ms
Maxtor	IDE	213 MB	12 ms
Maxtor	SCSI	213 MB	15 ms

for a set of spectra. The cost for this solution is simply that individual spectra are more difficult to access. This cost is more than offset by the increased disk storage capacity and time saved in saving spectra.

TABLE IV.
DISK CLUSTER SIZES

Disk Size		DOS Default Cluster Size	
Floppy Disks:			
360	KB	1024	Bytes
1.2	MB	512	Bytes
1.44	MB	512	Bytes
Hard Disks:			
0-16	MB	4096	Bytes
16-128	MB	2048	Bytes
128-256	MB	4096	Bytes
256-512	MB	8192	Bytes
512-1024	MB	16,384	Bytes
1024-2048	MB	32,768	Bytes

Computer limitations. The easiest of the hardware limitations to overcome are the computer limitations. The limitations in this category are related to the speed at which instructions may be carried out by the computer: processor speed limitations. Upgrading computer facilities is the only solution available. Some of the possible components which may be included in this upgrade are:

1) install a direct memory access (DMA) board,
2) install a newer I/O board,
3) replace the current computer with one which has a faster processor.

Generally, replacing the computer with one which has a faster processor will have the greatest impact on the speed of accessing and saving data. Installing a DMA board will improve the speed of the data transfer from memory to disk, but has little impact on how fast the other instructions are performed. A newer I/O board will allow faster data collection from the IMS, but it won't improve the speed of the data transfer to disk, or perform other instructions faster. Improving the processor speed will improve the speed at which each instruction is performed, which minimizes the total time necessary to complete the task of data transfer and manipulation.

Software related limitations.

There are two basic types of software related limitations. The first are those related to the disk operating system, DOS, and the second are those related to program overhead. These limitations are generally outside the control of the researcher.

Disk operating system limitations. The most important function of DOS is the control of access to the disks in the computer. Disk access and file allocation of disk space is performed as requested by the program, with space being allocated one cluster at a time. The allocation algorithm used by DOS is called the Next Available Cluster algorithm[3]. Each time the program sends a command to write to the disk, the algorithm starts at the cluster where the last write occurred, and then searches for the next free cluster to begin writing the data. After that cluster is written, the next free cluster is located, and the write continues until the data is written. Because the next available cluster is used, the data file may be spread over a large amount of the disk, depending upon where the next available cluster is located, and the file becomes fragmented. In addition to writing the data, the computer's operating system must place the pointers of which clusters belong to which files in the File allocation Table, FAT, and place a directory listing for the file in the proper directory listing. If duplicate filenames are used within the same directory, the current directory listing and FAT pointers must be removed from the FAT and the new listings and pointers entered. This results in increased time required to write successive files, as shown in Table V, where the number of files written in each second is seen to decrease as the number of files increases.

The solution to this limitation is again to write the data to a single data file for each set of spectra collected. Thus, the next available cluster will often be the current cluster (until it is filled with data). The directory listing must only be made once, and only the FAT listing must be updated.

Program overhead limitations. Program overhead limitations may be imposed upon the researcher and programmer by DOS, as seen above, or by the programmer himself. The limitations that the programmer places on the data collection are related to such mundane tasks as: reading the system clock to determine how much time has expired since the last spectrum was collected, keeping track of how many spectra have been collected to date, monitoring for trigger pulses, and maintaining a check on the status of data transfers to the disk. Each of these steps may be eliminated, but the price which must be paid is an increased level of uncertainty as to the nature of the data. For example, failure to read the system clock will result in not knowing when a particular sample was collected. Thus, its place in the series of spectra which have been collected is unknown. Not monitoring for trigger pulses is a particularly unpleasant idea when taking GC-IMS data, because the GC retention time is unknown, and the information gained from performing the GC separation is lost. Monitoring the status of the data transfer to disk is the most dangerous of the program overhead steps to eliminate, because it is not just information you may lose, you run the risk of losing the data itself.

The greatest burden on program overhead is the desire of the researcher to view the data as it is being collected. This necessitates the programmer putting in graphics routines. Graphics routines generally require additional programming steps related to scaling the data to fit the graphics windows and

TABLE V.
PARTIAL DIRECTORY LISTING FOR SUCCESSIVELY CREATED SPECTRA

TIME0000.ACQ	1334 10-03-94	1:41p		TIME0262.ACQ	1334 10-03-94	1:49p
TIME0001.ACQ	1334 10-03-94	1:41p		TIME0263.ACQ	1334 10-03-94	1:49p
TIME0002.ACQ	1334 10-03-94	1:41p		TIME0264.ACQ	1334 10-03-94	1:49p
TIME0003.ACQ	1334 10-03-94	1:41p		TIME0265.ACQ	1334 10-03-94	1:49p
TIME0004.ACQ	1334 10-03-94	1:41p		TIME0266.ACQ	1334 10-03-94	1:50p
TIME0005.ACQ	1334 10-03-94	1:41p		TIME0357.ACQ	1334 10-03-94	1:57p
TIME0006.ACQ	1334 10-03-94	1:41p		TIME0358.ACQ	1334 10-03-94	1:58p
TIME0007.ACQ	1334 10-03-94	1:41p		TIME0359.ACQ	1334 10-03-94	1:58p
TIME0008.ACQ	1334 10-03-94	1:41p		TIME0360.ACQ	1334 10-03-94	1:58p
TIME0009.ACQ	1334 10-03-94	1:41p		TIME0361.ACQ	1334 10-03-94	1:58p
TIME0010.ACQ	1334 10-03-94	1:41p		TIME0362.ACQ	1334 10-03-94	1:58p
TIME0011.ACQ	1334 10-03-94	1:41p		TIME0363.ACQ	1334 10-03-94	1:58p
TIME0012.ACQ	1334 10-03-94	1:41p		TIME0364.ACQ	1334 10-03-94	1:58p
TIME0013.ACQ	1334 10-03-94	1:41p		TIME0365.ACQ	1334 10-03-94	1:58p
TIME0014.ACQ	1334 10-03-94	1:41p		TIME0366.ACQ	1334 10-03-94	1:58p
TIME0015.ACQ	1334 10-03-94	1:41p		TIME0367.ACQ	1334 10-03-94	1:59p
TIME0016.ACQ	1334 10-03-94	1:41p		TIME0598.ACQ	1334 10-03-94	2:34p
TIME0017.ACQ	1334 10-03-94	1:41p		TIME0599.ACQ	1334 10-03-94	2:35p
TIME0018.ACQ	1334 10-03-94	1:41p		TIME0600.ACQ	1334 10-03-94	2:35p
TIME0019.ACQ	1334 10-03-94	1:41p		TIME0601.ACQ	1334 10-03-94	2:35p
TIME0020.ACQ	1334 10-03-94	1:41p		TIME0602.ACQ	1334 10-03-94	2:35p
TIME0021.ACQ	1334 10-03-94	1:41p		TIME0603.ACQ	1334 10-03-94	2:35p
TIME0022.ACQ	1334 10-03-94	1:41p		TIME0604.ACQ	1334 10-03-94	2:36p
TIME0023.ACQ	1334 10-03-94	1:42p		TIME0605.ACQ	1334 10-03-94	2:36p
TIME0252.ACQ	1334 10-03-94	1:48p		TIME0606.ACQ	1334 10-03-94	2:36p
TIME0253.ACQ	1334 10-03-94	1:49p		TIME0607.ACQ	1334 10-03-94	2:36p
TIME0254.ACQ	1334 10-03-94	1:49p		TIME0608.ACQ	1334 10-03-94	2:36p
TIME0255.ACQ	1334 10-03-94	1:49p		TIME0609.ACQ	1334 10-03-94	2:37p
TIME0256.ACQ	1334 10-03-94	1:49p		TIME0610.ACQ	1334 10-03-94	2:37p
TIME0257.ACQ	1334 10-03-94	1:49p		TIME0611.ACQ	1334 10-03-94	2:37p
TIME0258.ACQ	1334 10-03-94	1:49p		TIME0612.ACQ	1334 10-03-94	2:37p
TIME0259.ACQ	1334 10-03-94	1:49p		TIME0613.ACQ	1334 10-03-94	2:37p
TIME0260.ACQ	1334 10-03-94	1:49p		TIME0614.ACQ	1334 10-03-94	2:38p
TIME0261.ACQ	1334 10-03-94	1:49p				

refreshing the screen when the next data set is collected. The time necessary to perform these steps increases in direct proportion to the number of points being displayed in the graphics routine. While it is often desirable to monitor the data as it being collected, it is a step which must be eliminated when maximizing the rate at which spectra are collected.

It becomes apparent that program overhead has many items which may be eliminated easily, but the price for eliminating these items is steep indeed. It is possible to minimize the number of times that you perform the monitoring procedures, but they cannot be eliminated. They are simply the price that must be paid to collect data. A realistic determination of what is important to monitor must be made before finalizing the data collection routines.

Data related limitations.

The data related limitations are both the easiest and most difficult limitation to deal with. The limitations are the necessity to store the data, and the nature of the data itself. The researcher has total control over each of these limitations. He may decide that a particular set of data, or portion of a GC run, contains no useful information, and thus doesn't need to be saved. He must accept the fact, however, that he may be wrong and may lose some important data. This loss of data is dependent upon the researcher's knowledge and experience. It is possible that a researcher only wishes to perform a cursory scan of the data; to get an idea of what information is available from the sample. It is quite possible, even probable, that there is no necessity to store the data; the result being that speed of the data collection is increased.

The researcher also has control over the nature of the data. This does not mean that one has control over the IMS spectrum, just what information is germane. There may be only a window of data that is of importance to collect and save. In the GC-IMS, it may be a window of GC retention times, a window of IMS drift time, or both. This is dependent upon the nature of the information that the researcher is attempting to obtain. There is other data which may be important to the researcher as well. A determination of what additional information is important, whether or not to collect the information, and how often to collect the information must be made. Information of this type includes the date and time the data is collected, the GC retention time, the temperature of the locale where the data is collected, the temperature of the GC inlet, the temperature of the GC column, and the temperature and pressure of the IMS cell.

RESULTS

After taking all of these limitations into account, we have developed a software package which is capable of collecting up to 20 spectra per second, or 83 percent of the spectra which are produced by the GC-IMS. Along with the spectra, we monitor and collect the information contained in Table VI.

To achieve the 20 spectra per second rate, it was necessary do eliminate the graphics procedures. Using graphics displays to view data while it is being collected, reduces the rate at which data can be collected to 7 spectra per second. The elimination of the graphics does not prohibit viewing of the data; it only delays the viewing until after all the data has been collected. A typical spectrum obtained using this new data collection routine is shown in Figure 4. The spectra in Figure 4 are plotted in contour format to ease in the visualization of the data.

CONCLUSIONS

At first glance, collecting data from a GC-IMS appears to be a simple task; turn on the computer and the GC-IMS, then take data. It is possible to collect the GC-IMS data at 33 spectra per second, or at least the 24 spectra per second that the GC-IMS produces, but important information is lost and other information is hidden. Information that is hidden is the elapsed time since the AVS sampled the environment. This information is hidden only if there was one sampling pulse at the beginning of the data collection, otherwise it is lost. Information that is lost are cell temperature, cell pressure, AVS temperature, and GC temperature. Thus, the simplistic approach to data collection must be abandoned in the face of reality. There are limitations to be addressed at every turn: limitations related to hardware, software, and data. Choices must be made as to what information is to be retained, and is superfluous to the data. The more aware a researcher is of the limitations, the better job he can do on collecting the data.

TABLE VI
PARAMETERS COLLECTED WITH A GC-IMS SYSTEM, AND THE FREQUENCY WITH WHICH THEY ARE COLLECTED

Parameters collected only at the beginning of the GC-IMS data collection.

IMS Mode	- Positive or negative ions
Comment	- Information about the sample, column type, etc.
Filename	- Name under which the data is stored
Length of filename	- used to control how data is written to the datafile
Length of comment	- used to control how data is written to the datafile
RATE	- The rate at which data points in a spectrum will be collected
NOSAMP	- Number of points in each spectrum collected

Parameters collected or monitored with each spectrum

Count	- How many spectra have been collected
TEMPAVS	- Temperature of the AVS Inlet
TEMPCOL	- Temperature of the GC Column
TEMPCELL	- Temperature of the IMS Cell
PRESSCELL	- Pressure inside the IMS Cell
DURATION	- GC Retention Time
PULSE	- Is the AVS actively Sampling?
DISKFULL	- Is the Disk full ?

REFERENCES

1. Snyder, A.P., Harden, C.S., Brittain, A.H., Kim, M.-G., Arnold, N.S., and Meuzelaar, H.L.C. Portable Hand-Held Gas Chromatography/Ion Mobility Spectrometry Device. *Anal. Chem*, **65**, 299-306 (1993).

2. Dworzanski, J.P., Kim, M.-G., Snyder, A.P., Arnold, N.S., and Meuzelaar, H.L.C. Performance advances in ion mobility spectrometry through combination with high speed vapor sampling, preconcentration and sepaeation techniques. *Anal. Chim. Acta*, **293**, 219-235 (1994).

3. Mueller, S. and Elliot, A.C. Que's Guide to Data Recovery, Que, Carmel, IN, 1991, pp 76-84.

269
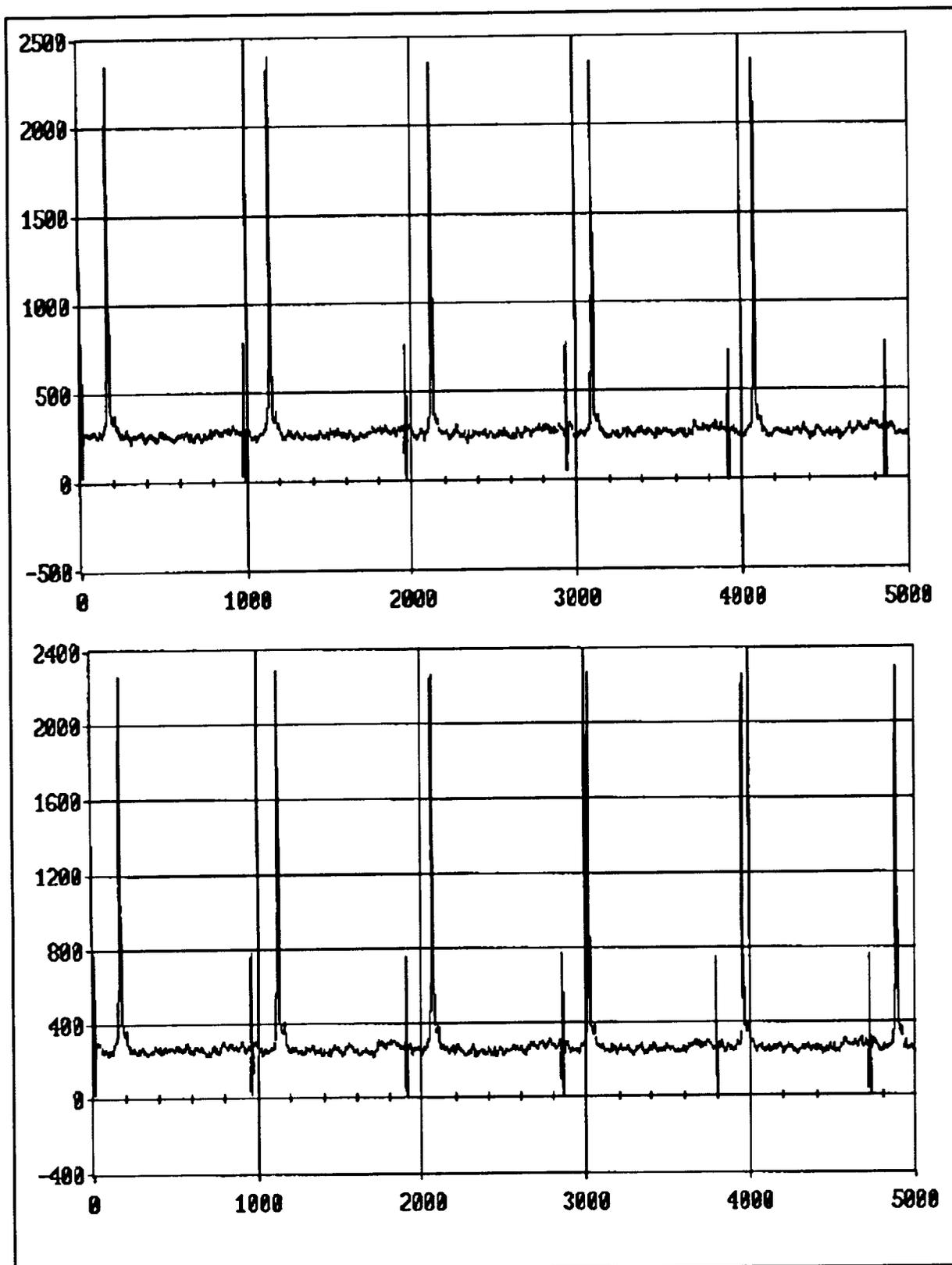
Figure 1. Two series of IMS spectra showing the inconsistency in the gating pulse rate.

270
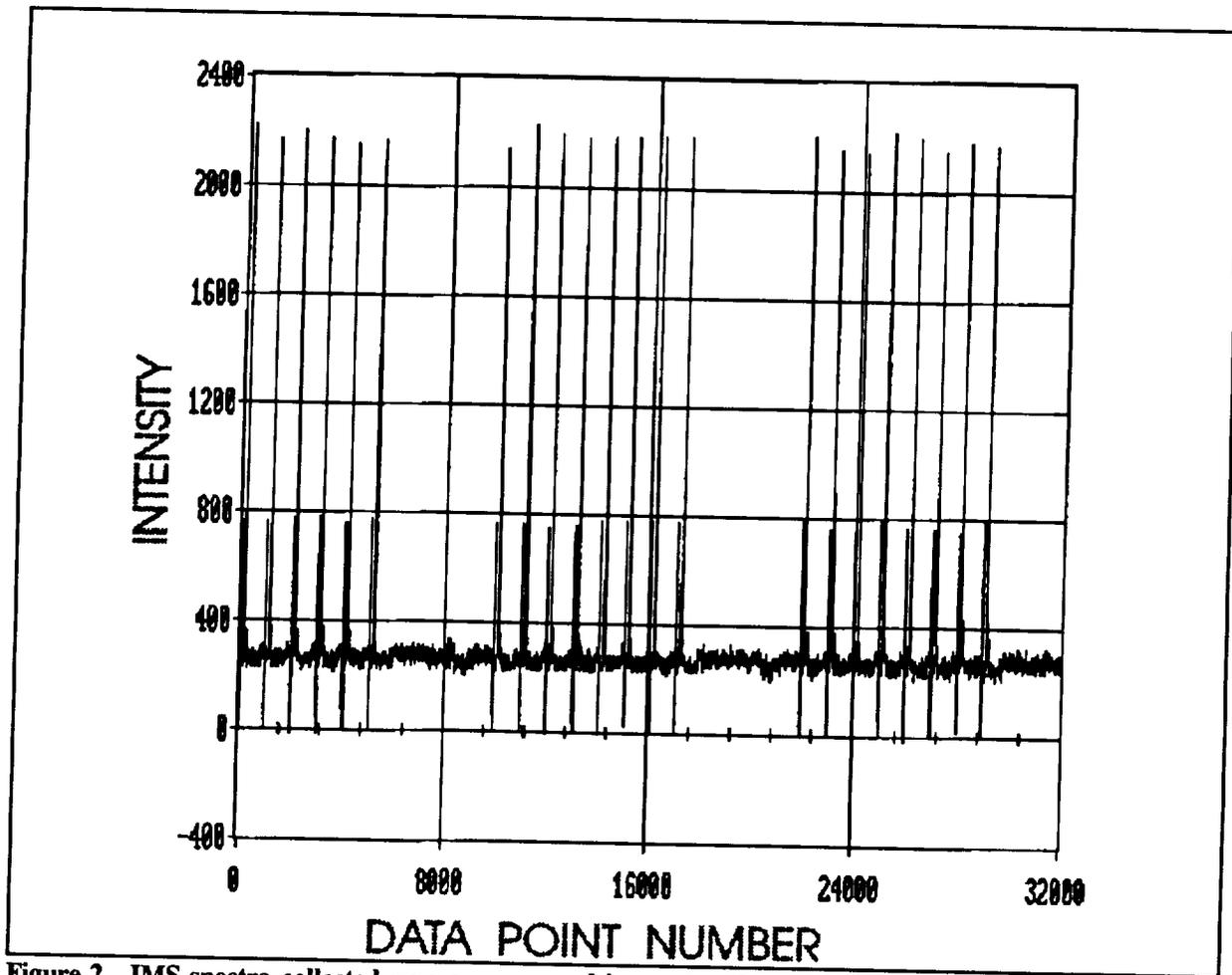
Figure 2. IMS spectra collected over a one second interval. Thirty thousand data points were collected at a data rate of 30,000 Hz.
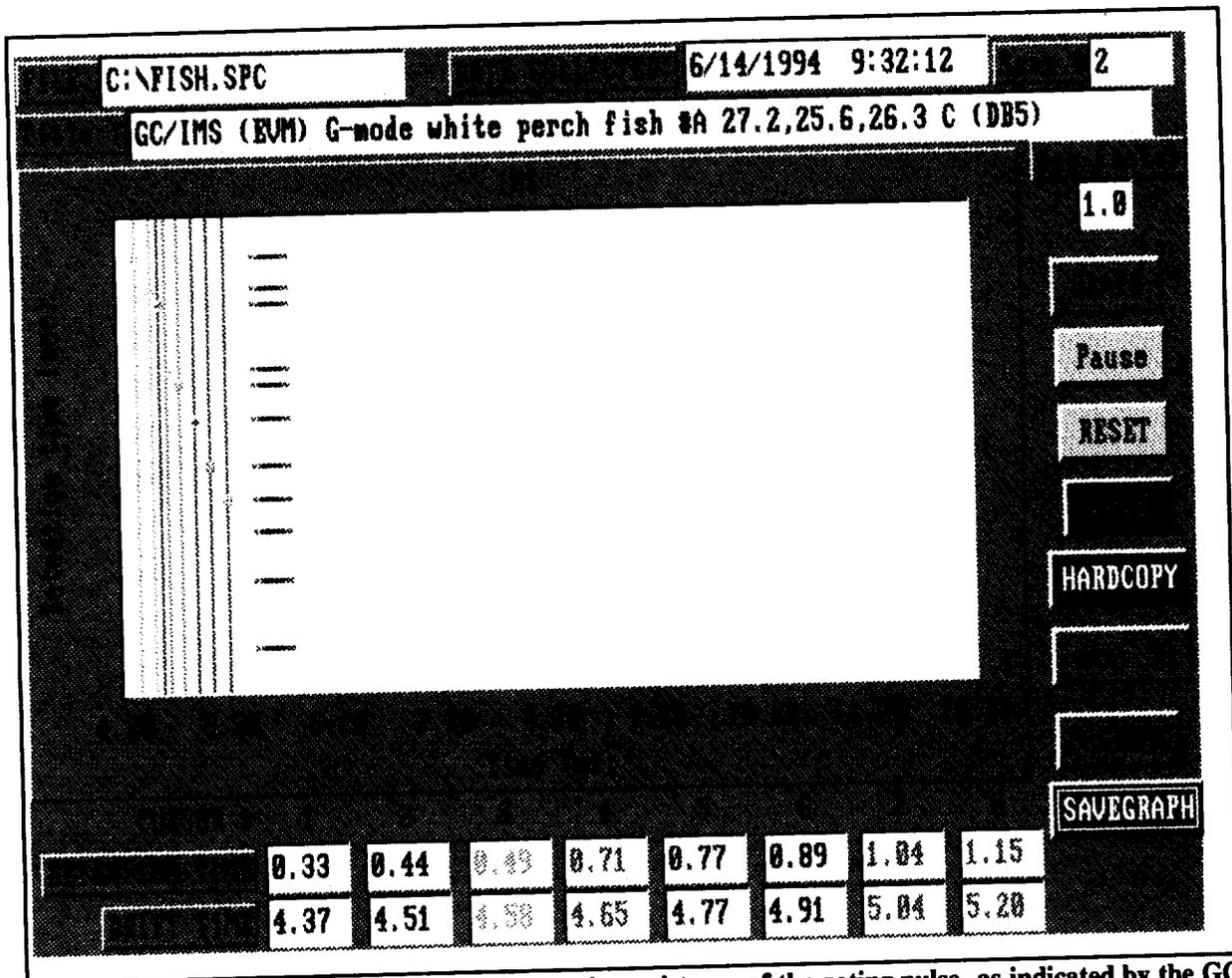
Figure 3. GC-IMS contour spectra showing the inconsistency of the gating pulse, as indicated by the GC retention times of each spectrum.

C-4.
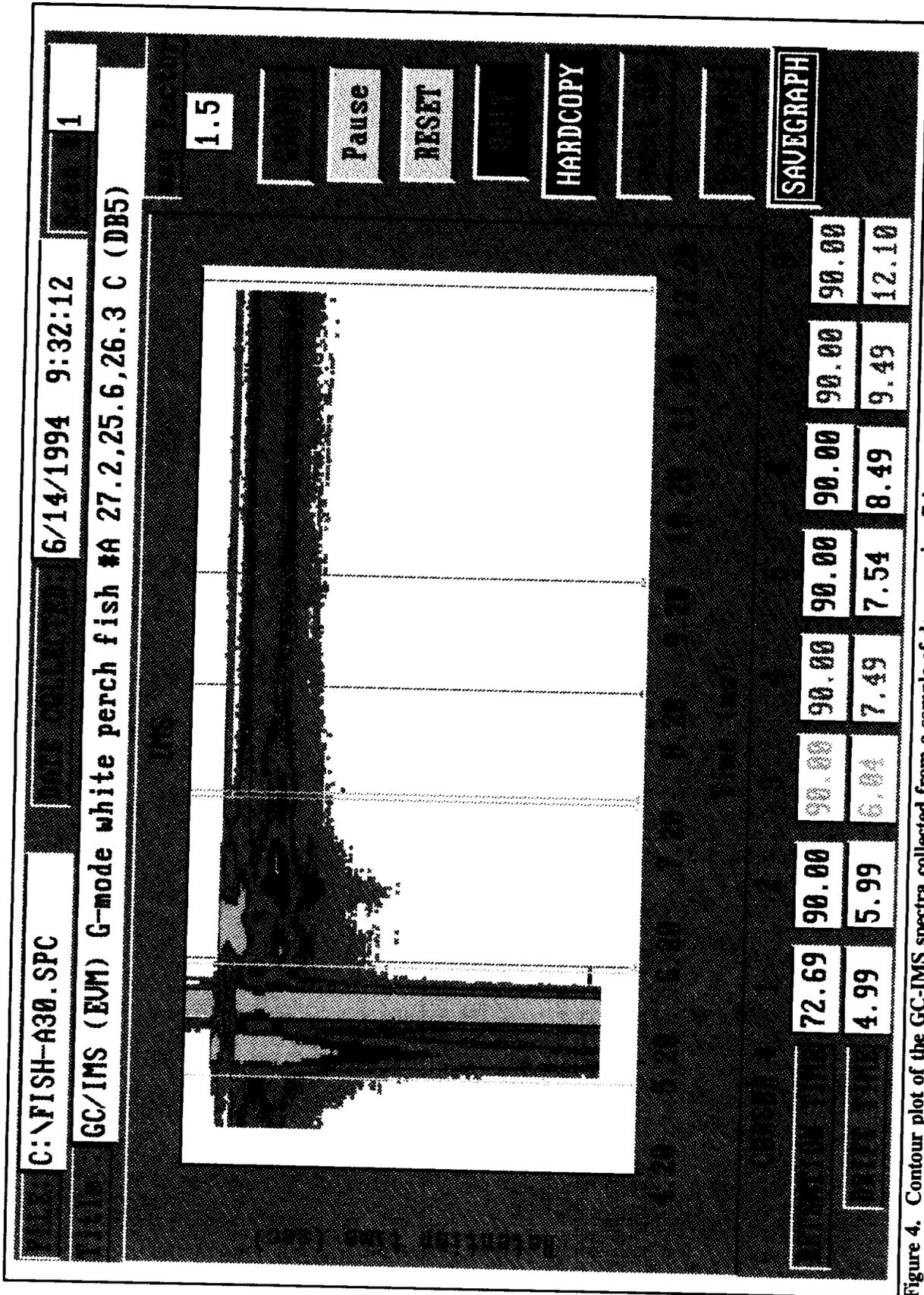
Figure 4. Contour plot of the GC-IMS spectra collected from a sample of decomposing fish.

IMS SOFTWARE DEVELOPMENTS FOR THE DETECTION OF CHEMICAL WARFARE AGENT

St. Klepel, U. Gräfenhain, R. Lippe, J. Stach and V. Starrock*)

Bruker-Saxonia Analytik GmbH, Permoserstr. 15, 04318 Leipzig, F.R.G.

*)Federal Armed Forces NBC Establishment, P.O. Box 1142, 296233 Munster, F.R.G.

Interference compounds like gasoline, diesel, burning wood or fuel etc. are present in common battlefield situations. These compounds can cause detectors to respond as a false positive or interfere with the detector's ability to respond to target compounds such as chemical warfare agents. To ensure proper response of the ion mobility spectrometer to chemical warfare agents, two special software packages were developed and incorporated into the Bruker RAID-1. The programs suppress interfering signals caused by car exhaust or smoke gases resulting from burning materials and correct the influence of variable sample gas humidity which is important for detection and quantification of blister agents like mustard gas or lewisite.

1. SUPPRESSION OF INTERFERENCE GASES

Many interference gases can be found in battle field scenarios. Typical compounds are nitrogen oxides, sulfur dioxide, chlorine, ammonia, formaldehyde or carbonmonoxide and carbondioxide. Others like gasoline, diesel or smoke gases from burning materials consist of many organic compounds. The latter cause "broad band" ion mobility spectra without any structure in most cases. Fig 1 shows a typical series of ion mobility spectra of burning fuel and wood.

In case of the above described spectra it is likely that standard ion mobility spectra analysis will come up with typical CWA peaks hidden somewhere under the broadband smoke ion mobility spectrum. Fig. 2 shows an evaluated spectrum of wood and fuel smoke gases recorded in the positive ion mode. After deconvolution, all nerve agents stored in the library are identified. This means a false positive alarm is given by the device if it is used in the stand alone mode.

274
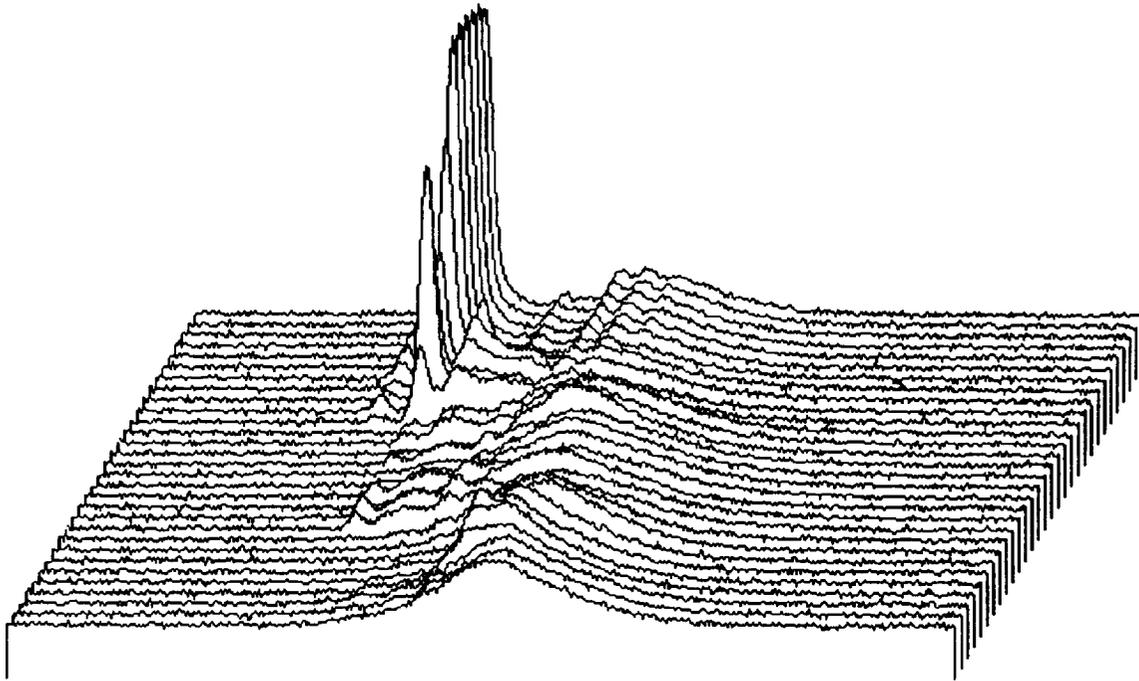
Fig. 1: Series of ion mobility spectra of positive ions obtained from smoke gases from burning wood and fuel
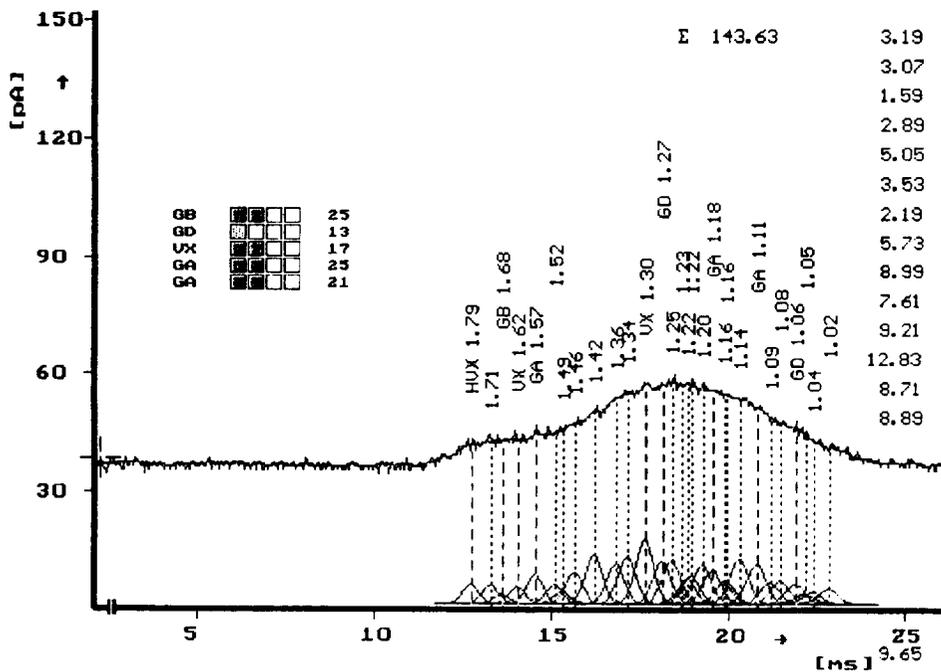
Fig. 2: Evaluated spectrum of smoke from burning wood and fuel: The nerve agents GA, GB, GD and VX were identified.

275

If vapours of nerve agents are added to smoke gases, the resulting ion mobility spectra show beside a broad peak discrete signals due to the formation of monomer and dimer ions of the phosphor organic compound. This means that substances with a high proton affinity are ionized by means of APCI processes also in presence of high amounts of smoke gases. A corresponding spectrum is shown in Fig. 3.
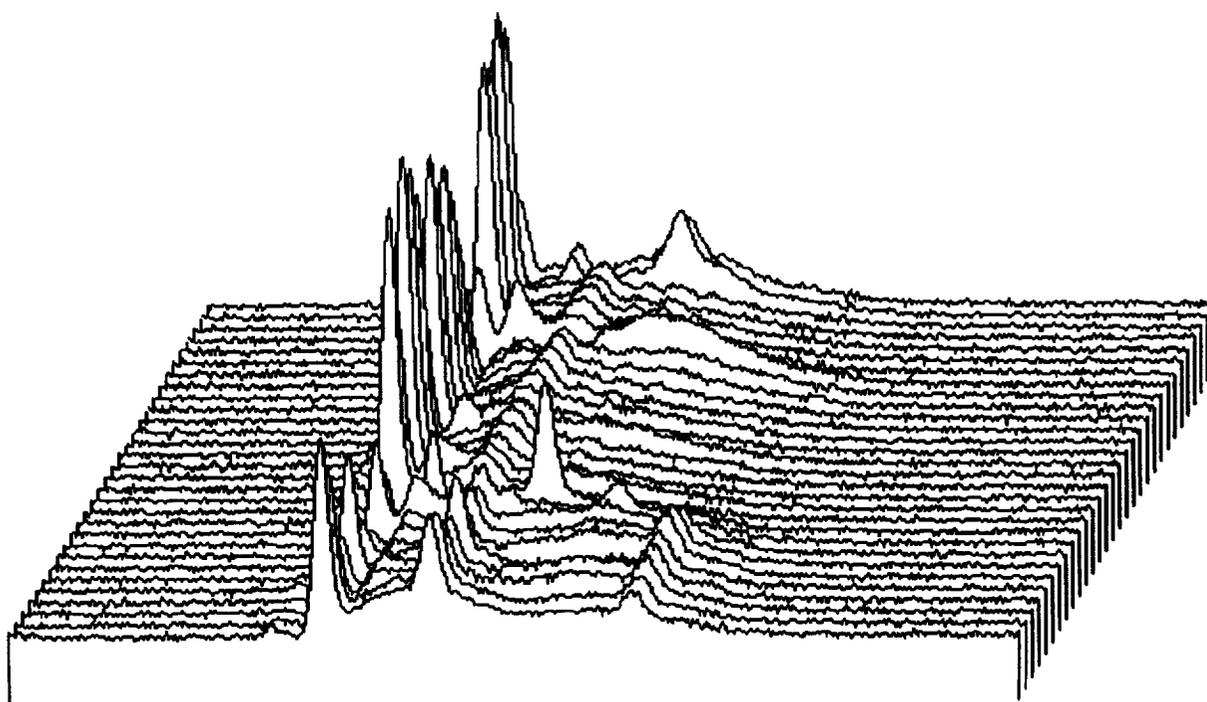
Fig. 3: Series of ion mobility spectra (positive ions) of smoke gases from burning fuel and isopropyldimethylphosphonate (IDMP)

These findings give the possibility to suppress broad signals caused by interfering substances. A special software package called "Partial Spectra Analysis" (PSA) uses base line correction and peak identification algorithms for the evaluation of ion mobility spectra. As shown in Fig. 4, the broad peak of the smoke gases is completely suppressed and the signals of the IDMP are identified by comparison with the data stored in the library.
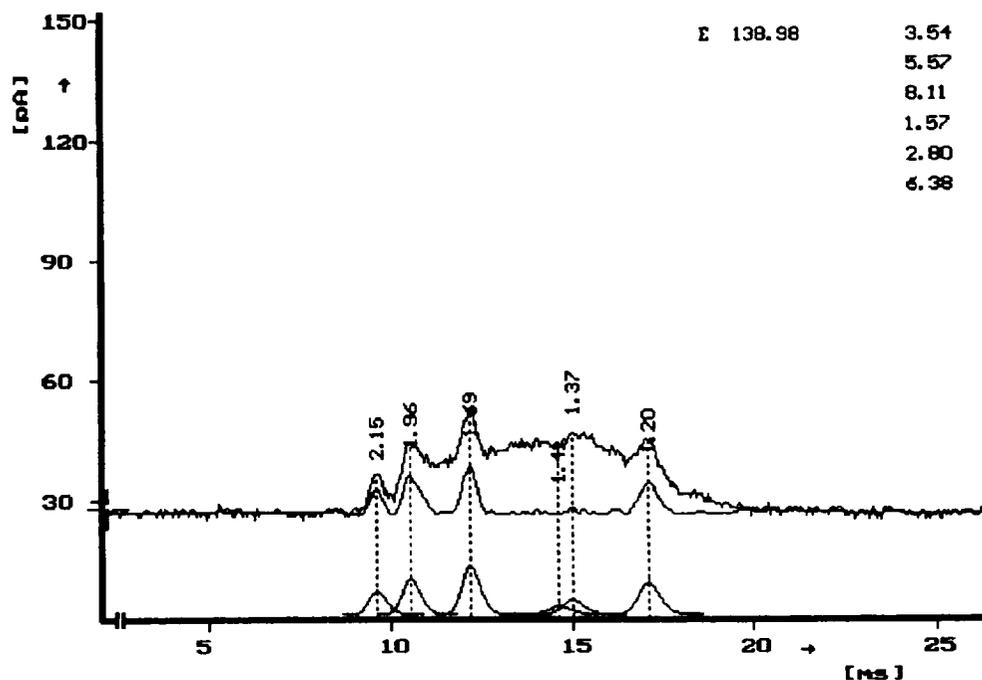
.Fig. 4: Evaluation of an ion mobility spectrum (positive Ions) of a sample of smoke gases and IDMP

2. INFLUENCE OF HUMIDITY ON ION MOBILITY SPECTRA OF CHEMICAL WARFARE AGENTS

The ion mobility spectra of chemical warfare agents especially blister agents like sulfur mustard (HD) depend strongly on the relative humidity of the ambient air. Fig. 5 shows a series of ion mobility spectra of sulfur mustard recorded with different humidity of the sample gas. Beside the mustard gas signal, $(HD)O_2^-$, peaks caused by Cl^-, $(H_2O)_2Cl^-$ and reactant ions are shown in Fig. 5. Another weak signal can be assigned to thiodiclycol a hydrolysis product of sulfur mustard. The identification of sulfur mustard in the RAID-1 is based on the $(HD)O_2^-$ and the Cl^- peak [2]. The formation of chloride ions or chloride water clusters is well known for chlorinated organic compounds [1]. In the case of mustard gas, this dissociative charge transfer reaction depends on the humidity of the sample gas. With increasing relative humidity the intensity of the $(HD)O_2^-$ signal decreases and the intensity of the chloride signal increases. Fig. 6 shows a three-dimensional plot the signal intensities with varying concentration and humidity.

277
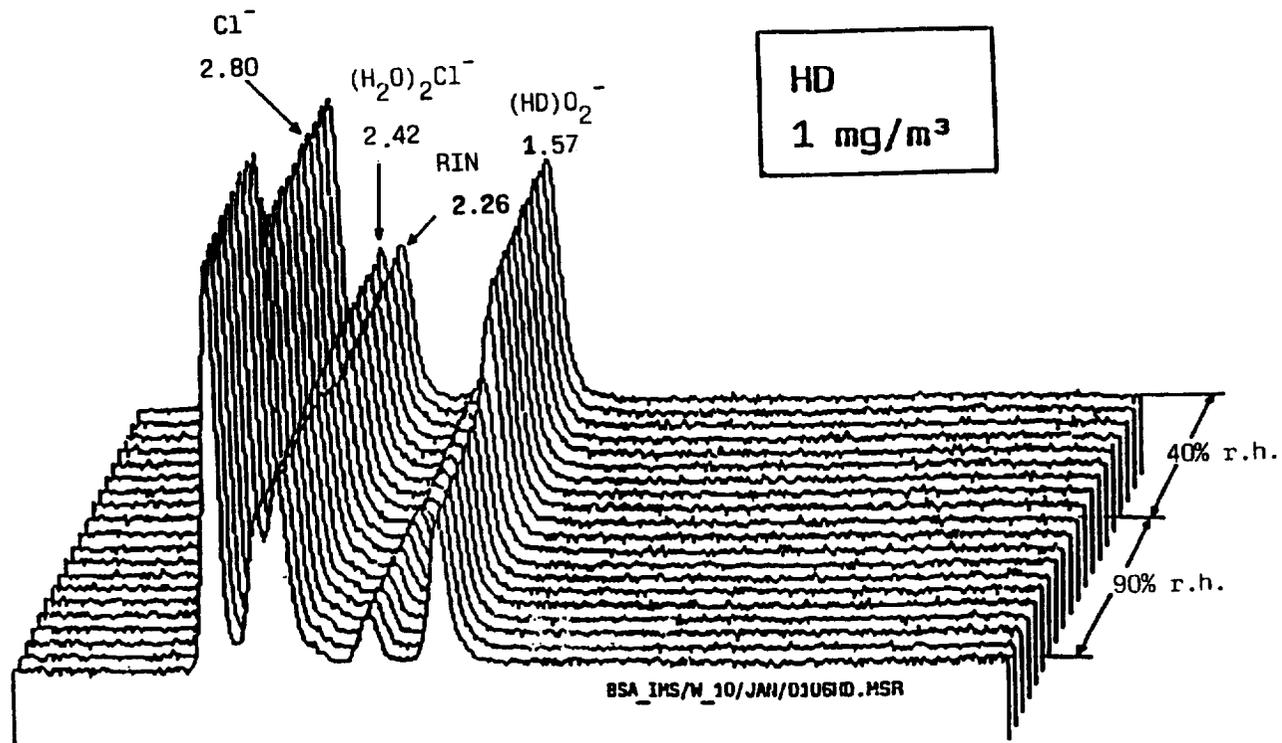
Fig. 5: Series of ion mobility spectra of sulfur mustard recorded at different humidities
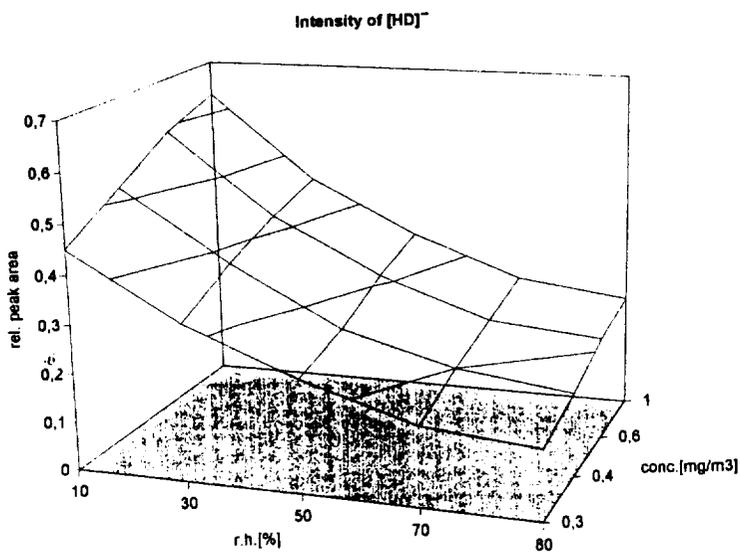
Fig 6. Dependence of the HD signal intensity on humidity and concentration.

The strong dependence of the HD signal on humidity causes strong deviations in the estimated concentrations if a calibration curve, recorded, e.g., for a medium humidity, is used for quantification. However, the reaction kinetics of the observed hydrolyses reactions of suflur mustard can be described regarding the reaction region of the ion mobility spectrometer as a "tube" reactor. On the basis of this model concentrations of HD can be calculated using the HD and the Cl⁻ peak areas. The result is shown by means of calibration curves for HD calculated without and with hydrolysis correction (see Fig. 7). Interferences of other chlorinated compounds which also form Cl⁻ ions in the ion mobility spectrometer are considered by this model.
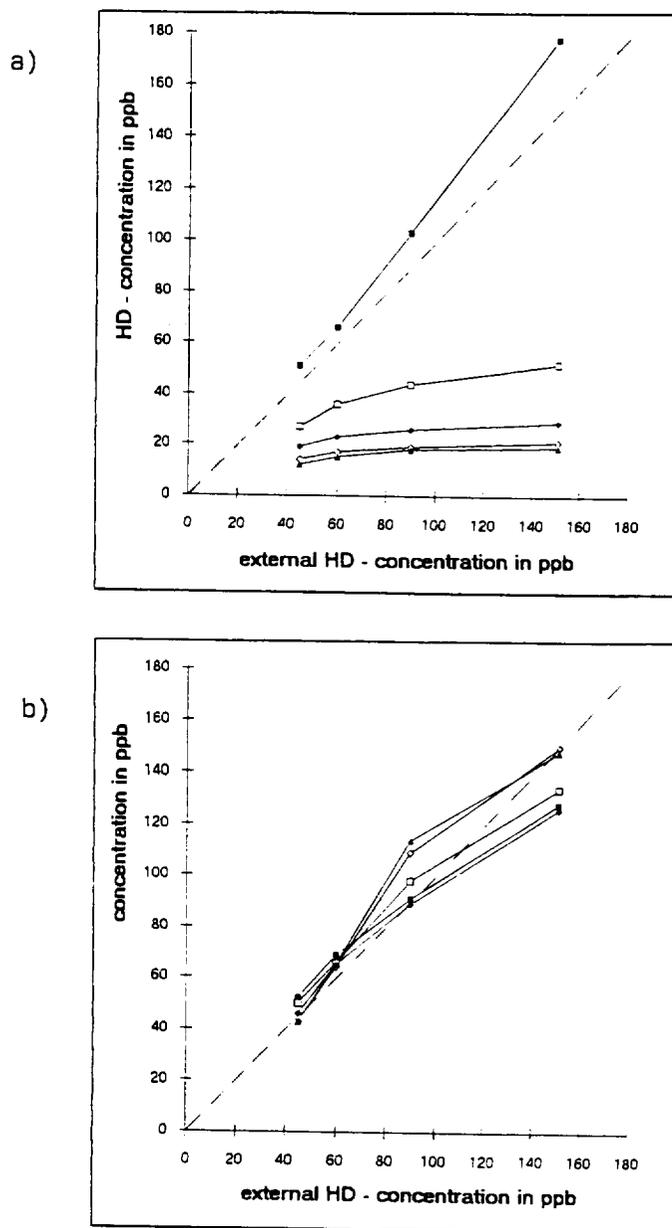
Fig. 7: Calibration curves for HD obtained for humidities of 10(•), 30(□), 50(♦), 70(◊) and 80 % (▲). Fig 7b shows the calibration curves calculated taking into account the hydrolysis of HD

279

3. LITERATURE

[1]   Miller, D.A. and Grimsrud, E.P.,   Anal. Chem. 51 (1979) 851.

[2]   Starrock, V., Krippendorf, A. and Döring, H.-R. Second International Workshop on Ion Mobility Spectrometry, Quebec City, Canada, 15.-18.8.1993.

A DIGITAL "BOXCAR INTEGRATOR" FOR IMS SPECTRA

Martin J. Cohen, Robert M. Stimac, and Roger F. Wernlund
PCP, inc., 2155 Indian Road, West Palm Beach, FL 33409
Donald C. Parker
Keystone Applications, 4791 Country Meadows Road, Brooklyn, WI 53521

When trying to detect or quantify a signal at or near the limit of detectability, it is invariably embeded in the noise. This statement is true for nearly all detectors of any physical phenomena and the limit of detectability, hopefully, occurs at very low signal-to-noise levels. This is particularly true of IMS (Ion Mobility Spectrometer) spectra due to the low vapor pressure of several chemical compounds of great interest and the small currents associated with the ionic detection process.

Gated Integrators and Boxcar Integrators or Averagers are designed to recover fast, repetitive analog signals. In a typical application, a time "Gate" or "Window" is generated, characterized by a set delay from a trigger or gate pulse and a certain width. A Gated Integrator amplifies and integrates the signal that is present during the time the gate is open, ignoring noise and interference that may be present at other times. Boxcar Integration refers to the practice of averaging the output of the Gated Integrator over many sweeps of the detector. Since any signal present during the gate will add linearly, while noise will add in a "random walk" fashion as the square root of the number of sweeps, averaging N sweeps will improve the "Signal-to-Noise Ratio" by a factor of the square root of N.

Many detection algorithms are in use today in various instruments. The simplest ones quantitize the signal from the IMS cell and then respond to the amplitude of a single largest data point within a fixed "window" or group of data points following each trigger pulse. Fundamentally, all detection algorithms, simple or sophisticated, are band pass filters designed to provide some attenuation to the noise frequencies involved with little attenuation at the signal frequencies involved. Improvement of the Signal-to-Noise Ratio will lower the minimum quantity or concentration of chemical vapors that can be detected. Multiple filtering occurs because there are several frequency bands involved in real world measurements.

The first filter section is inherent in the frequency response of the electrometer detector and any analog signal amplification prior to digitizing the ion spectrum. This is usually a low pass filter with a corner frequency of several kilohertz. The spectrum is then digitized. Figure #1 shows the typical single sweep background noise in the region where detected chemicals may appear. Figure #2 shows an idealized chemical signal ion peak. It would be superimposed on the noise signal. At the limit of detectability, it may be smaller in amplitude than the noise signal. Furthermore, if it is a real chemical signal, it will grow slowly for tens of sweeps, hold for a few more, and finally decay, frequently at a slower rate which yields a tail. This provides several opportunities to further filter the signal using different criteria. How wide (milliseconds or number of channels) is a typical ion peak in a spectrum? How long (seconds or number of sweeps) is the chemical present in the detector?

Our new computer program, KEY3, differs from earlier digital programs in several important respects. Indeed, it emulates the best features of the older analog Boxcar Integrator technology, in what we believe are novel ways.

If the operator preselects the chemical detection windows (up to 10) and background windows (up to 2) the program operates upon raw data from each and every sweep. This data may be stored on disk independently of the full spectrum storage. Thus the chemical detection or quantitation is separated from full spectrum averaging and storage criteria allowing independent parameter adjustments. The detection program can also be run or rerun from stored data, but for this analysis I will consider the case of real time raw data.

In Figure #3 the noise of Figure #1 and the signal of Figure #2 are added, thus showing what each sweep looks like prior to analysis. The signal window is centered over the drift time of the chosen chemical. The background windows are normally set to quiet regions of the spectrum before and after the signal window. We recommend that all window widths be set to about 110% of the IMS gate width to maximize the Signal-to-Noise Ratio of the data. The Signal Recovery Equations are shown in Figure #4. All of the data points within the windows are averaged, the two background window averages are averaged together and subtracted from the signal. This results in a single number, I_k , for each sweep, which represents the amplitude of the ion peak above background. This number is effectively the output of a band pass filter, since the background subtraction eliminates the DC response of the circuit. The upper corner frequency of the filter section is about 1 kilohertz and is tuned by the window width. The wider the window width, the lower the corner frequency of the filter. Essentially, this filter is optimized for the width of the ion signal in the IMS spectrum.

In Figure #5 we leave the drift time spectrum and consider another frequency domain, that of the chemical concentration in the IMS cell plotted against sweep number. The time axis may represent tens of seconds and hundreds of sweeps depending upon the Repetition Period of the IMS detector. The detected signal near the limit of detection is, by definition, small and hence noisy. Further smoothing is required to bring the signal out of the noise for reliable detection. Three of the smoothing functions commonly used in commercial programs are:

· Moving Average
· Weighted Moving Average
· Exponential average

In the moving average, one selects the number of data points to average and all data points have equal weight. In the weighted moving average one again selects the number of data points to average, but the most recent data point carries the most weight, since from the oldest to the newest, the weight of each point is 1, 2, 3,···, n.

Figure #6 shows the equations used for exponential averaging. Several commercial instruments use the first equation where the Time Constant is selected. Other programs use the second equation where the Damping Factor is operator selected. Both equations are equivalent where the Time Constant (T) and the Damping Factor (DF) are related as shown. We chose to implement our KEY3 program with the first equation based upon setting a time constant where $1.0 \geq T \geq 1024$. A_k is the most recent averaged output while I_k is the most recent input data point.

In Figure #7 we have shown equations for these three smoothing functions with certain parameter inputs. The number of points selected for each type of moving average and the time constant used for the exponential average were selected so that the most recent input, I_k, was 25% of the averaged output, A_k.

In Figure #8 we have evaluated these equations for certain parameter values. The weight of the seven most recent data points is given for each of the three functions. All three functions average or smooth the input data. They differ only in the relative weight that they give to the individual input data points making up the output of the circuit or function.

The response of these three functions, with the previously selected parameters, to a step input is plotted as Figure #9. It is evident that the moving average function exhibits the highest frequency response, the fastest convergence and is the poorest noise filter. The exponential average function has the poorest high frequency response, the slowest convergence and is the best noise filter of the three. Consequently, we have chosen to implement the exponential average smoothing function in our KEY3 program. The largest time constant (T) is selected that will allow nearly full response of the circuit to the chemical signal in typically 3T or 4T. The longer the signal is present, the greater the value of T that can be used.

From analog filter theory we understand that the high frequency response of the Exponential Average function rolls off at 6 db per octave above the corner frequency. We know that similar multiple filter sections roll off at 12, 18, ⋯ db per octave and, as shown in Figure #10 and that the effective time constant grows as the square root of the sum of the squares. Therefore four filter sections with T = 2 have a rise time similar to a single filter section with T = 4, but exhibit a sharper cutoff of 24 db/octave above the corner frequency. Hence multiple filter sections exhibit a greater reduction in high frequency noise for similar response to the signal frequency of the detected chemical as compared to single filter functions.

In Figure #11 we have plotted the exponential average response of four iterations with T = 4 and the response of one iteration with T = 8 to a step input. Note that the 10% to 90% Rise Time is essentially the same and that both converge within 2% after the same number of sweeps.

In Figure #12, using the same parameters, we plot these responses to an impulse. Note that the four iterations with T = 4 produce only half the output response of the single iteration with T = 8. The high frequencies inherent in the impulse driving function are more effectively filtered out with the multiple iterations.

In actual tests of an IMS explosive detector, we have demonstrated that a two stage analog "Boxcar" Exponential Signal Averager with background subtraction was able to reduce the Minimum Detectable Concentration of TNT to one half of the best values previously obtained. We would expect that the new digital KEY3 Data Acquisition and Reduction Program will do even better, since the number of iterations (filter sections) is so much greater, parameter settings are so much more flexible and the experiment can be rerun from disk memory to optimize the settings.

In summary, our new KEY3 Data Acquisition and Data Reduction Program allows signal averaging and storage of IMS spectra in the conventional manner. It also allows real time integration of selected drift time peaks within windows, with or without background substraction. For best quantitation or alarm results at low chemical concentrations, the window width for each chemical/background should be set to about 110% of the gate width. Thereafter, the integrated

"signal" can be processed by an exponential signal averaging function having a time constant of 25 to 35% of the rise time of the detected chemical. The best reliability of quantitation or alarm will occur if multiple recursions are made using a per iteration time constant that is the desired time constant divided by the square root of the number of recursions.

The specifications of our Peak Alarm/Monitor (PAM) follow.

KEY3 PROGRAM

PEAK ALARM/MONITOR (PAM) SPECIFICATIONS

- Number of Active Windows: 0 to 12

    · 0 to 10 Signal Windows

        · All with Digital Output Alarm Lines

        · Two with 0 to 10 volt, 11 bit Analog Output Lines

    · 0 to 2 Background Windows

- Window Width (PAM width): $1 \geq W \geq 55$ Dwell Channels
                                                    (odd integers only)

- Exponential Divisor (Time Constant): $1.0 \geq T \geq 1024$

- Recursion (Number of Filter Sections): $1 \geq R \geq 1024$
                                                    (integers only)

284
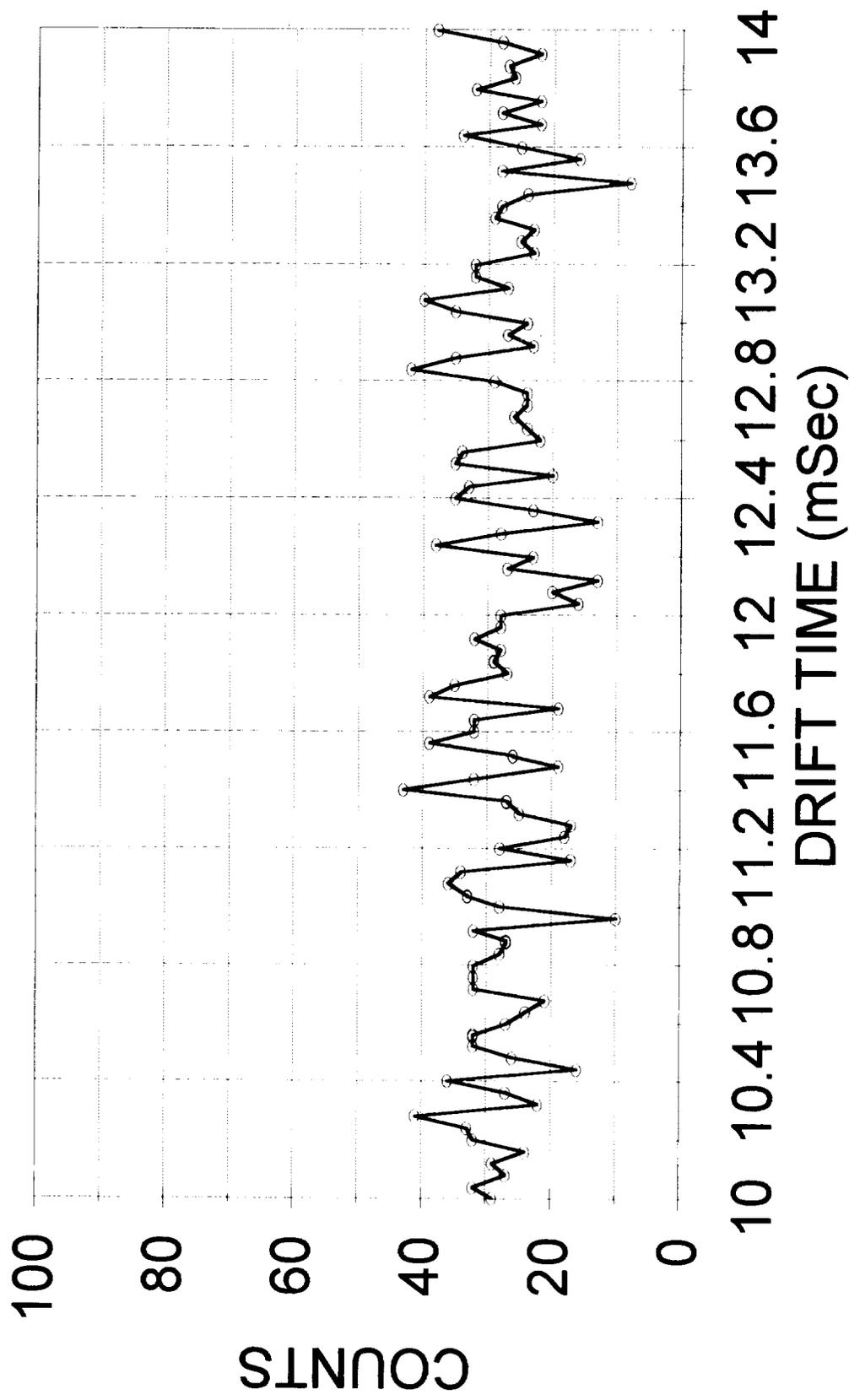
ONE SWEEP

TYPICAL NOISE

FIGURE No. 1

ONE SWEEP

TYPICAL SIGNAL
with windows
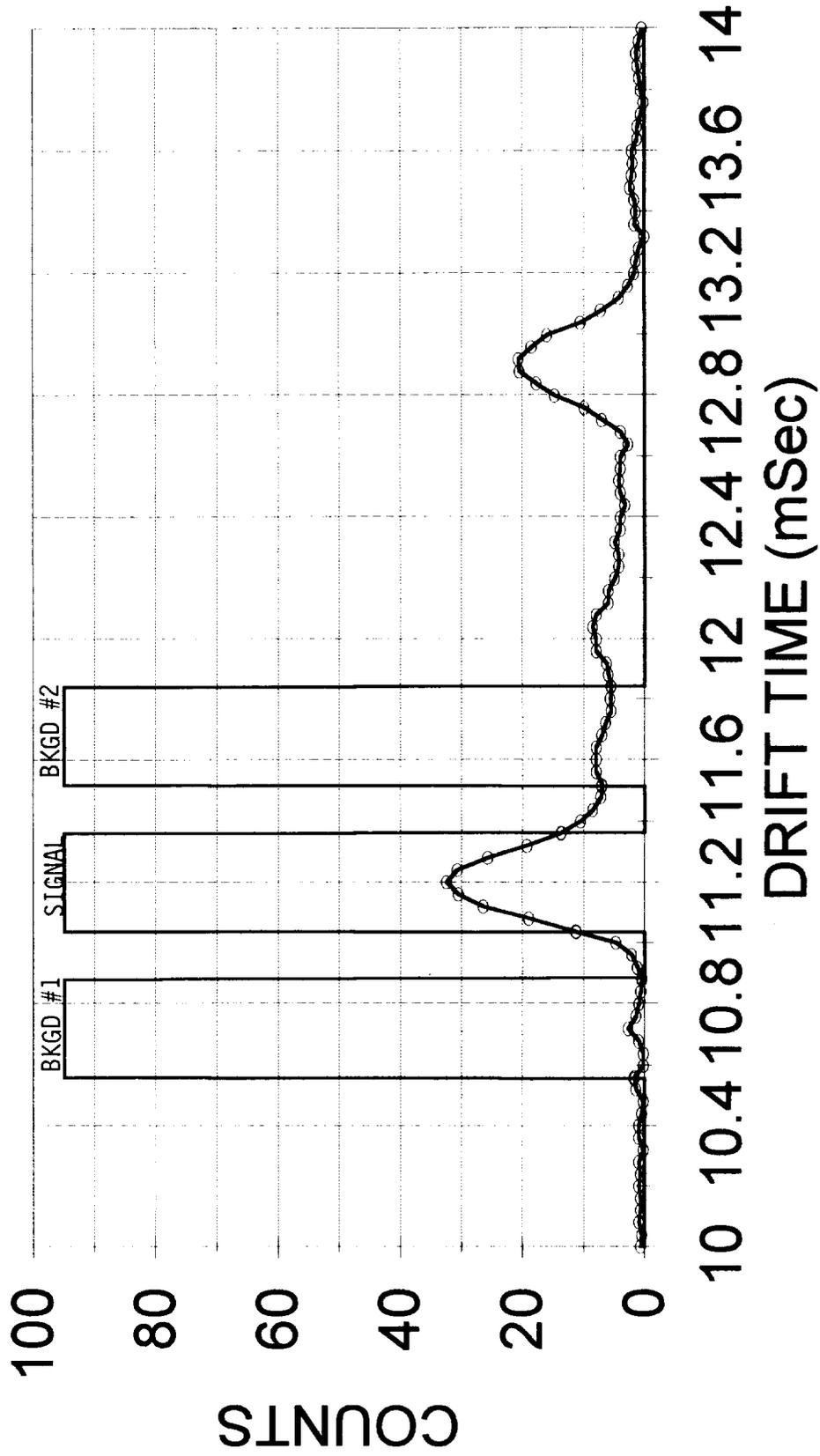
FIGURE No. 2

TYPICAL NOISY SIGNAL
with windows
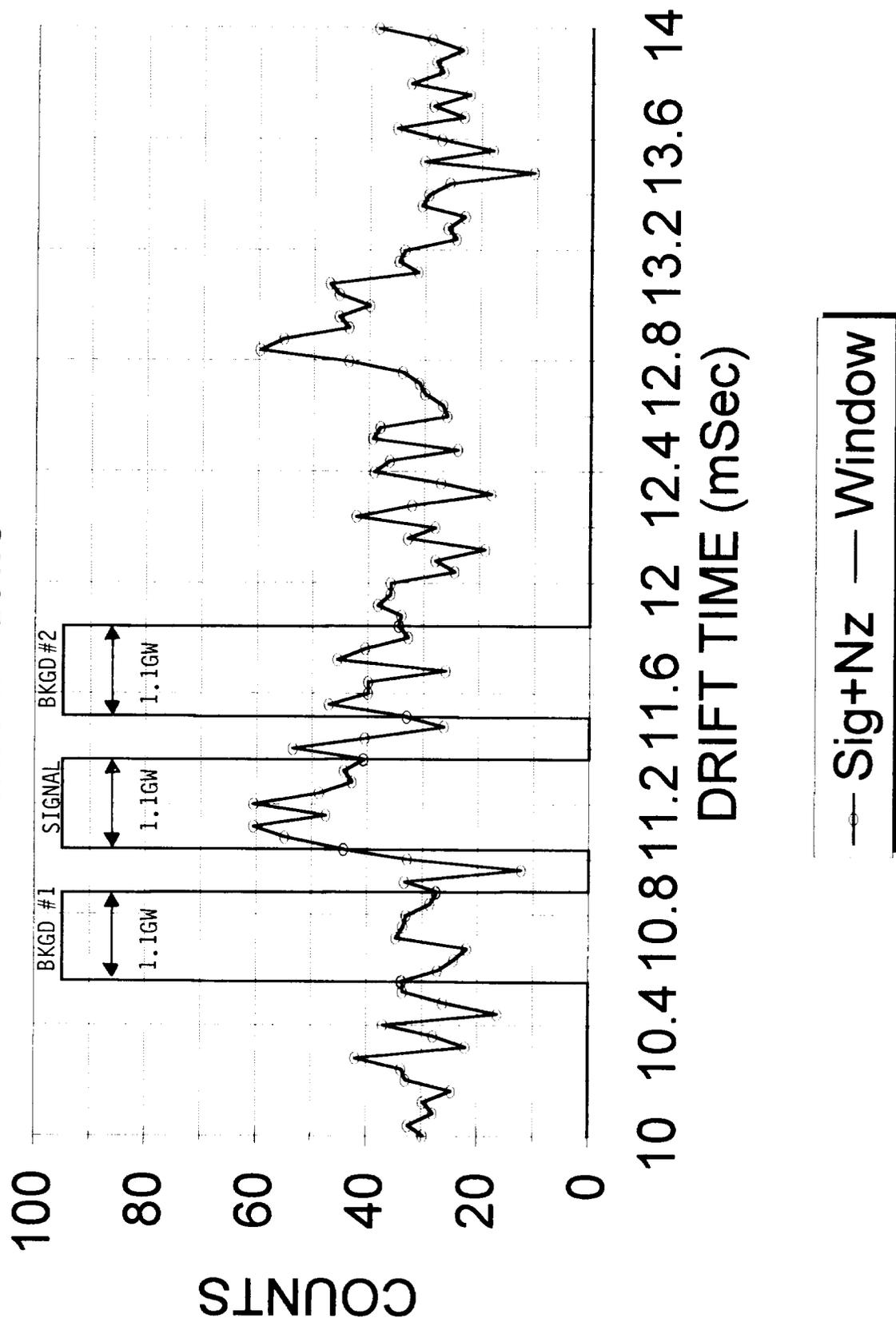
FIGURE No. 3

SIGNAL RECOVERY FROM IMS SPECTRUM

· Window Width = odd No. of channels - Centered on Ion Peak

· Best S/N: WW = 1.1 * GW

· Within Window: Avg = $[Y_1 + Y_2 + Y_3 + \cdots Y_n]/n$

· Three Averages: Signal, Background 1, Background 2

· Calculate after each Sweep:

    I_k = Signal - $[(Bkgd\ 1 + Bkgd\ 2)/2]$

· I_k is Avg Signal above Avg Baseline, new each sweep

FIGURE No. 4

SIGNAL-BACKGROUND

SMOOTHING FUNCTIONS
1.Mv Avg 2.Wt Mv Avg 3.Exp Avg
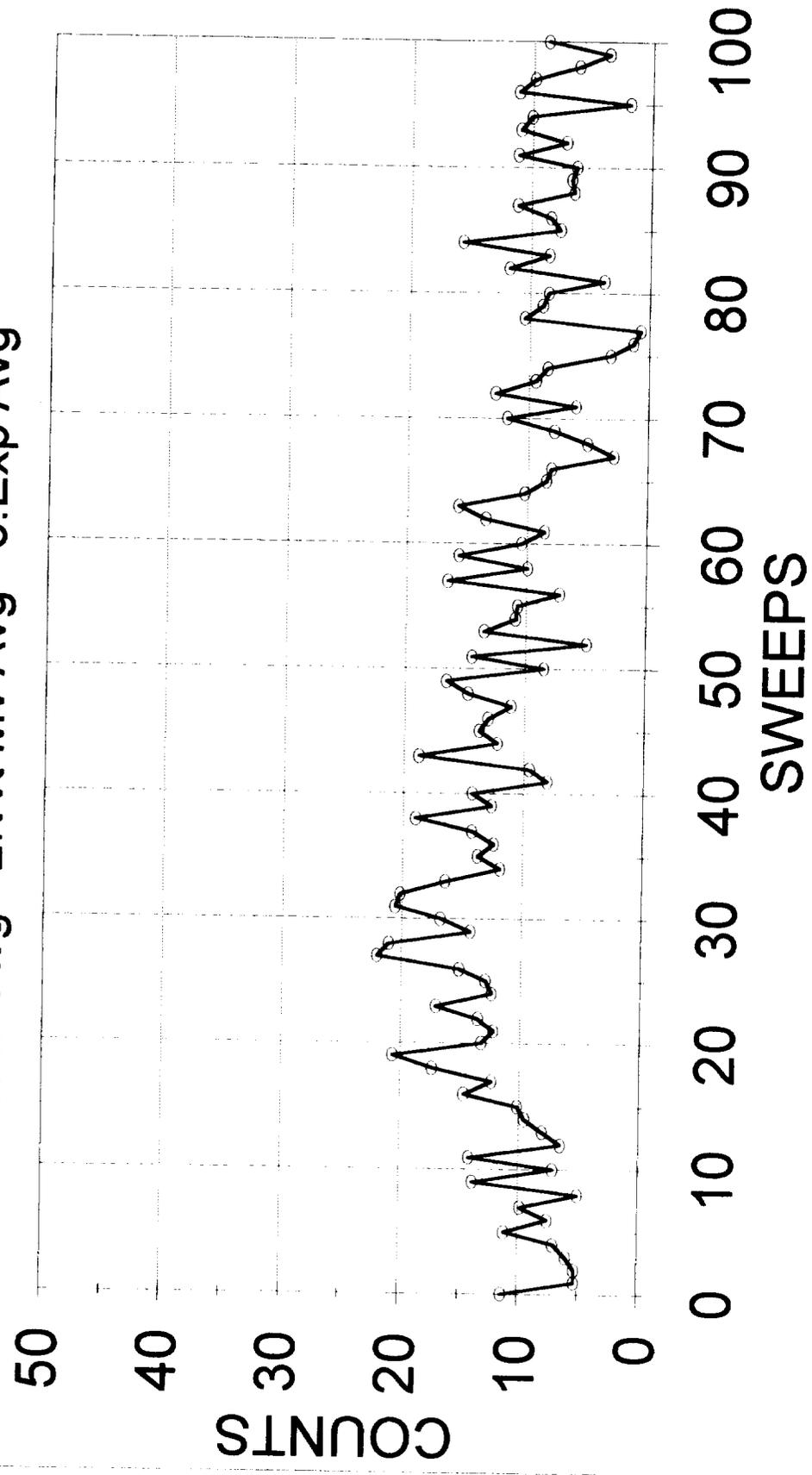
FIGURE No. 5

EXPONENTIAL AVERAGING (SMOOTHING) EQUATIONS

$$A_k = A_{k-1} + [(I_k - A_{k-1})/T]$$ where T = Time Constant (No. of Sweeps)

$$A_k = [(DF) * A_{k-1}] + [(1-DF) * I_k]$$ where DF = Damping Factor

$$DF = (T - 1)/T$$

$$T = 1/(1 - DF)$$

For KEY3 Program $1.0 \leq T \leq 1024$

FIGURE No. 6

290

GENERAL AVERAGING (SMOOTHING) EQUATIONS

1) Moving Average of 4 Points:

$$A_k = [I_k + I_{k-1} + I_{k-2} + I_{k-3}]/4$$

2) Weighted Moving Average of 7 Points:

$$A_k = [7I_k + 6I_{k-1} + 5I_{k-2} + 4I_{k-3} + 3I_{k-4} + 2I_{k-5} + I_{k-6}]/28$$

3) Exponential Averaging with T = 4, DF = 75%:

$$A_k = [I_k + (3/4)I_{k-1} + (9/16)I_{k-2} + (27/64)I_{k-3} + (81/256)I_{k-4}$$
$$+ (243/1024)I_{k-5} + (729/4096)I_{k-6} + \cdots]/4$$

FIGURE No. 7

GENERAL AVERAGING EQUATIONS TABLE

	I_k	I_{k-1}	I_{k-2}	I_{k-3}	I_{k-4}	I_{k-5}	I_{k-6}	Bal.	No. Sweeps to Converge
1) MOVING AVERAGE (Pt = 4)	.250	.250	.250	.250	-	-	-	.000	4
2) WEIGHTED MOVING AVERAGE (Pt = 7)	.250	.214	.179	.143	.107	.071	.036	.000	7
3) EXPONENTIAL AVERAGE (T = 4)	.250	.188	.141	.105	.079	.059	.044	.134	26
SUM 1: MOVING AVERAGE	.250	.500	.750	1.000	1.000	1.000	1.000	1.000	
SUM 2: WEIGHTED MOVING AVERAGE	.250	.464	.643	.786	.893	.964	1.000	1.000	
SUM 3: EXPONENTIAL AVERAGE	.250	.438	.579	.684	.763	.822	.866	1.000	

FIGURE No. 8

292

THREE AVERAGING (SMOOTHING) FUNCTIONS

STEP RESPONSE
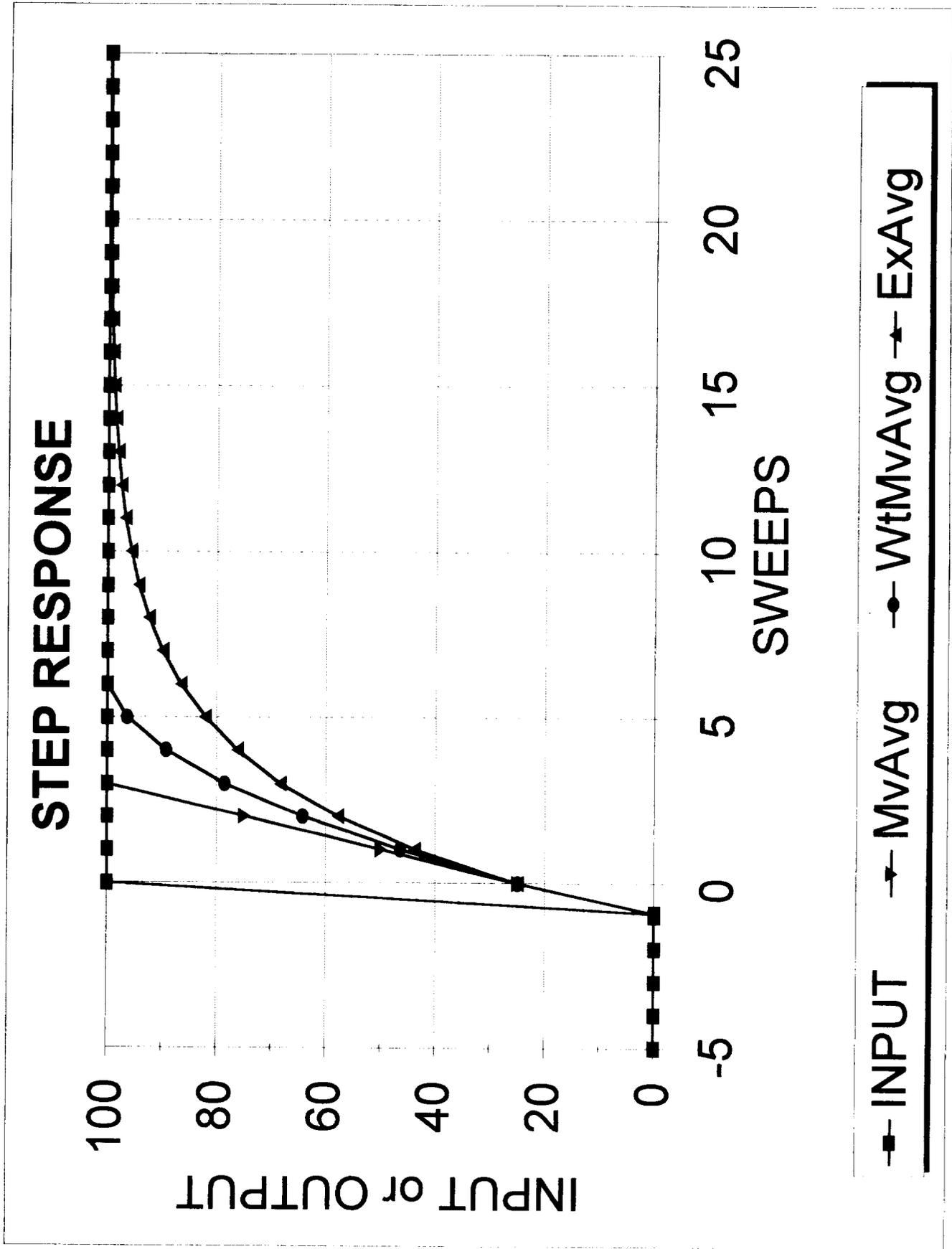
FIGURE No. 9

ANALOG RC EXPONENTIAL AVERAGING EQUATIONS WITH TABLE
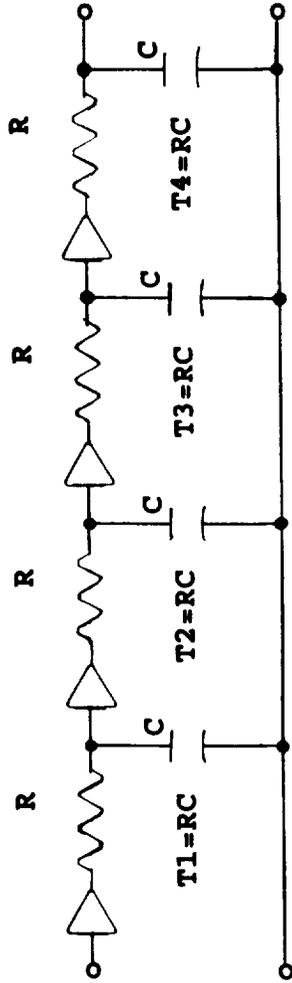
$$T = \sqrt{(T1)^2 + (T2)^2 + (T3)^2 + \cdots}$$

T1	T2	T3	T4	T	DF
2	-	-	-	2	50%
2	2	-	-	2.83	64.6%
2	2	2	-	3.46	71.1%
2	2	2	2	4	75%

FIGURE No. 10
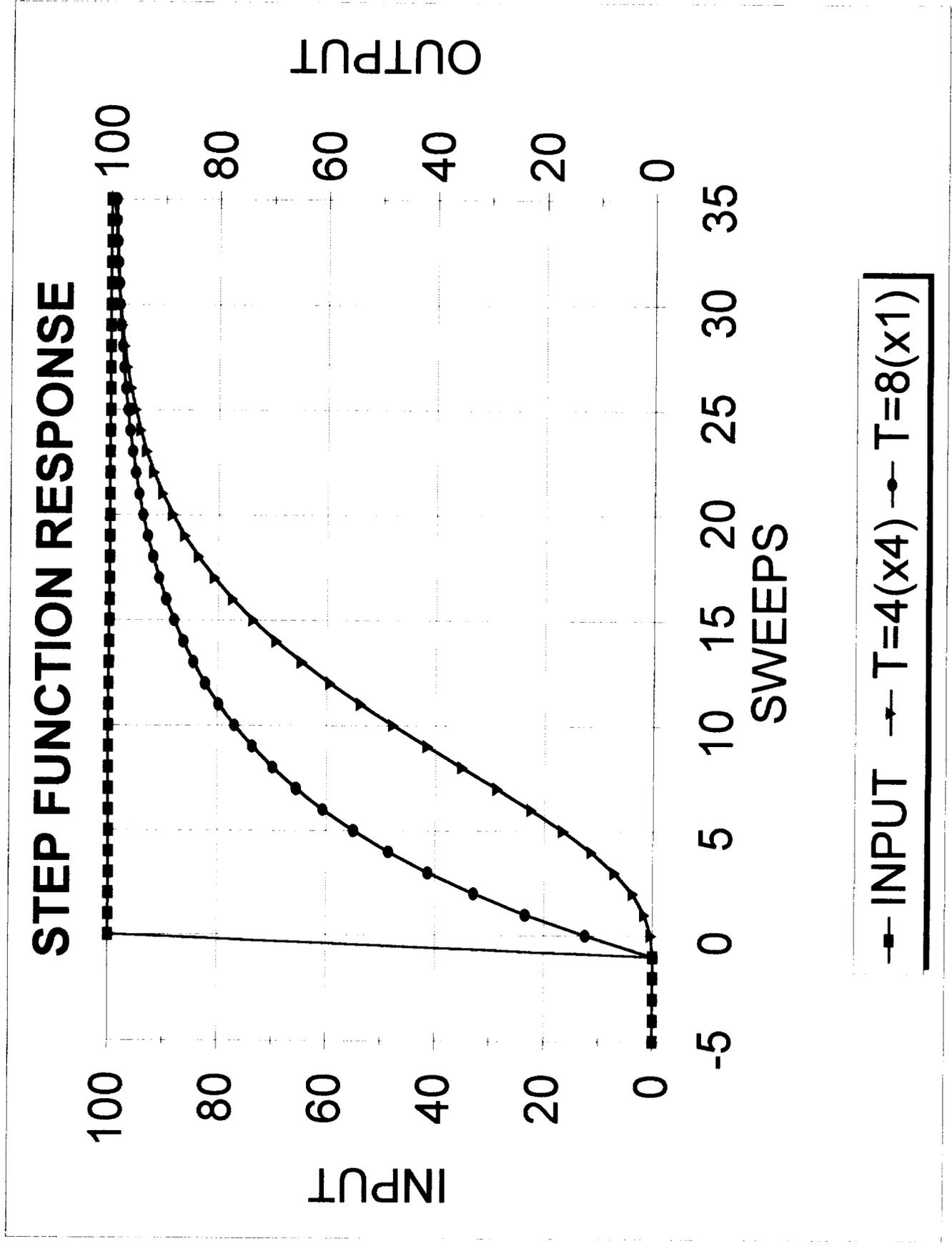
FIGURE No. 11

SINGLE SECTION vs EQUIVALENT 4 SECTION FILTER

IMPULSE FUNCTION RESPONSE
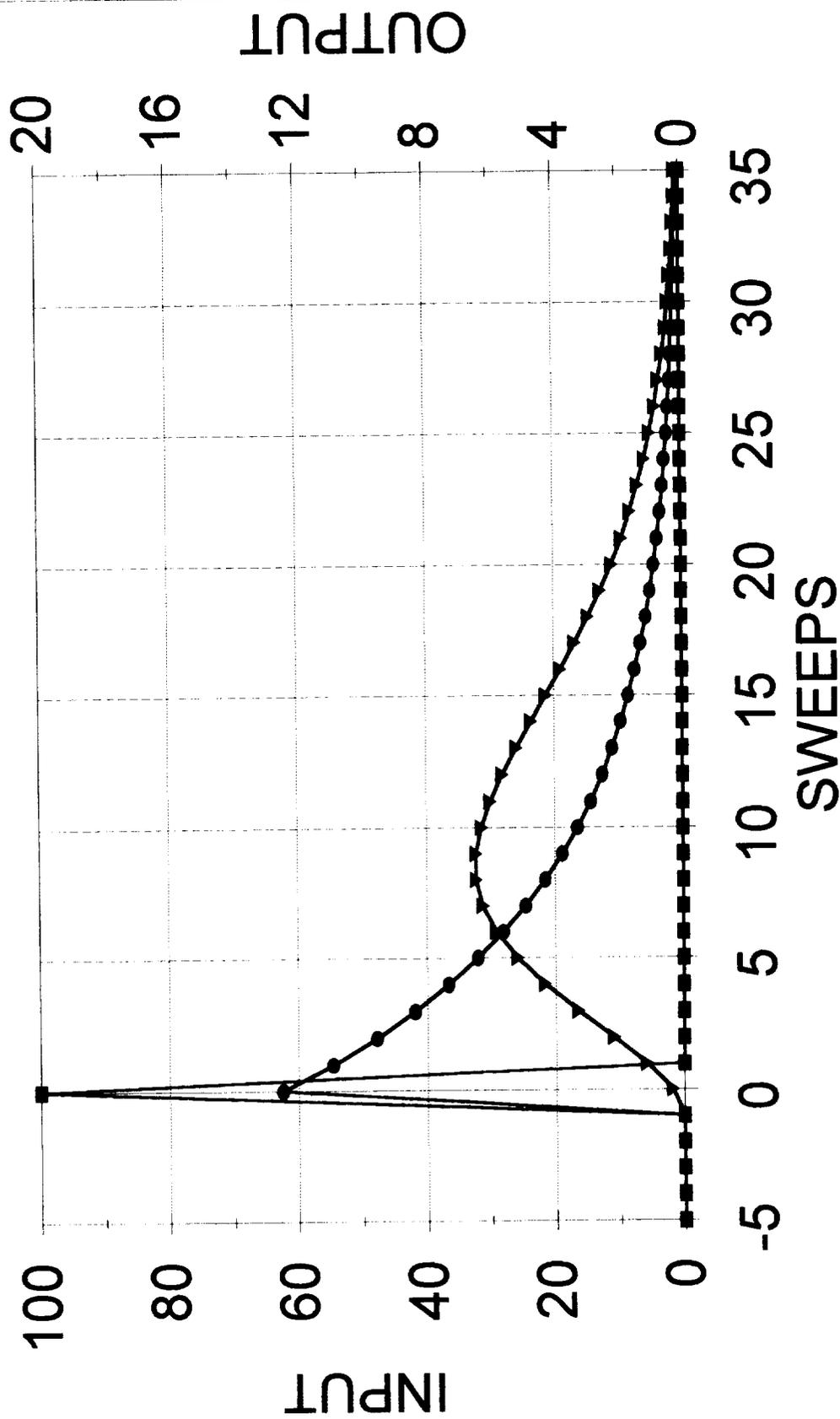
FIGURE No. 12

SIGNAL PROCESSING for ION MOBILITY SPECTROMETERS

by S. Taylor, M. Hinton, R. Turner, Graseby Dynamics Ltd, Odhams Trading Estate, St. Albans Road, Watford, Herts, WD2 5JX, UK

N95- 33289

ABSTRACT

Signal processing techniques for systems based upon Ion Mobility Spectrometry will be discussed in the light of 10 years of experience in the design of real-time IMS. Amongst the topics to be covered are compensation techniques for variations in the number density of the gas - the use of an internal standard (a reference peak) or pressure and temperature sensors. Sources of noise and methods for noise reduction will be discussed together with resolution limitations and the ability of deconvolution techniques to improve resolving power. The use of neural networks (either by themselves or as a component part of a processing system) will be reviewed.

1. BACKGROUND

Graseby Dynamics has been developing ion mobility spectrometers for over 15 years. We have produced systems that are capable of automatic detection of a number of chemical species :

Chemical warfare agents - for example nerve and blister agents

Drugs - heroin, cocaine, amphetamines etc.

Explosives - nitro-glycerine, TNT, RDX etc.

Hazardous chemicals - TDI , dimethyl sulphate etc.

2. OBJECTIVE

This paper will not consider how to present the sample to the analyser but only how to deal with the signals generated by an IMS after the sample has been induced.

The objective of the signal processing is to identify and quantify the analyte.

Most of the work that Graseby has done has been aimed at automatic identification - the spectrometers have to analyse, identify and quantify either completely unattended or at least without operator intervention.

Figure 1 depicts the overall signal processing system.

3. FUNDAMENTALS

What sort of signals ?

Ion currents - generally below the nanoamp region (though some ion sources may exceed this).

Time -varying and repetitive with repetition times between a few milliseconds to a few hundred milliseconds. (This assumes a single ion gate system with direct time of travel analysis).

What sort of noise ?

3.1 Statistical noise as a consequence of the ion numbers - generally not a significant factor:

Corresponds to a standard deviation of about 0.001 % at the 1pA level.

(save for the rather special case of low activity alpha sources which can be noisy as a result of the formation of bursts of ions along each alpha track.)

3.2. Classical noise sources in the amplifying system

Johnson (thermal) noise tends to predominate over other classical noise sources.

It is advantageous to employ a current-to-voltage converter as the first stage. This minimises effects of capacitance on the bandwidths since the input is a virtual earth.

The amplifying system needs a reasonable bandwidth to accurately amplify time varying signals.

Figure 2 depicts the measured bandwidth of a typical IMS spectrum - compared to the anticipated bandwidth of Gaussian shaped peak of the same half-height width.

Biggest value in the feedback resistor (R) of the current-to-voltage converter gives the best S/N since noise increases as square root of resistance whilst the gain is directly proportional to R.

3.3 Electrical noise

There is a need for efficient screening of the signal path both inside and outside the spectrometer itself - in CAM a significant amount of electrical noise can be generated from the various signals flying around the system - one of the LCD driver signals (10 volts peak-to-peak) was found to feed through a small gap in the screening and cause a significant degradation in S/N.

Poor screening within the drift tube can lead to noise on the field defining electrodes being passed onto the collector electrode.

In complete instrument systems there can be a galaxy of noise generators - digital lines, switch mode power supplies etc. and care must be taken to avoid other noise routes into the signal path. For example noise on the reference used for analogue to digital conversion can reflect directly onto the signal.

3.4 Mechanical noise

There are two main areas where mechanically induced noise may arise :

a) The ion collector / collector screen assembly within the drift tube.

and   b) The electrical leads taking the signal to the current-to-voltage converter.

The collector screen serves to shield the collector from variations in electric field - including that caused by an approaching cloud of ions. It is held in close proximity to the collector electrode but there is a fixed potential between the two. This arrangement is very like that of a condenser microphone. Movement of one component with respect to the other induces currents into the ion collector and unless great care is taken in order to achieve mechanical rigidity the arrangement is very susceptible to vibration.

If, for engineering reasons, the current-to-voltage converter cannot be mounted immediately beside the collector then a length of co-axial cable may have to be used. Mechanical vibration of the cable can induce charge separation between the inner and outer conductors of the cable by triboelectric and piezoelectric effects. This induced current is amplified at the current-to-voltage converter and significant microphony can result. Careful selection of the type of co-axial cable is required along with design steps to reduce the level of the vibration.

4. NOISE REDUCTION

4.1 Filtering

Clearly one needs to filter out as much noise as possible without distorting the signal significantly. Analogue filters with roll-off characteristics completely matching the frequency content of the IMS signal would be the ideal to apply. In practice, filters of standard types (Butterworth, Bessel, Chebyshev etc) tend to be applied. They provide the engineering compromise between the ideal and that achievable without adding spurious effects e.g. ringing and overshoot. In any event the frequency characteristic of an IMS product ion peak varies with the drift time associated with it due to peak broadening effects. The ideal filter would have to have a constantly varying frequency response.

We have applied both analogue and digital filtering methods. One should always apply analogue filter methods fully in addition to any further digital processing. There is a very large range of filter techniques available. We tend to favour using a Bessel filter of 5th order. The pass/stop transition region we select depending on the application. For instance, for our high temperature IMS systems we need a higher bandwidth to cater for the sharper peaks caused by the shorter travel time at the elevated temperatures.

Filtering methods introduce phase delays in the filtered signal. These can be significant and should be considered if the ultimate in reduced mobility calculation is required. One of the reasons for selecting a filter with a Bessel response rather than a Butterworth response is that the former gives a constant phase delay for any frequency within its pass band. Typically, the calculated phase shifts will be of the order of 100-200 µs and should be taken into account when calculating reduced mobility figures from first principles.

4.2 Averaging

The time-coherent addition of repetitive ion mobility spectra is very effective at improving the signal/noise ratio. In theory, for an average of N spectra, a $\sqrt{N}$ improvement in signal/noise ratio should result. The technique may be considered as a time-domain filter with a very narrow pass band i.e. it will only pass a signal that is in strict time coherence. In practice, the improvement is usually slightly less than $\sqrt{N}$. Some noise sources may have a small time

299

coherence for a small N e.g. a pump vibration induced noise may have a period similar to the repetition rate of the IMS. In this case a random time delay can be inserted between each trigger of the IMS to interrupt the time coherence between the IMS signal and the rotation rate of the pump motor.

The disadvantage of averaging is that fast changes in the spectrum will be smoothed out. This may lead to an apparent reduction in GC resolution in GC-IMS. The smoothing action can be vitally important if the effect is to delay warning a soldier that he should put on his gas mask. Dynamic averaging can be applied where the spectra are checked after an average of 4, say, if there is no significant change i.e. none above the noise, then the averaging process can add in the previous 4 spectra and recheck and so on. Such techniques attempt to optimise the speed of response to a signal/noise ratio that gives a trustworthy measurement.

A similar, but more comprehensive, approach could be adopted in GC-IMS if all the spectra were stored separately for later processing. This might entail conducting intelligent averaging whereby, if the spectra had fast-changing aspects, say, as a large sample pulse eluted from the column, then fewer averages or a rolling average could be conducted for this part of the time record. If the IMS peaks were small then more averaging would be conducted to increase the signal/noise ratio. In practice such advanced techniques have not proved necessary since with taking, say, averages of 16 spectra it is found that 10 or more data points may be acquired per GC peak.

5. RESOLUTION

The resolution of an IMS signal places fundamental limits on the ability of the IMS system to identify individual ion species. The resolution may be measured in a number of ways, but is essentially the ability of the instrument to separate and quantify packets of ions of slightly different mobility. In signal processing terms it relates to the width of the IMS peaks and the time separation between them.

IMS peak broadening is caused by a number of effects. Most notable amongst these are diffusion Gaussian broadening and space charge effects. For very small ion peaks (i.e. a small number of ions) the space charge effects may be ignored and the diffusion broadening then places an upper limit on the IMS resolution. In the absence of space charge effects, integration of the Boltzmann equation results in the resolution being proportional to the square root of the drift voltage. In the limit of increasing drift voltage the half-height width of the peak will tend towards the width of the gate pulse and then the resolution becomes proportional to the inverse of the drift voltage.

Figure 3 shows the variation in peak width with ion density (peak height) for the experiment where the ^{63}Ni ion source was placed at differing distances from the ion gate. This gives an indication of space charge effects on the peak widths.

6. RESOLUTION ENHANCEMENT

Deconvolution is a signal processing technique used to enhance the resolution by removing the peak broadening process suffered by the ion packet as it travels down the drift tube. In its simplest form the broadening process may be viewed as a transfer function acting on the signal (gate open pulse) applied to the system.

$$y = D*x$$

where y is the output signal,
x is the input signal
& D is the peak broadening operator

If we know this function perfectly (i.e. its impulse response is known and that there is no noise in the output) then the deconvolution process is to apply the inverse of the transfer function to the signal:-

$$x = D^{-1} * y$$

This may be achieved by the use of Fourier transforms.

However, when noise, n, is present, that is;

$$y = Dx + n$$

and we must determine:-

$$x = D^{-1}(y-n)$$

$D^{-1}n$ can be large for parts of the frequency spectrum and this simple method then amplifies noise in the signal and is unusable. A further problem is that small errors in determining D can lead to large errors in D-1 leading to spurious results and noise amplification.

There are many deconvolution schemes published in the literature. At Graseby Dynamics we have had some success with two deconvolution schemes. Both require a reasonable estimate of the impulse response of the system transfer function, but they have been shown to be substantially less prone to producing artefacts due to noise in the original signal.

A) Constrained Iterative Deconvolution

This uses an iterative approach, as described by Schafer et al[1] ,with the constraint that no part of the resultant output (deconvolved spectrum) of each iteration can be less than zero. This corresponds with the physical situation that charge of incorrect polarity cannot arrive at the collector electrode.

Figures 4 and 5 show a typical iteratively deconvolved spectrum

The resolution may be enhanced by a factor of about 3. The peak magnitude information can be unreliable after applying deconvolution. Peak height/area measurements should then be conducted on the original spectrum and the deconvolved spectrum be used solely for identification.

B) Maximum Entropy Deconvolution

Graseby Dynamics has used the services of Maximum Entropy Data Consultants Ltd[2] (MEDC) to conduct their deconvolution method on some trial spectra. Again an estimate has to be made of the impulse response of the system transfer function. For this and other studies we have found that a simple Gaussian shape is a reasonable first approximation, but a better approach is to take the spectrum produced by a single ion species e.g. for positive ion mode

that of acetone in an otherwise clean system. Since the stimulus of the system is almost an impulse, then the output (i.e. the acetone RIP) is the response to this and can be taken as the transfer function. MEDC applied their method, using an acetone RIP as the transfer function and obtained very good results. The resolution may be enhanced by a factor of about 8.

Figures 6 and 7 show the same spectrum as that in figure 4, but now deconvolved by the maximum entropy method.

As can be seen the MEM deconvolved peaks have the best resolution and the noise level is also reasonable. MEDC claim that the principles they incorporate in their processing are the only logical ones which should be applied to deconvolution. Further, they claim their processing allows for a rigorous, statistically based estimation of ion peak magnitudes in the deconvolved spectrum. That is, they can measure a peak magnitude and provide a confidence figure for the value's accuracy.

Of course, there has to be a disadvantage to such a powerful technique - it is very computationally intensive. It requires several hundred to a few thousand FFTs to perform a single deconvolution. It may not yet be a real time technique, but it may find use in those laboratory applications where resolution is paramount.

7. IDENTIFICATION

Having obtained a spectrum of low noise and high resolution, the next problem is to identify ion species by means of accurate reduced mobility measurements. Two methods may be adopted:-

a) Use of a standard reference compound. In which the ratio of the target compound ion drift time to that of a known reference ion gives the reduced mobility.

b) Use of pressure, temperature and drift voltage measurements. In which, these parameters, the drift length and the target compound ion drift time are used to calculate the reduced mobility.

Both methods have merits and disadvantages. In the reference compound method, the selection of the compound and the manner of its introduction to the system are vital. Many reduced mobilities are concentration and temperature dependent.

To measure the reduced mobility accurately from first principles requires an accurate knowledge of the ion drift time, the drift length, the drift voltage and the IMS internal temperature and pressure. Further, the drift field must be perfectly regular for the entire drift length and the influence of end effects and signal processing delays must be known. In practice the instrument will be calibrated using a compound producing a known, stable ion species, with an internationally accepted reduced mobility figure. The steps being taken to choose standard compounds are to be commended.

The calibration provides an instrument constant which includes the unknowns listed above. Thereafter, the drift voltage, drift tube temperature and pressure need to be accurately measured. An example of a most-likely error bound calculation is given below. The error figures quoted for each measurement are typical of what may be achieved in a commercial instrument.

$$Ko = \xi \frac{1}{t} \frac{P}{T} \frac{1}{V}$$

where ξ = a instrument constant determined using a reference compound

t = drift time

P = pressure

T = temperature

V = drift voltage

$$\left(\frac{\delta Ko}{Ko}\right)^2 \approx \left(\frac{\delta t}{t}\right)^2 + \left(\frac{\delta P}{P}\right)^2 + \left(\frac{\delta T}{T}\right)^2 + \left(\frac{\delta V}{V}\right)^2$$

With careful design:-

$$\left(\frac{\delta Ko}{Ko}\right)^2 \approx \left(\frac{10}{10000}\right)^2 + \left(\frac{5}{1000}\right)^2 + \left(\frac{0.15}{300}\right)^2 + \left(\frac{1}{1000}\right)^2$$

Giving $\left(\frac{\delta K0}{Ko}\right) \approx 0.5\%$

For most applications the selection of a small, low power pressure transducer means that the errors in this measurement tend to dominate the overall error. For this not to be the case one would need to measure the absolute pressure to +/- 1mbar.

Having decided by either method where to look for ion peaks in the spectrum, the next process is to determine the presence and position of peaks. This may achieved by means of peak searching routines followed by the application of a set of decision rules, i.e. if a peak appears within a time/mobility window then it must be compound, X. Our experience is that the set of decision rules often becomes increasingly complicated throughout the life of the instrument as new fields-of-use and interferents are encountered. We are now using combined positive and negative ion mode spectral data to identify compounds, collected simultaneously using twin drift tube systems, to enhance interferent rejection.

Increasingly, neural networks are being applied to conduct the identification function. The result of an experimental neural network is given in tables 1 & 2 below. The network was fed the spectra of 4 different compounds over a range of concentrations and the spectra of the clean system (no sample vapour present) Table 1 shows the values in the 5 output elements once the network has been trained on this set of data. Not surprisingly the output element associated with each compound gives a high value when offered the spectrum of that compound. More interestingly the network also performed reasonably well with the separate test set of spectra of the same compounds as shown in table 2.

Table 1 Neural Network Results (Training set)

Output element number (Compound ident)					Compound
1 (A)	2 (B)	3 (C)	4 (D)	5 (RIP)	
1	0	0	0	0	A
1	0	0	0	0	A
1	0	0	0	0	A
0	1	0	0	0	B
0	1	0	0	0	B
0	1	0	0	0	B
0	0	1	0	0	C
0	0	1	0	0	C
0	0	1	0	0	C
0	0	0	1	0	D
0	0	0	1	0	D
0	0	0	1	0	D
0	0	0	0	1	RIP
0	0	0	0	1	RIP
0	0	0	0	1	RIP

RIP refers to the spectrum from a clean system (no sample vapour).

Table 2 Neural Network Results (Test set)

Output element number (Compound ident)					Compound
1 (A)	2 (B)	3 (C)	4 (D)	5 (RIP)	
1	0	0	0	0	A
0.9	0	0	0	0.1	A
1	0	0	0	0	A
0	1	0	0	0	B
0	0.8	0	0	0.1	B
0	1	0	0	0	B
0	0	1	0	0	C
0	0	0.8	0	0.26	C *
0	0	1	0	0	C
0	0	0	1	0	D
0	0	0	1	0	D
0	0	0.3	0.9	0	D
0	0	0	0	0.9	RIP
0	0	0	0	1	RIP
0	0.1	0	0	0.9	RIP

Note that the result for the test labelled marked (*) was for a low concentration of compound, C, such that the RIP was near its full height. It is not surprising that the neural network considered that this spectrum was similar to that for a clean system. With a larger training set this, and other deviations from the expected result may have been avoided.

The above results were obtained using digitised spectra which were scaled for pressure and temperature (drift voltage assumed constant). The complete spectrum was offered to the

network in each case - not just peak positions and heights. This method can distinguish compounds that give very similar spectra. It is also found to give better interferent rejection and can be trained to reject specific interferent compounds.

8. QUANTIFICATION

A typical IMS spectrum consisting of 16 averages has a figure for the ratio (clean-system RIP/noise level) of approximately 100. This implies a dynamic range of about 2 orders of magnitude which could be extended by reducing the noise. A quiet system and with the spectra acquired using hundreds of averages the dynamic range may be extended to 3 orders of magnitude. Of course, only a small section of this range, usually at low concentrations, may be considered linear. At high concentrations functional forms for the quantitation need to be applied to deal with the appearance of dimers and trimers and they may also aid in overcoming some of the saturation effects. A functional form may be represented:-

$$\text{Measured value } = f(M, D, RIP)$$
$$\text{where } M = \text{monomer peak height}$$
$$D = \text{dimer peak height}$$
$$RIP = \text{RIP peak height}$$

These may take many forms, depending on the instrument and ion chemistry. A typical form might be:-

$$\text{Measured value } = M + D \text{ for } RIP > \text{Trip value}$$
$$\text{Measured value } = M + D + \alpha \frac{D}{M} \text{ for } RIP < \text{Trip value}$$
$$\text{where } \alpha \text{ is a constant derived from experiment}$$

In calibrating an IMS system at Graseby Dynamics we generally use look up tables to convert from the measured value to a concentration value. This allows for greater flexibility than trying to use a single equation to fit the response curve over the entire dynamic range of the instrument.

Peak areas may be used instead of peak heights and may be preferred if the increase in noise from the summing of several digitised samples within the spectrum is less than the increase in the signal. This suggests that one should only measure the central area of the peak, out to about the half-height position.

REFERENCES

1.   R. W. Schafer, R. M. Mersereau & M. A. Richards
Proc. IEEE vol 69 No4 p432 (April 1981)

2.   Maximum Entropy Data Consultants Ltd, St. John's College, Cambridge, CB2 1TP, U.K.
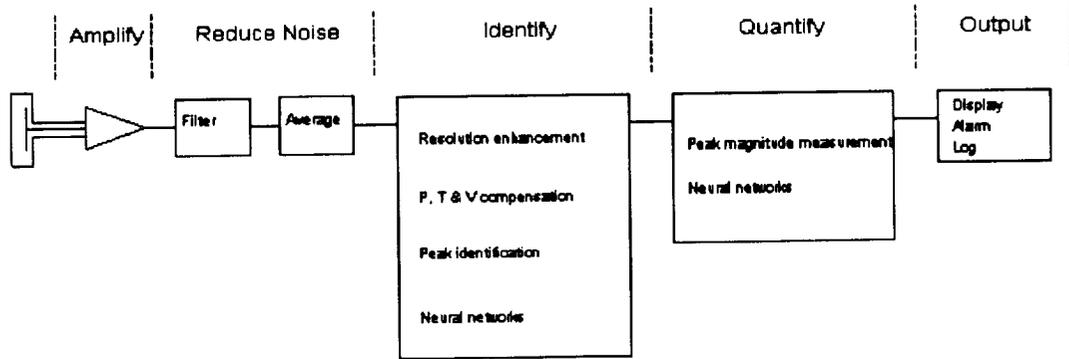
Figure 1. Overall signal processing path
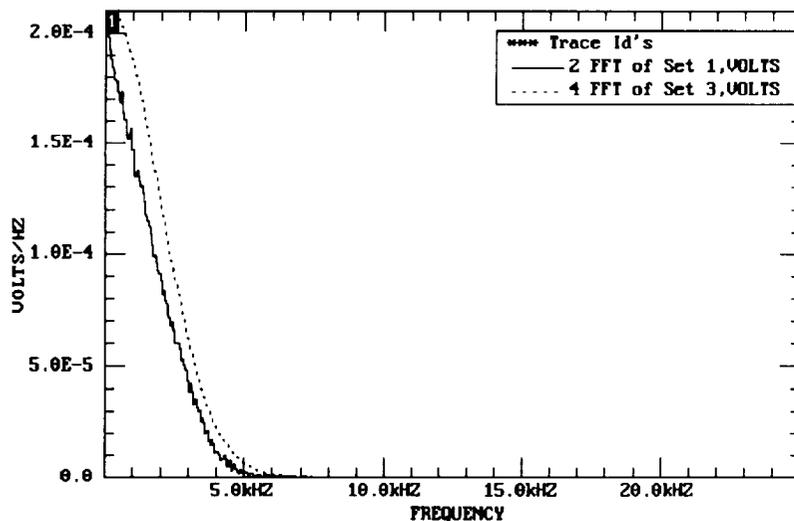
Figure 2. Typical frequency spectrum of an IMS signal (solid) and that of a calculated Gaussian peak of similar half-height width (dashed)

Figure 3. Ion peak half-height width versus ion peak height when the source-to-gate distance is varied.
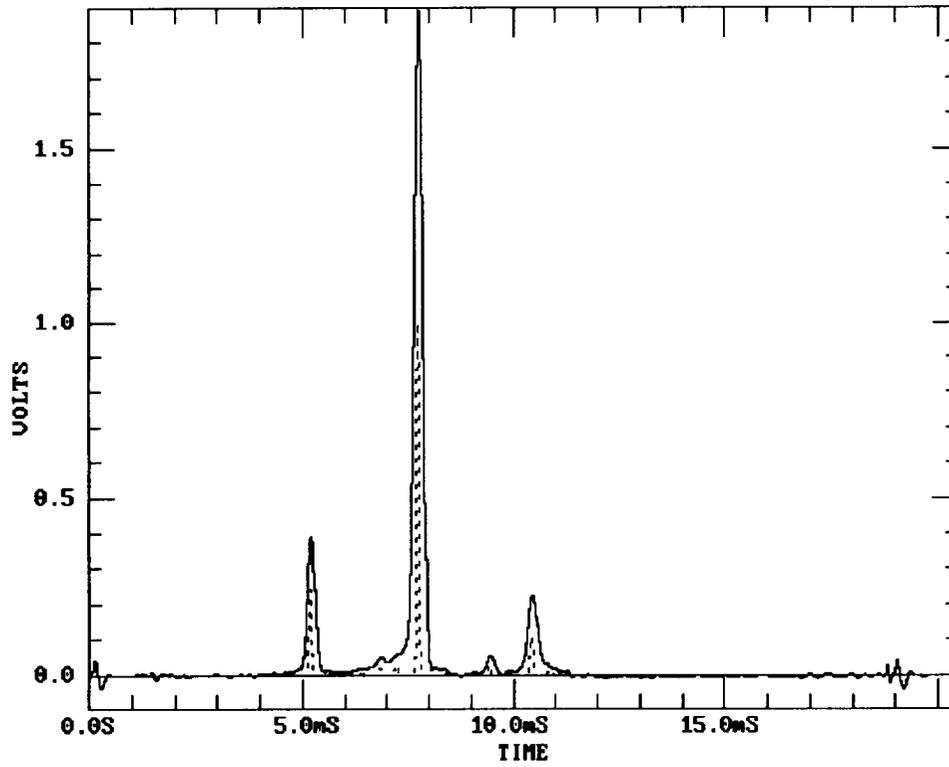
Figure 4. Typical original (solid) and iteratively deconvolved (dashed) spectrum
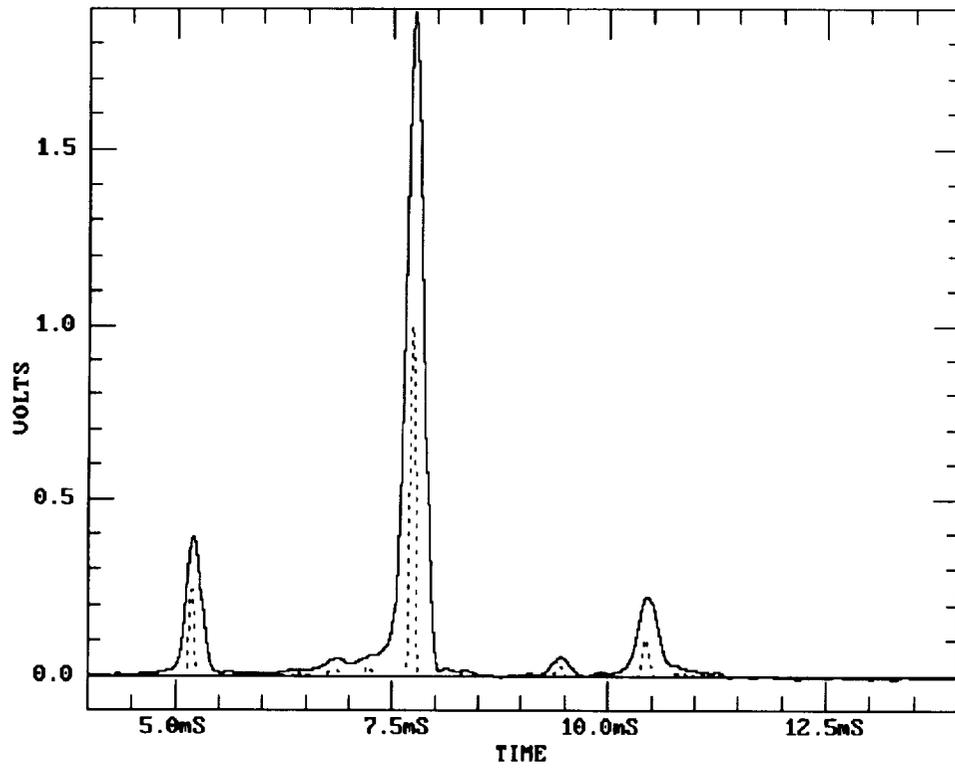
Figure 5. Spectrum from figure 4 on expanded timescale
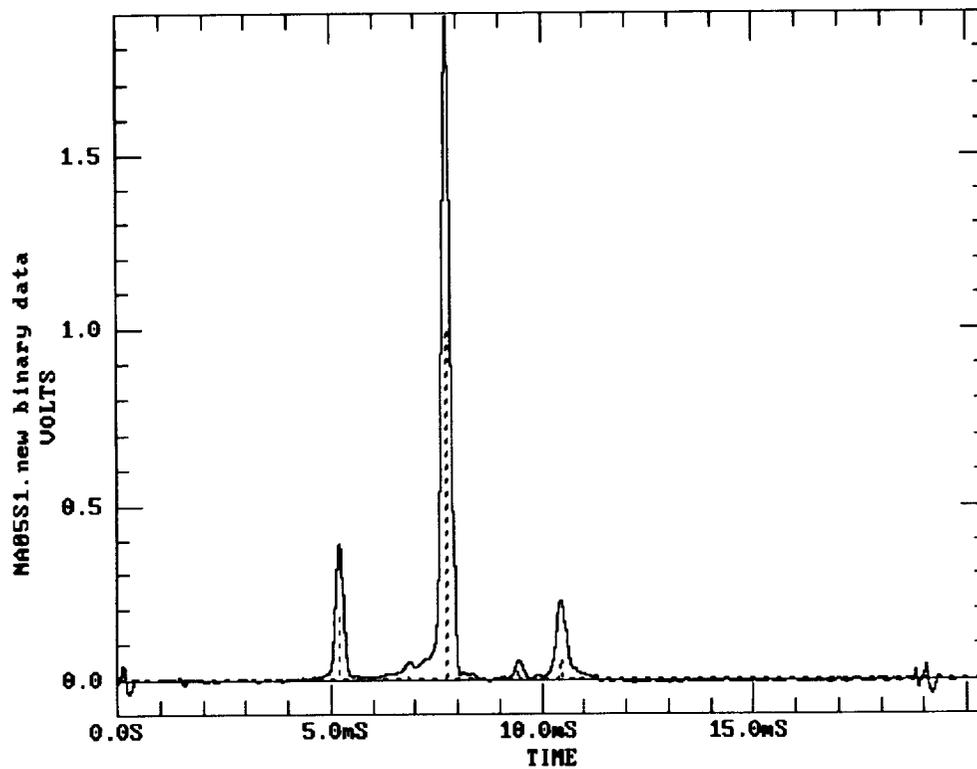
Figure 6. Typical original (solid) and maximum entropy deconvolved (dashed) spectrum
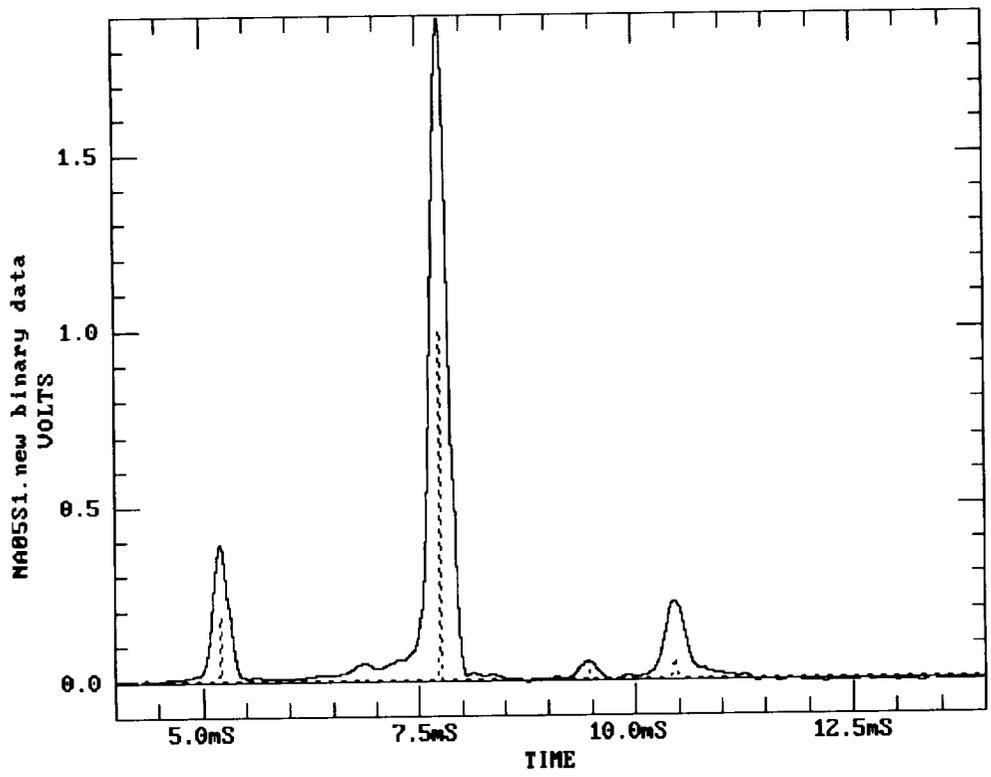
Figure 7. Spectrum from figure 6 on expanded timescale

Quantitative Analysis of Volatile Organic Compounds Using Ion Mobility Spectra and Cascade Correlation Neural Networks

Peter de B. Harrington* and Peng Zheng
Ohio University
Center for Intelligent Chemical Instrumentation
Department of Chemistry
Clippinger Laboratories
Athens, OH 45701-2979

Dennis M. Davis
U.S. Army Edgewood Research, Development and Engineering Center
Chemical and Biological Detection Research Team
Aberdeen Proving Ground, MD 21010-5423

ABSTRACT

Ion mobility spectrometry (IMS) is a powerful technique for trace organic analysis in the gas phase. Quantitative measurements are difficult, because IMS has a limited linear range. Factors that may affect the instrument response are pressure, temperature and humidity. Nonlinear calibration methods, such as neural networks, may be ideally suited for IMS. Neural networks have the capability of modeling complex systems. Many neural networks suffer from long training times and overfitting. Cascade correlation neural networks train at very fast rates. They also build their own topology, that is number of layers and number of units in each layer. By controlling the decay parameter in training neural networks, reproducible and general models may be obtained.

INTRODUCTION

IMS is a powerful technique for analysis of trace quantities of organic compounds in the gas phase. IMS is inexpensive, offers high sensitivity, fast response and low detection limits. Sophisticated computer software coupled to an IMS instrument may allow a synergism to be obtained that will generate an intelligent or smart instrument. These instruments will incorporate expertise in data interpretation and processing as part of the hardware. There is great potential for automated identification and quantitation of volatile substances by IMS. The suitability of neural networks for IMS data analysis has already been demonstrated[1,2]. Automated systems may be developed for identification and classification of unknown materials.

A general system was presented for semi-quantitative measurements of volatile organic compounds in air that used backpropagation neural networks (BNNs)[3]. Although these systems are popular tools, they were abandoned for this project because of several disadvantages. The most important limitation is that BNNs train at slow rates. For difficult cases, BNNs may not converge to a satisfactory error. In addition, determining the network

---

*Corresponding author.

configuration (i.e., the number of layers and processing units) is a difficult and important step for building reliable models. The cascade correlation network (CCN) learns its own network configuration during training.[4] CCNs train faster than BNNs by adjusting a single unit at a time. The result is a network that configures its topology and trains at an astonishing rate. CCNs are valuable tools for obtaining general calibration models from IMS data. A CCN that identifies and quantitates a variety of organic solvents over a broad range of concentrations has been developed.

An IMS instrument consists of a sample inlet system, a reaction region, a drift region and an ion collector. The carrier gas (air or nitrogen) sweeps the sample into the reaction region where the sample gas is ionized. The ions formed in the reaction region are injected into the drift region where the time for ions to move through an applied electric field is measured. The drift velocity, V_d, of an ion is obtained by dividing the length of the drift region, L, by the drift time, t_d. The ion mobility, K, is obtained by dividing the drift velocity by the accelerating potential, E. The relationships are given in equations (1) and (2).

$$V_d = \frac{L}{t_d}$$

(1)

$$K = \frac{V_d}{E}$$

(2)

The mobility value may be corrected to standard gas density, 2.687×10^{19} molecule/cm that corresponds to standard conditions of 273 Kelvin and 760 torr. The reduced mobility K_0 is obtained by

$$K_0 = K \left(\frac{P}{760} \right) \left(\frac{273}{T} \right)$$

(3)

for which P and T are the experimental pressure and temperature, respectively.

Factors that affect K_0 include imprecise determination of the electric field, imprecise temperature measurements of the drift space, temperature gradients, pressure fluctuation, and humidity of the drift gas. Pressure fluctuations are important when the drift gas flow rate is pump controlled. Variable water content of the drift gas affects the water content of the clustered reactant ions. Sample introduction may saturate the system and contaminants or multiple analytes may interact in a complex manner. Under saturated conditions, multiple peaks due to contaminants in the sample, oligomer formation, and ion-molecule reactions in the drift space are common. Also K_0 values are dependent on the drift gas. In general, K_0 changes as a function of the polarizability, α, of the drift gas.

The drift tube of the instrument is continually swept with air or nitrogen, to clear neutral sample molecules from the drift tube, and to serve as the drift gas of the instrument.

313

The most common form of primary ionization is by β-particle radiation from a ^{63}Ni foil in the reaction region of the IMS cell. A series of cascading reactions progresses and results in the formation of a set of reactant ions. Sample vapors are introduced into the reaction region via a carrier gas where reactant ions collide with sample vapor molecules and product ions are formed. The predominant mechanism of formation for positive ions is proton transfer from $(H_2O)_nH^+$ reactant ions to the sample molecule, which is followed by a number of possible complex reactions. Typical reactions are with additional sample molecules present, reactions with water vapor molecules, and reaction with other neutral molecules present in the reaction region of the mobility spectrometer. Product ions containing one analyte molecule are referred to as "monomers", two analyte molecules, "dimers", and so forth.

Ions are injected into the drift region of the instrument using an electric shutter. Characteristic constant velocities are attained for particular ions which form a near-Gaussian distribution during drift tube traversal. At the end of the drift region, ions strike a collector electrode (Faraday cup) and generate a weak source signal (typically 10-100 pA) at a frequency of 30-40 Hz.

EXPERIMENTAL SECTION

The ion mobility spectrometer used to obtain spectra was a hand-held IMS device, the Airborne Vapor Monitor, AVM, (Graseby Ionics, Ltd. Watford, Herts, U.K.). Spectra from the ion mobility spectrometer were collected on an IBM-compatible 80386 25MHz personal computer using Advanced Signal Processor Software (ASP, Graseby Ionics, Ltd.). Typical data collection parameters are given in Table I.

Table I. Typical Operating Conditions for the AVM

Ionization Source	^{63}Ni
Gating Pulse Repetition Rate	33 Hz
Cell Temperature	30 °C
Cell Pressure	760 torr
Drift Gas	Clean dry air
Drift Gas Flow	400 mL/min
Spectral Mode	Positive Ion
Points Per Spectrum	640
Sampling Frequency	33 KHz
Delay to Start of Sampling	0 μs

Data acquisition is initiated at the midpoint of the gating pulse. A spectrum is collected at a user specified sampling frequency. In practice, an analog signal is converted with a flash analog-to-digital converter (ADC) which has twelve bit resolution. The spectra

are stored in binary format and can be converted to ASCII format as required.

All laboratory vapors were generated using a vapor generator called the Q5. The Q5 generator, Figure 1, has 15 component parts. These parts are: (1) an equilibrator assembly, (2) an air supply stopcock, (3) a constant pressure regulator (stabilizer) for the air supply, (4) a flowmeter (manometer) for the air supply, (5) a constant pressure regulator (stabilizer) for the diluent air supply, (6) stopcocks for the stabilizers, (7) a stopcock for the flow of air from the equilibrator to the mixing chamber, (8) a flowmeter (manometer) for the diluent air supply, (9) a mixing chamber, (10) a reservoir, (11) a reservoir exhaust stopcock, (12) sampling stopcocks, (13) a charcoal trap on the exhaust of the reservoir, (14) a charcoal canister on the sampling line, (15) and sampling bubblers.

The equilibrator assembly is the liquid test reagent container of the dilution apparatus. Dry air, under a constant controlled pressure, flows into the equilibrator. This air stream passes over the surface of the test reagent, and becomes saturated with the reagent vapor. The dry air-test vapor mixture flows from the equilibrator assembly to the mixing chamber where it is diluted with dry air to the required concentration of milligrams test vapor per liter of dry air. The equilibrator is maintained at a constant temperature by partial immersion in a constant temperature water bath. The water bath is maintained at 25 °C. Included in the equilibrator is a porous alundum oxide cylinder to produce a greater surface area for the liquid-vapor equilibration.

The flow of air through the equilibrator is controlled by a stopcock in the air supply line, a constant pressure regulator for the air supply, and a flowmeter. The stopcock is located at the inlet of the equilibrator, and acts as the shutoff valve for the air supply, from the flowmeter to the equilibrator. The constant pressure for the air supply is maintained by bubbling the dry air through a constant level of fluid, e.g., water, in the stabilizer. By raising or lowering the level of the fluid in the stabilizer, the pressure of the air supply is increased or decreased. The level of the fluid is raised by adding fluid to the stabilizer, and lowered by draining fluid through the stabilizer stopcock that is located on the bottom of the stabilizer. Changing the pressure of the air supply in this way increases or decreases the flow of the test vapor through the dilution apparatus. Excess air that passes through the stabilizer is vented to the laboratory hood. The flowmeter measures the flow rate of the dry air-test vapor mixture in milliliters per minute. The flow rate of the diluent air is controlled in the same way as the equilibrator air supply. The flowmeter for the diluent air is measured in liters per minute. The nominal concentration of the test vapor can be calculated by

$$C = \frac{fp}{(F+f)\,P} \tag{4}$$

for which C is the concentration of the test vapor in parts per million, f is flow rate of air through the equilibrator, F is the flow rate of the diluent air, p is the vapor pressure of the test reagent at the temperature of the experiment, and P is the atmospheric pressure. Thus, the concentration of the test vapor may be easily changed by varying either the flow rate of air through the equilibrator or the flow rate of the diluent air. In practice, it works best to change the flow rate of the diluent air, when possible, because the efficiency of the vapor generation in the equilibrator decreases as the flow rate increases.

The dry air-test vapor mixture from the equilibrator and the diluent air are passed into the mixing chamber located at the entrance of the reservoir. The dilute test vapor is thoroughly mixed by a swirling circular motion of the air in the mixing chamber before entering the reservoir. The reservoir is the container for the diluted test vapor, from which samples are taken for concentration analysis and for testing purposes. There is a charcoal canister located on the exhaust of the reservoir. This canister serves as a scrubber to remove test vapors passing from the reservoir to the atmosphere in the laboratory hood. There are two sampling ports on the reservoir, one for taking samples for concentration analysis; the other for removing the vapor for testing purposes.

IMS data was collected for the following solvents and concentration ranges given in Table II. This set of data was split almost equally into calibration and prediction sets of data with the following exception. The prediction set had 9 more reactant ion spectra for which solvent vapors were present during data collection.

Table II. Spectra used in the Evaluation (Number of Calibration:Prediction).

Acetic Acid	100 ppb (3:3)	1 ppm (4:4)	10 ppm (5:4)		
Acetic Anhydride	100 ppb (2:3)	1 ppm (5:4)	5 ppm (4:4)		
Acetone	1 ppm (3:3)	10 ppm (2:2)	100 ppm (3:4)	1000 ppm (10:8)	
Diethyl Ether	4 ppm (4:4)	40 ppm (3:3)	400 ppm (4:4)		
Isooctane	3.5 ppm (6:6)	35 ppm (6:5)	350 ppm (3:3)		
Isopropanol	4 ppm (4:4)	40 ppm (2:2)	400 ppm (2:2)		
Methyl Benzoate	5 ppb (3:2)	10 ppb (5:5)	20 ppb (5:5)	50 ppb (3:2)	100 ppb (3:3)
o-Nitro Toluene	2.5 ppb (5:4)	25 ppb (9:10)	250 ppb (4:3)		
Toluene	15 ppb (3:2)	230 ppb (3:3)	1.7 ppm (3:4)	10 ppm (4:5)	
Reactant Ions	(29:38)				

All data analyses were run on a 60 MHz Pentium PC operating under DOS 6.2. Code was developed with Watcom's 32 bit C++ compiler version 9.5b. The cascade correlation program is shareware that is available from Carnegie Mellon University. The program was modified to use an improved random number generator. The ANSI C 16 bit random number

generator should be avoided for neural network programs.[5]

The IMS data were corrected for baseline by subtracting the average intensity from the range of 1.5-3.0 ms. The spectra were reduced by removing all the points less than 3.0 ms and greater than 16.0 ms. For CCN evaluations, each spectrum was scaled with respect to intensity by dividing every point in the spectrum by 1000. After preprocessing each spectrum was composed of 390 single precision floating point intensities.

The CCNs were trained with a sigmoid prime offset of 0.1. The output learning rate was 0.1 and the hidden unit learning rate was 0.001. For two CCN training configurations, the decay rates were either a factor of ten greater than the learning rates, or zero. The output units were trained for a maximum of 400 epochs and the hidden units were trained for a maximum of 200 epochs. If the error decreased less than 0.1% or 3% in 12 epochs, then training terminated for the hidden and output units, respectively. Twenty hidden units were trained simultaneously with the one yielding the highest correlation being used. Both output and hidden units were trained with a quickprop maximum step threshold value (μ) of 2.0. The networks were trained until the relative training error (i.e., error divided by the variance of the outputs) was 5%.

DATA ANALYSIS

Nine dependent variables were obtained for each spectrum. Each variable corresponds to the identity of a compound in the training set. The concentration values were transformed to p-values (i.e., $-\log_{10}$). Reactant ions were included from each compound acquisition. Their p-values were arbitrarily assigned values of 10, which corresponds to an arbitrary detection limit of the instrument. This transformation is necessary so that the concentration values will be equally weighted. Otherwise the networks must recognize small differences in concentration that result in bivariate predictions of either high or low concentration. This problem occurs because the differences between low concentration design points will be less than the variance about the high concentration design point. All the dependent variables are assigned values of 10, except that the variable corresponding to the compound is set to the p-concentration value. This approach is beneficial, because the identity of a compound is given by the prediction variable with the smallest output. The outputs correspond to concentrations, and spectra of multiple compounds may be modeled without modification.

Neural networks are powerful pattern recognizers and are susceptible to overfitting training data. It is always a good idea to implement control methods of pattern recognition for evaluation of a neural network's performance. Partial least squares (PLS) was chosen as a control methods.[6] The PLS model was constructed so that the number of latent variables furnished a minimum error for prediction set of data.

Errors were reported as standard error prediction (SEP) and relative standard error of prediction (RSEP) as given below.

317

$$SEP = \sqrt{\frac{\sum\limits_{j=1}^{p} \sum\limits_{i=1}^{n} (y_{i,j} - \hat{y}_{i,j})^2}{np}} \qquad (5)$$

$$RSEP = \sqrt{\frac{\sum\limits_{j=1}^{p} \sum\limits_{i=1}^{n} \left(\frac{y_{i,j} - \hat{y}_{i,j}}{y_{i,j}}\right)^2}{np}} \qquad (6)$$

The SEP has the same units as the prediction variables which are p-concentrations and RSEP is unitless and is reported as a percentage. The number of outputs in the network is given by p and the number of observations in the prediction set is given by n. The prediction set is an external set of validation data. The predicted value is $\hat{y}_{i,j}$ and the target output is $y_{i,j}$ for the j output and i observation.

The CCN is an alternative method to the more popular BNN. The differences between the two methods are that a CCN trains at a substantially faster rate and CCNs determine their own topology (i.e., number of layers and units). CCNs train by adjusting only a single unit at a time. Because CCNs fix all previously trained units, they have the capability of incremental learning. Therefore, if a new compound needs to be added to the calibration, the network can be added to its existing structure and save time during training.

CCNs like other neural networks train by adjusting weights so that the training error is minimized. Like any nonlinear optimization, the procedure is iterative and dependent on the initial conditions. For neural networks, the initial conditions are the random weight values assigned to weights prior to training. It has been shown that these initial conditions introduce a modeling error into neural network models.[7] Therefore all neural network results should be accompanied by figures of merit indicating this lack of precision.

The CCNs initiate training with only output units. These units are adjusted until a minimum prediction error is obtained. A candidate unit is added as hidden unit. The unit is trained so that the absolute value of the covariance between the unit's output and the residual error is maximized. The covariance is given as

$$s_j = \sum_{k=1}^{p} \left| \sum_{i=1}^{n} (o_{i,j} - \bar{o}_j)(e_{i,k} - \bar{e}_k) \right| \qquad (7)$$

for which s_j is the covariance of unit j. The number of output units is given by p, and n is the number of observations in the training set. The average output per epoch is given by $\bar{o}_j$ and the average error per epoch is given by $\bar{e}_k$. After a hidden unit's covariance is maximized, its weights are fixed. The output of the hidden unit is connected to the output units, and the output units are adjusted until the prediction error is minimized. The next hidden unit is added so that the previous hidden unit feeds into it. Therefore, the hidden units have a

cascading architecture because each new unit receives the outputs from all the previously added hidden units as well as the inputs, i.e., the spectra. The cascading architecture allows the CCN to model higher order functions that would be impossible for backpropagation networks. Because only one unit is adjusted at a time, the other units in the network can cache their outputs, and the network can train with fewer computations.

The networks presented in this study are all trained in batch mode with decay and sigmoid prime offsets. The basic training model for adjusting component j of weight vector for output unit k is given by

$$\Delta w_{j,k}(t+1) = -dw_{j,k}(t) + \eta \sum_{i=1}^{n} (y_{i,k} - \hat{y}_{i,k}) x_{i,j} \qquad (8)$$

for which t indicates training cycle (i.e., one pass through the training set). A training cycle is a complete pass through the n spectra in the training set, and is referred to as an epoch. A decay parameter (d) causes weights that are not pertinent (i.e., independent of prediction error) to decrease in magnitude. The learning rate is designated as η, $y_{i,k}$ is the target output and $\hat{y}_{i,k}$ is the predicted output of unit k and observation i, $x_{i,j}$ is the j component of input i. The training errors are summed for the number of observations in the training set (n). The hidden units are adjusted in a similar process.

$$\Delta w_{j,k}(t+1) = -dw_{j,k}(t) + \eta \sum_{i=1}^{n} s_i x_{i,j}(f'(net_{i,k}) + spo) \qquad (9)$$

The hidden units have sigmoid activation functions. Therefore the first derivative of the sigmoid function, $f'(net_{i,k})$, is needed for the weight adjustment. Network paralysis may be minimized by the sigmoid prime offset parameter (spo). This parameter propagates errors back through units whose sigmoid derivatives are zero or small. The value of s_i is given by

$$s_i = \sum_{k=1}^{p} \sigma_k [(y_{i,k} - \hat{y}_{i,k}) - \overline{(y_{i,k} - \hat{y}_{i,k})}] \qquad (10)$$

for which σ_k is the sign of the covariance of a hidden unit and the residual error of an output unit k for a training epoch. The other terms are the residual error and the average residual error for an entire training epoch. The CCN network uses the quickprop algorithm which is beyond the scope of this paper[8].

An important parameter for neural network generalization is the decay parameter. If this parameter is large, spurious weight values may be removed and the networks avoid overfitting the data. The networks may model large variances in the training data. However, if this value is too large the networks may never converge, because the weights will decay to zero. Increasing the decay parameter also increases training time. The decay and training time for the CCN evaluations are given in Table III.

Discussion of Results

The inclusion of data below the detection limit of an instrument is often avoided in developing calibration models. If data below the detection limit is included, nonlinearities in the model may be introduced. Neural networks can accomplish nonlinear modeling. For example, changes in concentration below the detection limit may result in no change in signal. However, recognition of the absence of a sample is important. Therefore, background scans were used for both calibration and prediction. An arbitrary detection limit was set to 0.1 ppb, and this value was assigned to the background scans. Therefore, recognition of a sample is achieved by predictions greater than this minimum concentration.

PLS is used as the control method. From the monotonic decrease of calibration error in Figure 2, one can see that PLS models nonlinear relationships. However, after 35 latent variables are used in the model, the error in predicting an external set of data increases. A PLS model with 35 latent variables is used as a control for comparison with CCN predictions. The PLS predictions are biased in that the model was optimized with respect to the prediction set. The optimal SEP and RSEP from this model are 0.322 (p-conc.), and 4.1%, respectively.

The effect of the decay parameter was evaluated with two CCN training configurations that were identical except for the use of a decay parameter. One configuration did not use weight decay in training, and the other had the weight decay set to an order of magnitude greater than learning rate. The magnitude of the decay parameter was chosen to be as large as possible, yet still furnish a reduction in error for each training cycle. Each training configuration was used to construct five networks which differed in only the random initial weights. Five replicates are used to study modeling error, caused by different initial conditions for the nonlinear optimization of the network.

Table III. Summary of CCN Results

Evaluation	SEP $d/\eta=10$ (p-Conc.)	RSEP $d/\eta=10$ (%)	Number of Hidden Units	SEP $d/\eta=0$ (p-Conc.)	RSEP $d/\eta=0$ (%)	Number of Hidden Units
Run 1	0.13	1.8	114	1.1	13	6
Run 2	0.14	1.9	119	1.05	13	6
Run 3	0.13	1.8	125	1.04	12	6
Run 4	0.15	2.0	119	1.06	13	6
Run 5	0.14	1.9	126	1.06	13	5
Average	**0.14±0.01**	**1.9±0.1**	**121±5**	**1.06±0.02**	**12.8±0.5**	**5.8±0.5**
PLS	0.322	4.1				

Large decay values increase network training times. The networks without the weight decay term took approximately 40 minutes each to train on a personal computer. The networks that trained with the large weight decay values each took approximately 15 hours to train. The increase in time by using large weight decay values, also applies to

backpropagation networks, which would be on the order of several days. Note that the number of hidden units is approximately 20 times larger for the CCN with the high decay value.

Large decay values are advantageous in that the networks avoid overfitting. A prevailing belief among neural network practitioners is that the neural network should be as small as possible to minimize overfitting the data set with too many adjustable parameters. These results demonstrate that including more adjustable parameters (i.e., hidden units) may improve a network's ability to generalize as shown by a decrease in error with external prediction sets. Note that the errors with the network that did not use a decay parameter are six times larger, and the lack of precision caused by modeling error is five times greater. The external prediction set was not used in training the network, or selecting training parameters.

Figures 3A-3I give the predicted and measured concentrations for each compound class. The predicted concentrations are the outputs from each of the nine output units. The points in the figures correspond to the spectra in the prediction set. This data was obtained from the results of five replicate runs of the CCN with the decay parameter. The CCN data is given as 95% confidence levels for each point, which indicates the model error associated with a spectrum. Spectra with large modeling errors are indicative of outliers. The PLS predictions are included in the figures. The reference line in the figures gives the ideal response. The points at the reported p-concentration of 10 either are reactant ions or are different compounds from those of the compound class. Note that the CCN performs favorably when compared to PLS. Each output unit corresponds to a compound in the training set. A compound is identified by its smallest p-concentration value. No compounds were misidentified in these evaluations.

Conclusions

IMS is an exciting area for the application of neural networks. The CCN is an excellent tool for the chemist. It has the advantages of a self-configuring topology, fast training rate and incremental learning. The use of the decay parameter can help a neural network generalize by modeling larger variations in the spectra. Large decay values not only reduce modeling errors, but also reduce the network convergence rate. If training time is increased by the use of the decay parameter, networks that train efficiently are desirable.

This study presents a general model for both quantitation and identification of organic compounds by IMS. Neural networks can perform better than standard data analysis methods such as PLS. Neural networks are well suited for IMS because they can be trained to have a property of shift invariance. This property is important to IMS data analysis for which temperature, pressure and other atmospheric fluctuations may cause peak shifting in the spectra. Incremental learning with CCNs and the study of mixtures by IMS are areas of future research.

Acknowledgements
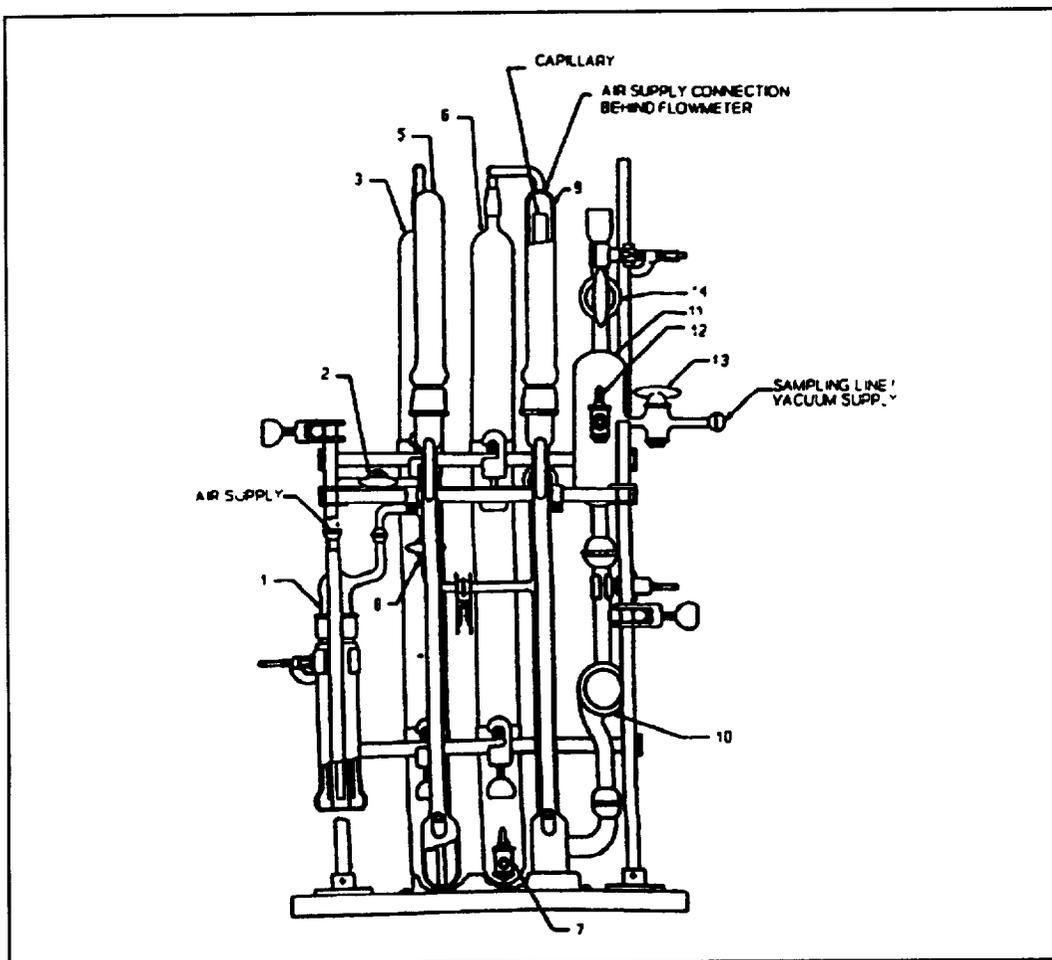
Figure 1. Schematic of the Q5 vapor generator.

322
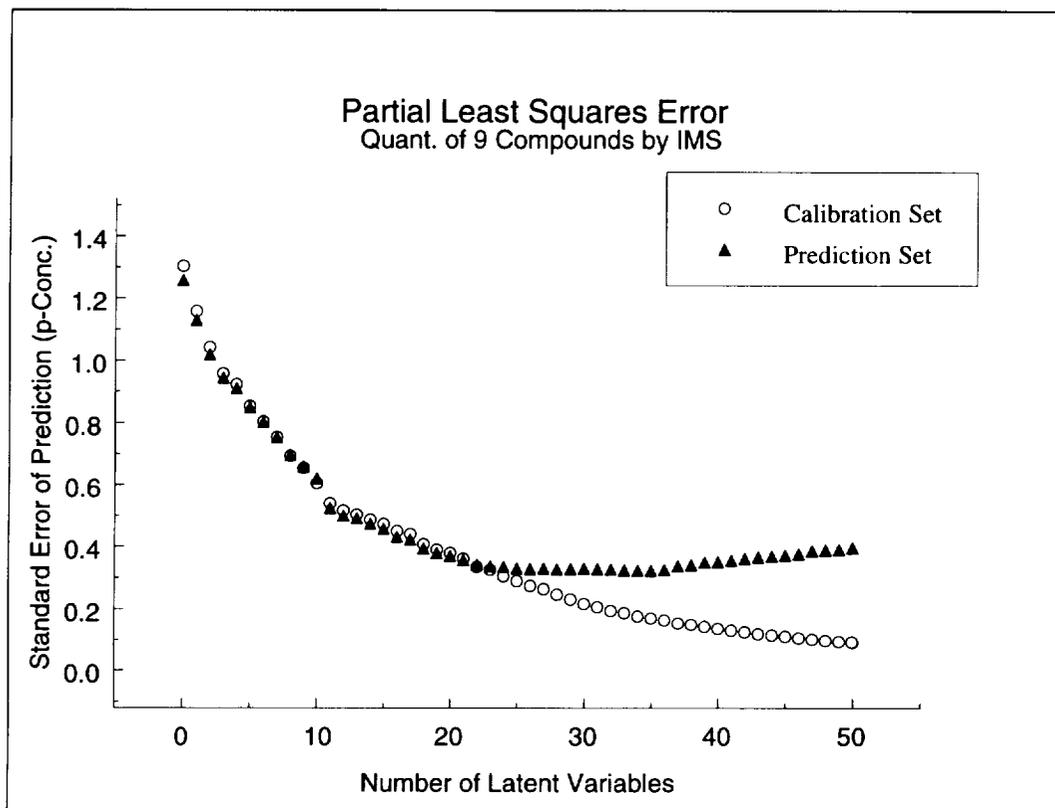
Figure 2.

CCN Prediction Data for Acetic Acid
95% Confidence Levels of 5 Replicated Networks
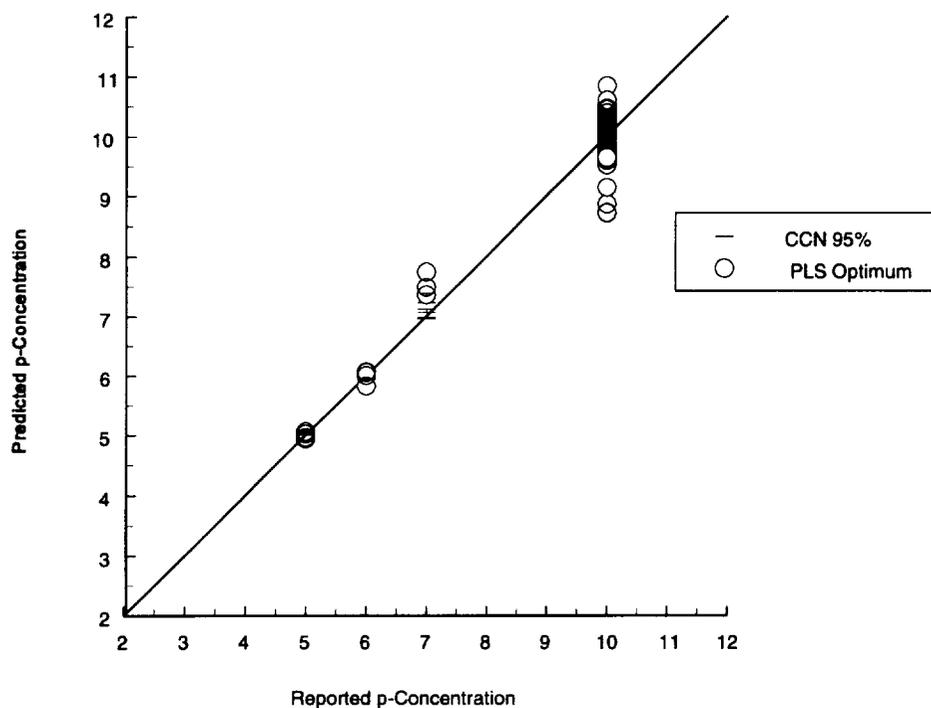
Figure 3A.

CCN Prediction Data for Acetic Anhydride
95% Confidence Levels of 5 Replicated Networks
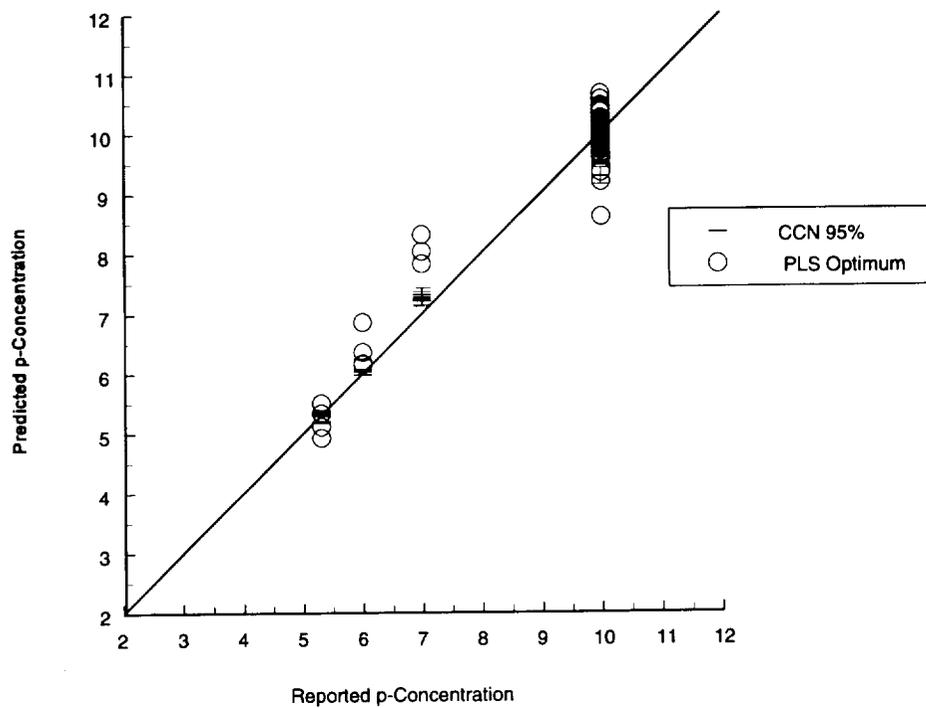
Figure 3B.

CCN Prediction Data for Acetone
95% Confidence Levels of 5 Replicated Networks
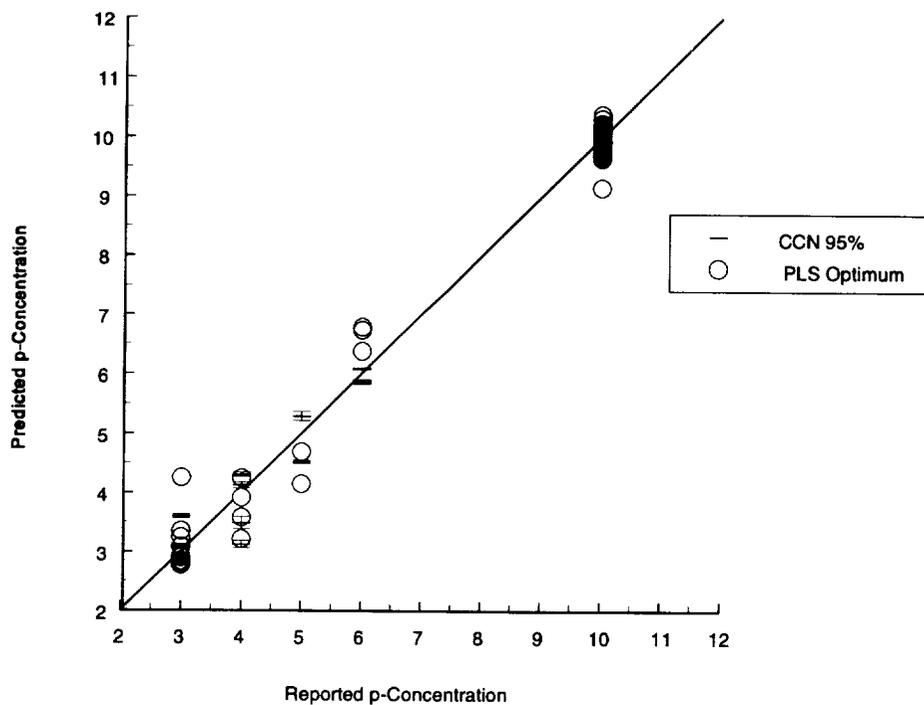
Figure 3C.

CCN Prediction Data for Diethyl Ether
95% Confidence Levels of 5 Replicated Networks
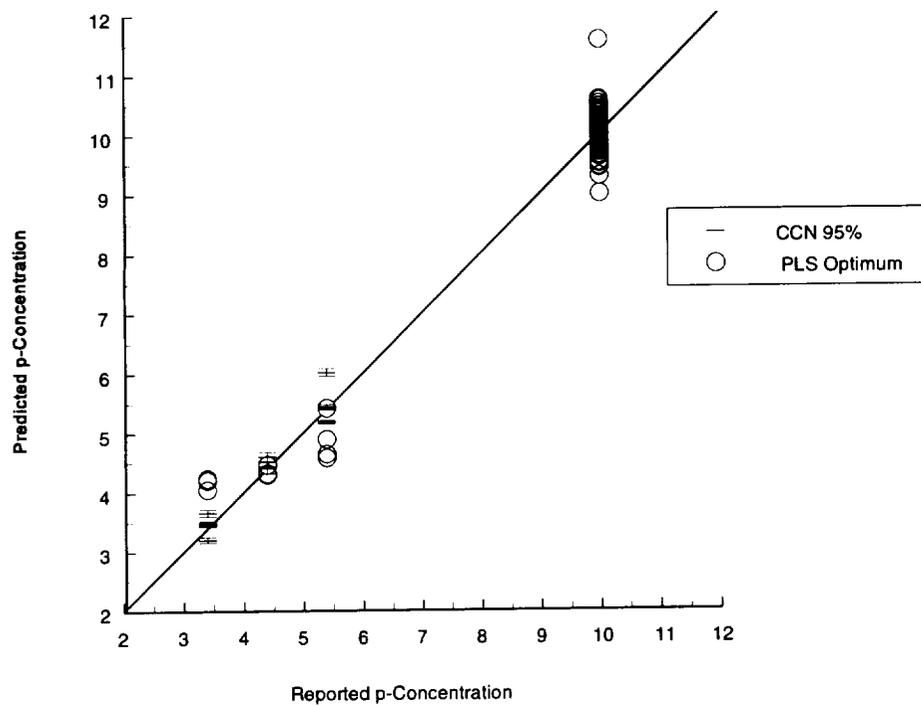
Figure 3D.

CCN Prediction Data for Isooctane
95% Confidence Levels of 5 Replicated Networks
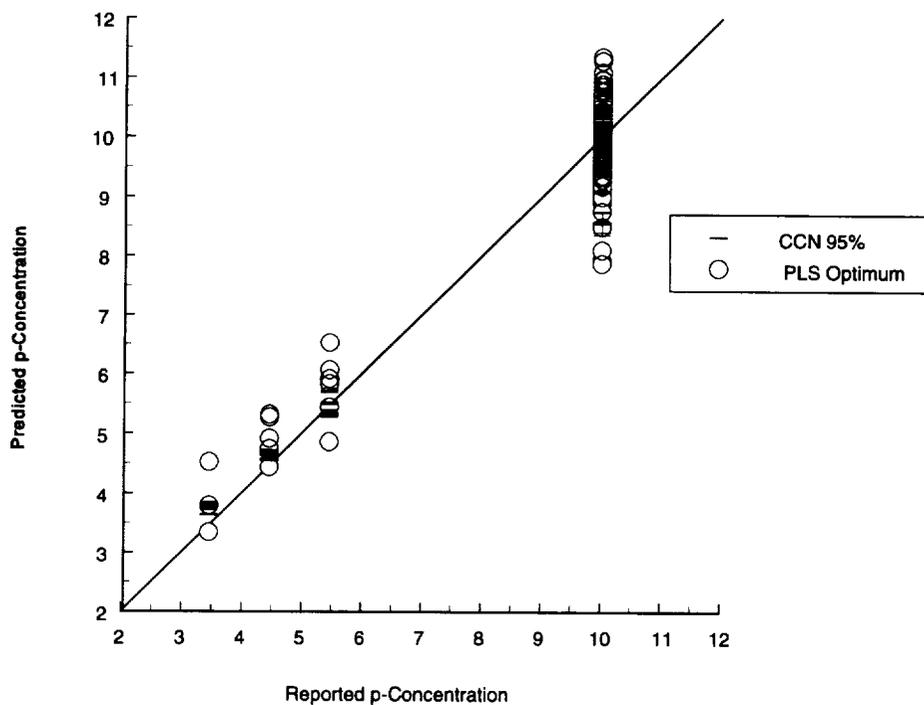
Figure 3E.

CCN Prediction Data for Isopropanol
95% Confidence Levels of 5 Replicated Networks
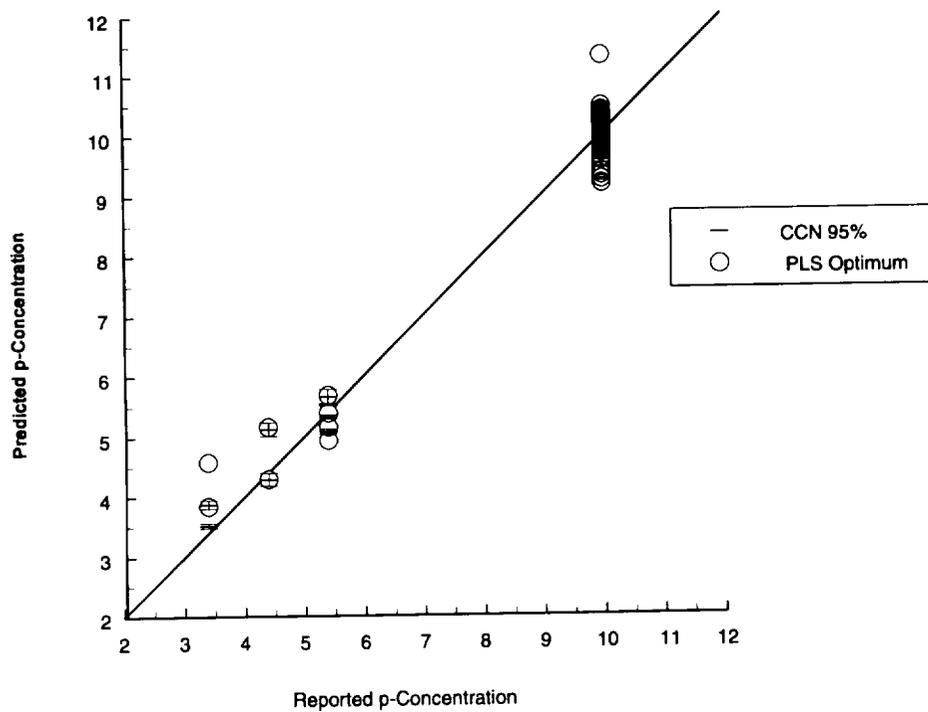
Figure 3F.

CCN Prediction Data for Methyl Benzoate
95% Confidence Levels of 5 Replicated Networks
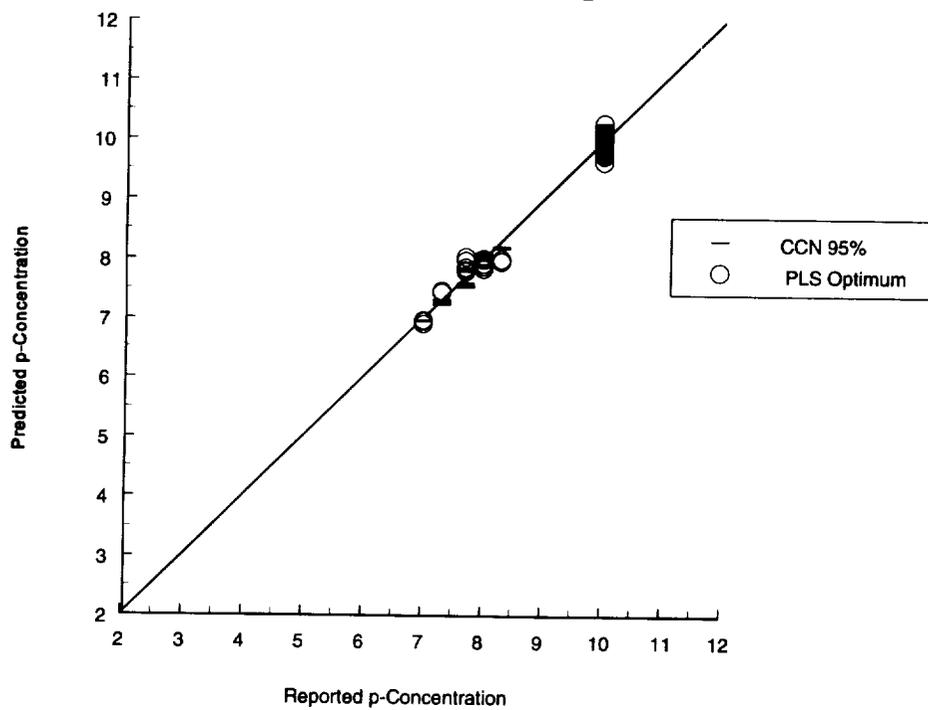
Figure 3G.

CCN Prediction Data for o-Nitro Toluene
95% Confidence Levels of 5 Replicated Networks

Figure 3H.

CCN Prediction Data for Toluene
95% Confidence Levels of 5 Replicated Networks
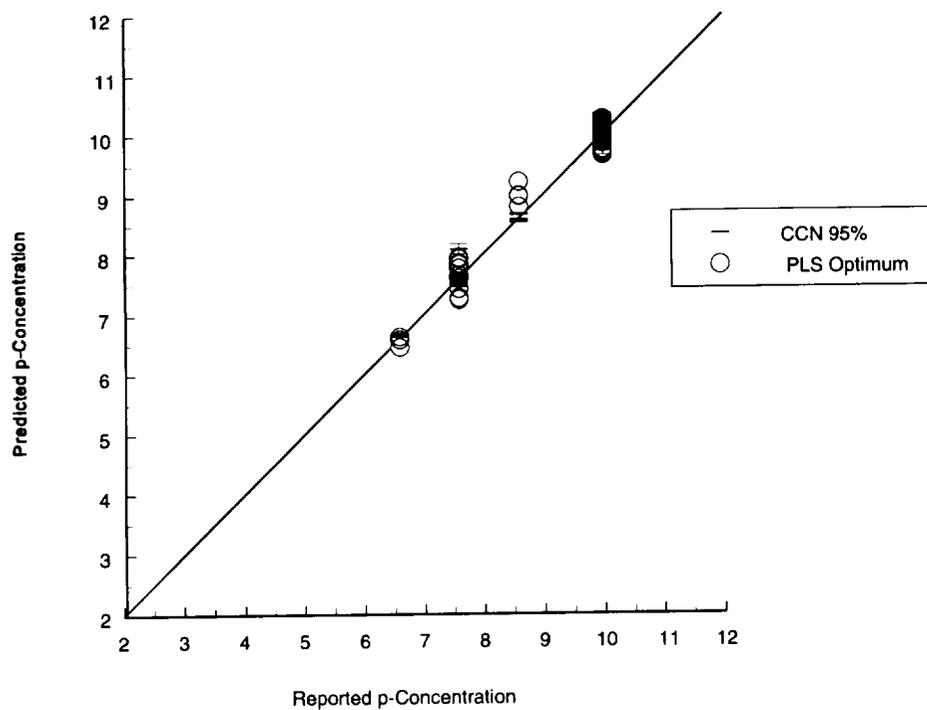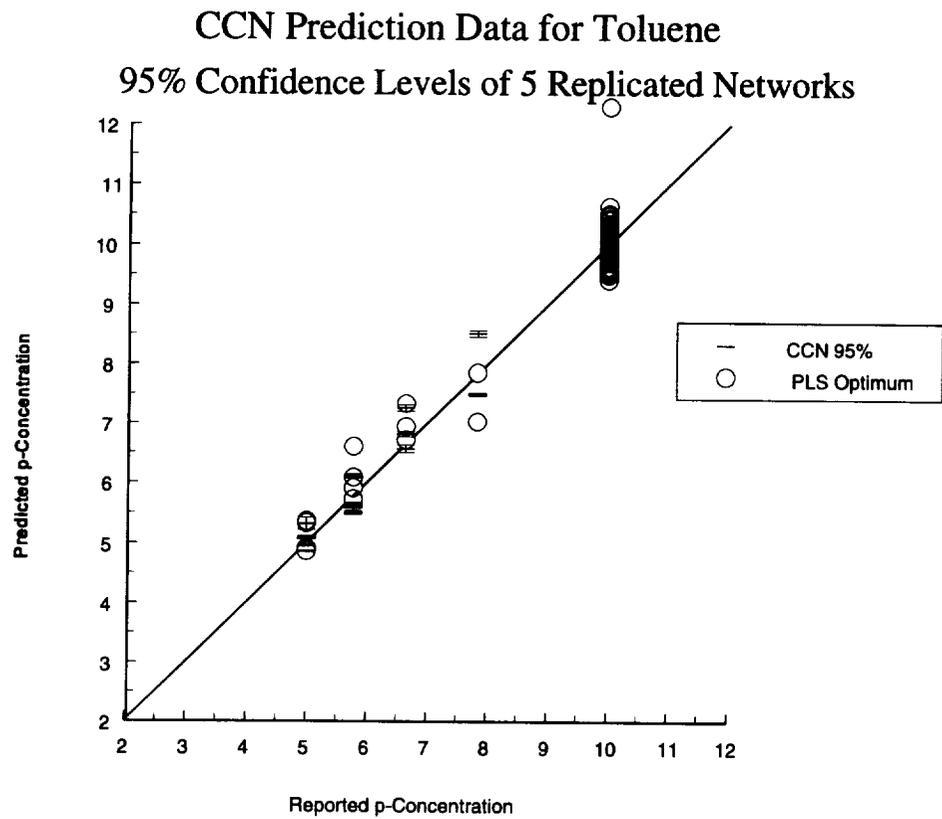
Figure 3I.

Citations

1. Bell, S.E., Mead, W.C., Jones, R.D., Eiceman, G.A., and Ewing, R.G. Connectionist Hyperprism Neural Network for the Analysis of Ion Mobility Spectra: An Empirical Evaluation. *J. Chem. Inf. Comput. Sci.*, **33**, 609-615 (1993).

2. Boger, Z. and Karpas, Z. Use of Neural Networks for Quantitative Measurements in Ion Mobility Spectrometry (IMS), *J. Chem. Inf. Comput. Sci.*, **34**, 576-580 (1994).

3. Zheng, P. Davis, D.M. and Harrington, P.B. Comparison of Backpropagation and Counterpropagation Neural Networks for Quantitative Analysis of Ion Mobility Spectra presented at the 1994 Pittsburgh Conference, Chicago, IL, March 1994, **641**.

4. Fahlman, S.E. and Lebiere C., The Cascade Correlation Architecture. Carnegie Mellon University Report **CMU-CS-90-100**, August 1991, 1-13.

5. Masters T. Practical Neural Network Recipes in C++. Academic Press, San Diego, CA, pp. 128-132.

6. Geladi, P and Kowalski, B.R. Partial Least-Squares Regression: A Tutorial. *Anal. Chim. Acta,* **185**, 1-17 (1986).

6. Harrington, P.B. Temperature-Constrained Backpropagation Neural Networks. *Anal. Chem.*, **66**, 802-807 (1994).

8. Fahlman, S.E. An Empirical Study of Learning Speed in Back-Propagation Networks. Carnegie Mellon University Report **CMU-CS-88-162**, September 1988, 1-17.

FTP-Server for exchange, interpretation, and database-search of ion mobility spectra, literature, preprints and software

J.I.Baumbach, A.v.Irmer

Institut für Spektrochemie und angewandte Spektroskopie,
Bunsen-Kirchhoff-Str. 11, D-44139 Dortmund, Germany

ABSTRACT

To assist current discussion in the field of ion mobility spectrometry, at the Institut für Spektrochemie und angewandte Spektroskopie, Dortmund, start with 4th of December, 1994 the work of an FTP-Server, available for all research groups at universities, institutes and research worker in industry. We support the exchange, interpretation, and database-search of ion mobility spectra through data format JCAMP-DX as well as literature retrieval, pre-print, notice and discussion board.

We describe in general lines the entrance conditions, local addresses and main code words. For further details monthly a news report will be prepared for all common user directly. To organise the first call, please contact BAUMBACH@HELIOS.ISAS-DORTMUND.DE or VONIRMER@HELIOS.ISAS-DORTMUND.DE. We send the password and account soon as possible.

EXCHANGE, INTERPRETATION, AND DATABASE-SEARCH OF SPECTRA

To assist peak assignment in ion mobility spectrometry it is important to have quality reference data. The reference collection should be stored in a database system which is capable of being searched using spectral or substance information. We propose to build such a database customized for ion mobility spectra. To start off with it is important to quickly reach a critical mass of data in the collection. We wish to obtain as many spectra combined with their IMS parameters as possible. Spectra suppliers will be rewarded for their participation with access to the database. To make the data exchange between users and system administration possible, it is important to define a file format specially made for the requirements of ion mobility spectra. The format should be computer readable and flexible enough for extensive comments to be included. In this document we propose a data exchange format, and we would like you to give comments on it.

For the international data exchange it is important, to have a standard data exchange format. We propose to base the definition of this format on the JCAMP-DX protocol, which was developed for the exchange of infrared spectra. This standard made by the <u>J</u>oint <u>C</u>ommittee on <u>A</u>tomic and <u>M</u>olecular <u>P</u>hysical Data is of a flexible design. The aim of this paper is to adopt JCAMP-DX to the special requirements of ion mobility spectra.

For further details see: "Exchange, interpretation, and database-search of ion mobility spectra supported by data format JCAMP-DX" by J.I.Baumbach, A. Davies, A.v.Irmer, P.Lampen.

FTP-SERVER & DATABASE

The main structure of the FTP-Server and Database is given in figure 1: The input includes ion mobility spectra themselves for pure components or mixtures and the different IMS configurations used in the experiments, commercial or home-made. Special boards for questions and answers and discussions are available. The retrieval system includes different literature databases from the IMS research community as well as news from the laboratories. A main point is the IMS-Preprint service. Please send pre-prints in your own word-processing system and pictures as TIFF files attached to the DATASERVER. Thus, very short

distributions time can be reached. The newest information will be available. Comments on papers are possible as well deep discussion on special topics to later main papers and publications.

IMS-Configuration · IMS-Preprints

IMS-Questions and Answers

IM-Spectrum

Discussions

FTP-Server & Database

Investigations

on Spectra

on Literature

interdisciplinary Information exchange about IMS
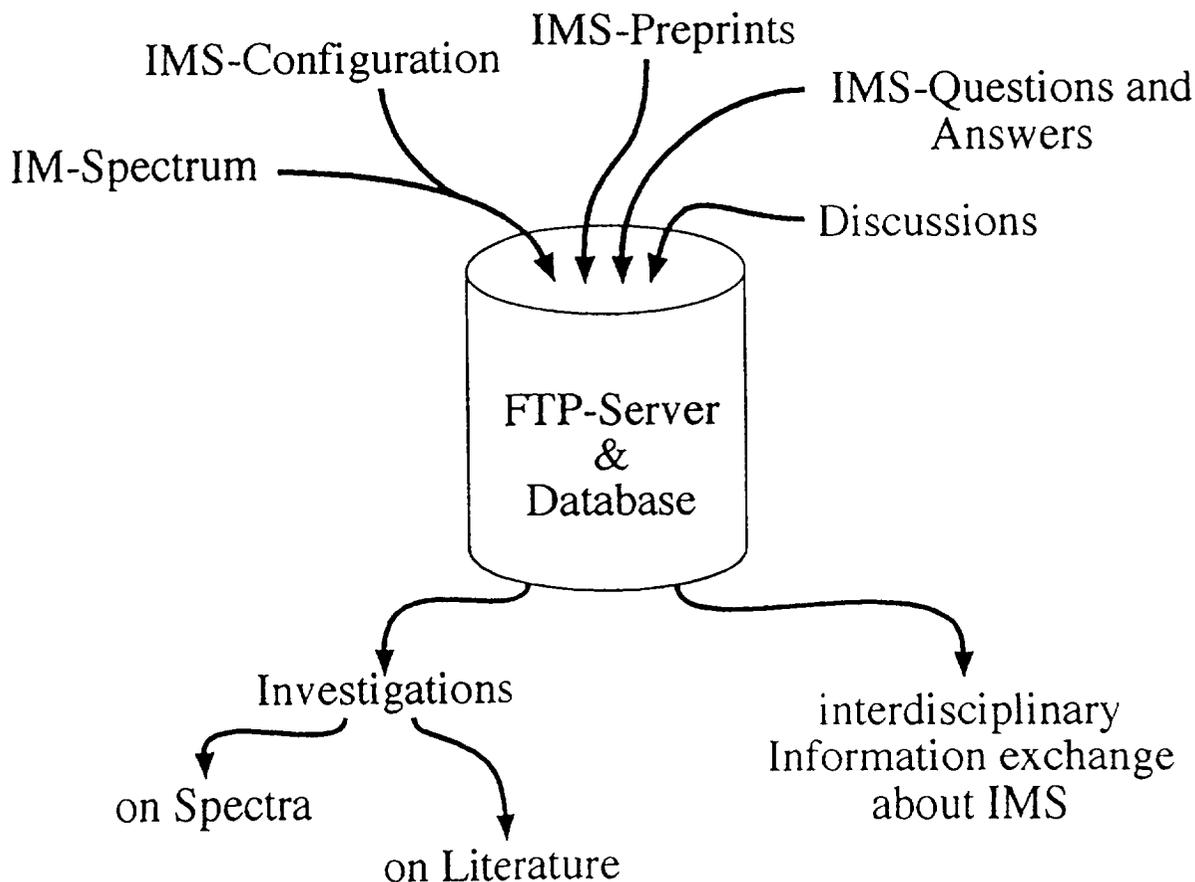
Figure 1: Main structure of FTP-Server & Database

ACCOUNT, PASSWORD AND FURTHER INFORMATION

The details of the server account are given in Table 1. This includes the FTP- oder TELNET-ACCOUNT to DATASERVER.ISAS.DE with the main password IMSDATA and the private password sended on request to the E-Mail addresses:

Table 1: General pass line to DATASERVER at the Institut für Spektrochemie und ange-wandte Spektroskopie, Dortmund	
TELNET	DATASERVER.ISAS.DE
FTP	DATASERVER.ISAS.DE
general password	IMSDATA
private password	will be sended on request
User	IMS

BAUMBACH@HELIOS.ISAS-DORTMUND.DE or
VONIRMER@HELIOS.ISAS-DORTMUND.DE soon to the participants. The USER name is
IMS. All details are readable on the page or will be sended on request.

HELPLINE AND SUPPORT

If an open question occurs, please don't hesitate to contact: Dr. Jörg Ingo Baumbach, Insitut
für Spektrochemie und angewandte Spektroskopie, Bunsen-Kirchhoff-Str. 11, D-44139
Dortmund, Telefon +49-231-1392-238, FAX +49-231-1392-120.

REPORT DOCUMENTATION PAGE

Form Approved
OMB No. 0704-0188

1. AGENCY USE ONLY (Leave Blank)	2. REPORT DATE April 1995	3. REPORT TYPE AND DATES COVERED NASA Conference Publication

4. TITLE AND SUBTITLE

Third International Workshop on Ion Mobility Spectrometry

5. FUNDING NUMBERS

6. AUTHOR(S)

John H. Cross*, Editor

7. PERFORMING ORGANIZATION NAME(S) AND ADDRESS(ES)

Lyndon B. Johnson Space Center
Medical Sciences Division
Houston, Texas 77058

8. PERFORMING ORGANIZATION REPORT NUMBERS

S-799

9. SPONSORING/MONITORING AGENCY NAME(S) AND ADDRESS(ES)

National Aeronautics and Space Administration
Washington, DC 20546-0001

10. SPONSORING/MONITORING AGENCY REPORT NUMBER

CP-3301

11. SUPPLEMENTARY NOTES

*KRUG Life Sciences, Houston, Texas

12a. DISTRIBUTION/AVAILABILITY STATEMENT

Unclassified/Unlimited
Available from the NASA Center for AeroSpace Information (CASI)
800 Elkridge Landing Road
Linthicum Heights, MD 21090-2934
(301) 621-0390

Subject Category: 25

12b. DISTRIBUTION CODE

13. ABSTRACT *(Maximum 200 words)*

Basic research in ion mobility spectrometry has given rise to rapid advancement in hardware development and applications. The Third International Workshop on Ion Mobility Spectrometry (IMS) was held October 16-19, 1994, at Johnson Space Center to provide a forum for investigators to present the most recent results of both basic and applied IMS research. Presenters included manufacturers and various users, including military research organizations and drug enforcement agencies. Thirty papers were given in the following five sessions: Fundamental IMS Studies, Instrument Development, Hyphenated IMS Techniques, Applications, and Data Reduction and Signal Processing. Advances in hardware development, software development, and user applications are described.

14. SUBJECT TERMS

Ion Motion, Mass Spectrometers, Gas Chromatography, Chemical Analysis, Ion Mobility Spectrometry, Conferences

15. NUMBER OF PAGES
344

16. PRICE CODE

17. SECURITY CLASSIFICATION OF REPORT	18. SECURITY CLASSIFICATION OF THIS PAGE	19. SECURITY CLASSIFICATION OF ABSTRACT	20. LIMITATION OF ABSTRACT
Unclassified	Unclassified	Unclassified	Unlimited

NSN 7540-01-280-5500

Standard Form 298 (Rev 2-89)
Prescribed by ANSI Std. 239-18
298-102